

- 1 J. McL. Emmerson: *Symmetry principles in particle physics* (1972)
- 2 J. M. Irvine: *Heavy nuclei, superheavy nuclei, and neutron stars* (1975)
- 3 I. S. Towner: *A shell-model description of light nuclei* (1977)
- 4 P. E. Hodgson: *Nuclear heavy-ion reactions* (1978)
- 5 R. D. Lawson: *Theory of the nuclear shell model* (1980)
- 6 W. E. Frahn: *Diffractive processes in nuclear physics* (1985)
- 7 S. S. M. Wong: *Nuclear statistical spectroscopy* (1986)
- 8 N. Ullah: *Matrix ensembles in the many-nucleon problem* (1987)
- 9 A. N. Antonov, P. E. Hodgson, and I. Zh. Petkov: *Nucleon momentum and density distributions in nuclei* (1988)
- 10 D. Bonatsos: *Interacting boson models of nuclear structure* (1988)
- 11 H. Ejiri and M. J. A. de Voigt: *Gamma-ray and electron spectroscopy in nuclear physics* (1989)
- 12 B. Castel and I. S. Towner: *Modern theories of nuclear moments* (1990)
- 13 R. F. Casten: *Nuclear structure* (1990)
- 14 I. Zh. Petkov and M. V. Stoitsov: *Nuclear density function theory* (1991)
- 15 E. Gadioli and P. E. Hodgson: *Pre-equilibrium nuclear reactions* (1992)
- 16 J. D. Walecka: *Theoretical nuclear and subnuclear physics* (1995)
- 17 D. N. Poenaru and W. Greiner (eds.): *Handbook of nuclear properties* (1995)
- 18 P. Fröbrich and R. Lipperheide: *Theory of nuclear reactions* (1996)

# Theory of Nuclear Reactions

P. FRÖBRICH

and

R. LIPPERHEIDE

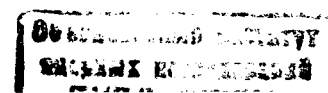
*Hahn-Meitner Institute, Berlin  
Free University of Berlin*

C 343  
F - 94

2011-15938

CLARENDON PRESS • OXFORD

1996



Oxford University Press, Walton Street, Oxford OX2 6DP

Oxford New York

Athens Auckland Bangkok Bombay

Calcutta Cape Town Dar es Salaam Delhi

Florence Hong Kong Istanbul Karachi

Kuala Lumpur Madras Madrid Melbourne

Mexico City Nairobi Paris Singapore

Taipei Tokyo Toronto

and associated companies in

Berlin Ibadan

Oxford is a trade mark of Oxford University Press

Published in the United States  
by Oxford University Press Inc., New York

© P. Fröbrich and R. Lipperheide, 1996

All rights reserved. No part of this publication may be reproduced, stored in a retrieval system, or transmitted, in any form or by any means, without the prior permission in writing of Oxford University Press. Within the UK, exceptions are allowed in respect of any fair dealing for the purpose of research or private study, or criticism or review, as permitted under the Copyright, Designs and Patents Act, 1988, or in the case of reprographic reproduction in accordance with the terms of licences issued by the Copyright Licensing Agency. Enquiries concerning reproduction outside those terms and in other countries should be sent to the Rights Department, Oxford University Press, at the address above.

This book is sold subject to the condition that it shall not, by way of trade or otherwise, be lent, re-sold, hired out, or otherwise circulated without the publisher's prior consent in any form of binding or cover other than that in which it is published and without a similar condition including this condition being imposed on the subsequent purchaser.

A catalogue record for this book is available from the British Library

Library of Congress Cataloging in Publication Data

(Data applied for)

ISBN 0 19 853783 2

Typeset by the authors using LaTeX

Printed in Great Britain by  
Biddles Ltd., Guildford and King's Lynn

## PREFACE

The present book has grown out of a course of lectures on the theory of nuclear reactions given to graduate students of the Freie Universität Berlin over the last decade. Its aim is to explain in a self-contained way the main formalisms used for describing nonrelativistic nuclear reactions. The reader is led from the basic laws to the final formulae employed in the calculation of those quantities which can directly be compared with the measured data. In order to do this adequately, we often have to take recourse to simplifications. The emphasis lies on explaining the basic notions and how these are consistently formulated in mathematical language. We have made an effort to be as explicit as possible, and to present the derivations in so much detail that the reader should generally be able to follow the arguments of the text without recourse to other literature.

The list of topics treated is, of course, not exhaustive. We did not aim at a comprehensive description of all formalisms for the various types of nuclear reactions. Thus we omitted the entire field of nuclear reactions at higher energies. Moreover, some well-established subjects of low-energy reaction theory have not been discussed, as for example, *R*-matrix theory, or the theories of pre-compound reactions and Ericson fluctuations. We note, in particular, that in the last chapter we restrict ourselves to the so-called surface-friction model, which allows us to analyze deep-inelastic collisions and fusion within a unified classical framework by methods of non-equilibrium statistical physics. We made this choice because, first, we are more familiar with this approach than with others, and second, because we are able, in this way, to make a fairly direct connection with measured data. Selected citations of work not discussed in these lectures can be found in the notes and references collected at the end of each chapter.

The material of the book is divided into five main topics. In (A) *Potential scattering* we discuss the quantum theory of scattering by a potential of the type commonly employed in the calculation of nuclear elastic cross sections. The semiclassical and wave-optical descriptions are introduced as approximations to the quantal theory which provide additional physical insight into the meaning of the calculated results.

The second topic is (B) *Formal theory*. Here the general formalism is developed which allows one to calculate the cross section for any type of nuclear reaction involving two fragments in the initial and final channels. To help the understanding, the formal theory is introduced for the already known case of potential scattering, and is then generalized to more complicated processes. Included in the formal part is a theory of the optical model.

In (C) *Direct reactions* the results of the formal part are applied explicitly to reactions involving only few degrees of freedom. Here the reaction mechanism is simple and can often be identified in detail in the formalism. Single-step processes and coupled-channel systems are discussed.

The next topic is (D) *The compound nucleus*. We employ the original Bohr hypothesis

according to which a compound-nucleus reaction is described as ‘fusion’ in the entrance channel followed by ‘decay’ in the exit channel. Thus we consider fusion first, and then go on to study the compound-nucleus reaction as a whole.

Finally, we discuss (E) *Dissipation and fluctuations*. The subjects treated under this heading are deep-inelastic collisions, fusion and heavy-ion induced fission in the presence of dissipation. It cannot be said that a universally accepted description of these phenomena has been achieved thus far. The approach which we have chosen in this book is only one of many. It is purely classical and allows for a straightforward interpretation of the observed effects. The dissipation and fluctuation phenomena are first described as they manifest themselves in experiment. Then a classical stochastic theory for the analysis of these phenomena is presented. Finally, the results of various cross section calculations are compared with experiment.

We have benefited greatly from comments by I. I. Gontchar, H.-J. Krappe, C. Mahaux, K. Möhring, G. Reiss, and U. Wille, to whom we express our appreciation. We also thank I. Lang and B. Bohne for drawing the figures.

Berlin  
August 1995

P. F.  
R. L.

## CONTENTS

### A POTENTIAL SCATTERING

<b>1 The quantum theory of potential scattering</b>	3
1.1 Introduction	3
1.2 Quantal scattering by a short-range potential	4
1.2.1 The differential cross section	4
1.2.2 Calculation of the scattering amplitude	8
1.2.3 Scattering by a complex potential	12
1.3 Charged-particle scattering	16
1.3.1 Rutherford scattering	16
1.3.2 Coulomb-plus-nuclear scattering	22
1.4 Scattering of identical particles	25
1.4.1 Classical scattering	25
1.4.2 Quantal scattering	27
1.5 An example of potential scattering	29
1.6 Notes and references	32
<b>2 Semiclassical scattering</b>	34
2.1 Introduction	34
2.2 Classical scattering	35
2.2.1 The deflection function	35
2.2.2 The classical cross section	37
2.2.3 Glory, rainbow, and orbiting	43
2.3 The semiclassical approximation (WKB)	47
2.3.1 The phase shifts in the semiclassical approximation	48
2.3.2 Evaluation of the scattering amplitude in WKB	56
2.4 Special features of semiclassical scattering	60
2.4.1 The glory	60
2.4.2 The rainbow	61
2.5 Semiclassical approximation for complex potentials	67
2.5.1 Phase shifts for integer angular momenta	67
2.5.2 Complex angular momenta: saddle points	69
2.6 Notes and references	72
<b>3 The wave-optical description of potential scattering</b>	75
3.1 Introduction	75
3.2 Diffraction in optics and nuclear scattering	76
3.2.1 The scattering of light	76

3.2.2	Nuclear scattering	78
3.3	Diffraction by a black nucleus	80
3.3.1	Fraunhofer diffraction	80
3.3.2	Fresnel diffraction	83
3.4	The strong absorption model	87
3.5	Notes and references	88
<b>B FORMAL THEORY</b>		
<b>4</b>	<b>The formal theory of potential scattering</b>	93
4.1	Introduction	93
4.2	The time-dependent formalism	93
4.2.1	The free wave packet state	93
4.2.2	The time-dependent scattering state	97
4.3	The time-independent formalism	100
4.3.1	The stationary scattering states	100
4.3.2	The Lippmann–Schwinger equation	102
4.3.3	Orthogonality and completeness	104
4.3.4	The $T$ -matrix	105
4.3.5	The $S$ -matrix	108
4.3.6	The unitarity of the $S$ -matrix. The optical theorem	109
4.4	Asymptotic properties and the cross section	111
4.4.1	The asymptotic stationary scattering wave function	111
4.4.2	Asymptotic wave packets. The cross section	112
4.5	Coherence properties of particle beams	115
4.5.1	The structure of the physical probability current	115
4.5.2	A model for the incident beam	117
4.6	Notes and references	119
<b>5</b>	<b>The formal theory of reactions</b>	121
5.1	Introduction	121
5.2	The general formalism for two-body channels	122
5.2.1	Channels	122
5.2.2	Reaction states	125
5.2.3	The $T$ - and $S$ -matrices	130
5.2.4	The optical theorem	132
5.2.5	The cross section	133
5.2.6	The principle of micro-reversibility	134
5.3	The differential reaction cross section	136
5.3.1	Spin-coupled channel states	136
5.3.2	The spin-coupled scattering matrices	137
5.3.3	The unpolarized differential cross section	138
5.4	Single-step approximations	141
5.4.1	The plane-wave Born approximation (PWBA)	141
5.4.2	The distorted-wave Born approximation (DWBA)	141

5.5	Coupled channels	143
5.5.1	The coupled-channel formalism for inelastic scattering	144
5.5.2	The coupled-channel Born approximation (CCBA)	146
5.5.3	Coupled reaction channels	147
5.6	Notes and references	149
<b>6</b>	<b>The optical model</b>	151
6.1	Introduction	151
6.2	The generalized optical potential (GOP)	152
6.2.1	The general form of the GOP operator	152
6.2.2	A schematic model: the model space	154
6.2.3	Derivation of the model-GOP	156
6.2.4	Analyticity, non-locality, and the Pauli principle	161
6.3	The optical potential	164
6.3.1	The elastic $S$ -matrix	164
6.3.2	Compound-elastic and shape-elastic scattering	167
6.3.3	The optical potential in the proper sense	170
6.3.4	The relation between the GOP and the optical potential	172
6.4	The equivalent local optical potential	174
6.4.1	The trivially equivalent local potential	174
6.4.2	The equivalent local potential in WKB	175
6.5	Dispersion relations	181
6.5.1	Derivation of the dispersion relation	181
6.5.2	An application of the dispersion relation	184
6.6	Notes and references	187
<b>C DIRECT REACTIONS</b>		
<b>7</b>	<b>Single-step approximations</b>	193
7.1	Introduction	193
7.2	PWBA for nucleon transfer	194
7.2.1	The $T$ -matrix in PWBA	194
7.2.2	Interpretation of the $T$ -matrix for nucleon transfer	198
7.2.3	The target structure factor	204
7.2.4	The (d,p) reaction in PWBA	206
7.3	DWBA for nucleon transfer	210
7.3.1	The general expression for the $T$ -matrix in DWBA	210
7.3.2	The (d,p) reaction in DWBA	214
7.3.3	The zero-range approximation	217
7.3.4	Finite-range calculations	220
7.4	Classical selection rules	223
7.5	An example of single-nucleon transfer between heavy ions	227
7.6	Notes and references	230

<b>8 The coupled-channel description of direct reactions</b>	232	<b>10 Compound-nucleus reactions</b>	322
8.1 Introduction	232	10.1 Introduction	322
8.2 The coupled-channel (CC) formalism for inelastic scattering	233	10.2 The compound reaction cross section	323
8.2.1 The CC equations in the partial-wave decomposition	233	10.2.1 The fluctuation cross section	323
8.2.2 The calculation of the inelastic cross section	236	10.2.2 The Hauser–Feshbach formula	325
8.2.3 Spin–orbit coupling	238	10.2.3 The angle-differential cross section	327
8.3 Inelastic excitation of collective states	239	10.2.4 The energy-differential cross section	329
8.3.1 The general form of the matrix elements	239	10.3 The nuclear level density	331
8.3.2 Rotational excitations	245	10.3.1 The level density in the Fermi gas model	331
8.3.3 Vibrational excitations	248	10.3.2 The level density in the nuclear shell model	338
8.4 The Coulomb polarization potential	251	10.3.3 On the derivation of the level density formulae	340
8.4.1 The generalized Coulomb polarization potential	251	10.3.4 A practical level density formula	342
8.4.2 The equivalent local Coulomb polarization potential	253	10.4 Decay modes of the compound nucleus	343
8.4.3 Examples	257	10.4.1 The evaporation cross section	344
8.5 The coupled-channel Born approximation (CCBA) for transfer	260	10.4.2 Rates of fusion, evaporation, fission, and $\gamma$ -decay	346
8.6 Coupled-reaction-channel calculations (CRC)	262	10.4.3 Evaporation cascades in light systems	357
8.7 Notes and references	265	10.5 Notes and references	358

## D THE COMPOUND NUCLEUS

<b>9 Fusion</b>	271
9.1 Introduction	271
9.2 The compound nucleus	273
9.2.1 The compound nucleus and its decay	273
9.2.2 Stability in the mass	274
9.2.3 Stability in angular momentum	278
9.3 Fusion above the barrier	279
9.3.1 The classical fusion cross section	279
9.3.2 Compound nucleus stability and the fusion cross section	284
9.3.3 The yrast-line limitation	286
9.3.4 The critical distance	287
9.3.5 Summary of the classical description of fusion	289
9.3.6 A classification of nuclear reactions	291
9.4 Sub-barrier fusion	293
9.4.1 The transmission coefficient in the WKB approximation	293
9.4.2 Tunnelling through a parabolic barrier	297
9.4.3 Semiclassical transmission in nuclear fusion	300
9.4.4 Quantal barrier penetration	302
9.5 Fusion in the presence of nuclear excitations	304
9.5.1 A schematic two-channel model	306
9.5.2 The zero-point fluctuation formula	308
9.5.3 The full coupled-channel description	313
9.6 Description of fusion in the optical model	316
9.7 Notes and references	319

## E DISSIPATION AND FLUCTUATIONS

<b>11 Deep-inelastic collisions. Phenomena and theory</b>	363
11.1 Introduction	363
11.2 Dissipative phenomena	364
11.2.1 The spin distribution of nuclear reactions	364
11.2.2 Characteristic features of deep-inelastic collisions (DIC)	367
11.2.3 The friction hypothesis	370
11.3 The Langevin description	371
11.3.1 A model Lagrangian and its equations of motion	371
11.3.2 The renormalized potential	373
11.3.3 The frictional force	373
11.3.4 The Langevin force	375
11.3.5 The fluctuation-dissipation theorem	378
11.3.6 The Langevin equations; their applicability to DIC	379
11.3.7 Discretization of the Langevin equations	380
11.4 The Fokker–Planck description	382
11.4.1 The Kramers–Moyal expansion	382
11.4.2 The connection with the Langevin equations	383
11.4.3 The Fokker–Planck equation	384
11.4.4 Simple examples	385
11.5 Methods of solving for the distribution function	392
11.5.1 The Gaussian solution of the Fokker–Planck equation	392
11.5.2 Computer simulation of the Langevin process	396
11.6 Notes and references	400

<b>12 Analysis of deep-inelastic collisions, fusion, and heavy-ion induced fission</b>	404
12.1 Introduction	404
12.2 Classical trajectories in the surface-friction model	405
12.2.1 Rigid nuclei	405
12.2.2 Deformable nuclei	410
12.2.3 DIC: The energy–angle correlation	415
12.2.4 Fusion above the barrier. The extra push	418
12.3 Fluctuations in deep-inelastic collisions and fusion	424
12.3.1 Gaussian solution of the Fokker–Planck equation	425
12.3.2 Monte Carlo sampling of Langevin trajectories	430
12.3.3 Bifurcation into fusion and DIC close to the barrier	432
12.3.4 The spin distributions of fusion and DIC	434
12.3.5 Superheavy elements	438
12.3.6 $\delta$ -electrons as an atomic clock for DIC	439
12.4 Dynamical effects in heavy-ion induced fission	441
12.4.1 The dynamical phase of fission	442
12.4.2 The stationary phase of fission	449
12.4.3 Example. Fission probabilities and neutron multiplicities	456
12.5 Notes and references	458
<b>Index</b>	463

## Part A

### Potential scattering

## THE QUANTUM THEORY OF POTENTIAL SCATTERING

### 1.1 Introduction

Potential scattering is the scattering of two collision partners whose mutual interaction is described by a static potential. This potential depends in general on the structure of the collision partners, in particular, on their size and shape (usually taken as spherical), but once the potential is specified and the centre-of-mass motion is separated out, the scattering problem in the remaining relative coordinate reduces to the description of the motion of a point-particle with a mass equal to the reduced mass of the two collision partners in the static field of the interaction potential. Only *elastic* scattering can be described in this way.

Actual elastic scattering of nuclei is in general rather more complicated. It is coupled to the internal degrees of freedom of the collision partners, and as a consequence the latter may temporarily change in shape and structure during the scattering process. When this is the case, the description of the elastic part of the collision process in terms of a simple potential would seem to be no longer adequate. However, one should not conclude from this that the potential approach must be dismissed, for one can account rather well for the nuclear elastic scattering phenomena by employing a potential of a more general nature, the ‘optical potential’. Moreover, in a rigorous treatment of general nuclear reactions, parts of the process, especially in the initial and final stages, are indeed of potential-scattering type.

Potential scattering involves only a minimum number of degrees of freedom, and the formalism for its description is simple. It is well suited for introducing many of the basic concepts and approximations of reaction theory, and for demonstrating in detail how concrete calculations of the actually measured quantities, namely the cross sections, are carried out.

The scattering of nuclei is a quantum phenomenon. We shall, therefore, begin with the *quantum theory of potential scattering*. In some instances the particle aspects of nuclear scattering are more pronounced, whereas in others, the wave nature of the process predominates. Both cases allow for simplifying approximations, which will be treated in later chapters.

In the present chapter several features of potential scattering will be discussed. In Section 1.2 we define the *elastic scattering cross section*, and explain its relation to the asymptotic form of the wave function. For the calculation of this wave function we consider a central, i.e. spherically symmetric, potential of short range. A decomposition of the three-dimensional scattering wave function into partial waves then reduces the

problem to the solution of a one-dimensional radial Schrödinger equation for each partial wave separately.

In order to account for the loss of probability current in quantal elastic scattering due to non-elastic processes, one introduces an absorptive, imaginary part in the scattering potential. The potential is thus generalised to the complex *optical potential*, which in addition to the elastic cross section, allows one also to calculate the reaction cross section.

In Section 1.3 we turn to *charged-particle scattering*, which is obviously an important aspect of any nuclear collision, since all nuclei carry charge. We first discuss Rutherford (i.e. point-Coulomb) scattering, for which the scattering amplitude can be written down in closed form. One is thus able to avoid the expansion in partial waves which, here, is not absolutely convergent owing to the slow fall-off of the Coulomb field at large distances. Thereafter we show how the partial-wave method can be adapted to calculate the scattering amplitude for a combined Coulomb-plus-nuclear potential.

The scattering of *identical particles* gives rise to special quantal effects which are described in Section 1.4. Finally, in Section 1.5, we discuss a practical example of potential scattering for the purpose of illustration.

## 1.2 Quantal scattering by a short-range potential

### 1.2.1 The differential cross section

We consider the scattering of two collision partners whose interaction is described by the central potential  $V(r)$ , where  $r = |\mathbf{r}_1 - \mathbf{r}_2|$  is the distance between the two particles. The potential is assumed to be less singular than  $1/r^2$  at the origin and of ‘short range’, i.e. it is supposed to vanish faster than  $1/r$  at large distances,

$$rV(r) \rightarrow 0 \text{ for } r \rightarrow \infty.$$

This condition is sufficient to guarantee that the wave function goes over into a *free* wave function at large distances. Actually, we shall simply require that the potential vanishes beyond some distance  $a$ ,

$$V(r) = 0 \text{ for } r \geq a. \quad (1.1)$$

The nuclear potentials usually considered fall off exponentially at large distances, and for these the condition (1.1) is effectively valid.

The two-body problem is reduced to the problem of a point particle in a fixed potential field by separating off the centre-of-mass motion. Let the projectile have mass  $m_1$  and coordinate  $\mathbf{r}_1$ , and the target, mass  $m_2$  and coordinate  $\mathbf{r}_2$ . We introduce the centre-of-mass coordinate  $\mathbf{R}$  and the relative coordinate  $\mathbf{r}$ ,

$$\begin{aligned} \mathbf{R} &= \frac{m_1\mathbf{r}_1 + m_2\mathbf{r}_2}{m_1 + m_2}, \\ \mathbf{r} &= \mathbf{r}_1 - \mathbf{r}_2, \end{aligned} \quad (1.2)$$

and correspondingly the total momentum  $\mathbf{P}$  and the relative momentum  $\mathbf{p}$ ,

$$\begin{aligned} \mathbf{P} &= \mathbf{p}_1 + \mathbf{p}_2, \\ \mathbf{p} &= \frac{m_2\mathbf{p}_1 - m_1\mathbf{p}_2}{m_1 + m_2}. \end{aligned} \quad (1.3)$$

The total Hamiltonian then separates into the centre-of-mass kinetic energy  $\mathbf{P}^2/2M$  and the Hamiltonian  $H$  for the relative motion,

$$H_{\text{tot}} = \frac{\mathbf{p}_1^2}{2m_1} + \frac{\mathbf{p}_2^2}{2m_2} + V(r) = \frac{\mathbf{P}^2}{2M} + H \quad (1.4)$$

with

$$H = \frac{\mathbf{p}^2}{2\mu} + V(r); \quad (1.5)$$

here  $M = m_1 + m_2$  is the total, and  $\mu = m_1m_2/(m_1 + m_2)$  the reduced mass. In explicit operator form we have

$$\mathbf{P} = \frac{\hbar}{i}\nabla_R, \quad H = -\frac{\hbar^2}{2\mu}\nabla^2 + V(r), \quad (1.6)$$

where  $\nabla^2$  is the Laplacian in the relative coordinate  $\mathbf{r}$ .

The two-body eigenfunction of  $H_{\text{tot}}$ ,  $\Psi(\mathbf{r}_1, \mathbf{r}_2)$ , factorizes into a plane wave representing the centre-of-mass motion and a function  $\psi(\mathbf{r})$  describing the relative motion,

$$\Psi(\mathbf{r}_1, \mathbf{r}_2) = e^{i\mathbf{K}\cdot\mathbf{R}}\psi(\mathbf{r}), \quad (1.7)$$

where the constant vector  $\mathbf{K} = \mathbf{P}/\hbar$  is the wave vector, i.e. the momentum in units of  $\hbar$ , of the free centre-of-mass motion. The wave function  $\psi(\mathbf{r})$  satisfies the stationary one-body Schrödinger equation

$$H\psi(\mathbf{r}) = E\psi(\mathbf{r}), \quad (1.8)$$

where  $E$  is the energy of the relative motion.

As a boundary condition on the scattering solution  $\psi(\mathbf{r})$  we require that at large distances it consists of an incident plane wave with momentum  $\mathbf{p}$ , where  $\mathbf{p}^2/2\mu = E$ , plus a scattered part which has the form of an outgoing spherical wave emerging from the scattering centre,

$$\psi(\mathbf{r}) \rightarrow e^{i\mathbf{k}\cdot\mathbf{r}} + f(\Omega)\frac{e^{ikr}}{r} \text{ for } r \rightarrow \infty; \quad (1.9)$$

here  $\mathbf{k} = \mathbf{p}/\hbar$ , and  $\Omega$  is the angular part of the coordinate  $\mathbf{r}$ . The  $z$ -axis is chosen along the direction of the incoming relative momentum  $\hbar\mathbf{k}$ , and the solid angle  $\Omega$  is referred to this axis. The amplitude  $f(\Omega)$  determining the strength of the scattered wave is called the *scattering amplitude*.

The wave function (1.9) is indeed a solution of eqn (1.8) for  $r \rightarrow \infty$ : in this limit one has  $H = -(\hbar^2/2\mu)\nabla^2$ , and both terms on the right-hand side of eqn (1.9) are eigenstates of this operator with eigenvalue  $E = \hbar^2k^2/2\mu$ , namely

$$-\frac{\hbar^2}{2\mu}\nabla^2 e^{i\mathbf{k}\cdot\mathbf{r}} = \frac{\hbar^2 k^2}{2\mu} e^{i\mathbf{k}\cdot\mathbf{r}} = E e^{i\mathbf{k}\cdot\mathbf{r}},$$

and to leading order in  $1/r$  (cf. eqn (1.19) for the behaviour of  $\nabla^2$  at large distances)

$$\begin{aligned} -\frac{\hbar^2}{2\mu} \nabla^2 f(\Omega) \frac{e^{ikr}}{r} &= \left[ -\frac{\hbar^2}{2\mu} r \frac{\partial^2}{\partial r^2} + \mathcal{O}\left(\frac{1}{r^2}\right) \right] f(\Omega) \frac{e^{ikr}}{r} \\ \rightarrow f(\Omega) \frac{\hbar^2 k^2}{2\mu} \frac{e^{ikr}}{r} &= E f(\Omega) \frac{e^{ikr}}{r} \quad \text{for } r \rightarrow \infty. \end{aligned}$$

Using the quantal expression for the probability current density (probability current per unit area, or *flux*),

$$\mathbf{j} = \frac{\hbar}{2\mu i} (\psi^* \nabla \psi - \psi \nabla \psi^*), \quad (1.10)$$

we obtain for the probability current density of the incident wave  $\psi = \exp(i\mathbf{k} \cdot \mathbf{r})$

$$\mathbf{j}_{\text{in}} = \frac{\hbar \mathbf{k}}{\mu} = \mathbf{v}, \quad (1.11)$$

where  $\mathbf{v}$  is the initial velocity. For the outgoing radial probability current through the area  $r^2 d\Omega$  we find similarly

$$\begin{aligned} j_r r^2 d\Omega &= \frac{\hbar}{2\mu i} \left[ f^* \frac{e^{-ikr}}{r} \frac{\partial}{\partial r} \left( f \frac{e^{ikr}}{r} \right) - f \frac{e^{ikr}}{r} \frac{\partial}{\partial r} \left( f^* \frac{e^{-ikr}}{r} \right) \right] r^2 d\Omega \\ \rightarrow v |f(\Omega)|^2 d\Omega &\quad \text{for } r \rightarrow \infty. \end{aligned} \quad (1.12)$$

The *differential cross section*  $d\sigma(\Omega)$  for elastic scattering is defined as the ratio of the asymptotic probability current flowing radially into an element of solid angle  $d\Omega = \sin\theta d\theta d\varphi$  in the direction of the solid angle  $\Omega = \{\theta, \varphi\}$ , over the probability current density of the incident wave,

$$d\sigma(\Omega) = \frac{\text{probability current into } d\Omega \text{ in the direction } \Omega}{\text{probability current density of the incident wave}}. \quad (1.13)$$

The asymptotic current flowing into  $d\Omega$  is the current through the area  $R^2 d\Omega$  at a large distance  $R$  from the scattering centre (cf. Fig. 1.1). It is given by formula (1.12) with  $r = R$ . Together with the current density of the incident wave (1.11) the definition (1.13) yields for the differential cross section per unit solid angle the formula

$$\frac{d\sigma}{d\Omega} = \frac{j_r R^2}{|\mathbf{j}_{\text{in}}|} = |f(\Omega)|^2. \quad (1.14)$$

For a spherical potential the scattering solution  $\psi(\mathbf{r})$  is symmetric about the  $z$ -axis, i.e. independent of the azimuthal angle  $\varphi$ . The scattering amplitude is thus a function of  $\theta$  only,  $f(\Omega) = f(\theta)$ .

The *total elastic scattering cross section*  $\sigma_{\text{el}}$  is obtained by integrating the differential cross section (1.14) over the full solid angle  $4\pi$ ,

$$\sigma_{\text{el}} = \int_{4\pi} d\Omega \frac{d\sigma}{d\Omega} = 2\pi \int_{-1}^1 d(\cos\theta) |f(\theta)|^2. \quad (1.15)$$

**It should be emphasized that the cross section (1.13) refers to a single projectile described by a probability current impinging on a single target nucleus.** The scattered particle can only be detected *once*, and at *one* scattering angle, and thus the cross section

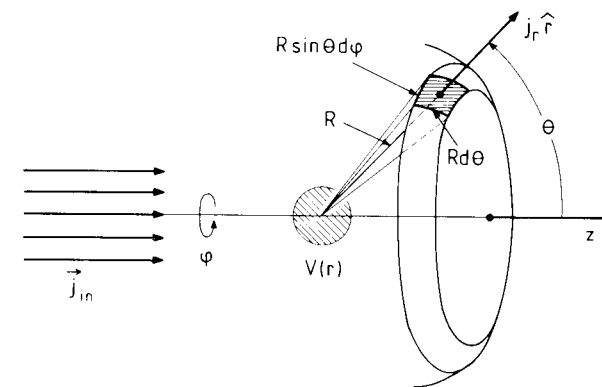


**Figure 1.1** Schematic drawing of the incident and outgoing probability currents for the definition of the differential cross section.

(1.13) describes the relative *probability* for observing this particle at this angle. Now in an actual experiment, the collisions of individual particles with individual nuclei can generally be considered as independent events, whose probabilities add up. If the incident particle beam is sufficiently homogeneous and if the number of scattering particles is large, the relative number of particles passing through a given area in unit time is equal to the relative probability for a single particle to do so. That is, the *particle current density* can be identified with the *probability current density*, and the same holds for the scattered current. In this sense, the *experimental cross section*  $d\sigma^{\text{exp}}(\Omega)$  for a beam of particles, which is defined as

$$d\sigma^{\text{exp}}(\Omega) = \frac{\text{particle current into } d\Omega \text{ in the direction } \Omega}{\text{particle current density of the incident particles}}, \quad (1.16)$$

can be identified with the quantal cross section (1.13),

$$d\sigma^{\text{exp}}(\Omega) = d\sigma(\Omega). \quad (1.17)$$

The preceding discussion is rather heuristic. It makes use of the stationary solution of the Schrödinger equation which extends over all space, and in which the incident and outgoing waves interfere everywhere. For a more careful treatment we shall, in Section 4.4.2, consider the **time-dependent formulation** of the scattering process, in which we describe a moving particle in terms of a *localized* wave packet. In Section 4.5 we discuss, moreover, the structure of the incident beam, with particular attention given to the question of the coherence of the wave packets representing the particles.

### 1.2.2 Calculation of the scattering amplitude

The scattering amplitude  $f(\Omega)$  is obtained by solving the three-dimensional Schrödinger equation (1.8) with the Hamiltonian  $H$  of eqn (1.5),

$$\left( -\frac{\hbar^2}{2\mu} \nabla^2 + V(r) \right) \psi(\mathbf{r}) = E\psi(\mathbf{r}). \quad (1.18)$$

We write the kinetic energy operator in spherical coordinates as

$$-\frac{\hbar^2}{2\mu} \nabla^2 = -\frac{\hbar^2}{2\mu} \frac{1}{r} \frac{\partial^2}{\partial r^2} r + \frac{\mathbf{L}^2}{2\mu r^2}, \quad (1.19)$$

where  $\mathbf{L}^2/2\mu r^2$  is the centrifugal energy containing the square of the angular momentum operator,

$$\mathbf{L}^2 = -\hbar^2 \left[ \frac{1}{\sin\theta} \frac{\partial}{\partial\theta} \left( \sin\theta \frac{\partial}{\partial\theta} \right) + \frac{1}{\sin^2\theta} \frac{\partial^2}{\partial\varphi^2} \right] \quad (1.20)$$

(cf. Messiah 1972, eqn (IX.12)). As mentioned earlier, the scattering by a central potential is axially symmetric about the  $z$ -axis, and the dependence on the azimuthal angle  $\varphi$  drops out.

#### Partial-wave expansion

We first consider the plane wave  $\exp(i\mathbf{k} \cdot \mathbf{r}) = \exp(ikr \cos\theta)$ , i.e. the solution of eqn (1.18) with  $V(r) = 0$ . It can be expanded in the complete set of Legendre polynomials  $P_l(\cos\theta)$ ,

$$e^{ikr \cos\theta} = \sum_{l=0}^{\infty} (2l+1)i^l j_l(kr) P_l(\cos\theta). \quad (1.21)$$

The polynomials  $P_l(\cos\theta)$  are eigenfunctions of the square of the angular momentum operator,

$$\mathbf{L}^2 P_l(\cos\theta) = \hbar^2 l(l+1) P_l(\cos\theta), \quad (1.22)$$

where the non-negative integer  $l = 0, 1, \dots$  is the angular-momentum quantum number; they satisfy the orthogonality relation

$$\int_{-1}^1 d(\cos\theta) P_l(\cos\theta) P_{l'}(\cos\theta) = \frac{2}{2l+1} \delta_{ll'}. \quad (1.23)$$

The radial functions  $j_l(kr)$  are the spherical Bessel functions (cf. Messiah 1972, B. §6); their asymptotic form is

$$j_l(kr) \rightarrow \frac{\sin(kr - \frac{\pi}{2}l)}{kr} = i^{-l} \frac{e^{ikr} - (-)^l e^{-ikr}}{2ikr} \quad \text{for } r \rightarrow \infty. \quad (1.24)$$

The complete wave solution  $\psi(\mathbf{r}) = \psi(r, \theta)$  of eqn (1.18) and the scattering amplitude  $f(\theta)$  can also be expanded in the set of Legendre polynomials  $P_l(\cos\theta)$ ,

$$\psi(r, \theta) = \frac{1}{kr} \sum_{l=0}^{\infty} (2l+1)i^l y_l(r) P_l(\cos\theta), \quad (1.25)$$

### 1.2 Quantal scattering by a short-range potential

$$f(\theta) = \sum_{l=0}^{\infty} (2l+1) f_l P_l(\cos\theta); \quad (1.26)$$

the phase factor  $i^l$  has been introduced in eqn (1.25) in order to conform with the corresponding expansion (1.21) for the free wave.

The Schrödinger equation (1.18) now becomes

$$\sum_{l=0}^{\infty} \left( -\frac{\hbar^2}{2\mu} \frac{1}{r} \frac{\partial^2}{\partial r^2} r + \frac{\hbar^2}{2\mu r^2} l(l+1) + V(r) - E \right) (2l+1)i^l \frac{y_l(r)}{kr} P_l(\cos\theta) = 0. \quad (1.27)$$

Multiplying from the left by  $P_{l'}(\cos\theta)$  and integrating over  $\cos\theta$  from  $-1$  to  $+1$ , we obtain, using the orthogonality relation (1.23), an ordinary differential equation for the radial function  $y_l(r)$ ,

$$\left( \frac{d^2}{dr^2} - \frac{l(l+1)}{r^2} - \frac{2\mu}{\hbar^2} V(r) + k^2 \right) y_l(r) = 0, \quad (1.28)$$

where  $k^2 = 2\mu E/\hbar^2$ . Since the wave function (1.25) must be finite everywhere including the origin, we require  $y_l(0) = 0$ .

The asymptotic form of eqn (1.28) is, because of the vanishing of the potential  $V(r)$  and the centrifugal term  $-l(l+1)/r^2$ ,

$$\left( \frac{d^2}{dr^2} + k^2 \right) y_l(r) = 0 \quad \text{for } r \rightarrow \infty. \quad (1.29)$$

The solution of this equation is some general trigonometric function  $a \sin(kr + \alpha)$ ; since the wave function (1.25) must reduce to the plane wave (1.21) for  $V(r) = 0$ , it is convenient to write the asymptotic radial function  $y_l(r)$  in the form

$$\begin{aligned} y_l(r) &\rightarrow a_l \sin(kr - \frac{\pi}{2}l + \delta_l) \\ &= a_l [\cos \delta_l \sin(kr - \frac{\pi}{2}l) + \sin \delta_l \cos(kr - \frac{\pi}{2}l)] \quad \text{for } r \rightarrow \infty \end{aligned} \quad (1.30)$$

or

$$y_l(r) \rightarrow a_l \frac{i^{-l} e^{i\delta_l} e^{ikr} - i^l e^{-i\delta_l} e^{-ikr}}{2i} \quad \text{for } r \rightarrow \infty. \quad (1.31)$$

Here the amplitude  $a_l$  is arbitrary for the moment, since the differential equation (1.28) is homogeneous. The *phase shift*  $\delta_l$  arises from the presence of the potential, and it has been introduced here in such a way as to vanish when the potential is absent. For real potentials  $V(r)$  the solution  $y_l(r)$  is real except for a possible overall phase factor, and hence the phase shift  $\delta_l$  is also real.

The scattering amplitude (1.26), or rather the partial amplitudes  $f_l$  into which it is expanded, can be expressed in terms of the phase shifts  $\delta_l$ . To this end we again write down the asymptotic form (1.9) of the wave function in terms of the angle  $\theta$ ,

$$\psi(r, \theta) \rightarrow e^{ikr \cos\theta} + f(\theta) \frac{e^{ikr}}{r} \quad \text{for } r \rightarrow \infty. \quad (1.32)$$

Using eqns (1.21), (1.24) and (1.26), we can rewrite this expression as

$$\psi(r, \theta) \rightarrow \frac{1}{2ik} \sum_{l=0}^{\infty} (2l+1) \left( (-)^{l+1} \frac{e^{-ikr}}{r} + (1+2ikf_l) \frac{e^{ikr}}{r} \right) P_l(\cos \theta) \quad \text{for } r \rightarrow \infty. \quad (1.33)$$

On the other hand, the asymptotic form of the solution (1.25) with  $y_l$  given by expression (1.31) is

$$\psi(r, \theta) \rightarrow \frac{1}{2ik} \sum_{l=0}^{\infty} (2l+1) a_l \left( (-)^{l+1} e^{-i\delta_l} \frac{e^{-ikr}}{r} + e^{i\delta_l} \frac{e^{ikr}}{r} \right) P_l(\cos \theta) \quad \text{for } r \rightarrow \infty. \quad (1.34)$$

Comparing the coefficients of  $e^{-ikr}/r$  and  $e^{ikr}/r$  in eqns (1.33) and (1.34) for each  $l$ , we find

$$1 = a_l e^{-i\delta_l} \quad (1.35)$$

and

$$1 + 2ikf_l = a_l e^{i\delta_l}. \quad (1.36)$$

Eliminating  $a_l$ , we have

$$f_l = \frac{1}{2ik} (e^{2i\delta_l} - 1) = \frac{1}{k} e^{i\delta_l} \sin \delta_l, \quad (1.37)$$

and therefore

$$f(\theta) = \frac{1}{2ik} \sum_{l=0}^{\infty} (2l+1) (S_l - 1) P_l(\cos \theta), \quad (1.38)$$

where the quantity

$$S_l = e^{2i\delta_l} \quad (1.39)$$

is the *S-function* for elastic scattering (often called the *S-matrix* since it generalizes to a matrix when more complicated scattering systems are considered).

The differential cross section

$$\frac{d\sigma}{d\Omega} = |f(\theta)|^2 \quad (1.40)$$

is now a double sum over the angular momenta  $l$ , in which the contributions of different angular momenta interfere,

$$\frac{d\sigma}{d\Omega} = \frac{1}{4k^2} \sum_{l,l'=0}^{\infty} (2l+1)(2l'+1) (S_l - 1)(S_{l'}^* - 1) P_l(\cos \theta) P_{l'}(\cos \theta). \quad (1.41)$$

The total elastic scattering cross section (1.15) is obtained by integrating expression (1.41) over angles. Using the orthogonality relation (1.23) for the Legendre polynomials we find

$$\sigma_{\text{el}} = 2\pi \int_{-1}^1 d(\cos \theta) \frac{d\sigma}{d\Omega} = \frac{\pi}{k^2} \sum_{l=0}^{\infty} (2l+1) |S_l - 1|^2, \quad (1.42)$$

which, owing to eqn (1.39), can also be written as

$$\sigma_{\text{el}} = \frac{4\pi}{k^2} \sum_{l=0}^{\infty} (2l+1) \sin^2 \delta_l. \quad (1.43)$$

Each angular momentum  $l$  contributes incoherently to the total elastic cross section.

For a short-range potential the expansion of the scattering amplitude (1.38) effectively breaks off after a finite number of terms. This is seen as follows. Consider the Schrödinger equation (1.28) for the partial-wave solution  $y_l(r)$ . Since the potential has a range  $a$ , it affects the solution only if the latter reaches into the region  $r < a$ ; outside this region the partial-wave solution is subject only to the centrifugal barrier potential  $l(l+1)/r^2 \approx l^2/r^2$  (here all energies are understood in units of  $\hbar^2/2\mu$ ). Now, at a distance equal to the nuclear potential range  $a$  this barrier is higher than the energy  $k^2$  for all angular momenta  $l > ka$ . Thus the partial-wave solution for  $l > ka$  must penetrate into the classically *forbidden* region of the centrifugal barrier in order to ‘feel’ the nuclear potential. Since the solution is strongly suppressed there, the potential will have a negligible effect on the solution as a whole. Thus the phase shift for partial waves with  $l > ka$  will vanish,  $\delta_l = 0$  or  $S_l = 1$ , and the expansion (1.38) breaks off at the cut-off angular momentum

$$l_c = ka. \quad (1.44)$$

Anticipating the classical discussion of the following chapter, we may also say in much simpler language that particles incident on trajectories corresponding to angular momenta  $l > l_c = ka$  (or impact parameters  $b = l/k > a$ ) pass by the scattering centre outside the interaction region  $r \leq a$ . They are therefore not scattered.

#### Calculation of the phase shifts

The phase shifts are calculated in the following way. First, we solve eqn (1.28) for  $y_l(r)$  with the condition  $y_l(0) = 0$ ,  $y'_l(0) \neq 0$ , where the prime denotes the derivative with respect to  $r$ ,  $y' = dy/dr$ . Integrating out to the radius  $a$  (there are only a few potentials for which this can be done analytically; almost always one has to resort to numerical integration), we then form the logarithmic derivative

$$\rho_l = \left. \frac{dy_l(r)/dr}{y_l(r)} \right|_{r=a}. \quad (1.45)$$

We now turn to the solution in the region  $r \geq a$ , where  $V(r)$  vanishes. Here the differential equation (1.28) reduces to

$$\left( \frac{d^2}{dr^2} - \frac{l(l+1)}{r^2} + k^2 \right) y_l(r) = 0. \quad (1.46)$$

Its solution has the general form

$$\frac{y_l(r)}{kr} = b_l j_l(kr) + c_l n_l(kr) \quad \text{for } r \geq a, \quad (1.47)$$

where  $j_l(x)$  and  $n_l(x)$  are the spherical Bessel and Neumann functions (cf. Messiah 1972, B. §6). We choose Messiah’s definition of  $n_l(x)$  because it conforms to the definition of the corresponding irregular Coulomb function  $G_l(\eta, kr)$  (cf. eqn (1.121));

it differs in sign from the traditional definition of the Neumann function. The spherical Bessel and Neumann functions satisfy the equation ( $g_l(x) = j_l(x), n_l(x)$ )

$$\left( \frac{d^2}{dx^2} - \frac{l(l+1)}{x^2} + 1 \right) x g_l(x) = 0. \quad (1.48)$$

Since

$$\begin{aligned} j_l(x) &\rightarrow \frac{1}{x} \sin\left(x - \frac{\pi}{2}l\right) \quad \text{for } x \rightarrow \infty, \\ n_l(x) &\rightarrow \frac{1}{x} \cos\left(x - \frac{\pi}{2}l\right) \quad \text{for } x \rightarrow \infty, \end{aligned} \quad (1.49)$$

$y_l(r)$  becomes asymptotically

$$y_l(r) \rightarrow b_l \sin\left(kr - \frac{\pi}{2}l\right) + c_l \cos\left(kr - \frac{\pi}{2}l\right) \quad \text{for } r \rightarrow \infty. \quad (1.50)$$

Comparing with eqn (1.30) we find that the coefficients  $b_l$  and  $c_l$  are related to  $a_l$  and  $\delta_l$  in the following way,

$$\begin{aligned} b_l &= a_l \cos \delta_l, \\ c_l &= a_l \sin \delta_l, \end{aligned} \quad (1.51)$$

and eqn (1.47) can be written as

$$\frac{y_l(r)}{kr} = a_l [\cos \delta_l j_l(kr) + \sin \delta_l n_l(kr)] \quad \text{for } r \geq a. \quad (1.52)$$

The logarithmic derivative of the partial-wave solution outside the range of the potential is, therefore (here the prime denotes the derivative  $d/da$ ),

$$\frac{dy_l(r)/dr}{y_l(r)} \Big|_{r=a} = \frac{\cos \delta_l [aj_l(ka)]' + \sin \delta_l [an_l(ka)]'}{\cos \delta_l [aj_l(ka)] + \sin \delta_l [an_l(ka)]}. \quad (1.53)$$

By continuity the quantity (1.53) must be equal to the logarithmic derivative  $\rho_l$  of eqn (1.45) obtained by integrating eqn (1.28) out from  $r = 0$ . Replacing the left-hand side of eqn (1.53) with  $\rho_l$  and solving for the phase shift  $\delta_l$ , we obtain finally

$$\delta_l = -\arctan \left( \frac{[aj_l(ka)]' - \rho_l aj_l(ka)}{[an_l(ka)]' - \rho_l an_l(ka)} \right). \quad (1.54)$$

The procedure for calculating the phase shift is therefore as follows. Integrate eqn (1.28) for  $y_l(r)$  from the origin with  $y_l(0) = 0, y'_l(0) = \text{arbitrary} \neq 0$ , up to radius  $r = a$ ; form the logarithmic derivative  $\rho_l = y'_l(a)/y_l(a)$  from this solution, and calculate the phase shift  $\delta_l$  according to eqn (1.54). The matching radius  $a$  does not have to be identical with the range  $a$  of the potential defined by eqn (1.1); any matching radius will do as long as it is larger than, or equal to, the range  $a$ .

### 1.2.3 Scattering by a complex potential

#### The equation of continuity

So far we have considered real potentials  $V$ , as in classical particle scattering. In quantum mechanics, on the other hand, the potential governs the *wave motion* of the probability

amplitude, and it may be made to account for absorption by providing it with an imaginary part  $W$  in analogy to the absorptive imaginary part of the index of refraction in wave optics. Such a complex potential is called an *optical potential*,

$$V_{\text{opt}}(r) = V(r) + iW(r), \quad (1.55)$$

which is to be substituted for the formerly real potential. The Schrödinger equation in this *optical model* is

$$\left( -\frac{\hbar^2}{2\mu} \nabla^2 + V_{\text{opt}}(r) \right) \psi(\mathbf{r}) = E\psi(\mathbf{r}). \quad (1.56)$$

In order to see the effect of introducing an imaginary part in the potential, we write down the divergence of the current density (1.10) using eqns (1.55) and (1.56),

$$\begin{aligned} \nabla \cdot \mathbf{j} &= \frac{\hbar}{2\mu i} (\psi^* \nabla^2 \psi - \psi \nabla^2 \psi^*) \\ &= \frac{1}{\hbar} (\psi^* W \psi + \psi W \psi^*) = \frac{2}{\hbar} |\psi|^2 W. \end{aligned} \quad (1.57)$$

With the probability density  $\rho = |\psi|^2$  we then obtain the *equation of continuity*

$$\nabla \cdot \mathbf{j}(\mathbf{r}) = \frac{2}{\hbar} \rho(\mathbf{r}) W(r). \quad (1.58)$$

This relation shows that absorption, corresponding to a current sink (loss of flux,  $\nabla \cdot \mathbf{j}(\mathbf{r}) < 0$ ), requires a *negative* imaginary part of the optical potential,  $W(r) < 0$ , at the points  $\mathbf{r}$  where this absorption occurs.

#### The reaction cross section

The removal of probability current in elastic scattering is related to the fact that processes other than elastic ones may occur in a nuclear collision, which absorb some of this current. A quantitative measure for the absorption is provided by the *absorption cross section*  $\sigma_a$ . It is defined as the ratio of the net ingoing probability current (total ingoing minus total outgoing current) over the probability current density of the incident wave,

$$\sigma_a = \frac{\text{net ingoing probability current}}{\text{probability current density of the incident wave}}. \quad (1.59)$$

This quantity is here identified with the *reaction cross section*, and in this chapter we henceforth replace the notation  $\sigma_a$  with  $\sigma_r$ . (We shall see in Chapter 6 that the two cross sections are *not* the same in general.) The equality of this quantal cross section with the *experimental* reaction cross section holds in the same sense as for the elastic cross section in Section 1.2.1.

The net ingoing probability current is given by

$$-\int d\mathbf{F} \cdot \mathbf{j}(\mathbf{r}) = -\int d^3r \nabla \cdot \mathbf{j}(\mathbf{r}) = -\frac{2}{\hbar} \int d^3r \rho(\mathbf{r}) W(r), \quad (1.60)$$

where we have used the Gauss theorem and eqn (1.58). Therefore the reaction cross section is given by an integral of the imaginary part of the potential  $W(r)$  weighted with

the probability density  $\rho(\mathbf{r})$  of the scattering wave function,

$$\sigma_r = -\frac{2}{\hbar v} \int d^3r \rho(\mathbf{r}) W(r). \quad (1.61)$$

The reaction cross section can be written as a sum of partial-wave contributions by substituting in eqn (1.61)  $\rho(\mathbf{r}) = |\psi(\mathbf{r})|^2$ , where  $\psi(\mathbf{r})$  is given by the expansion (1.25). We find, using the orthogonality relation (1.23),

$$\sigma_r = -\frac{2}{\hbar v} \frac{4\pi}{k^2} \sum_{l=0}^{\infty} (2l+1) \int_0^{\infty} dr |y_l(r)|^2 W(r). \quad (1.62)$$

We thus have

$$\sigma_r = \sum_{l=0}^{\infty} \sigma_r(l), \quad (1.63)$$

where the partial reaction cross section  $\sigma_r(l)$  is given by

$$\sigma_r(l) = \frac{\pi}{k^2} (2l+1) T_l \quad (1.64)$$

with

$$T_l = -\frac{8}{\hbar v} \int_0^{\infty} dr |y_l(r)|^2 W(r). \quad (1.65)$$

The quantity  $T_l$  is called **transmission coefficient** for reasons which will become clear presently when we express the reaction cross section in terms of the asymptotic current, i.e. of the phase shifts.

A complex potential in the Schrödinger equation will lead to complex scattering solutions, and hence to complex phase shifts. The formulae of Section 1.2.2 remain unchanged, with the understanding that the function  $y_l(r)$  and the phase shift  $\delta_l$  are now complex. Only eqn (1.43) for the total elastic cross section must be modified in that it is replaced with

$$\sigma_{el} = \frac{4\pi}{k^2} \sum_{l=0}^{\infty} (2l+1) |e^{i\delta_l} \sin \delta_l|^2. \quad (1.66)$$

Just like the elastic cross section, the reaction cross section can also be written in terms of the phase shifts. This is achieved by evaluating the net ingoing current density directly in the asymptotic region at  $r = R \rightarrow \infty$ ,

$$-\int d\mathbf{F} \cdot \mathbf{j} = -\frac{\hbar}{2\mu i} R^2 2\pi \int_{-1}^1 d(\cos \theta) \left( \psi^* \frac{\partial \psi}{\partial r} - \psi \frac{\partial \psi^*}{\partial r} \right)_{r=R}, \quad (1.67)$$

with the asymptotic wave function for  $R \rightarrow \infty$  given by (cf. eqns (1.33), (1.37) and (1.39))

$$\psi(r, \theta) \rightarrow \frac{1}{2ik} \sum_{l=0}^{\infty} (2l+1) \left( (-)^{l+1} \frac{e^{-ikr}}{r} + S_l \frac{e^{ikr}}{r} \right) P_l(\cos \theta). \quad (1.68)$$

We use the orthogonality relation for the Legendre polynomials (1.23) and find on the right-hand side of eqn (1.67)

$$\begin{aligned} & -\frac{\hbar}{2\mu i} R^2 2\pi \frac{1}{4k^2 R^2} \sum_{l=0}^{\infty} 2(2l+1) \left\{ \left[ (-)^{l+1} e^{ikR} + S_l^* e^{-ikR} \right] \right. \\ & \times \left. \left[ (-)^{l+1} (-ik)e^{-ikR} + ikS_l e^{ikR} \right] - \text{c.c.} \right\} = \frac{\hbar\pi}{\mu k} \sum_{l=0}^{\infty} (2l+1)(1 - |S_l|^2). \end{aligned}$$

Dividing this expression by the incident flux  $v = \hbar k / \mu$ , we obtain for the reaction cross section

$$\sigma_r = \frac{\pi}{k^2} \sum_{l=0}^{\infty} (2l+1)(1 - |S_l|^2). \quad (1.69)$$

The reaction cross section contains the **reflection coefficient**

$$\eta_l = |S_l|^2. \quad (1.70)$$

It is seen from eqn (1.68) that  $\eta_l$  is the ratio of the outgoing over the ingoing radial current in the asymptotic spherical wave with angular momentum  $l$ . For an absorptive potential we have less outgoing than ingoing current, that is,

$$|S_l|^2 = e^{-4\text{Im } \delta_l} < 1 \text{ or } \text{Im } \delta_l > 0. \quad (1.71)$$

Comparing expression (1.69) with eqns (1.63) and (1.64), we find the relation

$$T_l = 1 - |S_l|^2, \quad (1.72)$$

so that the reaction cross section is given by

$$\sigma_r = \frac{\pi}{k^2} \sum_{l=0}^{\infty} (2l+1) T_l. \quad (1.73)$$

The right-hand side of eqn (1.72) represents that part of the radial current which is *not* reflected, but absorbed or ‘transmitted’ into the inner region of the target nucleus without re-emission. The quantity  $T_l$  is therefore called the **transmission coefficient** (the name ‘absorption coefficient’ would be more appropriate, cf. also Section 9.4.4).

The general behaviour of the transmission coefficient as function of the angular momentum  $l$  is shown in Fig. 1.2. The absorption is practically complete ( $S_l \approx 0$  or  $T_l \approx 1$ ) for small  $l$  and vanishes beyond the cut-off value  $l_c$ . The reason for this behaviour is the same as in the discussion in Section 1.2.2, and can be understood from eqn (1.65): as  $l$  increases, the centrifugal barrier pushes the wave function  $y_l(r)$  away from the origin so that it ceases to have any overlap with the imaginary potential  $W(r)$ .

### The total cross section

The sum of the total elastic and reaction cross sections is the **total cross section**,

$$\sigma_{tot} = \sigma_{el} + \sigma_r. \quad (1.74)$$

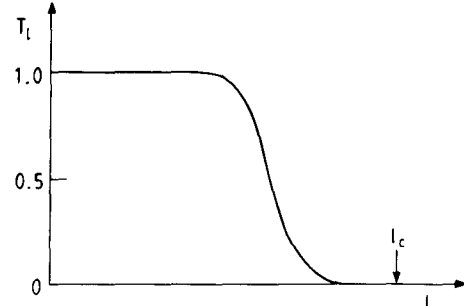


**Figure 1.2** The transmission coefficient  $T_l$  as function of the angular momentum  $l$ . The approximate position of the cut-off angular momentum  $l_c$  is indicated.

Adding the expressions (1.42) and (1.69), we obtain

$$\sigma_{\text{tot}} = \frac{2\pi}{k^2} \sum_{l=0}^{\infty} (2l+1)(1 - \text{Re } S_l). \quad (1.75)$$

The total cross section is seen to be *linearly* related to the set of  $S$ -functions  $S_l$ .

#### The optical theorem

Comparing the imaginary part of eqn (1.38) (using  $P_l(\cos 0) = P_l(1) = 1$ ) with eqn (1.75), we find

$$\sigma_{\text{tot}} = \frac{4\pi}{k} \text{Im } f(\theta = 0). \quad (1.76)$$

This is the *optical theorem*. It derives its name from the observation, first made in wave optics, that the removal of current from the incident wave by scattering or absorption generates a shadow in the forward direction  $\theta = 0$ , i.e. must induce a forward-scattered wave which interferes destructively with the incident wave in the direction  $\theta = 0$ . The optical theorem expresses the fact that the intensity of this shadow, determined by the forward elastic scattering amplitude  $f(0)$ , is proportional to the removed current, which is measured by the total cross section. The appearance of the imaginary part of the forward scattering amplitude is an indication that the *phase* of this amplitude comes into play, and that therefore interference effects are essential in producing the shadow.

## 1.3 Charged-particle scattering

### 1.3.1 Rutherford scattering

The Coulomb potential  $Z_1 Z_2 e^2 / r$  between two point-charges  $Z_1 e$  and  $Z_2 e$  scattering off each other (point-Coulomb or Rutherford scattering) does not fulfil the condition (1.1) for short-range potentials. Therefore a separate discussion is needed. In the centre-of-mass

system the stationary Schrödinger equation is here

$$\left( -\frac{\hbar^2}{2\mu} \nabla^2 + \frac{Z_1 Z_2 e^2}{r} - E \right) \psi_C(\mathbf{r}) = 0. \quad (1.77)$$

Let us write this equation in the form ( $z = r \cos \theta$ )

$$\left( -\nabla^2 + \frac{2\eta k}{r} - k^2 \right) \psi_C(r, z) = 0, \quad (1.78)$$

where

$$\eta = \frac{Z_1 Z_2 e^2}{\hbar v} \quad (1.79)$$

is the Sommerfeld parameter with  $v = \hbar k / \mu$ ; again, the wave function does not depend on the azimuthal angle  $\varphi$  (cf. Section 1.2.1).

The Coulomb scattering amplitude can be obtained in closed form. To show this we introduce the *parabolic coordinates*

$$\begin{aligned} \xi &= r - z, \\ \zeta &= r + z, \end{aligned} \quad (1.80)$$

where  $r = (x^2 + y^2 + z^2)^{1/2}$ . With

$$\begin{aligned} \frac{\partial}{\partial x} &= \frac{x}{r} \left( \frac{\partial}{\partial \xi} + \frac{\partial}{\partial \zeta} \right), \\ \frac{\partial}{\partial y} &= \frac{y}{r} \left( \frac{\partial}{\partial \xi} + \frac{\partial}{\partial \zeta} \right), \\ \frac{\partial}{\partial z} &= \frac{z}{r} \left( \frac{\partial}{\partial \xi} + \frac{\partial}{\partial \zeta} \right) - \frac{\partial}{\partial \xi} + \frac{\partial}{\partial \zeta} \end{aligned} \quad (1.81)$$

we have

$$\nabla^2 = \frac{\partial^2}{\partial x^2} + \frac{\partial^2}{\partial y^2} + \frac{\partial^2}{\partial z^2} = \frac{2}{r} \left[ \frac{\partial}{\partial \xi} \left( \xi \frac{\partial}{\partial \xi} \right) + \frac{\partial}{\partial \zeta} \left( \zeta \frac{\partial}{\partial \zeta} \right) \right]. \quad (1.82)$$

For  $\eta = 0$  the Coulomb wave function  $\psi_C$  must go over into a plane wave, and it is therefore useful to separate off the latter,

$$\psi_C(r, z) = \psi_C(\xi, \zeta) = e^{ikz} F(\xi, \zeta) = e^{ik(\zeta-\xi)/2} F(\xi, \zeta). \quad (1.83)$$

The differential equation for the function  $F(\xi, \zeta)$  separates in the variables  $\xi$  and  $\zeta$ . Using eqns (1.82) and (1.83) in eqn (1.78), we find

$$\left( \xi \frac{\partial^2}{\partial \xi^2} + (1 - ik\xi) \frac{\partial}{\partial \xi} + \zeta \frac{\partial^2}{\partial \zeta^2} + (1 + ik\zeta) \frac{\partial}{\partial \zeta} - k\eta \right) F(\xi, \zeta) = 0. \quad (1.84)$$

Writing  $F(\xi, \zeta) = F_1(\xi)F_2(\zeta)$ , we obtain the two equations

$$\left( \xi \frac{\partial^2}{\partial \xi^2} + (1 - ik\xi) \frac{\partial}{\partial \xi} - kf_1 \right) F_1(\xi) = 0, \quad (1.85)$$

$$\left( \zeta \frac{\partial^2}{\partial \zeta^2} + (1 + ik\zeta) \frac{\partial}{\partial \zeta} - kf_2 \right) F_2(\zeta) = 0, \quad (1.86)$$

with  $f_1 + f_2 = \eta$ .

As is seen by substitution in the last two equations, the solutions  $F_1(\xi)$  and  $F_2(\zeta)$  behave in the following way for large values of the argument,

$$F_1(\xi) \rightarrow a_1 \xi^{if_1} \left( 1 - i \frac{f_1^2}{k\xi} \right) + b_1 \xi^{-if_1} \frac{e^{ik\xi}}{\xi} \quad \text{for } |\xi| \rightarrow \infty, \quad (1.87)$$

$$F_2(\zeta) \rightarrow a_2 \zeta^{-if_2} \left( 1 + i \frac{f_2^2}{k\zeta} \right) + b_2 \zeta^{if_2} \frac{e^{-ik\zeta}}{\zeta} \quad \text{for } |\zeta| \rightarrow \infty. \quad (1.88)$$

With the plane wave  $\exp(ikz)$  multiplied onto it, the function  $F_1(\xi)$  represents asymptotically a sum of a plane wave propagating in the  $z$ -direction and an outgoing spherical wave; correspondingly, the function  $F_2(\zeta)$  becomes a plane wave plus an *ingoing* spherical wave. In order to exclude the latter we set  $F_2(\zeta)$  equal to a constant. Equation (1.86) then requires  $f_2 = 0$  and therefore  $f_1 = \eta$ . We now have

$$\Psi_C(r, z) = e^{ikz} A F_1(\xi), \quad (1.89)$$

where  $F_1(\xi)$  satisfies the equation

$$\xi \frac{d^2 F_1}{d\xi^2} + (1 - ik\xi) \frac{dF_1}{d\xi} - \eta k F_1 = 0, \quad (1.90)$$

and can be identified with the confluent hypergeometric function (cf. Messiah 1972, Appendix B. §1)

$$F_1(\xi) = F(-i\eta, 1, ik\xi). \quad (1.91)$$

We now follow Schiff (1968, Section 21), and represent the function (1.91) by the expansion

$$F(a, b, x) = \sum_{n=0}^{\infty} \frac{\Gamma(a+n)\Gamma(b)}{\Gamma(a)\Gamma(b+n)} \frac{x^n}{n!}, \quad (1.92)$$

where the  $\Gamma$ -function, an analytic continuation of the factorial into the complex plane, is defined as (cf. Abramowitz and Stegun 1965, eqn (6.1.1))

$$\Gamma(z) = \int_0^{\infty} dt e^{-t} t^{z-1} \quad \text{for } \operatorname{Re} z > 0. \quad (1.93)$$

The hypergeometric function is equal to unity at the origin,

$$F(-i\eta, 1, 0) = 1, \quad (1.94)$$

and has the following asymptotic behaviour for  $\xi \rightarrow \infty$  (compare with eqn (1.87)),

$$F(-i\eta, 1, ik\xi) \rightarrow \frac{e^{\eta\pi/2}}{\Gamma(1+i\eta)} \left[ (k\xi)^{i\eta} \left( 1 - i \frac{\eta^2}{k\xi} \right) + \frac{\Gamma(1+i\eta)}{i\Gamma(-i\eta)} (k\xi)^{-i\eta-1} e^{ik\xi} \right]. \quad (1.95)$$

Choosing  $A = \Gamma(1+i\eta)e^{-\eta\pi/2}$  in eqn (1.89) we find for  $r \rightarrow \infty$  (with  $\theta \neq 0$ , so that  $\xi = r - z = r(1 - \cos\theta) \rightarrow \infty$ )

$$\Psi_C(r, z) \rightarrow e^{i(kz+\eta\ln[k(r-z)])} + f_C(\theta) \frac{e^{i[kr-\eta\ln(2kr)]}}{r}, \quad (1.96)$$

where

$$f_C(\theta) = \frac{\Gamma(1+i\eta)}{i\Gamma(-i\eta)} \frac{1}{2k} \left( \frac{1 - \cos\theta}{2} \right)^{-i\eta-1}. \quad (1.97)$$

With  $-i\eta\Gamma(-i\eta) = \Gamma(1-i\eta)$  and  $1 - \cos\theta = 2\sin^2(\theta/2)$  we can rewrite expression (1.97) in the standard form of the **Coulomb scattering amplitude**,

$$f_C(\theta) = -\frac{\eta}{2k\sin^2(\theta/2)} e^{-i\eta \ln \sin^2(\theta/2) + 2i\sigma_0}, \quad (1.98)$$

where

$$\sigma_0 = \frac{1}{2i} \ln \left( \frac{\Gamma(1+i\eta)}{\Gamma(1-i\eta)} \right) = \arg \Gamma(1+i\eta) \quad (1.99)$$

is the **Coulomb phase shift** for  $l = 0$  (cf. eqn (1.11)). Comparing the asymptotic wave function for charged-particle scattering (1.96) with that for short-range potential (neutral-particle) scattering, eqn (1.32), we find that the incident plane wave and the outgoing spherical wave are distorted by **logarithmic phase factors**. Deriving the corresponding asymptotic current densities for  $r \rightarrow \infty$  in the same way as for particles scattered by a short-range potential (cf. eqns (1.11) and (1.12)) we collect contributions from the logarithmic phases which are proportional to  $\eta$ ,

$$\mathbf{j}_{\text{in}} \rightarrow \frac{\hbar k}{\mu} \hat{\mathbf{z}} + \frac{\hbar\eta}{\mu} \frac{\hat{\mathbf{r}} - \hat{\mathbf{z}}}{2r \sin^2(\theta/2)},$$

$$j_r r^2 \rightarrow |f_C(\theta)|^2 \frac{\hbar}{\mu} \left( k - \frac{\eta}{r} \right) \quad \text{for } r \rightarrow \infty, \quad (1.100)$$

where  $\hat{\mathbf{z}}$  and  $\hat{\mathbf{r}}$  are unit vectors. The terms containing  $r$  in the denominator can be discarded, and the **asymptotic current densities thus remain unaffected by the logarithmic phase factors**. From eqn (1.13) we find for the cross section

$$\frac{d\sigma_C}{d\Omega} = |f_C(\theta)|^2 = \frac{\eta^2}{4k^2 \sin^4(\theta/2)} = \left( \frac{Z_1 Z_2 e^2}{4E \sin^2(\theta/2)} \right)^2. \quad (1.101)$$

This happens to be just the **classical Rutherford cross section** (cf. eqn (2.22)). It diverges in the forward direction, a fact which evidently is connected with the slow fall-off of the Coulomb potential (like  $1/r$ ), since we have seen in Section 1.2 that the cross section is finite everywhere for short-range potentials, which do not have an infinitely long ‘Coulomb tail’.

### Screening

A Coulomb field reaching out to infinity is an idealization. Atomic nuclei are surrounded by an electron cloud which extends to a distance of the order of the atomic radius  $R_{\text{at}} \approx 1 \text{ \AA} = 10^5 \text{ fm}$ . Because of their small mass and the relative weakness of their interaction, the electrons do not in general affect the collision between atomic nuclei. However, for partial waves with such high angular momenta that the centrifugal barrier keeps them outside the atom altogether, the electrons screen off the nuclear charge, and the electric potential vanishes: **the Coulomb field is cut off at the radius  $R_{\text{at}}$** . Since the screening occurs far away from the nucleus where the unscreened Coulomb field is very

small anyway, it influences only the very weakly scattered waves, i.e. the scattering into forward angles.

The screening of the Coulomb potential can be taken into account by introducing an exponential cut-off of the form

$$V_C^{\text{screen}}(r) = \frac{Z_1 Z_2 e^2}{r} e^{-r/R_{\text{at}}}. \quad (1.102)$$

In the Born approximation, which is sufficient for our purpose (cf. Taylor 1972, Chapter 14.a), we find for the corresponding scattering amplitude (using eqns (4.120) and (4.87) with  $\Psi_{\mathbf{k}}^+(\mathbf{r}) = (2\pi)^{-3/2} \exp(i\mathbf{k} \cdot \mathbf{r})$ )

$$f_C^{\text{screen}}(\theta) = -\frac{\mu}{2\pi\hbar^2} \int d^3r e^{-i\mathbf{q} \cdot \mathbf{r}} V_C^{\text{screen}}(r) = -\frac{2\mu Z_1 Z_2 e^2 / \hbar^2}{q^2 + 1/R_{\text{at}}^2}, \quad (1.103)$$

where  $\mathbf{q} = k\hat{\mathbf{r}} - \mathbf{k}$  is the momentum transfer,  $q^2 = 4k^2 \sin^2(\theta/2)$ . The scattering cross section for the screened Coulomb potential is then obtained as

$$\frac{d\sigma_C^{\text{screen}}}{d\Omega} = \frac{4k^2 \eta^2}{[4k^2 \sin^2(\theta/2) + 1/R_{\text{at}}^2]^2}. \quad (1.104)$$

It is seen from this formula that the effect of screening is noticeable in the cross section only for angles which satisfy  $4k^2 \sin^2(\theta/2) \leq 1/R_{\text{at}}^2$  or  $\theta \leq 1/kR_{\text{at}}$ . For the scattering of  $^{16}\text{O}$  on  $^{16}\text{O}$  with centre-of-mass energy  $E = 10 \text{ MeV}$  we have  $k = (16m_N c^2 E)^{1/2}/\hbar c \approx 2 \text{ fm}^{-1}$  (here  $m_N$  is the nucleon mass); in this case the effect would be visible only for the very small angles  $\theta < 1/kR_{\text{at}} \approx 0.5 \times 10^{-5}$  radians. Usually screening is disregarded in the description of nuclear collisions.

#### Gamow factor

The value of the Coulomb wave function (1.89) at the origin is

$$\Psi_C(0, 0) = AF(-i\eta, 1, 0) = A = \Gamma(1 + i\eta)e^{-\eta\pi/2}, \quad (1.105)$$

so that (cf. Abramowitz and Stegun 1965, eqn (6.1.31))

$$|\Psi_C(0, 0)|^2 = |\Gamma(1 + i\eta)|^2 e^{-\pi\eta} = \frac{2\pi\eta}{e^{2\pi\eta} - 1}. \quad (1.106)$$

For positively charged nuclei we have  $\eta > 0$ , and if the collision speed  $v$  is small,  $\eta \gg 1$ ; then

$$|\Psi_C(0, 0)|^2 \simeq 2\pi\eta e^{-2\pi\eta}. \quad (1.107)$$

This is of relevance for astrophysics where nuclear reactions take place at very low energies ( $v$  is very small). For a nuclear reaction to occur, the nuclei have to approach each other to within a distance of the sum of their nuclear radii. This distance is small enough to be replaceable with zero in the Coulomb wave function  $\psi_C(r, z)$ , representing the probability amplitude for the two nuclei with incident flux  $v$  (cf. eqn (1.100)) to come as close as the distance  $r$ . The probability for the nuclei to overlap is therefore given by expression (1.107), which is the dominant factor in the rate of an astrophysical nuclear reaction. The exponential  $e^{-2\pi\eta}$  is called the **Gamow factor** and is very small indeed

in stellar processes. It is essentially the probability for two nuclei to tunnel through the classically forbidden region of the repulsive Coulomb barrier between them.

#### The partial-wave expansion

It is fortunate that the Coulomb scattering amplitude can be obtained in the closed form (1.98), because its expansion in partial waves similar to eqn (1.38) presents problems, as we shall now discuss.

The partial-wave expansion of the Coulomb wave function  $\psi_C(r, z) = \psi_C(r, \theta)$  is written, in analogy to eqn (1.25),

$$\psi_C(r, \theta) = \frac{1}{kr} \sum_{l=0}^{\infty} (2l+1)i^l e^{i\sigma_l} F_l(\eta, kr) P_l(\cos \theta). \quad (1.108)$$

Here the factor  $\exp(i\sigma_l)$  is introduced for later convenience; the phase  $\sigma_l$  will be defined presently.

The radial Coulomb function  $F_l(\eta, kr)$  satisfies the differential equation

$$\left( \frac{d^2}{dr^2} - \frac{l(l+1)}{r^2} - \frac{2\eta k}{r} + k^2 \right) F_l(\eta, kr) = 0 \quad (1.109)$$

and the boundary condition  $F_l(\eta, 0) = 0$ ; it is called the *regular Coulomb function* (cf. Messiah 1972, B. §5). Its asymptotic behaviour is

$$F_l(\eta, kr) \rightarrow \sin[kr - \eta \ln(2kr) - \frac{\pi}{2}l + \sigma_l] \quad \text{for } r \rightarrow \infty. \quad (1.110)$$

Besides the logarithmic phase  $\eta \ln(2kr)$ , which, as we have seen, does not contribute to the asymptotic current, this function contains the *Coulomb phase shift*

$$\sigma_l = \frac{1}{2i} \ln \left( \frac{\Gamma(l+1+i\eta)}{\Gamma(l+1-i\eta)} \right) = \arg \Gamma(l+1+i\eta). \quad (1.111)$$

The Coulomb phase shift does *not* vanish for large  $l$ : using Stirling's formula (cf. Abramowitz and Stegun 1965, eqn (6.1.40)),

$$\ln \Gamma(z) \rightarrow (z - \frac{1}{2}) \ln z - z + \frac{1}{2} \ln(2\pi) \quad \text{for } |z| \rightarrow \infty,$$

we have, with  $z = l + 1 + i\eta$ ,

$$\sigma_l \rightarrow \text{Im} [(l + \frac{1}{2} + i\eta) \ln(l + 1 + i\eta) - i\eta] \rightarrow \eta \ln l \quad \text{for } l \rightarrow \infty, \quad (1.112)$$

so that the Coulomb phase shift *increases with  $l$* . This is understood from eqn (1.109): for  $r \rightarrow \infty$  the Coulomb potential  $2\eta k/r$  predominates over the centrifugal potential  $l(l+1)/r^2$  for *any* value of the angular momentum  $l$ , and is thus expected to produce a non-vanishing phase shift even for the largest  $l$  (see the discussion in Section 1.2.2). Therefore the Coulomb *S*-function

$$S_l^C = e^{2i\sigma_l} \quad (1.113)$$

does not become equal to unity for large  $l$ , and an expansion of the Coulomb amplitude (1.98) analogous to eqn (1.38),

$$f_C(\theta) = \frac{1}{2ik} \sum_{l=0}^{\infty} (2l+1)(e^{2i\sigma_l} - 1) P_l(\cos \theta), \quad (1.114)$$

would *not* converge absolutely.

We note that the expansion of the Coulomb wave function (1.108) *does* converge for any finite value of  $r$ . The non-convergence of the Coulomb scattering amplitude arises because here the limit  $r \rightarrow \infty$  in the partial waves (1.110) is taken *first*, and the sum over  $l$  afterwards.

### 1.3.2 Coulomb-plus-nuclear scattering

In order to describe the interaction of actual nuclei, the short-range nuclear optical potential must be supplemented with the Coulomb potential generated by the nuclear charge distributed over the volumes of the nuclei. Usually one assumes uniform charge distributions (ucd), so that the Coulomb interaction for spherical nuclei has the form

$$V_C^{\text{ucd}}(r) = \begin{cases} Z_1 Z_2 e^2 / (2R_C) [3 - (r/R_C)^2] & \text{for } r < R_C, \\ Z_1 Z_2 e^2 / r & \text{for } r > R_C, \end{cases} \quad (1.115)$$

where the *Coulomb radius*  $R_C$  is the sum of the charge radii of projectile and target, which may differ slightly from the sum of the nuclear density radii or the sum of the nuclear interaction radii appearing in the optical potential.

The total interaction  $V_C^{\text{ucd}}(r) + V_N(r)$  now has a Coulomb tail which behaves like  $1/r$  for  $r \rightarrow \infty$ , and we are faced with the same difficulties in regard to the convergence of the partial-wave expansion as in the pure Coulomb case. Since, however, the Coulomb solution is known in closed form, it is possible to separate out the Coulomb part of the wave function, and to treat only the remainder in terms of partial waves.

The Schrödinger equation for Coulomb-plus-nuclear scattering is

$$\left( -\nabla^2 + \frac{2\mu}{\hbar^2} [V_C^{\text{ucd}}(r) + V_N(r)] - k^2 \right) \psi(\mathbf{r}) = 0. \quad (1.116)$$

In the wave function  $\psi(\mathbf{r})$  we separate out the Coulomb wave function  $\psi_C(\mathbf{r})$  by writing

$$\psi(\mathbf{r}) = \psi_C(\mathbf{r}) + \psi_N(\mathbf{r}). \quad (1.117)$$

The function  $\psi_C$  contains the incident wave. Therefore, the additional term  $\psi_N(\mathbf{r})$  due to the potential  $V_N(r)$  is purely outgoing asymptotically. It includes the logarithmic phase term  $-\eta \ln(2kr)$  since the total wave function  $\psi$  must contain this type of outgoing wave, independently of any short-range nuclear interaction,

$$\psi_N(\mathbf{r}) \rightarrow f_N(\theta) \frac{e^{i[kr - \eta \ln(2kr)]}}{r} \quad \text{for } r \rightarrow \infty. \quad (1.118)$$

Here  $f_N(\theta)$  is the *nuclear* scattering amplitude contributed by the nuclear potential  $V_N$ .

For a numerical solution of the wave equation (1.116) we must again reduce it to a one-dimensional problem by expanding in partial waves in analogy to eqn (1.25),

$$\psi(r, \theta) = \frac{1}{kr} \sum_{l=0}^{\infty} (2l+1) i^l e^{i\sigma_l} y_l(r) P_l(\cos \theta). \quad (1.119)$$

The wave equation for the radial functions  $y_l(r)$  is now

$$\left( \frac{d^2}{dr^2} - \frac{l(l+1)}{r^2} - \frac{2\mu}{\hbar^2} [V_C^{\text{ucd}}(r) + V_N(r)] + k^2 \right) y_l(r) = 0. \quad (1.120)$$

The corresponding equation for the Coulomb radial wave function is eqn (1.109), which has as its regular solution the regular Coulomb function  $F_l(\eta, x)$ . Its irregular solution is the *irregular Coulomb function*  $G_l(\eta, x)$ , whose asymptotic behaviour is, in analogy to eqn (1.110) (cf. Messiah 1972, B. §5),

$$G_l(\eta, kr) \rightarrow \cos[kr - \eta \ln(2kr) - \frac{\pi}{2}l + \sigma_l] \quad \text{for } r \rightarrow \infty. \quad (1.121)$$

In the case of neutral particles, when  $\eta = 0$ , we have  $F_l(0, x) = x j_l(x)$  and  $G_l(0, x) = x n_l(x)$ .

For  $r > a$ , where  $a$  is the range of the nuclear potential  $V_N$ , the total wave function  $\psi(\mathbf{r})$  is subject only to the Coulomb potential  $2\eta k/r$ , and can be written as a superposition of regular and irregular Coulomb functions,

$$\psi(\mathbf{r}) = \frac{1}{kr} \sum_{l=0}^{\infty} (2l+1) i^l e^{i\sigma_l} [g_l^N F_l(\eta, kr) + f_l^N G_l(\eta, kr)] P_l(\cos \theta) \quad \text{for } r > a \quad (1.122)$$

or

$$\psi(\mathbf{r}) = \psi_C(r, \theta) + \frac{1}{kr} \sum_{l=0}^{\infty} (2l+1) i^l e^{i\sigma_l} [(g_l^N - 1 - i f_l^N) F_l(\eta, kr) + f_l^N H_l^{(+)}(\eta, kr)] P_l(\cos \theta) \quad \text{for } r > a. \quad (1.123)$$

Here we have used eqn (1.108) and introduced the *outgoing Coulomb function*

$$H_l^{(+)}(\eta, kr) = G_l(\eta, kr) + i F_l(\eta, kr) \quad (1.124)$$

with the asymptotic behaviour

$$H_l^{(+)}(\eta, kr) \rightarrow \exp[i[kr - \eta \ln(2kr) - \frac{\pi}{2}l + \sigma_l]] \quad \text{for } r \rightarrow \infty. \quad (1.125)$$

The sum on the right-hand side of eqn (1.123) represents the expansion of the nuclear part of the wave function,  $\psi_N(\mathbf{r})$ ; this sum *converges* even after the limit  $r \rightarrow \infty$  has been taken. It must be purely outgoing at large distances in order to be consistent with eqn (1.118); therefore we must set, in view of eqns (1.110) and (1.125),

$$g_l^N = 1 + i f_l^N. \quad (1.126)$$

We thus have

$$\psi(\mathbf{r}) = \psi_C(r, \theta) + \frac{1}{kr} \sum_{l=0}^{\infty} (2l+1) i^l e^{i\sigma_l} f_l^N H_l^{(+)}(\eta, kr) P_l(\cos \theta)$$

for  $r > a$ . (1.127)

It is convenient to write the complex coefficient  $f_l^N$  in the form

$$f_l^N = \frac{1}{2i} (S_l^N - 1), (1.128)$$

and to introduce the **nuclear phase shift**  $\delta_l^N$  via the relation

$$S_l^N = e^{2i\delta_l^N}. (1.129)$$

This implies no restriction on the value of the quantity  $f_l^N$  as long as the nuclear phase shift is not restricted to real values from the outset.

The asymptotic form of the nuclear part of the wave function (1.123) is now (cf. eqn (1.125))

$$\begin{aligned} \psi_N(\mathbf{r}) \rightarrow & \frac{1}{2ikr} \sum_{l=0}^{\infty} (2l+1) i^l e^{i\sigma_l} (e^{2i\delta_l^N} - 1) \\ & \times \exp[i[kr - \eta \ln(2kr) - \frac{\pi}{2}l + \sigma_l]] P_l(\cos \theta) \quad \text{for } r \rightarrow \infty, \end{aligned} (1.130)$$

and comparing with expression (1.118) we find for the nuclear scattering amplitude

$$f_N(\theta) = \frac{1}{2ik} \sum_{l=0}^{\infty} (2l+1) e^{2i\sigma_l} (e^{2i\delta_l^N} - 1) P_l(\cos \theta). (1.131)$$

The partial-wave expansion (1.131) converges absolutely because the nuclear scattering amplitude  $f_N(\theta)$  is generated by the *short-range* nuclear potential  $V_N$ ; for angular momenta  $l$  larger than some cut-off value  $l_c$  the nuclear phase shifts  $\delta_l^N$  vanish and  $\exp(2i\delta_l^N) = 1$ . Using the same arguments as in the neutral case, we determine the **cut-off angular momentum**  $l_c$  as that value of  $l$  above which the partial-wave solution of eqn (1.120) is prevented by the centrifugal-plus-Coulomb barrier from penetrating into the region  $r < a$  where the nuclear potential acts. For the cut-off condition we find, considering eqn (1.120) with  $V_N = 0$  and  $(2\mu/\hbar^2)V_C^{\text{ucd}} = 2\eta k/r$ , and setting  $l_c(l_c + 1) \approx l_c^2$ ,

$$\frac{l_c^2}{a^2} + \frac{2k\eta}{a} = k^2,$$

which yields

$$l_c = ka \sqrt{1 - \frac{2\eta}{ka}}. (1.132)$$

Again, this relation has a simple classical interpretation (cf. Fig. 2.1 and eqn (2.17)): it gives the value of the angular momentum  $l_c$  (or impact parameter  $b_c = l_c/k$ ) of the Coulomb trajectory for which the distance of closest approach is equal to the range  $a$  of the nuclear potential.

The cut-off value  $l_c$  for charged-particle scattering is *smaller* than  $ka$ , the cut-off value for the neutral case. We see that the nuclear phase shifts  $\delta_l^N$  for charged particles behave differently from the phase shifts one would obtain if the Coulomb term  $V_C^{\text{ucd}}$  in eqn (1.116) were turned off; this was to be expected, because the former are defined with respect to Coulomb functions and the latter with respect to spherical Bessel functions. For example, the nuclear phase shifts  $\delta_l^N$  of the proton are *not* the same as the phase shifts of the neutron, even if both are calculated using the same nuclear potential  $V_N$ .

The complete scattering amplitude is finally given by

$$f(\theta) = f_C(\theta) + f_N(\theta), (1.133)$$

where  $f_C(\theta)$  is the Coulomb scattering amplitude (1.98). The cross section for Coulomb-plus-nuclear scattering becomes

$$\frac{d\sigma}{d\Omega} = |f(\theta)|^2 = \frac{d\sigma_C}{d\Omega} + 2\text{Re}[f_C^*(\theta)f_N(\theta)] + |f_N(\theta)|^2, (1.134)$$

which contains a characteristic Coulomb–nuclear interference term.

#### Calculation of the nuclear phase shifts

The nuclear phase shifts  $\delta_l^N$  are calculated in complete analogy to the neutral case. The spherical Bessel and Neumann functions in eqn (1.54) (multiplied by  $a$ ) are simply replaced with the corresponding regular and irregular Coulomb functions,

$$\delta_l^N = -\arctan\left(\frac{F'_l(\eta, ka) - \rho_l F_l(\eta, ka)}{G'_l(\eta, ka) - \rho_l G_l(\eta, ka)}\right), (1.135)$$

where

$$\rho_l = \left. \frac{dy_l(r)/dr}{y_l(r)} \right|_{r=a}; (1.136)$$

here  $y_l(r)$  is the regular solution of eqn (1.120) with  $y_l(0) = 0$ .

If the nuclear potential  $V_N(r)$  in eqn (1.120) is real, the solutions  $y_l(r)$  are real as well, and so are the nuclear phase shifts given by formula (1.135). They become complex if the nuclear potential is complex.

## 1.4 Scattering of identical particles

### 1.4.1 Classical scattering

When projectile and target particles are identical, the cross section exhibits certain features which are characteristically different in classical and quantal scattering. We begin with classical scattering.

Consider a beam of particles 1 (with unit current density) incident on a target consisting of particles 2 which are identical with the particles 1 (cf. Fig. 1.3). In the centre-of-mass system, where the total momentum of the particles is zero before and after the collision, particles 1 and 2 must always move in opposite directions. Thus the current of particles 1 scattered into a solid angle  $d\Omega$  in the direction  $\theta$ , which determines the cross section  $d\sigma_1(\theta)$ , is counter-balanced by an equally strong current of recoiling particles 2 in the opposite direction  $\pi - \theta$ , and one obtains a cross section  $d\sigma_2(\pi - \theta)$  for particles 2 in this direction which satisfies the equality  $d\sigma_2(\pi - \theta) = d\sigma_1(\theta)$ . This

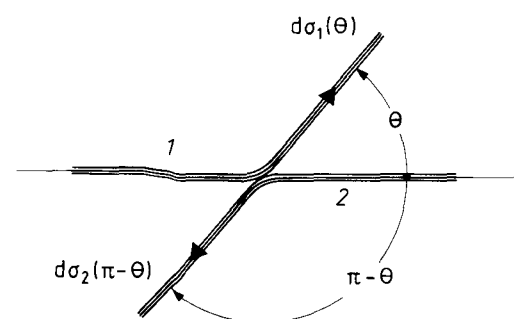


**Figure 1.3** The scattering of identical particles in the centre-of-mass system.

holds for any scattering angle  $\theta$ , and after the relabelling  $\pi - \theta \rightarrow \theta$  we therefore have

$$\frac{d\sigma_2}{d\Omega}(\theta) = \frac{d\sigma_1}{d\Omega}(\pi - \theta).$$

Since the detector does not distinguish between particles 1 and 2, the scattering cross section at a given angle  $\theta$  accounts for the currents of both particles scattered into this angle,

$$\frac{d\sigma}{d\Omega}(\theta) = \frac{d\sigma_1}{d\Omega}(\theta) + \frac{d\sigma_2}{d\Omega}(\theta),$$

or

$$\frac{d\sigma}{d\Omega}(\theta) = \frac{d\sigma_1}{d\Omega}(\theta) + \frac{d\sigma_1}{d\Omega}(\pi - \theta). \quad (1.137)$$

Thus the identical-particle cross section at angle  $\theta$  is given by the cross section for the particle regarded as distinguishable plus its value in the opposite direction. The *integrated cross section* for identical-particle scattering, since it adds the scattered currents of particles 1 and 2 while the incident current consists only of particles 1, is *twice* as large as for non-identical-particle scattering,

$$\int_{4\pi} d\Omega \frac{d\sigma}{d\Omega} = 2 \int_{4\pi} d\Omega \frac{d\sigma_1}{d\Omega}.$$

For identical as well as for non-identical particles, the integral on the right-hand side (without the factor 2) can be identified with the current removed from the incident beam of unit flux by elastic scattering, i.e. with the total elastic cross section  $\sigma_{\text{el}}$ . Therefore,

$$\int_{4\pi} d\Omega \frac{d\sigma}{d\Omega} = 2\sigma_{\text{el}}. \quad (1.138)$$

Note the difference between this equation and eqn (1.15) for non-identical particle scattering.

### 1.4.2 Quantal scattering

The scattering potential must be invariant under the exchange of identical particles, that is, under the reversal of the relative coordinate  $\mathbf{r}$ . This is of course the case for spherical potentials which depend only on  $r = |\mathbf{r}_1 - \mathbf{r}_2|$ . The spatial wave functions of two identical particles can then be classified according to their symmetry under the operation  $\mathbf{r} \rightarrow -\mathbf{r}$  or  $\{r, \theta, \varphi\} \rightarrow \{r, \pi - \theta, \varphi + \pi\}$ . Instead of the asymptotic scattering wave function (1.9) we have therefore the two functions

$$\psi_{\pm}(\mathbf{r}) \rightarrow (e^{i\mathbf{k} \cdot \mathbf{r}} \pm e^{-i\mathbf{k} \cdot \mathbf{r}}) + [f(\theta) \pm f(\pi - \theta)] \frac{e^{ikr}}{r} \quad \text{for } r \rightarrow \infty, \quad (1.139)$$

where we have replaced the solid angle  $\Omega$  in the argument of the scattering amplitude with the only relevant angle,  $\theta$ . The upper sign refers to the symmetric and the lower sign to the antisymmetric wave function.

The scattering amplitudes in the wave functions (1.139) are

$$f_{\pm}(\theta) = f(\theta) \pm f(\pi - \theta), \quad (1.140)$$

and the radial probability currents through the solid angle  $d\Omega$  in the direction  $\theta$  are equal to

$$v |f(\theta) \pm f(\pi - \theta)|^2 d\Omega.$$

As it appears in expression (1.139), the first term represents a standing wave,  $2\cos(\mathbf{k} \cdot \mathbf{r})$  or  $2i\sin(\mathbf{k} \cdot \mathbf{r})$ , implying that the incident part of the scattering wave function has vanishing current density (1.10). However, we must remember that the asymptotic stationary scattering solution (1.139) is an idealization. In reality we have the following situation. In the centre-of-mass system the incident wave function consists of a set of plane waves  $\exp(i\mathbf{k}' \cdot \mathbf{r})$  with momenta  $\mathbf{k}'$  very nearly equal to the momentum  $\mathbf{k}$  used in the stationary equation (1.139), bundled into a wave packet moving towards the scattering centre from one side (cf. Section 4.2.1), and a similar wave packet of plane waves  $\exp(-i\mathbf{k}' \cdot \mathbf{r})$  moving in from the opposite side. The two wave packets do not overlap, and the incident current is to be calculated from the wave packet *on one side only*, where the beam source is located. The density of the incident probability current (of the indistinguishable particles 1 or 2) is therefore equal to  $v$ , and the differential cross section is

$$\frac{d\sigma_{\pm}}{d\Omega}(\theta) = |f_{\pm}(\theta)|^2 \quad (1.141)$$

or

$$\frac{d\sigma_{\pm}}{d\Omega}(\theta) = \frac{d\sigma}{d\Omega}(\theta) + \frac{d\sigma}{d\Omega}(\pi - \theta) \pm 2\text{Re}[f(\theta)^* f(\pi - \theta)], \quad (1.142)$$

where  $d\sigma(\theta)/d\Omega = |f(\theta)|^2$ . The interference term in expression (1.142) distinguishes the quantal cross section for identical particles from the corresponding classical cross section (1.137).

We remark that because of the parity property of the Legendre polynomials,  $P_l[\cos(\pi - \theta)] = (-)^l P_l(\cos \theta)$ , the partial-wave expansion (1.38) for the symmetric scattering amplitude is

$$f_+(\theta) = \frac{1}{ik} \sum_{l=\text{even}} (2l+1)(S_l - 1) P_l(\cos \theta), \quad (1.143)$$

and correspondingly for the antisymmetric scattering amplitude  $f_-(\theta)$ , where the sum goes over all odd  $l$ .

### Particles with spin

So far, we have regarded the colliding identical particles as spinless. Now particles with spin  $I$  are *bosons* if  $I$  is an integer ( $2I$  even), and *fermions* if  $I$  is a half-integer ( $2I$  odd). The total identical-particle wave function including spatial and spin coordinates must be symmetric under the exchange of the two particles for bosons, and antisymmetric for fermions.

We assume that the scattering amplitude is independent of the spin projections  $M = -I, \dots, I$  of the individual particles. If, moreover, the detector is insensitive to the spin projections, each individual spin state contributes to the measured cross section with equal weight. For the two-particle system there are  $(2I+1)^2$  such different states. In  $2I+1$  of these the two particles have the same spin projection, they are indistinguishable and their scattering cross section is given by formula (1.142). In the other  $2I(2I+1)$  states the two particles have *different* spin projections and could be distinguished if the measuring apparatus were sensitive to the spin components. In the present instance this is not the case, but the distinguishability-in-principle implies that the two-particle wave function must not be symmetrized (or antisymmetrized), and as in classical scattering the cross sections for the scattered and recoiling particles simply add up; the cross section is here given by formula (1.142) without the interference term. The sum of the cross sections for all spin states is then equal to

$$(2I+1) \left( \frac{d\sigma}{d\Omega}(\theta) + \frac{d\sigma}{d\Omega}(\pi-\theta) \pm 2\text{Re}[f(\theta)^* f(\pi-\theta)] \right) + \\ 2I(2I+1) \left( \frac{d\sigma}{d\Omega}(\theta) + \frac{d\sigma}{d\Omega}(\pi-\theta) \right).$$

This cross section represents the sum of the contributions from  $(2I+1)^2$  different two-particle states in spin space. Dividing by this number we obtain for the average cross section for an unpolarized beam, using  $\pm 1 = (-1)^{2I}$  for bosons and fermions, respectively,

$$\frac{d\sigma^{\text{unpol}}}{d\Omega}(\theta) = \frac{d\sigma}{d\Omega}(\theta) + \frac{d\sigma}{d\Omega}(\pi-\theta) + \frac{(-1)^{2I}}{2I+1} 2\text{Re}[f(\theta)^* f(\pi-\theta)]. \quad (1.144)$$

This short argument is taken from Schiff (1968, Section 40), where a more detailed derivation of the identical-particle cross section formula can also be found.

### Mott formula

For the *Coulomb scattering of identical particles* the cross section (1.144) can be written down explicitly using formula (1.98),

$$\frac{d\sigma}{d\Omega}(\theta) = \frac{\eta^2}{4k^2} \left( \frac{1}{\sin^4(\theta/2)} + \frac{1}{\cos^4(\theta/2)} \right. \\ \left. + \frac{(-1)^{2I}}{2I+1} \frac{8}{\sin^2\theta} \cos[2\eta \ln \tan(\theta/2)] \right). \quad (1.145)$$

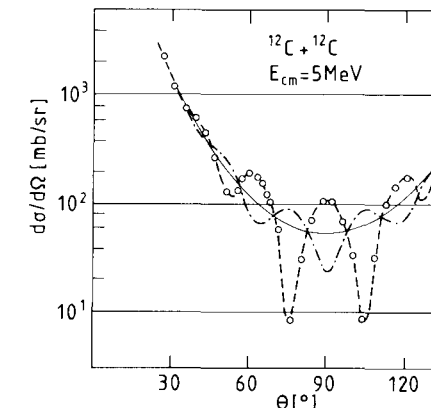


**Figure 1.4** Elastic cross section for the scattering of  $^{12}\text{C}$  by  $^{12}\text{C}$  at  $E = 5$  MeV in the centre-of-mass system. The open circles represent the experimental data of Bromley *et al.* (1960), which are well fitted by the Mott formula with  $I = 0$  (dashed curve). The Mott cross section for  $I = \frac{1}{2}$  (dashed-dotted curve) and the classical cross section (thin solid curve) are also shown for comparison.

This is the *Mott formula*. In general, the interference term oscillates rapidly about zero, the more so the larger the Sommerfeld parameter  $\eta$ . In the limit  $\eta \rightarrow \infty$  the oscillations become so fast that the unavoidable averaging over small angular regions in any actual experiment will reduce the interference term to zero. The Mott formula then goes over into the classical formula corresponding to eqn (1.137).

As an illustration Fig.1.4 shows the cross section for the scattering of  $^{12}\text{C}$  by  $^{12}\text{C}$  at  $E = 5$  MeV in the centre-of-mass system. This energy is so low that the repulsive Coulomb forces keep the colliding nuclei outside the region of nuclear interaction. The scattering is, therefore, governed by the Coulomb interaction alone. The spin of  $^{12}\text{C}$  is zero, so that the Mott formula with  $I = 0$  is to be used. The Mott cross section oscillates about the classical symmetrized Rutherford cross section.

In order to demonstrate the effect of the spin on the scattering cross section we also show the calculated Mott cross section for the same parameters as for  $^{12}\text{C}$  but with spin  $I = \frac{1}{2}$ . This corresponds essentially to the replacement of  $^{12}\text{C}$  with  $^{13}\text{C}$ . As is seen in the figure, the oscillations are now in opposite phase to those for  $I = 0$ , and their amplitude is reduced by the factor  $\frac{1}{2}$ .

## 1.5 An example of potential scattering

As an example of potential scattering we consider the elastic scattering of  $^{12}\text{C}$  by  $^{28}\text{Si}$  at three energies, and compare the calculated differential cross section with the data. For the nuclear potential  $V_N$  we use a phenomenological optical potential of Woods-Saxon

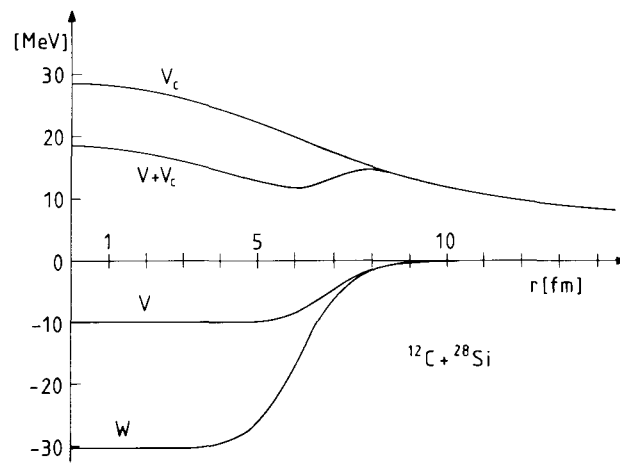


**Figure 1.5** Optical potential  $V_{\text{opt}} = V + iW$ , Coulomb potential  $V_C$  and the real part of the total potential  $\text{Re } V_{\text{tot}} = V + V_C$  for the elastic scattering of  $^{12}\text{C}$  by  $^{28}\text{Si}$ .

shape (cf. Woods and Saxon 1954)

$$V_{\text{opt}}(r) = V f_1(r) + iW f_2(r), \quad f_i(r) = \frac{1}{1 + e^{(r-R_i)/a_i}}, \quad (1.146)$$

with the parameters  $V = -10.0$  MeV,  $W = -30.0$  MeV,  $R_1 = 6.9238$  fm,  $a_1 = 0.617$  fm,  $R_2 = 6.1782$  fm, and  $a_2 = 0.609$  fm. To this is added the Coulomb potential of a homogeneous charge distribution (1.115) with Coulomb radius  $R_C = 6.3912$  fm. These parameters have been obtained by a fitting procedure to obtain an optimal reproduction of the data of DeVries (1977). The potential is displayed in Fig. 1.5. The calculated differential cross section divided by the Rutherford cross section,  $(d\sigma/d\Omega)/(d\sigma_C/d\Omega)$ , is shown in Fig. 1.6 for the system  $^{12}\text{C} + ^{28}\text{Si}$  at the three energies  $E_{\text{lab}} = 24.0$ ,  $49.3$ , and  $186.4$  MeV. The results of the optical-model calculation reproduce the experimental data with surprising accuracy. The pattern of the angular distribution changes with energy; at low energy it is smooth while pronounced diffractive structures show up with increasing energy. The diffraction at low energy is of *Fresnel* type and turns into a *Fraunhofer* pattern at high energy. This will be discussed in detail in Chapter 3. Using the optical potential obtained from a fit of the elastic cross section one can also calculate the reflection coefficient (1.70), which is shown in Fig. 1.7 for the three energies in question. From Fig. 1.5 we may take  $a = 12.0$  fm as the cut-off radius in the sense of eqn (1.1); then formula (1.132) yields the cut-off angular momenta  $l_c = 19.7$ ,  $37.6$ , and  $83.5$ , respectively, which are also indicated in Fig. 1.7. For heavier systems and higher energies the cut-off angular momenta can rise up to values of several thousand.

We have chosen the above-mentioned example because it presents a case where one and the same optical potential fits the experimental data at different energies. In gen-

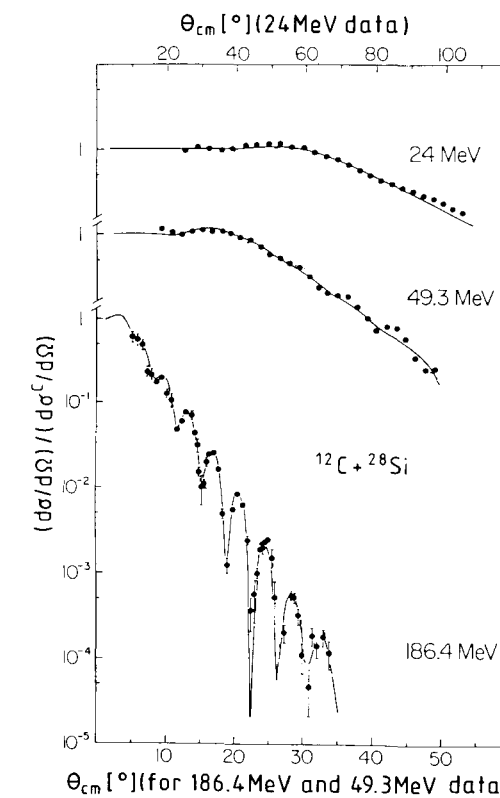


**Figure 1.6** Comparison of the optical-model (solid curves) and experimental (dots) differential cross sections for the elastic scattering of  $^{12}\text{C}$  by  $^{28}\text{Si}$  at the energies  $E_{\text{lab}} = 24.0$ ,  $49.3$ , and  $186.4$  MeV (cf. DeVries 1977). Note the difference in angular scale for the lowest and the two higher energies.

eral, however, the optical potentials must be taken as energy-dependent. In contrast to the present example, the real part of the potential is usually deeper than the imaginary part. Finding an optical potential which adequately reproduces the experimental scattering cross sections often demands much experience. Commonly one assumes a certain parametrized shape, such as the Woods-Saxon form or a more complicated one, and performs a search on the parameters to achieve the best fit to the data. Often no unique answer is found. A more deductive way of finding the potential from the data would be to solve the *inverse scattering problem*, that is, to employ an algorithm which allows one to calculate uniquely the potential from the cross section, or rather, the scattering phase shifts. This procedure is also not without difficulties, and has given rise to a literature of its own (cf., e.g., Chadan and Sabatier 1989; Krappe and Lipperheide 1985).

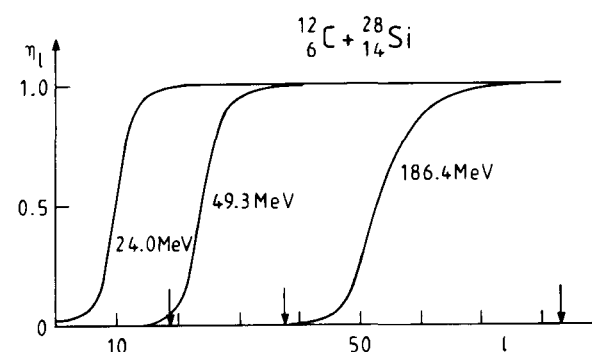


**Figure 1.7** The reflection coefficient  $\eta_l = |S_l|^2$  as function of the angular momentum  $l$  in the elastic scattering of  $^{12}\text{C}$  by  $^{28}\text{Si}$  at the energies  $E_{\text{lab}} = 24.0$ ,  $49.3$ , and  $186.4$  MeV. The corresponding cut-off angular momenta  $l_c$  are indicated by arrows.

## 1.6 Notes and references

The subject matter of the present chapter is treated in most standard textbooks on quantum mechanics (cf., e.g., Schiff 1968; Messiah 1972). A thorough and extensive discussion of many aspects of quantal potential scattering can be found in Newton (1982) and de Alfaro and Regge (1965). A modified optical theorem for charged particles, which in the form (1.76) would yield the useless relation  $\infty = \infty$ , has been given by Marty (1983) and Lipperheide (1987).

### References

- Abramowitz, M. and Stegun, I. A. (1965). *Handbook of mathematical functions*, Dover, New York.
- Bromley, D. A., Kuehner, J. A. and Almquist, E. (1960). *Phys. Rev. Lett.* **4** 365.
- Chadan, K. and Sabatier, P. C. (1989). *Inverse problems in quantum scattering theory*, Springer, Berlin.
- de Alfaro, V. and Regge, T. (1965). *Potential scattering*, North-Holland, Amsterdam.
- DeVries, R. M. (1977). *Proc. symposium on heavy-ion elastic scattering*, ed. DeVries, R. M., University of Rochester, p. 1.
- Krappe, H. J. and Lipperheide, R., eds. (1985). *Advanced methods in the evaluation of nuclear scattering data, Lecture notes in physics*, vol. 236, Springer, Berlin.
- Lipperheide, R. (1987). *Nucl. Phys.* **A469** 190.
- Marty, C. (1983). *Z. Physik* **A309** 261.
- Messiah, A. (1972). *Quantum mechanics*, vol. I, North-Holland, Amsterdam.
- Newton, R. G. (1982). *Scattering theory of waves and particles*, 2nd edn, Springer, Berlin.

- Schiff, L. I. (1968). *Quantum mechanics*, 3rd edn, McGraw-Hill, New York.
- Taylor, J. R. (1972). *Scattering theory*, Wiley, New York.
- Woods, R. and Saxon, D. S. (1954). *Phys. Rev.* **95** 577.

## 2

## SEMICLASSICAL SCATTERING

## 2.1 Introduction

Although the nuclear scattering systems are so small that their quantitative description must generally be based on quantum theory, it is often found that a *classical* treatment is quite adequate. In fact, it was the application of purely classical laws of motion to the scattering of  $\alpha$ -particles which led Rutherford to the discovery of the nucleus in 1911, years before the corresponding quantum laws had been formulated. Therefore, the question arises whether quantum scattering theory can be formulated in such a way that the connection with classical mechanics is uncovered; and whether one may then define conditions under which the quantum expressions can be approximately written in terms of purely classical quantities. This is indeed the case. The corresponding approximation is the *semiclassical approximation*. The condition under which it is valid is essentially that the wavelength characterizing the scattering wave function is small compared with the relevant dimensions of the scattering system.

In the semiclassical approximation the dynamics of the scattering is classical, and is described in terms of classical notions like trajectories, impact parameters, turning points, and so on. The classical dynamical quantities enter in the calculation of the amplitude and phase of the wave function. Typical quantal interference effects are preserved in the semiclassical approximation, and are indeed made physically interpretable in terms of the ‘interference of trajectories’.

The interference effects disappear in the truly classical limit where they give rise to an extremely rapidly oscillating interference pattern, and will therefore be averaged out in an actual physical situation. Quantum theory then yields the same results as classical mechanics.

We begin by discussing purely *classical scattering* in Section 2.2. Here the essential physical quantity is the deflection function, i.e. the deflection angle as a function of the impact parameter. It determines directly the cross section, and its features give rise to certain characteristic effects like glories, rainbows, and orbiting.

With the concepts of classical scattering established, we proceed in Section 2.3 to the *semiclassical* or Wentzel–Kramers–Brillouin (WKB) approximation of quantum scattering. The starting point is the expansion of the quantum scattering amplitude in terms of the scattering phase shifts. The latter will be determined by the classical action function evaluated along trajectories with different impact parameters.

The special features of classical scattering will also be encountered in semiclassical scattering, but generally the singularities appearing in the classical description will be

smoothed out. Section 2.4 is devoted to this topic, with particular attention given to the rainbow.

Finally, in Section 2.5 we treat the scattering by *complex potentials* in the WKB approximation via analytic continuation of the classical equations of motion. This is of importance for nuclear scattering, which is commonly described in terms of complex optical potentials.

## 2.2 Classical scattering

## 2.2.1 The deflection function

As in the quantum theory discussed in the preceding chapter, the problem of the classical scattering of one particle by another reduces in the centre-of-mass system to the problem of the scattering of a point-particle with the reduced mass  $\mu$  by a potential, which for simplicity is taken as central,  $V = V(r)$ . The trajectory  $\mathbf{r} = \mathbf{r}(t)$  of this particle is a solution of Newton’s equations. For a central potential it is confined to the scattering plane. It is reflection-symmetric about the bisector of the angle between the initial and final asymptotes (cf. Fig. 2.1), which it intersects at the distance  $r = a$  from the origin.

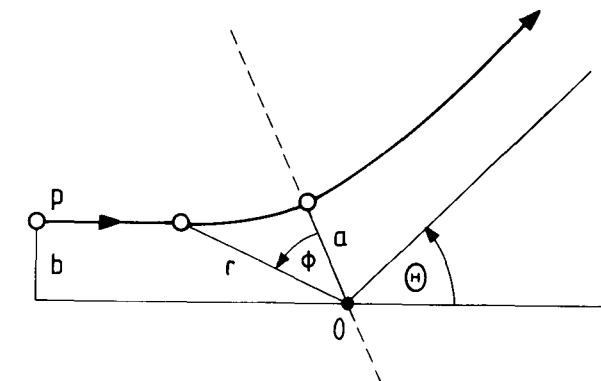


Figure 2.1 Coordinates and parameters of a classical trajectory in the scattering plane.

Let us introduce the radius  $r$  and the angle  $\phi$  with respect to this bisector. The trajectory is determined by two constants of motion, the energy

$$E = \frac{\mu}{2} \left( \frac{dr}{dt} \right)^2 + \frac{L^2}{2\mu r^2} + V(r) \quad (2.1)$$

and the angular momentum perpendicular to the scattering plane

$$L = \mu r^2 \frac{d\phi}{dt}. \quad (2.2)$$

These two equations can be regarded as differential equations in the variables  $r$  and  $\phi$ , which we rewrite in the form

$$\begin{aligned}\frac{dr}{dt} &= \sqrt{(2/\mu)[E - V(r) - L^2/2\mu r^2]}, \\ \frac{d\phi}{dt} &= \frac{L}{\mu r^2};\end{aligned}\quad (2.3)$$

dividing one equation by the other we obtain

$$\frac{d\phi}{dr} = \frac{L}{r^2 \sqrt{2\mu[E - V(r) - L^2/2\mu r^2]}}. \quad (2.4)$$

The angle  $\phi = \phi(r)$  is integrated from the point  $r = a$  out to infinity (this determines only the ingoing half of the trajectory; the outgoing half is obtained by reflection about the bisector, cf. Fig. 2.1). The point  $r = a$  defines the distance of closest approach, or *turning point*. At this point the radial velocity vanishes,  $dr/dt = 0$ , so that according to eqn (2.1)

$$E - V(a) - \frac{L^2}{2\mu a^2} = 0. \quad (2.5)$$

Since  $\phi = 0$  for  $r = a$ , the form of the trajectory is obtained by integration of eqn (2.4) as

$$\phi(r) = \int_a^r dr' \frac{L}{r'^2 \sqrt{2\mu[E - V(r') - L^2/2\mu r'^2]}}. \quad (2.6)$$

The integrand in expression (2.6) generally diverges at the lower limit like the reciprocal of a square root,  $1/\sqrt{r - a}$ , but it is still integrable. In the case of orbiting, however, the integrand diverges more strongly, and the integral becomes infinite (cf. Section 2.2.3).

It is instructive to consider the *radial* motion of the particle as determined by the first of eqns (2.3). This motion is governed by the *effective potential*

$$V_L(r) = V(r) + \frac{L^2}{2\mu r^2}, \quad (2.7)$$

in which the centrifugal potential  $L^2/2\mu r^2$  is added to the original potential. The effective potential is shown in Fig. 2.2 together with the trajectory, which is represented by the horizontal line at energy  $E$ . The turning point lies at the radius  $r = a$  where the trajectory hits the effective potential (cf. eqn (2.5)).

On the left of Fig. 2.1 we read off  $L = bp = b\sqrt{2\mu E}$ , where  $b$  is the *impact parameter* (the distance between the initial asymptote and its parallel through the scattering centre) and  $p$  the initial momentum. The *deflection angle*  $\Theta$  is obtained from the solution (2.6) for  $r \rightarrow \infty$ ,

$$\Theta = \pi - 2\phi(\infty); \quad (2.8)$$

it depends on the impact parameter  $b$  in the following way,

$$\Theta(b) = \pi - 2 \int_a^\infty dr \frac{b}{r^2 \sqrt{1 - V(r)/E - b^2/r^2}}. \quad (2.9)$$

This function is the classical *deflection function*. Positive deflection angles,  $0 < \Theta \leq \pi$ , correspond to net repulsion, whereas negative angles,  $\Theta < 0$ , result from net attraction.

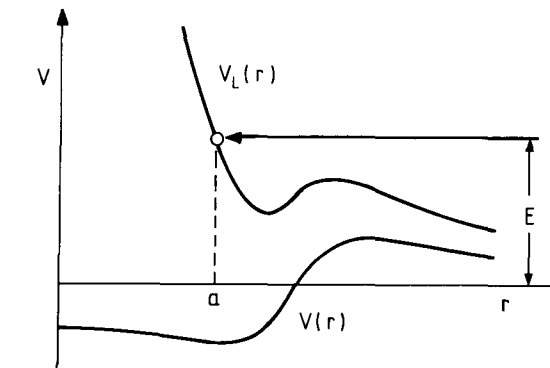


**Figure 2.2** Radial motion in the effective potential  $V_L(r)$ . The potential  $V(r)$  represents schematically a real Coulomb-plus-nuclear potential.

## 2.2.2 The classical cross section

The cross section  $d\sigma$  for particle scattering has been defined in Chapter 1. The definition (1.16) is repeated here for convenience,

$$d\sigma = \frac{\text{particle current into } d\Omega \text{ in the direction } \Omega}{\text{particle current density of the incident particles}}. \quad (2.10)$$

Figure 2.3 illustrates repulsive scattering,  $0 < \Theta \leq \pi$ . The incident flux of particles is regarded as uniform, and is set equal to  $J$ . Let us consider the part of the beam inside the volume bounded by the trajectories with impact parameters  $b$  and  $b + db$  with cross-sectional area  $bdbd\varphi$ . In view of the cylindrical symmetry of the problem, the form of the trajectories is independent of the azimuthal angle  $\varphi$ . The number of particles per unit time passing through the area  $bdbd\varphi$  is the current  $J bdbd\varphi$ . By current conservation this is also the value of the current inside the solid angle  $d\Omega = \sin \Theta |d\Theta| d\varphi$  into which the particles are deflected.

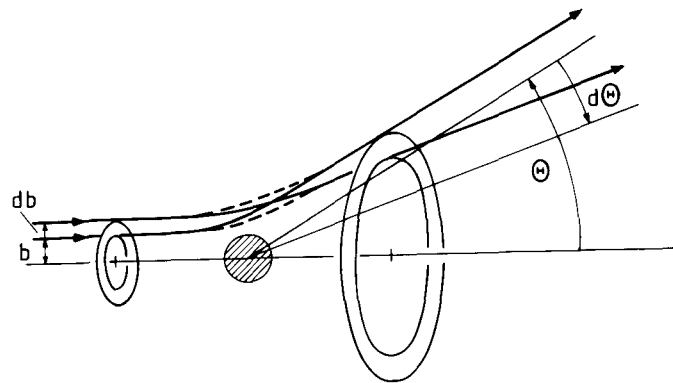
In the case of repulsive scattering ( $\Theta > 0$ ) the deflection angle  $\Theta$  is equal to the *scattering angle*  $\theta$  appearing in the definition of the cross section (cf. Fig. 1.1). The latter is measured in the positive direction and is restricted to the range  $0 \leq \theta \leq \pi$ . For attractive scattering ( $\Theta < 0$ ) the relation between the deflection angle and the corresponding scattering angle has the form

$$\theta = |\Theta \text{ modulo } 2\pi|, \quad (2.11)$$

where ‘ $\Theta$  modulo  $2\pi$ ’ must lie in the interval  $[-\pi, \pi]$ . More explicitly eqn (2.11) reads

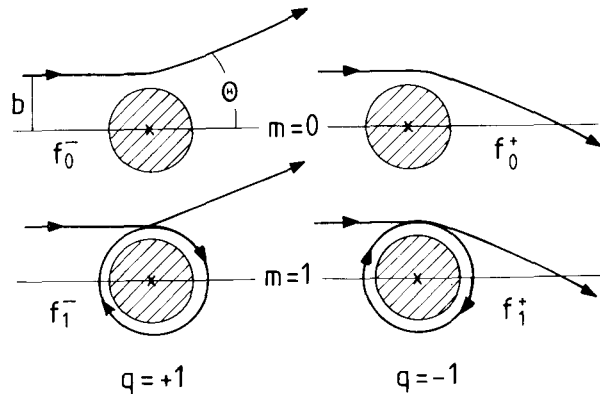
$$\Theta = q\theta - m2\pi \text{ with } q = \pm 1; m = 0, 1, 2, \dots \quad (2.12)$$

Figure 2.4 illustrates a few cases. For  $q = +1$  the trajectory ends asymptotically on the side of the scattering axis from where it has entered (*nearside scattering*), and for



**Figure 2.3** Schematic drawing of trajectories for the determination of the classical cross section. The trajectories with impact parameter values between  $b$  and  $b + db$  stay inside the envelope represented by the dashed curves.

$q = -1$ , on the opposite side (*farside scattering*). The integer  $m$  is the number of turns the trajectory makes around the scattering centre.



**Figure 2.4** Various classical trajectories associated with the same scattering angle  $\theta$ ; the cases  $m = 0, 1$  are shown. The labels  $f_m^\pm$  refer to the semiclassical amplitudes discussed in Section 2.3.2.

For repulsive as well as attractive scattering the definition (2.10) of the cross section yields

$$d\sigma = \frac{J bdbd\varphi}{J}. \quad (2.13)$$

Dividing by  $d\Omega = |\sin \Theta d\Theta| d\varphi$  we have

$$\frac{d\sigma}{d\Omega} = \frac{bdbd\varphi}{|\sin \Theta d\Theta| d\varphi}$$

or

$$\frac{d\sigma}{d\Omega} = \frac{b}{\sin \Theta |d\Theta| / b}, \quad (2.14)$$

here we have taken into account the relation (2.12). The classical differential cross section is completely determined by the deflection function  $\Theta(b)$ .

#### Rutherford scattering

For an example, we consider classical Rutherford scattering, i.e. scattering by a point-Coulomb potential. This case has already been discussed as a quantal problem in Section 1.3.1. The Coulomb potential has the form

$$V(r) = \frac{Z_1 Z_2 e^2}{r} = \frac{2\eta E}{kr}, \quad (2.15)$$

where  $\eta$  is the Sommerfeld parameter (1.79). Equation (2.6) with  $L = \hbar kb$  yields for the Coulomb trajectory

$$\begin{aligned} \phi(r) &= \int_a^r dr' \frac{b}{r'^2 \sqrt{1 - (2\eta/k r') - b^2/r'^2}} = -\arcsin\left(\frac{\eta/k + b^2/r'}{\sqrt{(\eta/k)^2 + b^2}}\right)|_a^r \\ &= \frac{\pi}{2} - \arcsin\left(\frac{\eta/k + b^2/r}{\sqrt{(\eta/k)^2 + b^2}}\right), \end{aligned} \quad (2.16)$$

where we have used the turning-point condition (cf. eqn (2.5))

$$1 - 2\eta/ka - b^2/a^2 = 0. \quad (2.17)$$

For the Coulomb deflection function we then find from eqn (2.8)

$$\begin{aligned} \Theta(b) &= \pi - 2\phi(\infty) = 2 \arcsin\left(\frac{\eta/k}{\sqrt{(\eta/k)^2 + b^2}}\right) \\ &= 2 \arctan\left(\frac{\eta}{kb}\right). \end{aligned} \quad (2.18)$$

The relation between the deflection angle  $\Theta$  and the impact parameter  $b$  for a Coulomb trajectory is therefore

$$b = \frac{\eta}{k} \cot\left(\frac{\Theta}{2}\right). \quad (2.19)$$

Using this equation and eqn (2.17), we find for the distance of closest approach

$$a = \frac{\eta}{k} + \sqrt{\left(\frac{\eta}{k}\right)^2 + b^2} = \frac{\eta}{k} \left(1 + \frac{1}{\sin(\Theta/2)}\right). \quad (2.20)$$

Differentiating the deflection function (2.18) we have

$$\frac{d\Theta}{db} = -\frac{2\eta/k}{(\eta/k)^2 + b^2} = -\frac{2k}{\eta} \sin^2\left(\frac{\Theta}{2}\right), \quad (2.21)$$

where we have expressed  $b$  in terms of  $\Theta$  using eqn (2.19). Then formula (2.14) for the cross section yields, after the deflection angle  $\Theta$  has been replaced with the scattering angle  $\theta$  in the argument of the sine function,

$$\frac{d\sigma}{d\Omega} = \frac{\eta^2}{4k^2 \sin^4(\theta/2)}. \quad (2.22)$$

This is the *Rutherford cross section*. It is given by the same formula as the quantal cross section for Coulomb scattering, eqn (1.101).

The Rutherford cross section diverges strongly at forward angles (like  $\theta^{-4}$ ). This can be explained as follows. Owing to the long range of the Coulomb potential all trajectories are deflected (even if only weakly so) no matter how large their impact parameter. Since the incident current has been introduced in an idealized form, extending uniformly over all space, it contains all impact parameters up to infinitely large ones. The large impact parameters contribute in the near-forward direction, and for scattering into forward angles the target therefore appears to be infinitely large. Analogous arguments in relation to the probability current hold for the quantal Rutherford cross section (1.101).

#### Turning points, trajectories, and the deflection function

The Coulomb deflection function (2.18) just discussed is a monotonic positive function in conformance with the monotonic behaviour of the repulsive Coulomb potential. However, in actual nuclear scattering the potential  $V(r)$  is a sum of both Coulomb and nuclear contributions (assumed real for the moment) and contains repulsive and attractive parts. The deflection function for such a potential at a given energy  $E$  will in general have a non-monotonic and even singular shape. This is shown schematically in Fig. 2.5, in which several features can be discerned. They give rise to phenomena whose names will be given here, but which will be explained only later on.

First we indicate a case of *multiple trajectories*: three trajectories with different impact parameters  $b_n$  end at the same positive deflection angle  $\Theta$ , and therefore, at the same scattering angle  $\theta$ ,  $\Theta(b_n) = \theta$  (three points of intersection of the deflection function with the horizontal line at the angle  $\theta$ ;  $n=1,2,3$ ). This scattering angle is also reached by trajectories with deflection angle  $\Theta = -\theta$  and  $\Theta = \pm\theta - m2\pi$ ,  $m = 1, 2, \dots$ , in accordance with eqn (2.12) (not shown in the figure).

We further note that the cross section (2.14) is singular for  $\sin\theta = 0$ , i.e. at those impact parameters  $b_g$  for which  $\sin[\Theta(b_g)] = 0$  or  $\Theta(b_g) = \pi - m\pi$ ,  $m = 0, 1, 2, \dots$ . These singularities define *glories*. In Fig. 2.5 a *forward glory* at  $\Theta(b_g) = 0$  and a *backward glory* at  $\Theta(b_g) = -\pi$  are shown, each with two intersection points corresponding to different glory angular momenta  $b_g$ .

The cross section (2.14) also becomes singular at the points where  $d\Theta/db = 0$ . This happens at the maximum of the deflection function of Fig. 2.5, which defines a *rainbow* at the rainbow impact parameter  $b_r$  and the rainbow angle  $\theta_r$ . Finally, the deflection function itself has a singularity at  $b = b_o$ , which is related to *orbiting*. For a detailed understanding of the connection between the position of the turning points, the associated trajectories and the deflection function, we turn to Fig. 2.6, which illustrates typically the scattering of a particle with energy  $E$  by a potential  $V_L(r) = V_b(r)$  of the type shown in Fig. 2.2.

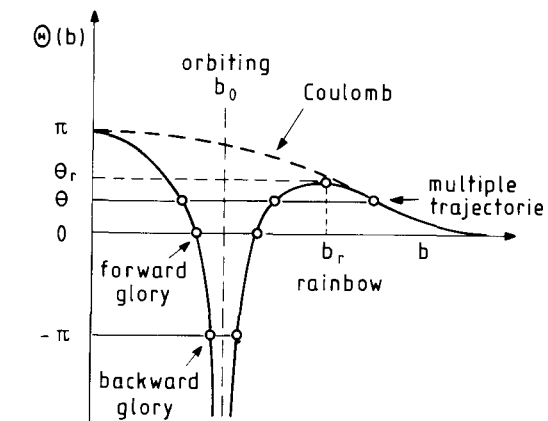


**Figure 2.5** Schematic deflection function  $\Theta(b)$  for scattering by a real Coulomb-plus-nuclear potential. The Coulomb deflection function is shown for comparison (dashed curve).

Figure 2.6a shows the trajectory of the particle, represented by the horizontal line at energy  $E$ , and the effective potential  $V_L(r)$  of eqn (2.7), which in terms of the impact parameter  $b = L/\sqrt{2\mu E}$  is given by

$$V_b(r) = V(r) + E \frac{b^2}{r^2}. \quad (2.23)$$

We now discuss the principal features of classical scattering in their dependence on the value of the impact parameter.

(i) For the largest impact parameter considered in Fig. 2.6a,  $b > b_o$ , the trajectory of the particle has one turning point  $a = a(b)$  according to the condition (2.5), which we rewrite as

$$V_b(a) = E. \quad (2.24)$$

A drawing of this trajectory in the scattering plane is shown in Fig. 2.6b (here, for once, positive angles describe clockwise directions). In this figure the potential  $V(r)$  may be visualized as a circular mould (like a soup-plate) onto which the particle impinges along a trajectory with the impact parameter  $b$ . The trajectory comes closest to the scattering centre at some point on the ‘turning circle’ whose radius is given by the turning point  $a$ . In the present instance the trajectory passes so far away from the scattering centre that it is affected only by the repulsive Coulomb tail of the potential  $V(r)$ , which deflects it to a small positive angle; the corresponding point in the plot of the deflection function  $\Theta(b)$  is shown in Fig. 2.6c.

As the impact parameter  $b$  decreases, three turning points come up, of which the outer one is the effective turning point at which the particle actually turns around, while the two interior turning points are classically inaccessible.

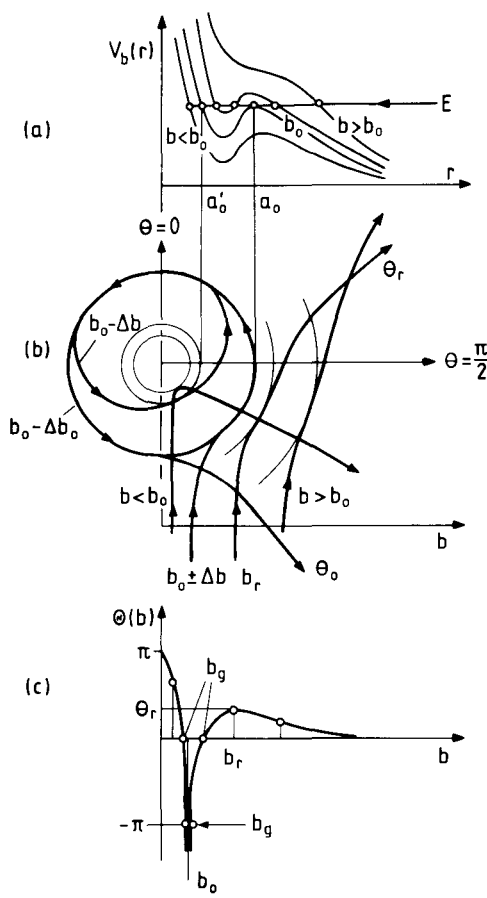


**Figure 2.6** Particle scattering at energy  $E$ . (a) Effective potential  $V_b(r)$  for various impact parameters  $b$  and the associated turning points. (b) The corresponding trajectories in the scattering plane. (c) The deflection function.

(ii) With decreasing impact parameter the trajectory moves closer to the scattering centre where the Coulomb repulsion becomes stronger, and is therefore first deflected to larger angles. At the rainbow impact parameter  $b = b_r$  the deflection angle reaches a maximum at the rainbow angle  $\Theta_r$ ; for impact parameters  $b < b_r$  the attractive nuclear field acts more strongly on the particle, and bends the trajectory back toward smaller deflection angles. The rainbow maximum is shown in the plot of the deflection function in Fig. 2.6c. The trajectory with impact parameter  $b = b_r$  corresponds to  $d\Theta(b)/db = 0$ , which gives rise to the **rainbow singularity** in the cross section.

(iii) As the impact parameter becomes still smaller, the trajectory passes through the forward direction,  $\Theta = 0$ , corresponding to a forward glory. The impact parameter

for which this happens is the glory impact parameter  $b_g$ , where the deflection function goes through zero,  $\Theta(b_g) = 0$ . There is another forward glory impact parameter at smaller  $b$ . In Fig. 2.6c we also show backward glory impact parameters  $b_g$ , for which  $\Theta(b_g) = -\pi$ .

(iv) At the orbiting impact parameter  $b = b_0$  the trajectory just reaches the top of the barrier of the effective potential at the orbiting radius  $r = a_0$  (cf. Fig. 2.6a), which is the point where the two outer turning points coalesce. If the trajectory hits the barrier slightly below the top, i.e. if  $b = b_0 + \Delta b$  (where  $\Delta b > 0$  and very small), it winds around the scattering centre just outside the orbiting circle with radius  $a_0$ , and finally emerges at some deflection angle  $\Theta_o$  (cf. Fig. 2.6b). On the other hand, if the trajectory goes over the top, i.e. if  $b = b_0 - \Delta b$ , it again winds around the scattering centre, first on the outside of the orbiting circle, then on the inside, and thereafter leaves for the interior to be reflected at the smaller circle with the radius  $r = a'_0$  corresponding to the inner turning point. The rounding of the inner turning circle adds  $-2\pi$  to the deflection angle. On the way out the trajectory winds through the orbiting circle for the second time and leaves at a deflection angle  $\Theta_o - 2\pi$ , where  $\Theta_o$  is now the part of the deflection angle contributed by the inward and outward rounds along the orbiting circle. For  $b = b_0$  the trajectory encircles the scattering centre infinitely many times, and thus produces the orbiting singularity in the deflection function.

(v) For trajectories with  $b < b_0$  there is only one turning point on the inner flank of the effective potential.

The various features of classical scattering will be discussed quantitatively in the following. The simplest case is that of multiple trajectories, with which we conclude this subsection. Glory, rainbow, and orbiting will be dealt with subsequently.

#### Multiple trajectories

We have noted above that *several* trajectories, which start out with different impact parameters  $b_n$ , may lead to the *same* scattering angle  $\theta$ . The contributions from all these trajectories must be added to obtain the classical cross section

$$\frac{d\sigma}{d\Omega} = \sum_n \frac{d\sigma_n}{d\Omega} = \sum_n \frac{b_n}{\sin \theta |d\Theta/db|_n}; \quad (2.25)$$

here, in accordance with eqn (2.12), the index  $n$  labels the points of intersection of  $\Theta(b)$  with the horizontal lines  $\pm\theta - m2\pi$ , where  $m$  is a non-negative integer,  $m = 0, 1, 2, \dots$ . Only those terms contribute appreciably for which the slope of the deflection function  $|d\Theta/db|_n$  is not too large.

#### 2.2.3 Glory, rainbow, and orbiting

##### The glory

We have already noted that the presence of the function  $\sin \theta$  in the denominator of the cross section (2.14) causes the latter to become infinite for  $\theta = 0$ , i.e.  $\Theta = -2m\pi$  (forward glory), and for  $\theta = \pi$ , i.e.  $\Theta = -(2m+1)\pi$  (backward glory), where  $m = 0, 1, 2, \dots$ . We have omitted the backward deflection angle  $\Theta = \pi$  because it corresponds to repulsive backscattering which can occur only in a central collision, for

which  $b = 0$ ; since the expression (2.14) for the cross section contains the factor  $b$ , the contribution of this trajectory is suppressed.

The glory singularity in the cross section does not have its origin in the deflection function  $\Theta(b)$ . However, it is affected by the behaviour of this function. Indeed, for a glory to arise at all, the deflection function must attain a forward or backward glory angle, and it must provide sufficiently many trajectories which nearly go into these directions, i.e. it must have a sufficiently small derivative  $d\Theta/db$  at the glory angle (cf. Fig. 2.5).

**One does not measure an infinite cross section in the forward or backward directions.**

**What is measured is a cross section integrated over a small but finite solid angle  $\Delta\Omega$ ,**

$$\Delta\sigma = \int_{\Delta\Omega} d\Omega \frac{d\sigma}{d\Omega} = \int_{\Delta\theta} \sin\theta d\theta d\varphi \frac{d\sigma}{d\Omega}. \quad (2.26)$$

The factor  $\sin\theta$  appearing in the integrand cancels the term  $\sin\theta$  in the denominator of the glory cross section  $d\sigma/d\Omega$ ; the cross section (2.26) is therefore finite.

The name ‘glory’ for the enhancement in the forward and backward directions is taken from a similar effect in the scattering of light by water drops (cf. Newton 1982, Sections 3.7 and 5.5). The backward glory is observed when looking at the shadow of an aeroplane on a cloud below, or by regarding one’s own shadow in a fog bank (‘Brockengespenst’). The glory is also responsible for the brilliant reflection properties of the special paint used on traffic signs and car licence plates. The meteorological glory is discussed extensively by Bryant and Jarmie (1974) and by Nussenzweig (1979). For applications in *nuclear* scattering the glory becomes of interest in its semiclassical form (cf. Section 2.4.1).

#### The rainbow

The formula for the classical scattering cross section (2.14) diverges when  $d\Theta/db = 0$ , i.e. when the deflection function has an extremum. This happens at the *rainbow impact parameter*  $b_r$  and the corresponding *rainbow angle*  $\Theta_r$ , where two trajectories belonging to a set of multiple trajectories, i.e. having different impact parameters  $b$  but the same deflection angle  $\Theta$ , merge into one (cf. Figs. 2.5 and 2.6). This singularity is again removable by integrating over a small neighbourhood of the rainbow angle: since the rainbow corresponds to an extremum of the deflection function, the latter has a quadratic behaviour near  $\Theta_r$ ,  $\Theta \approx \Theta_r + c(b - b_r)^2$ , and therefore  $|d\Theta/db| \approx 2|c(b - b_r)| \approx 2|c(\Theta - \Theta_r)|^{1/2}$ ; near the singularity the cross section thus behaves like the reciprocal of a square root, and is therefore integrable.

The name ‘rainbow’ derives from the analogy with the geometrical-optics description of the scattering of light by rain drops (cf. Newton 1982, Section 3.6; Child 1974, Section 2.2), where the rainbow angle determines the radius of the meteorological rainbow; the dependence of the rainbow angle on the wavelength is responsible for the colouring of the rainbow. For an extensive discussion of the meteorological rainbow cf. Nussenzweig (1977).

#### Orbiting

Glory and rainbow are connected with singularities of the scattering cross section. Now the deflection function itself may become singular as well, that is, the integral in eqn

(2.9) may *diverge*. This happens when the effective potential for the radial motion (2.23) has a maximum (which implies a vanishing effective force),

$$\left. \frac{\partial V_b(r)}{\partial r} \right|_{r=a} = 0, \quad (2.27)$$

at the turning point  $a$  given by

$$V_b(a) = E. \quad (2.28)$$

For fixed energy  $E$  these two equations determine the *orbiting radii*  $a_o$  and  $a'_o$  and the *orbiting impact parameter*  $b_o$  (cf. Fig. 2.6).

As will be shown presently, the deflection function (2.9) becomes negative infinite at the impact parameter  $b_o$ . Trajectories with impact parameters near  $b_o$  are deflected into negative angles  $\Theta$  which can be larger in magnitude than many multiples of  $2\pi$ : the particle revolves many times around the scattering centre in a near-circular orbit (the radial velocity nearly vanishes) with radius  $a_o$ . The phenomenon is thus rightly called ‘orbiting’. We now derive the corresponding cross section.

Precisely at the orbiting impact parameter  $b = b_o$  we have for  $r \approx a_o$ , using eqns (2.27) and (2.28),

$$1 - \frac{V_{b_o}(r)}{E} = -\frac{1}{2E} \left. \frac{\partial^2 V_{b_o}(r)}{\partial r^2} \right|_{r=a_o} (r - a_o)^2 + \dots, \quad (2.29)$$

so that the integral in the deflection function (2.9) is logarithmically divergent: with the definition ( $V''_{b_o}(a_o) < 0$ )

$$\kappa = \frac{b_o}{a_o^2} \sqrt{\frac{-2E}{V''_{b_o}(a_o)}} \quad (2.30)$$

we find

$$\Theta(b_o) \approx \pi - 2\kappa \int_{a_o} dr \frac{1}{r - a_o} = \text{const} + 2\kappa \ln(r - a_o)|_{r \rightarrow a_o} \rightarrow -\infty.$$

This divergence is shown in Fig. 2.5.

In order to investigate the behaviour of the deflection function in the neighbourhood of  $b_o$ , we write the impact parameter as

$$b = b_o + \Delta b, \quad (2.31)$$

and correspondingly the turning-point radius as

$$a = a(b) = a_o + \Delta a. \quad (2.32)$$

The small quantities  $\Delta b$  and  $\Delta a$  are the deviations of the variables  $b$  and  $a$  from their orbiting values. Equation (2.28) defines the functional dependence of the variables  $a$  and  $b$  on each other. To lowest order in  $\Delta b$  and  $\Delta a$  it yields, with account of eqn (2.27),

$$\Delta V_b(a) = \left. \frac{\partial}{\partial b} V_b(a) \right|_o \Delta b + \frac{1}{2} \left. \frac{\partial^2}{\partial a^2} V_b(a) \right|_o (\Delta a)^2 = 0,$$

or, using eqn (2.23),

$$\frac{2b_0 E}{a_0^2} \Delta b + \frac{1}{2} \frac{\partial^2}{\partial a^2} V_b(a) \Big|_0 (\Delta a)^2 = 0$$

(here the index ‘o’ implies that we have set  $a = a_0$  and  $b = b_0$ ). Near orbiting the shift of the turning point  $\Delta a$  caused by a change  $\Delta b$  of the impact parameter is therefore

$$(\Delta a)^2 = \frac{2a_0^2}{b_0} \kappa^2 \Delta b, \quad (2.33)$$

where we have used eqn (2.30). We see that for  $\Delta b > 0$  (raising the centrifugal barrier from its height for  $b = b_0$ ) the outer turning point lies to the right of  $a_0$  by the amount  $|\Delta a|$  (cf. Fig. 2.6). On the other hand, when  $\Delta b < 0$  (lowering the centrifugal barrier), eqn (2.33) has no *real* solution for  $\Delta a$ , and there is no turning point near  $a_0$ ; the trajectory passes over the barrier and is reflected at the internal turning point  $a'_0$ .

Expanding now the argument of the square root in the integral of eqn (2.9) in the variable  $b$  about  $b_0$  to first order in  $\Delta b$  (or  $|\Delta a|^2$ ), and in the variable  $r$  about  $a_0$  to second order in  $x$ , where  $x = r - a_0$ , we find with the help of eqns (2.23), (2.29), and (2.30)

$$1 - \frac{V_b(r)}{E} = \frac{b_0^2}{a_0^4 \kappa^2} (x^2 \mp |\Delta a|^2) + \dots, \quad (2.34)$$

where the minus sign corresponds to  $\Delta b > 0$  and the plus sign to  $\Delta b < 0$ . Then the leading part of the deflection function for  $\Delta b > 0$  is

$$\Theta(b) \approx -2\kappa \int_{\Delta a}^{x_1} \frac{dx}{\sqrt{x^2 - |\Delta a|^2}} = 2\kappa \ln|\Delta a| + \dots = \kappa \ln \Delta b + \dots \quad (2.35)$$

(here  $x_1$  is some point to the right of  $a_0$ ). On the other hand, for  $\Delta b < 0$ , the leading part of the deflection function comes from the integral along the trajectory passing over the barrier,

$$\begin{aligned} \Theta(b) &\approx -2\kappa \int_{-x_1}^{x_1} \frac{dx}{\sqrt{x^2 + |\Delta a|^2}} = -4\kappa \int_0^{x_1} \frac{dx}{\sqrt{x^2 + |\Delta a|^2}} \\ &= 4\kappa \ln|\Delta a| + \dots = 2\kappa \ln|\Delta b| + \dots. \end{aligned} \quad (2.36)$$

The deflection function in the neighbourhood of the orbiting impact parameter  $b_0$  therefore has the form, finally,

$$\Theta(b) \approx \begin{cases} \Theta_1 + \kappa \ln[(b - b_0)/b_0] & \text{for } b > b_0, \\ \Theta_2 + 2\kappa \ln[(b_0 - b)/b_0] & \text{for } b < b_0. \end{cases} \quad (2.37)$$

Here  $\Theta_1$  and  $\Theta_2$  are the non-singular parts of the deflection function. The factor 2 in the deflection function for the lower impact parameter values reflects the fact that the corresponding trajectory ‘orbits’ *twice*, as described in connection with Fig. 2.6.

For the calculation of the cross section we need the derivative of the deflection function in the neighbourhood of the orbiting impact parameter  $b_0$ , which is obtained

from eqn (2.37) as

$$\frac{d\Theta(b)}{db} = \begin{cases} \kappa/(b - b_0) = (\kappa/b_0)\exp[-(\Theta - \Theta_1)/\kappa] & \text{for } b > b_0, \\ -2\kappa/(b_0 - b) = -2(\kappa/b_0)\exp[-(\Theta - \Theta_2)/2\kappa] & \text{for } b < b_0. \end{cases} \quad (2.38)$$

The orbiting cross section at a particular scattering angle  $\theta$  consists of contributions from all deflection angles  $\Theta$  satisfying eqn (2.12). The cross section then becomes, with account of eqn (2.38),

$$\begin{aligned} \frac{d\sigma}{d\Omega} &= \frac{b_0}{\sin \theta} \sum_{q=\pm 1} \left( \frac{b_0}{\kappa} e^{(q\theta - \Theta_1)/\kappa} \sum_{m=0}^{\infty} e^{-m2\pi/\kappa} \right. \\ &\quad \left. + \frac{b_0}{2\kappa} e^{(q\theta - \Theta_2)/2\kappa} \sum_{m=0}^{\infty} e^{-m\pi/\kappa} \right) \\ &= \frac{b_0^2}{\kappa \sin \theta} \left( 2 \cosh(\theta/\kappa) e^{-\Theta_1/\kappa} / (1 + e^{-2\pi/\kappa}) \right. \\ &\quad \left. + \cosh(\theta/2\kappa) e^{-\Theta_2/2\kappa} / (1 + e^{-\pi/\kappa}) \right). \end{aligned} \quad (2.39)$$

For  $\kappa \gg 2\pi$  (wide effective barrier top) this formula simplifies to

$$\frac{d\sigma}{d\Omega} = \frac{3}{2} \frac{b_0^2}{\kappa \sin \theta}, \quad (2.40)$$

and for  $\kappa \ll 2\pi$  (narrow effective barrier top) to

$$\frac{d\sigma}{d\Omega} = \frac{b_0^2}{\kappa \sin \theta} \left( e^{(\theta - \Theta_1)/\kappa} + \frac{1}{2} e^{(\theta - \Theta_2)/2\kappa} \right). \quad (2.41)$$

### 2.3 The semiclassical approximation (WKB)

Having discussed classical scattering, we now turn to quantum scattering under semiclassical conditions, which allow one to replace the quantum scattering amplitude with an expression which contains purely classical quantities. What these conditions are is best described after the appropriate formalism has been established.

We consider the quantum scattering amplitude (1.38) written in the form

$$f(\theta) = \frac{1}{2ik} \sum_{l=0}^{\infty} (2l+1)(e^{2i\delta_l} - 1) P_l(\cos \theta). \quad (2.42)$$

The semiclassical scattering amplitude is obtained from expression (2.42) in four steps.

(i) The phase shifts  $\delta_l$  are calculated in the WKB approximation, where they can be written as the difference of the full and free classical actions. (ii) The Legendre polynomials are replaced with their asymptotic forms for large values of  $l$ . (iii) The sum over angular momenta is changed to an integral. Finally (iv) the whole expression is evaluated by the method of stationary phase.

We begin with the calculation of the WKB phase shifts. The next two steps are then immediate, whereas the evaluation of the WKB scattering amplitude in the stationary-phase approximation will again require some elaboration.

### 2.3.1 The phase shifts in the semiclassical approximation

#### The semiclassical condition

Let us consider the partial-wave expansion of the scattering wave function (cf. eqn (1.25)),

$$\psi(\mathbf{r}) = \frac{1}{kr} \sum_{l=0}^{\infty} (2l+1)i^l y_l(r) P_l(\cos \theta). \quad (2.43)$$

Here the radial wave function  $y_l(r)$  satisfies the equation (cf. eqn (1.28))

$$y_l'' + \frac{[p_l(r)]^2}{\hbar^2} y_l = 0, \quad (2.44)$$

where we have introduced the local momentum

$$p_l(r) = +[F_l(r)]^{1/2} \quad (2.45)$$

with

$$F_l(r) = p_l^2(r) = 2\mu[E - V_l(r)]; \quad (2.46)$$

the term

$$V_l(r) = V(r) + \frac{\hbar^2 l(l+1)}{2\mu r^2} \quad (2.47)$$

is the effective potential for the partial wave with angular momentum quantum number  $l$ .

We write the solution  $y_l(r)$  in the form

$$\begin{aligned} y_l(r) &= A_l(r) e^{\frac{i}{\hbar} S_l(r)} \\ &= A_l(r) \{ \cos[S_l(r)/\hbar] + i \sin[S_l(r)/\hbar] \}. \end{aligned} \quad (2.48)$$

Here we *do not* introduce the functions  $A_l$  and  $S_l$  as intrinsically real, because we shall later consider analytic continuations of them which are complex. Instead, we regard the solution (2.48) as a function of  $\hbar$ , and require both  $A_l$  and  $S_l$  to be *even* functions of  $\hbar$  (cf. Messiah 1972, Section VI.6; the dependence on  $\hbar$  is not indicated explicitly). This requirement is met by defining the functions  $A_l$  and  $S_l$  in the following way:

$$\begin{aligned} A_l(r) &= \sqrt{y_l(r)\bar{y}_l(r)}, \\ \tan(S_l(r)/\hbar) &= -i[y_l(r) - \bar{y}_l(r)]/[y_l(r) + \bar{y}_l(r)], \end{aligned} \quad (2.49)$$

where  $\bar{y}_l(r)$  denotes the function  $y_l(r)$  in which  $\hbar$  is replaced with  $-\hbar$ .

Equation (2.44) now becomes an equation connecting the functions  $A_l(r)$  and  $S_l(r)$ ,

$$\hbar^2 A_l'' - S_l'^2 A_l + i\hbar(S_l'' A_l + 2S_l' A_l') + p_l^2 A_l = 0, \quad (2.50)$$

where the prime stands for the radial derivative  $d/dr$ . Regarded as a function of  $\hbar$  the left-hand side of eqn (2.50) can be separated into an even and an odd part, which must

vanish separately. For the odd part we find

$$S_l'' A_l + 2S_l' A_l' = 0 \text{ or } \frac{1}{2} \frac{S_l''}{S_l'} + \frac{A_l'}{A_l} = 0, \quad (2.51)$$

so that

$$A_l = \text{const} (S_l')^{-1/2}. \quad (2.52)$$

The even part has the form

$$\hbar^2 A_l'' - S_l'^2 A_l + p_l^2 A_l = 0$$

or

$$\frac{S_l'^2}{p_l^2} = 1 + \lambda^2 \frac{A_l''}{A_l}, \quad (2.53)$$

where we have introduced the *reduced local wavelength*

$$\lambda(r) = \frac{\lambda(r)}{2\pi} = \frac{\hbar}{p_l(r)}. \quad (2.54)$$

Substituting eqn (2.52) in (2.53), we find

$$\frac{S_l'^2}{p_l^2} = 1 + \lambda^2 \left[ \frac{3}{4} \left( \frac{S_l''}{S_l'} \right)^2 - \frac{1}{2} \frac{S_l'''}{S_l'} \right]. \quad (2.55)$$

Let us now assume that the second term on the right-hand side is small compared to unity; then we have to lowest order

$$[S_l']^2 \approx [p_l(r)]^2 = F_l(r). \quad (2.56)$$

Replacing  $\hbar^2 l(l+1)$  in the local momentum  $p_l(r)$  with the square of the classical angular momentum  $L^2$ , we see that in this approximation the term  $S_l(r)$  in the phase of the wave function  $y_l(r)$ , and owing to eqn (2.52) also the pre-factor  $A_l(r)$ , are both given purely in terms of classical quantities. This is what we wanted to achieve. The quantum aspect of this *semiclassical approximation* rests entirely in the explicit appearance of the reduced Planck constant  $\hbar$  in the phase.

The condition for the validity of the semiclassical approximation is that the second term on the right-hand side of eqn (2.55) is small compared to unity. Using the approximation (2.56), we write this term in the form

$$\lambda^2 \left[ \frac{3}{4} \left( \frac{p_l'}{p_l} \right)^2 - \frac{1}{2} \frac{p_l''}{p_l} \right] = -\frac{1}{4} \lambda'^2 + \frac{1}{2} \lambda \lambda''. \quad (2.57)$$

The condition that this quantity is small compared to unity reduces to the requirement that the term  $-\frac{1}{4} \lambda'^2$  is so, since generally the term  $\frac{1}{2} \lambda \lambda''$  is small if the first term is. The condition therefore becomes

$$|\lambda'(r)| \ll 1. \quad (2.57)$$

In view of eqns (2.46) and (2.54) this means for the effective scattering potential  $V_l(r)$

$$\frac{\hbar \mu |V_l(r)|}{2\mu [E - V_l(r)]^{3/2}} \ll 1 \text{ or } \frac{1}{2} \left| \frac{|V_l(r)| \cdot \lambda(r)}{[p_l(r)]^2 / 2\mu} \right| \ll 1. \quad (2.58)$$

Thus the variation of the potential  $V_l(r)$  over the distance of a reduced local wavelength must be small compared to the local kinetic energy  $[p_l(r)]^2/(2\mu)$ . In particular, one must stay away from the turning points where  $p_l^2 = 2\mu(E - V_l) = 0$ .

We can also interpret the semiclassical condition (2.57) directly in terms of the reduced local wavelength. Writing it in the form

$$|\lambda(r)'| \cdot \lambda(r) \ll \lambda(r), \quad (2.59)$$

one can formulate this condition as follows: the change of the local wavelength over a distance equal to the local wavelength must be small compared to this wavelength.

### The partial wave function in WKB

Turning now to the calculation of the wave function (2.48) in the WKB approximation, we find that its exponent is determined by (cf. eqn (2.56))

$$S'_l = \pm p_l, \quad (2.60)$$

which yields

$$S_l(r) = \pm \int^r p_l(r) dr. \quad (2.61)$$

For the partial wave function we therefore have, using eqn (2.52),

$$y_l^{\text{WKB}}(r) = \frac{1}{[p_l(r)]^{1/2}} e^{\pm \frac{i}{\hbar} \int^r p_l(r) dr}. \quad (2.62)$$

At the turning point  $r = a$ , where the function  $F_l(r)$  vanishes together with the local momentum  $p_l(r)$  (cf. eqn (2.46)), the WKB wave function diverges. On the other hand, near this point the WKB approximation is not valid anyway. Fortunately, we are interested only in the phase shifts; in order to calculate these one only requires the wave function away from the turning point, i.e. for  $r \rightarrow \infty$  and near the origin  $r = 0$ . This calculation will be carried out in the following.

We consider the situation illustrated in Fig. 2.7, where the effective potential gives rise to a single turning point only. To the left of the turning point,  $r < a$ ,  $F_l(r)$  is

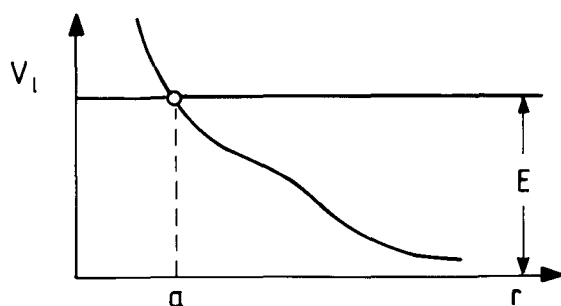


Figure 2.7 An effective potential with a single turning point.

negative, the local momentum  $p_l(r)$  is imaginary, and the WKB solution has the form

$$y_l^{\text{WKB}}(r) = \frac{C_0}{[-F_l(r)]^{1/4}} e^{\pm \frac{1}{\hbar} \int_a^r [-F_l(r')]^{1/2} dr'} \quad \text{for } r < a. \quad (2.63)$$

From now on we shall make the replacement  $l(l+1) \rightarrow (l + \frac{1}{2})^2$  in the centrifugal potential  $\hbar^2 l(l+1)/r^2$  (cf. Langer 1937). This **Langer modification** guarantees the correct behaviour of the semiclassical wave function at the origin. For  $r \rightarrow 0$  we have then  $-F_l(r) \rightarrow (\hbar/r)^2(l + \frac{1}{2})^2$  and the evaluation of the wave function (2.63) yields  $y_l^{\text{WKB}} \propto r^{1/2} r^{\pm(l+1/2)}$ . When  $r \rightarrow 0$  we therefore find  $y_l^{\text{WKB}} \propto r^{l+1}$  for the plus sign in the exponent in eqn (2.63), and  $y_l^{\text{WKB}} \propto r^{-l}$  for the minus sign. Since the wave function has to be regular at the origin, we must choose the plus sign, and the wave function to the left of the turning point is given by

$$y_l^{\text{WKB}}(r) = \frac{1}{2[-F_l(r)]^{1/4}} e^{\pm \frac{1}{\hbar} \int_a^r [-F_l(r')]^{1/2} dr'} \quad \text{for } r < a. \quad (2.64)$$

Here we have set  $C_0 = \frac{1}{2}$  for later convenience.

To the right of the turning point,  $r > a$ ,  $F_l(r)$  is positive according to eqn (2.46), and the local momentum  $p_l(r)$  is therefore real, so that the general form of the WKB solution is a superposition of the solutions (2.62),

$$y_l^{\text{WKB}}(r) = \frac{1}{[F_l(r)]^{1/4}} \left( C_1 e^{\frac{i}{\hbar} \int_a^r [F_l(r')]^{1/2} dr'} + C_2 e^{-\frac{i}{\hbar} \int_a^r [F_l(r')]^{1/2} dr'} \right) \quad \text{for } r > a. \quad (2.65)$$

The exact wave function  $y_l(r)$  is the regular solution of the Schrödinger equation (2.44) and is analytic as a function of  $r$ . Therefore, the WKB approximations to the left and to the right of the turning point, in the regions where they approximate well the exact quantal solution, must be analytic continuations of each other. Such an analytic continuation leads to a **connecting formula** between the two WKB solutions. With some sacrifice of rigour we can obtain this connection formula by the following argument (cf. Landau and Lifshitz 1965, §47).

We replace  $F_l(r)$  near the turning point with its linear approximation,  $F_l(r) = c^2(r - a)$ , where  $c > 0$ ; then we have from eqn (2.64)

$$y_l^{\text{WKB}}(r) = \frac{1}{2c^{1/2}(a - r)^{1/4}} e^{-\frac{2}{3\hbar} c(a - r)^{3/2}} \quad \text{for } r < a, \quad (2.66)$$

and from eqn (2.65)

$$y_l^{\text{WKB}}(r) = \frac{1}{c^{1/2}(r - a)^{1/4}} \left( C_1 e^{\frac{i}{\hbar} \frac{2c}{3}(r - a)^{3/2}} + C_2 e^{-\frac{i}{\hbar} \frac{2c}{3}(r - a)^{3/2}} \right) \quad \text{for } r > a \quad (2.67)$$

The analytic continuation from the left to the right of the turning point now amounts to the determination of the coefficients  $C_1$  and  $C_2$ . To this end we match the two functions (2.66) and (2.67) in a region of the complex  $r$ -plane where the WKB expressions are good approximations to the quantal solutions, that is, sufficiently far away from the turning point (but the linear approximation for  $F_l(r)$  must of course still be valid). This matching is described next (cf. Fig. 2.8).

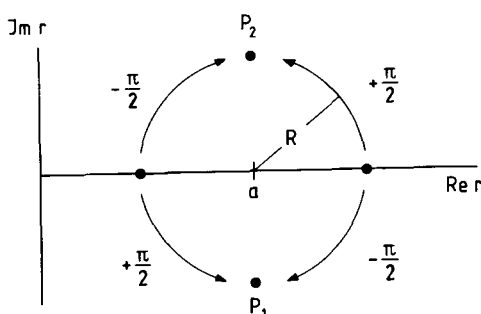


**Figure 2.8** Analytic continuation of the WKB solutions in the complex  $r$ -plane.

We continue solution (2.66) from the real axis into the lower half-plane to the point  $P_1$  by the rotation  $a - r = |a - r| = R \rightarrow Re^{i\pi/2}$ . There the solution (2.66) becomes

$$y_l^{\text{WKB}}(P_1) = \frac{1}{2c^{1/2}R^{1/4}e^{i\pi/8}} e^{-\frac{2}{3}\frac{c}{\hbar}R^{3/2}e^{i3\pi/4}}. \quad (2.68)$$

The continuation of solution (2.67) from the real axis to the point  $P_1$  by the rotation  $r - a = |a - r| = R \rightarrow Re^{-i\pi/2}$  yields

$$y_l^{\text{WKB}}(P_1) = \frac{1}{c^{1/2}R^{1/4}e^{-i\pi/8}} \left( C_1 e^{i\frac{2}{3}\frac{c}{\hbar}R^{3/2}e^{-i3\pi/4}} + C_2 e^{-i\frac{2}{3}\frac{c}{\hbar}R^{3/2}e^{-i3\pi/4}} \right). \quad (2.69)$$

At the point  $P_1$  the first term in the parentheses has an exponent with real part  $\frac{2}{3}\frac{c}{\hbar}R^{2/3}/\sqrt{2}$ , and the second term has an exponent with real part  $-\frac{2}{3}\frac{c}{\hbar}R^{2/3}/\sqrt{2}$ . The first term predominates over the second term, so that the latter can be neglected. The solutions (2.68) and (2.69) then are seen to have the same dependence on  $R$ , and comparison of their pre-factors yields

$$C_1 = \frac{1}{2}e^{-i\pi/4}. \quad (2.70)$$

With the help of an analogous analytical continuation for solution (2.66) (with  $R \rightarrow Re^{-i\pi/2}$ ) and solution (2.67) (with  $R \rightarrow Re^{i\pi/2}$ ) into the upper half-plane to the point  $P_2$  (now the term multiplied by  $C_1$  is negligible) we obtain

$$C_2 = \frac{1}{2}e^{i\pi/4}. \quad (2.71)$$

With formulae (2.70) and (2.71) we have established the connection between the WKB solution (2.64) for  $r < a$  and the WKB solution for  $r > a$ , which becomes, from expression (2.65),

$$\begin{aligned} y_l^{\text{WKB}}(r) &= \frac{1}{[F_l(r)]^{1/4}} \cos \left( \frac{1}{\hbar} \int_a^r [F_l(r')]^{1/2} dr' - \frac{\pi}{4} \right) \quad \text{for } r > a \\ &\rightarrow \frac{1}{(\hbar k)^{1/2}} \sin \left( kr + \int_a^\infty [p_l(r')/\hbar - k] dr' - ka + \frac{\pi}{4} \right) \\ &\quad \text{for } r \rightarrow \infty; \end{aligned} \quad (2.72)$$

### 2.3 The semiclassical approximation (WKB)

it contains the phase  $\frac{\pi}{4}$  which is typical for WKB.

We remark that an alternative method for obtaining the connecting formula is to solve the Schrödinger equation (2.44) analytically in the neighbourhood of the turning point after replacing the potential by its linear approximation, so that  $p_l^2 \approx c^2(r - a)$ . This leads to a solution in the form of an Airy function, from whose asymptotic behaviour one recovers the phase factor (cf. Landau and Lifshitz 1965, §24).

◇ *The free wave.* It is instructive to consider the case of a free partial wave, when  $V(r) = 0$  in the function  $F_l(r)$  of eqns (2.46) and (2.47), so that only the centrifugal potential remains,

$$F_l(r) = 1 - \frac{(l + \frac{1}{2})^2}{r^2}; \quad (2.73)$$

here we have set  $\hbar = k = 1$  and applied the Langer modification  $l(l+1) \rightarrow (l + \frac{1}{2})^2$ .

The exact regular quantal solution is in this case (cf. eqn (1.48))

$$y_l(r) = r j_l(r), \quad (2.74)$$

which is analytic in  $r$ . The WKB approximations to the left and right of the turning point  $a = l + \frac{1}{2}$  (cf. eqns (2.64) and (2.72)) can be given explicitly,

$$y_l^{\text{WKB}}(r) = \frac{1}{2} \frac{r^{l+1}}{(a^2 - r^2)^{1/4}} \frac{1}{[a + (a^2 - r^2)^{1/2}]^a} e^{(a^2 - r^2)^{1/2}} \quad \text{for } r < a, \quad (2.75)$$

$$y_l^{\text{WKB}}(r) = \frac{r^{1/2}}{(r^2 - a^2)^{1/4}} \cos \left[ (r^2 - a^2)^{1/2} + (l + \frac{1}{2}) \arcsin(a/r) - (l + 1)\frac{\pi}{2} \right] \quad \text{for } r > a; \quad (2.76)$$

they have a branch point at  $r = a$ . For  $r \rightarrow \infty$  the WKB solution becomes proportional to  $\sin(r - l\frac{\pi}{2})$  and yields the correct ‘centrifugal’ phase shift  $-l\frac{\pi}{2}$ . For  $r \rightarrow 0$  the coefficient of  $r^{l+1}$  is  $1/[\sqrt{2}(2l+1)^{l+1}]e^{l+1/2}$ , which is to be compared with the exact value  $1/(2l+1)!! = 1/(1 \cdot 3 \cdot \dots \cdot (2l+1))$ ; for an angular momentum as low as  $l = 3$  the agreement is within 2% : 0.0097526 (WKB) versus 0.0095238 (exact). ◇

#### Determination of the phase shifts

We now compare the asymptotic WKB wave function (cf. the second line of eqn (2.72)) with the asymptotic form of the quantal solution (1.30),

$$y_l(r) \rightarrow a_l \sin(kr - \frac{\pi}{2}l + \delta_l) \quad \text{for } r \rightarrow \infty; \quad (2.77)$$

ignoring the difference in the normalization we read off the *WKB phase shift* from the argument of the sine function,

$$\delta_l^{\text{WKB}} = \frac{\pi}{2}(l + \frac{1}{2}) + \int_a^\infty dr [p_l(r)/\hbar - k] - ka. \quad (2.78)$$

This phase shift has a simple classical interpretation. We recall that the WKB wave function for  $r > a$  (cf. the first line of eqn (2.72)) contains the function

$$s_l(r) = \int_a^r [F_l(r')]^{1/2} dr' = \int_a^r p_l(r') dr'. \quad (2.79)$$

This quantity is the radial part of the action calculated along a trajectory with angular momentum  $l$  from the turning point  $a$  to a distance  $r$  on the outgoing branch (by the symmetry of the trajectory with respect to the turning point, the radial action along the ingoing branch has the same value, cf. Fig. 2.1). In an analogous fashion we introduce the free radial action  $s_l^0(r)$ , for which the turning point is given by  $a = (l + \frac{1}{2})/k$ ,

$$s_l^0(r) = \int_{(l+\frac{1}{2})/k}^r p_l^0(r') dr', \quad (2.80)$$

where

$$[p_l^0(r)]^2 = 2\mu E - \frac{\hbar^2(l + \frac{1}{2})^2}{r^2}. \quad (2.81)$$

The free radial action can be evaluated as

$$s_l^0(r) = \hbar[kr - \frac{\pi}{2}(l + \frac{1}{2})] \text{ for } r \rightarrow \infty. \quad (2.82)$$

We therefore find for the WKB phase shift

$$\delta_l^{\text{WKB}} = \lim_{r \rightarrow \infty} \frac{1}{\hbar} [s_l(r) - s_l^0(r)]. \quad (2.83)$$

The radial action  $s_l(r)$  is a classical quantity. The same is true for the free radial action (2.82), which may be written as

$$s_l^0(r) = pr - \frac{\pi}{2}L \text{ for } r \rightarrow \infty,$$

where  $L = \hbar(l + \frac{1}{2})$  is the classical angular momentum. Equation (2.83) expresses the WKB phase shift as the difference of the full and free radial actions taken from the turning point out to infinity (or half this difference along the whole trajectory) divided by the reduced Planck constant  $\hbar$ .

Using eqn (2.83) we can set up a new scheme for the calculation of the WKB phase shift. The previous formula (2.78) gives the phase shift associated with the angular momentum  $l$ , i.e. with the classical trajectory having impact parameter  $b = \hbar(l + \frac{1}{2})/k$ , in the form of an integral of the corresponding radial momentum. The trajectory is determined by the integral (2.6). Instead of evaluating these closed expressions as such, we consider the Newtonian equations of motion for each value of  $l$ ,

$$\begin{aligned} \dot{r} &= p_l(r)/\mu, \\ \dot{p}_l(r) &= -V'_l(r), \\ \dot{\phi}(r) &= \hbar(l + \frac{1}{2})/\mu r^2, \end{aligned} \quad (2.84)$$

where the dot stands for the time derivative  $d/dt$  and the prime for the radial derivative  $\partial/\partial r$ . The last equation is decoupled from the others and is needed only for the calculation of the form of the trajectory.

We now introduce the phase function

$$\delta_l(r) = \frac{1}{\hbar} [s_l(r) - s_l^0(r)], \quad (2.85)$$

whose radial derivative, according to eqns (2.79) and (2.80), is given by

$$\delta_l'(r) = \frac{1}{\hbar} [p_l(r) - p_l^0(r)]. \quad (2.86)$$

Combining the first two eqns (2.84) with eqn (2.86) we have

$$\begin{aligned} \dot{r} &= p_l(r)/\mu, \\ \dot{p}_l(r) &= -V'_l(r), \\ \dot{\delta}_l(r) &= \frac{1}{\hbar} [p_l(r) - p_l^0(r)]\dot{r}. \end{aligned} \quad (2.87)$$

The procedure for calculating the WKB phase shift is to integrate the system of eqns (2.87) for a fixed value of  $l$ ; the initial conditions at time  $t = t_i$  with the radius  $r = r_i$  outside the range of the potential  $V(r)$  are  $p_l(r_i) = p_l^0(r_i)$  and  $\delta_l(r_i) = 0$ . The phase function  $\delta_l(r)$  will reach a constant limit once the integration has passed through the turning point and left the region of interaction at a large distance  $r = r_f$ . This constant is the WKB phase shift,

$$\delta_l^{\text{WKB}} = \delta_l(r_f). \quad (2.88)$$

The WKB approximation of the nuclear phase shift for charged-particle scattering (cf. Section 1.3.2) can be obtained in an analogous way. Inspection shows that the procedure is again described by eqns (2.79) to (2.88) where the effective potential  $V_l(r)$  and the corresponding local momentum now include the Coulomb potential, and where the free action is replaced with the Coulomb action.

In the system of equations (2.87) we recognize the essence of the semiclassical method. The dynamics, that is, the effect of the potential field on the motion of the particle, is determined by the classical Newtonian equations of motion, which constitute the first two equations. The third equation yields the phase shift  $\delta_l^{\text{WKB}}$  as the difference (2.83) of the full and free classical radial actions; it allows one to calculate the quantal scattering amplitude (2.42) in terms of purely classical quantities.

Solving the system of eqns (2.87) yields of course the same trajectories and the same values of the phase shifts as the previous procedure employing the integrals of motion, energy  $E$  and angular momentum  $L = \hbar(l + \frac{1}{2})$ . However, the integration of the system (2.87) is more convenient from the computational point of view, especially when the WKB method is extended to complex potentials, as in Section 2.5. More importantly, when energy or angular momentum are not conserved in the scattering system, as in the presence of friction, solving classical equations of motion of the kind (2.87) numerically is the only way of calculating trajectories and cross sections. We shall come back to this point in Chapter 12.

Finally, we find from eqn (2.78), using eqns (2.45) to (2.47) with  $l(l+1) \rightarrow (l + \frac{1}{2})^2$ ,

$$2 \frac{d\delta_l^{\text{WKB}}}{dl} = \pi - 2 \int_a^\infty \frac{\hbar(l + \frac{1}{2}) dr}{r^2 \sqrt{2\mu[E - V(r)] - \hbar^2(l + \frac{1}{2})^2/r^2}}. \quad (2.89)$$

Setting  $\hbar(l + \frac{1}{2}) = b\sqrt{2\mu E}$  we see that the expression on the right-hand side is nothing but the classical deflection function  $\Theta(b)$  of eqn (2.9), so that

$$2 \frac{d\delta_l^{\text{WKB}}}{dl} = \Theta(b) \quad \text{with } b = (l + \frac{1}{2})/k. \quad (2.90)$$

This relation enables us, incidentally, to calculate a classical deflection function from the quantal scattering phases (even for complex potentials) by setting approximately

$$\Theta(l) = 2 \operatorname{Re} \frac{\delta_{l+1} - \delta_l}{(l+1) - l} = 2 \operatorname{Re} (\delta_{l+1} - \delta_l) \quad \text{for } l \gg 1. \quad (2.91)$$

### 2.3.2 Evaluation of the scattering amplitude in WKB

In order to obtain a closed expression for the scattering amplitude (2.42) in the WKB approximation, we first replace the Legendre polynomials  $P_l(\cos \theta)$  with more elementary functions, using their asymptotic form (cf. Newton 1982, eqn (3.73))

$$\begin{aligned} P_l(\cos \theta) &\approx 2[(2l+1)\pi \sin \theta]^{-1/2} \cos[\frac{\pi}{4} - (l + \frac{1}{2})\theta] \\ &= (2\lambda \sin \theta)^{-1/2} (e^{i(\pi/4-\lambda\theta)} + e^{-i(\pi/4-\lambda\theta)}) \end{aligned} \quad (2.92)$$

for  $\lambda \sin \theta \gtrsim 1$  or  $\theta, \pi - \theta \gtrsim 1/\lambda$ ;

here we have introduced the angular momentum variable  $\lambda = l + \frac{1}{2}$ , which is a convenient notation in semiclassical analyses. This approximation excludes angular momenta  $l$  near zero. These do not contribute significantly to the partial-wave sum in the semiclassical regime, i.e. for large energies and heavier nuclei, and can therefore be discarded. It is seen that the formula is not valid near  $\theta = 0$  or  $\pi$ .

Secondly, we replace the sum over angular momenta in the scattering amplitude (2.42) with an integral. This is done by applying the *Poisson sum formula* (cf. Morse and Feshbach 1953, Section 4.8; Brink 1985, Section 4.2),

$$\sum_{l=0}^{\infty} g_l = \sum_{m=-\infty}^{\infty} e^{-im\pi} \int_0^{\infty} d\lambda g(\lambda) e^{i2\pi m\lambda}, \quad (2.93)$$

which holds for a set of numbers  $g_l$ ,  $l = 0, 1, 2, \dots$ , with an analytic continuation  $g_l \rightarrow g(\lambda)$  on the real axis of  $\lambda = l + \frac{1}{2}$ ,  $0 < \lambda < \infty$ . For the terms appearing in the sum (2.42) this continuation is given by using eqns (2.78) and (2.92).

◇ The Poisson sum formula is obtained by writing  $g(\lambda) = g(l + x)$  for fixed  $l$  as a Fourier series in the range  $0 < x < 1$ ,

$$g(l+x) = \sum_{m=-\infty}^{\infty} g_m^{(l)} \exp(-i2m\pi x) \quad \text{for } 0 < x < 1, \quad (2.94)$$

with Fourier coefficients

$$g_m^{(l)} = \int_0^1 dx g(l+x) \exp[i2m\pi(l+x)] = \int_l^{l+1} d\lambda g(\lambda) \exp(i2m\pi\lambda).$$

Setting  $x = \frac{1}{2}$  in eqn (2.94) and summing over the integers  $l$ , one obtains eqn (2.93). ◇

### 2.3 The semiclassical approximation (WKB)

In rewriting the scattering amplitude (2.42) we omit the term  $-1$  in the second parentheses because it contributes only for  $\theta = 0$ ,

$$\sum_{l=0}^{\infty} (2l+1) P_l(\cos \theta) = \delta(\theta).$$

Applying eqn (2.93) together with the approximation (2.92), we then find

$$f(\theta) = \sum_{m=-\infty}^{\infty} [f_m^+(\theta) + f_m^-(\theta)], \quad (2.95)$$

where we have defined

$$f_m^{\pm}(\theta) = -\frac{i}{k} \int_0^{\infty} d\lambda \frac{\lambda^{1/2}}{(2\pi \sin \theta)^{1/2}} e^{i\phi_{\pm}(\lambda)} \quad (2.96)$$

with the phase

$$\phi_{\pm}(\lambda) = 2\delta^{\text{WKB}}(\lambda) \pm \lambda\theta \mp \frac{\pi}{4} + 2m\pi\lambda - m\pi. \quad (2.97)$$

#### The stationary-phase approximation

The amplitudes (2.96) are given by integrals of the general form

$$I = \int_0^{\infty} d\lambda g(\lambda) e^{i\phi(\lambda)}, \quad (2.98)$$

where  $g(\lambda)$  is a slowly varying function of  $\lambda$ , while the phase factor  $\exp[i\phi(\lambda)]$ , in general, oscillates rapidly because its phase is essentially the classical radial action in units of  $\hbar$ , which is large. Thus for most values of  $\lambda$  the contributions from neighbouring points will cancel out except near a *stationary point*  $\lambda = \lambda_0$  at which the phase is non-varying ('stationary'),

$$\frac{d\phi}{d\lambda} = 0. \quad (2.99)$$

The integral is determined by the integrand near this point, for here the contributions from neighbouring points are in phase and add up constructively. The function  $g(\lambda)$  is then approximated by its value for  $\lambda = \lambda_0$ ,  $g(\lambda) \approx g(\lambda_0)$ , and the phase is expanded about  $\lambda_0$  up to second order in  $\lambda$ ,

$$\phi(\lambda) = \phi(\lambda_0) + \frac{1}{2} \frac{d^2\phi}{d\lambda^2} \Big|_{\lambda_0} (\lambda - \lambda_0)^2 + \dots \quad (2.100)$$

If there is one positive stationary point ( $\lambda_0 > 0$ ), the lower limit of the integral (2.98) can be shifted to  $-\infty$ . The integral then becomes

$$\begin{aligned} I &\approx g(\lambda_0) e^{i\phi(\lambda_0)} \int_{-\infty}^{\infty} d\lambda \exp[i\frac{1}{2}\phi''(\lambda_0)(\lambda - \lambda_0)^2] = g(\lambda_0) e^{i\phi(\lambda_0)} \sqrt{\frac{2\pi i}{\phi''(\lambda_0)}} \\ &= g(\lambda_0) e^{i\phi(\lambda_0)} \sqrt{\frac{2\pi}{|\phi''(\lambda_0)|}} \exp[i(\frac{\pi}{4} - \frac{1}{2}\arg\phi''(\lambda_0))]. \end{aligned} \quad (2.101)$$

If there is more than one stationary point one has to sum over their contributions.

Let us now apply the stationary-phase approximation to the integrals (2.96). The stationary points  $\lambda_0$  of the phases (2.97) are given as solutions of  $d\phi_{\pm}/d\lambda = 0$ , or

$$2 \frac{d\delta^{\text{WKB}}(\lambda)}{d\lambda} \pm \theta + m2\pi = 0. \quad (2.102)$$

Introducing the deflection function via eqn (2.90) we therefore have

$$\Theta(\lambda_0) = \mp\theta - m2\pi \text{ for } f_m^{\pm}(\theta), \quad (2.103)$$

where  $m$  is a positive integer or zero. This equation is identical with the classical relation (2.12). Solving it for  $\lambda_0$  with  $\lambda_0 = kb$  yields the impact parameter  $b$  of the trajectory or trajectories along which the particle scatters into the scattering angle  $\theta$ . Thus the semiclassical scattering amplitude for angle  $\theta$  is determined by the classical trajectory (-ies) leading to that angle.

Since the scattering angle is positive,  $0 < \theta < \pi$ , the sign of the deflection function determines which of the two phases  $\phi_{\pm}$  is stationary, i.e. which of the terms  $f_m^{\pm}(\theta)$  contributes to the scattering amplitude. The deflection function  $\Theta(\lambda)$  varies between  $-\infty$  and  $\pi$ , so that  $m$  has to be a non-negative integer. Therefore,  $\phi_+$  is stationary for  $\Theta(\lambda) < 0$  (attractive farside scattering:  $f_m^+(\theta)$ ), and  $\phi_-$  is stationary for  $\Theta(\lambda) > 0$  (nearside scattering:  $f_m^-(\theta)$ , repulsive if  $m = 0$  and attractive if  $m > 0$ ). These cases are illustrated in Fig. 2.4 for  $m = 0, 1$ .

The number  $m$  counts how often a trajectory encircles the scattering centre. Usually, and especially in heavy-ion scattering, the cases with  $m > 0$  can be disregarded because the corresponding trajectories encircle the scattering centre in a region of nuclear attraction, which generally is also the region of absorption; they do not contribute to the elastic cross section. We therefore restrict ourselves to the terms with  $m = 0$ .

The second derivative of the phase (2.97) is equal to the first derivative of the deflection function,

$$\frac{d^2\phi_{\pm}}{d\lambda^2}\Big|_{\lambda_0} = \frac{d\Theta(\lambda)}{d\lambda}\Big|_{\lambda_0}. \quad (2.104)$$

Then the contribution of the stationary point  $\lambda_0$  to the scattering amplitude (2.96), for example, for the + branch with  $m = 0$  becomes, according to eqn (2.101) with  $g(\lambda_0) = -(i/k)\lambda_0^{1/2}(2\pi \sin \theta)^{-1/2}$ ,

$$f_0^+(\theta) = -\frac{i}{k} \frac{\sqrt{\lambda_0}}{\sqrt{\sin \theta}} \exp \left[ i \left( \phi_+(\lambda_0) + \frac{\pi}{4} - \frac{1}{2} \arg \frac{d\Theta}{d\lambda}\Big|_{\lambda_0} \right) \right] \left| \frac{d\Theta(\lambda)}{d\lambda} \right|_{\lambda_0}^{-1/2}; \quad (2.105)$$

here  $\lambda_0 = \lambda_0(\theta)$  is a function of the angle  $\theta$  which is determined by the solution of eqn (2.103). The corresponding cross section is given by

$$\frac{d\sigma}{d\Omega} = |f_0^+(\theta)|^2 = \frac{\lambda_0}{k^2 \sin \theta |d\Theta/d\lambda|_{\lambda_0}}, \quad (2.106)$$

which, with  $\lambda_0 = kb_0$ , is seen to be equal to the classical cross section (2.14),

$$\frac{d\sigma}{d\Omega} = \frac{b_0}{\sin \theta |d\Theta/db|_{b_0}}. \quad (2.107)$$

We emphasize that owing to the conditions stated in eqn (2.92) this formula *does not* hold for  $\theta \approx 0$  or  $\pi$  in the semiclassical approximation.

◇ *The Coulomb scattering amplitude.* It is remarkable that one obtains the *exact* Coulomb scattering amplitude (1.98) by applying the stationary-phase approximation to the integral (cf. eqn (2.96))

$$f_0^-(\theta) = -\frac{i}{k} \int_0^\infty d\lambda \frac{\lambda^{1/2}}{(2\pi \sin \theta)^{1/2}} e^{i(2\sigma_{\lambda} - \lambda\theta + \pi/4)}, \quad (2.108)$$

and writing the Coulomb phases  $\sigma_{\lambda}$  in the form of eqn (3.35). ◇

### Multiple trajectories

If the integral for the scattering amplitude at a given scattering angle contains more than one stationary point (that is, if several trajectories lead to the same scattering angle, cf. Section 2.2.2), their contributions have to be summed (again for  $m = 0$ ),

$$f(\theta) = -\frac{i}{k\sqrt{\sin \theta}} \sum_n \frac{\lambda_n^{1/2}}{\sqrt{|d\Theta/d\lambda|_{\lambda_n}}} e^{i\phi_n}, \quad (2.109)$$

where

$$\phi_n = \phi_{\pm,n} + \frac{\pi}{4} - \frac{1}{2} \arg \frac{d\theta}{d\lambda}\Big|_{\lambda_n}. \quad (2.110)$$

When the absolute square of the scattering amplitude is taken to obtain the cross section, interference terms appear. These are the essential feature of the semiclassical cross section, which distinguishes it from the classical expression (2.25). In the case of two interfering trajectories we find for the semiclassical cross section

$$\frac{d\sigma}{d\Omega} = \frac{1}{k^2 \sin \theta} \left| \frac{\lambda_1^{1/2}}{\sqrt{|\Theta'_1|}} e^{i\phi_1} + \frac{\lambda_2^{1/2}}{\sqrt{|\Theta'_2|}} e^{i\phi_2} \right|^2 \quad (2.111)$$

or

$$\frac{d\sigma}{d\Omega} = \frac{d\sigma_1^{\text{cl}}}{d\Omega} + \frac{d\sigma_2^{\text{cl}}}{d\Omega} + 2\sqrt{\frac{d\sigma_1^{\text{cl}}}{d\Omega} \frac{d\sigma_2^{\text{cl}}}{d\Omega}} \cos(\phi_2 - \phi_1), \quad (2.112)$$

where the superfix ‘cl’ refers to the *classical* cross section of the type (2.106), and  $\phi_n = \phi[\lambda_n(\theta)]$ ,  $n = 1, 2$ . When the two stationary points define trajectories of the same type, the nearside type  $\phi_+$ , say, eqn (2.97) with  $m = 0$  yields for the phase difference in the argument of the cosine

$$\phi_2 - \phi_1 = 2\delta^{\text{WKB}}(\lambda_2) - 2\delta^{\text{WKB}}(\lambda_1) + (\lambda_2 - \lambda_1)\theta, \quad (2.113)$$

where the two interfering stationary angular momenta are functions of the scattering angle,  $\lambda_i = \lambda_i(\theta)$ ,  $i = 1, 2$ . For a small variation  $\Delta\theta$  of the scattering angle the phase difference changes by

$$\begin{aligned}\Delta(\phi_2 - \phi_1) &= \left\{ 2(d\delta^{\text{WKB}}/d\lambda_2)\lambda'_2(\theta) - 2(d\delta^{\text{WKB}}/d\lambda_1)\lambda'_1(\theta) \right. \\ &\quad \left. + \lambda_2 - \lambda_1 + [\lambda'_2(\theta) - \lambda'_1(\theta)]\theta \right\} \Delta\theta \\ &= \{\Theta(\lambda_2)\lambda'_2(\theta) - \Theta(\lambda_1)\lambda'_1(\theta) + [\lambda'_2(\theta) - \lambda'_1(\theta)]\theta + \lambda_2 - \lambda_1\} \Delta\theta \\ &= (\lambda_2 - \lambda_1)\Delta\theta;\end{aligned}\quad (2.114)$$

here the second equality follows from eqn (2.90), while the last line is a consequence of eqn (2.103), which yields for the two interfering trajectories  $\Theta(\lambda_2) = \Theta(\lambda_1) = \theta$ . Thus the interference term gives rise to oscillations in the angular dependence with a period  $\Delta\theta = 2\pi/|\lambda_2 - \lambda_1| = 2\pi\hbar/|L_2 - L_1|$ , where  $L$  is the classical angular momentum. In the classical limit, when the angular momenta are large compared to  $\hbar$ , this period is very small indeed, and the interference term oscillates extremely rapidly as a function of the angle. It will effectively be averaged out to zero.

## 2.4 Special features of semiclassical scattering

The particular features of classical scattering, glory, rainbow, and orbiting, also occur in a modified form in semiclassical scattering. The main alteration is here that the singularities in the classical cross section are removed owing to wave-mechanical ‘smoothing’.

### 2.4.1 The glory

The classical glory singularity (cf. Section 2.2.3) is caused by the zeros of the function  $\sin\theta$  in the denominator of the classical cross section (2.14). Since the semiclassical cross section formula (2.106) has been derived using the approximation (2.92), which is not valid near these points, we have to make a new start.

Instead of formula (2.92) we use the approximation (cf. Newton 1982, eqn (3.59))

$$P_l(\cos\theta) = (\cos\theta)^{\lambda-1/2} J_0(\lambda \sin\theta) \quad \text{for } \lambda \sin\theta \ll 1, \quad (2.115)$$

where  $J_0(z)$  is the Bessel function of order zero. Equation (2.115) holds in the forward and backward directions  $\theta \approx 0, \pi$ .

The forward glory at the deflection angle  $\Theta_g = -m2\pi$ ,  $m = 0, 1, 2, \dots$ , is generally masked by diffractive scattering from large impact parameters (cf. Child 1974; Newton 1982; or in heavy-ion scattering, Ostrowski *et al.* 1991). In the backward direction we have  $\Theta_g = -(2m+1)\pi$ . We consider only the case  $\Theta_g = -\pi$ . With the approximation (2.115) replacing (2.92) the scattering amplitude  $f_0^-(\theta)$  of eqn (2.96) becomes for  $\theta \approx |\Theta_g| = \pi$

$$f_0^-(\theta) \approx -\frac{i}{k} \int_0^\infty d\lambda (\cos\theta)^{\lambda-1/2} \lambda J_0(\lambda \sin\theta) e^{2i\delta^{\text{WKB}}(\lambda)}. \quad (2.116)$$

We introduce the glory angular momentum  $\lambda_g$  as the angular momentum for which  $\Theta = -\pi$ , (in Fig. 2.6c there are actually two such glory angular momenta). Next we

## 2.4 Special features of semiclassical scattering

expand the WKB phase shift around  $\lambda_g$ ,

$$\delta^{\text{WKB}}(\lambda) = \delta^{\text{WKB}}(\lambda_g) + \frac{1}{2}\Theta_g(\lambda - \lambda_g) + \frac{1}{4} \frac{d\Theta}{d\lambda} \Big|_{\lambda_g} (\lambda - \lambda_g)^2 + \dots \quad (2.117)$$

and set  $\theta = \pi$  in  $(\cos\theta)^{\lambda-1/2} \rightarrow e^{i\pi(\lambda-1/2)}$  and  $\lambda = \lambda_g$  in  $\lambda J_0(\lambda \sin\theta)$ . Then the scattering amplitude (2.116) becomes, with  $\Theta_g = -\pi$ ,

$$\begin{aligned}f_0^-(\theta) &\approx -\frac{i\lambda_g}{k} J_0(\lambda_g \sin\theta) e^{i\pi(\lambda_g-1/2)} e^{2i\delta^{\text{WKB}}(\lambda_g)} \int_{-\infty}^\infty d\lambda \exp\left[i\frac{1}{2}(d\Theta/d\lambda)_{\lambda_g}(\lambda - \lambda_g)^2\right] \\ &= -\frac{\lambda_g}{k} J_0(\lambda_g \sin\theta) e^{i\pi\lambda_g} e^{2i\delta^{\text{WKB}}(\lambda_g)} \sqrt{2\pi i/(d\Theta/d\lambda)_{\lambda_g}},\end{aligned}\quad (2.118)$$

and we find for the cross section in the backward direction, with  $\lambda_g \equiv kb_g$ ,

$$\frac{d\sigma}{d\Omega} = \frac{2\pi kb_g^2}{|d\Theta/db|_{b_g}} J_0^2(kb_g \sin\theta). \quad (2.119)$$

This cross section is an oscillatory function of the angle  $\theta$ . The frequency of the oscillations is determined by the glory angular momentum  $\lambda_g$ .

For an interpretation of  $\alpha-^{40}\text{Ca}$  scattering in terms of a backward glory effect see, for example, Takigawa and Lee (1977).

### 2.4.2 The rainbow

Rainbow scattering occurs at angular momenta  $\lambda = \lambda_r$  for which  $\Theta'(\lambda_r) = 0$ . The deflection function for nuclear scattering generally has two rainbows (cf. Fig. 2.9), a Coulomb rainbow at a large angular momentum, and a nuclear rainbow at a smaller angular momentum.

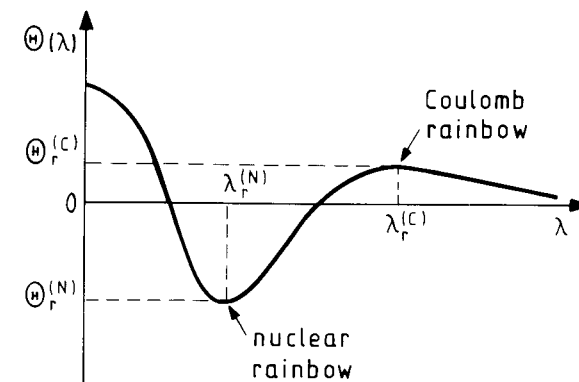


Figure 2.9 Deflection function with Coulomb and nuclear rainbows.

We have seen that the classical cross section diverges at the rainbow angle  $\Theta_r$ . This does not mean, however, that the semiclassical cross section does the same, because in this case it is *not* given by the ‘classical’ formula (2.106). The derivation of the latter

in the semiclassical approximation is based on the two-term expansion (2.100) of the phase  $\phi(\lambda)$ ; but because of

$$\Theta'(\lambda_r) = \phi''(\lambda_r) = 0 \quad (2.120)$$

the second term on the right-hand side of eqn (2.100) vanishes at the rainbow angular momentum  $\lambda_r$ , so that the stationary-phase evaluation of the integral (2.101) is invalid for the rainbow. Therefore, we have to go beyond the approximation (2.100). We may approximate the phase near  $\lambda_r$  by expanding it up to third order, or by mapping it onto an appropriate function in the neighbourhood of  $\lambda_r$ . These procedures result in the *primitive* and the *uniform Airy approximations*, respectively.

### (i) The primitive Airy approximation

Let us expand the phase  $\phi(\lambda)$  about the rainbow angular momentum  $\lambda_r$  up to third order, using the notation  $\phi_r = \phi(\lambda_r)$ ,  $\phi'_r = \phi'(\lambda_r)$  and  $\phi'''_r = \phi'''(\lambda_r)$ ,

$$\phi(\lambda) = \phi_r + \phi'_r \cdot (\lambda - \lambda_r) + \frac{1}{6} \phi'''_r \cdot (\lambda - \lambda_r)^3 + \dots; \quad (2.121)$$

here we have taken account of eqn (2.120). We now find for the integral (2.98)

$$I \approx g(\lambda_r) e^{i\phi_r} \int_{-\infty}^{\infty} d\lambda \exp\{i[\phi'_r \cdot (\lambda - \lambda_r) + \frac{1}{6} \phi'''_r \cdot (\lambda - \lambda_r)^3]\}. \quad (2.122)$$

We consider the nuclear rainbow for which  $\phi'''_r > 0$ , and introduce as a new variable of integration  $v = (\phi'''_r/2)^{1/3}(\lambda - \lambda_r)$ . Then we have

$$\begin{aligned} I &\approx g(\lambda_r) e^{i\phi_r} (\phi'''_r/2)^{-1/3} \int_{-\infty}^{\infty} dv \exp\{i[\phi'_r (\phi'''_r/2)^{-1/3} v + \frac{1}{3} v^3]\} \\ &= g(\lambda_r) e^{i\phi_r} (\phi'''_r/2)^{-1/3} 2\pi \text{Ai}\left[\phi'_r (\phi'''_r/2)^{-1/3}\right], \end{aligned} \quad (2.123)$$

where  $\text{Ai}(x)$  is the Airy function defined by (cf. Abramovitz and Stegun 1964, Section 10.4)

$$\text{Ai}(x) = \frac{1}{\pi} \int_0^{\infty} dt \cos(xt + \frac{1}{3}t^3) = \frac{1}{2\pi} \int_{-\infty}^{\infty} dt \exp[i(xt + \frac{1}{3}t^3)], \quad (2.124)$$

with  $x = \phi'_r (\phi'''_r/2)^{-1/3}$ .

For a nuclear rainbow we have from eqn (2.97) with  $m = 0$

$$\phi'_r = \phi'_+(\lambda_r) = \Theta(\lambda_r) + \theta \quad (2.125)$$

and

$$\phi'''_r = \phi'''(\lambda_r) = \Theta''(\lambda_r). \quad (2.126)$$

Therefore the argument of the Airy function is

$$x = \phi'_r (\phi'''_r/2)^{-1/3} = q^{-1/3}(\theta - \theta_r), \quad (2.127)$$

where we have introduced the rainbow scattering angle  $\theta_r = -\Theta(\lambda_r) > 0$  (cf. Fig. 2.9) and  $q = \Theta''(\lambda_r)/2$ . Taking the absolute square of the scattering amplitude (2.123) with  $g(\lambda_r) = -(i/k)\lambda_r^{1/2}(2\pi \sin \theta)^{-1/2}$ , we arrive at the cross section

$$\frac{d\sigma}{d\Omega} \approx \frac{\lambda_r}{k^2 \sin \theta} 2\pi \frac{\{\text{Ai}[q^{-1/3}(\theta - \theta_r)]\}^2}{q^{2/3}} \text{ for } \theta \approx \theta_r. \quad (2.128)$$

The Airy function is shown in Fig. 2.10; it is seen to be finite everywhere, and therefore the cross section does not diverge at the rainbow angle: the singularity of the classical cross section has been removed. The part of the Airy function to the left of the origin ( $\theta < \theta_r$ ) describes the bright side of the rainbow, and the part to the right ( $\theta > \theta_r$ ) the

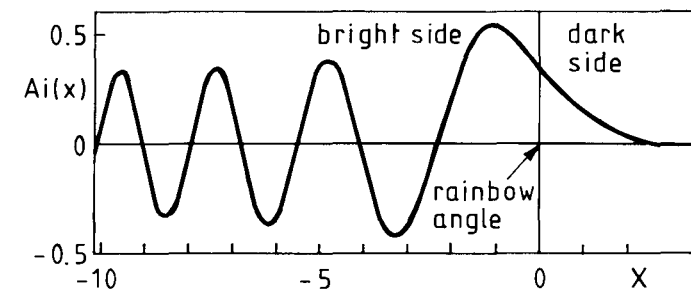


**Figure 2.10** The Airy function as a function of  $x = q^{-1/3}(\theta - \theta_r)$ . The rainbow angle corresponds to  $x = 0$ ; the dark and bright sides are indicated.

dark side (in classical scattering there would be no scattering into the latter region). Note that the maximum of the cross section *does not* lie at the rainbow angle  $\theta_r$ .

At the rainbow angular momentum two stationary points associated with the same deflection angle coalesce. The primitive Airy approximation describes the immediate neighbourhood of this point, but it is not valid when the two stationary points are still separated. An improved approximation encompassing both situations is the uniform Airy approximation, to which we turn next.

### (ii) The uniform Airy approximation

In the uniform approximation the phase  $\phi(\lambda) = \phi(\lambda, \theta)$  defined by eqn (2.97), instead of being expanded in  $\lambda$  near a point, is subjected to a conformal mapping. Introducing the new variable

$$y = y(\lambda) \quad (2.129)$$

near the point  $y(\lambda_r) = 0$ , we write the phase  $\phi(\lambda)$  in the form

$$\phi(\lambda, \theta) = A(\theta) - \zeta(\theta)y(\lambda) + \frac{1}{3}[y(\lambda)]^3 \quad (2.130)$$

(cf. Berry 1966; Brink 1985, Appendix C). This form of the mapping resembles the expansion in eqn (2.121).

The stationary points  $\lambda = \lambda_{1,2}(\theta)$  are the solutions of

$$\frac{\partial \phi}{\partial \lambda} = \left[ -\zeta(\theta) + y^2 \right] \frac{dy}{d\lambda} = 0, \quad (2.131)$$

which yields for  $dy/d\lambda \neq 0$

$$y_{1,2} = y[\lambda_{1,2}(\theta)] = \pm [\zeta(\theta)]^{1/2}. \quad (2.132)$$

The phases at these points are

$$\phi_{1,2}(\theta) = \phi[\theta, \lambda_{1,2}(\theta)] = A(\theta) \mp \frac{2}{3}\zeta^{3/2}(\theta). \quad (2.133)$$

From this equation we find for the coefficients of the mapping function

$$\begin{aligned} A(\theta) &= \frac{1}{2}[\phi_1(\theta) + \phi_2(\theta)], \\ \frac{2}{3}\zeta^{3/2}(\theta) &= \frac{1}{2}[\phi_2(\theta) - \phi_1(\theta)]. \end{aligned} \quad (2.134)$$

The integral (2.98) in the new variable  $y$  has the form

$$I \approx e^{iA} \int dy h(y) \exp[i(-\zeta y + \frac{1}{3}y^3)]; \quad (2.135)$$

here

$$h(y) = g(y)(d\lambda/dy) \quad (2.136)$$

is a function of which we must require that it yields the correct amplitudes  $g_{1,2} = g[\lambda_{1,2}(\theta)]$  at the two stationary points (2.132). A linear ansatz for  $h(y)$  will be sufficient for this,

$$h(y) = p_a + p_b y, \quad (2.137)$$

where the parameters  $p_{a,b}$  are determined by the two values of  $h(y)$  at the stationary points,

$$h_{1,2} = h(y_{1,2}) = p_a \pm p_b \zeta^{1/2}. \quad (2.138)$$

In order to relate  $h_{1,2}$  to  $g_{1,2}$  we must determine  $(d\lambda/dy)_{1,2}$  (cf. eqn (2.136)). To this end we consider

$$\frac{\partial^2 \phi}{\partial y^2} = \frac{\partial^2 \phi}{\partial \lambda^2} \left( \frac{d\lambda}{dy} \right)^2 + \frac{\partial \phi}{\partial \lambda} \frac{d^2 \lambda}{dy^2},$$

which, according to eqn (2.130), is to be identified with  $2y$ . At the stationary points  $\lambda_{1,2}$ , where  $\partial \phi / \partial \lambda = 0$ , we have

$$\frac{\partial^2 \phi}{\partial y^2} \Big|_{1,2} = \frac{\partial^2 \phi}{\partial \lambda^2} \Big|_{1,2} \left( \frac{\partial \lambda}{\partial y} \Big|_{1,2} \right)^2 = 2y_{1,2} = \pm 2\zeta^{1/2}, \quad (2.139)$$

and therefore

$$h_{1,2} = g_{1,2} \frac{d\lambda}{dy} \Big|_{1,2} = g_{1,2} \zeta^{1/4} \left( \frac{2}{\pm \phi''_{1,2}} \right)^{1/2}, \quad (2.140)$$

where  $\phi''_{1,2} = \partial^2 \phi(\lambda)/\partial \lambda^2|_{\lambda=\lambda_{1,2}(\theta)}$ . Thus we find from eqn (2.138)

$$p_{a,b} = \frac{\zeta^{\pm 1/4}}{\sqrt{2}} \left( \frac{g_1}{(\phi'_1)^{1/2}} \pm \frac{g_2}{(-\phi'_2)^{1/2}} \right). \quad (2.141)$$

In the integral (2.135) the variable  $y$  in the function  $h(y)$  can be replaced with the derivative  $i\partial/\partial \zeta$ , and the operator function  $h(i\partial/\partial \zeta)$  can then be taken outside the integral. We obtain finally, using eqn (2.137) and the notation  $\text{Ai}'$  for the derivative of the Airy function with respect to its argument,

$$\begin{aligned} I &\approx 2\pi e^{iA} [p_a \text{Ai}(-\zeta) - i p_b \text{Ai}'(-\zeta)] \\ &= \sqrt{2\pi} e^{iA} \left[ \left( \frac{g_1}{(\phi'_1)^{1/2}} + \frac{g_2}{(-\phi'_2)^{1/2}} \right) \zeta^{1/4} \text{Ai}(-\zeta) \right. \\ &\quad \left. - i \left( \frac{g_1}{(\phi'_1)^{1/2}} - \frac{g_2}{(-\phi'_2)^{1/2}} \right) \zeta^{-1/4} \text{Ai}'(-\zeta) \right]. \end{aligned} \quad (2.142)$$

Expression (2.142) is the general form of the uniform approximation with the cubic mapping (2.130). Because of the appearance of the Airy functions it is called the *uniform Airy approximation*. It contains the functions  $\phi'_{1,2}(\theta)$  in the denominators, which according to eqn (2.139) vanish when the two stationary points coalesce,  $y_1 = y_2$  or  $\zeta = 0$ ; this happens at the rainbow angle. However, closer inspection shows that in the coefficient of the function  $\text{Ai}(-\zeta)$  this singularity is cancelled by the factor  $\zeta^{1/4}$ , and in the coefficient of the function  $\text{Ai}'(-\zeta)$  it is removed when taking the difference inside the parenthesis. Therefore the uniform Airy approximation is finite everywhere.

Depending on the scattering angle the stationary solutions  $\lambda_{1,2}(\theta)$  are real when  $\zeta(\theta) > 0$  (classically allowed case, bright side of the rainbow), or conjugate complex,  $\lambda_2 = \lambda_1^*$ , when  $\zeta(\theta) < 0$  (classically forbidden case, dark side of the rainbow).

The uniform Airy approximation has two limits already known to us:

(a) *Two well separated real stationary points*. In this case  $\zeta$  is large. From the asymptotic form of the Airy function for  $\zeta \rightarrow \infty$  (cf. Abramowitz and Stegun 1965, formulae (10.4.60) and (10.4.62)),

$$\begin{aligned} \text{Ai}(-\zeta) &\rightarrow \pi^{-1/2} \zeta^{-1/4} \sin(\frac{2}{3}\zeta^{3/2} + \frac{\pi}{4}), \\ \text{Ai}'(-\zeta) &\rightarrow -\pi^{-1/2} \zeta^{1/4} \cos(\frac{2}{3}\zeta^{3/2} + \frac{\pi}{4}), \end{aligned} \quad (2.143)$$

we obtain

$$\zeta^{1/4} \text{Ai}(-\zeta) \pm i \zeta^{-1/4} \text{Ai}'(-\zeta) \rightarrow \pi^{-1/2} \exp[\pm i(\frac{2}{3}\zeta^{3/2} - \frac{\pi}{4})]. \quad (2.144)$$

Using this relation in eqn (2.142) we find

$$I \approx \sqrt{2\pi} i \left( \frac{g_1 e^{i\phi_1}}{(\phi'_1)^{1/2}} + \frac{g_2 e^{i\phi_2}}{(\phi'_2)^{1/2}} \right), \quad (2.145)$$

where the phases  $\phi_{1,2}$  are given by expression (2.133). Formula (2.145) agrees with eqn (2.101) extended to the case of two stationary points.

(b) *The primitive Airy approximation*. Here one identifies the mapping (2.130) with the expansion (2.121) by setting  $y = (\phi_r'''/2)^{1/3} \cdot (\lambda - \lambda_r)$ ,  $A = \phi_r$  and  $\zeta = -\phi_r'(\phi_r'''/2)^{-1/3}$ . This defines the argument in the Airy functions appearing in expression (2.142). The stationary phase condition  $d\phi/d\lambda|_{1,2} = 0$  applied to the phase (2.121) yields

$$\lambda_{1,2} - \lambda_r = \pm (-2\phi_r'/\phi_r''')^{1/2}. \quad (2.146)$$

We also calculate the second derivative from eqn (2.121),

$$\phi''|_{1,2} = \phi_r''' \cdot (\lambda_{1,2} - \lambda_r) = \pm 2(-\phi_r' \phi_r''')^{1/2}, \quad (2.147)$$

and set  $g_1 = g_2 = g(\lambda_r)$ . Substituting these expressions in formula (2.142) we obtain eqn (2.123), and using eqn (2.125) we recover the primitive Airy approximation expression (2.128).

(iii) *Example: a Coulomb rainbow*

An application of the uniform Airy approximation to the Coulomb rainbow has been made by Da Silveira (1973). For the heavy-ion system Ar + Se at  $E = 201$  MeV in the centre-of-mass system a parametrized deflection function  $\Theta(\lambda)$  is fitted to the

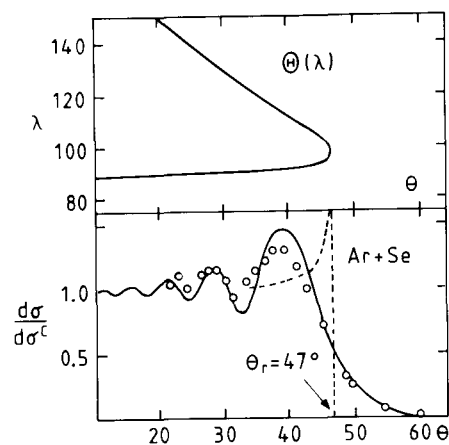


Figure 2.11 A Coulomb-rainbow effect. See text for description.

experimental data (cf. the upper part of Fig. 2.11). The argument of the Airy function is then found from eqn (2.134),

$$\zeta = \zeta(\theta) = \left\{ \frac{3}{4} [\phi_2(\theta) - \phi_1(\theta)] \right\}^{2/3},$$

where, on account of eqns (2.97) and (2.102),

$$\phi_2(\theta) - \phi_1(\theta) = \int_{\lambda_1(\theta)}^{\lambda_2(\theta)} (d\phi/d\lambda) d\lambda = \int_{\lambda_1(\theta)}^{\lambda_2(\theta)} \Theta(\lambda) d\lambda - [\lambda_2(\theta) - \lambda_1(\theta)]\theta.$$

The deflection function has a Coulomb-like tail for large angular momenta  $\lambda$  and bends down for  $\lambda < \lambda_r$  due to strong nuclear attraction; there are no contributions from low values of  $\lambda$ , since the corresponding trajectories are absorbed. The cross section calculated by taking the square of expression (2.142), divided by the Rutherford cross section, is shown in the lower part of the figure in comparison with experiment. The dashed curve represents the classical cross section (2.25), which diverges at the rainbow angle.

The cross section in Fig. 2.11 exhibits a pattern which is actually typical of Fresnel diffraction (cf. Section 3.3.2). We see here that it can also be interpreted as a rainbow effect.

#### Orbiting: barrier-top resonances

The case of orbiting in the semiclassical approximation is quite different from that in the purely classical description. This is plausible, since it is clear from Fig. 2.6 that the important contributions to the orbiting cross section come from the region near the top of the effective barrier. In this region the semiclassical calculation of the wave function has to take account of tunnelling through the barrier. In Chapter 9 on fusion we shall discuss this problem in connection with the calculation of barrier penetration probabilities. In

the present context of differential elastic cross sections we content ourselves with the remark that the semiclassical description is not based on trajectories which encircle the scattering centre, but makes use of quasi-bound states near the barrier top, which give rise to resonances in the scattering. These resonances are called *barrier-top resonances* and are treated in detail, for example, in Brink (1985), Section 6.3, Child (1974), Section 5.4, and by Friedman and Goebel (1977). Orbiting is discussed in terms of interferences of the contributions of particular partial waves for the case of elastic  $^{16}\text{O} + ^{28}\text{Si}$  scattering by Shastry and Parija (1983).

## 2.5 Semiclassical approximation for complex potentials

The results of the preceding sections can be extended to complex potentials, that is, optical potentials. This extension is achieved by analytical continuation of the classical equations of motion (2.87) and of the functions  $A_l(r)$  and  $S_l(r)$  appearing in the semiclassical wave function (2.48).

### 2.5.1 Phase shifts for integer angular momenta

For a real potential the trajectories and phase shifts are calculated from a large value of  $r$  inward up to the turning point  $a$ , where the radial momentum  $p_l(r)$  vanishes and changes sign, and then outward again (cf. Section 2.3.1). For a complex potential the radial momentum will become complex; the turning points defined as the zeros of this momentum become complex as well, and therefore move from the real axis into the complex plane (cf. Fig. 2.12). The trajectories must be taken around these turning points in the complex  $r$ -plane. In doing this one has to avoid possible singularities of the potential itself. Such singularities occur, for example, in the Woods-Saxon potential (1.146), which has poles for  $r = R + i(2n + 1)\pi a$ ,  $n = \text{integer}$ .

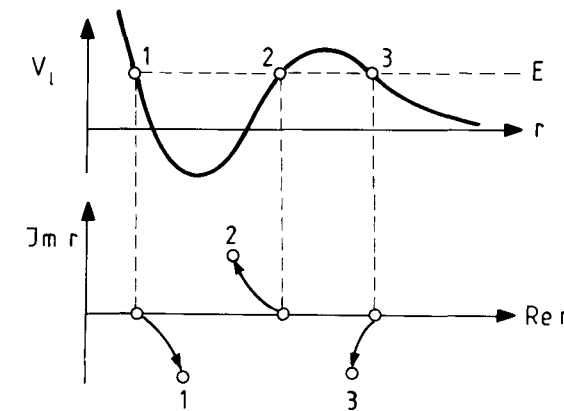
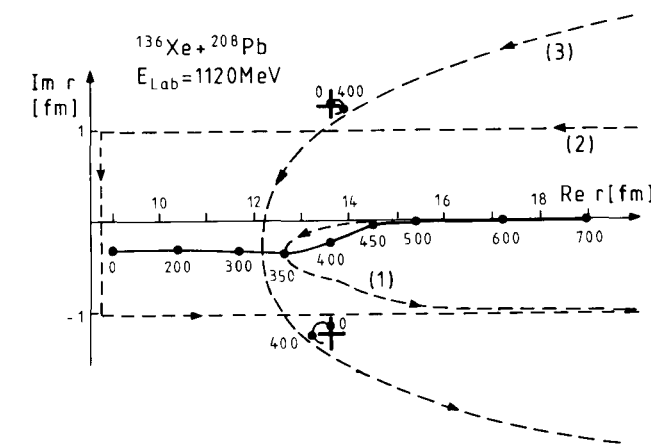


Figure 2.12 Shift of the turning points into the complex plane caused by a complex potential.

For an example we consider the cross section for the scattering of  $^{136}\text{Xe}$  by  $^{208}\text{Pb}$  at  $E_{\text{lab}} = 1120$  MeV calculated with the help of an optical potential (cf. Fröblich and Kaufmann 1978). Figure 2.13 shows the location of the turning points in the complex



**Figure 2.13** Location of the turning points (solid curves with dots) in the complex  $r$ -plane for the scattering of  $^{136}\text{Xe}$  by  $^{208}\text{Pb}$  at  $E_{\text{lab}} = 1120$  MeV. The numbers at the dots give the angular momentum  $l$  associated with the turning points. The crosses represent poles of the potential. Also shown are three trajectories (dashed curves).

$r$ -plane. Some of the turning points (marked by dots) are identified by the corresponding value of the angular momentum  $l$ . Regarding the turning point as a function of the angular momentum, we find three turning-point branches  $r = r(l)$  in the complex  $r$ -plane. The ‘physical’ branch, which makes the most important contribution to the cross section, runs close to the real axis and becomes real for large values of  $l$ . The two other branches have the shape of circles around the poles of the potential. They make negligible contributions to the cross section since they lead to large imaginary phase shifts.

In the figure we also show examples of trajectories solving the equations of motion (2.87). Trajectory (1) is obtained by straightforward integration of these equations with  $l = 350$ , using *real* time steps. It starts on the real axis for large  $r$ , meets the complex turning point for  $l = 350$  and returns parallel to the real axis. For use in the calculation of the WKB phase shift according to eqn (2.88), the trajectory can be arbitrarily deformed in the complex  $r$ -plane (this implies leaving the real time axis) as long as no singular point is crossed. Such a deformed trajectory is represented by the contour (2). Trajectory (3) is an example of a trajectory which is not allowed because it encircles the first pole of the Woods–Saxon potential in the lower half-plane.

The WKB phase shifts thus computed are then substituted in the partial-wave sum (2.42) to yield the cross section represented by the curve in Fig. 2.14. The same curve is obtained by a quantal calculation, which attests to the accuracy of the complex WKB approximation. The agreement with the experimental data (cf. Vandenbosch *et al.* 1976) is very good; this means that the optical potential chosen for calculation provides a good fit to experiment.

Other examples are discussed by Koeling and Malfliet (1975) and by Landowne *et*

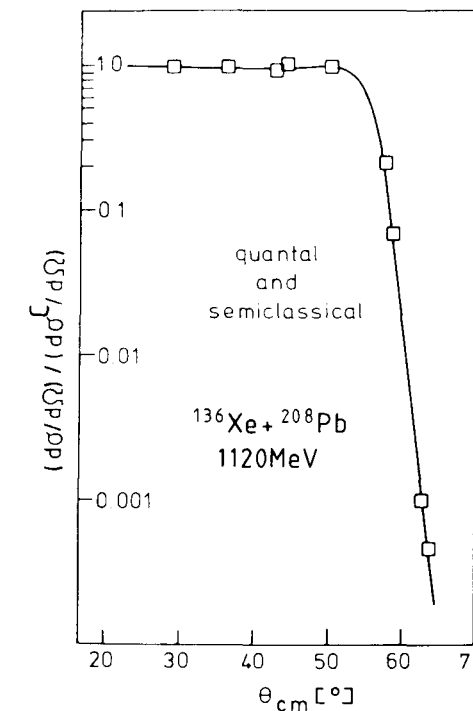


**Figure 2.14** The elastic cross section divided by the Rutherford cross section for the scattering of  $^{136}\text{Xe}$  by  $^{208}\text{Pb}$  at  $E_{\text{lab}} = 1120$  MeV, calculated with complex WKB phase shifts. The squares represent the experimental data of Vandenbosch *et al.* (1976).

*al.* (1976). Brink and Takigawa (1977) treat the scattering of low-energy  $\alpha$ -particles by Ca, a case where all three turning-point branches play a role.

## 2.5.2 Complex angular momenta: saddle points

An alternative procedure for applying the WKB approximation to complex potential scattering is to change the sum in the partial wave expansion for the scattering amplitude (2.42) into an integral of the type (2.98) and to evaluate the latter by integration in the complex plane. The stationary-phase method for real potentials is thus replaced with the *saddle-point method* (cf. Knoll and Schaeffer 1976).

We have previously determined the real stationary point(s)  $\lambda_0$  from the condition (2.103) for each (real) scattering angle  $\theta$ ; when the potential is complex, this relation becomes the saddle-point condition for one or more complex *saddle points*  $\lambda_0$  of the integral (2.98). We substitute these complex saddle points for the angular momentum  $l = \lambda - \frac{1}{2}$  in the system of eqns (2.87), which is supplemented with additional differential equations determining the derivative of the angle variable  $\phi(r)$  with respect to the initial

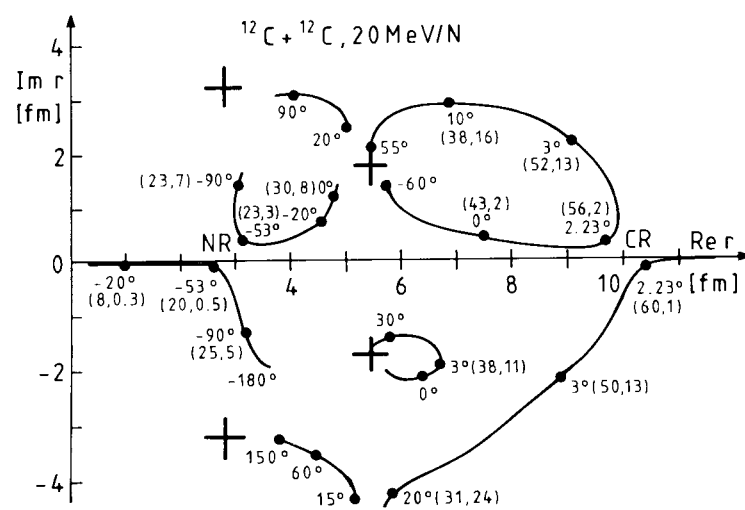


**Figure 2.15** Location of the turning points in the complex  $r$ -plane for the scattering system  $^{12}\text{C}+^{12}\text{C}$  at 20 MeV/nucleon. The scattering angle and the associated complex value of the angular momentum (in parentheses) are given for some of the turning points. The crosses indicate the singular points (poles) of the potential.

angular momentum,  $d\phi(r)/dl_i$ . At the end of the trajectory the latter quantity determines the derivative of the deflection function (cf. eqn (2.8)). The integration of this extended system of equations provides us with all the quantities needed for evaluating the scattering amplitude (2.109).

For an example we consider the system  $^{12}\text{C}+^{12}\text{C}$  at 20 MeV/nucleon described by a complex optical potential (cf. Bohlen *et al.* 1985). Its turning-point pattern is shown in Fig. 2.15. Several branches are found, where the same scattering angle  $\theta$  is attained by trajectories with different complex angular momenta  $\lambda$ . The turning points closest to the real axis affect the cross section most severely. One identifies a *nuclear rainbow* angle marked NR at  $\theta_R = -53^\circ$ , at which two almost real turning points of different branches, and therefore also two almost real angular momenta, come close to one another; they both lie at a distance  $\text{Re } r \approx 3 \text{ fm}$  from the origin, which is rather far inside the nucleus. This may be interpreted as evidence of *refractive scattering* (i.e. scattering by the *real* part of the potential) in the interior of the nucleus. The absorption is weak in this case, as the turning points connected with the nuclear rainbow are almost real. The weak absorption distinguishes the system  $^{12}\text{C} + ^{12}\text{C}$  from heavy systems, where the absorption inside the nucleus is strong and no refractive scattering is observed. The nuclear rainbow is seen as a hump in the angular distribution of the elastic cross section at about  $53^\circ$  (cf. Fig. 2.16). This effect can also be read off from the corresponding deflection function calculated from the quantal phase shifts with the help of eqn (2.91) (cf. Fig. 2.17). In Figs. 2.15 and

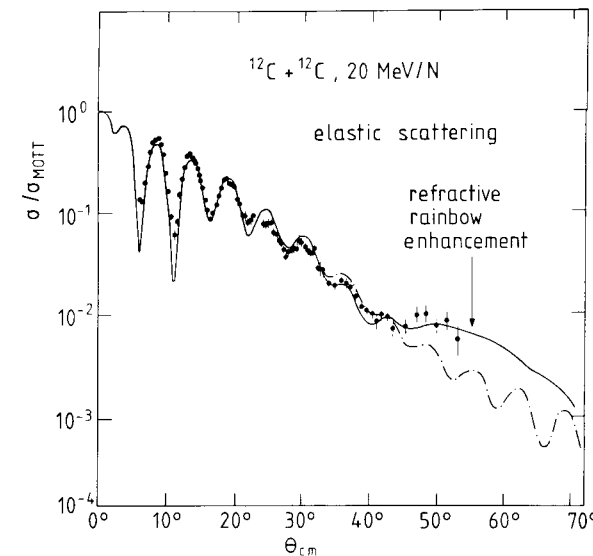


**Figure 2.16** The elastic scattering cross section divided by the Mott cross section for  $^{12}\text{C}+^{12}\text{C}$  at 20 MeV/nucleon, displaying a refractive nuclear rainbow enhancement around  $53^\circ$ .

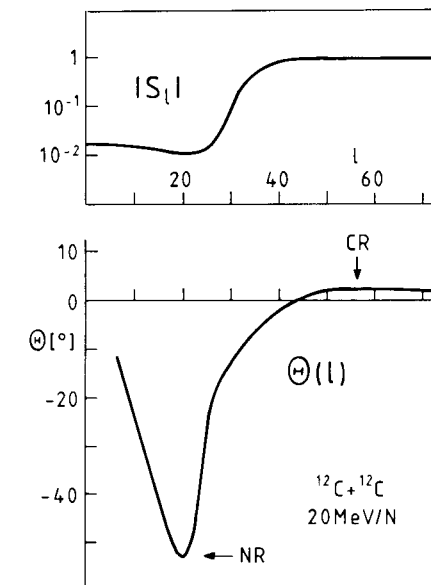


**Figure 2.17** The function  $|S_l|$  and the deflection function  $\Theta(l)$  for the system  $^{12}\text{C}+^{12}\text{C}$  at 20 MeV/nucleon.

Figs. 2.15 and 2.17 one notices a *Coulomb rainbow* (CR) at the small angle  $\theta_{\text{CR}} \approx 3^\circ$ , which involves trajectories with turning points near the surface of the nucleus,  $\text{Re } r \approx 10$  fm. The data points of the experimental cross section shown in Fig. 2.16 do not extend to this region.

An extensive analysis of the results of the WKB approximation for complex potentials (including an application of the uniform Airy approximation) has been carried out by Stiliaris *et al.* (1989) for the case of  $^{16}\text{O} + ^{16}\text{O}$  scattering at 350 MeV.

## 2.6 Notes and references

Classical scattering is treated in the standard texts on classical mechanics. Here we mention the book by Goldstein (1959) and the monograph on scattering theory by Newton (1982). For the meteorological phenomena from which the special features of classical scattering like glory and rainbow have taken their name, and beautiful pictures thereof, see the book by Greenler (1991). In nuclear physics the purely classical theory is mainly used for the description of *dissipative* scattering discussed in Chapters 11 and 12, because of the ease with which frictional forces can be incorporated in classical potential scattering (cf. Gross and Kalinowski 1978).

The theory of semiclassical scattering has been pioneered by Wheeler and co-workers (cf. Ford and Wheeler 1959; Ford *et al.* 1959). Reviews have been written by Child (1974), Brink (1985) and Nussenzweig (1992). The Airy uniform approximation, in particular, has been discussed by Berry (1966), whose work goes back to Chester *et al.* (1957). There exist other kinds of uniform approximations with mapping functions appropriate for particular topologies (cf., e.g., Brink 1985, Appendix C). A general theory, the ‘theory of catastrophes’, classifies the possible uniform mappings (cf. Thom 1975).

The semiclassical theory has been extended to more general dynamical processes than potential scattering under the general name of ‘classical S-matrix theory’. We quote the work of Berry and Mount (1972), Miller (1974), Marcus (1971) and Pechukas (1969). Here one constructs the S-matrix from contributions of interfering trajectories in a multi-dimensional space of dynamical variables. The turning points are generalized to caustics at which the semiclassical amplitudes experience a jump in phase, analogous to the term  $\frac{\pi}{4}$  found in the one-dimensional example of Section 2.3.1. How to deal with this problem and how to determine the number of phase jumps (the ‘Maslov index’) is discussed in the work by Möhring *et al.* (1980) and references therein.

The semiclassical description is employed in nuclear scattering mainly to interpret certain features of the cross section in terms of classical trajectories and their interference. Their actual calculation is nowadays carried out more efficiently by solving the exact quantal equations on modern computers.

For further papers on rainbow scattering in  $\alpha$ -scattering see Goldberg and Smith (1974), and in heavy-ion collisions, McVoy and Satchler (1984) and Fricke and McVoy (1987).

## References

- Abramowitz, M. and Stegun, I. A. (1965). *Handbook of mathematical functions*, Dover, New York.
- Berry, M. V. (1966). *Proc. Phys. Soc.* **89** 479.
- Berry, M. V. and Mount, K. E. (1972). *Rep. Prog. Phys.* **35** 315.
- Bohlen, H. G., Chen, X. S., Cramer, J. G., Fröblich, P., Gebauer, B., Lettau, H., von Oertzen, W., Ulrich, R. and Wilpert, T. (1985). *Z. Physik A* **322** 241.
- Brink, D. M. (1985). *Semiclassical methods for nucleus-nucleus scattering*, Cambridge University Press, Cambridge.
- Brink, D. M. and Takigawa, N. (1977). *Nucl. Phys.* **A279** 159.
- Bryant, H. C. and Jarmie, N. (1974). *Sci. Am.* **231** 60.
- Chester, C., Friedman, B. and Ursell, F. (1957). *Proc. Camb. Phil. Soc.* **53** 599.
- Child, M. S. (1974). *Molecular collision theory*, Academic Press, New York.
- Da Silveira, R. (1973). *Phys. Lett.* **B45** 211.
- Ford, K. W. and Wheeler, J. A. (1959). *Ann. Phys.* **7** 259, 287.
- Ford, K. W., Hill, D. L., Wakano, M. and Wheeler, J. A. (1959). *Ann. Phys.* **7** 239.
- Fricke, S. H. and McVoy, K. W. (1987). *Nucl. Phys.* **A467** 291.
- Friedman, W. A. and Goebel, C. J. (1977). *Ann. Phys. (N.Y.)* **104** 145.
- Fröblich, P. and Kaufmann, P. (1978). *Nucl. Phys.* **A307** 297.
- Goldberg, D. A. and Smith, S. M. (1974). *Phys. Rev. Lett.* **33** 715.
- Goldstein, H. (1959). *Classical mechanics*, Addison-Wesley, Cambridge, MA.
- Greenler, R. (1991). *Rainbows, halos, glories*, Cambridge University Press, Cambridge.
- Gross, D. H. E. and Kalinowski, H. (1978). *Phys. Rep.* **C45** 175.
- Knoll, J. and Schaeffer, R. (1976). *Ann. Phys.* **97** 307.
- Koeling, T. and Malfliet, R. (1975). *Phys. Rep.* **C22** 183.
- Landau, L. D. and Lifschitz, E. M. (1965). *Quantum mechanics*, Pergamon, Oxford.
- Landowne, S. M., Dasso, C. H., Nilsson, B. S., Broglia, R. A. and Winther, A. (1976). *Nucl. Phys.* **A259** 99.
- Langer, R. E. (1937). *Phys. Rev.* **51** 669.
- Marcus, R. A. (1971). *J. Chem. Phys.* **54** 3965.
- McVoy, K. W. and Satchler, G. R. (1984). *Nucl. Phys.* **A417** 157.
- Messiah, A. (1972). *Quantum mechanics*, North-Holland, Amsterdam.
- Miller, W. H. (1974). *Adv. Chem. Phys.* **25** 69.
- Möhring, K., Levit, S. and Smilansky, U. (1980). *Ann. Phys.* **127** 198.
- Morse, P. H. and Feshbach, H. (1953). *Methods of theoretical physics*, McGraw-Hill, New York.
- Newton, R. G. (1982). *Scattering theory of waves and particles*, Springer, Berlin.
- Nussenzweig, H. M. (1977). *Sci. Am.* **236** 116.
- Nussenzweig, H. M. (1979). *J. Opt. Soc. Am.* **69** 1068.
- Nussenzweig, H. M. (1992). *Diffraction effects in semiclassical scattering*, Cambridge University Press, Cambridge.
- Ostrowski, A. N., Tiereth, W. and Voit, H. (1991). *Phys. Rev.* **C44** 2082.
- Pechukas, P. (1969). *Phys. Rev.* **181** 166 and 174.
- Shastry, C. S. and Parija, I. (1983). *Phys. Rev.* **C27** 2042.

- Stiliaris, E., Bohlen, H. G., Fröbrich, P., Gebauer, B., Kolbert, D., von Oertzen, W., Wilpert, M. and Wilpert, Th. (1989). *Phys. Lett.* **B223** 291.  
 Takigawa, N. and Lee, S. Y. (1977). *Nucl. Phys.* **A292** 173.  
 Thom, R. (1975). *Structural stability and morphogenesis*, Benjamin, Reading, MA.  
 Vandenbosch, R. Webb, M. P. Thomas, T. D. and Zisman, M. S. (1976). *Nucl. Phys.* **A269** 210.

## THE WAVE-OPTICAL DESCRIPTION OF POTENTIAL SCATTERING

### 3.1 Introduction

In the preceding chapter we have discussed the semiclassical approximation to quantum scattering theory, where the dynamics is described in terms of classical trajectories. By analytic continuation of these trajectories into the complex plane the treatment has even been extended to the scattering by complex, i.e. absorptive, potentials.

We shall now consider the *optical aspects* of quantal scattering, recognizing that the Schrödinger equation for scattering by a potential has the same form as the Helmholtz equation for the propagation of light waves in optics, with the index of refraction playing the role of a potential. Therefore, under appropriate conditions, the characteristic phenomena of optics should also make their appearance in quantal scattering.

For short wavelengths we are dealing with geometrical optics, where the light rays follow trajectories of classical particles in the ‘potential’ defined by the index of refraction. For larger wavelengths interference effects appear. They can be described approximately by the WKB methods discussed in the last chapter, which also allow for absorption, i.e. for a complex index of refraction. If the absorption is strong it is advantageous to go over to a *wave-optical description* of the associated diffraction phenomena.

The *diffraction in optics* is briefly reviewed in Section 3.2. The two main types of diffraction, Fraunhofer and Fresnel diffraction, are discussed without derivation. Subsequently we state the conditions for their occurrence in nuclear scattering.

In Section 3.3 the quantum scattering amplitude for scattering on a spherical *black nucleus*, i.e. a nucleus which is totally absorbing over its whole volume, is calculated using the partial-wave expansion. The black nucleus is modelled by introducing a *cut-off* (*grazing*) angular momentum  $l_{\text{gr}}$  such that all partial waves with  $l < l_{\text{gr}}$  are completely absorbed, while those with  $l > l_{\text{gr}}$  experience no nuclear interaction at all. This *sharp-cut-off model* is used to derive the Fraunhofer and Fresnel diffraction amplitudes. The model allows for a qualitative description of the nuclear scattering cross section in the wave-optical domain.

Finally, Section 3.4 is devoted to a more realistic analysis of nuclear scattering in the framework of the so-called *strong absorption model* (SAM). Here a semi-empirical form of the *S*-function is proposed for scattering in the presence of strong absorption, which improves on the primitive black-nucleus model by introducing a smooth cut-off.

In these diffraction models the basic physical quantity used to describe the data is the *S*-function; it is this function which is parametrized, not the more fundamental potential, as is done in optical-model fitting.

### 3.2 Diffraction in optics and nuclear scattering

#### 3.2.1 The scattering of light

We recall some results of the Fresnel–Kirchhoff theory of diffraction by a screen (cf. Born and Wolf 1964, Chapter VIII; Sommerfeld 1964, §34; Frahn 1985, Chapter 4). In this theory a solution of the Helmholtz equation is established which is approximately valid in all space except the immediate neighbourhood of the edge of the screen. One requires that the wavelength  $\lambda$  of the light is small, not negligibly small as in geometrical optics, but small compared to the linear dimensions  $R$  of the absorbing screen,  $\lambda \ll R$ , or, using  $k = 2\pi/\lambda$ ,

$$kR \gg 1. \quad (3.1)$$

Consider now the experimental set-up shown schematically in Fig. 3.1. Light is emitted by the source S, scattered by the target screen T of radius  $R$  and detected by the observer O. There are two typical configurations which lead to the following two characteristic types of diffraction.

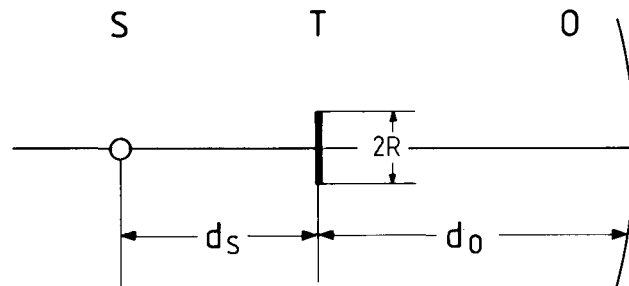


**Figure 3.1** Configuration of source S, target screen T of radius  $R$  and observer O in optical diffraction.

**Fraunhofer diffraction** is diffraction by the screen as a whole and occurs when both source and observer are located far away from the screen,  $R \ll d$ , where  $d$  is the shorter of the distances of the source,  $d_S$ , or the observer,  $d_O$ , from the screen. The requirements of the Fraunhofer regime are met if, together with eqn (3.1), the condition

$$(kR)(R/d) \ll 1. \quad (3.2)$$

is satisfied. The Fraunhofer diffraction pattern for scattering by a black circular screen is described by the following formula for the intensity  $I(\theta)$  (cf. Frahn 1985, eqn (4.6.12a)),

$$I(\theta) = R^2 [J_1(kR \sin \theta) / \sin \theta]^2, \quad (3.3)$$

where  $J_1(x)$  is the Bessel function of first order; the function  $I(\theta)/I(0) = [2J_1(x)/x]^2$  with  $x = kR \sin \theta$  is shown in Fig. 3.2. The Fraunhofer pattern has its main peak in the forward direction, followed by decreasing diffraction maxima as the scattering angle increases.

**Fresnel diffraction** is diffraction by the edge of the screen. Here either the source or the observer, or both, are located at a finite distance from the screen,  $d \gtrsim R$ ; together

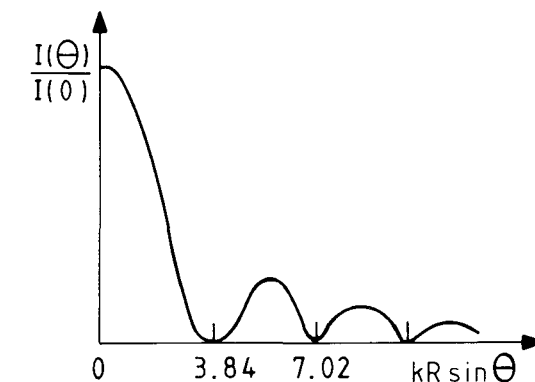


**Figure 3.2** The Fraunhofer diffraction pattern in optics.

with eqn (3.1) we have the Fresnel condition

$$(kR)(R/d) \gtrsim 1. \quad (3.4)$$

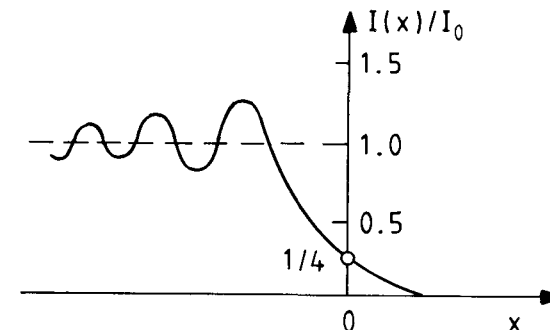


**Figure 3.3** The Fresnel diffraction pattern in optics.

In optics, Fresnel diffraction is usually considered as diffraction by a straight edge. The Fresnel diffraction pattern is described by the formula

$$I(\theta) = I(x) = \frac{1}{2} I_0 \left\{ \left[ \frac{1}{2} - C(x) \right]^2 + \left[ \frac{1}{2} - S(x) \right]^2 \right\}; \quad (3.5)$$

here the variable  $x$  is defined as

$$x = 2\sqrt{kds/\pi} \sin[\frac{1}{2}(\theta - \theta_{gr})], \quad (3.6)$$

where the *grazing angle*  $\theta_{\text{gr}}$  is the angle between the ray touching the screen edge and the optical axis. The functions  $C(x)$  and  $S(x)$  are the Fresnel functions explained in eqn (3.47) below. Figure 3.3 shows this diffraction pattern; on the bright side,  $\theta < \theta_{\text{gr}}$ , the intensity oscillates, whereas on the dark side,  $\theta > \theta_{\text{gr}}$ , it decreases exponentially. Under the Fresnel condition (3.4) the same diffraction pattern is observed in scattering by a *circular* screen (cf. Frahn 1972, Section II).

In the theory of the diffraction of light one usually considers the scattering by a planar screen, and uses geometrical arguments in three-dimensional space. The diffraction formulae (3.3) and (3.5) are commonly derived in this way. We do not present these derivations here, since we shall obtain the same results for nuclear scattering using an expansion in partial waves.

### 3.2.2 Nuclear scattering

The situation in nuclear, in particular, heavy-ion scattering, is similar to that of light scattering (cf. Frahn 1972). The source of the incident nuclear particles and the detector are of course always located at distances  $d$  from the target which are very much larger than the radius  $R$  of the target nucleus, suggesting that nuclear scattering always follows a Fraunhofer regime. However, this is not the case because here the role of the ratio  $R/d$  in distinguishing between the Fraunhofer and Fresnel regimes is taken over by another quantity.

Nuclei are charged, and the effect of the Coulomb forces on the nuclear scattering is characterized by the Sommerfeld parameter  $\eta = Z_1 Z_2 e^2 / \hbar v$  (cf. eqn (1.79)). Consider now the classical motion of a charged particle impinging on a completely absorbing ‘*black nucleus*’ with radius  $R$  (cf. Fig. 3.4). In the Coulomb field of the target nucleus an incident particle with impact parameter  $b$  is deflected to the angle  $\theta$ , which is connected with  $b$  through the relation (cf. eqn (2.19))

$$b = \frac{\eta}{k} \cot\left(\frac{\theta}{2}\right). \quad (3.7)$$

We define the *grazing impact parameter*  $b_{\text{gr}}$  as the impact parameter of the *grazing trajectory*, whose distance of closest approach is equal to the radius of the target, which can happen only if  $2\eta \leq kR$ . Then we have, using eqn (2.20),

$$\frac{\eta}{k} + \sqrt{\left(\frac{\eta}{k}\right)^2 + b_{\text{gr}}^2} = R \quad (3.8)$$

The corresponding deflection angle is the *grazing deflection angle*  $\theta_{\text{gr}}$ , for which we find from eqns (3.7) and (3.8),

$$\sin\left(\frac{\theta_{\text{gr}}}{2}\right) = \left(\frac{kR}{\eta} - 1\right)^{-1}. \quad (3.9)$$

Particles on trajectories with  $b > b_{\text{gr}}$ , i.e.  $\theta < \theta_{\text{gr}}$ , pass by the target, while those with  $b < b_{\text{gr}}$  are absorbed.

Figure 3.4, which is the same as Fig. 2.1 specialized to the case of Coulomb scattering, shows that the scattered particle appears to originate from a virtual source  $S$  close to the target. Since the trajectory is symmetric about the line connecting the turning point  $P$

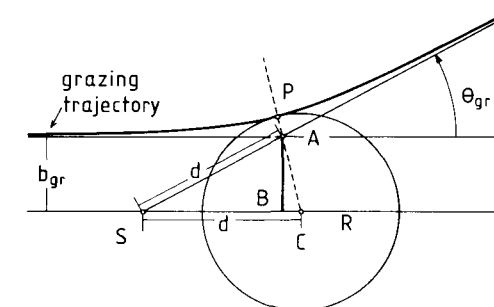


Figure 3.4 Scattering of a charged particle by a black nucleus.

with the scattering centre  $C$ , the triangle  $CSA$  is isosceles. Thus the distance  $SC$  from the source to the scattering centre is equal to the distance  $SA$ ,

$$d = \frac{b_{\text{gr}}}{\sin \theta_{\text{gr}}}. \quad (3.10)$$

On the other hand, by continuing the outgoing asymptote of the trajectory back to the virtual source point  $S$ , we see that the radius of the effective disk representing the target is no longer  $R$ , but the distance  $BA$ , which is equal to the impact parameter  $b_{\text{gr}}$ .

Defining the grazing angular momentum  $l_{\text{gr}} = kb_{\text{gr}}$  we replace the screen radius  $R$  appearing in eqns (3.1), (3.2), and (3.4) with  $b_{\text{gr}}$ , and  $d$  with  $b_{\text{gr}}/\sin \theta_{\text{gr}}$ . Then we arrive at the general condition for nuclear diffraction

$$l_{\text{gr}} \gg 1, \quad (3.11)$$

the Fraunhofer condition

$$l_{\text{gr}} \sin \theta_{\text{gr}} \ll 1 \quad (3.12)$$

and the Fresnel condition

$$l_{\text{gr}} \sin \theta_{\text{gr}} \gtrsim 1. \quad (3.13)$$

From eqns (3.8) and (3.9) we have

$$\sin \theta_{\text{gr}} = 2 \frac{\eta}{l_{\text{gr}}} \frac{1}{1 + (\eta/l_{\text{gr}})^2}. \quad (3.14)$$

Then the *Fraunhofer condition* becomes

$$\eta \ll 1, \quad (3.15)$$

and the *Fresnel condition*,

$$\eta \gtrsim 1. \quad (3.16)$$

We see that the shape of the diffraction pattern depends on the value of  $\eta$ , i.e. on the relative effect of the charge product  $Z_1 Z_2 e^2$  and the scattering energy  $E$  on the dynamics. We have *Fraunhofer diffraction* for small values of  $\eta$  (weak Coulomb field

or high energy), and Fresnel diffraction for large values of  $\eta$  (strong Coulomb field or low energy). In the first case we are dealing with undistorted waves approaching and leaving the target, which propagate along straight lines. Since source and detector are far removed from the nuclear target, we have the Fraunhofer regime. On the other hand, for large values of  $\eta$  the Coulomb field becomes effective and distorts the waves into Coulomb waves. The divergent waves reaching the target appear to be emitted by a virtual source S located near the target (cf. Fig. 3.4), and one observes Fresnel diffraction.

### 3.3 Diffraction by a black nucleus

We shall now describe nuclear diffraction in detail, starting from the quantum scattering amplitude (1.133),

$$f(\theta) = f_C(\theta) + f_N(\theta), \quad (3.17)$$

where

$$f_C(\theta) = -\frac{\eta}{2k \sin^2(\theta/2)} e^{-i\eta \ln \sin^2(\theta/2) + i2\sigma_l} \quad (3.18)$$

is the Coulomb scattering amplitude (1.98) and

$$f_N(\theta) = \frac{1}{2ik} \sum_{l=0}^{\infty} (2l+1) e^{2i\sigma_l} (S_l^N - 1) P_l(\cos \theta) \quad (3.19)$$

is the partial-wave expansion of the nuclear scattering amplitude (1.131), with

$$S_l^N = e^{2i\delta_l^N}; \quad (3.20)$$

the quantities  $\sigma_l$  are the Coulomb phase shifts and  $\delta_l^N$ , the complex nuclear phase shifts (1.129) generated by the optical potential representing the nuclear interaction of the particle with the target. When the imaginary part of the optical potential is large, as in heavy-ion scattering, we are dealing with strong absorption. In this case nuclear scattering may be regarded as scattering by a black sphere.

#### 3.3.1 Fraunhofer diffraction

The Fraunhofer diffraction pattern is obtained when  $\eta \ll 1$ , i.e. when the Coulomb effects are negligible (cf. eqn (3.15)). We then set  $f_C(\theta) = 0$  and  $\sigma_l = 0$ , and the scattering amplitude (3.17) becomes

$$f(\theta) = \frac{1}{2ik} \sum_{l=0}^{\infty} (2l+1) (S_l^N - 1) P_l(\cos \theta). \quad (3.21)$$

We introduce the grazing angular momentum  $l_{gr}$  which separates the partial waves which penetrate into the nucleus from those which do not. In a black nucleus all partial waves with angular momentum  $l < l_{gr}$  are completely absorbed, whereas those with  $l > l_{gr}$  remain unaffected by the nuclear potential. A completely absorbed partial wave function contains no outgoing wave, which implies  $S_l^N = 0$ ; since on the other hand  $S_l^N = 1$  for a partial wave which remains outside the range of the nuclear potential, we have

$$S_l^N = \begin{cases} 0 & \text{for } l < l_{gr}, \\ 1 & \text{for } l > l_{gr}. \end{cases} \quad (3.22)$$

### 3.3 Diffraction by a black nucleus

This means that the transmission coefficient (1.72),

$$T_l = 1 - |S_l|^2 = 1 - |S_l^N|^2, \quad (3.23)$$

which measures the absorption of the  $l$ th partial wave, has the form

$$T_l^N = \begin{cases} 1 & \text{for } l < l_{gr}, \\ 0 & \text{for } l > l_{gr} \end{cases} \quad (3.24)$$

(cf. Fig. 3.5). Equations (3.22) or (3.24) define the *sharp-cut-off model*

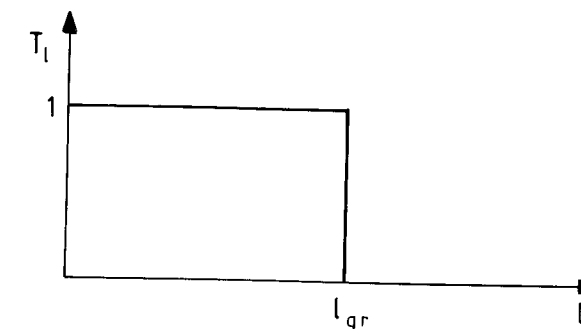


Figure 3.5 The transmission coefficient  $T_l$  for a black nucleus.

In this model, the scattering amplitude (3.21) takes the form (cf. Blair 1954, 1959)

$$f(\theta) = -\frac{1}{2ik} \sum_{l=0}^{l_{gr}} (2l+1) P_l(\cos \theta). \quad (3.25)$$

Using the relation (cf. Magnus *et al.* 1966, p. 232)

$$(2l+1) P_l(x) = \frac{d}{dx} [P_{l+1}(x) - P_{l-1}(x)] \quad \text{for } l \gtrsim 1, \quad (3.26)$$

we find, with  $P_0(x) = 1$  and  $P_1(x) = x$ ,

$$\begin{aligned} f(\theta) &= -\frac{1}{2ik} \left( 1 + \frac{d}{d \cos \theta} \sum_{l=1}^{l_{gr}} [P_{l+1}(\cos \theta) - P_{l-1}(\cos \theta)] \right) \\ &= \frac{i}{2k} \left( 1 + \frac{d}{d \cos \theta} [P_{l_{gr}+1}(\cos \theta) + P_{l_{gr}}(\cos \theta) - P_1(\cos \theta) - P_0(\cos \theta)] \right) \\ &= \frac{i}{2k} \frac{d}{d \cos \theta} [P_{l_{gr}+1}(\cos \theta) + P_{l_{gr}}(\cos \theta)] \approx \frac{i}{k} \frac{d}{d \cos \theta} P_{l_{gr}}(\cos \theta). \end{aligned} \quad (3.27)$$

The Legendre polynomials  $P_l(\cos \theta)$  with  $l \gg 1$  are peaked in the forward direction where they can be approximated by a Bessel function (cf. Abramowitz and Stegun 1965, eqn (9.1.71)),

$$P_l(\cos \theta) \approx J_0(l\theta) \quad \text{for } l \gg 1. \quad (3.28)$$

With eqn (9.1.28) of Abramowitz and Stegun (1965),

$$\frac{d}{dz} J_0(z) = -J_1(z), \quad (3.29)$$

one obtains for forward angles

$$\frac{d}{d \cos \theta} P_{l_{\text{gr}}}(\cos \theta) \approx -\frac{1}{\sin \theta} \frac{d}{d \theta} J_0(l_{\text{gr}} \theta) \approx \frac{l_{\text{gr}}}{\theta} J_1(l_{\text{gr}} \theta). \quad (3.30)$$

Since  $\eta \approx 0$  we find from eqn (3.8)  $b_{\text{gr}} = R$  and therefore  $l_{\text{gr}} = kR$ . We thus arrive at the *Fraunhofer amplitude*

$$f(\theta) = iR \frac{J_1(kR\theta)}{\theta}. \quad (3.31)$$

The Fraunhofer differential cross section then becomes

$$\frac{d\sigma}{d\Omega} = |f(\theta)|^2 = R^2 \left( \frac{J_1(kR\theta)}{\theta} \right)^2. \quad (3.32)$$

The angular distribution described by this formula is identical with the optical Fraunhofer pattern (3.3) if  $\sin \theta$  is replaced with  $\theta$ .

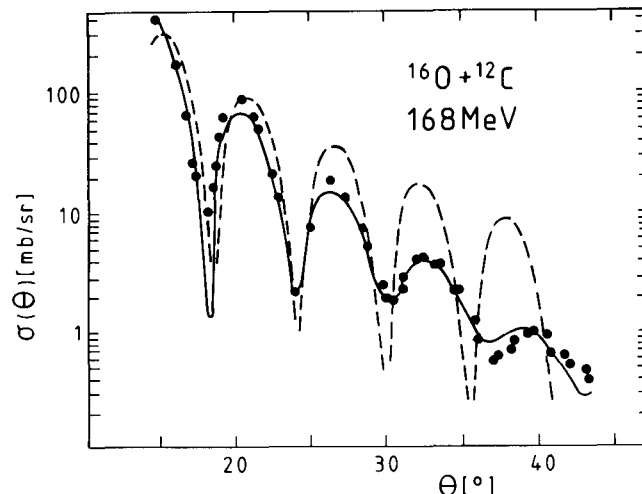


**Figure 3.6** Fraunhofer diffraction in the scattering of  $^{16}\text{O}$  by  $^{12}\text{C}$  at  $E_{\text{lab}}(^{16}\text{O}) = 168$  MeV. The data (dots) are compared with the Fraunhofer cross section (dashed curve) and with an optical model fit (solid curve) (cf. Hiebert and Garvey 1964).

For an example of nuclear scattering we consider the system  $^{16}\text{O} + ^{12}\text{C}$  at  $E_{\text{lab}}(^{16}\text{O}) = 168$  MeV (cf. Fig. 3.6). The data are qualitatively reproduced by the Fraunhofer distribution. From the near-periodic structure of the function  $J_1^2(x)$  with period  $\pi$  it can be seen that the angular spacing between successive maxima is  $\Delta\theta \approx \pi/kR = \pi/l_{\text{gr}}$ ;

this result can be employed to determine the grazing angular momentum  $l_{\text{gr}}$  directly from the data. In the above-given example we read off  $\Delta\theta \approx 6^\circ$ , so that  $l_{\text{gr}} \approx 30$ ; with  $k = (2\mu E_{\text{cm}}/\hbar^2)^{1/2} = 4.9 \text{ fm}^{-1}$  we therefore find  $R = l_{\text{gr}}/k \approx 6.1 \text{ fm}$ . The figure also shows that a more quantitative fit of the data can be obtained by an optical-model analysis (solid curve) of the type discussed in Section 1.5, which makes use of more parameters than just the one,  $R$ , appearing in the Fraunhofer model.

### 3.3.2 Fresnel diffraction

When the Fresnel condition  $\eta \gtrsim 1$  is satisfied (cf. eqn (3.16)), the Coulomb effects are strong. Then the Coulomb distortion of the waves can no longer be neglected as in the Fraunhofer regime.

The rigorous analytic treatment of Fresnel diffraction is not trivial. Here we present a non-rigorous derivation which provides some insight into how the physical conditions for Fresnel diffraction result in an angular distribution of the same form as the Fresnel pattern (3.5) in optics (cf. Frahn 1972).

Let us consider the nuclear scattering amplitude (3.19). We use the asymptotic formula (2.92) for the Legendre polynomials and replace the sum over  $l$  with an integral over  $\lambda = l + \frac{1}{2}$  employing the Poisson sum formula (2.93). We keep only the term with  $m = 0$  in this formula and find, in analogy to eqns (2.95) to (2.97),

$$f_N(\theta) = -\frac{i}{k} \int_0^\infty d\lambda \frac{\lambda^{1/2}}{(2\pi \sin \theta)^{1/2}} [S^N(\lambda) - 1] (e^{i\phi_+(\lambda)} + e^{i\phi_-(\lambda)}), \quad (3.33)$$

where

$$\phi_\pm(\lambda) = 2\sigma(\lambda) \pm \lambda\theta \mp \frac{\pi}{4}, \quad (3.34)$$

with the Coulomb phase shift  $\sigma(\lambda) = \sigma_l$  given by eqn (1.111). For this phase shift we can write (cf. eqn (1.111), and Messiah 1972, eqn (B.32b)), and applying the Poisson sum formula (2.93) with  $m = 0$ ,

$$\begin{aligned} \sigma(\lambda) &= \sigma_l = \arg \Gamma(l + 1 + i\eta) \\ &= \sigma_0 + \sum_{l'=1}^l \arctan \left( \frac{\eta}{l'} \right) \\ &\approx \sigma_0 + \int_{1/2}^\lambda d\lambda' \arctan \left( \frac{\eta}{\lambda'} \right). \end{aligned} \quad (3.35)$$

The integral (3.33) is now evaluated by the stationary-phase method introduced in Section 2.3.2. The stationary point  $\lambda_0$  for the term  $\exp[i\phi_-(\lambda)]$  in the parentheses is obtained from the condition

$$\frac{d\phi_-(\lambda)}{d\lambda} = 2 \frac{d\sigma(\lambda)}{d\lambda} - \theta = 2 \arctan \left( \frac{\eta}{\lambda} \right) - \theta = 0, \quad (3.36)$$

which yields

$$\lambda_0 = \eta \cot(\theta/2). \quad (3.37)$$

A similar formula holds for the term  $\exp[i\phi_+(\lambda)]$  in the parentheses in eqn (3.33), and leads to a stationary point on the negative  $\lambda$ -axis; this stationary point does not contribute to the integral (3.33). As should be expected from the discussion in Section 2.3.2, eqn

(3.37) is the classical relation (3.7) between the deflection angle  $\theta$  and the angular momentum  $\lambda_0$  of a Coulomb trajectory.

Owing to eqns (3.34) and (3.35), the phase at the stationary point is determined by an integral of the function  $\arctan(\eta/\lambda') = \text{arccot}(\lambda'/\eta)$  (cf. Gradshteyn and Ryzhik 1965, eqn (2.822.2)),

$$\begin{aligned}\phi_-(\lambda_0) &= 2\sigma_0 + 2 \int_{1/2}^{\lambda_0} d\lambda' \arccot(\lambda'/\eta) - \lambda_0\theta + \frac{\pi}{4} \\ &= 2\sigma_0 + 2[\lambda' \arccot(\lambda'/\eta) + (\eta/2) \ln(\eta^2 + \lambda'^2)]_{1/2}^{\lambda_0} - \lambda_0\theta + \frac{\pi}{4} \\ &= 2\sigma_0 - 2\eta \ln \sin(\theta/2) - \frac{\pi}{4} + \mathcal{O}(1/\eta),\end{aligned}\quad (3.38)$$

where we have used the stationarity condition (3.37).

The second derivative of the phase is

$$\frac{d^2\phi_-(\lambda)}{d\lambda^2} = \frac{d^2\sigma(\lambda)}{d\lambda^2} = 2 \frac{d}{d\lambda} \arctan\left(\frac{\eta}{\lambda}\right) = -\frac{2\eta}{\lambda^2 + \eta^2}, \quad (3.39)$$

and we find at the stationary point, using eqn (3.37),

$$\frac{d^2\phi_-}{d\lambda^2} \Big|_{\lambda_0} = -\frac{2}{\eta} \sin^2(\theta/2). \quad (3.40)$$

Expanding the phase  $\phi_-(\lambda)$  about  $\lambda_0$  up to second order,  $\phi_-(\lambda) = \phi_-(\lambda_0) + \phi''_-(\lambda_0)(\lambda - \lambda_0)^2 + \dots$ , replacing the slowly varying factor  $\lambda^{1/2}$  with  $\lambda_0^{1/2}$  and using again eqn (3.37), we find for the nuclear amplitude (3.33)

$$\begin{aligned}f_N(\theta) &= -\frac{i}{2k} \left( \frac{\eta}{\pi \sin^2(\theta/2)} \right)^{1/2} e^{-i\eta \ln \sin^2(\theta/2) + i2\sigma_0 - i\pi/4} \\ &\times \int_0^\infty d\lambda [S_N(\lambda) - 1] \exp \left\{ -(i/\eta)[\sin(\theta/2)(\lambda - \lambda_0)]^2 \right\}.\end{aligned}\quad (3.41)$$

We now introduce again the sharp-cut-off model (3.22) and obtain

$$\begin{aligned}f_N(\theta) &= \frac{i}{2k} \left( \frac{\eta}{\pi \sin^2(\theta/2)} \right)^{1/2} e^{-i\eta \ln \sin^2(\theta/2) + i2\sigma_0 - i\pi/4} \\ &\times \int_0^{\lambda_{\text{gr}}} d\lambda \exp \left\{ -(i/\eta)[\sin(\theta/2)(\lambda - \lambda_0)]^2 \right\}.\end{aligned}\quad (3.42)$$

After introduction of the new variable

$$\tau = \sqrt{2/\pi\eta} \sin(\theta/2)(\lambda - \lambda_0) \quad (3.43)$$

the lower limit of the integral in expression (3.42) changes to  $-\sqrt{2\eta/\pi} \cos(\theta/2)$ , which can be replaced with  $-\infty$  in the limit  $\eta \gg 1$ . Thus we have

$$f_N(\theta) = \frac{\eta}{2k \sin^2(\theta/2)} e^{-i\eta \ln \sin^2(\theta/2) + i2\sigma_0} \frac{e^{i\pi/4}}{\sqrt{2}} \int_{-\infty}^x d\tau e^{-i\pi\tau^2/2}, \quad (3.44)$$

where

$$x = x(\theta) = \tau(\lambda_{\text{gr}}) = \sqrt{2/\pi\eta} \sin(\theta/2)[\lambda_{\text{gr}} - \lambda_0(\theta)]. \quad (3.45)$$

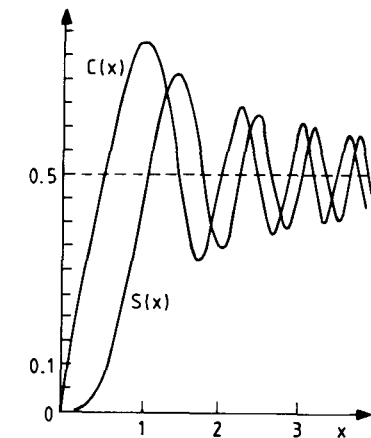


Figure 3.7 The Fresnel integrals  $C(x)$  and  $S(x)$ .

We decompose the integral in eqn (3.44) in the following way,

$$\int_{-\infty}^x d\tau e^{-i\pi\tau^2/2} = \left( \int_{-\infty}^0 + \int_0^x \right) d\tau e^{-i\pi\tau^2/2} = \frac{e^{-i\pi/4}}{\sqrt{2}} + C(x) - iS(x), \quad (3.46)$$

where we have introduced the Fresnel integrals (cf. Abramowitz and Stegun 1965, Section 7.3)

$$\begin{aligned}C(x) &= -C(-x) = \int_0^x dt \cos(\pi t^2/2), \quad C(\pm\infty) = \pm\frac{1}{2}; \\ S(x) &= -S(-x) = \int_0^x dt \sin(\pi t^2/2), \quad S(\pm\infty) = \pm\frac{1}{2}.\end{aligned}\quad (3.47)$$

These are plotted in Fig. 3.7.

The nuclear scattering amplitude eqn (3.44) now becomes, owing to eqn (3.18),

$$\begin{aligned}f_N(\theta) &= -f_C(\theta) \frac{e^{i\pi/4}}{\sqrt{2}} \left[ \frac{e^{-i\pi/4}}{\sqrt{2}} + C(x) - iS(x) \right] \\ &= -f_C(\theta) \frac{1}{2}(1+i) \left[ \frac{1}{2}(1-i) + C(x) - iS(x) \right] \\ &= -f_C(\theta) \left\{ \frac{1}{2} + \frac{1}{2}[C(x) + S(x)] + i\frac{1}{2}[C(x) - S(x)] \right\}.\end{aligned}\quad (3.48)$$

The full scattering amplitude (3.17) is obtained as

$$\begin{aligned}f(\theta) &= f_C(\theta) + f_N(\theta) \\ &= f_C(\theta) \left\{ \frac{1}{2} - \frac{1}{2}[C(x) + S(x)] - i\frac{1}{2}[C(x) - S(x)] \right\}.\end{aligned}\quad (3.49)$$

Dividing this expression by the Coulomb amplitude  $f_C(\theta)$ , we have

$$\frac{f(\theta)}{f_C(\theta)} = \frac{1}{2} \{1 - [C(x) + S(x)] - i[C(x) - S(x)]\}. \quad (3.50)$$

The differential cross section divided by the Rutherford cross section is therefore (cf. Frahn 1972)

$$\left( \frac{d\sigma}{d\Omega} / \frac{d\sigma_C}{d\Omega} \right) = \left| \frac{f(\theta)}{f_C(\theta)} \right|^2 = \frac{1}{2} \left\{ \left[ \frac{1}{2} - C(x) \right]^2 + \left[ \frac{1}{2} - S(x) \right]^2 \right\} \quad (3.51)$$

with  $x = x(\theta)$  given by eqn (3.45).

The function  $x(\theta)$  can be written explicitly as a function of the scattering angle  $\theta$  by inserting  $\lambda_0(\theta)$  from eqn (3.37) and writing for the grazing angular momentum  $\lambda_{gr}$

$$\lambda_{gr} = \eta \cot(\theta_{gr}/2). \quad (3.52)$$

Using the law of addition

$$\cot \beta - \cot \alpha = \sin(\alpha - \beta) / (\sin \alpha \sin \beta)$$

we arrive at

$$x(\theta) = 2\sqrt{\lambda_{gr}/\pi \sin \theta_{gr}} \sin[\frac{1}{2}(\theta - \theta_{gr})]. \quad (3.53)$$

We see that the grazing angle  $\theta_{gr}$  or the grazing angular momentum  $\lambda_{gr}$  (which, for given  $\eta$ , fix each other via eqn (3.52)) determine the shape of the angular distribution. Formula (3.51) together with the relations (3.53) and (3.10) is identical with the analogous optical formula (3.5) with the definition (3.6).

The Fresnel angular distribution for the elastic scattering of  $^{16}\text{O}$  by  $^{208}\text{Pb}$  at  $E_{\text{lab}}(^{16}\text{O}) = 170$  MeV is shown in Fig. 3.8, where it is compared with the experimental data (cf. Baker and McIntyre 1967). It is seen that the Fresnel formula (3.51) which contains as the only adjustable parameter the cut-off angular momentum  $\lambda_{gr}$ , reproduces the data qualitatively (dashed curve), but not quantitatively. A quantitative fit can be obtained via a quantal calculation using the smooth-cut-off strong-absorption model of Section 3.4 (solid curve).

Three particular values of the cross section  $d\sigma(\theta)/d\sigma_C(\theta)$  can be read off from Fig. 3.8, which are derived from eqn (3.51) in conjunction with eqns (3.47) and (3.53):

$$\theta \gg \theta_{gr} \quad \text{implies} \quad x \rightarrow \infty \quad \text{and therefore} \quad d\sigma/d\sigma_C \rightarrow 0,$$

$$\theta = 0 \quad \text{implies} \quad x \rightarrow -\infty \quad \text{and therefore} \quad d\sigma/d\sigma_C = 1,$$

and finally,

$$\theta = \theta_{gr} \quad \text{implies} \quad x = 0 \quad \text{and therefore} \quad d\sigma/d\sigma_C = \frac{1}{4}. \quad (3.54)$$

The last relation provides us with the ‘quarter-point recipe’: if an experimental differential cross section can be interpreted as a Fresnel distribution, the angle where it has dropped to one-quarter of the Rutherford cross section is the grazing angle  $\theta_{gr}$ , from which the grazing angular momentum  $\lambda_{gr}$  can be calculated with the help of eqn (3.52).

Interpreting cross sections of the type of Fig. 3.8 as Fresnel distributions is an alternative to the interpretation in terms of Coulomb rainbow scattering given in Section 2.4.2 (cf. also Brink 1985, Section 5.6).

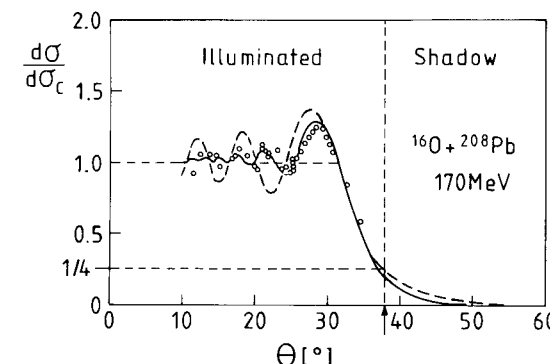


**Figure 3.8** Fresnel diffraction for  $^{16}\text{O} + ^{208}\text{Pb}$  at  $E_{\text{lab}}(^{16}\text{O}) = 170$  MeV. The open circles represent the experimental data of Baker and McIntyre (1967). The dashed curve results from employing the Fresnel formula with  $\eta = 31.2$  and  $\lambda_{gr} = 90.4$ ; the solid curve is calculated using the SAM parametrization of Section 3.4 and a partial-wave summation of the scattering amplitude (cf. Frahn 1971, 1972).

The Fresnel scattering formula (3.51) gives a qualitative description of heavy-ion scattering data for heavy systems or for light systems at not too high energy. For a quantitative fit of experimental angular distributions of elastic scattering the sharp-cut-off assumption is too crude. In Section 3.4 we shall therefore consider a more flexible parametrization of the  $S$ -function than that given by eqn (3.22).

◊ *Remark on the derivation of the diffraction formulae.* In the preceding discussion we have employed methods whose mathematical soundness is anything but obvious. Our aim has been to obtain in a simple, heuristic fashion the Fresnel formula (3.51) together with eqn (3.53), which is the analogue of formulae (3.5) and (3.6) in optics.

A more rigorous treatment should start from a smooth-cut-off description of the black nucleus as discussed in the next section. One must carefully consider the conditions under which a semiclassical asymptotic expansion with respect to a large parameter  $\propto 1/\hbar$  is valid. For an integral with a sharp cut-off, a naive stationary-phase evaluation is not justified from a rigorous mathematical point of view. These questions are discussed by Frahn and Gross (1976) and Gross (1976), and are summarized by Frahn (1985) and Brink (1985). ◊

### 3.4 The strong absorption model

We have seen in Chapter 1 that the absolute value of the  $S$ -function calculated with the use of a strongly absorbing optical potential of, for example, the Woods–Saxon type (cf. Fig. 1.7) has a behaviour as a function of angular momentum  $l$  which corresponds to a smoothed version of the sharp cut-off model (3.22); it can approximately be parametrized

in terms of the Fermi function

$$g(x) = \frac{1}{1 + e^x}, \quad (3.55)$$

just as the Woods–Saxon potential itself. It is therefore natural to adopt this kind of parametrization for the complex function  $S_l^N$  in general; one may then hope to achieve fits to the experimental cross sections which are of a quality similar to that of optical-model fits. This leads to the *strong absorption model* (SAM), where it is assumed that the absorption inside the nucleus, i.e. for partial waves with angular momenta  $\lambda < \lambda_{\text{gr}}$ , is no longer complete but still strong, with a smooth transition to vanishing absorption near the grazing angular momentum  $\lambda_{\text{gr}}$ .

As an example for such a smooth-cut-off model we quote here the parametrization of Frahn and Venter (1963) (cf. also Frahn 1971, 1972). This parametrization is given by

$$S_l^N = S^N(\lambda) = \left(1 + i\mu \frac{d}{d\lambda}\right) g\left(\frac{\lambda_{\text{gr}} - \lambda}{\Delta}\right), \quad (3.56)$$

where the function  $g(x)$  is the Fermi function (3.55). The SAM contains two new parameters, the width of the smooth-cut-off region  $\Delta$  and the strength of the imaginary part of the  $S$ -function  $\mu$ . An example of a SAM  $S$ -function is shown in Fig. 3.9 for the system  $^{16}\text{O} + ^{208}\text{Pb}$  at  $E_{\text{lab}}(^{16}\text{O}) = 170$  MeV, using the parameter values  $\lambda_{\text{gr}} = 90.4$ ,

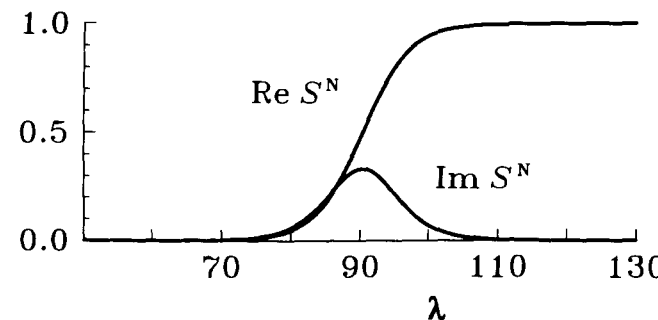


**Figure 3.9** Real and imaginary parts of the Frahn–Venter parametrization of the  $S$ -function with  $\lambda_{\text{gr}} = 90.4$ ,  $\Delta = 3.41$ , and  $\mu = 4.5$  for the system  $^{16}\text{O} + ^{208}\text{Pb}$  at  $E_{\text{lab}}(^{16}\text{O}) = 170$  MeV.

$\Delta = 3.41$ , and  $\mu = 4.5$ . Substituting the  $S$ -functions  $S_l^N = S^N(\lambda)$  in the partial-wave expansion (3.19) of the nuclear scattering amplitude, one obtains the cross section represented by the solid curve in Fig. 3.8; it fits the data rather well.

Other parametrizations than the one discussed in the present section have been proposed, for example, by McIntyre *et al.* (1960) and by Ericson (1966).

Closed expressions analogous to the Fraunhofer and Fresnel formulae have also been derived for the SAM cross sections (cf. Frahn 1985; Brink 1985). They are quite complicated and will not be quoted here.

### 3.5 Notes and references

The black-nucleus hypothesis was introduced by Blair (1954). The diffraction model as it is now generally employed has been developed mainly by Frahn (cf. the various

references given below). Reviews of the evaluation of nuclear scattering cross sections using parametrized SAM  $S$ -matrices are given by Frahn (1984, 1985) and Brink (1985).

The sharp-cut-off model allows for a qualitative, and the SAM, for a quantitative semi-phenomenological description of nuclear elastic scattering. These models are introduced on the level of the scattering function, which is a physical quantity close to the cross section, i.e. to the data. It provides an alternative to the semi-phenomenological optical model, where the modelled quantity is the potential. The latter is more removed from the data than the scattering function, and is often difficult to determine unambiguously; on the other hand, it is commonly regarded as the more fundamental quantity. The relation between the SAM scattering function and the corresponding optical potential has been investigated by inverse scattering methods (cf. Allen *et al.* 1991).

The similarity between the nuclear optical potential and the complex index of refraction in optics is especially close for low-energy neutron propagation in condensed matter. Neutron waves with large wavelength exhibit a behaviour which is completely analogous to that of light waves, and a whole discipline, *neutron optics*, is built on this analogy (cf., e.g., Sears 1989).

### References

- Abramowitz, M. and Stegun, I. A. (1965). *Handbook of mathematical functions*, Dover, New York.
- Allen, L. J., Fiedeldey, H., Sofianos, S. A., Amos, K. and Steward, C. (1991). *Phys. Rev.* **C44** 1606.
- Baker, S. D. and McIntyre, J. A. (1967). *Phys. Rev.* **161** 1200.
- Blair, J. S. (1954). *Phys. Rev.* **95** 1218.
- Blair, J. S. (1959). *Phys. Rev.* **115** 928.
- Born, M. and Wolf, E. (1964). *Principles of optics*, 4th edn, Pergamon Press, Oxford.
- Brink, D. M. (1985). *Semiclassical methods for nucleus–nucleus scattering*, Cambridge University Press, Cambridge.
- Ericson, T. E. D. (1966). In *Preludes in theoretical physics*, eds. de Shalit, A., Feshbach, H. and van Hove, L., North-Holland, Amsterdam, p. 321.
- Frahn, W. E. (1971). *Phys. Rev. Lett.* **26** 568.
- Frahn, W. E. (1972). *Ann. Phys. (N.Y.)* **72** 524.
- Frahn, W. E. (1984). In *Heavy-ion science*, vol. 1, ed. Bromley, D. A., Plenum Press, New York, p. 135.
- Frahn, W. E. (1985). *Diffractive processes in nuclear physics*, Clarendon Press, Oxford.
- Frahn, W. E. and Gross, D. H. E. (1976). *Ann. Phys. (N.Y.)* **101** 520.
- Frahn, W. E. and Venter, R. H. (1963). *Ann. Phys. (N.Y.)* **24** 243.
- Gradshteyn, I. S. and Ryzhik, I. M. (1965). *Tables of integrals, series and products*, Academic Press, New York.
- Gross, D. H. E. (1976). *Nucl. Phys.* **A260** 333.
- Hiebert, J. C. and Garvey, G. T. (1964). *Phys. Rev.* **135** B346.
- Magnus, W., Oberhettinger, F. and Soni, R. P. (1966). *Formulas and theorems for the special functions of mathematical physics*, Springer, Berlin.
- McIntyre, J. A., Wang, K. H. and Becker, L. C. (1960). *Phys. Rev.* **117** 1337.
- Messiah, A. (1972). *Quantum mechanics*, vol. I, North-Holland, Amsterdam.

- Sears, V. F. (1989). *Neutron optics*, Oxford University Press, Oxford.  
Sommerfeld, A. (1964). *Vorlesungen über theoretische Physik*, vol.IV (*Optik*),  
Akademische Verlagsgesellschaft, Leipzig.

## Part B

### Formal theory

## THE FORMAL THEORY OF POTENTIAL SCATTERING

### 4.1 Introduction

Since potential scattering describes solely elastic scattering it covers only a small, although important, aspect of nuclear collisions. For the treatment of general nuclear reactions like inelastic scattering or transfer of particles, a more general formalism is required. This formalism, the *formal theory of reactions*, will now be developed.

In the present chapter we introduce the formal theory on the example of potential scattering, since we are already familiar with the final results. The potential is assumed to be *real*. The generalization to a theory of reactions is immediate, and will be given in Chapter 5. These two chapters, together with the subsequent one on the optical model, are *formal*, but the physical meaning of the formalism will always be manifest. The detailed derivation of cross section formulae for numerical use, as well as the explicit discussion of various specific reaction types, will be deferred to later chapters.

The treatment given here is quantal and non-relativistic. For a correct description of the collision process which distinguishes between the asymptotic and interaction regions, we have to employ time-dependent normalizable and localized states, i.e. *wave packets*; this will be done in Section 4.2.

Actual calculations, however, are more conveniently performed in a time-independent, stationary formulation. It is shown in Section 4.3 how the latter emerges from the time-dependent theory. This is followed by a discussion of the *T*- and *S-matrices*, in terms of which the cross section is calculated for comparison with experiment.

In Section 4.4 we derive explicitly the asymptotic forms of the stationary as well as the time-dependent states. From these we can read off the expression for the *cross section* in a physically transparent manner.

Finally, in Section 4.5, we discuss the *coherence properties of the particle beams* employed in nuclear reactions, in order to gain a deeper understanding of the actual quantal scattering process.

### 4.2 The time-dependent formalism

#### 4.2.1 The free wave packet state

We begin by constructing a quantum state which represents a particle in free motion. Such a state must have a finite spatial extent corresponding to the volume within which the particle is localized, and the centre of this packet must move with the particle.

These requirements are met by the *free wave packet state*, which we shall now discuss. For ease of writing we use the bra-ket notation. We consider the solution  $|\Phi(t)\rangle$  of the

time-dependent Schrödinger equation without scattering potential,

$$i\hbar \frac{d}{dt} |\Phi(t)\rangle = T |\Phi(t)\rangle. \quad (4.1)$$

The operator  $T$  is the kinetic energy  $T = -\hbar^2 \nabla^2 / 2m$ , where  $m$  is the mass of the particle. The eigenstates of the kinetic energy operator are the plane-wave states  $|\mathbf{k}\rangle$  which satisfy the stationary equation

$$(T - E)|\mathbf{k}\rangle = 0 \quad (4.2)$$

with  $E = \hbar^2 k^2 / 2m$ , and which are normalized to a  $\delta$ -function,

$$\langle \mathbf{k}' | \mathbf{k} \rangle = \delta(\mathbf{k} - \mathbf{k}'). \quad (4.3)$$

In the coordinate representation the wave function of the plane wave is given by

$$\langle \mathbf{r} | \mathbf{k} \rangle = \frac{1}{(2\pi)^{3/2}} e^{i\mathbf{k} \cdot \mathbf{r}}. \quad (4.4)$$

A free wave packet state  $|\Phi_{\mathbf{k}_a}(t)\rangle$  is now defined as a solution of the Schrödinger equation (4.1) representing a localized bundle of waves which moves along a straight line with mean momentum  $\hbar \mathbf{k}_a$ . It can be written as a superposition of plane-wave states  $|\mathbf{k}\rangle$ ,

$$|\Phi_{\mathbf{k}_a}(t)\rangle = \int d^3k A(\mathbf{k} - \mathbf{k}_a) e^{-\frac{i}{\hbar} Et} |\mathbf{k}\rangle, \quad (4.5)$$

where the weight amplitude  $A(\boldsymbol{\kappa})$  is conveniently chosen as a real Gaussian,

$$A(\boldsymbol{\kappa}) = \left(\frac{2\Delta^2}{\pi}\right)^{3/4} e^{-\Delta^2 \boldsymbol{\kappa}^2}. \quad (4.6)$$

This amplitude corresponds to a normalized distribution  $[A(\boldsymbol{\kappa})]^2$  of momenta with root-mean-square width

$$\Delta_k = \frac{\sqrt{3}}{2\Delta}. \quad (4.7)$$

The state  $|\Phi_{\mathbf{k}_a}(t)\rangle$  is normalized to unity,

$$\begin{aligned} \langle \Phi_{\mathbf{k}_a}(t) | \Phi_{\mathbf{k}_a}(t) \rangle &= \int d^3k d^3k' A^*(\mathbf{k}' - \mathbf{k}_a) A(\mathbf{k} - \mathbf{k}_a) e^{-\frac{i}{\hbar}(E-E')t} \langle \mathbf{k}' | \mathbf{k} \rangle \\ &= \int d^3k |A(\mathbf{k} - \mathbf{k}_a)|^2 = 1, \end{aligned} \quad (4.8)$$

where we have used eqn (4.3).

In the coordinate representation the free wave packet is given by

$$\begin{aligned} \Phi_{\mathbf{k}_a}(\mathbf{r}, t) &= \langle \mathbf{r} | \Phi_{\mathbf{k}_a}(t) \rangle = \frac{1}{(2\pi)^{3/2}} \int d^3k A(\mathbf{k} - \mathbf{k}_a) e^{-\frac{i}{\hbar} Et} e^{i\mathbf{k} \cdot \mathbf{r}} \\ &= \frac{1}{(2\pi)^{3/2}} \left(\frac{2\Delta^2}{\pi}\right)^{3/4} \int d^3k e^{-\Delta^2 (\mathbf{k} - \mathbf{k}_a)^2} e^{i(\mathbf{k} \cdot \mathbf{r} - \hbar k^2 t / 2m)}. \end{aligned} \quad (4.9)$$

## 4.2 The time-dependent formalism

Changing the variable of integration in the integral to  $\mathbf{q} = \mathbf{k} - \mathbf{k}_a$ , we can rewrite the exponent in the integrand in the form

$$\begin{aligned} &- \Delta^2 (1 + i\hbar t / 2m\Delta^2) \left( \mathbf{q} - \frac{i(\mathbf{r} - \mathbf{v}_a t)}{2\Delta^2 (1 + i\hbar t / 2m\Delta^2)} \right)^2 \\ &- \frac{(\mathbf{r} - \mathbf{v}_a t)^2}{4\Delta^2 (1 + i\hbar t / 2m\Delta^2)} + i(\mathbf{k}_a \cdot \mathbf{r} - \hbar k_a^2 t / 2m), \end{aligned}$$

where

$$\mathbf{v}_a = \hbar \mathbf{k}_a / m \quad (4.10)$$

is the mean velocity of the wave packet. Performing the integration and separating real and imaginary terms in the remaining exponents we arrive at the following wave function for the wave packet,

$$\begin{aligned} \Phi_{\mathbf{k}_a}(\mathbf{r}, t) &= \exp[i(\mathbf{k}_a \cdot \mathbf{r} - \hbar k_a^2 t / 2m)] \exp\left(\frac{i\hbar t}{2m\Delta^2} \frac{(\mathbf{r} - \mathbf{v}_a t)^2}{4[\Delta(t)]^2}\right) \\ &\times \frac{1}{(2\pi\Delta^2)^{3/4}} \frac{1}{[1 + i\gamma(t)]^{3/2}} \exp\left(-\frac{(\mathbf{r} - \mathbf{v}_a t)^2}{4[\Delta(t)]^2}\right). \end{aligned} \quad (4.11)$$

Here

$$\gamma(t) = \frac{\hbar}{2m\Delta^2} t \quad (4.12)$$

is the spreading coefficient in the time-dependent width  $\Delta(t)$  of the wave packet,

$$\begin{aligned} \Delta(t) &= \Delta \sqrt{1 + [\gamma(t)]^2} \\ &\approx \begin{cases} \Delta(1 + \frac{1}{2}[\gamma(t)]^2) & \text{for } \gamma(t) \ll 1, \\ \Delta\gamma(t) = \hbar t / 2m\Delta & \text{for } \gamma(t) \gg 1. \end{cases} \end{aligned} \quad (4.13)$$

Formula (4.11) yields for the probability density distribution of the wave packet

$$|\Phi_{\mathbf{k}_a}(\mathbf{r}, t)|^2 = \frac{1}{[2\pi\Delta^2(t)]^{3/2}} \exp\left(-\frac{(\mathbf{r} - \mathbf{v}_a t)^2}{2[\Delta(t)]^2}\right) = W(|\mathbf{r} - \mathbf{v}_a t|), \quad (4.14)$$

which is a Gaussian centred at  $\mathbf{r} = \mathbf{v}_a t$  with width  $\Delta(t)$ . The probability density of the wave packet is localized around the origin at time  $t = 0$  with width  $\Delta(0) = \Delta$ ; it moves with mean velocity  $\mathbf{v}_a$  and has a width  $\Delta(t)$  which increases with time as prescribed by eqn (4.13). The spreading coefficient is proportional to the time  $t$ ; for very large times the width  $\Delta(t)$  will itself increase linearly with  $t$ , so that the wave packet will eventually disperse.

### The size of a wave packet

For a numerical idea of the width of the wave packet and its spreading in time we consider a wave packet describing a  $^{20}\text{Ne}$  nucleus moving with kinetic energy 100 MeV and an initial width of macroscopic dimension  $\Delta = 10^{-3}$  cm. This may be considered a reasonable estimate of the dimensions of a physical wave packet, considering the sizes of the ion source and of the beam tube of the accelerator (cf. Austern 1970, Chapter 1). The wave packet has the velocity  $v = \sqrt{2E/m_{\text{Ne}}} = 0.1 c \approx 3 \times 10^9 \text{ cm s}^{-1}$ ; it travels

a distance  $d = 10 \text{ m}$  in  $t = d/v \approx 0.3 \times 10^{-6} \text{ s}$ . Using eqns (4.12) and (4.13), we find that during this time the width of the wave packet increases by the fraction  $\frac{1}{2}[\gamma(t)]^2 \approx 10^{-11}$ , which is entirely negligible.

This example shows that in the usual nuclear reaction experiment the shape of the wave packet remains unchanged, and the quantal spreading of the wave packet can be disregarded. Only when the spreading coefficient  $\gamma(t)$  becomes of the order of unity does the wave packet begin to disperse. In our example this happens after  $\approx 0.07 \text{ s}$ , when the neon nucleus has travelled a distance of  $\approx 2000 \text{ km}$ .

In view of eqn (4.7) the assumed spatial width  $\Delta = 10^{-3} \text{ cm}$  corresponds to a momentum width  $\Delta_k \approx 10^3 \text{ cm}^{-1} = 10^{-10} \text{ fm}^{-1}$ , making the momentum distribution in the wave packet very sharp indeed compared to the momentum dependence of any nuclear amplitude.

#### Wave packet description of the relative motion of two particles

In nuclear scattering, *two* particles are involved, the projectile and target, which must each be described by a wave packet. For two non-interacting particles with masses  $m_1$  and  $m_2$  and momenta  $\mathbf{k}_{a1}$  and  $\mathbf{k}_{a2}$  which meet at the origin at the time  $t = 0$ , the wave packet function is given by

$$\begin{aligned}\Phi_{\mathbf{k}_{a1}, \mathbf{k}_{a2}}(\mathbf{r}_1, \mathbf{r}_2; t) &= \Phi_{\mathbf{k}_{a1}}(\mathbf{r}_1, t)\Phi_{\mathbf{k}_{a2}}(\mathbf{r}_2, t) \\ &= \frac{1}{(2\pi)^3} \left( \frac{2\Delta_1 \Delta_2}{\pi} \right)^{3/2} \int d^3 k_1 \int d^3 k_2 e^{-\Delta_1^2 (\mathbf{k}_1 - \mathbf{k}_{a1})^2} e^{-\Delta_2^2 (\mathbf{k}_2 - \mathbf{k}_{a2})^2} \\ &\quad e^{i(\mathbf{k}_1 \cdot \mathbf{r}_1 - \hbar k_1^2 t / 2m_1)} e^{i(\mathbf{k}_2 \cdot \mathbf{r}_2 - \hbar k_2^2 t / 2m_2)}.\end{aligned}\quad (4.15)$$

Introducing the total momentum  $\mathbf{K}$  and the relative momentum  $\mathbf{k}$ ,

$$\mathbf{K} = \mathbf{k}_1 + \mathbf{k}_2, \quad \mathbf{k} = (m_2 \mathbf{k}_1 - m_1 \mathbf{k}_2)/M, \quad (4.16)$$

where  $M = m_1 + m_2$  is the total mass, we have

$$\mathbf{k}_1 = (m_1/M)\mathbf{K} + \mathbf{k}, \quad \mathbf{k}_2 = (m_2/M)\mathbf{K} - \mathbf{k}, \quad (4.17)$$

and similarly for the mean momenta  $\mathbf{k}_{a1}$  and  $\mathbf{k}_{a2}$ .

For convenience we consider the particular case when

$$\Delta_i = \Delta \sqrt{\mu/m_i} \quad \text{with } i = 1, 2, \quad (4.18)$$

where  $\mu = m_1 m_2 / M$  is the reduced mass. We find that the two-particle wave packet function (4.15) separates into a wave packet function for the centre-of-mass coordinate  $\mathbf{R} = (m_1 \mathbf{r}_1 + m_2 \mathbf{r}_2)/M$  and one for the relative coordinate  $\mathbf{r} = \mathbf{r}_1 - \mathbf{r}_2$ ,

$$\begin{aligned}\Phi_{\mathbf{k}_{a1}, \mathbf{k}_{a2}}(\mathbf{r}_1, \mathbf{r}_2; t) &= \\ &\quad \frac{1}{(2\pi)^{3/2}} \left( \frac{2\mu \Delta^2}{M\pi} \right)^{3/4} \int d^3 K e^{-(\mu/M)\Delta^2 (\mathbf{K} - \mathbf{K}_a)^2} e^{i(\mathbf{K} \cdot \mathbf{R} - \hbar K^2 t / 2M)} \\ &\quad \times \frac{1}{(2\pi)^{3/2}} \left( \frac{2\Delta^2}{\pi} \right)^{3/4} \int d^3 k e^{-\Delta^2 (\mathbf{k} - \mathbf{k}_a)^2} e^{i(\mathbf{k} \cdot \mathbf{r} - \hbar k^2 t / 2\mu)}.\end{aligned}\quad (4.19)$$

## 4.2 The time-dependent formalism

Although this result has been obtained for weight amplitudes of the special form of Gaussians with the widths (4.18), it should be true in general, except for inessential modifications in the definition of the mean momenta and widths in the two wave packet functions. Since the motion of the centre of mass is unaffected by the interaction between the two particles, we shall from now on restrict the discussion to the relative motion. The particle mass  $m$  will accordingly be replaced with the reduced mass  $\mu$ . A detailed discussion of wave packets for a two-particle system can be found in Goldberger and Watson (1964, Chapter 3).

### 4.2.2 The time-dependent scattering state

Having discussed the free wave packet, we turn to the *scattering wave packet* for a particle moving in the field of a real scattering potential  $V$ . For the time being we assume that this potential is of short range, outside of which the motion is free. Thus we disregard Coulomb ‘tails’ which would give rise to the appearance of logarithmic phase factors in the asymptotic wave packets (cf. eqn (1.96)). The scattering wave packet, denoted by  $|\Psi(t)\rangle$ , is a solution of the time-dependent Schrödinger equation

$$i\hbar \frac{d}{dt} |\Psi(t)\rangle = H |\Psi(t)\rangle, \quad (4.20)$$

where

$$H = T + V. \quad (4.21)$$

The formal solution of eqn (4.20) is given by

$$|\Psi(t)\rangle = e^{-\frac{i}{\hbar} H(t-t_0)} |\Psi(t_0)\rangle, \quad (4.22)$$

where  $t_0$  is any fixed reference time. The exponential operator appearing on the right-hand side of eqn (4.22) is unitary, and the state has a constant norm which is set equal to unity,

$$\langle \Psi(t) | \Psi(t) \rangle = \langle \Psi(t_0) | \Psi(t_0) \rangle = 1. \quad (4.23)$$

The state  $|\Psi(t)\rangle$  must be constructed so as to be localized around the position of the particle at all times. For a potential centred at  $r = 0$  it is convenient to choose the origin of time such that the state  $|\Psi(t)\rangle$  is localized around  $r = 0$  at time  $t = 0$ . If the potential is absent, the scattering state is equal to the free wave packet state (4.5).

Although the scattering state is no longer identical with the free wave packet when the potential is introduced, it satisfies the free Schrödinger equation for  $t < -t_\infty$ , where  $-t_\infty$  is some time in the past when the wave packet has not yet been affected by the potential. It can therefore be identified with the free wave packet state at a *large negative* matching time  $t_0 < -t_\infty$ ,

$$|\Psi_{\mathbf{k}_a}(t_0)\rangle = |\Phi_{\mathbf{k}_a}(t_0)\rangle \quad \text{with } t_0 < -t_\infty. \quad (4.24)$$

Using eqn (4.22) we then have

$$|\Psi_{\mathbf{k}_a}(t)\rangle = e^{-\frac{i}{\hbar} H(t-t_0)} |\Phi_{\mathbf{k}_a}(t_0)\rangle \quad \text{with } t_0 < -t_\infty. \quad (4.25)$$

This is the state vector describing the motion of a wave packet with mean momentum  $\mathbf{k}_a$  which reaches the region of interaction near the origin  $r \approx 0$  at a time  $t \approx 0$ ; here it

is scattered by the potential  $V(\mathbf{r})$ . The structure of the scattering wave packet (4.25), in particular its width, is similar to the structure of the free wave packet state from which it evolves; however, its motion will be different.

The time-dependent scattering state (4.25) is defined for all times  $t$ . In the following we shall consider it for a fixed time somewhere in the interval  $[-t_\infty, t_\infty]$  inside of which the scattering wave packet is acted upon by the potential. For convenience we choose this time as  $t = 0$ , where we have

$$|\Psi_{\mathbf{k}_a}(0)\rangle = e^{\frac{i}{\hbar}Ht_0}|\Phi_{\mathbf{k}_a}(t_0)\rangle \text{ with } t_0 < -t_\infty. \quad (4.26)$$

The matching time  $t_0$  can be chosen freely as long as it satisfies  $t_0 < -t_\infty$ . It is convenient to take advantage of this circumstance in the following way. Instead of identifying the scattering state with the free state at one fixed remote time  $t_0$  as in eqn (4.24), we feed in the free state over the ‘infinitely long’ period from  $\tau = -\infty$  to  $\tau = -t_\infty$  (cf. Goldberger and Watson 1964, Section 5.1). We weight the contribution of a ‘feeding time interval’  $d\tau$  at time  $\tau$  by the factor  $(\eta/\hbar)d\tau \exp(\eta\tau/\hbar)$ , where  $\eta$  is a positive quantity which is *infinitesimal but non-zero*. Thus we replace the right-hand side of eqn (4.26), denoted by  $f(t_0)$ , with

$$\frac{\eta}{\hbar} \int_{-\infty}^{-t_\infty} d\tau e^{\frac{\eta}{\hbar}\tau} f(\tau).$$

Since  $\eta$  is infinitesimal, any *finite* interval of integration makes a vanishing contribution, and we can therefore replace the upper limit of integration  $-t_\infty$  with the time 0 in the limit  $\eta \rightarrow 0$ , which is taken at the end. The weight factor is normalized to unity,

$$\frac{\eta}{\hbar} \int_{-\infty}^0 d\tau e^{\frac{\eta}{\hbar}\tau} = 1. \quad (4.27)$$

For the scattering state at time  $t = 0$  we then have, instead of expression (4.26),

$$|\Psi_{\mathbf{k}_a}(0)\rangle = \frac{\eta}{\hbar} \int_{-\infty}^0 d\tau e^{\frac{\eta}{\hbar}\tau} e^{\frac{i}{\hbar}H\tau} |\Phi_{\mathbf{k}_a}(\tau)\rangle. \quad (4.28)$$

Since the free state satisfies eqn (4.1), we have

$$|\Phi_{\mathbf{k}_a}(\tau)\rangle = e^{-\frac{i}{\hbar}T\tau} |\Phi_{\mathbf{k}_a}(0)\rangle, \quad (4.29)$$

and we can rewrite eqn (4.28) in the form

$$|\Psi_{\mathbf{k}_a}(0)\rangle = \frac{\eta}{\hbar} \int_{-\infty}^0 d\tau e^{\frac{\eta}{\hbar}\tau} e^{\frac{i}{\hbar}H\tau} e^{-\frac{i}{\hbar}T\tau} |\Phi_{\mathbf{k}_a}(0)\rangle. \quad (4.30)$$

The procedure (4.28) of connecting the scattering state  $|\Psi_{\mathbf{k}_a}(0)\rangle$  with the free state  $|\Phi_{\mathbf{k}_a}(\tau)\rangle$  in a region of remote times  $\tau$  is to be preferred to the recipe (4.26) since it averages over uninteresting details of the wave packet at any particular instant  $\tau$ . More importantly, it has great formal advantages, as it allows us to introduce the stationary scattering states to be discussed in Section 4.3.

◊ *The Abelian limit.* The integral (4.30) is an operator form of the *Abelian limit*. The Abelian limit of a function  $f(t)$  for  $t \rightarrow -\infty$  is defined as

$$\lim_{t \rightarrow -\infty} f(t) = \lim_{\eta \rightarrow 0} \frac{\eta}{\hbar} \int_{-\infty}^0 d\tau e^{\frac{\eta}{\hbar}\tau} f(\tau). \quad (4.31)$$

This relation yields the limit  $f(-\infty)$  of the function  $f(\tau)$  if it exists,

$$\begin{aligned} \lim_{\eta \rightarrow 0} \frac{\eta}{\hbar} \int_{-\infty}^0 d\tau e^{\frac{\eta}{\hbar}\tau} f(\tau) &= \lim_{\eta \rightarrow 0} \int_{-\infty}^0 dx e^x f(\hbar x/\eta) \\ &= \lim_{\eta \rightarrow 0} f(\hbar x_0/\eta) \int_{-\infty}^0 dx e^x = f(-\infty), \end{aligned}$$

where  $x_0$  is some finite negative number. It also provides a definite limiting value for a function  $f(t)$  containing oscillating components of the type  $\sin(\omega t)$  by removing the latter,

$$\begin{aligned} \lim_{\eta \rightarrow 0} \frac{\eta}{\hbar} \int_{-\infty}^0 d\tau e^{\frac{\eta}{\hbar}\tau} \sin \omega \tau &= \lim_{\eta \rightarrow 0} \int_{-\infty}^0 dx e^x \sin(\omega \hbar x/\eta) \\ &= - \lim_{\eta \rightarrow 0} \frac{\omega \eta/\hbar}{\omega^2 + (\eta/\hbar)^2} = 0 \text{ for } \omega \neq 0. \end{aligned}$$

It is these kinds of components which describe the uninteresting details of the wave packet just alluded to. ◊

We now introduce the *Møller operator*

$$\Omega^{(+)} = \frac{\eta}{\hbar} \int_{-\infty}^0 d\tau e^{\frac{\eta}{\hbar}\tau} e^{\frac{i}{\hbar}H\tau} e^{-\frac{i}{\hbar}T\tau}, \quad (4.32)$$

in terms of which eqn (4.30) takes the form

$$|\Psi_{\mathbf{k}_a}^+(0)\rangle = \Omega^{(+)} |\Phi_{\mathbf{k}_a}(0)\rangle. \quad (4.33)$$

We have attached a plus sign to the Møller operator and to the scattering state in order to indicate that the scattering state  $|\Psi_{\mathbf{k}_a}^+(0)\rangle$  generated by applying the operator  $\Omega^{(+)}$  has evolved in a *positive time direction* from a free wave packet state at large negative times. We emphasize again that the parameter  $\eta$  in the definition (4.32) of the Møller operator is to be regarded as infinitesimal but *non-zero* in all manipulations under the integral. It is understood that the limit  $\eta \rightarrow 0$  is taken at the very end.

With the scattering state at  $t = 0$  given by eqn (4.33), the time-dependent scattering state at all times  $t$  can be written

$$|\Psi_{\mathbf{k}_a}^+(t)\rangle = e^{-\frac{i}{\hbar}Ht} \Omega^{(+)} |\Phi_{\mathbf{k}_a}(0)\rangle. \quad (4.34)$$

*Time-reversed* scattering states

We also can construct a scattering state  $|\Psi_{\mathbf{k}_a}^-(0)\rangle$  as that solution which has evolved backwards, in the *negative time direction*, from a free wave packet state  $|\Phi_{\mathbf{k}_a}(t_0)\rangle$ , where  $t_0 > t_\infty$  is now a large positive time,

$$|\Psi_{\mathbf{k}_a}^-(0)\rangle = e^{\frac{i}{\hbar}Ht_0} |\Phi_{\mathbf{k}_a}(t_0)\rangle \text{ with } t_0 > t_\infty. \quad (4.35)$$

Introducing the ‘time-reversed’ Møller operator

$$\Omega^{(-)} = \frac{\eta}{\hbar} \int_0^\infty d\tau e^{-\frac{\eta}{\hbar}\tau} e^{\frac{i}{\hbar}H\tau} e^{-\frac{i}{\hbar}T\tau} \quad (4.36)$$

we find for this scattering state

$$|\Psi_{\mathbf{k}_a}^-(0)\rangle = \Omega^{(-)} |\Phi_{\mathbf{k}_a}(0)\rangle. \quad (4.37)$$

In analogy to eqn (4.34) the time-dependent time-reversed state has the form

$$|\Psi_{\mathbf{k}_a}^-(t)\rangle = e^{-\frac{i}{\hbar}Ht} \Omega^{(-)} |\Phi_{\mathbf{k}_a}(0)\rangle. \quad (4.38)$$

### 4.3 The time-independent formalism

In the time-dependent formalism we have come to a point where the scattering state is connected, at the time  $t = 0$ , with the free wave packet state from which it has evolved (cf. eqn (4.33)), and similarly for the time-reversed state (cf. eqn (4.37)). Starting from these relations we shall now develop the time-independent, stationary formalism of potential scattering theory which is conventionally employed to calculate the dynamics of the scattering process.

#### 4.3.1 The stationary scattering states

Decomposing the free wave packet state on the right-hand side of eqn (4.33) into plane-wave states by using eqn (4.5) with  $t = 0$ , we write

$$|\Psi_{\mathbf{k}_a}(0)\rangle = \Omega^{(+)} \int d^3k A(\mathbf{k} - \mathbf{k}_a) |\mathbf{k}\rangle. \quad (4.39)$$

Since it is understood that the parameter  $\eta$  in expression (4.32) is non-vanishing, we can interchange the Møller operator and the integral over momentum,

$$|\Psi_{\mathbf{k}_a}^+(0)\rangle = \int d^3k A(\mathbf{k} - \mathbf{k}_a) |\mathbf{k}^+\rangle, \quad (4.40)$$

where we have introduced the *stationary scattering state*

$$|\mathbf{k}^+\rangle = \Omega^{(+)} |\mathbf{k}\rangle. \quad (4.41)$$

Using eqns (4.32) and (4.2), we find for the stationary scattering state

$$|\mathbf{k}^+\rangle = \frac{\eta}{\hbar} \int_{-\infty}^0 d\tau e^{\frac{\eta}{\hbar}\tau} e^{\frac{i}{\hbar}H\tau} e^{-\frac{i}{\hbar}T\tau} |\mathbf{k}\rangle = \frac{\eta}{\hbar} \int_{-\infty}^0 d\tau e^{-\frac{i}{\hbar}(E-H+i\eta)\tau} |\mathbf{k}\rangle \\ = \frac{i\eta}{E - H + i\eta} |\mathbf{k}\rangle. \quad (4.42)$$

We remark that the elementary evaluation of the integral in the preceding equation could *not* have been carried out in the Møller operator (4.32) itself, because there the integrand contains a product of exponentials of the two *non-commuting* operators  $H$  and  $T$ .

### 4.3 The time-independent formalism

The stationary scattering state (4.42) can be written in an alternative form by adding and subtracting the term  $E - H$  in the numerator and using the Schrödinger equation (4.2),

$$|\mathbf{k}^+\rangle = \frac{1}{E - H + i\eta} (E - H + i\eta + H - E) |\mathbf{k}\rangle \\ = |\mathbf{k}\rangle + \frac{1}{E - H + i\eta} (T + V - E) |\mathbf{k}\rangle \\ = |\mathbf{k}\rangle + \frac{1}{E - H + i\eta} V |\mathbf{k}\rangle. \quad (4.43)$$

Here and in the following the operator  $(E - H + i\eta)^{-1}$  is treated as non-singular for real values of  $E$  since  $H$  is Hermitian and  $\eta$  is finite.

Analogously we can write for the state  $|\Psi_{\mathbf{k}_a}^-(0)\rangle$

$$|\Psi_{\mathbf{k}_a}^-(0)\rangle = \int d^3k A(\mathbf{k} - \mathbf{k}_a) |\mathbf{k}^-\rangle \quad (4.44)$$

with the corresponding stationary scattering state

$$|\mathbf{k}^-\rangle = \Omega^{(-)} |\mathbf{k}\rangle. \quad (4.45)$$

Using eqn (4.36) we see that this state can be written as

$$|\mathbf{k}^-\rangle = \frac{-i\eta}{E - H - i\eta} |\mathbf{k}\rangle = |\mathbf{k}\rangle + \frac{1}{E - H - i\eta} V |\mathbf{k}\rangle. \quad (4.46)$$

The only change in regard to eqns (4.42) and (4.43) is the minus sign in front of the term  $i\eta$ .

The stationary scattering states  $|\mathbf{k}^\pm\rangle$  are eigenstates of the full Hamiltonian  $H$  with eigenvalue  $E$ , i.e. they satisfy the stationary Schrödinger equation

$$(H - E) |\mathbf{k}^\pm\rangle = 0. \quad (4.47)$$

This is seen by multiplying the states (4.42) or (4.46) by  $(E - H \pm i\eta)$ , respectively, and taking the limit  $\eta \rightarrow 0$ ,

$$\lim_{\eta \rightarrow 0} (E - H \pm i\eta) |\mathbf{k}^\pm\rangle = \lim_{\eta \rightarrow 0} (\pm i\eta) |\mathbf{k}\rangle = 0. \quad (4.48)$$

The fact that the states  $|\mathbf{k}^\pm\rangle$  are eigenstates of  $H$  justifies their name *stationary scattering states*. We shall call them *scattering states* for short.

Going back to the time-dependent normalized scattering states  $|\Psi_{\mathbf{k}_a}^\pm(t)\rangle$ , we find from eqns (4.22), (4.40), and (4.47), and analogously for the time-reversed state,

$$|\Psi_{\mathbf{k}_a}^\pm(t)\rangle = \int d^3k A(\mathbf{k} - \mathbf{k}_a) e^{-\frac{i}{\hbar}Et} |\mathbf{k}^\pm\rangle. \quad (4.49)$$

Comparing with eqn (4.5), we see that the time-dependent scattering state is obtained from the stationary scattering states  $|\mathbf{k}^\pm\rangle$  by folding with the same momentum distribution as in the construction of the *free* wave packet state from the corresponding stationary plane-wave states  $|\mathbf{k}\rangle$ .

From now on we omit the explicit integration over the momentum distribution amplitude  $A(\mathbf{k} - \mathbf{k}_a)$  needed to obtain a normalized state, and deal only with the states  $|\mathbf{k}^\pm\rangle$ , which are formally given by

$$|\mathbf{k}^\pm\rangle = \frac{\pm i\eta}{E - H \pm i\eta} |\mathbf{k}\rangle. \quad (4.50)$$

If one is interested in the behaviour of the time-dependent states one must perform the folding (4.49).

### 4.3.2 The Lippmann–Schwinger equation

In the following we often shall have to deal with different sets of stationary states. In order to simplify the notation and also to prepare for that of Chapter 5, we make the notational changes  $|\mathbf{k}\rangle \rightarrow |a\rangle$ ,  $|\mathbf{k}^\pm\rangle \rightarrow |a^\pm\rangle$ ,  $E \rightarrow E_a$ ,  $|\mathbf{k}'\rangle \rightarrow |b\rangle$ , etc. and  $\delta(\mathbf{k} - \mathbf{k}') \rightarrow \delta_{ab}$ .

Equation (4.50) becomes in the new notation

$$|a^\pm\rangle = \frac{\pm i\eta}{E_a - H \pm i\eta} |a\rangle. \quad (4.51)$$

By multiplying from the left first by  $(E_a - H \pm i\eta)$  and then by  $(E_a - T \pm i\eta)^{-1}$  on both sides of this equation, we find

$$\frac{1}{E_a - T \pm i\eta} (E_a - H \pm i\eta) |a^\pm\rangle = \frac{\pm i\eta}{E_a - T \pm i\eta} |a\rangle. \quad (4.52)$$

Since  $H = T + V$ , the left-hand side of eqn (4.52) can be decomposed in the following way,

$$\frac{1}{E_a - T \pm i\eta} (E_a - H \pm i\eta) |a^\pm\rangle = \left(1 - \frac{1}{E_a - T \pm i\eta} V\right) |a^\pm\rangle. \quad (4.53)$$

On the right-hand side of eqn (4.52), the operator  $T$  acts on its eigenstate  $|a\rangle$  and therefore can be replaced with its eigenvalue  $E_a$ , so that the right-hand side of eqn (4.52) is simply equal to  $|a\rangle$ . Setting this ket equal to the right-hand side of eqn (4.53) and shifting terms from one side to the other, we obtain the **Lippmann–Schwinger equation**

$$|a^\pm\rangle = |a\rangle + \frac{1}{E_a - T \pm i\eta} V |a^\pm\rangle. \quad (4.54)$$

This is the stationary integral equation for  $|a^\pm\rangle$  associated with the differential equation (4.47), which includes explicitly the free state  $|a\rangle$  corresponding to the initial solution for  $t \rightarrow \pm\infty$ .

It is instructive to write the Lippmann–Schwinger equation (4.54) in the coordinate representation by inserting unit operators in terms of complete sets of eigenstates of the position operator  $\mathbf{r}$ ,

$$\langle \mathbf{r} | a^\pm \rangle = \langle \mathbf{r} | a \rangle + \int d^3 r' \int d^3 r'' \langle \mathbf{r} | \frac{1}{E_a - T \pm i\eta} | \mathbf{r}' \rangle \langle \mathbf{r}' | V | \mathbf{r}'' \rangle \langle \mathbf{r}'' | a^\pm \rangle.$$

For a local potential we have

$$\langle \mathbf{r}' | V | \mathbf{r}'' \rangle = V(\mathbf{r}') \delta(\mathbf{r}' - \mathbf{r}''),$$

### 4.3 The time-independent formalism

so that we obtain, using eqn (4.4),  $\langle \mathbf{r} | a^\pm \rangle = \langle \mathbf{r} | \mathbf{k}^\pm \rangle = \Psi_\mathbf{k}^\pm(\mathbf{r})$  and  $E_a = E$ ,

$$\Psi_\mathbf{k}^\pm(\mathbf{r}) = \frac{1}{(2\pi)^{3/2}} e^{i\mathbf{k} \cdot \mathbf{r}} + \int d^3 r' G^\pm(\mathbf{r}, \mathbf{r}'; E) V(\mathbf{r}') \Psi_\mathbf{k}^\pm(\mathbf{r}'). \quad (4.55)$$

Here  $G^\pm(\mathbf{r}, \mathbf{r}'; E)$  is the *Green function* in the coordinate representation, 

$$\begin{aligned} G^\pm(\mathbf{r}, \mathbf{r}'; E) &= \langle \mathbf{r} | \frac{1}{E - T \pm i\eta} | \mathbf{r}' \rangle = \int d^3 k' \frac{\langle \mathbf{r} | \mathbf{k}' \rangle \langle \mathbf{k}' | \mathbf{r}' \rangle}{E - (\hbar^2 k'^2/2\mu) \pm i\eta} \\ &= \frac{1}{(2\pi)^3 \hbar^2} \int d^3 k' \frac{e^{i\mathbf{k}' \cdot (\mathbf{r} - \mathbf{r}')}}{k'^2 - k^2 \pm i\eta}. \end{aligned} \quad (4.56)$$

The integral in this equation can be evaluated as follows. We set  $\mathbf{s} = \mathbf{r} - \mathbf{r}'$  and  $\mathbf{k}' \cdot \mathbf{s} = k' s \cos \theta$ . Separating out the angular part of the volume element,  $d^3 k' = k'^2 dk' 2\pi d(\cos \theta)$ , and integrating over  $\cos \theta$ , we find

$$G^\pm(s; E) = \frac{2\mu}{i(2\pi)^2 \hbar^2} \int_0^\infty \frac{k' dk'}{k^2 - k'^2 \pm i\eta} \left( \frac{e^{ik's}}{s} - \frac{e^{-ik's}}{s} \right). \quad (4.57)$$

Let us first consider the integral with  $+i\eta$ ; since its integrand is even in  $k'$ , we may

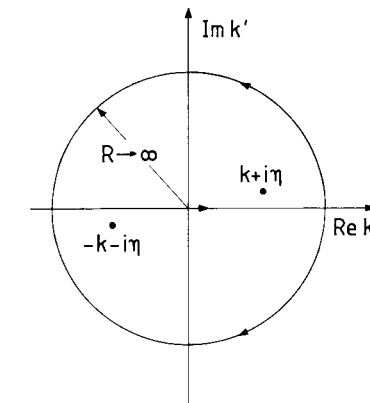


**Figure 4.1** Contours of integration for the evaluation of the Green function (4.58).

extend the integration over the entire  $k'$ -axis, and write it in the form (with  $k > 0$ )

$$\frac{1}{2} \int_{-\infty}^{\infty} \frac{k' dk'}{(k + i\eta + k')(k + i\eta - k')} \left( \frac{e^{ik's}}{s} - \frac{e^{-ik's}}{s} \right). \quad (4.58)$$

We close the contour along the real axis by a large non-contributing half-circle in the upper complex half-plane of  $k'$  for the first term in the parentheses, and by a large non-contributing half-circle in the lower half-plane for the second term (cf. Fig. 4.1). Using the residue theorem we find for the contributions of each term the same expression  $-(i\pi/2)(e^{iks}/s)$ . Similarly, the integral with  $-i\eta$  becomes  $-(i\pi/2)(e^{-iks}/s)$ . The

Green function (4.56) therefore is given by

$$G^\pm(\mathbf{r}, \mathbf{r}'; E) = G^\pm(s; E) = -\frac{\mu}{2\pi\hbar^2} \frac{e^{\pm iks}}{s}. \quad (4.59)$$

The function  $G^+(s; E)$  associated with  $+i\eta$  is an outgoing wave asymptotically, while the function  $G^-(s; E)$  describes the corresponding ingoing wave.

The Lippmann–Schwinger equation (4.55) now takes the explicit form

$$\Psi_k^\pm(\mathbf{r}) = \frac{1}{(2\pi)^{3/2}} e^{i\mathbf{k}\cdot\mathbf{r}} - \frac{\mu}{2\pi\hbar^2} \int d^3 r' \frac{e^{\pm ik|\mathbf{r}-\mathbf{r}'|}}{|\mathbf{r}-\mathbf{r}'|} V(\mathbf{r}') \Psi_k^\pm(\mathbf{r}'). \quad (4.60)$$

It is seen that, for a *real* potential, the Lippmann–Schwinger equation for  $\Psi_k^+(\mathbf{r})$  goes over into that for  $\Psi_k^-(\mathbf{r})$  by complex conjugation accompanied by a change of sign of the vector  $\mathbf{k}$  which appears in the incident wave; therefore we have

$$\Psi_k^-(\mathbf{r}) = [\Psi_k^+(\mathbf{r})]^*. \quad (4.61)$$

### 4.3.3 Orthogonality and completeness

#### Orthogonality

The adjoint of the equation (4.43) for a scattering state  $|b^+\rangle$  is

$$\langle b^+ | = \langle b | + \langle b | V \frac{1}{E_b - H - i\eta}, \quad (4.62)$$

where  $\langle b^+ |$  is the bra adjoint to the ket  $|b^+\rangle$ . Here we regard the potential  $V$  as real (the case of a complex optical potential will be discussed in Chapter 5). Multiplying by the ket  $|a^+\rangle$  from the right we obtain

$$\langle b^+ | a^+ \rangle = \langle b | a^+ \rangle + \langle b | V \frac{1}{E_b - H - i\eta} | a^+ \rangle. \quad (4.63)$$

The first term on the right-hand side is now written, using the Lippmann–Schwinger equation (4.54),

$$\langle b | a^+ \rangle = \langle b | a \rangle + \langle b | \frac{1}{E_a - T + i\eta} V | a^+ \rangle. \quad (4.64)$$

Letting the operator  $T$  act to the left, it operates on its eigenstate  $\langle b |$  and turns into its eigenvalue  $E_b$ , so that we have

$$\langle b | a^+ \rangle = \langle b | a \rangle + \frac{1}{E_a - E_b + i\eta} \langle b | V | a^+ \rangle. \quad (4.65)$$

In the second term on the right-hand side of eqn (4.63) the operator  $H$ , acting to the right, operates on its eigenstate  $|a^+\rangle$  and becomes  $E_a$ ; we have, therefore,

$$\langle b | V \frac{1}{E_b - H - i\eta} | a^+ \rangle = \langle b | V | a^+ \rangle \frac{1}{E_b - E_a - i\eta}. \quad (4.66)$$

The sum of the right-hand sides of eqns (4.65) and (4.66) yields the right-hand side of eqn (4.63). The terms containing the interaction potential  $V$  cancel out, and eqn (4.63)

### 4.3 The time-independent formalism

becomes the *orthogonality relation*

$$\langle b^+ | a^+ \rangle = \langle b | a \rangle = \delta_{ba}, \quad (4.67)$$

or more explicitly,

$$\langle \mathbf{k}'^+ | \mathbf{k}^+ \rangle = \langle \mathbf{k}' | \mathbf{k} \rangle = \delta(\mathbf{k}' - \mathbf{k}). \quad (4.68)$$

Here we have made use of the orthogonality (4.3) of the plane-wave states  $|a\rangle = |\mathbf{k}\rangle$ . The same relation can be proved for the time-reversed states, so that, finally,

$$\langle b^\pm | a^\pm \rangle = \delta_{ba} \quad (4.69)$$

or

$$\langle \mathbf{k}'^\pm | \mathbf{k}^\pm \rangle = \delta(\mathbf{k}' - \mathbf{k}). \quad (4.70)$$

#### Completeness

As eigenstates of the Hermitian operator  $H$  the scattering states  $|\mathbf{k}^\pm\rangle$  form *separate complete sets* if one adds the bound eigenstates  $|n\rangle$  of  $H$ ,

$$\int d^3 k |\mathbf{k}^\pm\rangle \langle \mathbf{k}^\pm | + \sum_n |n\rangle \langle n | = 1; \quad (4.71)$$

this relation is understood to hold separately for the upper and lower suffixes.

### 4.3.4 The *T*-matrix

The Lippmann–Schwinger equation (4.54) with the plus signs describes the transformation of the plane-wave state  $|a\rangle$  into the scattering state  $|a^+\rangle$  through the presence of the potential  $V$ . Using the completeness relation for the plane-wave states

$$\sum_b |b\rangle \langle b| = 1, \quad (4.72)$$

one can write

$$|a^+\rangle = \sum_b |b\rangle \langle b | a^+ \rangle, \quad (4.73)$$

and it is seen that the state  $|a^+\rangle$  is spread out over many plane-wave states besides the incident one. The projection of the scattering state  $|a^+\rangle$  on the plane-wave state  $|b\rangle$  is the momentum representation of this state, i.e. its *wave function in momentum space*,  $\langle b | a^+ \rangle = \langle \mathbf{k}' | a^+ \rangle = \Psi_k^+(\mathbf{k}')$ ; it can be written in the form (4.65),

$$\langle b | a^+ \rangle = \delta_{ba} + \frac{1}{E_a - E_b + i\eta} \langle b | V | a^+ \rangle. \quad (4.74)$$

We now introduce the *T-matrix*

$$T_{ba}^+ = \langle b | V | a^+ \rangle. \quad (\text{post}) \quad (4.75)$$

Equation (4.74) then becomes

$$\langle b | a^+ \rangle = \delta_{ba} + \frac{1}{E_a - E_b + i\eta} T_{ba}^+. \quad (4.76)$$

We see that the  $T$ -matrix  $T_{ba}^+$  determines the strength of the admixture of momentum states other than the initial state  $|a\rangle$ ; it contains the essential information on the scattering process.

In analogy to the preceding discussion we find from the adjoint of eqn (4.54) with the minus signs

$$\langle b^-|a\rangle = \delta_{ba} + \frac{1}{E_b - E_a + i\eta} T_{ba}^-, \quad (4.77)$$

where

$$T_{ba}^- = \langle b^-|V|a\rangle. \quad (\text{prior}) \quad (4.78)$$

In the post expression (4.75) the admixed state  $b$  is represented by a plane wave, while in the prior expression (4.78) it is the initial state  $a$  which is so; the names ‘post’ and ‘prior’ have been introduced in order to conform with the notation employed in Chapter 5 devoted to the description of general reactions (cf. Section 5.2.3).

#### The $T$ -operator; off-shell $T$ -matrices

The two  $T$ -matrices  $T_{ba}^\pm$  are formed by matrix elements of one and the same operator. This is proved by observing that we can write, using eqn (4.43),

$$T_{ba}^+ = \langle b|V|a^+ \rangle = \langle b| \left( V + V \frac{1}{E_a - H + i\eta} V \right) |a\rangle, \quad (4.79)$$

and similarly for  $T_{ba}^-$ , using the adjoint of eqn (4.46),

$$T_{ba}^- = \langle b^-|V|a\rangle = \langle b| \left( V + V \frac{1}{E_b - H + i\eta} V \right) |a\rangle. \quad (4.80)$$

Introducing the energy-dependent  $T$ -operator

$$T(E) = V + V \frac{1}{E - H + i\eta} V, \quad (4.81)$$

we can define a  $T$ -matrix as the matrix element of the  $T$ -operator between the plane-wave states  $|a\rangle$  and  $|b\rangle$ ,

$$T_{ba}(E) = \langle b|T(E)|a\rangle = \langle b| \left( V + V \frac{1}{E - H + i\eta} V \right) |a\rangle; \quad (4.82)$$

in general, all three energies  $E$ ,  $E_a$ , and  $E_b$  may be different, and in this case we have to do with a  $T$ -matrix which is *fully off-energy-shell*.

We can now write for the post and prior  $T$ -matrices

$$T_{ba}^+ = \langle b|V|a^+ \rangle = \langle b|T(E_a)|a\rangle \quad (4.83)$$

and

$$T_{ba}^- = \langle b^-|V|a\rangle = \langle b|T(E_b)|a\rangle. \quad (4.84)$$

These  $T$ -matrices are called *half off-shell* if  $E_a \neq E_b$ . Finally, on the energy shell, when  $E_a = E_b$ , we find

$$T_{ba}^+ = T_{ba}^- = T_{ba}, \quad (4.85)$$

where we have introduced the common notation  $T_{ba}$  for the on-shell post and prior  $T$ -matrices.

The  $T$ -matrix  $T_{ba}$  is formed by matrix elements of the  $T$ -operator with the label of the initial state  $a$  appearing to the right of that of the final state  $b$ . The natural ordering of the initial and final labels is the reverse, and we therefore introduce the on-shell notation

$$T_{a \rightarrow b} = T_{ba}. \quad (4.86)$$

The off-shell  $T$ -matrices are of no particular use in the potential scattering of a single particle, i.e. in the scattering of two isolated particles by each other. However, they are an essential input for exact calculations of the cross sections in three- and more-particle systems (cf., e.g. Lovelace 1964), or in the description of reactions leading to unbound nuclear states in the final channel (cf. Lipperheide 1970; Fuchs *et al.* 1972).

#### The principle of micro-reversibility

Writing the  $T$ -matrices (4.83) and (4.84) explicitly as integrals in the coordinate representation, we have

$$T_{\mathbf{k}',\mathbf{k}}^+ = \frac{1}{(2\pi)^{3/2}} \int d^3r e^{-i\mathbf{k}' \cdot \mathbf{r}} V(\mathbf{r}) \Psi_{\mathbf{k}}^+(\mathbf{r}) \quad (4.87)$$

and

$$T_{\mathbf{k}',\mathbf{k}}^- = \frac{1}{(2\pi)^{3/2}} \int d^3r [\Psi_{\mathbf{k}'}^-(\mathbf{r})]^* V(\mathbf{r}) e^{i\mathbf{k}' \cdot \mathbf{r}}. \quad (4.88)$$

Using eqn (4.61) we find

$$T_{\mathbf{k}',\mathbf{k}}^- = \frac{1}{(2\pi)^{3/2}} \int d^3r e^{i\mathbf{k}' \cdot \mathbf{r}} V(\mathbf{r}) \Psi_{-\mathbf{k}'}^+(\mathbf{r}) \quad (4.89)$$

and therefore,

$$T_{\mathbf{k}',\mathbf{k}}^- = T_{-\mathbf{k}',-\mathbf{k}}^+. \quad (4.90)$$

Now eqn (4.85) states that on the energy shell  $T_{\mathbf{k}',\mathbf{k}}^- = T_{\mathbf{k}',\mathbf{k}}^+ = T_{\mathbf{k}',\mathbf{k}}$ , so that eqn (4.90) becomes in this case

$$T_{\mathbf{k}',\mathbf{k}} = T_{-\mathbf{k}',-\mathbf{k}}. \quad (4.91)$$

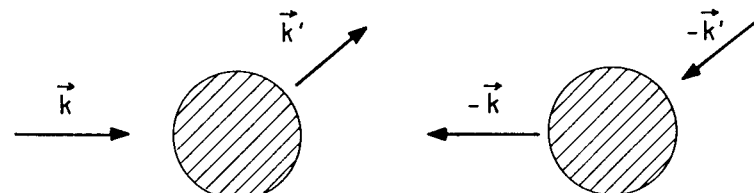


**Figure 4.2** The scattering processes  $\mathbf{k} \rightarrow \mathbf{k}'$  and  $-\mathbf{k}' \rightarrow -\mathbf{k}$  related by the principle of micro-reversibility.

For a more general notation we introduce the ‘time-reversed’ indices  $\tilde{a} = -\mathbf{k}$ ,  $\tilde{b} = -\mathbf{k}'$  corresponding to the reversed momenta, so that we can write eqn (4.91) more

succinctly as

$$T_{ba} = T_{\bar{a}\bar{b}}. \quad (4.92)$$

In the notation introduced in eqn (4.86) we therefore have

$$T_{a \rightarrow b} = T_{\bar{b} \rightarrow \bar{a}}, \quad (4.93)$$

This relation expresses the *principle of micro-reversibility*: the  $T$ -matrix for the scattering from the state  $a$  to the state  $b$  is equal to that for the scattering from the ‘time-reversed state’  $\bar{b}$  to the ‘time-reversed state’  $\bar{a}$ . As we shall see in Section 5.2.6, this is a consequence of *time reversal invariance*, which rests on our assumption that the potential  $V(\mathbf{r})$  used in deriving eqn (4.61) is *real*.

Equation (4.91) expresses the equality of two  $T$ -matrices. In the left-hand  $T$ -matrix the wave with momentum  $\mathbf{k}$  coming from the left (say) of the scattering centre is scattered into a wave with momentum  $\mathbf{k}'$  leaving to the right, whereas in the right-hand  $T$ -matrix the wave  $-\mathbf{k}'$  coming from the right is scattered into the wave  $-\mathbf{k}$  leaving to the left (cf. Fig. 4.2). Thus the principle of micro-reversibility relates the  $T$ -matrices for *physical* processes developing in a *positive* time direction.

### 4.3.5 The $S$ -matrix

The scalar product  $\langle \Psi_{\mathbf{k}_b}^-(0) | \Psi_{\mathbf{k}_a}^+(0) \rangle$  is the probability amplitude, at time  $t = 0$ , for the scattering state  $|\Psi_{\mathbf{k}_a}^+(0)\rangle$  (which has evolved from the free wave packet state with mean momentum  $\mathbf{k}_a$  at  $t < -t_\infty$ ), to contain the scattering state  $|\Psi_{\mathbf{k}_b}^-(0)\rangle$  (which will develop into the wave packet state with mean momentum  $\mathbf{k}_b$  at  $t > t_\infty$ ). In other words, it is the probability amplitude for the transition, through the action of the potential  $V$ , from a normalized free incident wave packet state with mean momentum  $\mathbf{k}_a$ , to an outgoing free wave packet state with momentum  $\mathbf{k}_b$ . Using eqns (4.40) and (4.44), we can write

$$\langle \Psi_{\mathbf{k}_b}^-(0) | \Psi_{\mathbf{k}_a}^+(0) \rangle = \int d^3 k' A^*(\mathbf{k}' - \mathbf{k}_b) \int d^3 k A(\mathbf{k} - \mathbf{k}_a) S_{\mathbf{k}', \mathbf{k}}, \quad (4.94)$$

where we have introduced the *S-matrix*

$$S_{\mathbf{k}', \mathbf{k}} = \langle \mathbf{k}'^- | \mathbf{k}^+ \rangle \quad (4.95)$$

or

$$S_{ba} = \langle b^- | a^+ \rangle. \quad (4.96)$$

The *S*-matrix (4.95) is the probability amplitude for the transition from the initial plane-wave state  $|\mathbf{k}\rangle$  to the final plane-wave state  $|\mathbf{k}'\rangle$  through the action of the potential  $V$ . According to eqn (4.94) the physical transition amplitude  $\langle \Psi_{\mathbf{k}_b}^-(0) | \Psi_{\mathbf{k}_a}^+(0) \rangle$  is obtained from the more formal *S*-matrix (4.95) by folding the initial and final momenta with the momentum distribution amplitude  $A(\kappa)$  in the free incoming and outgoing wave packets.

The *S*-matrix is simply related to the  $T$ -matrix. We consider the scattering states

$$|a^\pm\rangle = |a\rangle + \frac{1}{E_a - H \pm i\eta} V |a\rangle \quad (4.97)$$

and write

$$\frac{1}{x \pm i\eta} = \frac{x}{x^2 + \eta^2} \mp \frac{i\eta}{x^2 + \eta^2} = \frac{\mathcal{P}}{x} \mp i\pi\delta(x), \quad (4.98)$$

### 4.3 The time-independent formalism

where  $\mathcal{P}$  denotes the principal value. Then we have

$$|a^+\rangle - |a^-\rangle = -2\pi i\delta(E_a - H)V|a\rangle. \quad (4.99)$$

Multiplying from the left by  $\langle b^-|$  we obtain

$$\langle b^-|a^+\rangle - \langle b^-|a^-\rangle = -2\pi i\langle b^-|\delta(E_a - H)V|a\rangle. \quad (4.100)$$

We now use the orthogonality relation (4.69) for the scattering states  $|a^-\rangle$  and  $|b^-\rangle$  on the left-hand side, and let the operator  $H$  in the argument of the  $\delta$ -function act to the left so that it can be changed into its eigenvalue  $E_b$ ; we then find

$$\langle b^-|a^+\rangle = \delta_{ba} - 2\pi i\delta(E_a - E_b)\langle b^-|V|a\rangle \quad (4.101)$$

or, using the definition of the  $T$ -matrix (4.78) and eqn (4.85),

$$S_{ba} = \delta_{ba} - 2\pi i\delta(E_a - E_b)T_{ba}. \quad (4.102)$$

Because of the presence of the energy-conserving  $\delta$ -function in front of the  $T$ -matrix, the latter is here to be taken on the energy shell.

#### The on-shell *S*-matrix

In view of the relation

$$\delta_{ba} = \delta(\mathbf{k}_b - \mathbf{k}_a) = \frac{\hbar^2}{\mu k_a} \delta(E_b - E_a) \delta(\Omega_b - \Omega_a) \quad (4.103)$$

it is convenient to write the *S*-matrix (4.102) in the form

$$S_{ba} = \frac{\hbar^2}{\mu k_a} \delta(E_b - E_a) S_{ba}, \quad (4.104)$$

where the quantity  $S_{ba}$  is the *on-shell S-matrix*. It is given by

$$S_{ba} = \delta(\Omega_b - \Omega_a) - i\mu k_a \frac{2\pi}{\hbar^2} T_{ba} \text{ with } E_a = E_b \quad (4.105)$$

or, in terms of the momenta,

$$S_{\mathbf{k}', \mathbf{k}} = \delta(\Omega' - \Omega) - i\mu k \frac{2\pi}{\hbar^2} T_{\mathbf{k}', \mathbf{k}} \text{ with } E = E'. \quad (4.106)$$

#### 4.3.6 The unitarity of the *S*-matrix. The optical theorem

The *S*-matrix  $S_{ca} = \langle c^- | a^+ \rangle$  is unitary. In order to see this, we multiply it by its Hermitian conjugate  $S_{bc}^\dagger = S_{cb}^* = \langle c^- | b^+ \rangle^* = \langle b^+ | c^- \rangle$  and sum over the states  $c$ ,

$$\sum_c S_{bc}^\dagger S_{ca} = \sum_c \langle b^+ | c^- \rangle \langle c^- | a^+ \rangle. \quad (4.107)$$

Using the completeness relation (4.71) with the minus signs and observing that the bound states  $|n\rangle$  are orthogonal to any scattering state  $|\mathbf{k}^-\rangle = |c^-\rangle$ , we find that eqn (4.107) becomes

$$\sum_c S_{bc}^\dagger S_{ca} = \langle b^+ | a^+ \rangle. \quad (4.108)$$

In view of the orthogonality relation (4.69) with the plus signs this equation takes the form of the *unitarity relation*

$$\sum_c S_{bc}^\dagger S_{ca} = \delta_{ba}. \quad (4.109)$$

Similarly, using eqns (4.71) and (4.69) with the plus and minus signs, respectively, one obtains

$$\sum_c S_{bc} S_{ca}^\dagger = \delta_{ba}. \quad (4.110)$$

We thus have, in matrix notation,

$$S^\dagger S = \mathbf{1}, \quad S S^\dagger = \mathbf{1}. \quad (4.111)$$

Written in terms of the momenta, the relation (4.109) reads

$$\int d^3 k'' S_{\mathbf{k}'', \mathbf{k}}^* S_{\mathbf{k}'', \mathbf{k}} = \delta(\mathbf{k}' - \mathbf{k}). \quad (4.112)$$

Using eqns (4.103) and (4.104), we arrive at the unitarity relation for the on-shell  $S$ -matrix,

$$\int d\Omega'' S_{\mathbf{k}'', \mathbf{k}}^* S_{\mathbf{k}'', \mathbf{k}} = \delta(\Omega'' - \Omega) \text{ with } E'' = E' = E. \quad (4.113)$$

#### The optical theorem

The unitarity of the  $S$ -matrix implies a physically equivalent relation for the  $T$ -matrix. We have from eqn (4.113), using eqn (4.106),

$$\begin{aligned} \delta(\Omega' - \Omega) &= \\ &\int d\Omega'' \left( \delta(\Omega'' - \Omega') - i\mu k \frac{2\pi}{\hbar^2} T_{\mathbf{k}'', \mathbf{k}'} \right)^* \left( \delta(\Omega'' - \Omega) - i\mu k \frac{2\pi}{\hbar^2} T_{\mathbf{k}'', \mathbf{k}} \right) \\ &= \delta(\Omega' - \Omega) - i\mu k \frac{2\pi}{\hbar^2} (T_{\mathbf{k}', \mathbf{k}} - T_{\mathbf{k}, \mathbf{k}}^*) + (\mu k)^2 \left( \frac{2\pi}{\hbar^2} \right)^2 \int d\Omega'' T_{\mathbf{k}'', \mathbf{k}'}^* T_{\mathbf{k}'', \mathbf{k}} \\ &\quad \text{with } E'' = E' = E \end{aligned} \quad (4.114)$$

or

$$i(T_{\mathbf{k}', \mathbf{k}} - T_{\mathbf{k}, \mathbf{k}}^*) = \mu k \frac{2\pi}{\hbar^2} \int d\Omega'' T_{\mathbf{k}'', \mathbf{k}'}^* T_{\mathbf{k}'', \mathbf{k}} \text{ with } E'' = E' = E. \quad (4.115)$$

In the special case  $\mathbf{k}' = \mathbf{k}$  we obtain

$$-\text{Im } T_{\mathbf{k}, \mathbf{k}} = \mu k \frac{\pi}{\hbar^2} \int d\Omega'' |T_{\mathbf{k}'', \mathbf{k}}|^2 \text{ with } E'' = E. \quad (4.116)$$

This relation is the *optical theorem* for the  $T$ -matrix.

## 4.4 Asymptotic properties and the cross section

### 4.4.1 The asymptotic stationary scattering wave function

#### The scattering amplitude

Let us go back to the Lippmann–Schwinger equation (4.60) in the coordinate representation and consider its limit for large values of  $r$ . Since the variable  $\mathbf{r}'$  is effectively restricted to values within the range of the potential  $V(\mathbf{r}')$  we have  $r \gg r'$ , so that  $|\mathbf{r} - \mathbf{r}'| \rightarrow r - \hat{\mathbf{r}} \cdot \mathbf{r}'$ , where  $\hat{\mathbf{r}} = \mathbf{r}/r$  is the unit vector in the direction of  $\mathbf{r}$ . Expanding the exponent in the Green function in this way and using  $|\mathbf{r} - \mathbf{r}'| \rightarrow r$  in the denominator, we read off the asymptotic scattering solution, taking separately the upper and the lower sign,

$$\Psi_{\mathbf{k}}^\pm(\mathbf{r}) \rightarrow \frac{1}{(2\pi)^{3/2}} \left( e^{i\mathbf{k} \cdot \mathbf{r}} + f_{\mathbf{k}}^\pm(\hat{\mathbf{r}}) \frac{e^{\pm ikr}}{r} \right) \text{ for } r \rightarrow \infty, \quad (4.117)$$

where we have introduced the *scattering amplitudes*

$$f_{\mathbf{k}}^+(\hat{\mathbf{r}}) = -\mu \left( \frac{2\pi}{\hbar} \right)^2 T_{k\hat{\mathbf{r}}, \mathbf{k}} \quad (4.118)$$

and

$$f_{\mathbf{k}}^-(\hat{\mathbf{r}}) = -\mu \left( \frac{2\pi}{\hbar} \right)^2 T_{\mathbf{k}, -k\hat{\mathbf{r}}}^* \quad (4.119)$$

with the  $T$ -matrix element  $T_{\mathbf{k}', \mathbf{k}} = T_{\mathbf{k}', \mathbf{k}}^\pm$  defined in eqns (4.87) or (4.88). For spherical potentials,  $V(\mathbf{r}) = V(r)$ , the scattering amplitudes can depend only on the energy  $k^2 = k'^2$  and on the scalar product  $\mathbf{k}' \cdot \mathbf{k} = k^2 \cos \theta$ , i.e. on the angle  $\theta$  between the momenta of the outgoing and incident waves.

The scattering wave function  $\Psi_{\mathbf{k}}^+(\mathbf{r})$  as a solution of eqn (4.47) containing an incoming wave with momentum  $\mathbf{k}$  is, except for the normalization, nothing but the scattering solution  $\psi(\mathbf{r})$  of Section 1.2.1 with the asymptotic form (1.9). The scattering amplitude  $f_{\mathbf{k}}^+(\hat{\mathbf{r}})$  therefore is identical with the scattering amplitude  $f(\theta)$  introduced there,

$$f(\theta) = f_{\mathbf{k}}^+(\hat{\mathbf{r}}) = -\mu \left( \frac{2\pi}{\hbar} \right)^2 T_{k\hat{\mathbf{r}}, \mathbf{k}}. \quad (4.120)$$

This relation connects the  $T$ -matrix with the scattering amplitude. In Section 1.2.1 we have found that the absolute square of the scattering amplitude yields the cross section. However, the ‘derivation’ there was only heuristic, and we shall in the next section give a more rigorous and physical proof of this connection.

Writing the optical theorem (4.116) in terms of the scattering amplitude (4.120) we obtain

$$\text{Im } f_{\mathbf{k}}^+(0) = \frac{k}{4\pi} \int d\Omega' |f_{\mathbf{k}}^+(\theta')|^2 = \frac{k}{4\pi} \sigma_{\text{el}}. \quad (4.121)$$

Since the potential  $V$  is real there is no absorption and the total elastic cross section  $\sigma_{\text{el}}$  is equal to the total cross section  $\sigma_{\text{tot}}$ , eqn (4.121) agrees with eqn (1.76) of Section 1.2.3.

**Partial-wave S-matrix and phase shifts**

When the scattering potential is spherical it is useful to decompose the  $T$ -matrix  $T_{\mathbf{k}', \mathbf{k}}$  into multipole components, corresponding to the partial-wave expansion

$$T_{\mathbf{k}', \mathbf{k}} = \sum_{lm} Y_{lm}^*(\Omega') Y_{lm}(\Omega) T_l(k) = \sum_l \frac{2l+1}{4\pi} P_l(\cos \theta) T_l(k). \quad (4.122)$$

We do the same with the on-shell  $S$ -matrix  $S_{\mathbf{k}', \mathbf{k}}$ ,

$$S_{\mathbf{k}', \mathbf{k}} = \sum_{lm} Y_{lm}^*(\Omega') Y_{lm}(\Omega) S_l(k) = \sum_l \frac{2l+1}{4\pi} P_l(\cos \theta) S_l(k). \quad (4.123)$$

Using

$$\delta(\Omega' - \Omega) = \sum_{lm} Y_{lm}^*(\Omega') Y_{lm}(\Omega) = \sum_l \frac{2l+1}{4\pi} P_l(\cos \theta), \quad (4.124)$$

we then find from eqn (4.106)

$$T_l = \frac{i}{\mu k} \frac{\hbar^2}{2\pi} (S_l - 1). \quad (4.125)$$

Substituting expression (4.122) in eqn (4.120) using eqn (4.125) and comparing with eqn (1.38), we find that the  $S$ -function  $S_l$  introduced here is identical with the  $S$ -function (1.39) expressed in terms of the phase shifts  $\delta_l$ .

**4.4.2 Asymptotic wave packets. The cross section**

We have introduced the wave packets for the description of the scattering particle as a moving, localizable object, and we have seen how the Abelian limit procedure allows us to go over to the stationary formalism in which the scattering calculations are most conveniently performed. It remains for us to use the wave packet concept to derive the cross section formula in a more rigorous manner than we did in Section 1.2.1.

Let us consider the time-dependent scattering state (4.49) in the coordinate representation,

$$\Psi_{\mathbf{k}_a}^\pm(\mathbf{r}, t) = \langle \mathbf{r} | \Psi_{\mathbf{k}_a}^\pm(t) \rangle = \int d^3k A(\mathbf{k} - \mathbf{k}_a) e^{-\frac{i}{\hbar} Et} \Psi_{\mathbf{k}}^\pm(\mathbf{r}). \quad (4.126)$$

For large values of  $r$  we can use the asymptotic form of the stationary scattering states (4.117) and obtain

$$\Psi_{\mathbf{k}_a}^\pm(\mathbf{r}, t) \rightarrow \Phi_{\mathbf{k}_a}(\mathbf{r}, t) + \Psi_{\mathbf{k}_a}^{\pm, \text{scatt}}(\mathbf{r}, t) \quad \text{for } r \rightarrow \infty, \quad (4.127)$$

where  $\Phi_{\mathbf{k}_a}(\mathbf{r}, t)$  is the plane wave packet (4.9), and the scattered wave packet  $\Psi_{\mathbf{k}_a}^{\pm, \text{scatt}}(\mathbf{r}, t)$  is given by

$$\Psi_{\mathbf{k}_a}^{\pm, \text{scatt}}(\mathbf{r}, t) = \frac{1}{(2\pi)^{3/2}} \int d^3k A(\mathbf{k} - \mathbf{k}_a) e^{-\frac{i}{\hbar} Et} f_{\mathbf{k}}^\pm(\hat{\mathbf{r}}) \frac{e^{\pm ikr}}{r}. \quad (4.128)$$

The scattering amplitude  $f_{\mathbf{k}}^\pm(\hat{\mathbf{r}})$  changes as a function of momentum on a scale which is generally larger than  $\Delta k \approx 10^{-4} \text{ fm}^{-1}$  (since  $\Delta k = \sqrt{mc^2/2E} \Delta E/\hbar c$ , this value

corresponds approximately to a resonance width of 1 eV for a neutron of 10 eV, or to a resonance width of 1 keV for  $^{16}\text{O}$  at 10 MeV). Comparing this momentum variation with the width of  $10^{-10} \text{ fm}^{-1}$  of the momentum distribution amplitude  $A(\mathbf{k} - \mathbf{k}_a)$  of the wave packet (we adhere to the example given in Section 4.2.1), we see that the scattering amplitude  $f_{\mathbf{k}}^\pm(\hat{\mathbf{r}})$  can be moved outside the integral with  $\mathbf{k}$  replaced with  $\mathbf{k}_a$ . We then obtain

$$\Psi_{\mathbf{k}_a}^{\pm, \text{scatt}}(\mathbf{r}, t) = f_{\mathbf{k}_a}^\pm(\hat{\mathbf{r}}) \frac{1}{r} \Phi_{\mathbf{k}_a}^{\text{spher}}(\pm r, t), \quad (4.129)$$

where  $\Phi_{\mathbf{k}_a}^{\text{spher}}(\pm r, t)$  is the **spherical wave packet**

$$\Phi_{\mathbf{k}_a}^{\text{spher}}(\pm r, t) = \frac{1}{(2\pi)^{3/2}} \int d^3k A(\mathbf{k} - \mathbf{k}_a) e^{-\frac{i}{\hbar} Et} e^{\pm ikr}. \quad (4.130)$$

In the integral on the right-hand side we write  $kr = \mathbf{k} \cdot \hat{\mathbf{k}}r$  and replace  $\hat{\mathbf{k}}$  with  $\hat{\mathbf{k}}_a$ , which is allowed since the weight amplitude  $A(\mathbf{k} - \mathbf{k}_a)$  restricts the direction of  $\mathbf{k}$  to a narrow cone around  $\mathbf{k}_a$ . We then have (cf. eqn (4.9))

$$\Phi_{\mathbf{k}_a}^{\text{spher}}(\pm r, t) = \Phi_{\mathbf{k}_a}(\pm \hat{\mathbf{k}}_a r, t). \quad (4.131)$$

The probability distribution of the spherical wave packet is, according to eqn (4.14), given by

$$|\Phi_{\mathbf{k}_a}^{\text{spher}}(\pm r, t)|^2 = \frac{1}{(2\pi\Delta^2)^{3/2}} \exp\left(-\frac{(r \mp v_a t)^2}{2\Delta^2}\right) = W(r \mp v_a t) \quad (4.132)$$

where the wave packet width  $\Delta$  is taken as constant, i.e. the spreading of the wave packet is neglected as discussed in Section 4.2.1. The probability distribution of this spherical wave packet has the shape of a spherical shell with constant thickness  $\Delta$ ; as the time  $t$  increases, this shell expands (for the upper sign) or shrinks (for the lower sign) with velocity  $v_a = \hbar k_a / \mu$ . Since  $r > 0$ , the spherical wave  $\Phi_{\mathbf{k}_a}^{\text{spher}}(\pm r, t)$  vanishes for  $t \rightarrow \mp\infty$ , respectively.

As a result we find that the time-dependent scattering wave function (4.127) consists asymptotically of an undisturbed wave packet which propagates in the direction of the momentum  $\hbar \mathbf{k}_a$ , and an out- or ingoing spherical wave packet. The spherical wave packet appears in the physical state (which is the one with the plus sign) at times  $t \rightarrow \infty$ ,

$$\begin{aligned} \Psi_{\mathbf{k}_a}^+(\mathbf{r}, t) &\rightarrow \Phi_{\mathbf{k}_a}(\mathbf{r}, t) & \text{for } t \rightarrow -\infty, \\ \Psi_{\mathbf{k}_a}^+(\mathbf{r}, t) &\rightarrow \Phi_{\mathbf{k}_a}(\mathbf{r}, t) + f_{\mathbf{k}_a}^+(\hat{\mathbf{r}}) \frac{1}{r} \Phi_{\mathbf{k}_a}^{\text{spher}}(r, t) & \text{for } t \rightarrow \infty, \end{aligned} \quad (4.133)$$

and in the time-reversed state (the one with the minus sign) at times  $t \rightarrow -\infty$ :

$$\begin{aligned} \Psi_{\mathbf{k}_a}^-(\mathbf{r}, t) &\rightarrow \Phi_{\mathbf{k}_a}(\mathbf{r}, t) + f_{\mathbf{k}_a}^-(\hat{\mathbf{r}}) \frac{1}{r} \Phi_{\mathbf{k}_a}^{\text{spher}}(-r, t) & \text{for } t \rightarrow -\infty, \\ \Psi_{\mathbf{k}_a}^-(\mathbf{r}, t) &\rightarrow \Phi_{\mathbf{k}_a}(\mathbf{r}, t) & \text{for } t \rightarrow \infty. \end{aligned} \quad (4.134)$$

Formulae (4.133) and (4.134) are illustrated in Fig. 4.3. In the first case, the scattering solution consists of a free wave packet with mean momentum  $\mathbf{k}_a$  at early times to which,

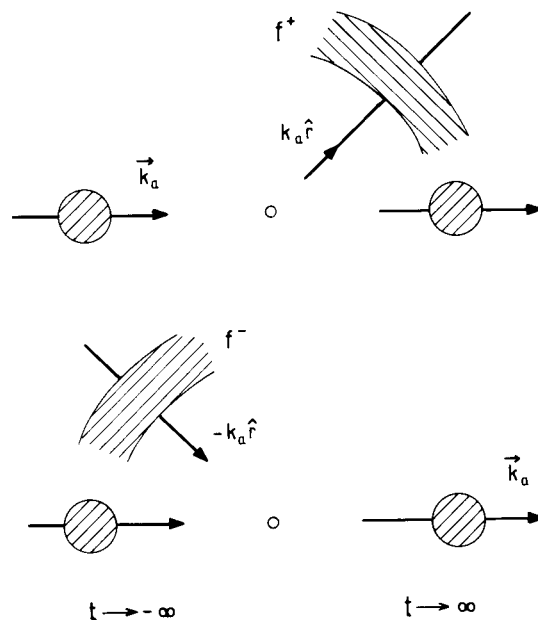


**Figure 4.3** Asymptotic behaviour of the time-dependent scattering wave function. The upper part of the figure refers to the physical state  $\Psi_{\mathbf{k}_a}^+(\mathbf{r}, t)$ , the lower part to the time-reversed state  $\Psi_{\mathbf{k}_a}^-(\mathbf{r}, t)$ .

by the action of the potential  $V$ , an outgoing spherical wave with amplitude  $f_{\mathbf{k}_a}^+(\hat{\mathbf{r}})$  is added at late times. In the second case, the solution consists at early times of a free wave packet with mean momentum  $\mathbf{k}_a$  plus an incoming spherical wave with precisely the right complex amplitude  $f_{\mathbf{k}_a}^-(\hat{\mathbf{r}})$  to be ‘swallowed up’ by the plane wave packet in the region of the potential, so that this plane wave packet is the only one remaining at late times. From another point of view one may say that the wave packets  $\Psi_{\mathbf{k}_a}^\pm(\mathbf{r}, t)$  describe scattering with the *same* initial momentum  $\mathbf{k}_a$ , one starting at  $t \rightarrow -\infty$  and proceeding in a positive time direction, the other starting at  $t \rightarrow \infty$  and ‘running backwards’ in time. The present situation is different from the one shown in Fig. 4.2, which illustrates the principle of micro-reversibility. The latter connects a pair of initial states  $|\mathbf{k}\rangle$ ,  $|-\mathbf{k}'\rangle$  which both develop in a *positive* time sense.

#### The cross section

The elastic scattering cross section can now be obtained immediately. It is seen from eqn (4.14) that the incident wave packet impinges on the target nucleus with a probability current density  $v_a W(0)$ , where the probability density  $W(0)$  is the density inside the incident wave packet which has a spatial width larger than nuclear dimensions by

many orders of magnitude. On the other hand, the scattered spherical wave packet reaches the detector at position  $\mathbf{r}$ , where  $r$  is large, with the probability current density  $|f_{\mathbf{k}_a}^+(\hat{\mathbf{r}})|^2 v_a W(0)/r^2$  (cf. eqns (4.129) and (4.132)). The cross section is the ratio of the outgoing probability current through the surface element  $r^2 d\Omega$  divided by the incident probability current density  $v_a W(0)$ , and is therefore given by

$$\frac{d\sigma}{d\Omega} = |f_{\mathbf{k}_a}^+(\hat{\mathbf{r}})|^2. \quad (4.135)$$

This is in agreement with the expression (1.40) for the differential elastic scattering cross section.

Using eqn (4.118), we can write eqn (4.135) in the alternative form

$$\frac{d\sigma}{d\Omega} = \left(\frac{2\pi}{\hbar}\right)^4 \mu^2 |T_{\mathbf{k}_a \hat{\mathbf{r}}, \mathbf{k}_a}|^2. \quad (4.136)$$

## 4.5 Coherence properties of particle beams

In deriving the cross section formula (4.135) for the scattering of a single particle by a potential, we considered an incident plane wave packet of the form (4.9) which is scattered into the wave packet (4.129). The incident wave packet is made up of eigenfunctions of momentum,  $\exp(i\mathbf{k} \cdot \mathbf{r})$ , folded with a narrow momentum distribution amplitude  $A(\mathbf{k} - \mathbf{k}_a)$ . The simple amplitude (4.6) was assumed only for convenience; it could well be of a more general form  $A_{\mathbf{k}_a}(\mathbf{k})$ , and may, in particular, be complex. The essential point is that via the ‘bundling’ of the momenta one is able to *localize* and *normalize* the wave function of the particle. The distribution amplitude  $A(\mathbf{k} - \mathbf{k}_a)$  was assumed to be a well-behaved function, so that the wave packet is in a *pure quantum state* and has a definite width in the coordinate representation (4.11).

We localized the wave function of the scattering particle since this is required for a clean mathematical formulation of the scattering theory. Let us now turn to the discussion of the *real* situation. We shall see that owing to the way the particle beams are produced in accelerators and reactors, the measured results in the usual kind of scattering experiment do not depend on whether the particle is represented by a coherent wave packet or not.

### 4.5.1 The structure of the physical probability current

Considering actual experiments, it is indeed hard to imagine that a nuclear particle emerging from an accelerator (or, for neutrons, from a reactor) is in a pure quantum state. Its production in the source is a statistical process, and during its acceleration it is subject to stochastic interactions with the surroundings. Therefore, in place of the pure free wave packet state (4.9), it is more realistic to deal with another kind of ‘wave packet’ (cf. McCarthy 1968; Bernstein and Low 1987),

$$\phi_{\mathbf{k}_a}(\mathbf{r}, t; \mathbf{r}_e) = \frac{1}{(2\pi)^{3/2}} \int d^3 k a_{\mathbf{k}_a}(\mathbf{k}) e^{-\frac{i}{\hbar} E(t-t_e)} e^{i\mathbf{k} \cdot (\mathbf{r}-\mathbf{r}_e)}, \quad (4.137)$$

which is described as follows. We have not fixed the centre of the free wave packet at  $\mathbf{r} = 0$  for  $t = 0$ , i.e. at the place and time of the scattering by the target nucleus as in eqn (4.9), but at some location  $\mathbf{r}_e$  near the exit window of the accelerator tube at a given

exit time  $t_e$ . The exact position of the wave packet at the exit time is unknown within a macroscopic volume  $\Delta V$  (of linear dimension  $10^{-3}$  cm, say, as we always assume here for the sake of argument). Moreover, because of the stochastic interactions which the particle has suffered before it reaches the exit window, the ‘amplitude’  $a_{\mathbf{k}_a}(\mathbf{k})$  for fixed  $\mathbf{k}_a$  is to be regarded as an ensemble of more or less random complex numbers which depend on  $\mathbf{k}$ . The extent to which the amplitudes for different values of  $\mathbf{k}$  are correlated is difficult to estimate; if the amplitudes are completely uncorrelated, the product  $a_{\mathbf{k}_a}(\mathbf{k})a_{\mathbf{k}_a}^*(\mathbf{k}')$  is a matrix whose ensemble average  $\overline{a_{\mathbf{k}_a}(\mathbf{k})a_{\mathbf{k}_a}^*(\mathbf{k}')}$  is diagonal in the variables  $\mathbf{k}$  and  $\mathbf{k}'$ .

In order to deal with this situation we go over to a formalism which accommodates both coherent and partially or fully random amplitudes  $a_{\mathbf{k}_a}(\mathbf{k})$ , and introduce the density matrix

$$\phi_{\mathbf{k}_a}(\mathbf{r}, t; \mathbf{r}_e)\phi_{\mathbf{k}_a}^*(\mathbf{r}', t; \mathbf{r}_e) \quad (4.138)$$

to describe the incident particle. The corresponding density matrix for the scattered particle is then given by

$$\psi_{\mathbf{k}_a}^{\pm, \text{scatt}}(\mathbf{r}, t; \mathbf{r}_e)\psi_{\mathbf{k}_a}^{\pm, \text{scatt}*}(\mathbf{r}', t; \mathbf{r}_e), \quad (4.139)$$

where we have defined the scattered wave packet

$$\psi_{\mathbf{k}_a}^{\pm, \text{scatt}}(\mathbf{r}, t; \mathbf{r}_e) = \frac{1}{(2\pi)^{3/2}} \frac{1}{r} \int d^3k a_{\mathbf{k}_a}(\mathbf{k}) f_{\mathbf{k}}^{\pm}(\hat{\mathbf{r}}) e^{-\frac{i}{\hbar}E(t-t_e)} e^{\pm ikr} e^{-i\mathbf{k}\cdot\mathbf{r}_e} \quad (4.140)$$

in analogy to the plane wave packet (4.137).

Since the precise position  $\mathbf{r}_e$  within the macroscopic volume  $\Delta V$  is unknown, we average over it. Averaging also over the density matrix (4.138), we find for the incident probability current at position  $\mathbf{r}$  impinging on a unit area perpendicular to the beam direction  $\hat{\mathbf{k}}_a$ ,

$$J_{\text{incid}}(\mathbf{r}, t) = \frac{1}{\Delta V} \int_{\Delta V} d^3r_e \overline{\phi_{\mathbf{k}_a}^*(\mathbf{r}, t; \mathbf{r}_e)[\hat{\mathbf{k}}_a \cdot \mathbf{j}(\mathbf{r})]\phi_{\mathbf{k}_a}(\mathbf{r}, t; \mathbf{r}_e)}; \quad (4.141)$$

here the current operator  $\mathbf{j}(\mathbf{r})$  is defined by

$$\mathbf{j}(\mathbf{r}) = \frac{\hbar}{2\mu i} (\vec{\nabla} - \vec{\nabla}), \quad (4.142)$$

where the arrows affixed to the  $\nabla$ -operator indicate the direction in which this operator acts. The current (4.141) is the probability current of a particle moving with mean velocity  $v_a = \hbar k_a / \mu$  as before, but owing to the averaging over the initial position it is at all times localized only within the confines of the moving volume  $\Delta V$ . Evaluating the current inside this volume, we find

$$\begin{aligned} J_{\text{incid}} &= \frac{1}{\Delta V} \int_{\Delta V} d^3r_e \int d^3k' \int d^3k \overline{a_{\mathbf{k}_a}^*(\mathbf{k}')a_{\mathbf{k}_a}(\mathbf{k})} \\ &\times \left( \hat{\mathbf{k}}_a \cdot \frac{\hbar(\mathbf{k} + \mathbf{k}')}{2\mu} \right) \frac{1}{(2\pi)^3} e^{[i(\mathbf{k}-\mathbf{k}')\cdot(\mathbf{r}-\mathbf{r}_e) - \frac{i}{\hbar}(E-E')(t-t_e)]}. \end{aligned} \quad (4.143)$$

Let us perform the integration over the position  $\mathbf{r}_e$  first. Since the volume of integration  $\Delta V$  is of macroscopic size this integration can effectively be extended over all space,

producing a term  $(2\pi)^3 \delta(\mathbf{k} - \mathbf{k}')$ . One of the momentum integrals is then evaluated trivially, and we obtain for the probability current density of the incident beam inside the moving volume  $\Delta V$

$$J_{\text{incid}} = \frac{v_a}{\Delta V} \int d^3k \rho_{\mathbf{k}_a}(\mathbf{k}), \quad (4.144)$$

where  $\rho_{\mathbf{k}_a}(\mathbf{k})$  is the absolute square of the amplitude at a given wave number  $\mathbf{k}$ , or the *wave number spectrum* of the incident beam,

$$\rho_{\mathbf{k}_a}(\mathbf{k}) = |\overline{a_{\mathbf{k}_a}(\mathbf{k})}|^2. \quad (4.145)$$

The current (4.144) is independent of  $\mathbf{r}$  and  $t$  inside the volume  $\Delta V$ .

Similarly we find for the probability current of the outgoing particle impinging on an area  $r^2 d\Omega$  perpendicular to the radius vector, using eqn (4.140),

$$J_{\text{out}} = \frac{v_a}{\Delta V} \int d^3k |f_{\mathbf{k}}^+(\hat{\mathbf{r}})|^2 \rho_{\mathbf{k}_a}(\mathbf{k}). \quad (4.146)$$

It thus turns out that the incident and outgoing currents are *independent of the phases* of the different plane-wave contributions  $a_{\mathbf{k}_a}(\mathbf{k})$  in the ‘wave packets’ (4.137) and (4.140). Only their spectral distribution (4.145) matters.

When deriving the cross section in the wave-packet description (cf. Section 4.4.2), we argued that the width of the momentum distribution amplitude  $A(\mathbf{k} - \mathbf{k}_a)$  is generally so small on the scale of the momentum variation of the scattering amplitude  $f_{\mathbf{k}}^+(\hat{\mathbf{r}})$  that the latter can be moved outside the integral (4.128). Making the same assumption in regard to the width of the wave number spectrum  $\rho_{\mathbf{k}_a}(\mathbf{k})$ , we can write the outgoing current (4.146) in the form

$$J_{\text{out}} = \frac{v_a}{\Delta V} |f_{\mathbf{k}_a}^+(\hat{\mathbf{r}})|^2 \int d^3k \rho_{\mathbf{k}_a}(\mathbf{k}). \quad (4.147)$$

Then the differential cross section  $d\sigma/d\Omega = J_{\text{out}}/J_{\text{incid}}$  is again given by formula (4.135).

Owing to the uncertainties in the initial position of the particle (one could also have included uncertainties in the ‘time of release’ of the accelerated particle), the cross section contains no information on the coherence properties of the initial particle state. The lesson of this discussion is that the measured results in a scattering experiment do not depend on whether the scattering particle is described by a coherent wave packet state or by an incoherent mixture of plane-wave states. Each plane-wave component  $|\mathbf{k}\rangle$  in the initial system scatters independently, and its phase relative to the other components in the wave packet is irrelevant.

#### 4.5.2 A model for the incident beam

Bernstein and Low (1987) have discussed the following model for the structure of the probability current of a *single incident particle*. The ‘amplitude’  $a_{\mathbf{k}_a}(\mathbf{k})$  is decomposed into  $N$  coherent wave packet amplitudes  $A_{\mathbf{k}_a}^{(i)}(\mathbf{k})$ ,  $i = 1, \dots, N$  (which may be identical

to the simple Gaussian amplitude  $A(\mathbf{k} - \mathbf{k}_a)$  of eqn (4.6)) with random coefficients  $c_i$ ,

$$a_{\mathbf{k}_a}(\mathbf{k}) = \sum_{i=1}^N c_i A_{\mathbf{k}_a}^{(i)}(\mathbf{k}) \quad (4.148)$$

where

$$\bar{c}_i = 0, \quad \overline{c_i c_j} = p_i \delta_{ij}, \quad \sum_{i=1}^N p_i = 1. \quad (4.149)$$

This model for the incident particle is equivalent to a description in terms of the density operator (cf. Messiah 1972, Section VIII, §21)

$$\rho = \sum_{i=1}^N |\Phi_i\rangle p_i \langle \Phi_i| \text{ with } \langle \Phi_i|\Phi_i\rangle = 1, \quad (4.150)$$

where the states

$$|\Phi_i\rangle = |\Phi_i(t)\rangle = \int d^3 k A_{\mathbf{k}_a}^{(i)}(\mathbf{k}) e^{-\frac{i}{\hbar} E t} |\mathbf{k}\rangle \quad (4.151)$$

are the free wave packets (4.5). The quantities  $p_i \geq 0$  are the probabilities with which each wave packet appears in the ensemble of amplitudes  $a_{\mathbf{k}_a}(\mathbf{k})$ . The particle is thus regarded statistically as consisting of  $N$  ‘sub-particles’.

It is instructive to consider the distribution of the momenta in this model. Let us define the mean value of the momentum in the pure wave packet state  $|\Phi_i\rangle$ ,

$$\mathbf{k}_i = \langle \Phi_i | \mathbf{k} | \Phi_i \rangle = \int d^3 k \mathbf{k} |A_{\mathbf{k}_a}^{(i)}(\mathbf{k})|^2, \quad (4.152)$$

and correspondingly the variance of the momentum in that state, i.e. the momentum spread of the wave packet,

$$(\Delta \mathbf{k}_i)^2 = \langle \Phi_i | (\mathbf{k} - \mathbf{k}_i)^2 | \Phi_i \rangle = \langle \Phi_i | \mathbf{k}^2 | \Phi_i \rangle - \mathbf{k}_i^2. \quad (4.153)$$

The ensemble average of the momentum is, then, using eqns (4.150) and (4.152),

$$\bar{\mathbf{k}} = \text{trace}(\rho \mathbf{k}) = \sum_{i=1}^N p_i \langle \Phi_i | \mathbf{k} | \Phi_i \rangle = \sum_i p_i \mathbf{k}_i. \quad (4.154)$$

For the ensemble average of the variance of the momentum we have

$$\begin{aligned} \overline{\Delta_k^2} &= \overline{(\mathbf{k} - \bar{\mathbf{k}})^2} = \bar{\mathbf{k}}^2 - \bar{\mathbf{k}}^2 \\ &= \sum_i p_i \langle \Phi_i | \mathbf{k}^2 | \Phi_i \rangle - \bar{\mathbf{k}}^2 \\ &= \sum_i p_i (\langle \Phi_i | \mathbf{k}^2 | \Phi_i \rangle - \mathbf{k}_i^2) + \sum_i p_i \mathbf{k}_i^2 - \bar{\mathbf{k}}^2 \\ &= \sum_i p_i (\Delta \mathbf{k}_i)^2 + \sum_i p_i (\mathbf{k}_i - \bar{\mathbf{k}})^2 \end{aligned} \quad (4.155)$$

or

$$\overline{\Delta_k^2} = (\Delta \mathbf{k}_{\text{av}})^2 + \sum_{i=1}^N p_i (\mathbf{k}_i - \bar{\mathbf{k}})^2 > (\Delta \mathbf{k}_{\text{av}})^2, \quad (4.156)$$

where

$$(\Delta \mathbf{k})_{\text{av}}^2 = \sum_i p_i (\Delta \mathbf{k}_i)^2 \quad (4.157)$$

is the average momentum spread in the wave packets.

The ensemble average of the momentum spread is to be identified with the *observed* spread; therefore, the average momentum spread within the wave packets is *smaller* than the observed momentum spread  $\overline{\Delta_k^2}$ , so that conversely, the average *spatial* spread of the wave packets is *larger* than the ‘observed’ value  $3/4 \overline{\Delta_k^2}$  (we recall from Section 4.2.1 that the relation between spatial width  $\Delta$  and momentum width  $\Delta_k$  is  $\Delta = \sqrt{3}/2 \Delta_k$ ).

If each particle in an incident beam of  $M$  independent particles is described by a single coherent wave packet  $|\Phi^n\rangle$  with  $\langle \Phi^n | \Phi^n \rangle = 1$ ,  $n = 1, \dots, M$ , the beam is to be associated with the density operator

$$\rho_{\text{beam}} = \sum_{n=1}^M |\Phi^n\rangle \langle \Phi^n|, \quad (4.158)$$

where each wave packet appears with unit probability. If now, in line with the present model, each particle is sub-divided into  $N$  ‘sub-particles’ described by wave packets  $|\Phi_i^n\rangle$ ,  $i = 1, \dots, N$ , this density operator becomes

$$\rho_{\text{beam}} = \sum_{n=1}^M \sum_{i=1}^N |\Phi_i^n\rangle \langle \Phi_i^n|. \quad (4.159)$$

In a beam of  $M$  physical particles we then have  $N \times M$  statistically independent wave packets, and the one-to-one assignment of wave packets to particles is no longer warranted. Each wave packet is scattered by the potential as if the others were not present, and makes an independent contribution to the scattering cross section.

In Section 1.2.1 we have made a distinction between the cross section for the *probability current of a single particle* and that for a *particle current of a beam of many particles*. In the light of the preceding discussion we now see that for the interpretation of an actual scattering experiment we need not differentiate between the two.

## 4.6 Notes and references

The formal theory of collisions has been developed in the pioneering papers of Möller (1945), Lippmann and Schwinger (1950), Gell-Mann and Goldberger (1953), and the review article of Brenig and Haag (1959). Treatments of this subject can also be found in the books of Goldberger and Watson (1964), Rodberg and Thaler (1967), Messiah (1972), Joachain (1975), and Newton (1982).

The question of the coherence properties of cold neutron beams has recently attracted considerable attention (cf. Comsa 1983; Kaiser *et al.* 1983; Klein *et al.* 1983; Bernstein and Low 1987; Sears 1989). In generalization of the results of Section 4.5 it can be shown that any nuclear reaction using the usual kind of ‘passive’, i.e. static target would not yield information on the coherence properties of particle beams. For an actual observation of the coherence properties of particle beams more refined experiments have been proposed, involving time-dependent so-called ‘active’ targets (cf. Golub and Lamoreaux 1992).

## References

- Astern, N. (1970). *Direct nuclear reaction theories*, Wiley, New York.
- Bernstein, H. J. and Low, F. E. (1987). *Phys. Rev. Lett.* **59** 951.
- Brenig, W. and Haag, R. (1959). *Fortschritte der Physik* **7** 183; translated in *Quantum scattering theory* (1963), ed. Ross, M., Indiana University Press, Bloomington.
- Comsa, G. (1983). *Phys. Rev. Lett.* **51** 1105.
- Fuchs, H., Homeyer, H., Oeschler, H., Lipperheide, R. and Möhring, K. (1972). *Nucl. Phys.* **A196** 286.
- Gell-Mann, M. and Goldberger, M. L. (1953). *Phys. Rev.* **91** 398.
- Goldberger, M. L. and Watson, K. M. (1964). *Collision theory*, Wiley, New York.
- Golub, R. and Lamoreaux, S. K. (1992). *Phys. Lett.* **162A** 122.
- Joachain, C. J. (1975). *Quantum collision theory*, North-Holland, Amsterdam.
- Kaiser, H., Werner, S. A. and George, E. A. (1983). *Phys. Rev. Lett.* **50** 560.
- Klein, A. G., Opat, G. I. and Hamilton, W. A. (1983). *Phys. Rev. Lett.* **50** 563.
- Lipperheide, R. (1970). *Phys. Lett.* **32B** 555.
- Lippmann B. A. and Schwinger, J. (1950). *Phys. Rev.* **79** 469.
- Lovelace, C. (1964). *Phys. Rev.* **135** B1225.
- McCarthy, I. E. (1968). *Introduction to nuclear physics*, Wiley, New York.
- Messiah, A. (1972). *Quantum mechanics*, North-Holland, Amsterdam.
- Møller, C. (1945). *Kgl. Danske Videnskab. Selskab, Mat.-Fys. Medd.* **23** No. 1.
- Newton, R. G. (1982). *Scattering theory of waves and particles*, Springer, Berlin.
- Rodberg, L. S. and Thaler, R. M. (1967). *Introduction to the quantum theory of scattering*, Academic Press, New York.
- Sears, V. (1989). *Neutron optics*, Oxford University Press, Oxford.

## THE FORMAL THEORY OF REACTIONS

## 5.1 Introduction

The formal theory of potential scattering developed in the preceding chapter can immediately be generalized to a formal theory of reactions.

We recall that in potential scattering a plane-wave state with the initial momentum  $\mathbf{k}$  makes a transition to a plane-wave state with the final momentum  $\mathbf{k}'$ . Since energy is conserved, only the direction of the momentum changes. For a general reaction the definition of the initial and final states requires more than the specification of only their relative momenta. Additional quantum numbers are needed to characterize the *internal states* of the collision partners, which may be excited and gain or lose nucleons as a result of their mutual interaction. Nevertheless, the formalism of potential scattering carries over to nuclear reactions in general if the state labels  $a$  and  $b$  are understood to include these additional degrees of freedom.

The concepts and derivations introduced in the formal theory of potential scattering also apply to nuclear reactions, sometimes in an appropriately modified form. It is only in the explicit evaluation of the formal expressions for the transition amplitudes and in the specific approximation schemes for different reaction types that the formal theory of reactions becomes much more complicated and richer in detail than potential scattering.

In Section 5.2 we introduce the concept of a *channel*, which serves to define the asymptotic state of the system of collision partners far away from the region of interaction, i.e. before or after the collision. A particular partition of the total number of nucleons between the collision partners defines an *arrangement channel*; particle transfer during a collision then causes a *rearrangement*, i.e. a transition from one arrangement channel to another. The analogue of a free state in potential scattering is a *channel state*, which is a state in a particular channel with the interaction between the two collision partners switched off. We further discuss the *reaction states* in generalization of the scattering states of the previous chapter. The time-dependent reaction states are solutions of the time-dependent Schrödinger equation in which the reaction system is in a particular initial, or entrance, channel at the initial time. The corresponding stationary reaction states are then defined in analogy to those in potential scattering. They satisfy Lippmann-Schwinger equations and orthogonality relations.  $T$ - and  $S$ -matrices can be derived as before. The unitarity relation for the  $S$ -matrix and the optical theorem are generalized to the multichannel case, and the reciprocity relation between the cross section of a reaction and that of the corresponding time-reversed process is derived.

The establishment of explicit expressions for the  $T$ - and  $S$ -matrices to be used in the calculation of reaction cross sections as functions of energy and reaction angle is a

complicated procedure involving the coupling of various angular-momentum eigenstates. This will be discussed in Section 5.3.

The next two sections are devoted to approximation schemes. Since it is impossible to solve the many-nucleon Schrödinger problem exactly, simplifications have to be made. Two important approximations are discussed. In Section 5.4 the reaction mechanism is reduced to a *single-step mechanism*, in which the transition from the initial to the final channel state is assumed to proceed ‘directly’; only the quantum numbers of these two states are involved with the exclusion of all others. This approximation is particularly useful for the treatment of rearrangement processes.

An extension of this single-step mechanism is the *coupled-channel scheme* discussed in Section 5.5. Here one includes a certain number of intermediate channels which are coupled to the initial and final channel states, as well as among themselves. The reaction is thus described as a multistep process.

These approximation schemes will only be discussed formally in the present chapter. Their use for the explicit calculation of cross sections of direct reactions is deferred to Chapters 7 and 8.

## 5.2 The general formalism for two-body channels

### 5.2.1 Channels

In order to classify the initial and final states of a nuclear reaction we introduce the concept of an *arrangement channel*. More specifically, we consider a *two-body arrangement channel*, which is a particular partition of the total number of interacting nucleons into two fragments, or collision partners. We disregard more-than-two-body channels which occur in break-up and fragmentation reactions. Thus we are concerned with reactions of the type



where  $x, A$  are the fragments in the entrance channel, and  $y, B$  those in the exit channel. It is important to note that the **two fragments must be bound**; unbound states of the nuclei of a particular partition are counted among arrangement channels with a correspondingly larger number of reaction partners, which we disregard. We also omit one-body channels since they describe bound states of the *total system* which are stable against nuclear decay. They do not occur in a reaction.

◊ Here we regard a particular state of a nucleus as bound if it is stable over macroscopic times, i.e. times long compared with the time during which the reaction takes place. In this sense the ground and lowest excited states of naturally occurring nuclei are bound, although (cf., e.g. Bohr and Mottelson 1969, Fig. 2.4) all nuclei heavier than iron have less binding energy per nucleon than iron itself, and can in principle decay into two or more daughter nuclei, but often only after an enormously long time, even on a macroscopic scale. In the same vein, we disregard the instability of excited nuclear states against  $\gamma$ - and  $\beta$ -decay, since these processes generally are much slower than nuclear reactions. ◊

A particular arrangement channel consisting of two nuclei,  $x$  and  $A$ , is labelled by the index  $\alpha = (A_x, Z_x; A_A, Z_A)$ , which we abbreviate as  $\alpha = (x, A)$ ; here  $A_i, Z_i$  are the

## 5.2 The general formalism for two-body channels

mass number and charge of the nucleus  $i$  ( $i = x, A$ ), respectively. This index determines only the partitioning of the nucleons between the fragments in a channel. For a complete characterization of a **two-body channel  $a$**  we introduce, besides the arrangement index  $\alpha$ , the complete set of quantum numbers of the channel,

$$a = \{\alpha; a_x, a_A; \mathbf{k}_a\}, \quad (5.2)$$

where  $a_x = \{\epsilon_x, I_x, M_x, T_x, M_x^T, \pi_x\}$  and  $a_A = \{\epsilon_A, I_A, M_A, T_A, M_A^T, \pi_A\}$  are the internal quantum numbers of the fragments  $x$  and  $A$ :  $\epsilon_i$  is the intrinsic energy,  $I_i$  the spin with  $z$ -component  $M_i$ ,  $T_i$  the isospin with  $z$ -component  $M_i^T$ , and  $\pi_i$  the parity of the nucleus  $i$ , where  $i = x, A$ ; finally,

$$\mathbf{k}_a = \frac{m_A \mathbf{k}_x - m_x \mathbf{k}_A}{m_x + m_A} \quad (5.3)$$

is the relative momentum of the collision partners  $x$  and  $A$ , or **channel momentum**. The kinetic energy associated with the channel momentum is the **channel energy**

$$\mathcal{E}_a = \frac{\hbar^2 k_a^2}{2\mu_\alpha}, \quad (5.4)$$

where  $\mu_\alpha = m_x m_A / (m_x + m_A)$  is the reduced mass in the arrangement channel  $\alpha$ .

The channel  $a$  is defined in terms of the *non-interacting* partners  $x$  and  $A$ . As the reaction proceeds from the entrance channel, where the nuclei  $x$  and  $A$  are usually in their ground states and far apart from one another, many other excited and rearranged channels will be coupled in, until in a particular exit channel  $b$  the two final partners  $y$  and  $B$  are again far apart and non-interacting.

### Channel states

The plane-wave state  $|\mathbf{k}\rangle$  of the previous chapter is now generalized to the **free channel state  $|a\rangle$**  for two non-interacting nuclei in arrangement channel  $\alpha$  with relative momentum  $\mathbf{k}_a$  (the motion of the centre of mass has been separated out),

$$|a\rangle = |a; \mathbf{k}_a\rangle = |a_x, a_A; \mathbf{k}_a\rangle = |a_x, a_A\rangle |\mathbf{k}_a\rangle = |a_x\rangle |a_A\rangle |\mathbf{k}_a\rangle, \quad (5.5)$$

where  $|a_x\rangle$  and  $|a_A\rangle$  are *bound internal states* of the nuclei  $x$  and  $A$ , and  $|\mathbf{k}_a\rangle$  is the plane-wave state of the relative motion of  $x$  and  $A$  with momentum  $\mathbf{k}_a$ . In eqn (5.5) we have adopted the convention that  $a$  denotes the full set of channel quantum numbers except when the relative momentum  $\mathbf{k}_a$  is specified, in which case the set  $a$  includes only the arrangement channel label  $\alpha$  and the internal quantum numbers  $\{a_x, a_A\}$ . It is sometimes necessary to specify explicitly the spins of the internal states; in this case we write

$$|a_x, a_A; \mathbf{k}_a\rangle = |\underline{a}; I_x M_x, I_A M_A; \mathbf{k}_a\rangle = |\underline{a}; I_x M_x, I_A M_A\rangle |\mathbf{k}_a\rangle \quad (5.6)$$

and

$$\begin{aligned} |a_x\rangle &= |\underline{a}_x; I_x M_x\rangle, \\ |a_A\rangle &= |\underline{a}_A; I_A M_A\rangle, \end{aligned} \quad (5.7)$$

where  $\underline{a}$  includes all internal quantum numbers not explicitly specified.

The free Hamiltonian in the arrangement channel  $\alpha$  is defined as

$$H_\alpha = T_\alpha + h_\alpha, \quad (5.8)$$

where

$$T_\alpha = -\frac{\hbar^2}{2\mu_\alpha} \nabla_\alpha^2 \quad (5.9)$$

is the kinetic energy of the relative motion. The operator  $h_\alpha$  is the sum of the internal Hamiltonians of the reaction partners,

$$h_\alpha = h_x + h_A. \quad (5.10)$$

The internal states  $|a_x\rangle$  and  $|a_A\rangle$  are bound eigenstates of the Hamiltonians  $h_x$  and  $h_A$ , respectively,

$$\begin{aligned} h_x|a_x\rangle &= \epsilon_x|a_x\rangle, \\ h_A|a_A\rangle &= \epsilon_A|a_A\rangle, \end{aligned} \quad (5.11)$$

so that

$$h_\alpha|a_x, a_A\rangle = \epsilon_a|a_x, a_A\rangle \text{ with } \epsilon_a = \epsilon_x + \epsilon_A, \quad (5.12)$$

where we have introduced the *internal energy*  $\epsilon_a$  of the channel  $a$ . Then we can write

$$(H_\alpha - E_a)|a\rangle = 0 \quad (5.13)$$

with

$$E_a = \mathcal{E}_a + \epsilon_a, \quad (5.14)$$

where  $\mathcal{E}_a$  is the channel energy (5.4). Equation (5.13) is the analogue of eqn (4.2) for the plane-wave state  $|\mathbf{k}\rangle$ .

Because the Hamiltonians in different arrangement channels are different, two channel states  $|a\rangle = |a_x\rangle|a_A\rangle|\mathbf{k}_a\rangle$  and  $|b\rangle = |b_y\rangle|b_B\rangle|\mathbf{k}_b\rangle$  are not orthogonal to each other if they belong to *different* arrangement channels. Only if these states belong to the *same* arrangement channel will the internal states be eigenstates of the same internal Hamiltonian, and the plane-wave states of the relative motion, eigenstates of the same kinetic energy operator; then they *are* orthogonal. That is, we have

$$\begin{aligned} \langle a|b\rangle &= \delta_{ab} \text{ if } \alpha = \beta, \\ \langle a|b\rangle &\neq \delta_{ab} \text{ if } \alpha \neq \beta. \end{aligned} \quad (5.15)$$

In analogy to eqn (4.5) a free, normalized time-dependent state in channel  $a$  is given by

$$|\Phi_a(t)\rangle = \int d^3k'_a A(\mathbf{k}'_a - \mathbf{k}_a)e^{-\frac{i}{\hbar}E'_a t}|a; \mathbf{k}'_a\rangle. \quad (5.16)$$

It satisfies the free time-dependent Schrödinger equation

$$i\hbar \frac{d}{dt}|\Phi_a(t)\rangle = H_\alpha|\Phi_a(t)\rangle. \quad (5.17)$$

### Distorted channel states

One may generalize the free channel state, in which the two nuclei do not interact, to a *distorted channel state*, where the nuclei interact via a *distorting potential*  $U_\alpha$  which

depends only on the relative coordinate between them. In the coordinate representation such a potential (if assumed to be spherical) has the form  $U_\alpha(r_\alpha)$ , where  $r_\alpha$  is the distance between the centres of mass of the two nuclei in the arrangement channel  $\alpha$ . The channel Hamiltonian then becomes

$$H_\alpha^U = H_\alpha + U_\alpha. \quad (5.18)$$

The corresponding distorted channel state is now a scattering state, and there exist two of these, an incoming and an outgoing one,

$$|a_U^\pm\rangle = |a; \mathbf{k}_{a,U}^\pm\rangle = |a_x, a_A; \mathbf{k}_{a,U}^\pm\rangle. \quad (5.19)$$

If the distorting potential is real, both states (5.19) satisfy the equation

$$(H_\alpha^U - E_a)|a_U^\pm\rangle = 0. \quad (5.20)$$

A common example of a distorting potential is the Coulomb potential, in which case the distorted channel wave functions are the Coulomb wave functions. In the distorted-wave method to be discussed in Section 5.4.2 we shall use *complex* optical potentials as distorting potentials; in this case the two types of scattering states *do not* satisfy the same Schrödinger equation (cf. eqns (5.138) and (5.139)). In the following we shall always consider *free* channels for simplicity. The extension to distorted channels is immediate.

### The *Q*-value

In a general reaction the system in the entrance channel  $a$  makes a transition to the exit channel  $b$ . The total energy in the entrance channel is  $E_a$  and in the exit channel,  $E_b$ . Since energy is conserved, we have

$$E_a = E_b \quad (5.21)$$

or

$$\mathcal{E}_a + \epsilon_a = \mathcal{E}_b + \epsilon_b. \quad (5.22)$$

Except in elastic scattering, the internal energies are not the same in the entrance and exit channels; their difference is called the *Q-value* of the reaction (cf. Blatt and Weisskopf 1952, Chapter VIII),

$$Q_{a \rightarrow b} = \epsilon_a - \epsilon_b. \quad (5.23)$$

Using eqn (5.22), we can also write the *Q-value in terms of the channel energies*,

$$Q_{a \rightarrow b} = \mathcal{E}_b - \mathcal{E}_a. \quad (5.24)$$

In a reaction with positive *Q*-value the kinetic energy in the final channel is higher than in the initial channel; speaking in thermochemical terms, the reaction ‘produces heat’ and is therefore called *exothermic*,  $Q_{a \rightarrow b} > 0$ . In the opposite case it is *endothermic*,  $Q_{a \rightarrow b} < 0$ .

### 5.2.2 Reaction states

The total Hamiltonian  $H$  of the system is

$$H = T_\alpha + h_\alpha + V_\alpha = H_\alpha + V_\alpha, \quad (5.25)$$

where the internuclear interaction  $V_\alpha$  in the arrangement channel  $\alpha$  is given by

$$V_\alpha = \sum_{i \in x, j \in A} V_{ij}; \quad (5.26)$$

here  $V_{ij}$  is the two-body interaction between nucleon  $i$  in nucleus  $x$  and nucleon  $j$  in nucleus  $A$ . In the coordinate representation we have  $V_{ij} = v(\mathbf{r}_{ij})$ , which is assumed to be of short range. In view of the fact that the internal Hamiltonian  $h_\alpha$  contains the internal kinetic and interaction energies of all the nucleons bound in the fragments  $x$  and  $A$ , it is clear that the two terms on the right-hand side of eqn (5.25) together represent the sum of all the kinetic and two-nucleon interaction energies of the total system, with the kinetic energy of the centre-of-mass motion omitted, of course.

In eqn (5.25) the total Hamiltonian  $H$  has been decomposed into its free and interacting parts in arrangement channel  $\alpha$ . This can evidently be done in any other arrangement channel  $\beta$  as well. Each such decomposition sums up the same nucleonic operators, only in a different order; we can therefore write

$$H = H_\alpha + V_\alpha = H_\beta + V_\beta. \quad (5.27)$$

In analogy to the potential scattering state  $|\Psi_{\mathbf{k}}(t)\rangle$  of eqn (4.25), the physical time-dependent reaction state  $|\Psi_a(t)\rangle$  is now defined as a solution to the time-dependent many-body Schrödinger equation

$$i\hbar \frac{d}{dt} |\Psi_a(t)\rangle = H |\Psi_a(t)\rangle \quad (5.28)$$

evolving from the free state (5.16) in channel  $a$ , which it equals at large negative times  $t_0 < -t_\infty$ . It is given by the formal solution

$$|\Psi_a(t)\rangle = e^{-\frac{i}{\hbar} H(t-t_0)} |\Phi_a(t_0)\rangle \quad \text{with } t_0 < -t_\infty. \quad (5.29)$$

For  $t = 0$  we have

$$|\Psi_a^+(0)\rangle = e^{\frac{i}{\hbar} H t_0} |\Phi_a(t_0)\rangle \quad \text{with } t_0 < -t_\infty, \quad (5.30)$$

where we have added the label  $+$  to the reaction state vector in order to indicate that it is the physical solution which has developed in a *positive* time direction. This is the analogue of eqn (4.26), where the time-dependence of the wave function  $|\Phi_a(t_0)\rangle$  is now governed by the Hamiltonian  $H_\alpha$  in arrangement channel  $\alpha$  and not by the kinetic energy  $T$ .

The wave packet arguments of Chapter 4 can also be applied in the present instance. If the state  $|\Phi_a(t)\rangle$  describes a normalized free wave packet, then the state  $|\Psi_a^+(t)\rangle$  describes a normalized ‘interacting’ wave packet. Proceeding as in Section 4.2, we again go over to the Abelian limit and introduce the Møller operator (cf. eqn (4.32)) appropriate for the entrance arrangement channel  $\alpha$ ,

$$\Omega_\alpha^{(+)} = \frac{\eta}{\hbar} \int_{-\infty}^0 d\tau e^{\frac{\eta}{\hbar}\tau} e^{\frac{i}{\hbar} H \tau} e^{-\frac{i}{\hbar} H_\alpha \tau}. \quad (5.31)$$

The full, interacting stationary reaction state is then defined by

$$|a^+\rangle = \Omega_\alpha^{(+)} |a\rangle. \quad (5.32)$$

In analogy to eqns (4.42) and (4.43), this reduces to the simple formal expression

$$|a^+\rangle = \frac{i\eta}{E_a - H + i\eta} |a\rangle = |a\rangle + \frac{1}{E_a - H + i\eta} V_\alpha |a\rangle \quad (5.33)$$

in terms of the initial channel state  $|a\rangle$ , the full Hamiltonian  $H$  and the internuclear interaction  $V_\alpha$ .

One can also define the ‘time-reversed’ state

$$|\Psi_a^-(0)\rangle = e^{\frac{i}{\hbar} H t_0} |\Phi_a(t_0)\rangle \quad \text{with } t_0 > t_\infty, \quad (5.34)$$

the ‘time-reversed’ Møller operator

$$\Omega_\alpha^{(-)} = \frac{\eta}{\hbar} \int_0^\infty d\tau e^{-\frac{\eta}{\hbar}\tau} e^{\frac{i}{\hbar} H \tau} e^{-\frac{i}{\hbar} H_\alpha \tau} \quad (5.35)$$

and the ‘time-reversed’ reaction state

$$|a^-\rangle = \Omega_\alpha^{(-)} |a\rangle. \quad (5.36)$$

We then have

$$|a^-\rangle = \frac{-i\eta}{E_a - H - i\eta} |a\rangle = |a\rangle + \frac{1}{E_a - H - i\eta} V_\alpha |a\rangle. \quad (5.37)$$

The stationary reaction states  $|a^\pm\rangle$  satisfy the stationary Schrödinger equation

$$(H - E_a) |a^\pm\rangle = 0; \quad (5.38)$$

we call them *reaction states* for short. The time-dependent scattering states  $|\Psi_a^\pm(t)\rangle$  are given, in analogy to eqn (4.49), by

$$|\Psi_a^\pm(t)\rangle = \int d^3 k'_a A(\mathbf{k}'_a - \mathbf{k}_a) e^{-\frac{i}{\hbar} E'_a t} |a; \mathbf{k}'_a \pm\rangle. \quad (5.39)$$

*The Lippmann–Schwinger equation*

As in Section 4.3.2 we can derive the Lippmann–Schwinger equation

$$|a^\pm\rangle = |a\rangle + \frac{1}{E_a - H_\alpha \pm i\eta} V_\alpha |a^\pm\rangle, \quad (5.40)$$

whose formal solutions  $|a^\pm\rangle$  are given by eqns (5.33) and (5.37), respectively.

*Orthogonality*

We now turn to the orthogonality of the reaction states. We cannot proceed as in Section 4.3.3, where we made use of the orthogonality of the free channel states  $|a\rangle$ , because this orthogonality does not hold for free states belonging to different arrangement channels (cf. eqn (5.15)).

Taking recourse to a different approach, we consider two different time-dependent reaction states  $|\Psi_a^+(t)\rangle$  and  $|\Psi_b^+(t)\rangle$ . Both are solutions of the Schrödinger equation

(5.28), and therefore their scalar product is independent of time,

$$\begin{aligned}\frac{d}{dt}\langle\Psi_b^+(t)|\Psi_a^+(t)\rangle &= \left(\frac{d}{dt}\langle\Psi_b^+(t)|\right)|\Psi_a^+(t)\rangle + \langle\Psi_b^+(t)|\left(\frac{d}{dt}|\Psi_a^+(t)\rangle\right) \\ &= -\frac{1}{i\hbar}\langle\Psi_b^+(t)|(H^\dagger - H)|\Psi_a^+(t)\rangle = 0,\end{aligned}\quad (5.41)$$

since  $H$  is Hermitian,  $H^\dagger = H$ . We thus find

$$\begin{aligned}\langle\Psi_b^+(0)|\Psi_a^+(0)\rangle &= \langle\Psi_b^+(t_0)|\Psi_a^+(t_0)\rangle \\ &= \langle\Phi_b^+(t_0)|\Phi_a^+(t_0)\rangle \text{ for } t_0 < -t_\infty;\end{aligned}\quad (5.42)$$

here we have used eqn (5.29) in the second line.

We first prove that for  $t_0 < -t_\infty$

$$\langle\Phi_b^+(t_0)|\Phi_a^+(t_0)\rangle = \delta_{ba} \int d^3k'_a A^*(\mathbf{k}'_a - \mathbf{k}_b) A(\mathbf{k}'_a - \mathbf{k}_a), \quad (5.43)$$

where  $\delta_{ba}$  is a Kronecker symbol involving the internal states of the nuclei in an arrangement channel:

(i) If the channels  $a$  and  $b$  are in *different* arrangement channels,  $\alpha \neq \beta$ , the two free states  $|\Phi_a^+(t_0)\rangle$  and  $|\Phi_b^+(t_0)\rangle$  have no overlap for  $t_0 < -t_\infty$  because at least one nucleon in a given fragment in channel  $a$  belongs to a *different* fragment in channel  $b$ , and there is no overlap between the fragments in the remote past owing to the finite size of the wave packets; therefore the right-hand side contains a factor  $\delta_{ab}$ , which is equivalent to the factor  $\delta_{ab}$  in the present instance.

(ii) If the channels  $a$  and  $b$  are in the *same* arrangement channel,  $\alpha = \beta$ , the channel states  $|a\rangle$  and  $|b\rangle$  are orthogonal to each other according to the first of eqns (5.15), which we write more explicitly as

$$\langle b; \mathbf{k}'_b | a; \mathbf{k}''_a \rangle = \delta_{ba} \delta(\mathbf{k}'_b - \mathbf{k}''_a), \text{ for } \alpha = \beta; \quad (5.44)$$

computing the scalar product of the states  $|\Phi_a(t_0)\rangle$  and  $|\Phi_b(t_0)\rangle$  in the form (5.16), we arrive at eqn (5.43).

Owing to eqn (5.42) we therefore find from eqn (5.43)

$$\langle\Psi_b^+(0)|\Psi_a^+(0)\rangle = \delta_{ba} \int d^3k'_a A^*(\mathbf{k}'_a - \mathbf{k}_b) A(\mathbf{k}'_a - \mathbf{k}_a). \quad (5.45)$$

Having evaluated the scalar product of the states  $|\Psi_a^+(0)\rangle$  and  $|\Psi_b^+(0)\rangle$  in the form (5.45), we now calculate it *again*, this time using the representation (5.39) in terms of the stationary reaction states,

$$\langle\Psi_b^+(0)|\Psi_a^+(0)\rangle = \iint d^3k'_a d^3k'_b A^*(\mathbf{k}'_b - \mathbf{k}_b) A(\mathbf{k}'_a - \mathbf{k}_a) \langle b; \mathbf{k}'_b | a; \mathbf{k}'_a \rangle. \quad (5.46)$$

The orthogonality relation for the reaction states  $|a; \mathbf{k}'_a\rangle$  and  $|a; \mathbf{k}'_a\rangle$  can now be obtained from a comparison of eqns (5.45) and (5.46). To this end we use the Gaussian form (4.6) of the weight amplitudes  $A(\boldsymbol{\kappa})$ ,

$$A(\boldsymbol{\kappa}) = \left(\frac{2\Delta^2}{\pi}\right)^{3/4} e^{-\Delta^2 \boldsymbol{\kappa}^2}, \quad (5.47)$$

so that eqn (5.45) becomes

$$\begin{aligned}\langle\Psi_b^+(0)|\Psi_a^+(0)\rangle &= \delta_{ba} \left(\frac{2\Delta^2}{\pi}\right)^{3/2} \int d^3k'_a e^{-\Delta^2[(\mathbf{k}'_a - \mathbf{k}_b)^2 + (\mathbf{k}'_a - \mathbf{k}_a)^2]} \\ &= \delta_{ba} \left(\frac{2\Delta^2}{\pi}\right)^{3/2} e^{-\Delta^2(\mathbf{k}_a - \mathbf{k}_b)^2/2} \int d^3k'_a e^{-2\Delta^2[\mathbf{k}'_a - (\mathbf{k}_a + \mathbf{k}_b)/2]^2} \\ &= \delta_{ba} e^{-\Delta^2(\mathbf{k}_a - \mathbf{k}_b)^2/2}.\end{aligned}\quad (5.48)$$

On the other hand, eqn (5.46) takes the form

$$\langle\Psi_b^+(0)|\Psi_a^+(0)\rangle = \left(\frac{2\Delta^2}{\pi}\right)^{3/2} \iint d^3k'_a d^3k'_b e^{-\Delta^2[(\mathbf{k}'_b - \mathbf{k}_b)^2 + (\mathbf{k}'_a - \mathbf{k}_a)^2]} \langle b; \mathbf{k}'_b | a; \mathbf{k}'_a \rangle. \quad (5.49)$$

Expression (5.48) vanishes unless channels  $a$  and  $b$  are identical and the momenta  $\mathbf{k}_a$  and  $\mathbf{k}_b$  are equal within a small bandwidth  $1/\Delta$ . Now, expression (5.49) must behave in the same way. This requires that the scalar product  $\langle b; \mathbf{k}'_b | a; \mathbf{k}'_a \rangle$  contains the factor  $\delta_{ba}$ . Moreover, it must vanish unless the momenta  $\mathbf{k}'_a$  and  $\mathbf{k}'_b$  are equal within a bandwidth at least as small as  $1/\Delta$ . Since this scalar product is independent of  $\Delta$ , its momentum dependence must reduce to a  $\delta$ -function, and we have

$$\langle b; \mathbf{k}'_b | a; \mathbf{k}'_a \rangle = \delta_{ba} \delta(\mathbf{k}'_a - \mathbf{k}'_b). \quad (5.50)$$

Expressions (5.48) and (5.49) then become equal.

The same orthogonality relation holds for the time-reversed states  $|a; \mathbf{k}_a^-\rangle$ , and we can write, therefore,

$$\langle b; \mathbf{k}_b^\pm | a; \mathbf{k}_a^\pm \rangle = \delta_{ba} \delta(\mathbf{k}_a - \mathbf{k}_b) \quad (5.51)$$

or in a more formal manner,

$$\langle b^\pm | a^\pm \rangle = \delta_{ba}, \quad (5.52)$$

where the indices  $a$  and  $b$  now refer to the intrinsic states as well as to the relative motion. Equation (5.52) is the *orthogonality relation* for the reaction states.

Equations (5.41) and (5.48) imply that the time-dependent reaction states  $|\Psi_a^+(t)\rangle$  are orthogonal ‘within the width  $1/\Delta$ ’ for all times  $t$ ,

$$\langle\Psi_b^+(t)|\Psi_a^+(t)\rangle = \delta_{ba} \int d^3k' A^*(\mathbf{k}' - \mathbf{k}_b) A(\mathbf{k}' - \mathbf{k}_a). \quad (5.53)$$

This is *not* in general the case for the *free* states  $|\Phi_a^+(t)\rangle$  and  $|\Phi_b^+(t)\rangle$ : when the channels  $a$  and  $b$  belong to different arrangement channels,  $\alpha \neq \beta$ , these two states are solutions to *different* Hamiltonians  $H_\alpha$  and  $H_\beta$ ; their scalar product is no longer independent of time, and vanishes only for  $t \rightarrow \pm\infty$ . This is the time-dependent corollary of the stationary relations (5.15).

### Completeness

As before, the states  $|c^\pm\rangle$ , which we have restricted to be *two-body* states, form a complete set when all other non-two-body channels, including the ones where the entire system of nucleons is bound and the ones where all nucleons are unbound (and interacting via

$H$ ), are added in. Symbolically, we write

$$\sum_c |c^\pm\rangle\langle c^\pm| + \sum_{\text{non-two-body states}} = 1. \quad (5.54)$$

### 5.2.3 The $T$ - and $S$ -matrices

The  $T$ -matrix

We consider the adjoint of eqn (5.33) for the bra  $\langle b^+|$ ,

$$\langle b^+| = \langle b| + \langle b|V_\beta \frac{1}{E_b - H - i\eta}, \quad (5.55)$$

and multiply from the right by the ket  $|a^+\rangle$ . Using the orthogonality relation (5.52) for the product  $\langle b^+|a^+\rangle$ , we find

$$\langle b|a^+\rangle = \delta_{ba} + \langle b|V_\beta \frac{1}{H - E_b + i\eta}|a^+\rangle. \quad (5.56)$$

Letting the Hamiltonian  $H$  in the denominator operate to the right, it acts on its eigenstate  $|a^+\rangle$  and can be replaced with its eigenvalue  $E_a$ . We then have

$$\langle b|a^+\rangle = \delta_{ba} + \frac{1}{E_a - E_b + i\eta} T_{ba}^+, \quad (5.57)$$

where we have introduced the *post*  $T$ -matrix

$$T_{ba}^+ = \langle b|V_\beta|a^+\rangle. \quad (\text{post}) \quad (5.58)$$

Proceeding as in Section 4.3.4, we also introduce the *prior*  $T$ -matrix

$$T_{ba}^- = \langle b^-|V_\alpha|a\rangle. \quad (\text{prior}) \quad (5.59)$$

The names ‘post’ and ‘prior’ indicate here that in one case the internuclear interaction in the final channel,  $V_\beta$ , appears explicitly in the expression for the  $T$ -matrix while in the other case it is the interaction in the initial channel,  $V_\alpha$ . The internuclear interaction in both  $T$ -matrices occurs in that arrangement channel  $\beta$  or  $\alpha$  which is represented by the free channel state  $b$  or  $a$ , respectively.

As in Section 4.3.4, the post and prior forms are equal on the energy shell  $E_a = E_b$ . This is proved in the same way as in Section 4.3.4, except that now two different internuclear interactions,  $V_\alpha$  and  $V_\beta$ , are in general involved. Consider

$$\begin{aligned} \langle b|V_\beta|a^+\rangle &= \langle b|V_\beta \left(1 + \frac{1}{E_a - H + i\eta} V_\alpha\right)|a\rangle \\ &= \langle b|V_\beta|a\rangle + \langle b|V_\beta \frac{1}{E_a - H + i\eta} V_\alpha|a\rangle. \end{aligned} \quad (5.60)$$

First we show that

$$\langle b|V_\beta|a\rangle = \langle b|V_\alpha|a\rangle. \quad (5.61)$$

### 5.2 The general formalism for two-body channels

This relation is trivially true when the arrangement channel does not change during the reaction,  $\alpha = \beta$ . On the other hand, for  $\alpha \neq \beta$ , we can write

$$\begin{aligned} \langle b|V_\alpha|a\rangle &= \langle b|(H - H_\alpha)|a\rangle \\ &= \langle b|(H_\beta + V_\beta - H_\alpha)|a\rangle \\ &= \langle b|(E_b + V_\beta - E_a)|a\rangle = \langle b|V_\beta|a\rangle \quad \text{for } E_a = E_b. \end{aligned}$$

Here we have used eqn (5.13) and its adjoint, and obtained the eigenvalue  $E_a$  by acting with  $H_\alpha = T_\alpha + h_\alpha$  to the right, and the eigenvalue  $E_b$  by acting with  $H_\beta = T_\beta + h_\beta$  to the left. The last step can be justified by using Green’s theorem in the coordinate representation in the arrangement channel  $\beta$ , where  $T_\beta \propto \nabla_\beta^2$ , and by observing that the surface terms in the integration by parts are equal to zero: this is so because the relative wave function  $\langle \mathbf{r}_\alpha | b \rangle$  (in the  $\alpha$ -arrangement channel representation) of the  $\beta$ -arrangement channel state  $|b\rangle = |b_y\rangle|b_B\rangle|\mathbf{k}_b\rangle$  vanishes for  $|\mathbf{r}_\alpha| \rightarrow \infty$ , since this limit implies that an *internal* coordinate in the wave function of the state  $|b_y\rangle|b_B\rangle$  goes to infinity. Equation (5.61) is thus proved for reactions with and without rearrangement, and eqn (5.60) becomes, for  $E_a = E_b$ ,

$$\begin{aligned} \langle b|V_\beta|a^+\rangle &= \langle b|V_\alpha|a\rangle + \langle b|V_\beta \frac{1}{E_b - H + i\eta} V_\alpha|a\rangle \\ &= \langle b| \left(1 + V_\beta \frac{1}{E_b - H + i\eta}\right) V_\alpha|a\rangle \\ &= \langle b^-|V_\alpha|a\rangle, \end{aligned} \quad (5.62)$$

where we have used the adjoint of eqn (5.37).

Since the post and prior  $T$ -matrices (5.58) and (5.59) are equal on the energy shell, we introduce the common on-shell notation

$$T_{a \rightarrow b} = T_{ba} = T_{ba}^+ = T_{ba}^-. \quad (5.63)$$

Comparing the first line of eqn (5.60) with the second line of eqn (5.62), we see that on the energy shell,  $E = E_a = E_b$ , the  $T$ -matrix can be written in the form

$$T_{a \rightarrow b} = \langle b| \left(V_\beta + V_\beta \frac{1}{E - H + i\eta} V_\alpha\right) |a\rangle \quad (5.64)$$

or

$$T_{a \rightarrow b} = \langle b| \left(V_\alpha + V_\beta \frac{1}{E - H + i\eta} V_\alpha\right) |a\rangle, \quad (5.65)$$

whichever one prefers.

The  $T$ -operator

As in Section 4.3.4, we may introduce the  $T$ -operator acting between the arrangement channels  $\alpha$  and  $\beta$ ,

$$T_{\beta\alpha}(E) = V_\beta + V_\beta \frac{1}{E - H + i\eta} V_\alpha; \quad (5.66)$$

the fully off-energy-shell  $T$ -matrix is then given by (cf. eqn (4.82))

$$T_{ba}(E) = \langle b|T_{\beta\alpha}(E)|a\rangle, \quad (5.67)$$

where all three energies  $E$ ,  $E_a$ , and  $E_b$  are different. The on-shell  $T$ -matrix is

$$T_{a \rightarrow b} = \langle b | T_{\beta\alpha}(E_a) | a \rangle \quad \text{with } E_a = E_b. \quad (5.68)$$

### The $S$ -matrix

Again we define the  $S$ -matrix

$$S_{ba} = \langle b^- | a^+ \rangle. \quad (5.69)$$

Its relation to the  $T$ -matrix is derived in the same way as in Section 4.3.5, and has the form

$$S_{ba} = \delta_{ba} - 2\pi i \delta(E_a - E_b) T_{ba}. \quad (5.70)$$

Following the procedure of Section 4.3.6, we find from the completeness relation (5.54) with the minus signs the unitarity relation

$$\sum_c S_{bc}^\dagger S_{ca} = \delta_{ba}, \quad (5.71)$$

where the sum goes over all channel states except the totally bound one-body state.

In analogy to eqn (4.104) we may further write the  $S$ -matrix (5.69) in terms of the **on-shell  $S$ -matrix**  $S_{ba}$ ,

$$S_{ba} = \frac{\hbar^2}{\sqrt{\mu_\alpha \mu_\beta k_a k_b}} \delta(E_b - E_a) S_{ba}. \quad (5.72)$$

From eqns (5.70) and (5.71) we then obtain the analogue of eqn (4.105),

$$S_{ba} = \delta_{ba} \delta(\Omega_b - \Omega_a) - i \sqrt{\mu_\alpha \mu_\beta k_a k_b} \frac{2\pi}{\hbar^2} T_{ba}, \quad (5.73)$$

and the unitarity relation (cf. eqn (4.113))

$$\sum_c S_{bc}^\dagger S_{ca} = \delta_{ba} \delta(\Omega_b - \Omega_a) \quad \text{with } E_a = E_b = E_c. \quad (5.74)$$

### 5.2.4 The optical theorem

As in Section 4.3.6, we derive an optical theorem for the  $T$ -matrix, using the unitarity relation (5.74) together with eqn (5.73),

$$i(T_{ba} - T_{ba}^\dagger) = \frac{2\pi}{\hbar^2} \sum_c \mu_\gamma k_c \int d\Omega_c T_{bc}^\dagger T_{ca} \quad \text{with } E_a = E_b = E_c; \quad (5.75)$$

here the sum goes over all states except the totally bound one-body state. For  $a = b$  we have, with  $T_{bc}^\dagger = T_{cb}^*$ ,

$$- \text{Im } T_{aa} = \frac{\pi}{\hbar^2} \sum_c \mu_\gamma k_c \int d\Omega_c |T_{ca}|^2 \quad \text{with } E_a = E_b = E_c. \quad (5.76)$$

We isolate in the sum on the right-hand side the terms which represent *elastic* channels relative to channel  $a$ , i.e. all the terms whose set of quantum numbers  $c$  equals the set  $a$  except for the direction  $\Omega_c$  of the outgoing momentum  $\mathbf{k}_c$  relative to the direction of the

ingoing momentum  $\mathbf{k}_a$ ,

$$\begin{aligned} -\text{Im } T_{\{a;\mathbf{k}_a\} \rightarrow \{a;\mathbf{k}_a\}} &= \mu_\alpha k_a \frac{\pi}{\hbar^2} \int d\Omega'_a |T_{\{a;\mathbf{k}'_a\},\{a;\mathbf{k}_a\}}|^2 \\ &+ \frac{\pi}{\hbar^2} \sum_c \mu_\gamma k_c \int d\Omega_c |T_{ca}|^2 \quad (c : \text{all non-elastic channels}). \end{aligned} \quad (5.77)$$

With the help of eqn (4.120) we can write the elastic  $T$ -matrices in eqn (5.77) in terms of the elastic scattering amplitude  $f_{\mathbf{k}_a}^+(\Omega)$ , and find

$$\frac{4\pi}{k_a} \text{Im } f_{\mathbf{k}_a}^+(0) = \int d\Omega' |f_{\mathbf{k}_a}^+(\Omega')|^2 + \sigma_r; \quad (5.78)$$

here  $\Omega$  is the scattering angle, and we have identified the term referring to the non-elastic channels with the reaction cross section  $\sigma_r$ . This is the **generalized form of the optical theorem** (1.76).

### 5.2.5 The cross section

The cross section for a general reaction can be derived in analogy to the potential scattering case. Considering the momentum representation (5.57) of the stationary reaction state, we set in the denominator

$$E_a - E_b + i\eta = \mathcal{E}_a - \mathcal{E}_b + \epsilon_a - \epsilon_b + i\eta = \mathcal{E}_a - \mathcal{E}_b + Q_{a \rightarrow b} + i\eta. \quad (5.79)$$

In the coordinate representation in the arrangement channel  $\beta$ , the asymptotic form of the stationary reaction state is found, in analogy to eqn (4.117), as

$$(b; \mathbf{r}_\beta | a^+) \rightarrow \frac{1}{(2\pi)^{3/2}} \left( e^{i\mathbf{k}_a \cdot \mathbf{r}_\alpha} \delta_{ba} + f_{ba}^+(\hat{\mathbf{r}}_\beta) \frac{e^{i\mathbf{k}_b r_\beta}}{r_\beta} \right) \quad \text{for } r_\beta \rightarrow \infty, \quad (5.80)$$

where the reaction amplitude  $f_{ba}^+(\hat{\mathbf{r}}_\beta)$  is given by

$$f_{ba}^+(\hat{\mathbf{r}}_\beta) = -\mu_\beta \left( \frac{2\pi}{\hbar} \right)^2 T_{a \rightarrow b} \quad (5.81)$$

and

$$k_b = \sqrt{(2\mu_\beta/\hbar^2) \mathcal{E}_b} = \sqrt{(2\mu_\beta/\hbar^2) (\mathcal{E}_a + Q_{a \rightarrow b})}. \quad (5.82)$$

Since the **incident current density is equal to  $v_a$**  and the **outgoing current through a surface element  $r^2 d\Omega$  equal to  $v_b |f_{ba}^+(\hat{\mathbf{r}}_\beta)|^2$** , the **differential reaction cross section as function of the reaction angle  $\Omega_b$  (the angle between the outgoing direction  $\hat{\mathbf{r}}_\beta$  and the incoming beam)** is found to be given by

$$\frac{d\sigma_{a \rightarrow b}}{d\Omega_b} = \frac{v_b}{v_a} |f_{ba}^+(\Omega_b)|^2 \quad (5.83)$$

or, using eqn (5.81),

$$\frac{d\sigma_{a \rightarrow b}}{d\Omega_b} = \left( \frac{2\pi}{\hbar} \right)^4 \mu_\alpha \mu_\beta \frac{k_b}{k_a} |T_{a \rightarrow b}|^2. \quad (5.84)$$

A more explicit form of the angular distribution of the reaction cross section including angular momentum couplings will be derived in Section 5.3.

### 5.2.6 The principle of micro-reversibility

Owing to time reversal invariance, i.e. the fact that the Hamiltonian describing nuclear reactions is the same for processes evolving in a forward or backward time sense, one can derive a relation between the cross sections for a reaction and its reverse,

$$x + A \rightleftharpoons y + B. \quad (5.85)$$

This relation will be the generalization of eqn (4.93) expressing the principle of micro-reversibility for potential scattering.

Reading eqn (5.85) from left to right, we have as initial state the asymptotic free state  $|a\rangle$  with quantum numbers (cf. eqn (5.2); we omit isospin and parity)

$$a = \{\alpha; a_x = \underline{a}_x, I_x, M_x; a_A = \underline{a}_A, I_A, M_A; \mathbf{k}_a\}, \quad (5.86)$$

and similarly for the final state  $|b\rangle$ .

Since under time reversal the momenta and spins reverse their direction, we define the ‘time-reversed state’  $|\tilde{a}\rangle$  as the state with the quantum numbers

$$\tilde{a} = \{\alpha; \tilde{a}_x = \underline{a}_x, I_x, -M_x; \tilde{a}_A = \underline{a}_A, I_A, -M_A; -\mathbf{k}_a\}; \quad (5.87)$$

an analogous definition holds for the final state  $|\tilde{b}\rangle$ .

The time-reversed state  $|\tilde{a}\rangle$  is related to the original state  $|a\rangle$  by the transformation (cf. Messiah 1972, Chapter XV §17, 18)

$$|\tilde{a}\rangle = K|a\rangle, \quad (5.88)$$

where the *time reversal operator*  $K$  is defined in the coordinate representation of the orbital states, and in the standard representation of the spin states where the nucleon spin operators  $s_x$  and  $s_z$  are real and  $s_y$  is imaginary. Its explicit form is

$$K = Y K_0. \quad (5.89)$$

Here the operator

$$Y = e^{-i\pi S_y/\hbar} \text{ with } S_y = \sum s_y \text{ (over all nucleons)} \quad (5.90)$$

reverses the signs of the spin components  $M_x$  and  $M_A$ , and the operator  $K_0$  takes the complex conjugate of the quantity standing to its right. We have  $YK_0 = K_0Y$ ,  $Y^\dagger Y = 1$  and  $K_0^2 = 1$ . The formal expression of time reversal invariance of the Hamiltonian  $H$  is

$$[H, K] = 0. \quad (5.91)$$

Let us now consider the  $T$ -matrix for the transition from the state  $\tilde{b}$  to  $\tilde{a}$ , referring back to eqn (5.64):

$$T_{\tilde{b} \rightarrow \tilde{a}} = T_{\tilde{a}\tilde{b}} = \langle \tilde{a} | \left( V_\alpha + V_\alpha \frac{1}{E - H + i\eta} V_\beta \right) | \tilde{b} \rangle. \quad (5.92)$$

Taking the adjoint of eqn (5.88) we have on the left of the matrix element on the right-hand side

$$\langle \tilde{a} | = \langle a | \overset{\leftarrow}{K}_0 Y^\dagger, \quad (5.93)$$

where the complex conjugation operator  $K_0$  acts to the left. It can be replaced with  $K_0$  operating to the right if afterwards the complex conjugate of the entire matrix element

is taken:

$$\begin{aligned} T_{\tilde{b} \rightarrow \tilde{a}} &= T_{\tilde{a}\tilde{b}} = \langle \tilde{a} | \left( V_\alpha + V_\alpha \frac{1}{E - H + i\eta} V_\beta \right) | \tilde{b} \rangle \\ &= \langle a | \overset{\leftarrow}{K}_0 Y^\dagger \left( V_\alpha + V_\alpha \frac{1}{E - H + i\eta} V_\beta \right) Y K_0 | b \rangle \\ &= \langle a | Y^\dagger K_0 \left( V_\alpha + V_\alpha \frac{1}{E - H + i\eta} V_\beta \right) Y K_0 | b \rangle^* \\ &= \langle a | \left( V_\alpha + V_\alpha \frac{1}{E - H - i\eta} V_\beta \right) Y^\dagger K_0 Y K_0 | b \rangle^* \\ &= \langle a | \left( V_\alpha + V_\alpha \frac{1}{E - H - i\eta} V_\beta \right) | b \rangle^* \\ &= \langle b | \left( V_\beta + V_\beta \frac{1}{E - H + i\eta} V_\alpha \right) | a \rangle = T_{ba} = T_{a \rightarrow b}. \end{aligned} \quad (5.94)$$

In the fourth line we have used eqn (5.91), which also implies  $[V_\alpha, K] = [V_\beta, K] = 0$ . In summary, we have proved the relation of **micro-reversibility for general nuclear reactions**

$$T_{\tilde{b} \rightarrow \tilde{a}} = T_{a \rightarrow b}. \quad (5.95)$$

*The unpolarized differential cross section and the principle of detailed balance*

The unpolarized differential cross section for the reaction  $a \rightarrow b$ , i.e.

$$\{\underline{a}; I_x(M_x); I_A(M_A); \mathbf{k}_a\} \rightarrow \{\underline{b}; I_y(M_y); I_B(M_B); \mathbf{k}_b\},$$

is defined as the cross section (5.84) summed over the final, and averaged over the initial spin projections,

$$\frac{d\sigma_{a \rightarrow b}}{d\Omega_b} = \left( \frac{2\pi}{\hbar} \right)^4 \mu_\alpha \mu_\beta \frac{k_b}{k_a} \frac{1}{(2I_x + 1)(2I_A + 1)} \sum_{M_x M_A} \sum_{M_y M_B} |T_{a \rightarrow b}|^2; \quad (5.96)$$

we do not introduce a special notation for the unpolarized cross section, since it will always be clear whether the spin projections are considered explicitly or summed over.

A similar relation holds for the reverse reaction:

$$\frac{d\sigma_{\tilde{b} \rightarrow \tilde{a}}}{d\Omega_{\tilde{a}}} = \left( \frac{2\pi}{\hbar} \right)^4 \mu_\alpha \mu_\beta \frac{k_a}{k_b} \frac{1}{(2I_y + 1)(2I_B + 1)} \sum_{M_x M_A} \sum_{M_y M_B} |T_{\tilde{b} \rightarrow \tilde{a}}|^2. \quad (5.97)$$

Solving eqns (5.96) and (5.97) for the quantities  $\sum |T|^2$  and setting them equal according to eqn (5.95), we obtain

$$(2I_x + 1)(2I_A + 1) k_a^2 \frac{d\sigma_{a \rightarrow b}}{d\Omega_b} = (2I_y + 1)(2I_B + 1) k_b^2 \frac{d\sigma_{\tilde{b} \rightarrow \tilde{a}}}{d\Omega_{\tilde{a}}}. \quad (5.98)$$

This relation expresses the **principle of detailed balance**. It is a relation between the unpolarized cross sections for a transition  $a \rightarrow b$  and its ‘time reverse’  $\tilde{b} \rightarrow \tilde{a}$ .

### 5.3 The differential reaction cross section

The differential reaction cross section (5.84) is a function of the reaction angle  $\Omega_b$ , which is given by the direction of the outgoing momentum  $\mathbf{k}_b$  in a reference system where the ingoing momentum  $\mathbf{k}_a$  lies in the  $z$ -direction. It is expressed in terms of the  $T$ -matrix  $T_{a \rightarrow b}$ , where the channel state  $|\underline{a}\rangle$  is defined by eqn (5.6) in terms of the individual nuclear spins of the reaction partners and the relative momentum  $\mathbf{k}_a$ ; the definition of the state  $|\underline{b}\rangle$  is analogous. For an explicit evaluation of the angular dependence of the  $T$ -matrix it is convenient to go over to a channel state definition in terms of *angular momenta*, since the  $T$ -matrix is diagonal in the total angular momentum quantum number  $J$  and its projection  $M$  because of the rotational invariance of the full Hamiltonian. We shall do this in the next subsection, following Blatt and Biedenharn (1952).

#### 5.3.1 Spin-coupled channel states

##### Eigenstates of the channel spin

We introduce the *channel spin*  $\mathbf{S}_a$  with projection  $M_a$  as the sum of the spins of the two nuclei  $x, A$  in the channel  $a$ ,

$$\mathbf{S}_a = \mathbf{I}_x + \mathbf{I}_A, \quad M_a = M_x + M_A, \quad (5.99)$$

so that the channel state is now characterized by the quantum numbers  $\{\underline{a}; S_a M_a; \mathbf{k}_a\}$ , where  $\underline{a}$  comprises all quantum numbers of the set  $a$  except  $\{S_a M_a; \mathbf{k}_a\}$ . We then define the channel state

$$|\underline{a}; S_a M_a; \mathbf{k}_a\rangle = |\underline{a}; S_a M_a\rangle |\mathbf{k}_a\rangle, \quad (5.100)$$

which is the product of the plane-wave state  $|\mathbf{k}_a\rangle$  and the internal state

$$|\underline{a}; S_a M_a\rangle = \sum_{M_x M_A} (I_x M_x; I_A M_A | S_a M_a) |\underline{a}; I_x M_x, I_A M_A\rangle, \quad (5.101)$$

where  $(I_x M_x; I_A M_A | S_a M_a)$  is a Clebsch–Gordan coefficient.

##### Eigenstates of the total spin

Introducing the channel energy (5.4) we may further decompose the plane-wave state  $|\mathbf{k}_a\rangle$  into energy and orbital angular momentum states with quantum numbers  $\{\mathcal{E}_a l_a m_a\}$ ,

$$|\mathbf{k}_a\rangle = \sum_{l_a m_a} i^{l_a} Y_{l_a m_a}^*(\hat{\mathbf{k}}_a) |\mathcal{E}_a l_a m_a\rangle, \quad (5.102)$$

where the argument  $\hat{\mathbf{k}}_a$  of the spherical harmonic defines the direction of the momentum  $\mathbf{k}_a$ . The phase term  $i^{l_a}$  has been introduced in order to conform with the notation in eqn (1.21) and that of Blatt and Biedenharn (1952). We can now couple the orbital angular momentum  $\mathbf{l}_a$  and the channel spin  $\mathbf{S}_a$  to the total spin  $\mathbf{J}$ ,

$$\mathbf{J} = \mathbf{l}_a + \mathbf{S}_a, \quad M = m_a + M_a, \quad (5.103)$$

and may thus define another type of channel state in terms of the quantum numbers  $\{\underline{a}; l_a S_a, JM, \mathcal{E}_a\}$ . This state is given in terms of the uncoupled states by the relation

$$|\mathcal{E}_a; l_a S_a; JM\rangle = \sum_{m_a M_a} (l_a m_a; S_a M_a | JM) |\mathcal{E}_a l_a m_a\rangle |\underline{a}; S_a M_a\rangle, \quad (5.104)$$

### 5.3 The differential reaction cross section

whose inverse is

$$|\mathcal{E}_a l_a m_a\rangle |\underline{a}; S_a M_a\rangle = \sum_{JM} (l_a m_a; S_a M_a | JM) |\mathcal{E}_a; l_a S_a; JM\rangle. \quad (5.105)$$

Combining eqns (5.100), (5.102), and (5.105), we obtain

$$\begin{aligned} |\underline{a}; S_a M_a; \mathbf{k}_a\rangle &= |\underline{a}; S_a M_a\rangle \sum_{l_a m_a} i^{l_a} Y_{l_a m_a}^*(\hat{\mathbf{k}}_a) |\mathcal{E}_a l_a m_a\rangle \\ &= \sum_{JM l_a m_a} (l_a m_a; S_a M_a | JM) i^{l_a} Y_{l_a m_a}^*(\hat{\mathbf{k}}_a) |\mathcal{E}_a; l_a S_a; JM\rangle. \end{aligned} \quad (5.106)$$

#### 5.3.2 The spin-coupled scattering matrices

##### The $T$ -matrix

The  $T$ -matrix as we have introduced it in Section 5.2.3 describes the transition between states (5.6) with specified spins and spin projections of the individual collision partners (cf. eqn (5.68)),

$$\begin{aligned} T_{\{\underline{a}; I_x M_x; I_A M_A; \mathbf{k}_a\} \rightarrow \{\underline{b}; I_y M_y; I_B M_B; \mathbf{k}_b\}} \\ = \langle \underline{b}; I_y M_y; I_B M_B; \mathbf{k}_b | T(E_a) | \underline{a}; I_x M_x; I_A M_A; \mathbf{k}_a \rangle. \end{aligned} \quad (5.107)$$

Let us now consider the  $T$ -matrix for the transition between states specified by the *channel spins* and their projections,

$$T_{\{\underline{a}; S_a M_a; \mathbf{k}_a\} \rightarrow \{\underline{b}; S_b M_b; \mathbf{k}_b\}} = \langle \underline{b}; S_b M_b; \mathbf{k}_b | T(E_a) | \underline{a}; S_a M_a; \mathbf{k}_a \rangle. \quad (5.108)$$

We invert eqn (5.101) using the orthogonality properties of the Clebsch–Gordan coefficients, and find that the two  $T$ -matrices are related by the equation

$$\begin{aligned} T_{\{\underline{a}; I_x M_x; I_A M_A; \mathbf{k}_a\} \rightarrow \{\underline{b}; I_y M_y; I_B M_B; \mathbf{k}_b\}} &= \sum_{S_a M_a} \sum_{S_b M_b} (I_x M_x; I_A M_A | S_a M_a) \\ &\times (I_y M_y; I_B M_B | S_b M_b) T_{\{\underline{a}; S_a M_a; \mathbf{k}_a\} \rightarrow \{\underline{b}; S_b M_b; \mathbf{k}_b\}}. \end{aligned} \quad (5.109)$$

We go one step further and introduce similarly the  $T$ -matrix for transitions between the *fully* spin-coupled states (5.104). As a consequence of the rotational invariance of the Hamiltonian  $H$ , this  $T$ -matrix is diagonal in  $J$  and  $M$ , and its diagonal matrix element is independent of  $M$  (from now on we omit the indices  $\mathcal{E}_a$  and  $\mathcal{E}_b$  and include them in the summary indices  $\underline{a}$  and  $\underline{b}$ , respectively),

$$\begin{aligned} T_{\{\underline{a}; l_a S_a; JM\} \rightarrow \{\underline{b}; l_b S_b; J' M'\}} &= \langle \underline{b}; l_b S_b; J' M' | T(E_a) | \underline{a}; l_a S_a; JM \rangle \\ &= T_{\{\underline{a}; l_a S_a\} \rightarrow \{\underline{b}; l_b S_b\}}^J \delta_{JJ'} \delta_{MM'}. \end{aligned} \quad (5.110)$$

Using eqn (5.106), we then obtain the relation

$$\begin{aligned} T_{\{\underline{a}; S_a M_a; \mathbf{k}_a\} \rightarrow \{\underline{b}; S_b M_b; \mathbf{k}_b\}} &= \sum_{JM} \sum_{l_a m_a} \sum_{l_b m_b} (l_a m_a; S_a M_a | JM) i^{l_a} Y_{l_a m_a}^*(\hat{\mathbf{k}}_a) \\ &\times (l_b m_b; S_b M_b | JM) i^{-l_b} Y_{l_b m_b}(\hat{\mathbf{k}}_b) T_{\{\underline{a}; l_a S_a\} \rightarrow \{\underline{b}; l_b S_b\}}^J. \end{aligned} \quad (5.111)$$

**The S-matrix**

In analogy to the on-shell  $S$ -matrix (5.73) defined in terms of the uncoupled states (5.6) we consider now the corresponding fully spin-coupled on-shell  $S$ -matrix, which is found from expression (5.73) by writing

$$\delta(\Omega_b - \Omega_a) = \sum_{LM} Y_{LM}(\hat{\mathbf{k}}_b) Y_{LM}^*(\hat{\mathbf{k}}_a), \quad (5.112)$$

and applying the same transformations as for the  $T$ -matrix,

$$S_{\{\underline{a}; l_a S_a\} \rightarrow \{\underline{b}; l_b S_b\}}^J = \delta_{\underline{b}\underline{a}} \delta_{l_b l_a} \delta_{S_b S_a} - i \sqrt{\mu_\alpha \mu_\beta k_a k_b} \frac{2\pi}{\hbar^2} T_{\{\underline{a}; l_a S_a\} \rightarrow \{\underline{b}; l_b S_b\}}^J. \quad (5.113)$$

For this  $S$ -matrix we have, in analogy to eqn (5.74), the unitarity relation

$$\sum_{\underline{c} \in \mathcal{S}_c} S_{\{\underline{b}; l_b S_b\} \rightarrow \{\underline{c}; l_c S_c\}}^{J^\dagger} S_{\{\underline{c}; l_c S_c\} \rightarrow \{\underline{a}; l_a S_a\}}^J = \delta_{\underline{b}\underline{a}} \delta_{l_b l_a} \delta_{S_b S_a}. \quad (5.114)$$

**5.3.3 The unpolarized differential cross section**

The unpolarized differential cross section for the transition from the physical initial state  $\{\underline{a}; I_x, I_A; \mathbf{k}_a\}$  to the final state  $\{\underline{b}; I_y, I_B; \mathbf{k}_b\}$  is, according to eqn (5.96), given by

$$\begin{aligned} \frac{d\sigma_{\{\underline{a}; I_x I_A\} \rightarrow \{\underline{b}; I_y I_B\}}}{d\Omega_b} &= \left(\frac{2\pi}{\hbar}\right)^4 \mu_\alpha \mu_\beta \frac{k_b}{k_a} \frac{1}{(2I_x + 1)(2I_A + 1)} \\ &\times \sum_{M_x M_A} \sum_{M_y M_B} |T_{\{\underline{a}; I_x M_x; I_A M_A; \mathbf{k}_a\} \rightarrow \{\underline{b}; I_y M_y; I_B M_B; \mathbf{k}_b\}}|^2. \end{aligned} \quad (5.115)$$

Substituting here eqn (5.109) and using the orthogonality properties of the Clebsch–Gordan coefficients, we find

$$\begin{aligned} \frac{d\sigma_{\{\underline{a}; I_x I_A\} \rightarrow \{\underline{b}; I_y I_B\}}}{d\Omega_b} &= \frac{1}{(2I_x + 1)(2I_A + 1)} \\ &\times \sum_{\substack{I_x + I_A \\ S_a = |I_x - I_A|}} \sum_{\substack{I_y + I_B \\ S_b = |I_y - I_B|}} \frac{(2S_a + 1)}{(2S_a + 1)} \frac{d\sigma_{\{\underline{a}; S_a\} \rightarrow \{\underline{b}; S_b\}}}{d\Omega_b}, \end{aligned} \quad (5.116)$$

where we have introduced the unpolarized differential cross section for a transition from channel spin  $S_a$  to channel spin  $S_b$ ,

$$\frac{d\sigma_{\{\underline{a}; S_a\} \rightarrow \{\underline{b}; S_b\}}}{d\Omega_b} = \left(\frac{2\pi}{\hbar}\right)^4 \mu_\alpha \mu_\beta \frac{k_b}{k_a} \frac{1}{2S_a + 1} \sum_{M_a M_b} |T_{\{\underline{a}; S_a M_a; \mathbf{k}_a\} \rightarrow \{\underline{b}; S_b M_b; \mathbf{k}_b\}}|^2. \quad (5.117)$$

Using eqn (5.111), we can now write the cross section (5.117) in terms of the fully spin-coupled  $T$ -matrix (5.110) which does not depend on the directions of the initial or final momenta, so that the angular dependence of the differential cross section is contained exclusively in the spherical harmonics. We choose a reference system whose  $z$ -axis points in the direction of  $\mathbf{k}_a$ , so that  $Y_{l_a m_a}(\Omega_a = 0) = \delta_{m_a 0} \sqrt{(2l_a + 1)/4\pi}$ . We

**5.3 The differential reaction cross section**

then find

$$\begin{aligned} \frac{d\sigma_{\{\underline{a}; S_a\} \rightarrow \{\underline{b}; S_b\}}}{d\Omega_b} &= \frac{1}{2S_a + 1} \mu_\alpha \mu_\beta \frac{k_b}{k_a} \left(\frac{2\pi}{\hbar^2}\right)^2 \\ &\times \sum_{Jl_a l_b} \sum_{J'l'_a l'_b} K(Jl_b l_a; J'l'_b l'_a; S_b S_a; \Omega_b) i^{l_b - l_a - l'_b + l'_a} \\ &\times T_{\{\underline{a}; l_a S_a\} \rightarrow \{\underline{b}; l_b S_b\}}^{J*} T_{\{\underline{a}; l'_a S_a\} \rightarrow \{\underline{b}; l'_b S_b\}}^{J'}, \end{aligned} \quad (5.118)$$

where the coefficient  $K(Jl_b l_a; J'l'_b l'_a; S_b S_a; \Omega_b)$  is a purely geometrical quantity involving only angular momentum quantum numbers,

$$\begin{aligned} K(Jl_b l_a; J'l'_b l'_a; S_b S_a; \Omega_b) &= \pi \sqrt{(2l_a + 1)(2l'_a + 1)} \\ &\times \sum_{MM'} \sum_{M_a M_b} \sum_{mbm'_b} (l_a 0; S_a M_a | JM)(l'_a 0; S_a M_a | J'M') \\ &\times (l_b m_b; S_b M_b | JM)(l'_b m'_b; S_b M_b | J'M') Y_{l_b m_b}^*(\Omega_b) Y_{l'_b m'_b}(\Omega_b). \end{aligned} \quad (5.119)$$

For the further reduction of the spin couplings of the cross section formula (5.118) we refer to Blatt and Biedenharn (1952) (as corrected by Huby 1954), and write down the final result for the *unpolarized differential reaction cross section*,

$$\frac{d\sigma_{\{\underline{a}; S_a\} \rightarrow \{\underline{b}; S_b\}}}{d\Omega_b} = \frac{1}{k_a^2} \frac{1}{2S_a + 1} \sum_{L=0}^{\infty} B_L(\underline{b} S_b; \underline{a} S_a) P_L(\cos \theta). \quad (5.120)$$

Here the coefficient  $B_L$  is given by

$$\begin{aligned} B_L(\underline{b} S_b; \underline{a} S_a) &= \frac{1}{4} (-)^{S_b - S_a} \mu_\alpha \mu_\beta k_a k_b \left(\frac{2\pi}{\hbar^2}\right)^2 \sum_{Jl_a l_b} \sum_{J'l'_a l'_b} \tilde{Z}(l_a Jl'_a J', S_a L) \\ &\times \tilde{Z}(l_b Jl'_b J', S_b L) \text{Re} \left[ T_{\{\underline{a}; l_a S_a\} \rightarrow \{\underline{b}; l_b S_b\}}^{J*} T_{\{\underline{a}; l'_a S_a\} \rightarrow \{\underline{b}; l'_b S_b\}}^{J'} \right], \end{aligned} \quad (5.121)$$

or in terms of the on-shell  $S$ -matrix (5.113),

$$\begin{aligned} B_L(\underline{b} S_b; \underline{a} S_a) &= \frac{1}{4} (-)^{S_b - S_a} \sum_{Jl_a l_b} \sum_{J'l'_a l'_b} \tilde{Z}(l_a Jl'_a J', S_a L) \tilde{Z}(l_b Jl'_b J', S_b L) \\ &\times \text{Re} \left[ \left( S_{\{\underline{a}; l_a S_a\} \rightarrow \{\underline{b}; l_b S_b\}}^{J*} - \delta_{\underline{b}\underline{a}} \delta_{l_b l_a} \delta_{S_b S_a} \right) \right. \\ &\left. \times \left( S_{\{\underline{a}; l'_a S_a\} \rightarrow \{\underline{b}; l'_b S_b\}}^{J'} - \delta_{\underline{b}\underline{a}} \delta_{l'_b l'_a} \delta_{S_b S_a} \right) \right]. \end{aligned} \quad (5.122)$$

The  $\tilde{Z}$ -coefficient for the initial state is defined as

$$\begin{aligned} \tilde{Z}(l_a Jl'_a J', S_a L) &= \sqrt{(2l_a + 1)(2l'_a + 1)} \sqrt{(2J + 1)(2J' + 1)} \\ &\times W(l_a Jl'_a J', S_a L) (l_a 0; l'_a 0 | L 0), \end{aligned} \quad (5.123)$$

and similarly for the final state. The quantity  $W(l_a Jl'_a J', S_a L)$  is a Racah coefficient (cf. Edmonds 1957, Section 6.2).

We note that our  $\tilde{Z}$ -coefficient differs from the usual  $Z$ -coefficient used by Blatt and Biedenharn (1952) and elsewhere in the literature by an additional phase,

$$Z(lJl'J', SL) = i^{L-l-l'} \tilde{Z}(lJl'J', SL). \quad (5.124)$$

In the special case of elastic scattering of spinless particles we have  $\underline{a} = \underline{b}$  and  $S_i = 0$  for all  $i$ . Setting  $l_a = l$ ,  $k_a = k$ ,  $T_{\{\underline{a}; l_a\} \rightarrow \{\underline{a}; l_a\}} = T_l$  and using

$$W(l_a J l'_a J', 0L) = (-)^{J+l_a'-L} (2J+1)^{-\frac{1}{2}} (2l_a'+1)^{-\frac{1}{2}} \delta_{l_a J} \delta_{l'_a J'}$$

(cf. Biedenharn *et al.* 1952, eqn (30)), we then find from eqns (5.120), (5.121), and (5.123)

$$\frac{d\sigma}{d\Omega} = \frac{1}{4k^2} \mu^2 k^2 \left( \frac{2\pi}{\hbar^2} \right)^2 \sum_{ll'L} (2l+1)(2l'+1) (l0l'0|L0)^2 T_l^* T_{l'} P_L(\cos\theta). \quad (5.125)$$

This result is identical with eqn (1.41) if account is taken of (cf. Edmonds 1957, eqn (4.6.5))

$$P_l(\cos\theta) P_{l'}(\cos\theta) = \sum_L (l0l'0|L0)^2 P_L(\cos\theta), \quad (5.126)$$

and the identification

$$T_l = \frac{i}{\mu k} \frac{\hbar^2}{2\pi} (S_l - 1) \quad (5.127)$$

is made in accordance with eqn (4.125).

#### The angle-integrated reaction cross section

Integrating the differential cross section (5.120) over angles, using  $\int P_L(\cos\theta)d\Omega = 4\pi \delta_{L0}$ , we obtain the unpolarized integrated reaction cross section

$$\sigma_{\{\underline{a}; S_a\} \rightarrow \{\underline{b}; S_b\}} = \frac{1}{k_a^2} \frac{4\pi}{2S_a + 1} B_0(\underline{b} S_b; \underline{a} S_a). \quad (5.128)$$

In evaluating  $B_0$  with the help of eqns (5.121) and (5.123) we obtain from the Clebsch-Gordan coefficients a factor  $\delta_{l_a l'_a} \delta_{l_b l'_b}$ , therefore  $J = J'$ , and with  $W(l_a J l_a J, S_a 0) = (-)^{S_a + l_a + J} (2J+1)^{-1/2} (2l_a+1)^{-1/2}$  (cf. Edmonds 1957, eqns (6.2.4), (6.2.13), and (6.3.2)) the integrated cross section becomes a sum

$$\sigma_{\{\underline{a}; S_a\} \rightarrow \{\underline{b}; S_b\}} = \frac{1}{2S_a + 1} \sum_J \sum_{l_a=|J-S_a|}^{J+S_a} \sum_{l_b=|J-S_b|}^{J+S_b} \sigma_{\{\underline{a}; l_a S_a\} \rightarrow \{\underline{b}; l_b S_b\}}^J, \quad (5.129)$$

where the separate terms are the *partial reaction cross sections*

$$\sigma_{\{\underline{a}; l_a S_a\} \rightarrow \{\underline{b}; l_b S_b\}}^J = \pi \mu_\alpha \mu_\beta \frac{k_b}{k_a} \left( \frac{2\pi}{\hbar^2} \right)^2 (2J+1) |T_{\{\underline{a}; l_a S_a\} \rightarrow \{\underline{b}; l_b S_b\}}^J|^2; \quad (5.130)$$

these are defined as the cross sections for the transition  $\{\underline{a}; l_a S_a\} \rightarrow \{\underline{b}; l_b S_b\}$  with the whole system in a state with total angular momentum  $J$ .

#### The principle of detailed balance for total angular momentum $J$

The  $T$ -matrices appearing in the cross section (5.130) obey the principle of micro-reversibility, and in analogy to Section 5.2.6 we arrive at the principle of detailed balance for the cross sections in a state with total angular momentum  $J$ ,

$$k_a^2 \sigma_{\{\underline{a}; l_a S_a\} \rightarrow \{\underline{b}; l_b S_b\}}^J = k_b^2 \sigma_{\{\underline{b}; l_b S_b\} \rightarrow \{\underline{a}; l_a S_a\}}^J. \quad (5.131)$$

In this equation the sets of quantum numbers  $\underline{a}$  and  $\underline{b}$  contain no spin projections nor the direction of the relative momentum; therefore (cf. eqns (5.86) and (5.87)) they remain unchanged under time reversal, and we may omit the tilde denoting the time-reversed quantum numbers.

## 5.4 Single-step approximations

In order to calculate the  $T$ -matrix exactly one would have to solve the many-nucleon Schrödinger equation (5.38). Since this is impossible, one must resort to approximations. In the following we discuss the plane-wave Born approximation (PWBA) and the distorted-wave Born approximation (DWBA) for inelastic scattering and transfer. In these approximations the process is assumed to proceed in a *single step* from the initial to the final state.

### 5.4.1 The plane-wave Born approximation (PWBA)

The simplest and most radical approximation consists in replacing the full reaction state  $|a^+\rangle$  in the  $T$ -matrix (5.58) with the free state  $|a\rangle$ . This is the Born approximation; it is here called plane-wave Born approximation (PWBA) in order to distinguish it from its modified form, the distorted-wave Born approximation to be discussed in the next subsection. In PWBA we thus have

$$T_{ba}^{\text{PWBA}} = \langle b | V_\beta | a \rangle, \quad (\text{post}) \quad (5.132)$$

which can be interpreted as describing the simple one-step mechanism where the system makes a direct transition from the entrance channel  $a$  to the exit channel  $b$  with the interaction potential  $V_\beta$  acting only once.

We can also take eqn (5.59) as our starting point, as long as we are on the energy shell,  $E_a = E_b$ ; replacing  $\langle b^- |$  with  $\langle b |$  we find

$$T_{ba}^{\text{PWBA}} = \langle b | V_\alpha | a \rangle. \quad (\text{prior}) \quad (5.133)$$

Equations (5.132) and (5.133) are the post and prior forms of the  $T$ -matrix in PWBA. The equality of the post and prior forms has already been proved for the exact  $T$ -matrices. In PWBA both forms are also equal as is seen from eqn (5.61).

As an example for the application of the PWBA we discuss the (d,p) reaction in Chapter 7.

### 5.4.2 The distorted-wave Born approximation (DWBA)

The PWBA can be improved considerably by taking approximate account of the elastic scattering in the entrance and exit channels. For this purpose we add a *single-particle* distorting potential  $U_\beta(\mathbf{r}_\beta)$  in the exit channel  $\beta$ , thus introducing a distorting Hamiltonian

in that channel,

$$H_\beta^U = T_\beta + h_\beta + U_\beta; \quad (5.134)$$

we thus work in the distorted-channel space introduced in Section 5.2.1. The total Hamiltonian (5.27) is then written in the form

$$H = H_\beta^U + W_\beta, \quad (5.135)$$

where

$$W_\beta = V_\beta - U_\beta \quad (5.136)$$

is the *residual interaction*, in which the distorting potential is subtracted from the full interaction.

The stationary eigenstates of the Hamiltonian  $H_\beta^U$  are denoted by  $|b^{U+}\rangle$ . We allow the distorting potential  $U_\beta$  to be non-Hermitian, since we want it to describe the elastic scattering in channel  $b$  as realistically as possible, i.e. we take it to represent a complex *optical potential*. The time-reversed state  $|b^{U-}\rangle$  must then be defined as an eigenstate of the Hamiltonian

$$\tilde{H}_\beta^U = T_\beta + h_\beta + U_\beta^\dagger, \quad (5.137)$$

where  $U_\beta^\dagger$  is the Hermitian conjugate of  $U_\beta$ . We therefore have

$$H_\beta^U |b^{U+}\rangle = E_b |b^{U+}\rangle \quad (5.138)$$

and

$$\tilde{H}_\beta^U |b^{U-}\rangle = E_b |b^{U-}\rangle, \quad (5.139)$$

or taking the adjoint

$$\langle b^{U-} | H_\beta^U = \langle b^{U-} | E_b, \quad (5.140)$$

where the operator  $H_\beta^U$  acts to the left.

The formal solutions of eqns (5.138) and (5.139) are, in analogy to eqns (4.43) and (4.46),

$$|b^{U+}\rangle = |b\rangle + \frac{1}{E_b - H_\beta^U + i\eta} U_\beta |b\rangle, \quad (5.141)$$

$$|b^{U-}\rangle = |b\rangle + \frac{1}{E_b - \tilde{H}_\beta^U - i\eta} U_\beta^\dagger |b\rangle. \quad (5.142)$$

We can in turn express the full time-reversed reaction state  $|b^{-}\rangle$  in terms of the distorted state (5.142),

$$|b^{-}\rangle = |b^{U-}\rangle + \frac{1}{E_b - H - i\eta} W_\beta^\dagger |b^{U-}\rangle. \quad (5.143)$$

We now consider the prior form of the  $T$ -matrix on the energy shell (5.59) and transform it in the following way,

$$\begin{aligned} T_{ba} &= \langle b^{-} | V_\alpha | a \rangle = \langle b^{U-} | \left( 1 + W_\beta \frac{1}{E_b - H + i\eta} \right) V_\alpha | a \rangle \\ &= \langle b^{U-} | V_\alpha | a \rangle + \langle b^{U-} | W_\beta \frac{1}{E_b - H + i\eta} V_\alpha | a \rangle \\ &= \langle b^{U-} | V_\alpha | a \rangle + \langle b^{U-} | W_\beta (|a^{+}\rangle - |a\rangle), \end{aligned}$$

where we have used the adjoint of eqn (5.143) in the first line and eqn (5.33) in the last line, setting  $E_a = E_b$ . We thus obtain

$$T_{ba} = \langle b^{U-} | (V_\alpha - W_\beta) | a \rangle + \langle b^{U-} | W_\beta | a^{+} \rangle. \quad (5.144)$$

The first term on the right-hand side of eqn (5.144) vanishes if  $a$  and  $b$  are in different arrangement channels,  $\alpha \neq \beta$ . This is seen in the following way. We write

$$\begin{aligned} \langle b^{U-} | (V_\alpha - W_\beta) | a \rangle &= \langle b^{U-} | [(H - H_\alpha) - (H - H_\beta^U)] | a \rangle \\ &= -\langle b^{U-} | H_\alpha | a \rangle + \langle b^{U-} | H_\beta^U | a \rangle \\ &= \langle b^{U-} | (-E_a + E_b) | a \rangle = 0 \text{ for } E_a = E_b, \end{aligned}$$

where in the last line we have applied eqns (5.13) and (5.140) (cf. also Section 5.2.3). On the other hand, for transitions without rearrangement,  $\alpha = \beta$ , the first term of eqn (5.144) becomes simply  $\langle b^{U-} | U_\beta | a \rangle$ . In both cases we thus arrive at the formula

$$T_{ba} = \langle b^{U-} | U_\beta | a \rangle \delta_{\beta\alpha} + \langle b^{U-} | W_\beta | a^{+} \rangle. \quad (5.145)$$

Relation (5.145) is the so-called two-potential formula of Gell-Mann and Goldberger, generalized to the case of rearrangement reactions (cf. Goldberger and Watson 1964). If the distorting potential  $U_\beta$  is set equal to the Coulomb potential, the decomposition of the full Hamiltonian is the same as in Coulomb-plus-nuclear potential scattering (cf. Section 1.3.2). The first term of eqn (5.145) is then the Coulomb amplitude written in the prior form, and the second term is the nuclear part involving as residual interaction  $W_\beta$  the nuclear potential  $V_N$ .

In the *distorted-wave Born approximation (DWBA)* it is assumed that the residual interaction  $W_\beta$  is so small that it does not affect appreciably the full reaction state  $|a^{+}\rangle$ . The latter can then be replaced with the distorted wave state  $|a^{U+}\rangle$

$$T_{ba}^{\text{DWBA}} = \langle b^{U-} | U_\beta | a \rangle \delta_{\beta\alpha} + \langle b^{U-} | W_\beta | a^{U+} \rangle. \quad (\text{post}) \quad (5.146)$$

This is the post form of the DWBA  $T$ -matrix. We note without proof that it is equal to its prior form

$$T_{ba}^{\text{DWBA}} = \langle b | U_\alpha | a^{U+} \rangle \delta_{\beta\alpha} + \langle b^{U-} | W_\alpha | a^{U+} \rangle \quad (\text{prior}) \quad (5.147)$$

on the energy shell,  $E_a = E_b$ .

Examples for the application of the DWBA are discussed in Chapter 7.

## 5.5 Coupled channels

In PWBA the  $T$ -matrix for the transition from channel  $a$  to channel  $b$  is calculated with complete disregard for the existence of any other than the entrance and exit channels. Moreover, the relative motion in these two channels is described by plane waves, that is, the nuclei do not even scatter elastically before or after the *single-step* transition from state  $a$  to state  $b$  is made. The latter shortcoming is remedied in the DWBA, where elastic scattering in the entrance and exit channels is introduced via the replacement of the plane waves with distorted waves generated by phenomenological optical potentials. One could

then proceed to a two-step mechanism by introducing the second Born approximation, either with plane or with distorted waves, and so on, but this becomes rather cumbersome, and there is generally no guarantee of convergence.

However, in the special case of *inelastic scattering*, where no net rearrangement occurs, and when, moreover, the indirect effect of rearrangement channels can be neglected, a calculation of the  $T$ -matrix to all orders in the inelastic interaction is possible by the method of *coupled channels*.

The coupled-channel method for the inelastic channels can be combined with the single-step approximation for rearrangement transitions in the *coupled-channel Born approximation* (CCBA), which improves on the DWBA  $T$ -matrix by replacing the phenomenological distorted-wave states with reaction states calculated by the coupled-channel method. Finally, in the *coupled reaction channel approximation* (CRC) one approximately treats rearrangement channels to better than Born approximation.

### 5.5.1 The coupled-channel formalism for inelastic scattering

We consider a *single* arrangement channel  $\alpha = (x, A)$ , so that we may write all operators without this index. We select  $N$  channels with *internal* states  $|b\rangle = |b_x\rangle|b_A\rangle$  in the notation of eqn (5.7). In this restricted space of channels we define a reaction state which we denote by  $|a^+(\text{inel})\rangle$  since it can describe no more than *inelastic* transitions; we call it the *inelastic scattering state*. It is labelled by the index  $a$  which denotes the elastic channel, i.e. the channel which contains the incident wave.

The reaction state  $|a^+(\text{inel})\rangle$  satisfies the full Schrödinger equation (5.38) only in the  $N$ -channel space, i.e. only projected on the  $N$  channels  $|b\rangle$  in this space,

$$\langle b|(H - E)|a^+(\text{inel})\rangle = 0 \quad \text{for } b = 1, \dots, N. \quad (5.148)$$

Here  $H = T + h + V$ , where  $T = -\hbar^2\nabla^2/2\mu$  is the kinetic energy of the relative motion,  $h$  is the Hamiltonian of the internal states, and

$$V = \sum_{i \in x, j \in A} V_{ij} = \sum_{i \in x, j \in A} v(\mathbf{r}_i, \mathbf{r}_j) = V(\mathbf{r}; \xi) \quad (5.149)$$

is the interaction between the scattering partners. In the last equation we have written the nucleon coordinates in terms of the relative coordinate  $\mathbf{r}$  between the nuclei and the internal variables  $\xi$ . The state  $|a^+(\text{inel})\rangle$  contains only  $N$  (usually the lowest) internal states of the nuclei  $x$  and  $A$  denoted summarily by  $|b\rangle$ , which satisfy the orthonormality relation  $\langle b|c\rangle = \delta_{bc}$ .

In the coordinate representation the internal states have the wave functions

$$\phi_b(\xi) = \langle \xi | b \rangle, \quad (5.150)$$

which satisfy the internal Schrödinger equation

$$h\phi_b(\xi) = \epsilon_b \phi_b(\xi) \quad (5.151)$$

and the orthogonality relation

$$\int d\xi \phi_b^*(\xi) \phi_c(\xi) = \delta_{bc}. \quad (5.152)$$

For the scattering states we have

$$\psi_a^{(+)\text{inel}}(\mathbf{r}, \xi) = \langle \mathbf{r}, \xi | a^+(\text{inel}) \rangle = \sum_{b=1}^N \psi_{ab}^{(+)}(\mathbf{r}) \phi_b(\xi), \quad (5.153)$$

where the *channel wave function*

$$\psi_{ab}^{(+)}(\mathbf{r}) = \int d\xi \phi_b^*(\xi) \psi_a^{(+)\text{inel}}(\mathbf{r}, \xi) \quad (5.154)$$

describes the relative motion in channel  $b$ . The label  $a$  indicates the particular channel which includes the incident wave. As a rule this is the ground-state channel, where both collision partners are in their internal ground states.

In the coordinate representation the equations (5.148) take the form

$$\int d\xi \phi_b^*(\xi) \left( -\frac{\hbar^2}{2\mu} \nabla^2 + h(\xi) + V(\mathbf{r}, \xi) - E \right) \sum_{c=1}^N \psi_{ac}^{(+)}(\mathbf{r}) \phi_c(\xi) = 0 \\ \text{for } b = 1, \dots, N. \quad (5.155)$$

Using eqn (5.151) and the orthogonality relation (5.152), we obtain

$$\left( -\frac{\hbar^2}{2\mu} \nabla^2 + V_{bb}(\mathbf{r}) - \mathcal{E}_b \right) \psi_{ab}^{(+)}(\mathbf{r}) = - \sum_{c(c \neq b)} V_{bc}(\mathbf{r}) \psi_{ac}^{(+)}(\mathbf{r}), \quad (5.156)$$

where

$$\mathcal{E}_b = E - \epsilon_b \quad (5.157)$$

is the channel energy in channel  $b$ . The channels are coupled via the channel coupling matrix

$$V_{bc}(\mathbf{r}) = \int d\xi \phi_b^*(\xi) V(\mathbf{r}; \xi) \phi_c(\xi). \quad (5.158)$$

The system of coupled equations (5.156) is to be solved for the  $N$ -channel wave functions  $\psi_{ab}^{(+)}(\mathbf{r})$  with the boundary condition that all channel wave functions contain only outgoing waves except the entrance channel wave function  $\psi_{aa}^{(+)}(\mathbf{r})$ , which includes an ingoing wave normalized to the ingoing current density  $v_a = \sqrt{2\mathcal{E}_a/\mu}$ . The wave function (5.153) calculated in this manner can then be substituted in the expression (5.58) for the  $T$ -matrix, which determines the transition amplitude for the transition from the entrance channel  $a$  to the exit channel  $b$ . The cross section is given by eqn (5.84).

However, the practical way of calculating the elastic and inelastic cross sections is the one suggested by the procedure of Section 5.2.5. One calculates the channel wave functions  $\psi_{ab}^{(+)}(\mathbf{r})$  from eqns (5.156) and considers their asymptotic behaviour, which is similar to that given in eqn (5.80), generalized to include the Coulomb interaction (cf. eqn (1.118)),

$$\psi_{ab}^{(+)} \rightarrow \psi_C(\eta_a, k_a; \mathbf{r}) \delta_{ab} + f_{ba}^+(\Omega) \frac{e^{i[k_b r - \eta_b \ln(2k_b r)]}}{r} \\ \text{for } r \rightarrow \infty, \quad b = 1, \dots, N, \quad (5.159)$$

where  $\psi_C(\eta_a, k_a; \mathbf{r})$  is the Coulomb wave function, and the outgoing spherical wave is Coulomb-distorted. The differential cross sections for the elastic ( $b = a$ ) and the inelastic scattering ( $b \neq a$ ) are then given by (cf. eqn (5.83))

$$\frac{d\sigma_{a \rightarrow b}}{d\Omega} = \frac{k_b}{k_a} |f_{ba}^+(\Omega)|^2. \quad (5.160)$$

A detailed discussion of the coupled-channel approach to inelastic scattering is deferred to Chapter 8; there we shall also compare the results of calculations with experimental cross sections.

### 5.5.2 The coupled-channel Born approximation (CCBA)

The coupled-channel formalism can be combined with the DWBA to improve the accuracy of the DWBA  $T$ -matrix (cf. Tamura 1974). To this end we go back to Section 5.4.2 and replace the distorting potential  $U_\beta$  appearing in the DWBA  $T$ -matrix of eqn (5.146) with the true internuclear interaction  $V_\beta$  projected on  $N$  selected channels in the arrangement channel  $\beta$ ,

$$\mathcal{U}_\beta = P_\beta V_\beta P_\beta, \quad (5.161)$$

where

$$P_\beta = \sum_{b'=1}^N |\beta; b'\rangle \langle \beta; b'| \quad (5.162)$$

is a projection operator in the final arrangement channel  $\beta$ . In the space projected out by this operator the final channel  $|\beta; b\rangle$  couples inelastically to the other  $N - 1$  channels  $|\beta; b'\rangle$ .

The final state  $|b^{U^-}\rangle$  in eqn (5.146) is now replaced with the adjoint of the state vector  $|b^-(\text{inel})\rangle$ . In the coordinate representation for the relative motion of the two nuclei this vector has a form analogous to expression (5.153),

$$\langle \mathbf{r}_\beta, \xi | b^-(\text{inel}) \rangle = \sum_{b'=1}^N \psi_{bb'}^{(-)}(\mathbf{r}_\beta) \phi_{b'}(\xi), \quad (5.163)$$

where the label  $b$  denotes the exit channel which contains a plane wave, the waves in the other channels being purely ingoing.

The vector  $|b^-(\text{inel})\rangle$  satisfies the Schrödinger equation

$$(T_\beta + h_\beta + \mathcal{U}_\beta - E_b) |b^-(\text{inel})\rangle = 0 \quad (5.164)$$

in the space of  $N$  channels. The term  $\mathcal{U}_\beta$  is a Hermitian  $N \times N$  matrix in this space. Written out explicitly in the coordinate representation, the equation (5.164) has the coupled-channel form (5.156).

The asymptotic form of the solution is given, in analogy to eqn (5.159),

$$\psi_{bb'}^{(-)}(\mathbf{r}) \rightarrow \psi_C(\eta_b, k_b; \mathbf{r}) \delta_{bb'} + f_{bb'}^{(-)}(\Omega) \frac{e^{-i[k_b'r - \eta_{b'} \ln(2k_b'r)]}}{r}$$

for  $r \rightarrow \infty$ ,  $b' = 1, \dots, N$ . (5.165)

Introducing now an interaction  $\mathcal{U}_\alpha$  in the entrance arrangement channel  $\alpha \neq \beta$  and replacing the vector  $|a^{U^+}\rangle$  with the vector  $|a^+(\text{inel})\rangle$ , we can generalize the DWBA

amplitude (5.146) to the following expression for a rearrangement process  $a \rightarrow b$  (e.g. nucleon transfer):

$$T_{ba}^{\text{CCBA}} = \langle b^-(\text{inel}) | W_\beta | a^+(\text{inel}) \rangle. \quad (5.166)$$

The state  $|a^+(\text{inel})\rangle$  is an  $N$ -component vector in the space of channels  $|\alpha; n\rangle$  in the arrangement channel  $\alpha$ ; if we replace it with the single state  $|a^{U^+}\rangle$ , and similarly  $\langle b^-(\text{inel}) |$  with  $\langle b^{U^-} |$ , we recover the form (5.146) of the DWBA amplitude for  $\alpha \neq \beta$ .

Results of CCBA calculations will be given in Chapter 8.

### 5.5.3 Coupled reaction channels

An approximate way of treating rearrangement reactions in better than Born approximation is provided by the method of *coupled reaction channels*, which should more appropriately be called the method of *coupled arrangement channels*. To keep the discussion as simple as possible we consider only the case of two channels (cf. Low 1976), which is illustrated schematically in Fig. 5.1.

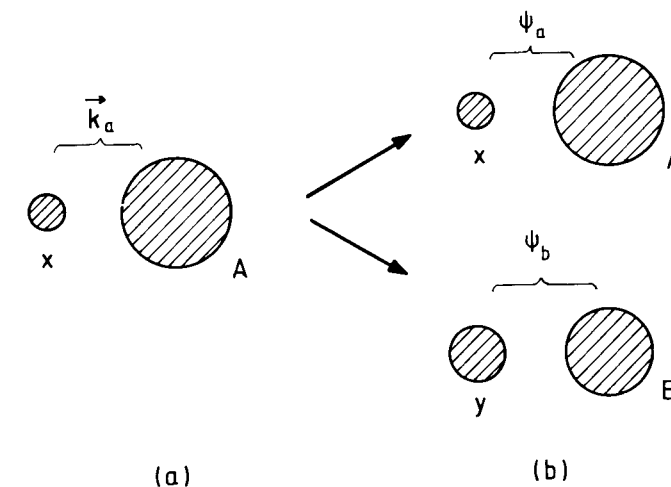


Figure 5.1 The two-channel case of the CRC theory.

We assume that the entire state vector  $|a^+\rangle$  consists of only two component parts, one in the entrance arrangement channel  $\alpha$  with the internal state in the ground state,  $|\alpha; 0\rangle$ , and another, which is not orthogonal to the first part, in the exit arrangement channel  $\beta$  in some internal state  $|\beta; b\rangle$ .

$$|a^+\rangle = \psi_\alpha |\alpha; 0\rangle + \psi_\beta |\beta; b\rangle. \quad (5.167)$$

Here the states describing the relative motion in the two different arrangement channels are written as wave functions in some unspecified representation,  $\psi_\alpha$  and  $\psi_\beta$ .

Again, since the state (5.167) is defined in the space of only two channels, it cannot satisfy the full Schrödinger equation (5.38). But we may require this for the Schrödinger

equation projected on these two channel states, which for brevity we denote by

$$|a\rangle = |\alpha; 0\rangle \text{ and } |b\rangle = |\beta; b\rangle. \quad (5.168)$$

We then obtain

$$\begin{aligned} \langle a|(H - E)|a^+\rangle &= 0, \\ \langle b|(H - E)|a^+\rangle &= 0, \end{aligned} \quad (5.169)$$

or

$$\begin{aligned} \langle a|(H - E)|a\rangle\psi_a + \langle a|(H - E)|b\rangle\psi_b &= 0, \\ \langle b|(H - E)|a\rangle\psi_a + \langle b|(H - E)|b\rangle\psi_b &= 0. \end{aligned} \quad (5.170)$$

The Hamiltonian can be decomposed in two ways (cf. eqn (5.27)),

$$H = h_\alpha + T_\alpha + V_\alpha = h_\beta + T_\beta + V_\beta, \quad (5.171)$$

where the internal Hamiltonians  $h_\alpha$  and the channel interactions  $V_\alpha$  are defined in Sections 5.2.1 and 5.2.2. Employing this decomposition appropriately we can rewrite eqns (5.170), using eqns (5.12) and (5.157), as

$$\begin{aligned} \langle a|(T_\alpha + V_\alpha - \mathcal{E}_a)|a\rangle\psi_a &= -\langle a|(T_\beta + V_\beta - \mathcal{E}_b)|b\rangle\psi_b, \\ \langle b|(T_\alpha + V_\alpha - \mathcal{E}_a)|a\rangle\psi_a &= -\langle b|(T_\beta + V_\beta - \mathcal{E}_b)|b\rangle\psi_b. \end{aligned} \quad (5.172)$$

As in the DWBA, we now introduce distorting potentials  $U_\alpha(\mathbf{r}_\alpha)$  and  $U_\beta(\mathbf{r}_\beta)$  in the arrangement channels  $\alpha$  and  $\beta$ ; their function is to replace as best they can the many-body interactions  $V_\alpha$  and  $V_\beta$ . To achieve this we choose the distorting potentials in the form

$$U_\alpha = \langle a|V_\alpha|a\rangle \text{ and } U_\beta = \langle b|V_\beta|b\rangle. \quad (5.173)$$

Equations (5.172) then become, adding and subtracting  $U_\alpha$  or  $U_\beta$  in the parentheses on the right-hand sides,

$$(T_\alpha + U_\alpha - \mathcal{E}_a)\psi_a = -\langle a|(V_\beta - U_\beta)|b\rangle\psi_b - \langle a|b\rangle(T_\beta + U_\beta - \mathcal{E}_b)\psi_b, \quad (5.174)$$

$$(T_\beta + U_\beta - \mathcal{E}_b)\psi_b = -\langle b|(V_\alpha - U_\alpha)|a\rangle\psi_a - \langle b|a\rangle(T_\alpha + U_\alpha - \mathcal{E}_a)\psi_a. \quad (5.175)$$

These are the coupled-reaction-channel equations. From the asymptotic forms of the solutions  $\psi_a$  and  $\psi_b$  the scattering and reaction amplitudes can be determined, and from these the cross sections.

The residual interactions  $V - U$  are the same as they occur in the DWBA description. The most troublesome terms are the ‘non-orthogonality terms’ containing the factor  $\langle a|b\rangle = \langle \alpha; 0|\beta; b\rangle$ . These terms are often simply neglected.

Equations (5.174) and (5.175) yield the DWBA amplitude for the transition  $a \rightarrow b$  if the residual interactions  $W_\alpha = V_\alpha - U_\alpha$  or  $W_\beta = V_\beta - U_\beta$  are taken into account to first order only and if the non-orthogonality terms are discarded. On the right-hand side of eqn (5.175) only the first term then remains; it contains the residual interaction  $W_\alpha$ , and therefore the wave function  $\psi_\alpha$  appearing there is taken in zeroth order in  $W_\beta$ , i.e. it is replaced with the solution of eqn (5.174) with the right-hand side set equal to zero. This last equation is then simply the Schrödinger equation for the distorted wave  $\psi_a^U$ .

Solving now the inhomogeneous equation (5.175) for the function  $\psi_\beta$  and isolating the outgoing wave in its asymptotic form, one finds for the reaction amplitude

$$f_{ba}^+(Q_b) = -\mu_\beta \left( \frac{2\pi}{\hbar^2} \right)^2 \langle b; \psi_b^{(-)} | W_\alpha | a; \psi_a^{(+)} \rangle \quad (5.176)$$

(for details cf. Austern 1970, Section 3.3; there the distorted-wave states have a normalization different from ours, so that an additional factor  $(2\pi)^{-3}$  appears). Recalling eqn (5.81) we see that this result is identical with the DWBA formula (5.146) for  $\alpha \neq \beta$ .

## 5.6 Notes and references

The basic literature for the formal theory of reactions is the same as that quoted in Chapter 4, *viz.* Brenig and Haag (1959), Goldberger and Watson (1964), Rodberg and Thaler (1967), Messiah (1972), Newton (1982) and Joachain (1975).

Various monographs have been written on the single-step approximations and on the coupled-channel method, for example, Tobocman (1961), Austern (1970), Glendenning (1983), and Satchler (1983). In Chapters 7 and 8 we shall make use of some of this material.

An important topic in the theory of nuclear reactions is the effect of the *Pauli principle*. If neutron and proton are treated as the ‘up-’ and ‘down-’ states of a nucleon with isospin  $\frac{1}{2}$ , all nucleons are identical fermions in a description which includes isospin coordinates. The wave functions must therefore be antisymmetric in all nucleons. The technical implementation of the Pauli principle is in general quite cumbersome. We do not discuss this problem here. We remark only that well-known methods of nuclear structure theory exist for the antisymmetrization of those nucleons which form an internal state of the *same bound nucleus*. We do not have to concern ourselves with this aspect since we regard the bound internal states as given entities which are constructed in conformance with the Pauli principle. It is the antisymmetrization between nucleons belonging to different nuclei which causes the complications in nuclear reaction theory. Here we refer to the discussion, for example, in Feshbach (1992, Sections III.5 and VI.2), in Goldberger and Watson (1964, Sections 4.2 to 4.4), or, for direct reactions, in Austern (1970, Sections 3.5, 4.8, and 4.9).

Often the Pauli principle does not affect a particular reaction in a characteristic manner, and this is why the theory of nuclear reactions has been successfully applied in many instances without account of the antisymmetrization of the nucleons in different nuclei. However, there are also some reaction mechanisms where the Pauli principle plays an essential role and can, at the same time, be built into the formalism in a clear and easy manner. One such example is the case of the elastic scattering of identical nuclei discussed in Section 1.4. Another example is provided by reactions of the type  $^{12}\text{C} + ^{13}\text{C} \rightarrow ^{12}\text{C} + ^{13}\text{C}$ , in which the amplitude for the elastic scattering of  $^{12}\text{C}$  by  $^{13}\text{C}$  interferes with the amplitude for the transfer of a neutron from  $^{13}\text{C}$  to  $^{12}\text{C}$ , forming the ground state of  $^{13}\text{C}$  (‘elastic transfer’). Here the Pauli principle for the two nuclei  $^{12}\text{C}$  has to be taken into account, which has been done by v. Oertzen and Bohlen (1975).

## References

- Austern, N. (1970). *Direct nuclear reaction theories*, Wiley, New York.
- Biedenharn, L. C., Blatt, J. M. and Rose, M. E. (1952). *Rev. Mod. Phys.* **24** 249.
- Blatt, J. M. and Biedenharn, L. C. (1952). *Rev. Mod. Phys.* **24** 258.
- Blatt, J. M. and Weisskopf, V. F. (1952). *Theoretical nuclear physics*, Wiley, New York.
- Bohr, A. and Mottelson, B. R. (1969). *Nuclear structure*, vol. I, Benjamin, New York.
- Brenig, W. and Haag, R. (1959). *Fortschritte der Physik* **7** 183; translated in *Quantum scattering theory* (1963), ed. Ross, M., Indiana University Press, Bloomington.
- Edmonds, A. R. (1957). *Angular momentum in quantum mechanics*, Princeton University Press, Princeton.
- Feshbach, H. (1992). *Theoretical nuclear physics: nuclear reactions*, Wiley, New York.
- Glendenning, N. K. (1983). *Direct nuclear reactions*, Academic Press, New York.
- Goldberger, M. L. and Watson, K. M. (1964) *Collision theory*, Wiley, New York.
- Huby, R. (1954). *Proc. Phys. Soc. (London)* **A67** 1103.
- Joachain, C. J. (1975). *Quantum collision theory*, North-Holland, Amsterdam.
- Low, K. S. (1976). *J. de Physique Colloque C5* **37** 15.
- Messiah, A. (1972). *Quantum mechanics*, North-Holland, Amsterdam.
- Newton, R. G. (1982). *Scattering theory of waves and particles*, Springer, Berlin.
- v. Oertzen, W. and Bohlen, H. G. (1975). *Phys. Reports* **19C** 1.
- Rodberg, L. S. and Thaler, R. M. (1967). *Introduction to the quantum theory of scattering*, Academic Press, New York.
- Satchler, R. G. (1983). *Direct nuclear reactions*, Clarendon Press, Oxford.
- Tamura, T. (1974). *Phys. Reports* **14** 59.
- Tobocman, W. (1961). *Theory of direct nuclear reactions*, Oxford University Press, Oxford.

## 6

## THE OPTICAL MODEL

## 6.1 Introduction

In Chapter 1 we introduced the optical potential in order to account for the loss of current in the elastic channel owing to the coupling to non-elastic channels. The treatment there was purely phenomenological. It was based on an analogy with optics, where a complex index of refraction fulfils the function of a scattering potential for light waves in the presence of absorption.

We shall now show that this ‘optical model’ can actually be raised to the status of a formal theory of elastic scattering. In fact, one can derive an operator, the **generalized optical potential (GOP)**, which, when introduced in the place of a potential in the Schrödinger equation for elastic scattering, takes account of the effect of the coupling to all other non-elastic channels. The solution of such a Schrödinger equation is the exact elastic channel state vector, i.e. the projection of the full reaction state vector on the target and projectile ground states. The GOP will turn out to have a simple formal structure, but it is in general very complicated when evaluated explicitly.

A formal expression for the GOP will be derived in Section 6.2. In order to gain some physical insight into this operator, we construct a schematic reaction model for which the GOP has a simple explicit form. From this model we can draw general conclusions about the structure of the GOP.

The elastic scattering amplitude calculated from the GOP generally has a complicated energy dependence, and it is convenient to decompose it into an **energy-averaged part and a fluctuating part**. It will be seen in the schematic model that the **fluctuating part arises from a mechanism in which the scattering system passes through many compound resonances**. Now the optical potential, as it is introduced phenomenologically, is not meant to produce the scattering amplitude in detail. This phenomenological potential, that is the **optical potential in the proper sense**, will be defined as that potential which generates only the **energy-averaged** part of the elastic scattering amplitude. The absolute square of this averaged amplitude defines the **shape-elastic cross section**. The fluctuating, compound part of the elastic scattering amplitude, on the other hand, does not contribute to the ‘optical’ or shape-elastic scattering. Its energy-averaged absolute square yields the **compound-elastic cross section**; it affects the shape-elastic scattering only in the form of absorption, in addition to that caused by the non-elastic couplings. The optical potential in the proper sense and its relation to the GOP will be discussed in detail in Section 6.3.

Both the GOP and the optical potential in the proper sense are non-local in space, i.e. they do not simply multiply the spatial wave function but act on it as integral operators.

Although modern computers are able to handle such operators, one would like to deal with a *local* optical potential which can be interpreted as a local complex index of refraction in the optical sense. It is indeed possible to construct an *equivalent local potential* which produces the same scattering amplitude as the original non-local one. This is the subject of Section 6.4.

Finally, in Section 6.5, we discuss the energy dependence of the optical potential. The latter is shown to be an analytic function in the upper half-plane of the complex energy variable. This can be traced back to the causal nature of the processes giving rise to the energy dependence. The analytic properties of the optical potential as a function of energy imply the existence of a dispersion relation between its real and imaginary parts, which is helpful for the explanation of energy structures in that potential.

## 6.2 The generalized optical potential (GOP)

### 6.2.1 The general form of the GOP operator

We consider the stationary reaction state  $|a^+\rangle$  with an incident plane wave in channel  $a$  of the form  $|a\rangle|\mathbf{k}_a\rangle$ , where  $|a\rangle$  is the product of the ground states of the two collision partners (in this chapter, we use the notation  $|a\rangle$  for the product of the *internal states* of the nuclei). The reaction state  $|a^+\rangle$  has components in many channels other than  $a$ ; these contain asymptotically only outgoing waves. The elastic channel component itself is that in which target and projectile remain in the ground state. It is obtained from the full reaction state by projecting the latter on the combined target-projectile ground state  $|a\rangle$ . To this end we introduce the projection operator

$$P = |a\rangle\langle a|, \quad P^2 = P, \quad (6.1)$$

which projects on the elastic channel space. Then

$$P|a^+\rangle = |a\rangle\langle a|a^+\rangle = |a\rangle|\mathbf{k}_a^+\rangle \quad (6.2)$$

is the elastic channel component of the reaction state. The state  $|\mathbf{k}_a^+\rangle$  describes the relative motion of the collision partners and is to be identified with the state  $|\mathbf{k}^+\rangle$  of eqn (4.41) (there the index  $a$  was omitted since no explicit reference was made to channels other than the elastic one).

The reaction state  $|a^+\rangle$  satisfies the Schrödinger equation (5.38) with the change in notation  $E_a \rightarrow E$ ,

$$(H - E)|a^+\rangle = 0. \quad (6.3)$$

We now obtain an equation for  $P|a^+\rangle$  by introducing the operator  $Q$  which projects on the space complementary to  $P$ , i.e. on all the non-elastic channels,

$$Q = 1 - P, \quad QP = PQ = 0, \quad Q^2 = Q, \quad (6.4)$$

and writing eqn (6.3) in the form

$$(H - E)(P + Q)|a^+\rangle = 0. \quad (6.5)$$

Projecting this equation on the spaces  $P$  and  $Q$ , we find

$$(PHP + PHQ)|a^+\rangle = EP|a^+\rangle, \quad (6.6)$$

$$(QHQ + QHP)|a^+\rangle = EQ|a^+\rangle. \quad (6.7)$$

## 6.2 The generalized optical potential (GOP)

Since  $H = T_\alpha + h_\alpha + V_\alpha$  and  $h_\alpha|a\rangle = \epsilon_a|a\rangle$  we have  $Ph_\alpha = \epsilon_a P$ , and therefore,

$$(T_\alpha + \epsilon_a - E + PV_\alpha P)P|a^+\rangle = -PV_\alpha Q|a^+\rangle, \quad (6.8)$$

$$(QHQ - E)Q|a^+\rangle = -QV_\alpha P|a^+\rangle. \quad (6.9)$$

Observing that the space  $Q$  contains only outgoing solutions, we obtain from eqn (6.9)

$$Q|a^+\rangle = \frac{1}{E + i\eta - QHQ} QV_\alpha P|a^+\rangle, \quad (6.10)$$

where the infinitesimal term  $+i\eta$  produces outgoing waves, as discussed in Section 4.3.2. Substituting the expression (6.10) in eqn (6.8) and multiplying from the left by  $\langle a|$ , we arrive at the following Schrödinger equation for the relative motion of the two fragments in the elastic channel,

$$(T_\alpha + V_\alpha - E_a)|\mathbf{k}_a^+\rangle = 0. \quad (6.11)$$

Here  $E_a = \hbar^2 k_a^2 / 2\mu_\alpha = E - \epsilon_a$  is the channel energy in the elastic channel (which we denoted by  $\mathcal{E}_a$  in eqn (5.4)), and

$$\mathcal{V}_\alpha = \mathcal{V}_\alpha(E) = \langle a|V_\alpha|a\rangle + \langle a|V_\alpha Q \frac{1}{E + i\eta - QHQ} QV_\alpha|a\rangle \quad (6.12)$$

is the *generalized optical potential (GOP)* first derived by Feshbach (1958a).

Using the relation

$$\frac{1}{x + i\eta} = \frac{\mathcal{P}}{x} - i\pi\delta(x), \quad (6.13)$$

where  $\mathcal{P}$  denotes the principal value, we see that the GOP has a Hermitian part ('real part' for short)

$$\text{Re } \mathcal{V}_\alpha = \langle a|V_\alpha|a\rangle + \langle a|V_\alpha Q \frac{\mathcal{P}}{E - QHQ} QV_\alpha|a\rangle \quad (6.14)$$

and a negative anti-Hermitian part ('imaginary part' for short)

$$\text{Im } \mathcal{V}_\alpha = -\pi\langle a|V_\alpha Q\delta(E - QHQ)QV_\alpha|a\rangle. \quad (6.15)$$

The first term in expression (6.12),

$$V_{\text{stat}} = \langle a|V_\alpha|a\rangle, \quad (6.16)$$

is a *static potential in the usual sense*, i.e. it provides a real force field for the motion of the two fragments in the elastic channel  $a$  which is *independent of the dynamical parameters determining the solution and in particular, of the energy  $E$* . The remainder of the GOP takes account of the effect of the non-elastic channels in the space  $Q$ , which are coupled to the elastic channel via the interaction  $QV_\alpha P$ . The excitation of the non-elastic channels is a dynamical process which depends in an essential way on the energy of the elastic channel state. The second, energy-dependent term in expression (6.12) is therefore the *dynamical part of the GOP*.

Some general features of the energy dependence of the GOP can be deduced immediately from the formal expression (6.12). Since the operator  $QHQ$  is Hermitian and therefore has real eigenvalues, the resolvent  $(E + i\eta - QHQ)^{-1}$  in the dynamical part of  $\mathcal{V}_\alpha(E)$  is regular for  $\text{Im } E + \eta \neq 0$ . *The GOP is thus regular in the entire complex*

*E*-plane except along the straight line  $\text{Im } E = -\eta$  just below the real axis, where it may have poles or branch cuts. Defining the physical sheet of the Riemann surface as the one which contains the physical, real values of  $E$ , we see that the GOP is an analytic function of  $E$  of the form

$$\mathcal{V}_\alpha(E) = (a|V_\alpha|a) + (a|V_\alpha Q \frac{1}{E - QHQ} QV_\alpha|a) \text{ for } E \text{ complex}, \quad (6.17)$$

whose physical values at real  $E$  are obtained by approaching the  $E$ -axis from above, i.e. the physical GOP is given by  $\mathcal{V}_\alpha(E) = \mathcal{V}_\alpha(E + i\eta)$  for real  $E$ .

The optical potential  $\mathcal{V}_\alpha(E)$  has physical meaning not only for real energies  $E > 0$  (scattering) but also for  $E < 0$  (bound states), when the Schrödinger equation (6.11) defines an eigenvalue problem yielding the bound eigenstates of the full Hamiltonian  $H$  projected on the space  $P$ .

## 6.2.2 A schematic model: the model space

To gain better insight into the physical nature of the GOP we now consider a simple schematic model in which the salient features of the optical potential are brought out rather clearly. This model is constructed within the framework of the shell-model theory of nuclear reactions (cf. Mahaux and Weidenmüller 1969).

Let us consider a neutron of mass  $m_n$  which impinges on a target nucleus consisting of  $A$  nucleons. We regard the target as infinitely heavy. The target wave function may be antisymmetric in the nucleon coordinates, but for simplicity the incident neutron is treated as distinguishable from the other nucleons. It is labelled by the index 0, while the target nucleons carry the labels  $i = 1, \dots, A$ .

The space of reaction states for the  $(A + 1)$ -nucleon system is spanned by eigenstates of the shell-model Hamiltonian

$$H_S = \sum_{i=0}^A [T(i) + V_S(i)], \quad (6.18)$$

here the potential  $V_S$  is the shell-model potential which binds or scatters the nucleons. This shell-model space is restricted to three subspaces,  $P$ ,  $Q_1$  and  $Q_2$  (cf. Fig. 6.1). The elastic channel space  $P$  consists of a neutron in the scattering state  $|S : \mathbf{k}_0^+\rangle$  of the potential  $V_S$ , and a target nucleus containing  $A$  independent nucleons in the shell-model ground state  $|0\rangle$ ,

$$\sum_{i=1}^A [T(i) + V_S(i)]|0\rangle = \epsilon_0|0\rangle. \quad (6.19)$$

The corresponding projection operator can be written in the form

$$P = |0\rangle\langle 0| \cdot \int d^3k_0 |S : \mathbf{k}_0^+\rangle\langle S : \mathbf{k}_0^+|. \quad (6.20)$$

The space  $Q_1$  contains  $N$  ‘bound states embedded in the continuum’  $|S : \lambda\rangle$ , i.e. shell-model states where all nucleons are bound although their total energy  $E_\lambda$  lies above the threshold for particle emission. The operator projecting on this

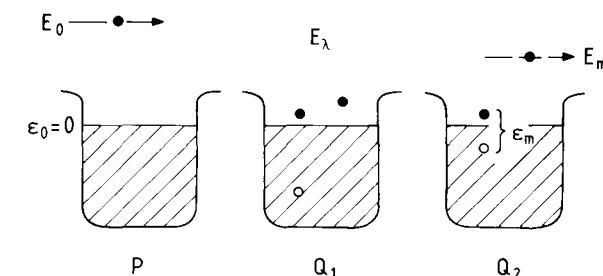


Figure 6.1 The three types of shell-model states in the spaces  $P$ ,  $Q_1$ , and  $Q_2$ . The incident neutron is considered distinguishable from the target nucleons. The ground-state energy  $\epsilon_0$  is normalized to zero.

space is

$$Q_1 = \sum_{\lambda=1}^N |S : \lambda\rangle\langle S : \lambda|. \quad (6.21)$$

Finally, the space  $Q_2$  contains  $M$  inelastic continuum states. Each of these consists of an excited target state  $|m\rangle$  of the particle-hole type, which is a solution of the  $A$ -nucleon Schrödinger equation (6.19) with the ground-state energy  $\epsilon_0$  replaced with the excited-state energy  $\epsilon_m$ , and a neutron in a shell-model continuum state,  $|S : \mathbf{k}_m^+\rangle$ . The operator projecting on the  $Q_2$  space has the form

$$Q_2 = \sum_{m=1}^M |m\rangle\langle m| \cdot \int d^3k_m |S : \mathbf{k}_m^+\rangle\langle S : \mathbf{k}_m^+|. \quad (6.22)$$

The states in the spaces  $P$ ,  $Q_1$ , and  $Q_2$  satisfy

$$(H_S - \epsilon_0 - E_0)|0\rangle|S : \mathbf{k}_0^+\rangle = 0 \text{ with } E_0 = \frac{\hbar^2 k_0^2}{2m_n}, \quad (6.23)$$

$$(H_S - E_\lambda)|S : \lambda\rangle = 0, \quad (6.24)$$

and

$$(H_S - \epsilon_m - E_m)|m\rangle|S : \mathbf{k}_m^+\rangle = 0 \text{ with } E_m = \frac{\hbar^2 k_m^2}{2m_n}. \quad (6.25)$$

All these shell-model states are mutually orthogonal. In the following we normalize the ground-state energy  $\epsilon_0$  to zero,  $\epsilon_0 = 0$ ; then the energies  $\epsilon_m$  are the excitation energies of the particle-hole states  $|m\rangle$ , and the channel energy  $E_0$  in the elastic channel, i.e. the incident energy, is equal to the total energy  $E$ .

The spaces  $P$  and  $Q_2$  are made up of distorted channel states (cf. Section 5.2.1) consisting of two fragments (the neutron and the target nucleus  $A$ ) whose relative motion is described by the shell-model continuum states  $|S : \mathbf{k}_0^+\rangle$  and  $|S : \mathbf{k}_m^+\rangle$ , respectively. On the other hand, the states  $|S : \lambda\rangle$  in the space  $Q_1$  are bound shell-model states of a single fragment consisting of  $A + 1$  nucleons. Their energy lies in the continuum, and when

the residual interaction between the nucleons is taken into account, these states become unstable and decay into one of the two-fragment states in the spaces  $P$  and  $Q_2$ .

The reaction state for a neutron with momentum  $\mathbf{k}$  ( $k^2 = 2m_n E/\hbar^2$ ) incident on the target in its ground state  $|0\rangle$  can now be written in the form

$$|0; \mathbf{k}^+\rangle = |a^+\rangle = |0^+\rangle + |1\rangle + |2^+\rangle, \quad (6.26)$$

where we have introduced the components in the three shell-model spaces,

$$|0^+\rangle = P|a^+\rangle = |0\rangle|\mathbf{k}^+\rangle = |0\rangle \cdot \int d^3k_0 c_0(\mathbf{k}, \mathbf{k}_0)|S : \mathbf{k}_0^+\rangle, \quad (6.27)$$

$$|1\rangle = Q_1|a^+\rangle = \sum_{\lambda=1}^N c_\lambda(\mathbf{k})|S : \lambda\rangle, \quad (6.28)$$

and

$$|2^+\rangle = Q_2|a^+\rangle = \sum_{m=1}^M |m\rangle \cdot \int d^3k_m c_m(\mathbf{k}, \mathbf{k}_m)|S : \mathbf{k}_m^+\rangle. \quad (6.29)$$

### 6.2.3 Derivation of the model-GOP

The coupling between the shell-model states is effected by the *residual interaction*  $V_{\text{res}}$ , which is equal to the sum of the two-body interactions between the nucleons in the  $(A+1)$ -nucleon system minus the total shell-model potential,

$$V_{\text{res}}(0, 1, \dots, A) = \sum_{j>i=0}^A v(i, j) - \sum_{i=0}^A V_S(i). \quad (6.30)$$

The total Hamiltonian is then given by

$$H = H_S + V_{\text{res}}, \quad (6.31)$$

and the Schrödinger equation (6.3) becomes

$$(H_S + V_{\text{res}} - E)|a^+\rangle = 0. \quad (6.32)$$

Using eqn (6.26), we find in the three spaces  $P$ ,  $Q_1$ , and  $Q_2$ , respectively,

$$[T(0) + V_S(0) + V_{00} - E]|0^+\rangle + V_{01}|1\rangle + V_{02}|2^+\rangle = 0, \quad (6.33)$$

$$V_{10}|0^+\rangle + (H_{11} - E)|1\rangle + V_{12}|2^+\rangle = 0, \quad (6.34)$$

$$V_{20}|0^+\rangle + V_{21}|1\rangle + (H_{22} - E)|2^+\rangle = 0, \quad (6.35)$$

where  $H_{11} = Q_1 H Q_1$ ,  $V_{00} = P V_{\text{res}} P$ ,  $V_{01} = P H Q_1 = P V_{\text{res}} Q_1$ , etc., and  $V_{ij} = V_{ji}$ ;  $i, j = 0, 1, 2$ . In eqn (6.33) we have used eqns (6.19) and (6.23) and have set  $E_0 = E$ , i.e.  $\epsilon_0 = 0$ .

We now consider two limiting cases of the coupling between the three shell-model spaces.

#### (i) Direct channel-channel coupling

We assume, first, that the elastic and inelastic channels do not couple to the intermediate states  $|S : \lambda\rangle$  of space  $Q_1$ , i.e. we set  $V_{01} = V_{21} = 0$ . Then eqns (6.33) and (6.35)

become

$$(T(0) + V_S(0) + V_{00} - E)|0^+\rangle + V_{02}|2^+\rangle = 0, \quad (6.36)$$

$$V_{20}|0^+\rangle + (H_{22} - E)|2^+\rangle = 0; \quad (6.37)$$

eqn (6.34) is decoupled and can be disregarded.

Following the steps from eqns (6.6) to (6.11), we arrive at a Schrödinger equation for the elastic channel alone,

$$(H_{\text{eff}} - E)|0^+\rangle = 0. \quad (6.38)$$

The effective Hamiltonian for the neutron in the elastic channel space  $P$  becomes

$$(0|H_{\text{eff}}|0) = T(0) + \mathcal{V}^{\text{dir}}, \quad (6.39)$$

where the  $\mathcal{V}^{\text{dir}}$  is the GOP for direct channel-channel coupling,

$$\mathcal{V}^{\text{dir}} = V_S(0) + (0|V_{00}|0) + (0|V_{02} \frac{1}{E + i\eta - H_{22}} V_{20}|0). \quad (6.40)$$

In the quantity  $H_{22} = Q_2(H_S + V_{\text{res}})Q_2$  the residual interaction term is not essential for understanding the structure of the GOP, and we shall omit it in the following. Then  $H_{22}$  has as eigenstates the inelastic continuum states  $|m\rangle|S : \mathbf{k}_m^+\rangle$  of eqn (6.25) with continuous eigenenergies  $E_m + \epsilon_m$ , and the GOP of eqn (6.40) can be written in the form

$$\mathcal{V}^{\text{dir}} = V_{\text{stat}} + \sum_{m=1}^M \int d^3k_m \frac{|V_{0m}(\mathbf{k}_m)\rangle \langle V_{0m}(\mathbf{k}_m)|}{E + i\eta - \epsilon_m - E_m}, \quad (6.41)$$

where the terms

$$|V_{0m}(\mathbf{k}_m)\rangle = (0|V_{\text{res}}|m\rangle|S : \mathbf{k}_m^+\rangle) \quad (6.42)$$

are kets in the single-particle space of the neutron.

The first term in the GOP of eqn (6.41) is the static term,

$$V_{\text{stat}} = V_S(0) + (0|V_{\text{res}}|0), \quad (6.43)$$

which is Hermitian and independent of the energy. It is equal to the sum of the shell-model potential and the target ground-state expectation value of the residual interaction between the neutron and the target nucleons.

The sum on the right-hand side of eqn (6.41) is of dynamical origin and takes account of the coupling to the excited states  $|m\rangle$  outside the space  $P$ . Writing

$$\int d^3k_m = \int_0^{4\pi} d\Omega_m \int_0^\infty dE_m \frac{k_m^2 dk_m}{dE_m} = \int_0^{4\pi} d\Omega_m \int_0^\infty dE_m \frac{m_n k_m}{\hbar^2} \quad (6.44)$$

and using eqn (6.13) in the integrands,

$$\frac{1}{E + i\eta - \epsilon_m - E_m} = \frac{\mathcal{P}}{E - \epsilon_m - E_m} - i\pi\delta(E - \epsilon_m - E_m). \quad (6.45)$$

we find that the real part of this sum consists of principal-value integrals as in eqn (6.14), whereas the imaginary part is given by

$$\text{Im } \mathcal{V}^{\text{dir}}(E) = -\pi \sum_{m=1}^M \frac{m_n k_m}{\hbar^2} \int d\Omega_m |V_{0m}(\mathbf{k}_m)\rangle \langle V_{0m}(\mathbf{k}_m)| \theta(E - \epsilon_m) \\ \text{with } k_m^2 = 2m_n(E - \epsilon_m)/\hbar^2. \quad (6.46)$$

The unit step functions  $\theta(E - \epsilon_m)$ , where  $\theta(x) = 1(0)$  for  $x > (<) 0$ , appear here because the integration over  $k_m$  in the integrals on the right-hand side of eqn (6.41) starts at  $E_m = 0$  (cf. eqn (6.44)). The excitation energy  $\epsilon_m$  is the *threshold energy* at which the inelastic channel  $m$  opens and contributes to the imaginary part of the GOP; the latter is seen to be negative, i.e. absorptive.

The *direct* GOP (6.41) is weakly energy-dependent. An explicit example of this potential will be discussed in Section 8.4.

### (ii) Coupling via the bound states embedded in the continuum

Let us now consider the case opposite to the one just discussed, and assume that the residual interaction does not couple the spaces  $P$  and  $Q_2$  directly, which implies  $PV_{\text{res}}Q_2 = 0$ , but only indirectly, via the bound states embedded in the continuum of the space  $Q_1$ . The system of equations (6.33) to (6.35) then becomes

$$(T(0) + V_S(0) + V_{00} - E)|0^+\rangle + V_{01}|1\rangle = 0, \quad (6.47)$$

$$V_{10}|0^+\rangle + (H_{11} - E)|1\rangle + V_{12}|2^+\rangle = 0, \quad (6.48)$$

$$V_{21}|1\rangle + (H_{22} - E)|2^+\rangle = 0. \quad (6.49)$$

We solve eqn (6.49) for the continuum states  $|2^+\rangle$ ,

$$|2^+\rangle = \frac{1}{E + i\eta - H_{22}} V_{21} |1\rangle, \quad (6.50)$$

and insert these in eqn (6.48). Solving then for the set of bound states  $|1\rangle$  we obtain

$$|1\rangle = \frac{1}{E + i\eta - H_{11} - V_{12}(E + i\eta - H_{22})^{-1}V_{21}} V_{10} |0^+\rangle. \quad (6.51)$$

Substitution of this set of states in eqn (6.47) yields again an equation of the type (6.38) in the elastic channel, where the effective Hamiltonian  $H_{\text{eff}}$  is now given by

$$H_{\text{eff}} = T(0) + V_S(0) + V_{00} \\ + V_{01} \frac{1}{E + i\eta - H_{11} - V_{12}(E + i\eta - H_{22})^{-1}V_{21}} V_{10}. \quad (6.52)$$

For simplicity we neglect the residual interaction in the diagonal operators  $H_{11}$  and  $H_{22}$ . Then the effective Hamiltonian in the elastic channel space  $P$  becomes

$$\langle 0 | H_{\text{eff}} | 0 \rangle = T(0) + \mathcal{V}^{\text{cpd}}, \quad (6.53)$$

where

$$\mathcal{V}^{\text{cpd}} = V_{\text{stat}} \\ + \sum_{\lambda=1}^N \frac{|V_{0\lambda}\rangle \langle V_{0\lambda}|}{E + i\eta - E_{\lambda} - \sum_{m=1}^M \int d^3k_m |V_{\lambda m}(\mathbf{k}_m)|^2 (E + i\eta - \epsilon_m - E_m)^{-1}}, \quad (6.54)$$

is called the *compound GOP* for reasons which will become clear presently.

The compound GOP arises from the coupling of the elastic (entrance) channel 0 to the bound states embedded in the continuum  $|S : \lambda\rangle$  via the quantities

$$|V_{0\lambda}\rangle = \langle 0 | V_{\text{res}} | S : \lambda \rangle \quad (6.55)$$

in the numerators, which are kets in the single-particle space of the neutron. In turn, the matrix elements

$$V_{\lambda m}(\mathbf{k}_m) = \langle S : \lambda | V_{\text{res}} | m \rangle |S : \mathbf{k}_m^+ \rangle \quad (6.56)$$

in the denominators of the sum on the right-hand side of eqn (6.54) couple the states  $|S : \lambda\rangle$  to the inelastic channels  $m = 1, \dots, N$ . Let us now examine the structure of this sum, i.e. of the dynamical part of the compound GOP.

In the region  $E < \epsilon_1$  the compound GOP has poles at the energies  $E = E_{\lambda}^{(\text{pole})}$ , where the  $E_{\lambda}^{(\text{pole})}$  are real zeros of the denominators in formula (6.54),

$$D_{\lambda}(E_{\lambda}^{(\text{pole})}) = E_{\lambda}^{(\text{pole})} - E_{\lambda} - \sum_{m=1}^M \int d^3k_m \frac{|V_{\lambda m}(\mathbf{k})|^2}{E_{\lambda}^{(\text{pole})} - \epsilon_m - E_m} = 0. \quad (6.57)$$

These real poles lead to a violent energy dependence of the optical potential.

Above the first inelastic threshold,  $E > \epsilon_1$ , the GOP (6.54) will become *complex*. In this region of energies probability current is lost from the elastic channel to the inelastic channels via the states  $|S : \lambda\rangle$ , leading to absorption in the elastic channel. This is seen explicitly by considering the integral in the denominators of the expression (6.54). Here we have

$$\sum_{m=1}^M \int d^3k_m \frac{|V_{\lambda m}(\mathbf{k}_m)|^2}{E + i\eta - \epsilon_m - E_m} = \Delta_{\lambda} - i\frac{1}{2}\Gamma_{\lambda}, \quad (6.58)$$

where, using eqn (6.13), we have defined the *energy shift*

$$\Delta_{\lambda} = \sum_{m=1}^M \mathcal{P} \int d^3k_m \frac{|V_{\lambda m}(\mathbf{k}_m)|^2}{E - \epsilon_m - E_m} \quad (6.59)$$

and the *partial width*

$$\Gamma_{\lambda} = \frac{2\pi m_n}{\hbar^2} \sum_{m=1}^M k_m \int d\Omega_m |V_{\lambda m}(\mathbf{k}_m)|^2. \quad (6.60)$$

The dynamical part of the compound GOP (6.54) can thus be written as

$$\sum_{\lambda} \frac{|V_{0\lambda}\rangle \langle V_{0\lambda}|}{E - E_{\lambda} - \Delta_{\lambda} + i\theta(E - \epsilon_1) \frac{1}{2}\Gamma_{\lambda}}.$$

It has the form of a sum of resonances. Each resonance is associated with a bound state embedded in the continuum  $|S : \lambda\rangle$ . Its position is given by the energy  $E_\lambda$  of the latter, shifted by the amount  $\Delta_\lambda$ . Its width (6.60) has a very direct physical interpretation. We see, referring, for example, to Messiah (1972, eqns (XVII. 50 and 52)) (there the additional factor  $(2\pi)^{-3}$  stems from the normalization of the states  $|\mathbf{k}^+\rangle$ , which differs from ours), that  $\Gamma_\lambda/\hbar$  is the probability per unit time, or transition rate, for the decay of the state  $|S : \lambda\rangle$  to the inelastic channels labelled by  $m$ . The width  $\Gamma_\lambda$  is called partial because it refers only to the decay into inelastic channels. The width for the decay back into the elastic channel does not appear explicitly in the GOP but will turn up in the scattering amplitude calculated with the help of this potential (cf. Section 6.3.1). The energy shift  $\Delta_\lambda$  and the width  $\Gamma_\lambda$  depend weakly on the energy  $E$ .

In the present model we have restricted the space of bound states embedded in the continuum  $Q_1$  to two-particle-one-hole states, which moreover are non-interacting ( $V_{11} = 0$ ). However, in any but the lightest nuclei the space  $Q_1$  contains a large number of complicated interacting many-particle-many-hole states. The residual two-particle interaction  $V_{\text{res}}$  does not couple these states directly to the elastic channel (which in general will also be more complicated than the simple one-particle-no-hole state of the model) but via a hierarchy of states in which the two-particle-one-hole states act as so-called doorway states. The many-particle-many-hole states give rise to a large number of resonances in the GOP. The widths of these resonances are an (inverse) measure of the lifetime of the associated complicated bound states embedded in the continuum. These generally take so long to decay on a nuclear scale that one may consider them as intermediary states of the joint system of projectile and target which we call a compound nucleus. In this sense they are compound states through which the system passes during the scattering process. It is now clear why the potential  $\mathcal{V}^{\text{cpd}}$  of eqn (6.54) has been called the compound GOP: it determines the part of the elastic scattering which proceeds via compound states (cf. also Section 6.3.2).

The inclusion of higher-order nucleon configurations in the formalism does not alter the general structure of the GOP in an important way. We therefore keep the formulae derived above, except that it is understood that the index  $\lambda$  now refers to a large number  $N$  of narrowly spaced compound states or resonances. This applies also to the states associated with the real poles  $E_\lambda^{(\text{pole})}$  of the GOP, which do not decay to inelastic channels because they lie below the threshold energy, but which acquire an elastic width when they appear in the scattering amplitude (cf. Section 6.3.1).

### (iii) The complete model-GOP

The GOP containing both the direct and compound contributions now has the general structure

$$\begin{aligned} \mathcal{V} &= V_{\text{stat}} + \sum_{m=1}^M \int d^3 k_m \frac{|V_{0m}(\mathbf{k}_m)\rangle \langle V_{0m}(\mathbf{k}_m)|}{E + i\eta - \epsilon_m - E_m} \\ &\quad + \sum_{\lambda=1}^N \frac{|V_{0\lambda}\rangle \langle V_{0\lambda}|}{E + i\eta - E_\lambda - \sum_{m=1}^M \int d^3 k_m |V_{\lambda m}(\mathbf{k}_m)|^2 (E + i\eta - \epsilon_m - E_m)^{-1}}. \end{aligned} \quad (6.61)$$

Here we have simply added the contributions of the direct and compound parts, eqns (6.41) and (6.54), respectively. In a rigorous treatment these two mechanisms cannot be treated as independent, making purely additive contributions. But for our schematic discussion this will do.

#### 6.2.4 Analyticity, non-locality, and the Pauli principle

We now discuss some specific features of the GOP as they manifest themselves in the schematic model.

##### Analyticity

We have seen above that the GOP, as a function of the real energy  $E$ , contains poles  $E_\lambda^{(\text{pole})}$  arising from the coupling to the compound states, and integrals which become complex for energies above the various thresholds  $\epsilon_m$ ; the latter occur both in the direct and the compound contributions. Extracting the real poles and calling the remainder the continuous part of the GOP,  $\mathcal{V}^{\text{cont}}(E)$ , we may write expression (6.61) for the GOP as

$$\mathcal{V} = \mathcal{V}(E) = \sum_{\lambda(\text{poles})} \frac{|\tilde{V}_{0\lambda}\rangle \langle \tilde{V}_{0\lambda}|}{E + i\eta - E_\lambda^{(\text{pole})}} + \mathcal{V}^{\text{cont}}(E). \quad (6.62)$$

The residues of the pole terms are given by (cf. eqns (6.54) and (6.57))

$$|\tilde{V}_{0\lambda}\rangle = [D'_\lambda(E_\lambda^{(\text{pole})})]^{-1} |V_{0\lambda}\rangle. \quad (6.63)$$

The continuous part has the form

$$\begin{aligned} \mathcal{V}^{\text{cont}}(E) &= V_{\text{stat}} + \sum_{m=1}^M \int d^3 k_m \frac{|V_{0m}(\mathbf{k}_m)\rangle \langle V_{0m}(\mathbf{k}_m)|}{E + i\eta - \epsilon_m - E_m} \\ &\quad + \sum_{\lambda(\text{cont})} \frac{|V_{0\lambda}\rangle \langle V_{0\lambda}|}{E - E_\lambda - \sum_{m=1}^M \int d^3 k_m |V_{\lambda m}(\mathbf{k}_m)|^2 (E + i\eta - \epsilon_m - E_m)^{-1}}, \end{aligned} \quad (6.64)$$

where in the sum over  $\lambda(\text{cont})$  the contributions of the real poles  $E_\lambda^{(\text{pole})}$  are omitted.

Since the integration over  $E_m$  runs from 0 to  $\infty$  (cf. eqn (6.44)) the integrals in expression (6.64) can be regarded as analytic functions in the complex  $E$ -plane with branch points at the thresholds  $E = \epsilon_m$ . They have branch cuts running from the points  $\epsilon_m$  along the real  $E$ -axis to infinity, and they are evaluated at the upper rims of these cuts,  $E + i\eta$ , where  $\eta \rightarrow 0$  and  $E$  is real. The Riemann surface for the function  $\mathcal{V}^{\text{cont}}(E)$  as a whole, with  $E$  complex, consists of the total number  $2M$  of sheets connected through these cuts. The sheet on which this function has the value (6.64) on the real axis (with  $\eta \rightarrow 0$ ) is called the physical sheet. The  $M$  branch cuts all lie on top of each other, starting at the lowest inelastic threshold  $\epsilon_1$ .

On the real axis the continuous part can be written, using eqn (6.58),

$$\begin{aligned} \mathcal{V}^{\text{cont}}(E) &= V^{\text{dir}} + i W^{\text{dir}} \theta(E - \epsilon_1) \\ &\quad + \sum_{\lambda(\text{cont})} \frac{|V_{0\lambda}\rangle \langle V_{0\lambda}|}{E - E_\lambda - \Delta_\lambda + i \theta(E - \epsilon_1) \frac{1}{2} \Gamma_\lambda}, \end{aligned} \quad (6.65)$$

where  $V^{\text{dir}}$  and  $W^{\text{dir}}$  are the real and imaginary parts of the direct contribution to the GOP, which depend only weakly on the energy. The imaginary part of the direct contribution has been shown to be negative in eqn (6.46); analogously, **the imaginary part of the compound contribution is also negative**,

$$\text{Im } \mathcal{V}^{\text{cpd}}(E) = - \sum_{\lambda(\text{cont})} |V_{0\lambda}\rangle\langle V_{0\lambda}| \frac{\frac{1}{2}\Gamma_\lambda}{(E - E_\lambda - \Delta_\lambda)^2 + \frac{1}{4}(\Gamma_\lambda)^2} \theta(E - \epsilon_m). \quad (6.66)$$

Thus the imaginary part of the entire GOP is negative, i.e. absorptive,  $\text{Im } \mathcal{V} < 0$ .

We summarize. **The GOP is an analytic function of the energy  $E$  on the physical sheet of the Riemann surface with no other singularities than real poles  $E_\lambda^{(\text{pole})}$  and a multiple branch cut on the real axis starting at  $\epsilon_1$**  (cf. the analogous discussion in Mahaux and Weidenmüller (1969, Section 7.3); there the Riemann surface for  $k$  associated with the  $S$ -matrix  $S(k)$  is considered). The real poles actually have an infinitesimal negative imaginary part  $-i\eta$ , which means that the path of integration in integrals over  $E$  along the real axis must pass *above* these poles. Such integrals will occur later when we calculate energy averages (cf. Section 6.3.3). For real  $E$  the branch cut contribution of the compound part is of the form (6.65), which has the *appearance* of containing a sum of complex ‘poles’ located in the lower half-plane (actually these poles do exist, namely on the other sheets reached through the branch cut). Later on, when we use the GOP for *real*  $E$  to calculate the  $S$ -matrix, we shall regard it as consisting of a sum of such real and complex ‘poles’, simply for ease of calculation.

#### Locality properties

The locality properties of the GOP in the coordinate representation,

$$\mathcal{V} = \mathcal{V}(\mathbf{r}_0, \mathbf{r}'_0), \quad (6.67)$$

can be easily displayed in the present model.

We consider first the static term  $V_{\text{stat}}$ . Using eqn (6.30), we find from eqn (6.43)

$$V_{\text{stat}} = (0| \sum_{i=1}^A v(0, i)|0) + (0| \left( \sum_{j>i=1}^A v(i, j) - \sum_{i=1}^A V_S(i) \right) |0). \quad (6.68)$$

The last term on the right-hand side contributes a constant which shifts the energy threshold  $\epsilon_0 = 0$  in the elastic channel; it can be made to vanish by adjusting the energy scale in the model appropriately. Then we have

$$V_{\text{stat}} = (0| \sum_{i=1}^A v(0, i)|0), \quad (6.69)$$

which in the coordinate representation becomes

$$V_{\text{stat}}(\mathbf{r}_0, \mathbf{r}'_0) = \langle \mathbf{r}_0 | V_{\text{stat}} | \mathbf{r}'_0 \rangle = V_{\text{fold}}(\mathbf{r}_0) \delta(\mathbf{r}_0 - \mathbf{r}'_0). \quad (6.70)$$

Here we have introduced the **folding potential**

$$V_{\text{fold}}(\mathbf{r}_0) = \int dA |\phi(A)|^2 \sum_{i=1}^A v(\mathbf{r}_0 - \mathbf{r}_i); \quad (6.71)$$

it is obtained by folding the interaction between the neutron and the target nucleons with the target density  $|\phi(A)|^2$ , where  $\phi(A)$  is the  $A$ -nucleon target wave function, and  $dA$  stands for the  $3A$ -dimensional element of integration over the target nucleon coordinates. The static part (6.70) of the model-GOP is seen to be *local*. We emphasize that this result rests on our assumption, made at the beginning of Section 6.2.2, that the neutron described by the coordinate  $\mathbf{r}_0$  is distinguishable from the nucleons in the target nucleus. We shall come back to this point shortly.

Besides the local static part, the GOP has a non-local part which stems from the **dynamical part in the expression (6.61)**. Here the numerators are operator-valued and account for the non-locality of the GOP. For example, in the compound contribution we have in the coordinate representation,

$$\langle \mathbf{r}_0 | V_{0\lambda} \rangle \langle V_{0\lambda} | \mathbf{r}'_0 \rangle = V_{\lambda 0}(\mathbf{r}_0) \cdot V_{\lambda 0}^*(\mathbf{r}'_0); \quad (6.72)$$

here

$$V_{\lambda 0}(\mathbf{r}_0) = \int dA \phi(A) \sum_{i=1}^A v(\mathbf{r}_0 - \mathbf{r}_i) \Phi_\lambda(A, \mathbf{r}_0), \quad (6.73)$$

where the functions  $\Phi_\lambda(A, \mathbf{r}_0)$  are the wave functions of the bound states  $|S : \lambda\rangle$ .

#### The effect of the Pauli principle

The channels defined in Chapter 5 and used in this section are made up of two bound fragments containing *identifiable* groups of nucleons. We mean by this that in Fig. 6.1 the nucleon 0 is the one which is scattered, and the nucleons  $1, \dots, A$  are the ones bound in the target. Now the nucleons are identical particles (if isospin is introduced, which we ignore here), and according to the Pauli principle the  $(A+1)$ -nucleon state must be antisymmetric in all nucleons. That is, the states in the spaces  $P$  and  $Q_2$  must be linear combinations which include states where any one of the nucleons  $1, \dots, A$  is in the continuum, while the nucleon 0 is bound. For the nucleon 0 the antisymmetrized form of the shell-model state  $|0\rangle|S : \mathbf{k}_0^+\rangle$  is therefore a state with components in  $A+1$  different arrangement channels. A coupled-channel formulation of nuclear reactions then becomes extremely complicated, and the same holds for a theory of the optical potential.

Here we restrict ourselves to some remarks concerning the static term only. Before total antisymmetrization, this term has the form (6.70) with the folding potential given by eqn (6.71). We assume that the target wave function is antisymmetrized in the  $A$  target nucleons, so that the ground-state wave function is a normalized Slater determinant constructed from the  $A$  lowest single-particle states  $\chi_j(\mathbf{r})$  in the shell-model potential  $V_S(\mathbf{r})$ . We then have for the folding potential

$$V_{\text{fold}} = \sum_{j=1}^A \int d^3 r_1 |\chi_j(\mathbf{r}_1)|^2 v(\mathbf{r}_0 - \mathbf{r}_1), \quad (6.74)$$

where we have replaced the sum over  $i$  in expression (6.71) with  $A$  times the first term (this factor  $A$  is cancelled by the normalization factor of the Slater determinant), and made use of the orthonormality of the states  $\chi_j(\mathbf{r}_i)$  in the integration over the nucleons  $i = 2, \dots, A$ .

If now the nucleon 0 is antisymmetrized with the others, the potential (6.74) must be replaced with an expression which, in analogy to the Hartree–Fock potential, projects out the states already present in the target wave function (these are ‘forbidden states’). The static potential thus becomes non-local.

Similarly, for an elastic channel containing, say, two  $^{16}\text{O}$  nuclei as collision partners, the static potential may admit no states which are occupied in the ground state of the oxygen nuclei. Microscopic calculations which take the Pauli principle fully into account yield potentials of this type (cf., e.g., Langanke and Friedrich 1986).

We conclude the discussion of this section with the remark that all the features which manifest themselves in the schematic-model GOP are also present in the general expression (6.12) for the GOP. The static term  $(a|V_\alpha|a)$  is local in the coordinate representation if the Pauli principle is disregarded. The GOP will contain a large number of real and complex ‘poles’ (in the sense explained above) corresponding to the large number of compound states existing in all but the lightest nuclei. These ‘poles’ have an imaginary part, i.e. a width, only if they lie above the first inelastic threshold. For low energies, this width will be rather small, corresponding to the small decay rate, or long lifetime, of the compound state. Thus the energy dependence of the GOP is characterized by strong fluctuations in this region.

As the energy increases the spacing of the compound states becomes denser, and at the same time their widths  $\Gamma_\lambda$  increase because more and more inelastic channels open up. The terms in the sum over compound resonances will then overlap and the compound part of the GOP becomes smoothly energy dependent.

### 6.3 The optical potential

We have seen that in the region of low energies, the GOP fluctuates strongly as a function of energy. The elastic scattering amplitude calculated from this GOP will exhibit a similar behaviour. Now the optical potential introduced phenomenologically in Chapter 1 is not intended to reproduce the elastic scattering amplitude in detail. The phenomenological potential is a smooth function of energy, leading to a cross section which is a certain average of the actual, in general strongly energy-dependent cross section. In the present section we shall discuss how such a potential, the *optical potential in the proper sense* (we call it *optical potential* for short), can be defined, and which average properties of the scattering it is able to describe (cf. Feshbach *et al.* 1954; Friedman and Weisskopf 1955). Its relation to the GOP can then be derived.

#### 6.3.1 The elastic S-matrix

The elastic scattering amplitude has the form (cf. eqn (1.38) with a slight change in notation),

$$f(E, \theta) = \frac{1}{2ik} \sum_{l=0}^{\infty} (2l+1)[S_l(E) - 1] P_l(\cos \theta). \quad (6.75)$$

For our purpose it is sufficient to consider only the s-wave S-matrix  $S(E) = S_0(E)$ . It can be calculated using the GOP of eqn (6.62) together with eqn (6.65). We simplify the

expression for the GOP by writing

$$\mathcal{V}(E) = \mathcal{V}^{\text{dir}} + \sum_{\lambda} \frac{|V_{0\lambda}\rangle\langle V_{0\lambda}|}{E - U_{\lambda}}, \quad (6.76)$$

where the term  $\mathcal{V}^{\text{dir}}$  includes the static potential  $V_{\text{stat}}$  and  $U_{\lambda}$  stands generically for the pole  $E_{\lambda}^{(\text{pole})} - i\eta$  infinitesimally below the real axis or for the complex ‘pole’  $E_{\lambda} + \Delta_{\lambda} - i\Gamma_{\lambda}/2$ . We have omitted the  $\theta$ -function multiplying the width  $\Gamma_{\lambda}$  in expression (6.65); this shifts slightly the threshold for the onset of absorption.

The direct part of the GOP alone gives rise to an *S*-matrix

$$\mathcal{S}^{\text{dir}} = \exp(2i\delta^{\text{dir}}), \quad (6.77)$$

where the phase shift  $\delta^{\text{dir}}$  is generally complex since  $\mathcal{V}^{\text{dir}}$  is so.

The *S*-matrix generated by the compound part is obtained in the following way. We consider a single term of the sum in expression (6.76). It is a separable operator, i.e. it factorizes in the dynamical variables, so that the corresponding Schrödinger equation (6.11) can be solved in analytic form. We keep only this term, and write in the momentum representation

$$\mathcal{V}(E) = \frac{V_{0\lambda}(\mathbf{k}') V_{0\lambda}^*(\mathbf{k}'')}{E - U_{\lambda}} = \frac{V_{0\lambda}(k') V_{0\lambda}^*(k'')}{E - U_{\lambda}}. \quad (6.78)$$

Then the Schrödinger equation in the momentum representation has the form

$$\left( \frac{\hbar^2 k'^2}{2m_n} - E \right) \psi_{\mathbf{k}}(\mathbf{k}') + \frac{V_{0\lambda}(k')}{E - U_{\lambda}} \int d^3 k'' V_{0\lambda}^*(k'') \psi_{\mathbf{k}}(\mathbf{k}'') = 0, \quad (6.79)$$

where  $E = \hbar^2 k^2 / 2m_n$ . Since  $V_{0\lambda}^*(k'')$  is spherically symmetric, the integration in eqn (6.79) removes all partial-wave components in the wave function  $\psi_{\mathbf{k}}(\mathbf{k}'')$  except the s-wave. Therefore, the GOP of eqn (6.78) gives rise to s-wave scattering only. Defining

$$c_{\lambda} = \int d^3 k' V_{0\lambda}^*(k') \psi_{\mathbf{k}}(\mathbf{k}') \quad (6.80)$$

we obtain for the solution of eqn (6.79)

$$\psi_{\mathbf{k}}(\mathbf{k}') = \delta(\mathbf{k} - \mathbf{k}') + \frac{V_{0\lambda}(k')}{E + i\eta - \hbar^2 k'^2 / 2m_n} \frac{c_{\lambda}}{E - U_{\lambda}}, \quad (6.81)$$

where the  $\delta$ -function is the solution with  $V_{0\lambda}(k') = 0$ . Substituting the function (6.81) in expression (6.80) and solving for  $c_{\lambda}$ , we find

$$c_{\lambda} = V_{0\lambda}^*(k) \frac{E - U_{\lambda}}{E - U_{\lambda} - \int d^3 k' |V_{0\lambda}(k')|^2 (E + i\eta - \hbar^2 k'^2 / 2m_n)^{-1}}. \quad (6.82)$$

Inserting the constant  $c_{\lambda}$  in eqn (6.81) we finally obtain for the wave function

$$\begin{aligned} \psi_{\mathbf{k}}(\mathbf{k}') &= \delta(\mathbf{k} - \mathbf{k}') + \frac{1}{E + i\eta - \hbar^2 k'^2 / 2m_n} \\ &\times \frac{V_{0\lambda}(k') V_{0\lambda}^*(k)}{E - U_{\lambda} - \int d^3 k'' |V_{0\lambda}(k'')|^2 (E + i\eta - \hbar^2 k''^2 / 2m_n)^{-1}}, \end{aligned} \quad (6.83)$$

which can be written in a form analogous to eqn (4.76),

$$\psi_{\mathbf{k}}(\mathbf{k}') = \delta(\mathbf{k} - \mathbf{k}') + \frac{1}{E - (\hbar^2 k'^2 / 2m_n) + i\eta} T_{\mathbf{k}', \mathbf{k}}^\lambda. \quad (6.84)$$

The  $T$ -matrix  $T_{\mathbf{k}', \mathbf{k}}^\lambda$  can be read off from eqn (6.83); on the energy shell, i.e. for  $k'^2 = k^2$ , it is given by

$$T_{\mathbf{k}', \mathbf{k}}^\lambda = \frac{\hbar^2}{8\pi^2 m_n k} \frac{\Gamma_\lambda^0}{E - U_\lambda - \Delta_\lambda^0 + i\frac{1}{2}\Gamma_\lambda^0}. \quad (6.85)$$

Here

$$\Delta_\lambda^0 = 4\pi \mathcal{P} \int k''^2 dk'' \frac{|V_{0\lambda}(k'')|^2}{E - \hbar^2 k''^2 / 2m_n} \quad (6.86)$$

is a shift suffered by the resonance energy owing to the coupling to the elastic channel, and

$$\Gamma_\lambda^0 = 8\pi^2 \frac{k^2 dk}{dE} |V_{0\lambda}(k)|^2 = \frac{8\pi^2 m_n k}{\hbar^2} |V_{0\lambda}(k)|^2 \quad (6.87)$$

is the partial width for the decay of the compound state to the elastic channel (cf. the discussion of formula (6.60)). Both quantities depend weakly on the energy  $E$ .

Equation (6.85) shows that the form of the energy dependence of a compound term in the GOP of eqn (6.76) is essentially retained in the corresponding scattering amplitude. In the case where  $U_\lambda$  stands for  $E_\lambda^{(\text{pole})}$ , the real pole  $E_\lambda^{(\text{pole})}$  acquires an elastic shift  $\Delta_\lambda^0$  and an elastic width  $\Gamma_\lambda^0$  associated with the decay of the associated compound state to the elastic channel. When  $U_\lambda = E_\lambda + \Delta_\lambda - i\Gamma_\lambda/2$ , the elastic shift and width are simply added to the inelastic one which appears already in the GOP. Instead of eqn (6.85) we may therefore write

$$T_{\mathbf{k}', \mathbf{k}}^\lambda = \frac{\hbar^2}{8\pi^2 m_n k} \frac{\Gamma_\lambda^0}{E - \mathcal{E}_\lambda + i\frac{1}{2}\Gamma_\lambda^{\text{tot}}}, \quad (6.88)$$

where  $\mathcal{E}_\lambda$  stands for  $E_\lambda^{(\text{pole})} + \Delta_\lambda^0$  (a shifted real pole of the GOP) or  $E_\lambda + \Delta_\lambda + \Delta_\lambda^0$  (the shifted real part of a complex pole of the GOP), and

$$\Gamma_\lambda^{\text{tot}} = \Gamma_\lambda + \Gamma_\lambda^0 \quad (6.89)$$

is the *total* width of the compound state  $\lambda$  for the decay into elastic and non-elastic channels. Since the  $T$ -matrix (6.88) depends only on the absolute value of the momentum  $\mathbf{k}$ , its partial-wave expansion (4.122) contains only the s-wave term

$$T_0^\lambda(k) = 4\pi T_{\mathbf{k}', \mathbf{k}}^\lambda = \frac{\hbar^2}{2\pi m_n k} \frac{\Gamma_\lambda^0}{E - \mathcal{E}_\lambda + i\frac{1}{2}\Gamma_\lambda^{\text{tot}}}. \quad (6.90)$$

In the region of *low energies*, which is the case of interest in the following, the widths  $\Gamma_\lambda^{\text{tot}}$  are smaller than the average distance  $D$  between the levels,  $\Gamma_\lambda^{\text{tot}} \ll D$ , and the  $T$ -matrices (6.90) for different resonances  $\lambda$  do not overlap. Therefore the  $T$ -matrix generated by the sum of levels in the GOP of eqn (6.76) has the form

$$T^{\text{cpd}} = \frac{\hbar^2}{2\pi m_n k} \sum_\lambda \frac{\Gamma_\lambda^0}{E - \mathcal{E}_\lambda + i\frac{1}{2}\Gamma_\lambda^{\text{tot}}}. \quad (6.91)$$

The  $S$ -matrix associated with this  $T$ -matrix is, according to eqn (4.125),

$$S^{\text{cpd}} = 1 - i \frac{2\pi m_n k}{\hbar^2} T^{\text{cpd}} = 1 - \sum_\lambda \frac{i\Gamma_\lambda^0}{E - \mathcal{E}_\lambda + i\frac{1}{2}\Gamma_\lambda^{\text{tot}}}. \quad (6.92)$$

In analogy to what has been said in Section 6.2.4 about the analytic structure of the GOP, the complex poles of the  $T$ - or  $S$ -matrices do not lie on the physical sheet, but on other sheets reached through a branch cut on the real axis. Nevertheless, for the integrations over  $E$  to be performed in the next subsection we may again regard functions of the type (6.92) as functions with no singularities other than poles.

For the  $S$ -matrix containing the direct as well as the compound contributions we take the product

$$S(E) = S^{\text{dir}} \cdot S^{\text{cpd}}(E). \quad (6.93)$$

This relation, which implies that the  $S$ -matrix of a sum of potentials is simply the product of the individual  $S$ -matrices (and the total phase shift is the sum of the individual phase shifts), is not rigorously true and may in some cases even be quite wrong. However, it is valid when the direct and the compound scattering are both weak, and we adopt it here purely for reasons of simplicity.

### 6.3.2 Compound-elastic and shape-elastic scattering

In the following we shall consider various cross sections averaged over an energy interval  $2I$  large enough to contain many compound resonances. It is convenient to define the *energy average* of a function  $f(E)$  in the form

$$\overline{f(E)} = \frac{1}{\pi} \int_{-\infty}^{\infty} dE' \frac{I}{(E' - E)^2 + I^2} f(E'). \quad (6.94)$$

The functions  $f(E)$  which we shall average in this way are analytic in the upper half of the complex  $E$ -plane including the real axis, and bounded by a constant for large  $E$ . Evaluating the integral in expression (6.94) with the help of the residue theorem, we find

$$\begin{aligned} \overline{f(E)} &= \frac{1}{\pi} \int_{-\infty}^{\infty} dE' \frac{I}{(E' - E - iI)(E' - E + iI)} f(E') \\ &= f(E + iI). \end{aligned} \quad (6.95)$$

In the last line we have closed the contour of integration in the upper half-plane where  $f(E')$  is analytic; the integral converges since the denominator increases like the square of  $E'$ . As a result, taking the average of a function  $f(E)$  of the above-defined type reduces to replacing the argument  $E$  with  $E + iI$ .

#### The compound-elastic cross section

The compound part of the  $S$ -matrix is given by eqn (6.92). Its contribution to the elastic cross section is, assuming that the resonances do not overlap,

$$\begin{aligned} \sigma^{\text{cpd}}(E) &= \frac{\pi}{k^2} |S^{\text{cpd}} - 1|^2 \\ &= \frac{\pi}{k^2} \sum_\lambda \frac{(\Gamma_\lambda^0)^2}{(E - \mathcal{E}_\lambda)^2 + \frac{1}{4}(\Gamma_\lambda^{\text{tot}})^2}. \end{aligned} \quad (6.96)$$

It is a sum of resonance terms which are of *Breit–Wigner* form (cf., e.g., Hodgson 1971, Section 14.2).

We now take the energy average of this quantity over an interval  $2I$  which is large compared with the width  $\Gamma_\lambda^{\text{tot}}$ ,  $I \gg \Gamma_\lambda^{\text{tot}}/2$ . In order to apply the averaging procedure of eqn (6.95) we write the denominators in the previous expression in a form where only a pole in the lower half of the  $E$ -plane appears,

$$\frac{\pi}{k^2} \frac{1}{(E - \mathcal{E}_\lambda)^2 + \frac{1}{4}(\Gamma_\lambda^{\text{tot}})^2} = \text{Re} \left\{ \frac{2i\pi}{k^2 \Gamma_\lambda^{\text{tot}}} \frac{1}{E - \mathcal{E}_\lambda + i\frac{1}{2}\Gamma_\lambda^{\text{tot}}} \right\}. \quad (6.97)$$

Instead of calculating the average of the real quantity on the left-hand side of eqn (6.97), we calculate the average of the complex expression in the curly brackets on the right-hand side and take the real part afterwards. The latter expression has a pole at  $E = \mathcal{E}_\lambda - i\Gamma_\lambda^{\text{tot}}/2$ , and therefore is a function of  $E$  which is analytic in the upper half-plane. Taking the average converts this pole into one at  $E = \mathcal{E}_\lambda - i(\Gamma_\lambda^{\text{tot}}/2 + I) \approx \mathcal{E}_\lambda - iI$ . The averaged terms to be summed in eqn (6.96) are now smooth functions of the energy, and the sum over  $\lambda$  can be replaced with an integral,

$$\begin{aligned} \sum_\lambda \frac{2i\pi(\Gamma_\lambda^0)^2}{k^2 \Gamma_\lambda^{\text{tot}}} \frac{1}{E - \mathcal{E}_\lambda + iI} &\approx \frac{2i\pi}{k^2} \int \frac{d\mathcal{E}}{D(\mathcal{E})} \frac{[\Gamma^0(\mathcal{E})]^2}{\Gamma^{\text{tot}}(\mathcal{E})} \frac{1}{E - \mathcal{E} + iI} \\ &\approx \frac{\pi}{k^2} \frac{2[\Gamma^0(E)]^2}{D(E)\Gamma^{\text{tot}}(E)} \int d\mathcal{E} \left( i \frac{E - \mathcal{E}}{(E - \mathcal{E})^2 + I^2} + \frac{I}{(E - \mathcal{E})^2 + I^2} \right), \end{aligned} \quad (6.98)$$

where  $D(\mathcal{E})$  is the level spacing, i.e. the average distance between the levels. The quantity  $D(\mathcal{E})$  and the widths  $\Gamma^0(\mathcal{E})$  and  $\Gamma^{\text{tot}}(\mathcal{E})$  have been assumed to be smoothly varying functions of the level position  $\mathcal{E}$ , and moved outside the integral at energy  $E$ . The condition for the replacement of the sum over  $\lambda$  with an integral over  $\mathcal{E}$  is that many levels  $\mathcal{E}_\lambda$  lie within the averaging interval  $I$ , that is,  $D(\mathcal{E}) \ll 2I$ .

The integral in the second line of eqn (6.98) receives its main contribution from the region near  $\mathcal{E} = E$ , and the limits of integration can therefore be extended to  $\pm\infty$  in first approximation. Then the contribution of the first term in the integrand vanishes because this term is odd. The integral over the second term yields the value  $\pi$ , and the sum (6.98) becomes real. The average of the compound contribution to the elastic cross section, called the *compound-elastic cross section*, is then given by

$$\sigma_{ce}(E) = \frac{\pi}{k^2} \frac{2\pi\Gamma^0(E)}{D(E)} \frac{\Gamma^0(E)}{\Gamma^{\text{tot}}(E)}. \quad (6.99)$$

The *shape-elastic cross section*

The compound-elastic cross section is only a part of the complete average elastic cross section

$$\overline{\sigma}_{\text{el}} = \frac{\pi}{k^2} \overline{|S(E) - 1|^2}. \quad (6.100)$$

Let us decompose the  $S$ -matrix  $S(E)$  into its energy average  $\overline{S}(E)$  and a fluctuating part  $S^{(\text{fl})}(E)$ ,

$$S(E) = \overline{S(E)} + S^{(\text{fl})}(E) \quad (6.101)$$

with

$$\overline{S^{(\text{fl})}(E)} = 0; \quad (6.102)$$

then expression (6.100) becomes

$$\overline{\sigma}_{\text{el}} = \frac{\pi}{k^2} (\overline{|\bar{S} - 1|^2} + \overline{|S^{(\text{fl})}|^2}). \quad (6.103)$$

Thus the average elastic cross section is the sum of two parts,

$$\overline{\sigma}_{\text{el}} = \sigma_{\text{se}} + \sigma_{\text{fl}}. \quad (6.104)$$

Here we have introduced the *shape-elastic cross section*

$$\sigma_{\text{se}} = \frac{\pi}{k^2} |\bar{S} - 1|^2 \quad (6.105)$$

calculated from the average elastic  $S$ -matrix, and the *fluctuation cross section*

$$\sigma_{\text{fl}} = \frac{\pi}{k^2} \overline{|S^{(\text{fl})}|^2}, \quad (6.106)$$

which is given by the average of the absolute square of the fluctuating  $S$ -matrix  $S^{(\text{fl})}$ . The shape-elastic cross section is mainly determined by the static part  $\mathcal{V}_{\text{stat}}$  of the GOP, i.e. by its geometrical shape; whence its name.

Using eqns (6.77), (6.92), and (6.95), and evaluating the sum over  $\lambda$  as in eqn (6.98), we find for the average  $S$ -matrix (6.93)

$$\begin{aligned} \bar{S} &= e^{2i\delta^{\text{dir}}} \overline{\left( 1 - \sum_\lambda \frac{i\Gamma_\lambda^0}{E - \mathcal{E}_\lambda + i\frac{1}{2}\Gamma_\lambda^{\text{tot}}} \right)} \\ &= e^{2i\delta^{\text{dir}}} \left( 1 - \frac{\pi\Gamma^0}{D} \right). \end{aligned} \quad (6.107)$$

The *fluctuation cross section*

We next calculate the fluctuation cross section (6.106), which contains the quantity (cf. eqn (6.101))

$$\overline{|S|}^2 = \overline{|S|^2} - |\bar{S}|^2. \quad (6.108)$$

For low energies the direct phase shift  $\delta^{\text{dir}}$  is real and we have from eqns (6.92) and (6.93)

$$\overline{|S|^2} = 1 - 2\text{Re} \sum_\lambda \overline{\left( \frac{i\Gamma_\lambda^0}{E - \mathcal{E}_\lambda + i\frac{1}{2}\Gamma_\lambda^{\text{tot}}} \right)} + \sum_\lambda \overline{\left( \frac{(\Gamma_\lambda^0)^2}{(E - \mathcal{E}_\lambda)^2 + \frac{1}{4}(\Gamma_\lambda^{\text{tot}})^2} \right)}, \quad (6.109)$$

which becomes

$$\overline{|S|^2} = 1 - \frac{2\pi\Gamma^0}{D} + \frac{2\pi(\Gamma^0)^2}{D\Gamma^{\text{tot}}}. \quad (6.110)$$

With (cf. eqn (6.107))

$$|\bar{S}|^2 = \left( 1 - \frac{\pi\Gamma^0}{D} \right)^2 = 1 - \frac{2\pi\Gamma^0}{D} + \left( \frac{\pi\Gamma^0}{D} \right)^2 \quad (6.111)$$

we then find from eqns (6.106) and (6.108)

$$\begin{aligned}\sigma_{\text{fl}} &= \frac{\pi}{k^2} \left[ \frac{2\pi(\Gamma^0)^2}{D\Gamma^{\text{tot}}} - \left( \frac{\pi\Gamma^0}{D} \right)^2 \right] = \frac{\pi}{k^2} \frac{2\pi(\Gamma^0)^2}{D\Gamma^{\text{tot}}} \left( 1 - \frac{\pi}{2} \frac{\Gamma^{\text{tot}}}{D} \right) \\ &\approx \frac{\pi}{k^2} \frac{2\pi\Gamma^0}{D} \frac{\Gamma^0}{\Gamma^{\text{tot}}},\end{aligned}\quad (6.112)$$

where we have used  $\Gamma^{\text{tot}} \ll D$ , which holds for the low energies we are considering here.

It follows from a comparison of eqn (6.112) with eqn (6.99) that the fluctuation cross section is equal to the compound-elastic cross section,

$$\sigma_{\text{fl}} = \sigma_{\text{ce}}. \quad (6.113)$$

Instead of eqn (6.104) we can also write, therefore,

$$\overline{\sigma_{\text{el}}} = \sigma_{\text{se}} + \sigma_{\text{ce}}. \quad (6.114)$$

### 6.3.3 The optical potential in the proper sense

The optical potential in the proper sense is defined in such a way that it generates the average elastic cross section *without* the compound-elastic contribution. The compound-elastic scattering is not considered part of the elastic scattering generated by the optical potential, but is regarded as an absorptive process.

From eqn (6.114) it is clear that the non-compound part of the elastic cross section is the shape-elastic cross section, which is determined by the average scattering amplitude. The *optical potential in the proper sense*,  $V_{\text{opt}}$ , therefore must produce the energy-averaged S-matrix (6.107). We thus define  $V_{\text{opt}}$  as that operator which in the Schrödinger equation analogous to eqn (6.11) (we have left out the channel index  $\alpha$ ),

$$(T + V_{\text{opt}} - E)|\mathbf{k}^+\rangle_{\text{opt}} = 0, \quad (6.115)$$

determines an *optical scattering state*  $|\mathbf{k}^+\rangle_{\text{opt}}$ , whose S-matrix  $S_{\text{opt}}$  is equal to the energy average of the scattering function calculated from the GOP,

$$S_{\text{opt}} = \bar{S}. \quad (6.116)$$

The optical S-matrix  $S_{\text{opt}}$  determines, besides the shape-elastic cross section, an *absorption cross section*

$$\sigma_a = \frac{\pi}{k^2} (1 - |S_{\text{opt}}|^2) = \frac{\pi}{k^2} (1 - |\bar{S}|^2). \quad (6.117)$$

Comparing this with the average reaction cross section

$$\begin{aligned}\overline{\sigma_r} &= \frac{\pi}{k^2} (1 - |S|^2) \\ &= \frac{\pi}{k^2} (1 - |\bar{S}|^2 - \overline{|S^{\text{fl}}|^2}),\end{aligned}\quad (6.118)$$

we see from eqns (6.106) and (6.113) that the absorption cross section is made up of the average reaction cross section and the compound-elastic cross section,

$$\sigma_a = \overline{\sigma_r} + \sigma_{\text{ce}}. \quad (6.119)$$

As required, the absorption cross section calculated from the optical S-matrix counts the compound-elastic scattering as a non-elastic process whose cross section is added to the true average reaction cross section.

It is customary to introduce an optical transmission coefficient

$$T_{\text{opt}} = 1 - |\bar{S}|^2, \quad (6.120)$$

in terms of which the absorption cross section (6.117) has the form

$$\sigma_a = \frac{\pi}{k^2} T_{\text{opt}}. \quad (6.121)$$

Substituting the optical S-matrix (6.107) in expression (6.120) we obtain, with  $\delta^{\text{dir}} = \text{real}$  and  $\Gamma^0/D \ll 1$ ,

$$T_{\text{opt}} = \frac{2\pi\Gamma^0}{D} \quad (6.122)$$

and

$$\sigma_a = \frac{\pi}{k^2} \frac{2\pi\Gamma^0}{D}. \quad (6.123)$$

In setting  $\delta^{\text{dir}} = \text{real}$  we have assumed that the direct processes are elastic so that in this case the absorption cross section  $\sigma_a$  is equal to the cross section for compound-nucleus formation. Then the compound-elastic cross section (6.99) can be written in the form

$$\sigma_{\text{ce}}(E) = \sigma_a(E) \frac{\Gamma^0(E)}{\Gamma^{\text{tot}}(E)}, \quad (6.124)$$

i.e. as the absorption cross section times the probability  $\Gamma^0/\Gamma^{\text{tot}}$  for the decay back into the elastic channel.

Finally, the *average total cross section* (cf. eqn (1.75)) can be directly calculated from the optical S-matrix,

$$\overline{\sigma_{\text{tot}}} = \frac{2\pi}{k^2} (1 - \text{Re } \bar{S}) = \frac{2\pi}{k^2} (1 - \text{Re } S_{\text{opt}}). \quad (6.125)$$

Writing

$$\overline{\sigma_{\text{tot}}} = \frac{2\pi}{k^2} (1 - \text{Re } \bar{S}) = \frac{\pi}{k^2} (|1 - \bar{S}|^2 + 1 - |\bar{S}|^2), \quad (6.126)$$

we find

$$\overline{\sigma_{\text{tot}}} = \sigma_{\text{se}} + \sigma_a. \quad (6.127)$$

In the optical model the total cross section is the sum of the shape-elastic and absorption cross sections. On the other hand, eqns (6.114), (6.119), and (6.127) lead to the result

$$\overline{\sigma_{\text{tot}}} = \overline{\sigma_{\text{el}}} + \overline{\sigma_r}, \quad (6.128)$$

which holds of course also without the averaging bars.

The relations (6.114), (6.119), (6.127), and (6.128) are summarized symbolically in Fig. 6.2. The average reaction cross section is in general also a sum of compound and non-compound contributions. The latter come from direct reactions,  $\sigma_{\text{dir}}$ , or deep-inelastic collisions,  $\sigma_{\text{DIC}}$ , which will be discussed in later chapters. The compound reaction cross section  $\sigma_{\text{cr}}$  combines with the compound-elastic cross section  $\sigma_{\text{ce}}$  to make

up the compound part of the absorption cross section, i.e. the cross section for compound nucleus formation or *fusion*,  $\sigma_F$  (cf. Chapter 9). The general form of eqn (6.124) for the compound-elastic cross section is then

$$\sigma_{ce}(E) = \sigma_F(E) \frac{\Gamma^0(E)}{\Gamma^{\text{tot}}(E)}. \quad (6.129)$$

$\overline{\sigma_{\text{tot}}}$		
$\overline{\sigma_{\text{el}}}$	$\overline{\sigma_r}$	
$\sigma_{se}$	$\sigma_a$	
$\sigma_{ce}$	$\sigma_{cr}$	$\sigma_{\text{DIC}} + \sigma_{\text{dir}}$
$\sigma_F$		

Figure 6.2 The cross sections in the optical model.

The optical potential yields the non-fluctuating, smoothly energy-dependent part of the elastic scattering amplitude; therefore, it describes the *fast* components of the scattering process. On the other hand, the strongly energy-dependent fluctuating part of the scattering amplitude, whose averaged square is the compound-elastic cross section, is associated with the *slow* processes of compound nucleus formation; these can be shown to suffer a time delay of the order of the lifetime of the compound states (for a detailed discussion see Friedman and Weisskopf (1955); Messiah (1972, Section X, §15)).

### 6.3.4 The relation between the GOP and the optical potential

We have defined the optical potential as that potential which generates the energy-averaged  $S$ -matrix. The  $S$ -matrix is obtained from eqns (6.92) and (6.93) by writing  $\mathcal{E}_\lambda = U_\lambda + \Delta_\lambda^0 + i\frac{1}{2}\Gamma_\lambda$  (the quantity  $U_\lambda$  has been defined after eqn (6.76)),

$$S = e^{2i\delta^{\text{dir}}} \left( 1 - \sum_\lambda \frac{i\Gamma_\lambda^0}{E - U_\lambda - \Delta_\lambda^0 + i\frac{1}{2}\Gamma_\lambda^0} \right). \quad (6.130)$$

Since the function  $S = S(E)$  has no singularities in the upper  $E$  plane, averaging over the energy interval  $2I$  yields

$$\bar{S} = e^{2i\delta^{\text{dir}}} \left( 1 - \sum_\lambda \frac{i\Gamma_\lambda^0}{E - U_\lambda - \Delta_\lambda^0 + iI + i\frac{1}{2}\Gamma_\lambda^0} \right). \quad (6.131)$$

We now observe, by retracing the earlier derivation of the unaveraged  $S$ -matrix from the GOP, that the energy-averaged  $S$ -matrix (6.131) can be obtained by solving the Schrödinger equation (6.115) with a potential  $V_{\text{opt}}$  which is simply given by the GOP (6.76) with  $U_\lambda$  replaced with  $U_\lambda - iI$ .

These schematic considerations make it plausible that quite generally the optical potential  $V_{\text{opt}}$  is essentially given by the GOP of eqn (6.12) with the energy shifted upward into the complex plane by the amount  $iI$ , where  $2I$  is the energy interval over which the  $S$ -matrix is averaged,

$$V_{\text{opt}}(E) = \mathcal{V}_\alpha(E + iI) = (a|V_\alpha|a) + (a|V_\alpha Q \frac{1}{E + iI - QHQ} Q V_\alpha|a), \quad (6.132)$$

or

$$V_{\text{opt}}(E) = \overline{\mathcal{V}_\alpha(E)}. \quad (6.133)$$

◇ It is instructive to demonstrate explicitly how the averaging over the energy fluctuations in the generalized optical potential  $\mathcal{V}(E)$  gives rise to an imaginary optical potential  $V_{\text{opt}}$  which describes compound-elastic absorption. We consider the GOP of eqn (6.76) and for the sake of argument drop the direct part and set  $U_\lambda = \mathcal{E}_\lambda - i\eta$ , thus omitting the terms  $\Delta_\lambda$  and  $\Gamma_\lambda$  in the denominators. Then the GOP becomes *real* for all real energies  $E$  and diverges at the isolated poles  $\mathcal{E}_\lambda$ . As explained in Section 6.2.4, the added infinitesimal part  $-i\eta$  merely serves as a reminder that integrations over the physical (real) values of  $E$  must pass these singularities on the *upper* side.

The GOP fluctuates strongly as a function of energy owing to the presence of the many closely spaced poles. From this GOP, which is analytic in the upper half of the  $E$ -plane including the real axis, we obtain the optical potential

$$V_{\text{opt}}(E) = \sum_\lambda \frac{|V_{0\lambda}\rangle\langle V_{0\lambda}|}{E - \mathcal{E}_\lambda + iI}. \quad (6.134)$$

Replacing the sum with an integral as in eqn (6.98), we arrive at

$$V_{\text{opt}}(E) = -i\frac{\pi}{D} |V_{0\lambda}\rangle\langle V_{0\lambda}|. \quad (6.135)$$

The energy averaging has transformed the *fluctuating real* (singular) GOP into a *smooth complex* optical potential  $V_{\text{opt}}$  with a negative imaginary part (the real part happens to vanish here). As long as the energy dependence of expression (6.135) is weak over intervals of range  $2I$ , the optical potential is independent of the averaging interval  $2I$ . ◇

In the preceding discussion we have considered the optical potential only in the low-energy region where the widths are small and the levels are non-overlapping,  $\Gamma^{\text{tot}} \ll D$ . However, the definition (6.133) of the optical potential as the energy average of the GOP remains the same in the region of higher energies. Here  $\Gamma^{\text{tot}} > D$  and, moreover, the total width dominates over the elastic width,  $\Gamma^{\text{tot}} \gg \Gamma^0$ . Therefore, in view of eqn (6.99), the compound-elastic cross section practically vanishes, and so does the fluctuation cross section, because the levels overlap and the unaveraged  $S$ -matrix ceases to be violently energy dependent. Thus the GOP is smooth without averaging,

$$\mathcal{V}(E) = \overline{\mathcal{V}(E)},$$

and can be identified directly with the optical potential,

$$V_{\text{opt}} = \text{GOP} = \mathcal{V}(E) = \overline{\mathcal{V}(E)}. \quad (6.136)$$

## 6.4 The equivalent local optical potential

We have seen that the optical potential is a non-local operator. In order to use it as a space-dependent complex index of refraction as in optics, we should like to replace it with an equivalent *local* potential (ELP). The least one has to require of such a potential is that it produces the same phase shifts, that is, the same asymptotic wave function as the non-local one, even though the wave functions in the interior of the nucleus may differ. There are various ways of obtaining an ELP. We consider one trivial method, and another semiclassical one which in many cases is quite satisfactory.

### 6.4.1 The trivially equivalent local potential

Let us consider a non-local potential  $V = V(\mathbf{r}, \mathbf{r}')$ , which may be the GOP  $\mathcal{V}$  or the optical potential  $V_{\text{opt}}$ . The corresponding Schrödinger equation has the form

$$-\frac{\hbar^2}{2\mu} \nabla^2 \psi(\mathbf{r}) + \int d^3 r' V(\mathbf{r}, \mathbf{r}') \psi(\mathbf{r}') = E \psi(\mathbf{r}). \quad (6.137)$$

The *trivially equivalent local potential*  $V_{\text{TELP}}$  is obtained from the non-local potential  $V$  by first calculating the wave function for the latter, which is the true elastic channel wave function  $\psi(\mathbf{r})$ , and defining

$$V_{\text{TELP}}(\mathbf{r}) = \frac{\int d^3 r' V(\mathbf{r}, \mathbf{r}') \psi(\mathbf{r}')}{\psi(\mathbf{r})}. \quad (6.138)$$

Obviously, this local ‘potential’ produces the same wave function  $\psi(\mathbf{r})$  as the original non-local potential.

One may eliminate the non-local potential from the expression (6.138) with the help of the Schrödinger equation (6.137),

$$V_{\text{TELP}}(\mathbf{r}) = E + \frac{\hbar^2}{2\mu} \frac{\nabla^2 \psi(\mathbf{r})}{\psi(\mathbf{r})} = E + \frac{\hbar^2}{2\mu} \frac{\psi^*(\mathbf{r}) \nabla^2 \psi(\mathbf{r})}{|\psi(\mathbf{r})|^2}. \quad (6.139)$$

In order to interpret the right-hand side of eqn (6.139), we introduce the density  $\rho(\mathbf{r})$  and the current  $\mathbf{j}(\mathbf{r})$  of the elastic channel wave function,

$$\rho(\mathbf{r}) = |\psi(\mathbf{r})|^2, \quad \mathbf{j}(\mathbf{r}) = \frac{\hbar}{\mu} \text{Im} [\psi^*(\mathbf{r}) \nabla \psi(\mathbf{r})]. \quad (6.140)$$

We then find

$$\text{Re} [\psi^* \nabla^2 \psi] = \frac{1}{2} \nabla^2 \rho - |\nabla \psi|^2 \quad (6.141)$$

and

$$\text{Im} [\psi^* \nabla^2 \psi] = \frac{\mu}{\hbar} \nabla \cdot \mathbf{j}. \quad (6.142)$$

It is further seen that

$$(\nabla \rho)^2 + \frac{4\mu^2}{\hbar^2} \mathbf{j}^2 = 4\rho |\nabla \psi|^2. \quad (6.143)$$

Therefore we have

$$\text{Re} [\psi^* \nabla^2 \psi] = \frac{1}{2} \nabla^2 \rho - \frac{(\nabla \rho)^2 + 4\mu^2 \mathbf{j}^2 / \hbar^2}{4\rho}, \quad (6.144)$$

and the trivially equivalent local potential becomes

$$V_{\text{TELP}}(\mathbf{r}) = E + \frac{\hbar^2}{4\mu} \left( \frac{\nabla^2 \rho}{\rho} - \frac{(\nabla \rho)^2}{2\rho^2} \right) - \frac{\mu \mathbf{j}^2}{2\rho^2} + i \hbar \frac{\nabla \cdot \mathbf{j}}{2\rho}. \quad (6.145)$$

The ‘potential’ (6.138) or (6.145) fulfils the function of a true potential when inserted in the appropriate place in the Schrödinger equation, but it will generally depend on as many parameters (energy, angular momentum, angle, and so on) as the wave function itself. It fluctuates strongly as a function of the position coordinate (e.g., it generally becomes infinite at the nodes of the wave function) and produces only that specific wave function from which it has been calculated in the first place. It is really less a potential than a functional of the density and the current. In particular, its imaginary part is given by the divergence of the probability current density divided by the probability density.

One thing we can learn from these considerations is the following. Since the divergence of the elastic current density may be positive in some regions (namely, where locally more flux is transferred from the non-elastic channels to the elastic one than *vice versa*), the imaginary part of the optical potential may be *locally emissive*, although of course the overall effect of the optical potential must be absorptive. This holds for any ELP which reproduces, if only approximately, the true elastic wave function inside the nucleus, and is generally also true for others.

The trivially equivalent local potential is less fundamental than a true potential which is expected to have a more universal application than producing just one specific wave function. One may, however, use the prescription (6.138) in an approximate way by substituting a simple approximation for the wave function  $\psi(\mathbf{r})$ , for example, a plane wave function. In this form the trivially equivalent local potential may be useful, and we shall indeed have recourse to it in Chapter 8 where we calculate an approximate optical potential for Coulomb excitation (cf. Section 8.4).

### 6.4.2 The equivalent local potential in WKB

The non-locality of the optical potential (6.12) or (6.61) is contained in the non-static, dynamical term. Furthermore, we have seen that the static term becomes non-local as well when the Pauli principle is taken into account. The Pauli principle will of course also affect the dynamical term and change its nonlocality. The rigorous account of this effect is a very difficult problem indeed, and will not be considered in this book.

Fortunately, it turns out in practice that the leading term in the optical potential is usually the static term. For the determination of the equivalent local potential it is then reasonable, in a first step, to consider only the Pauli, or exchange, non-locality of the energy-independent static term. The derivation of the ELP in the WKB approximation mainly applies to this type of non-local potential. We follow Horiuchi (1980).

## WKB solution of the non-local Schrödinger equation

Consider again the Schrödinger equation for a non-local potential,

$$\left(\frac{1}{2\mu}\check{\mathbf{p}}^2 - E\right)\psi(\mathbf{r}) + \int d^3r' V(\mathbf{r}, \mathbf{r}')\psi(\mathbf{r}') = 0, \quad (6.146)$$

where  $\check{\mathbf{p}} = (\hbar/i)\nabla$  is the momentum operator. We introduce the new independent variable  $\mathbf{s} = \mathbf{r}' - \mathbf{r}$  instead of  $\mathbf{r}'$  and use the general relation for an arbitrary function  $f(\mathbf{r})$

$$f(\mathbf{r} + \mathbf{s}) = e^{\frac{i}{\hbar}\mathbf{s}\cdot\check{\mathbf{p}}}f(\mathbf{r}), \quad (6.147)$$

which is easily proved by expanding the left-hand side into a Taylor series about  $\mathbf{r}$ , and the translation operator  $\exp(i\mathbf{s}\cdot\check{\mathbf{p}}/\hbar)$  on the right-hand side into the corresponding power series. Then we can write

$$\int d^3r' V(\mathbf{r}, \mathbf{r}')\psi(\mathbf{r}') = G(\mathbf{r}, \check{\mathbf{p}})\psi(\mathbf{r}), \quad (6.148)$$

where we have introduced the operator form  $G(\mathbf{r}, \check{\mathbf{p}})$  of the non-local potential  $V(\mathbf{r}, \mathbf{r}')$ ,

$$G(\mathbf{r}, \check{\mathbf{p}}) = \int d^3s e^{\frac{i}{2\hbar}\mathbf{s}\cdot\check{\mathbf{p}}}V(\mathbf{r} - \frac{1}{2}\mathbf{s}, \mathbf{r} + \frac{1}{2}\mathbf{s})e^{\frac{i}{2\hbar}\mathbf{s}\cdot\check{\mathbf{p}}}. \quad (6.149)$$

When the momentum operator  $\check{\mathbf{p}}$  is replaced with the classical momentum the operator  $G(\mathbf{r}, \check{\mathbf{p}})$  becomes the classical *Wigner transform*  $G(\mathbf{r}, \mathbf{p})$  of the non-local potential  $V(\mathbf{r}, \mathbf{r}')$ . It is seen from eqn (6.149) that the function  $G(\mathbf{r}, \mathbf{p})$  depends on the reduced Planck constant  $\hbar$ ; the latter appears as a factor  $1/\hbar$  of the momentum variable  $\mathbf{p}$ .

With the ansatz

$$\psi(\mathbf{r}) = A(\mathbf{r})e^{\frac{i}{\hbar}\tilde{S}(\mathbf{r})} = e^{\frac{i}{\hbar}\tilde{S}(\mathbf{r})}, \quad (6.150)$$

where

$$\tilde{S}(\mathbf{r}) = S(\mathbf{r}) + \frac{\hbar}{i}\ln A(\mathbf{r}), \quad (6.151)$$

we go back to the Schrödinger equation (6.146) using eqns (6.148) and (6.149), and multiply from the left by  $\exp[-(i/\hbar)\tilde{S}(\mathbf{r})]$ ,

$$e^{-\frac{i}{\hbar}\tilde{S}(\mathbf{r})}\left(\frac{1}{2\mu}\check{\mathbf{p}}^2 + G(\mathbf{r}, \check{\mathbf{p}})\right)e^{\frac{i}{\hbar}\tilde{S}(\mathbf{r})} = E. \quad (6.152)$$

Let us consider the quantity  $e^{-(i/\hbar)\tilde{S}(\mathbf{r})}G(\mathbf{r}, \check{\mathbf{p}})e^{(i/\hbar)\tilde{S}(\mathbf{r})}$ . Substituting here the operator (6.149), we obtain

$$\begin{aligned} & e^{-\frac{i}{\hbar}\tilde{S}(\mathbf{r})}G(\mathbf{r}, \check{\mathbf{p}})e^{\frac{i}{\hbar}\tilde{S}(\mathbf{r})} \\ &= \int d^3s e^{-(i/\hbar)\tilde{S}(\mathbf{r})}e^{\frac{i}{2\hbar}\mathbf{s}\cdot\check{\mathbf{p}}}V(\mathbf{r} - \frac{1}{2}\mathbf{s}, \mathbf{r} + \frac{1}{2}\mathbf{s})e^{\frac{i}{2\hbar}\mathbf{s}\cdot\check{\mathbf{p}}}e^{(i/\hbar)\tilde{S}(\mathbf{r})}. \end{aligned} \quad (6.153)$$

We now investigate the action of the first two exponentials in the integrand on the remainder to their right, which we call  $f(\mathbf{r})$ . In this function we omit the variable  $\mathbf{s}$ , on which it also depends; we do this deliberately, because in the following we want to use the variable  $\mathbf{s}$  in the exponential preceding this function as a mere parameter which has nothing to do with the variable of the same name in the function  $f$ . Thus we write the

## 6.4 The equivalent local optical potential

integrand in the form

$$g(\mathbf{r}, \mathbf{s}) = e^{-\frac{i}{\hbar}\tilde{S}(\mathbf{r})}e^{\frac{i}{2\hbar}\mathbf{s}\cdot\check{\mathbf{p}}}f(\mathbf{r}) = e^{-\frac{i}{\hbar}\tilde{S}(\mathbf{r})}f(\mathbf{r} + \frac{1}{2}\mathbf{s}). \quad (6.154)$$

We then have

$$\begin{aligned} \nabla_{\mathbf{s}}g(\mathbf{r}, \mathbf{s}) &= e^{-\frac{i}{\hbar}\tilde{S}(\mathbf{r})}\nabla_{\mathbf{s}}f(\mathbf{r} + \frac{1}{2}\mathbf{s}) \\ &= \frac{1}{2}e^{-\frac{i}{\hbar}\tilde{S}(\mathbf{r})}\nabla_{\mathbf{r}}f(\mathbf{r} + \frac{1}{2}\mathbf{s}) \\ &= \frac{1}{2}\left(\nabla_{\mathbf{r}} + \frac{i}{\hbar}\nabla\tilde{S}(\mathbf{r})\right)g(\mathbf{r}, \mathbf{s}) \\ &= \frac{i}{2\hbar}[\check{\mathbf{p}} + \nabla\tilde{S}(\mathbf{r})]g(\mathbf{r}, \mathbf{s}). \end{aligned} \quad (6.155)$$

The last equation is a differential equation in the variable  $\mathbf{s}$ , with  $\mathbf{r}$  treated as a parameter. Its solution is

$$g(\mathbf{r}, \mathbf{s}) = e^{\frac{i}{2\hbar}\mathbf{s}\cdot[\check{\mathbf{p}} + \nabla\tilde{S}(\mathbf{r})]}g(\mathbf{r}, 0), \quad (6.156)$$

or, going back to the definition (6.154) of  $g(\mathbf{r}, \mathbf{s})$ ,

$$e^{-\frac{i}{\hbar}\tilde{S}(\mathbf{r})}e^{\frac{i}{2\hbar}\mathbf{s}\cdot\check{\mathbf{p}}}f(\mathbf{r}) = e^{\frac{i}{2\hbar}\mathbf{s}\cdot[\check{\mathbf{p}} + \nabla\tilde{S}(\mathbf{r})]}e^{-\frac{i}{\hbar}\tilde{S}(\mathbf{r})}f(\mathbf{r}). \quad (6.157)$$

Using this relation for the evaluation of the exponential to the left of the interaction  $V$  in expression (6.153), and then again for the exponential to the right of  $V$ , we obtain finally

$$e^{-\frac{i}{\hbar}\tilde{S}(\mathbf{r})}G(\mathbf{r}, \check{\mathbf{p}})e^{\frac{i}{\hbar}\tilde{S}(\mathbf{r})} = G[\mathbf{r}, \check{\mathbf{p}} + \nabla\tilde{S}(\mathbf{r})] \cdot 1. \quad (6.158)$$

The operator  $G$  on the right-hand side operates on the constant ‘1’, so that, for example,  $\check{\mathbf{p}} \cdot 1 = 0$ . From eqn (6.152) we then find

$$\left(\frac{[\check{\mathbf{p}} + \nabla\tilde{S}(\mathbf{r})]^2}{2\mu} + G[\mathbf{r}, \check{\mathbf{p}} + \nabla\tilde{S}(\mathbf{r})]\right) \cdot 1 = E; \quad (6.159)$$

in order to obtain the first term on the left-hand side, we have treated the operator  $\check{\mathbf{p}}^2$  as a special form of the general operator  $G(\mathbf{r}, \check{\mathbf{p}})$ .

We now introduce the WKB approximation in eqn (6.159). For this purpose we make the dependence on  $\hbar$  explicit by writing

$$\check{\mathbf{p}} + \nabla\tilde{S} = \nabla S + \frac{\hbar}{i}\left(\frac{\nabla A}{A} + \nabla\right)$$

and expanding the Wigner function  $G(\mathbf{r}, \check{\mathbf{p}} + \nabla\tilde{S})$  about the ‘classical term’  $\nabla S$ , noting the ordering of the operators in expression (6.149),

$$\begin{aligned} G\left[\mathbf{r}, \nabla S + \frac{\hbar}{i}\left(\frac{\nabla A}{A} + \nabla\right)\right] \cdot 1 &= \\ G(\mathbf{r}, \nabla S) + \frac{\hbar}{2i} &\left[\left(\frac{\nabla A}{A} + \nabla\right)\nabla_p G(\mathbf{r}, \mathbf{p})\Big|_{\mathbf{p}=\nabla S}\right. \\ &+ \left.\nabla_p G(\mathbf{r}, \mathbf{p})\Big|_{\mathbf{p}=\nabla S} \cdot \left(\frac{\nabla A}{A} + \nabla\right)\right] \cdot 1. \end{aligned} \quad (6.160)$$

Regarding eqn (6.159) as an identity in the ‘variable’  $\hbar$ , we separate the terms which are odd and even in  $\hbar$ , respectively. Now, owing to rotational invariance and symmetry in the variables  $\mathbf{r}$  and  $\mathbf{r}'$ , the potential  $V(\mathbf{r}, \mathbf{r}')$  has the form  $V(r^2, r'^2, (\mathbf{r} \cdot \mathbf{r}')^2)$ , so that correspondingly, the function  $G(\mathbf{r}, \mathbf{p})$  has the form  $G(r^2, p^2, (\mathbf{r} \cdot \mathbf{p})^2)$ ; it is therefore even in  $\hbar$ , as follows from the discussion after eqn (6.149). To lowest order in  $\hbar$  eqn (6.159) together with eqn (6.160) therefore yields for the even terms

$$\frac{(\nabla S)^2}{2\mu} + G(\mathbf{r}, \nabla S) = E, \quad (6.161)$$

and for the odd terms

$$\left(2\frac{\nabla A}{A} + \nabla\right) \left(\frac{1}{\mu} \nabla S + \nabla_p G(\mathbf{r}, \mathbf{p})|_{\mathbf{p}=\nabla S}\right) = 0. \quad (6.162)$$

Equation (6.161) has the form of a Hamilton–Jacobi equation for the action function  $S(\mathbf{r})$  of a system with a momentum-dependent potential  $G(\mathbf{r}, \mathbf{p})$ . Substituting its solution in eqn (6.162) one can then solve the latter for the amplitude function  $A(\mathbf{r})$ . For simplicity we consider the case of s-waves, where only the magnitudes  $r$  and  $p$  of the variables  $\mathbf{r}$  and  $\mathbf{p}$  are involved. The preceding equations then become

$$\frac{1}{2\mu} \left(\frac{\partial S}{\partial r}\right)^2 + G\left(r, \frac{\partial S}{\partial r}\right) = E \quad (6.163)$$

and

$$\left(\frac{2}{A} \frac{\partial A}{\partial r} + \frac{\partial}{\partial r}\right) \left(\frac{1}{\mu} \frac{\partial S}{\partial r} + \frac{\partial}{\partial p} G(r, p)\Big|_{p=\partial S/\partial r}\right) = 0. \quad (6.164)$$

Introducing the local momentum  $p(r) = \partial S(r)/\partial r$  as the solution of the algebraic Hamilton–Jacobi equation (6.163),

$$\frac{[p(r)]^2}{2\mu} + G[r, p(r)] = E, \quad (6.165)$$

we can evaluate the action function as

$$S(r) = \int^r dr' p(r'). \quad (6.166)$$

We now rewrite eqn (6.164) in the form

$$2\frac{\partial}{\partial r} \ln A = -\frac{\partial}{\partial r} \ln \left(\frac{p(r)}{\mu} + \frac{\partial}{\partial p} G(r, p)\right), \quad (6.167)$$

setting  $p = p(r)$  after the differentiations have been carried out. We then find

$$A(r) = \left(\frac{p(r)}{\mu} + \frac{\partial}{\partial p} G(r, p)\right)^{-1/2} \equiv \left(\frac{\mu}{p(r)}\right)^{1/2} F(r), \quad (6.168)$$

where

$$F(r) = \left(1 + \frac{\mu}{p} \frac{\partial}{\partial p} G(r, p)\right)^{-1/2} \quad \text{with } p = p(r). \quad (6.169)$$

The wave function for the non-local potential is then

$$\psi(r) = A(r) e^{\pm i \frac{\hbar}{\hbar} S(r)}, \quad (6.170)$$

with  $S(r)$  and  $A(r)$  given by eqns (6.166) and (6.168), respectively.

#### Determination of the ELP

It is the asymptotic behaviour of the action function  $S(r)$  which determines the scattering phase shift. Therefore, we define the ELP as that potential  $V_{\text{loc}}(r)$  which yields the same  $S(r)$  and thus also the same  $p(r)$  as the non-local one. The Hamilton–Jacobi equation for such a local potential is

$$\frac{[p(r)]^2}{2\mu} + V_{\text{loc}}(r) = E, \quad (6.171)$$

which together with eqn (6.165) yields an algebraic equation for the equivalent local potential  $V_{\text{loc}}(r)$ ,

$$V_{\text{loc}}(r) = G(r, \sqrt{2\mu[E - V_{\text{loc}}(r)]}). \quad (6.172)$$

It is clear from this equation that the ELP depends on energy,  $V_{\text{loc}}(r) = V_{\text{loc}}(r; E)$ . This energy dependence is not of dynamical origin as in the potentials we have discussed before, but is a consequence of the transformation from a non-local to a local potential.

#### The Perey factor

For the local potential  $V_{\text{loc}}(r)$  with local momentum  $p(r)$  the wave function has the form

$$\psi_{\text{loc}}(r) = \left(\frac{\mu}{p(r)}\right)^{1/2} e^{\pm i \frac{\hbar}{\hbar} S(r)}. \quad (6.173)$$

Thus the wave solution  $\psi_{\text{loc}}(r)$  for the ELP is related to the wave solution for the non-local potential,  $\psi(r)$ , (cf. eqns (6.168) and (6.170)) by

$$\psi(r) = F(r) \psi_{\text{loc}}(r). \quad (6.174)$$

The factor  $F(r)$  which converts the solution for the ELP into the true ‘non-local’ solution, is called the **Perey factor** (cf. Perey 1963; Austern 1965). This factor is given by eqn (6.169) in terms of the non-local potential, or more precisely, its Wigner transform  $G(r, p)$ .

When the non-local potential is independent of the energy  $E$ , as is the case for the static term of the optical potential with exchange effects, then the expression for the Perey factor can be written very simply in terms of the local equivalent potential  $V_{\text{loc}}(r; E)$ , as we shall now show. From eqn (6.172) we have

$$\frac{\partial}{\partial E} V_{\text{loc}}(r; E) = \frac{\mu}{p} \frac{\partial}{\partial p} G(r, p) \left(1 - \frac{\partial}{\partial E} V_{\text{loc}}(r; E)\right) \quad \text{with } p = p(r). \quad (6.175)$$

Solving this equation for  $(\partial/\partial p)G(r, p)$  and substituting in eqn (6.169) we have

$$F(r) = \left(1 - \frac{\partial}{\partial E} V_{\text{loc}}(r; E)\right)^{1/2}. \quad (6.176)$$

This relation does not contain the non-local potential explicitly. Therefore, when a local optical potential has been found phenomenologically and is known to be the equivalent of an energy-independent non-local potential, then the Perey factor, and thus the true solution for the non-local potential, can be calculated from the ELP alone, without reference to the underlying non-local potential.

As a simple example we consider a non-local potential of the Frahn–Lemmer type (cf. Frahn and Lemmer 1957),

$$V(\mathbf{r}, \mathbf{r}') = U(|\mathbf{r} + \mathbf{r}'|/2)H(|\mathbf{r} - \mathbf{r}'|), \quad (6.177)$$

where

$$H(s) = (\pi\beta^2)^{-3/2} \exp(-s^2/\beta^2); \quad (6.178)$$

the quantity  $\beta$  is the range of the non-locality. The Wigner transform of this potential is

$$G(r, p) = U(r) \exp\left[-\left(\frac{\beta p}{2\hbar}\right)^2\right] \quad (6.179)$$

(this is an even function of  $\hbar$ , as required above), and the equivalent local potential is obtained as the solution of eqn (6.172), which here takes the form

$$V_{\text{loc}}(r; E) = U(r) \exp\left(-\frac{\mu\beta^2}{2\hbar^2}[E - V_{\text{loc}}(r; E)]\right). \quad (6.180)$$

Taking the derivative of eqn (6.180) with respect to the energy we find

$$\frac{\partial}{\partial E} V_{\text{loc}}(r; E) = -\frac{\mu\beta^2}{2\hbar^2} V_{\text{loc}}(r; E) \left(1 - \frac{\partial}{\partial E} V_{\text{loc}}(r; E)\right), \quad (6.181)$$

and solving this equation for  $\partial V_{\text{loc}}(r; E)/\partial E$  and substituting in eqn (6.176), we obtain the Perey factor

$$F(r) = \left(1 - \frac{\mu\beta^2}{2\hbar^2} V_{\text{loc}}(r; E)\right)^{-1/2}. \quad (6.182)$$

For neutrons, for example, the potential  $V_{\text{loc}}(r; E)$  is everywhere negative, so that  $F(r) < 1$ . Thus the wave solution for the ELP has to be multiplied by a factor smaller than unity in order to produce the non-local wave function, which in some places has led to the habit of calling the Perey factor a ‘damping factor’. We emphasize, however, that there is nothing in principle which prevents the Perey factor from exceeding unity locally or globally.

#### The validity of the WKB approximation

The present derivation of the ELP is based on the WKB expansion (6.160). This expansion is justified only if the function  $G(\mathbf{r}, \mathbf{p})$  varies smoothly as a function of  $\mathbf{p}$ , or more precisely, if its momentum variation over the distance of a wavelength  $\lambda$  is small compared with the value of  $G$  itself,

$$\left(\nabla_p G \cdot \frac{d\mathbf{p}}{d\lambda}\right) \lambda \ll G. \quad (6.183)$$

For example, for the Frahn–Lemmer potential (6.177) together with eqn (6.178) this means, using eqn (6.179) and  $p = 2\pi\hbar/\lambda$ ,

$$\beta \ll \frac{\hbar}{p}. \quad (6.184)$$

This inequality states that the non-locality range  $\beta$  must be *smaller* than the minimal Heisenberg uncertainty  $\hbar/p$  for a given momentum  $p$ .

## 6.5 Dispersion relations

### 6.5.1 Derivation of the dispersion relation

*The dispersion relation for the GOP*

It has been shown in Section 6.2.4 that the GOP is a function of the energy  $E$ , consisting of a sum of real poles and a continuous part  $\mathcal{V}^{(\text{cont})}(E)$  with a branch cut along the real axis (cf. the explicit schematic form (6.62) together with expression (6.64)). For the continuous part we can write down the Cauchy relation

$$\mathcal{V}^{(\text{cont})}(E) = \frac{1}{2\pi i} \int_C dE' \frac{\mathcal{V}^{(\text{cont})}(E')}{E' - E - i\eta}, \quad (6.185)$$

which holds for all values of  $E$  in the upper half-plane including the real axis. The contour  $C$  runs along the real axis and is closed in an anti-clockwise direction along a large half-circle in the upper half-plane. Since  $\mathcal{V}^{(\text{cont})}(E')$  vanishes asymptotically on the half-circle, the contour  $C$  can be restricted to the real axis alone. The value of the function  $\mathcal{V}^{(\text{cont})}(E)$  on the real  $E$ -axis is given by  $\mathcal{V}^{(\text{cont})}(E) = \mathcal{V}^{(\text{cont})}(E + i\eta)$ , and we therefore have for the entire GOP of eqn (6.62)

$$\mathcal{V}(E) = V_{\text{stat}} + \sum_{\lambda} \frac{|V_{0\lambda}\rangle\langle V_{0\lambda}|}{E - E_{\lambda}^{(\text{pole})}} + \frac{1}{2\pi i} \int_{-\infty}^{\infty} dE' \frac{\mathcal{V}^{(\text{cont})}(E')}{E' - E - i\eta} \quad \text{for } \text{Im } E \geq 0. \quad (6.186)$$

For *real*  $E$  we may use relation (6.13) which yields

$$\begin{aligned} \mathcal{V}(E) = V_{\text{stat}} &+ \sum_{\lambda} \frac{|V_{0\lambda}\rangle\langle V_{0\lambda}|}{E - E_{\lambda}^{(\text{pole})}} \\ &+ \frac{\mathcal{P}}{2\pi i} \int_{-\infty}^{\infty} dE' \frac{\mathcal{V}^{(\text{cont})}(E')}{E' - E} + \frac{1}{2}\mathcal{V}^{(\text{cont})}(E) \quad \text{for real } E. \end{aligned} \quad (6.187)$$

Eliminating the term  $\frac{1}{2}\mathcal{V}^{(\text{cont})}$  with the help of eqn (6.62), we arrive at

$$\mathcal{V}(E) = V_{\text{stat}} + \sum_{\lambda} \frac{|V_{0\lambda}\rangle\langle V_{0\lambda}|}{E - E_{\lambda}^{(\text{pole})}} + \frac{\mathcal{P}}{\pi i} \int_{-\infty}^{\infty} dE' \frac{\mathcal{V}^{(\text{cont})}(E')}{E' - E} \quad \text{for real } E, \quad (6.188)$$

and taking the real part of this relation, we obtain

$$\text{Re } \mathcal{V}(E) = V_{\text{stat}} + \sum_{\lambda} \frac{|V_{0\lambda}\rangle\langle V_{0\lambda}|}{E - E_{\lambda}^{(\text{pole})}} + \frac{\mathcal{P}}{\pi} \int_{-\infty}^{\infty} dE' \frac{\text{Im } \mathcal{V}^{(\text{cont})}(E')}{E' - E} \quad \text{for real } E. \quad (6.189)$$

As discussed in Section 6.2.2, the imaginary part of the GOP vanishes for energies below the first inelastic threshold  $\epsilon_1$ . With  $\text{Im } \mathcal{V}^{(\text{cont})}(E) = \text{Im } \mathcal{V}(E)$  we thus obtain the

**dispersion relation for the GOP**

$$\operatorname{Re} \mathcal{V}(E) = V_{\text{stat}} + \sum_{\lambda} \frac{|V_{0\lambda}\rangle \langle V_{0\lambda}|}{E - E_{\lambda}^{(\text{pole})}} + \frac{\mathcal{P}}{\pi} \int_{\epsilon_1}^{\infty} dE' \frac{\operatorname{Im} \mathcal{V}(E')}{E' - E} \quad \text{for real } E. \quad (6.190)$$

Adding  $i \operatorname{Im} \mathcal{V}(E)$  on both sides of eqn (6.190) and using the relation (6.13), we have for real  $E$ , and by analytic continuation also for complex  $E$ ,

$$\mathcal{V}(E) = V_{\text{stat}} + \sum_{\lambda} \frac{|V_{0\lambda}\rangle \langle V_{0\lambda}|}{E - E_{\lambda}^{(\text{pole})}} + \frac{1}{\pi} \int_{\epsilon_1}^{\infty} dE' \frac{\operatorname{Im} \mathcal{V}(E')}{E' - E - i\eta}. \quad (6.191)$$

This equation exhibits explicitly the analytic properties of the GOP on the physical sheet of the complex  $E$ -plane.

**The dispersion relation for the optical potential**

Turning now to the optical potential in the proper sense, we recall that it is related to the GOP by  $\mathcal{V}_{\text{opt}}(E) = \mathcal{V}(E + iI)$ , and is therefore analytic in the half-plane  $\operatorname{Im} E > -I$ . Hence  $\mathcal{V}_{\text{opt}}(E)$  satisfies the same relations (6.185) to (6.189) as the potential  $\mathcal{V}(E)$ , except that now the formerly real poles have been shifted downward into the lower half-plane,  $E_{\lambda}^{(\text{pole})} \rightarrow E_{\lambda}^{(\text{pole})} - iI$ , so that the sum of poles becomes continuous on the real axis and can be included in the continuous part of the optical potential. Instead of eqn (6.189) we have then

$$\operatorname{Re} \mathcal{V}_{\text{opt}}(E) = V_{\text{stat}} + \frac{\mathcal{P}}{\pi} \int_{-\infty}^{\infty} dE' \frac{\operatorname{Im} \mathcal{V}_{\text{opt}}(E')}{E' - E} \quad \text{for real } E. \quad (6.192)$$

Now the imaginary part of the optical potential is obtained from the GOP of eqn (6.191) by writing

$$\begin{aligned} \operatorname{Im} \mathcal{V}_{\text{opt}}(E) &= \operatorname{Im} \mathcal{V}(E + iI) = \\ &= -I \sum_{\lambda} \frac{|V_{0\lambda}\rangle \langle V_{0\lambda}|}{(E - E_{\lambda}^{(\text{pole})})^2 + I^2} + \frac{I}{\pi} \int_{\epsilon_1}^{\infty} dE' \frac{\operatorname{Im} \mathcal{V}(E')}{(E' - E)^2 + I^2}, \end{aligned} \quad (6.193)$$

which implies that the energy at which  $\operatorname{Im} \mathcal{V}_{\text{opt}}(E)$  becomes non-vanishing is ‘smeared out’ by an amount  $2I$  around the lowest threshold energy  $\epsilon_1$  or the lowest of the energies  $E_{\lambda}^{(\text{pole})}$ , whichever is smallest. We may therefore introduce an effective threshold energy  $E_0$  for  $\operatorname{Im} \mathcal{V}_{\text{opt}}(E)$  somewhere between 0 and  $\epsilon_1$ , and obtain the **dispersion relation for the optical potential**

$$\operatorname{Re} \mathcal{V}_{\text{opt}}(E) = V_{\text{stat}} + \frac{\mathcal{P}}{\pi} \int_{E_0}^{\infty} dE' \frac{\operatorname{Im} \mathcal{V}_{\text{opt}}(E')}{E' - E} \quad \text{for real } E. \quad (6.194)$$

In analogy to eqn (6.191) we then obtain on the entire physical sheet in the complex  $E$ -plane

$$\mathcal{V}_{\text{opt}}(E) = V_{\text{stat}} + \frac{1}{\pi} \int_{E_0}^{\infty} dE' \frac{\operatorname{Im} \mathcal{V}_{\text{opt}}(E')}{E' - E - i\eta}. \quad (6.195)$$

On the real axis it is convenient to write the optical potential as a sum,

$$\mathcal{V}_{\text{opt}}(E) = V_{\text{stat}} + V_{\text{dyn}}(E), \quad (6.196)$$

where the dynamical part  $V_{\text{dyn}}(E)$  is the complex, energy-dependent contribution of the dispersion integral on the right-hand side of eqn (6.195), which we write as

$$V_{\text{dyn}}(E) = V_{\text{pol}}(E) + i \operatorname{Im} \mathcal{V}_{\text{opt}}(E). \quad (6.197)$$

Its imaginary part is the *absorptive* part of the optical potential, which takes account of the loss of shape-elastic current by direct coupling to the non-elastic channels as well as by compound-elastic scattering. The real part

$$V_{\text{pol}}(E) = \frac{\mathcal{P}}{\pi} \int_{E_0}^{\infty} dE' \frac{\operatorname{Im} \mathcal{V}_{\text{opt}}(E')}{E' - E} \quad (6.198)$$

is called the **dispersive or polarization part**, because it represents the polarizing effect of the non-elastic channels and the compound states on the real potential in the elastic channel.

**Causality**

The analytic properties of the optical potential and their consequence, the dispersion relation, are closely connected with the causal behaviour of the potential in a time-dependent description. Let us again write down the optical-model Schrödinger equation (6.115),

$$(T + \mathcal{V}_{\text{opt}}(E) - E)|\mathbf{k}^+\rangle_{\text{opt}} = 0. \quad (6.199)$$

This is a stationary Schrödinger equation, which can be transformed to a time-dependent equation by a Fourier transformation. To this end we write

$$\mathcal{V}_{\text{opt}}(E) = \int_{-\infty}^{\infty} dt e^{iEt/\hbar} \mathcal{V}_{\text{opt}}(t), \quad (6.200)$$

where we have expressed  $\mathcal{V}_{\text{opt}}(E)$  in terms of the *time-dependent* optical potential

$$\mathcal{V}_{\text{opt}}(t) = \frac{1}{2\pi} \int_{-\infty}^{\infty} dE e^{-iEt/\hbar} \mathcal{V}_{\text{opt}}(E), \quad (6.201)$$

which is the inverse Fourier transform of the potential (6.200). Introducing expression (6.200) in eqn (6.199), multiplying by  $A(\mathbf{k} - \mathbf{k}_a) \exp(-iEt/\hbar)$  and integrating over  $\mathbf{k}$ , we find

$$\begin{aligned} &\int d^3k A(\mathbf{k} - \mathbf{k}_a) e^{-iEt/\hbar} (T - E)|\mathbf{k}^+\rangle_{\text{opt}} \\ &+ \int_{-\infty}^{\infty} d\tau \mathcal{V}_{\text{opt}}(\tau) \int d^3k A(\mathbf{k} - \mathbf{k}_a) e^{-iE(t-\tau)/\hbar} |\mathbf{k}^+\rangle_{\text{opt}} = 0 \end{aligned} \quad (6.202)$$

or, using the definition (4.49) of the time-dependent scattering state  $|\Psi_{\mathbf{k}_a}^+(t)\rangle$ ,

$$\left( T + \frac{\hbar}{i} \frac{d}{dt} \right) |\Psi_{\mathbf{k}_a}^+(t)\rangle_{\text{opt}} + \int_{-\infty}^{\infty} dt' \mathcal{V}_{\text{opt}}(t - t') |\Psi_{\mathbf{k}_a}^+(t')\rangle_{\text{opt}} = 0. \quad (6.203)$$

The time-dependent optical potential (6.201) is an integral of the function  $\mathcal{V}_{\text{opt}}(E)$ , which according to eqn (6.195) consists of a constant part  $V_{\text{stat}}$  and a function of  $E$  which is analytic in the upper half-plane including the real axis. The constant part contributes a term  $V_{\text{stat}} \delta(t)$ . The integration over the  $E$ -dependent part  $\mathcal{V}_{\text{dyn}}(E)$  in expression (6.201)

vanishes for  $t < 0$ , because in this case the integration contour can be closed along a large half-circle in the upper half-plane (this half-circle does not contribute to the integral because  $V_{\text{dyn}}(E)\exp(-iEt/\hbar) \rightarrow 0$  for  $\text{Im } E > 0, |E| \rightarrow \infty$ ). Since the integrand is analytic inside the closed contour, the entire integral reduces to zero. Therefore the dynamical part of the optical potential contributes only for  $t > 0$ , and we have

$$V_{\text{opt}}(t) = V_{\text{stat}} \delta(t) + V_{\text{dyn}}(t) \theta(t). \quad (6.204)$$

The time-dependent optical-model Schrödinger equation (6.203) reads, finally,

$$\left(\frac{\hbar}{i} \frac{d}{dt} + T + V_{\text{stat}}\right) |\Psi_{\mathbf{k}_a}^+(t)\rangle_{\text{opt}} + \int_{-\infty}^t dt' V_{\text{dyn}}(t-t') |\Psi_{\mathbf{k}_a}^+(t')\rangle_{\text{opt}} = 0. \quad (6.205)$$

The action of the static part is instantaneous, while that of the dynamical part is *retarded*, i.e. its action at time  $t$  involves the scattering state at earlier times  $t' < t$ . This is a manifestation of *causality*.

### 6.5.2 An application of the dispersion relation

The dispersion relation has been used, for example, in the analysis of the so-called ‘threshold anomalies’ in heavy-ion scattering. These are enhancements of the attractive real part of the optical potential at energies near the top of the Coulomb barrier, and can be related to the onset of absorption in that energy region. We shall discuss this in the following.

Consider the imaginary part of an optical potential of Woods–Saxon shape, say, whose strength rises linearly from zero at the threshold energy  $E_0$  to a maximum  $W_0$  at  $E_1$  and then decreases again linearly to zero at the (large) energy  $E_2$ . This function

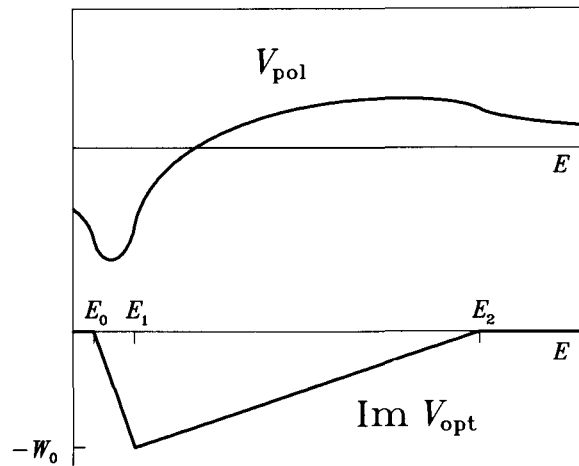


Figure 6.3 Absorptive and polarization parts of a schematic heavy-ion optical potential.

represents in a schematic fashion the energy dependence of the imaginary part of a heavy-ion optical potential (cf. Fig. 6.3), at least as far as the effects near threshold are

concerned. We thus have, with  $\Delta_0 = E_1 - E_0$ ,  $\Delta_2 = E_2 - E_1$ ,

$$\text{Im } V_{\text{opt}}(E) = \begin{cases} -(W_0/\Delta_0)(E - E_0) & \text{for } E_0 < E < E_1, \\ (W_0/\Delta_2)(E - E_2) & \text{for } E_1 < E < E_2, \\ 0 & \text{elsewhere.} \end{cases} \quad (6.206)$$

For the first interval we find from eqn (6.198)

$$\begin{aligned} V_{\text{pol}}^{(1)}(E) &= -\frac{W_0}{\pi \Delta_0} \int_{E_0}^{E_1} dE' \left( 1 + (E - E_0) \frac{\mathcal{P}}{E' - E} \right) \\ &= -\frac{W_0}{\pi} \left( 1 + \frac{E - E_0}{\Delta_0} \ln \frac{|E_1 - E|}{|E_0 - E|} \right), \end{aligned} \quad (6.207)$$

and similarly for the second interval,

$$V_{\text{pol}}^{(2)}(E) = \frac{W_0}{\pi} \left( 1 + \frac{E - E_2}{\Delta_2} \ln \frac{|E_2 - E|}{|E_1 - E|} \right). \quad (6.208)$$

Therefore,

$$\begin{aligned} V_{\text{pol}}(E) &= V_{\text{pol}}^{(1)}(E) + V_{\text{pol}}^{(2)}(E) \\ &= \frac{W_0}{\pi} \left( -\frac{E - E_0}{\Delta_0} \ln \frac{|E_1 - E|}{|E_0 - E|} + \frac{E - E_2}{\Delta_2} \ln \frac{|E_2 - E|}{|E_1 - E|} \right). \end{aligned} \quad (6.209)$$

In Fig. 6.3 we show the absorptive part and the corresponding polarization part as calculated from eqns (6.206) and (6.209). It is seen that the onset of absorption at the threshold energy  $E_0$  leads to an enhanced attraction in the real potential just above this energy.

#### Subtracted dispersion relations

The imaginary part  $W$  of the optical potential usually extends to rather high energies. Some authors (cf. Passatore 1967) let it assume a constant non-vanishing value at infinity. In the latter case the dispersion integral (6.198) diverges, and we must modify our treatment.

We go back to eqn (6.185), which holds for any function which is analytic in the upper half of the complex  $E$ -plane as long as the contour  $\mathcal{C}$  is closed around the point  $E$ , and write

$$\begin{aligned} &\mathcal{V}^{\text{cont}}(E) - \mathcal{V}^{\text{cont}}(E_R) \\ &= \frac{1}{2\pi i} \int_{\mathcal{C}} dE' \frac{\mathcal{V}^{\text{cont}}(E')}{E' - E - i\eta} - \frac{1}{2\pi i} \int_{\mathcal{C}} dE' \frac{\mathcal{V}^{\text{cont}}(E')}{E' - E_R - i\eta} \\ &= \frac{E - E_R}{2\pi i} \int_{\mathcal{C}} dE' \frac{\mathcal{V}^{\text{cont}}(E')}{(E' - E - i\eta)(E' - E_R - i\eta)}, \end{aligned} \quad (6.210)$$

where  $E_R$  is some conveniently chosen reference energy on the real axis. Since the integrand in the last line contains the square of  $E'$  in the denominator, the contribution along the large half-circle now vanishes even if  $\mathcal{V}^{\text{cont}}(E')$  is a constant there. Following the previous procedure, we then obtain instead of eqn (6.194) the *subtracted dispersion*

relation

$$\text{Re } V_{\text{opt}}(E) = \text{Re } V_{\text{opt}}(E_R) + (E - E_R) \frac{\mathcal{P}}{\pi} \int_{E_0}^{\infty} dE' \frac{\text{Im } V_{\text{opt}}(E')}{(E' - E)(E' - E_R)}. \quad (6.211)$$

Correspondingly we find for the polarization potential

$$V_{\text{pol}}(E) = V_{\text{pol}}(E_R) + (E - E_R) \frac{\mathcal{P}}{\pi} \int_{E_0}^{\infty} dE' \frac{\text{Im } V_{\text{opt}}(E')}{(E' - E)(E' - E_R)}. \quad (6.212)$$

The subtracted dispersion relations allow us to relate the real and imaginary parts of the optical potential if the latter becomes a non-vanishing constant at large energies. They can also be employed to improve the convergence of the dispersion integral of the imaginary part in general. The price to be paid for this advantage is the appearance of the unknown parameter  $V_{\text{pol}}(E_R)$  which allows us only to determine the energy dependence of the polarization potential, but not its absolute normalization.

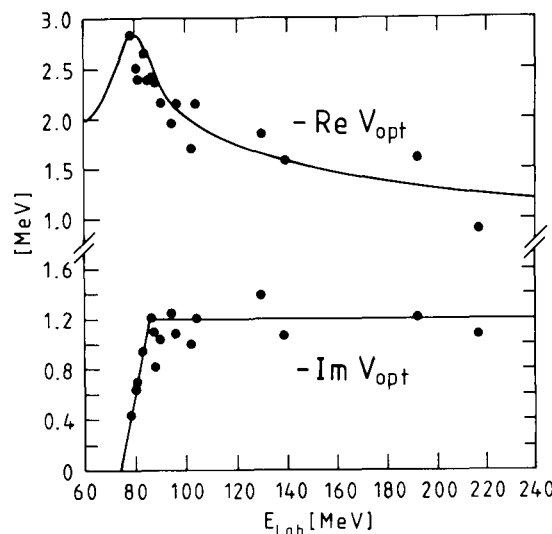


**Figure 6.4** Real and imaginary parts of the optical potential for the system  $^{16}\text{O} + ^{208}\text{Pb}$  evaluated at the radius  $r = 12.4$  fm. The real part is composed of the static potential and the polarization part. The end-point energy  $E_2$  in the imaginary part has here been removed to infinity. The dots represent empirical values.

As a realistic case we consider the system  $^{16}\text{O} + ^{208}\text{Pb}$ , where the energy dependence of the imaginary part of the phenomenological optical potential induces, via the dispersion relation, an enhancement around  $E = 80$  MeV in the real part. Such an ‘anomaly’ is indeed found in optical-model fits to the data, as shown in Fig. 6.4 (cf. Nagarajan *et al.* 1985). In this analysis, the imaginary part of the potential has been assumed to be constant and non-vanishing at large energies, i.e. its end-point  $E_2$  has been taken out to infinity. Therefore, a subtracted dispersion relation has been used (cf. Satchler 1991).

## 6.6 Notes and references

The optical model for nuclear scattering was introduced by Bethe (1940), Fernbach *et al.* (1949) and Pasternack and Snyder (1950). The first realistic calculations of elastic cross sections solving the Schrödinger equation with a complex potential were performed by Le Levier and Saxon (1952) and Woods and Saxon (1954). There exists a vast literature on phenomenological optical potentials. We refer to the early books by Jones (1960) and Hodgson (1963) and to more recent review articles by Beccetti and Greenlees (1969), Rapaport (1982) and Varner *et al.* (1991).

The first theories of the optical potential were based on a multiple-scattering formalism (cf. Lax 1951; Kerman *et al.* 1959; Takeda and Watson 1954, 1955; Riesenfeld and Watson 1956). The theory in the form discussed here was initiated by Feshbach (1958a), Brown (1959) and Agodi and Eberle (1960). Explicit microscopic calculations of the optical potential have been performed in this formalism, for example, by Bouyssy *et al.* (1981) and Rawitscher (1987). The effect of the Pauli principle has been discussed by Feshbach (1962), Coester and Kümmel (1958) and Lipperheide (1962).

The shell-model theory of nuclear reactions was considered in its principal features by Sachs (1953), Brenig (1959), and Brenig and Haag (1959). It has been developed in great detail by Mahaux and Weidenmüller (1969). Its use in the optical model was proposed by Lipperheide (1966).

The interpretation of the phenomenological optical potential as that potential which produces the energy average of the elastic scattering function was proposed by Feshbach *et al.* (1954). This idea has been worked out by Feshbach (1958a,b), Brown (1964), Lipperheide (1967), and Mahaux and Weidenmüller (1969).

Some key references for equivalent local potentials are Frahn and Lemmer (1957), Perey and Buck (1962), Fiedeldey (1967), and Horiuchi (1980). The Perey factor is discussed by Perey (1963) and Austern (1965).

Dispersion relations for the optical potential have first been mentioned by Feshbach (1958a), and their connection with causality has been pointed out by Cornwall and Ruderman (1962). Calculations have been carried out by Passatore (1967) and Lipperheide and Schmidt (1968) for nucleon scattering. Dispersion relations have been introduced in the description of heavy-ion scattering by Nagarajan *et al.* (1985). Reviews have been written by Hodgson (1991) and Satchler (1991).

The extension of the GOP formalism to include the description of bound states has been considered by Lipperheide (1966), Johnson *et al.* (1987), and Mahaux and Sartor (1989, 1991a). A review of the unified optical potential for scattering and bound states has been given by Hodgson (1990).

A large amount of work has also been done on the optical potential for nuclear matter, cf., for example, Jeukenne *et al.* (1976) and Mahaux *et al.* (1985). In particular, the connection between the optical potential as defined in the present chapter (the ‘Feshbach potential’) and its analogue in nuclear matter, the mass operator, has been discussed by Mahaux and Sartor (1991b) and Mahaux and Satchler (1993).

## References

Agodi, A. and Eberle, E. (1960). *Nuovo Cimento* **18** 718.

- Austern, N. (1965). *Phys. Rev.* **137** B752.  
 Beccetti, B. and Greenlees, G. (1969). *Phys. Rev.* **182** 1190.  
 Bethe, H. A. (1940). *Phys. Rev.* **57** 1125.  
 Bouyssy, A., Ngô, H. and Vinh Mau, N. (1981). *Nucl. Phys.* **A371** 173.  
 Brenig, W. (1959). *Nucl. Phys.* **13** 333.  
 Brenig, W. and Haag, R. (1959). *Fortschritte der Physik* **7** 183; translated in *Quantum scattering theory* (1963), ed. Ross, M., Indiana University Press, Bloomington.  
 Brown, G. E. (1959). *Rev. Mod. Phys.* **31** 893.  
 Brown, G. E. (1964). *Unified theory of nuclear models*, North-Holland, Amsterdam.  
 Coester, F. and Kümmel, H. (1958). *Nucl. Phys.* **9** 225.  
 Cornwall, J. M. and Ruderman, M. A. (1962). *Phys. Rev.* **128** 1474.  
 Fernbach, S., Serber, R. and Taylor, T. B. (1949). *Phys. Rev.* **75** 1352.  
 Feshbach, H. (1958a). *Ann. Phys. (N.Y.)* **5** 357.  
 Feshbach, H. (1958b). *Ann. Rev. Nucl. Sci.* **8** 49.  
 Feshbach, H. (1962). *Ann. Phys. (N.Y.)* **19** 287.  
 Feshbach, H., Porter, C. E. and Weisskopf, V. F. (1954). *Phys. Rev.* **96** 448.  
 Fiedeldey, H. (1967). *Nucl. Phys.* **A96** 463.  
 Frahn, W. E. and Lemmer, R. H. (1957). *Nuovo Cimento* **5** 523 and 1564.  
 Friedman, F. L. and Weisskopf, V. F. (1955). *Niels Bohr and the development of physics*, ed. Pauli, W., Pergamon, New York, p. 134.  
 Hodgson, P. E. (1963). *The optical model of elastic scattering*, Oxford University Press, Oxford.  
 Hodgson, P. E. (1971). *Nuclear reactions and nuclear structure*, Clarendon Press, Oxford.  
 Hodgson, P. E. (1990). *Contemporary Physics* **31** 295.  
 Hodgson, P. E. (1991). *Proc. int. conf. on nuclear data for science and technology, Jülich, Germany*.  
 Horiuchi, (1980). *Progr. Theor. Phys.* **64** 184.  
 Jeukenne, J. P., Lejeune, A. L. and Mahaux, C. (1976). *Phys. Rep.* **C25** 83.  
 Johnson, C. H., Horen, D. J. and Mahaux, C. (1987). *Phys. Rev.* **C36** 2252.  
 Jones, P. B. (1960). *The optical model in nuclear and particle physics*, Interscience, New York.  
 Kerman, A. K., McManus, H. and Thaler, R. (1959). *Ann. Phys. (N.Y.)* **8** 551.  
 Langanke, K. and Friedrich, H. (1986). *Adv. Nucl. Phys.* **17** 223.  
 Lax, M. (1951). *Rev. Mod. Phys.* **23** 287.  
 Le Levier, R. E. and Saxon, D. S. (1952). *Phys. Rev.* **87** 40.  
 Lipperheide, R. (1962). *Ann. Phys. (N.Y.)* **17** 114.  
 Lipperheide, R. (1966). *Nucl. Phys.* **89** 97.  
 Lipperheide, R. (1967). *Z. Physik* **202** 58.  
 Lipperheide, R. and Schmidt, A. K. (1968). *Nucl. Phys.* **A112** 65.  
 Mahaux, C. and Sartor, R. (1989). *Nucl. Phys.* **A493** 157.  
 Mahaux, C. and Sartor, R. (1991a). *Adv. Nucl. Phys.* **20** 1.  
 Mahaux, C. and Sartor, R. (1991b). *Nucl. Phys.* **A530** 303.  
 Mahaux, C. and Satchler, G. R. (1993). *Nucl. Phys.* **A560** 5.

- Mahaux, C. and Weidenmüller, H. A. (1969). *Shell model approach to nuclear reactions*, North-Holland, Amsterdam.  
 Mahaux, C., Bortignon, P. F., Broglia, R. A. and Dasso, C. H. (1985). *Phys. Rep.* **C120** 1.  
 Nagarajan, M. A., Mahaux, C. and Satchler, G. R. (1985). *Phys. Rev. Lett.* **54** 1136.  
 Messiah, A. (1972). *Quantum mechanics*, North-Holland, Amsterdam.  
 Passatore, G. (1967). *Nucl. Phys.* **A95** 694.  
 Pasternack, S. and Snyder, H. S. (1950). *Phys. Rev.* **80** 921.  
 Perey, F. G. (1963). *Proc. Conf. on direct interactions and nuclear reaction mechanisms*, eds. Clementel, E. and Villi, C., Gordon and Breach, New York, p. 125.  
 Perey, F. G. and Buck, B. (1962). *Nucl. Phys.* **32** 353.  
 Rapaport, J. (1982). *Phys. Rep.* **C87** 25.  
 Rawitscher, G. H. (1987). *Nucl. Phys.* **A475** 519.  
 Riesenfeld, W. B. and Watson, K. M. (1956). *Phys. Rev.* **102** 1157.  
 Sachs, R. G. (1953). *Nuclear Theory*, Addison-Wesley, Cambridge, MA.  
 Satchler, G. R. (1991). *Phys. Rep.* **C199** 147.  
 Takeda, G. and Watson, K. M. (1954). *Phys. Rev.* **94** 1087.  
 Takeda, G. and Watson, K. M. (1955). *Phys. Rev.* **97** 1336.  
 Varner, R. L., Thompson, W. J., McAbee, T. L., Ludwig, E. J. and Clegg, T. B. (1991). *Phys. Rep.* **C201** 57.  
 Woods, R. D. and Saxon, D. S. (1954). *Phys. Rev.* **95** 577.

## **Part C**

### Direct Reactions

## SINGLE-STEP APPROXIMATIONS

### 7.1 Introduction

The formal theory of reactions developed in Chapter 5 has provided us with rigorous expressions for the cross section of any type of transition from one two-body channel to another. These can be used as the starting point for the explicit calculation of reaction cross sections to be compared with experimental data. We shall demonstrate this using as examples a number of specific reactions for which the cross section will be derived in detail.

We first consider the so-called *direct reactions*, where only a few nucleons or excitation modes are involved, and where certain approximations, as for example, the Born approximation or the truncation of the channel space, are justified. We shall be obliged to introduce a further *element of non-rigour* by making use of phenomenological optical potentials. These simplifications are forced upon us because exact calculations of the cross sections of nuclear reactions are forbiddingly difficult, and have so far been attempted only for systems of very few particles.

In the present chapter we consider *single-step rearrangement reactions*, and in particular, the transfer of a nucleon between projectile and target in a single step. Here only the internal states in the entrance and exit channels are involved. The excitation of all other internal states is ignored. Apart possibly from the elastic scattering of the nuclei before and after the transfer, the only dynamical degrees of freedom taken into account are those of the transferred nucleon. These have a crucial effect on the cross section. In particular, the angular momentum of the transferred nucleon will be seen to determine the angular distribution of nuclei in the final channel. Since the angular momentum of the nucleon is determined by the difference of the spins of the nuclei between which it is exchanged, it yields information on the latter. This, together with the fact that the overlap of the initial and final internal states of the collision partners enters directly in the reaction amplitude, explains the extensive use of direct reactions for the determination of such structure parameters as nuclear spins and spectroscopic factors.

In Section 7.2 we discuss the *plane-wave Born approximation* (PWBA). Here the reaction amplitude is given by the matrix element of the transfer interaction between the unperturbed (plane-wave) initial and final states of the reaction. This allows us to exhibit the detailed reaction mechanism in a very perspicuous manner. The influence of the properties of the reaction partners on the reaction amplitude via the *structure factor* becomes clearly visible.

Unfortunately, the numerical results of the PWBA do not compare well with the experimental data. This can easily be remedied, however, by going over to the *distorted-*

wave Born approximation (DWBA), which is the topic of Section 7.3. In the latter approximation the reaction mechanism includes the elastic scattering of the nuclei before and after the actual transfer by introducing *distorted waves* in the entrance and exit channels: the plane-wave states for the relative motion in these channels are replaced with scattering states of phenomenological optical potentials. The cross sections calculated in this way are consistent with the experimental data and yield reliable values for the structure parameters of the nuclei involved in the reaction.

Section 7.4 is devoted to a discussion of simple *classical selection rules* for transfer processes. Such rules, which can of course only be approximate, are very useful for the interpretation of the experimental data, since the introduction of distorted waves complicates the calculations considerably and inhibits a direct interpretation of the quantal DWBA expressions for the cross sections.

Finally, in Section 7.5 we consider a specific example of *one-nucleon transfer* between heavy ions. Here the ability of a full DWBA calculation to reproduce the experimental data will be tested, and its conformance with the classical selection rules will be verified.

## 7.2 PWBA for nucleon transfer

As an example of an explicit calculation of a reaction cross section we consider the nucleon transfer reaction

$$x + A \rightarrow y + B, \quad (7.1)$$

where

$$x = z + y \quad \text{and} \quad B = z + A. \quad (7.2)$$

Regarding the nucleus  $x$  as the projectile and the nucleus  $A$  as the target, we are here dealing with a reaction in which a nucleon  $z$  is stripped off the projectile  $x = z + y$  through the interaction with the target  $A$ , and is transferred to the latter to form the final nucleus  $B = z + A$  (cf. Fig. 7.1). The nuclei  $y$  and  $A$  are the *core nuclei* to which the nucleon  $z$  is attached in the initial and final channels, respectively. Customarily one views a reaction from the projectile, and the reaction (7.1) together with (7.2) is, therefore, called a *stripping reaction*. In the centre-of-mass system one may, conversely, regard the nucleus  $A$  as the projectile and nucleus  $x$  as the target. Then the projectile  $A$  picks up the nucleon  $z$  to form the ejectile  $B = x + A$ , and the reaction is called a *pick-up reaction*.

### 7.2.1 The $T$ -matrix in PWBA

For the calculation of the PWBA form of the  $T$ -matrix for nucleon transfer, also called the *transfer amplitude*, we start from the post form of the formal  $T$ -matrix, eqn (5.132),

$$T_{a \rightarrow b} = T_{ba}^{\text{PWBA}} = \langle b | V_\beta | a \rangle. \quad (7.3)$$

Since the post and prior forms of the  $T$ -matrix are equal on the energy shell (cf. Section 5.2.3), we could just as well have taken the prior form as a starting point. However, we shall introduce further approximations below, for which the present approach is the most convenient one.

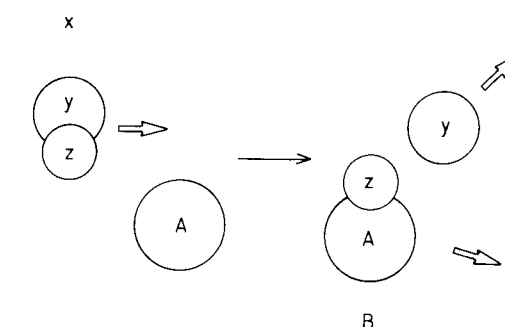


Figure 7.1 The nucleon transfer reaction.

In order to be explicit, we write the states  $|a\rangle$  and  $|b\rangle$  in the appropriate coordinate representations. The entrance channel state is the product of the internal state  $\Phi_{I_x M_x}^x(x)$  of nucleus  $x$  and the internal state  $\Phi_{I_A M_A}^A(A)$  of nucleus  $A$ , multiplied by a plane wave for the motion of the projectile  $x$  relative to the target  $A$  with the relative coordinate  $\mathbf{r}_\alpha = \mathbf{r}_{xA}$  (cf. Fig. 7.2) and relative momentum  $\mathbf{k}_\alpha = \mathbf{k}_{xA}$ ,

$$|a\rangle : \quad \Phi_{I_x M_x}^x(x) \Phi_{I_A M_A}^A(A) \frac{1}{(2\pi)^{3/2}} e^{i\mathbf{k}_\alpha \cdot \mathbf{r}_\alpha}. \quad (7.4)$$

The quantum numbers  $\{I_x M_x\}$  are the spin and spin projection of nucleus  $x$ , and the argument  $x$  comprises all its internal coordinates including the spin variables. The notation is analogous for the internal state of nucleus  $A$ .

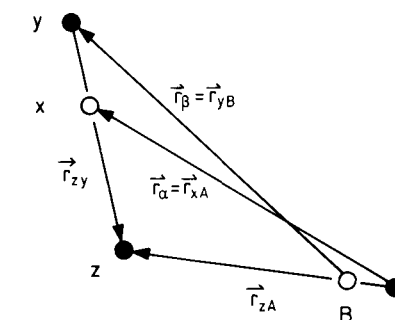


Figure 7.2 Coordinates used in the description of the nucleon transfer reaction.

Similarly, in the exit channel we have the adjoint state

$$\langle b | : \quad \frac{1}{(2\pi)^{3/2}} e^{-i\mathbf{k}_\beta \cdot \mathbf{r}_\beta} \Phi_{I_y M_y}^{y*}(y) \Phi_{I_B M_B}^{B*}(B); \quad (7.5)$$

here the plane wave describes the relative motion of the ejectile  $y$  with relative coordinate  $\mathbf{r}_\beta = \mathbf{r}_{yB}$  and relative momentum  $\mathbf{k}_\beta = \mathbf{k}_{yB}$  with respect to the final nucleus  $B$ .

The interaction in the exit channel is

$$V_\beta = V_{yB} = V_{zy} + V_{yA}, \quad (7.6)$$

which we have split up into the two terms

$$V_{zy} = \sum_{i \in y} v(\mathbf{r}_z - \mathbf{r}_i) = V_{zy}(\mathbf{r}_{zy}; y) \quad (7.7)$$

and

$$V_{yA} = \sum_{i \in y, j \in A} v(\mathbf{r}_i - \mathbf{r}_j) = V_{yA}(\mathbf{r}_{yA}; y, A). \quad (7.8)$$

For simplicity we disregard the possible spin dependence of the interactions.

It turns out that the effect of the interaction  $V_{yA}$  between the ejectile  $y$  and the target nucleus  $A$  is to provide only a smooth background to the final cross section, whereas the contribution of the interaction  $V_{zy}$  involving the transferred nucleon determines the structure of the angular distribution. Therefore we omit the term  $V_{yA}$  here. We shall see below that reducing the interaction  $V_\beta$  to the term  $V_{zy}$  will lead to an appealingly simple interpretation of the nucleon transfer amplitude. Eventually, the neglected interaction  $V_{yA}$  must be taken into account, and this will be done in the DWBA to be discussed in the next section.

We thus write for the  $T$ -matrix (7.3)

$$\begin{aligned} T_{a \rightarrow b}^{\text{PWBA}} &= T_{x \rightarrow yB}^{\text{PWBA}}(M_x M_A; \mathbf{k}_\alpha \rightarrow M_y M_B; \mathbf{k}_\beta) \\ &= \frac{1}{(2\pi)^3} \sum_{s_z} \int d^3 r_{yB} \int dy \int d^3 r_{zA} \int dA e^{-i\mathbf{k}_\beta \cdot \mathbf{r}_\beta} \Phi_{I_y M_y}^{y*}(y) \\ &\quad \times \Phi_{I_B M_B}^B(B) V_{zy}(\mathbf{r}_{zy}; y) \Phi_{I_x M_x}^x(x) \Phi_{I_A M_A}^A(A) e^{i\mathbf{k}_\alpha \cdot \mathbf{r}_\alpha}, \end{aligned} \quad (7.9)$$

where the set of coordinates  $B$  contains the internal coordinates  $A$  of the target nucleus and the coordinate  $\{\mathbf{r}_{zA}, s_z\}$  of the transferred nucleon relative to the former,  $B = \{\mathbf{r}_{zA}, s_z; A\}$ ; similarly we have  $x = \{\mathbf{r}_{zy}, s_z; y\}$ . Here  $s_z$  is the spin coordinate of the transferred nucleon.

The integrations over the internal coordinates  $y$  and  $A$  comprise a summation over the nucleonic spin variables. The variables of integration in the matrix element (7.9) are the set of coordinates  $\{\mathbf{r}_{yB}, \mathbf{r}_{zA}; y, A\}$  appropriate for the final arrangement channel (cf. Fig. 7.2): in accordance with the post-form expression (5.132) the integration goes over the *relative* coordinate  $\mathbf{r}_{yB}$  between the final fragments  $y$  and  $B$ , as well as over the *internal* coordinates  $y$  inside fragment  $y$  and the coordinates  $\{\mathbf{r}_{zA}; A\}$  inside fragment  $B$ . These variables are, however, not the most convenient ones for the evaluation of the integral in eqn (7.9). Since the interaction  $V_{zy}$  and the internal wave function  $\Phi^B$  contain the coordinates  $\{\mathbf{r}_{zy}\}$  and  $\{\mathbf{r}_{zA}\}$ , respectively, it is appropriate to go over to these as variables of integration. The transfer amplitude (7.9) will then factorize into a product of integrals.

From Fig. 7.2 we find

$$\begin{aligned} \mathbf{r}_\alpha &= \mathbf{r}_{xA} = \mathbf{r}_{zA} - \frac{m_y}{m_x} \mathbf{r}_{zy}, \\ \mathbf{r}_\beta &= \mathbf{r}_{yB} = -\mathbf{r}_{zy} + \frac{m_A}{m_B} \mathbf{r}_{zA}. \end{aligned} \quad (7.10)$$

We then rewrite the exponents in eqn (7.9) in the form

$$\begin{aligned} \mathbf{k}_\alpha \cdot \mathbf{r}_\alpha - \mathbf{k}_\beta \cdot \mathbf{r}_\beta &= \mathbf{k}_\alpha \cdot \left( \mathbf{r}_{zA} - \frac{m_y}{m_x} \mathbf{r}_{zy} \right) - \mathbf{k}_\beta \cdot \left( -\mathbf{r}_{zy} + \frac{m_A}{m_B} \mathbf{r}_{zA} \right) \\ &= \mathbf{k}_{zA} \cdot \mathbf{r}_{zA} - \mathbf{k}_{zy} \cdot \mathbf{r}_{zy}, \end{aligned} \quad (7.11)$$

where we have introduced the relative momenta

$$\boxed{\begin{aligned} \mathbf{k}_{zA} &= \mathbf{k}_\alpha - \frac{m_A}{m_B} \mathbf{k}_\beta, \\ \mathbf{k}_{zy} &= -\mathbf{k}_\beta + \frac{m_y}{m_x} \mathbf{k}_\alpha. \end{aligned}} \quad (7.12)$$

Furthermore, we insert unity in the form of a sum over the spin wave functions of the nucleon  $z$ ,

$$1 = \sum_{s_z} \delta_{s_z s'_z} = \sum_{s'_z} \sum_{M_z = \pm \frac{1}{2}} \chi_{\frac{1}{2} M_z}^*(s_z) \chi_{\frac{1}{2} M_z}^*(s'_z), \quad (7.13)$$

just in front of the projectile wave function. We then obtain the  $T$ -matrix (7.9) in the *factorized form*

$$T_{x \rightarrow yB}^{\text{PWBA}}(M_x M_A; \mathbf{k}_\alpha \rightarrow M_y M_B; \mathbf{k}_\beta) = \sum_{M_z} T_{M_x \rightarrow M_y M_z}^{x, yz}(\mathbf{k}_{zy}) F_{M_z M_A, M_B}^{BA}(\mathbf{k}_{zA}). \quad (7.14)$$

Owing to angular momentum conservation, the spin projection of the transferred nucleon  $M_z$  is fixed by the external spin projections,  $M_z = M_B - M_A = M_x - M_y$ , so that the sum over  $M_z$  actually reduces to a single term. For later convenience, however, we keep the sum.

In eqn (7.14) we have introduced the *projectile amplitude*

$$\begin{aligned} T_{M_x \rightarrow M_y M_z}^{x, yz}(\mathbf{k}_{zy}) &= \frac{1}{(2\pi)^{3/2}} \sum_{s_z} \int d^3 r_{zy} \int dy e^{-i\mathbf{k}_{zy} \cdot \mathbf{r}_{zy}} \chi_{\frac{1}{2} M_z}^*(s_z) \\ &\quad \times \Phi_{I_y M_y}^{y*}(y) V_{yz}(\mathbf{r}_{zy}; y) \Phi_{I_x M_x}^x(x) \end{aligned} \quad (7.15)$$

and the *target structure factor*

$$\begin{aligned} F_{M_z M_A, M_B}^{BA}(\mathbf{k}_{zA}) &= \frac{1}{(2\pi)^{3/2}} \sum_{s'_z} \int d^3 r_{zA} \int dA \Phi_{I_B M_B}^B(B) \\ &\quad \times \chi_{\frac{1}{2} M_z}^*(s'_z) \Phi_{I_A M_A}^A(A) e^{i\mathbf{k}_{zA} \cdot \mathbf{r}_{zA}}. \end{aligned} \quad (7.16)$$

These will be discussed in detail below.

### 7.2.2 Interpretation of the $T$ -matrix for nucleon transfer

The transfer amplitude (7.14) can be interpreted readily. The projectile amplitude (7.15) is the  $T$ -matrix (cf. eqn (5.58)) for the transition of the projectile nucleus  $x$  with spin projection  $M_x$  to a two-particle state consisting of particles  $z$  and  $y$  with spin projections  $M_z$  and  $M_y$  moving relative to one another in a plane-wave state with relative momentum  $\mathbf{k}_{zy}$  (projectile disintegration). Now the internal bound state of the projectile  $x$  has negative energy  $-\lvert\epsilon_x\rvert$ , and cannot decay into a state of two *free* particles. However, in the present case the projectile disintegrates into a state where one of the final particles, here the nucleon  $z$ , exists as a particle only for as long as it is not captured by the target  $A$ . In this intermediate phase the nucleon is free of any interaction, but it is not a free particle in the sense that the energy associated with its momentum, i.e. its kinetic energy  $\hbar^2 k_z^2 / 2m_z$  (a positive quantity), is equal to its total energy  $E_z$ , which is negative since the nucleon emerges from a bound state. The nucleon is, therefore, *off-energy-shell*. In this fashion we have extended the notion of the energy shell, introduced in Section 5.2.3 with reference to the  $T$ -matrix, to apply to particles as well.

The second factor in the transfer amplitude (7.14), the target structure factor (7.16), is an overlap integral of the wave function of the final nucleus  $B$  with spin projection  $M_B$  on one hand, and the wave functions of the target nucleus  $A$  with spin projection  $M_A$  and the nucleon  $z$  with spin projection  $M_z$ , both in a plane-wave state of relative motion with relative momentum  $\mathbf{k}_{zA}$ , on the other. The momenta  $\mathbf{k}_{zA}$  and  $\mathbf{k}_{zy}$  are fixed by the external momenta  $\mathbf{k}_\alpha$  and  $\mathbf{k}_\beta$  according to the relations (7.12).

The transfer amplitude is thus naturally given by the product of the projectile disintegration amplitude and the probability amplitude for the final nucleus  $B$  to contain the target nucleus  $A$  and the nucleon  $z$  with relative momentum  $\mathbf{k}_{zA}$ .



#### Feynman graph

The transfer amplitude (7.9) can be rewritten in a more symmetric form, which will lead us to another instructive interpretation of the PWBA mechanism. To this end we transform the target structure factor to a target transition amplitude analogous to the projectile amplitude. We write expression (7.16) as a bra-ket,

$$F_{M_z M_A, M_B}^{BA}(\mathbf{k}_{zA}) = \langle B; I_B M_B | zA; \frac{1}{2} M_z, I_A M_A; \mathbf{k}_{zA} \rangle, \quad (7.17)$$

and insert the quantity

$$\Delta = \epsilon_B - \epsilon_A - \frac{\hbar^2 k_z^2}{2\mu_{zA}} \quad (7.18)$$

between the bra and the ket. We then have

$$\Delta \cdot F_{M_z M_A, M_B}^{BA}(\mathbf{k}_{zA}) = \langle B; I_B M_B | \left( \epsilon_B - \epsilon_A - \frac{\hbar^2 k_z^2}{2\mu_{zA}} \right) | zA; \frac{1}{2} M_z, I_A M_A; \mathbf{k}_{zA} \rangle. \quad (7.19)$$

The final state  $\langle B; I_B M_B |$  satisfies the Schrödinger equation

$$\langle B; I_B M_B | h_B = \langle B; I_B M_B | \epsilon_B. \quad (7.20)$$

Similarly we have

$$\left( \epsilon_A + \frac{\hbar^2 k_z^2}{2\mu_{zA}} \right) | zA; \frac{1}{2} M_z, I_A M_A; \mathbf{k}_{zA} \rangle = (h_A + T_{zA}) | zA; \frac{1}{2} M_z, I_A M_A; \mathbf{k}_{zA} \rangle, \quad (7.21)$$

where  $T_{zA}$  is the kinetic energy operating on the state  $|\mathbf{k}_{zA}\rangle$ . Employing eqns (7.20) and (7.21) in eqn (7.19) we obtain

$$\Delta \cdot F_{M_z M_A, M_B}^{BA}(\mathbf{k}_{zA}) = \langle B; I_B M_B | (h_B - h_A - T_{zA}) | zA; \frac{1}{2} M_z, I_A M_A; \mathbf{k}_{zA} \rangle. \quad (7.22)$$

Since

$$h_B = T_{zA} + h_A + V_{zA}, \quad (7.23)$$

we find that all terms in the parentheses in eqn (7.22) cancel except the potential  $V_{zA}$ . Then the target structure factor can be written as

$$F_{M_z M_A, M_B}^{BA}(\mathbf{k}_{zA}) = \Delta^{-1} \cdot T_{M_z M_A \rightarrow M_B}^{zA, B}(\mathbf{k}_{zA}), \quad (7.24)$$

where

$$T_{M_z M_A \rightarrow M_B}^{zA, B}(\mathbf{k}_{zA}) = \langle B; I_B M_B | V_{zA} | zA; \frac{1}{2} M_z, I_A M_A; \mathbf{k}_{zA} \rangle. \quad (7.25)$$

Returning to the coordinate representation, we have

$$\begin{aligned} T_{M_z M_A \rightarrow M_B}^{zA, B}(\mathbf{k}_{zA}) &= \frac{1}{(2\pi)^{3/2}} \sum_{s_z} \int d^3 r_{zA} \int dA \Phi_{I_B M_B}^{B*}(B) V_{zA}(\mathbf{r}_{zA}; A) \\ &\quad \times \Phi_{I_A M_A}^A(A) \chi_{\frac{1}{2} M_z}(s_z) e^{i\mathbf{k}_{zA} \cdot \mathbf{r}_{zA}}. \end{aligned} \quad (7.26)$$

This quantity is the  $T$ -matrix  $T^{zA, B}$  for the synthesis of the final nucleus  $B$  with spin projection  $M_B$  from the nucleon  $z$  with spin projection  $M_z$  and the nucleus  $A$  with spin projection  $M_A$ , moving relative to each other with relative momentum  $\mathbf{k}_{zA}$ . As in the disintegration of the projectile, this is not an amplitude for the ‘fusion’ of a free nucleon  $z$  and a free nucleus  $A$  into a final nucleus  $B$ , for again, the nucleon is not on the energy shell.

The transfer amplitude (7.14) now takes the form

$$\begin{aligned} T_{x A \rightarrow y B}^{\text{PWBA}}(M_x M_A; \mathbf{k}_\alpha \rightarrow M_y M_B; \mathbf{k}_\beta) &= \\ \sum_{M_z} \frac{T_{M_x \rightarrow M_y M_z}^{x, zy}(\mathbf{k}_{zy}) T_{M_z M_A \rightarrow M_B}^{zA, B}(\mathbf{k}_{zA})}{\epsilon_{BA} - \hbar^2 k_z^2 / 2\mu_{zA}}, \end{aligned} \quad (7.27)$$

where

$$\epsilon_{BA} = \epsilon_B - \epsilon_A < 0 \quad (7.28)$$

is the negative of the binding energy of the nucleon  $z$  in the nucleus  $B$ . The transfer amplitude (7.27) is essentially given by the product of the off-energy-shell  $T$ -matrix  $T^{x, zy}$  for the projectile disintegration into the free ejectile  $y$  and the off-shell particle  $z$ , and the off-energy-shell  $T$ -matrix  $T^{zA, B}$  for the synthesis of nucleus  $B$  out of the off-shell particle  $z$  and the free target nucleus  $A$ . It is illustrated by the Feynman graph of Fig. 7.3, where the two sub- $T$ -matrices are represented by the vertices on the left and right. As part of the Feynman graph these  $T$ -matrices are called *vertex functions*. The

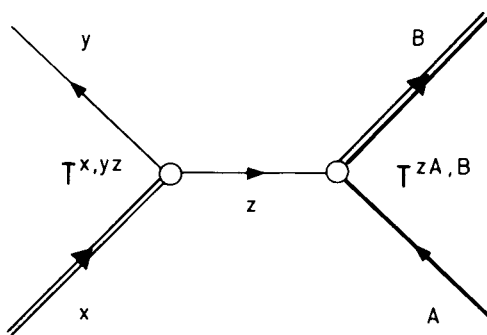


Figure 7.3 Feynman graph for nucleon transfer in PWBA.

Feynman graph exhibits the fact that nucleon transfer in the single-step approximation as defined in Section 5.4.1 has a natural *two-stage* interpretation.

The right-hand side of eqn (7.27) contains the energy denominator

$$\Delta^{-1} = \frac{1}{\epsilon_{BA} - \hbar^2 k_{zA}^2 / 2\mu_{zA}}, \quad (7.29)$$

which has turned up as a result of the replacement of the target structure factor with the synthesis amplitude (cf. eqn (7.24)). Expression (7.29) can be rewritten so as to refer to the nucleon  $z$  alone, by introducing the nucleon momentum

$$\mathbf{k}_z = \mathbf{k}_B - \mathbf{k}_A \quad (7.30)$$

and the nucleon energy

$$E_z = E_B - E_A, \quad (7.31)$$

where

$$E_A = \frac{\hbar^2 k_A^2}{2m_A} + \epsilon_A \quad (7.32)$$

and

$$E_B = \frac{\hbar^2 k_B^2}{2m_B} + \epsilon_B. \quad (7.33)$$

The relations (7.31) and (7.30) imply energy and momentum conservation at the right vertex of the Feynman graph 7.3, while eqns (7.32) and (7.33) are the on-energy-shell relations for the free particles  $A$  and  $B$ .

Expressing the sum of the kinetic energies of particles  $A$  and  $z$  through their centre-of-mass and relative energies,

$$\frac{\hbar^2 k_A^2}{2m_A} + \frac{\hbar^2 k_z^2}{2m_z} = \frac{\hbar^2 k_B^2}{2m_B} + \frac{\hbar^2 k_{zA}^2}{2\mu_{zA}}, \quad (7.34)$$

we find from eqns (7.31) to (7.33)

$$\epsilon_{BA} - \frac{\hbar^2 k_{zA}^2}{2\mu_{zA}} = E_z - \frac{\hbar^2 k_z^2}{2m_z}. \quad (7.35)$$

Since  $\epsilon_{BA} < 0$ , the left-hand side of this equation is negative definite, and therefore

$$E_z \neq \frac{\hbar^2 k_z^2}{2m_z}, \quad (7.36)$$

i.e. the nucleon  $z$  is off-energy-shell.

Relation (7.35) allows us to write for the  $T$ -matrix

$$T_{x_A \rightarrow y_B}^{\text{PWBA}}(M_x M_A; \mathbf{k}_\alpha \rightarrow M_y M_B; \mathbf{k}_\beta) = \sum_{M_z} \frac{T_{M_x \rightarrow M_y M_z}^{x,yz}(\mathbf{k}_{zy}) T_{M_z M_A \rightarrow M_B}^{zA,B}(\mathbf{k}_{zA})}{E_z - \hbar^2 k_z^2 / 2m_z}. \quad (7.37)$$

This formula expresses the transfer amplitude in a form which is now in exact correspondence with the Feynman graph of Fig. 7.3. The transfer amplitude is given by the product of the projectile disintegration vertex  $T^{x,yz}$  and the vertex  $T^{zA,B}$  for the synthesis of the final nucleus, multiplied by the *propagator* of the nucleon

$$\Delta^{-1} = \frac{1}{E_z - \hbar^2 k_z^2 / 2m_z}. \quad (7.38)$$

The propagator is represented by the nucleon line connecting the two vertices, and depends only on the energy and momentum of the nucleon. It would diverge if the nucleon were on the energy shell.

#### Interpretation of the propagator

The physical meaning of the propagator  $\Delta^{-1}$  is most easily explained in the present context by writing it again in the form (7.29), where  $\mathbf{k}_{zA}$  is the momentum and  $\epsilon_{BA} < 0$  the energy of the nucleon  $z$  in the rest system of the final nucleus  $B$ . This propagator is the momentum representation of the free Green function,

$$\Delta^{-1} = \frac{1}{\epsilon_{BA} - \hbar^2 k_{zA}^2 / 2\mu_{zA}} = G(\mathbf{k}_{zA}; \epsilon_{BA}) \quad (7.39)$$

(actually, the free Green function is diagonal in the momentum representation, i.e. it is proportional to a  $\delta$ -function in the momentum variables; expression (7.39) is the coefficient in front of this  $\delta$ -function).

Let us now discuss the nucleon transfer process in coordinate space (cf. Fig. 7.4). The coordinate representation of the free Green function has been given in eqn (4.59). In the present instance, where the energy is *negative*, it is of the form

$$G(|\mathbf{r}_{zA} - \mathbf{r}'_{zA}|; \epsilon_{BA}) = -\frac{\mu_{zA}}{2\pi\hbar^2} \frac{e^{-\kappa_{BA}|\mathbf{r}_{zA} - \mathbf{r}'_{zA}|}}{|\mathbf{r}_{zA} - \mathbf{r}'_{zA}|} \quad (7.40)$$

with  $\kappa_{BA}^2 = 2\mu_{zA}|\epsilon_{BA}|/\hbar^2$ .

The propagator (7.39) is the Fourier transform of expression (7.40),

$$\frac{1}{\epsilon_{BA} - \hbar^2 k_{zA}^2 / 2\mu_{zA}} = \int d^3 r_{yA} e^{-ik_{zA} \cdot (\mathbf{r}'_{zA} - \mathbf{r}_{yA} - \mathbf{r}_{zy})} G(|\mathbf{r}'_{zA} - \mathbf{r}_{yA} - \mathbf{r}_{zy}|; \epsilon_{BA}), \quad (7.41)$$

where we have introduced the relative coordinate  $\mathbf{r}_{yA}$  between the cores  $y$  and  $A$ . Using eqn (7.15) and eqn (7.26) we can now write instead of eqn (7.27) (for brevity we omit the spin indices and the summation over  $M_z$ ),

$$\begin{aligned} T_{xA \rightarrow yB}^{\text{PWBA}}(\mathbf{k}_\alpha \rightarrow \mathbf{k}_\beta) &= \frac{1}{(2\pi)^3} \int d^3 r_{yA} \int d^3 r'_{zA} \int d^3 r_{zy} e^{-ik_{zA} \cdot (\mathbf{r}'_{zA} - \mathbf{r}_{yA} - \mathbf{r}_{zy})} \\ &\times e^{ik_{zA} \cdot \mathbf{r}'_{zA}} \Gamma(\mathbf{r}'_{zA}; zA \rightarrow B) G(|\mathbf{r}'_{zA} - \mathbf{r}_{yA} - \mathbf{r}_{zy}|; \epsilon_{BA}) \\ &\times \Gamma(\mathbf{r}_{zy}; x \rightarrow zy) e^{-ik_{zy} \cdot \mathbf{r}_{zy}}. \end{aligned} \quad (7.42)$$

Here we have introduced the vertex interaction of the projectile

$$\Gamma(\mathbf{r}_{zy}; x \rightarrow zy) = \sum_{s_z} \int dy \chi_{\frac{1}{2}M_z}^*(s_z) \Phi_{I_y M_y}^y(y) V_{zy}(\mathbf{r}_{zy}; y) \Phi_{I_x M_x}^x(x), \quad (7.43)$$

which we interpret as the projectile source for nucleon  $z$  at  $\mathbf{r}_{zy}$ , and the vertex interaction of the target

$$\begin{aligned} \Gamma(\mathbf{r}'_{zA}; zA \rightarrow B) &= \sum_{s'_z} \int dA \Phi_{I_B M_B}^B(B) V_{zA}(\mathbf{r}'_{zA}; A) \\ &\times \Phi_{I_A M_A}^A(A) \chi_{\frac{1}{2}M_z}^*(s'_z), \end{aligned} \quad (7.44)$$

which is the corresponding target sink for the nucleon at  $\mathbf{r}'_{zA}$ .

The physical meaning of the propagator  $G(|\mathbf{r}'_{zA} - \mathbf{r}_{yA} - \mathbf{r}_{zy}|; \epsilon_{BA})$  is now evident from Fig. 7.4. It is the probability amplitude for the nucleon  $z$ , emitted via the source vertex function  $\Gamma(\mathbf{r}_{zy}; x \rightarrow zy)$  in the projectile at the point  $\mathbf{r}_{zy} = \mathbf{r}_{zA} - \mathbf{r}_{yA}$ , to propagate as a non-interacting particle to the position  $\mathbf{r}'_{zA}$ , where it is captured by the target nucleus  $A$  via the sink vertex function  $\Gamma(\mathbf{r}'_{zA}; zA \rightarrow B)$ . It is seen from expression (7.40) that the propagator has the range  $\kappa_{BA}^{-1} = \hbar/(2\mu_{zA}|\epsilon_{BA}|)^{1/2}$ ; the nucleon is transferred within a range of nuclear dimensions, which is the smaller the stronger the binding of the nucleon in the nucleus  $B$ .

The structure of the amplitude (7.42) becomes very simple if we assume, for the sake of argument, that the source and sink functions, i.e. the interactions at the two vertices, are of zero range,  $\Gamma(\mathbf{r}_{zy}; x \rightarrow zy) = \Gamma_y \delta(\mathbf{r}_{zy})$  and  $\Gamma(\mathbf{r}'_{zA}; zA \rightarrow B) = \Gamma_A \delta(\mathbf{r}'_{zA})$ . We then have

$$\begin{aligned} T_{xA \rightarrow yB}^{\text{PWBA}}(\mathbf{k}_\alpha \rightarrow \mathbf{k}_\beta) &= \frac{1}{(2\pi)^3} \int d^3 r_{yA} e^{ik_{zA} \cdot \mathbf{r}_{yA}} \Gamma_A G(r_{yA}; \epsilon_{BA}) \Gamma_y \\ &= \frac{1}{(2\pi)^3} \int d^3 r_{yA} e^{ik_{zA} \cdot \mathbf{r}_{yA}} V(\mathbf{r}_{yA}), \end{aligned} \quad (7.45)$$

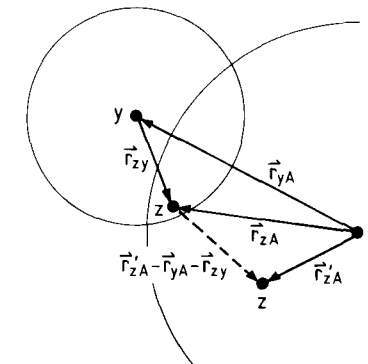


Figure 7.4 The nucleon transfer process in coordinate space.

where

$$V(\mathbf{r}_{yA}) = -\frac{\mu_{zA} \Gamma_A \Gamma_y}{2\pi \hbar^2} \frac{e^{-\kappa_{BA} r_{yA}}}{r_{yA}}. \quad (7.46)$$

This is recognized as the Born amplitude for the exchange of a nucleon  $z$  between the core nuclei  $y$  and  $A$  with momentum transfer  $\mathbf{k}_{zA} = \mathbf{k}_\alpha - (m_A/m_B)\mathbf{k}_\beta$  (cf. eqn (7.12)). The exchange of the nucleon  $z$  gives rise to the exchange potential (7.46) which has a similar form and interpretation as the well-known Yukawa potential.

Comparing the expression (7.42) for the transfer amplitude with the original expression (7.14) together with eqns (7.15) and (7.16), we observe that the former contains an extra folding of the Green function  $G(|\mathbf{r}'_{zA} - \mathbf{r}_{zA}|; \epsilon_{BA})$  with the interaction vertex  $\Gamma(\mathbf{r}'_{zA}; zA, B)$ . In expression (7.42) the transfer process is viewed as involving an *interaction* with the target at the point  $\mathbf{r}'_{zA}$ , while in expressions (7.14) to (7.16) we are dealing with a target *overlap* at the point  $\mathbf{r}_{zA}$ .

#### Concluding remarks on the interpretation of the nucleon transfer amplitude

We have derived the Feynman amplitude (7.37) in order to elucidate the nuclear transfer process as the succession of two sub-processes at the projectile and target vertices, which enter in a completely symmetric fashion. For this purpose we have rewritten the target structure factor as a synthesis amplitude multiplied by the propagator (cf. eqn (7.24)). Conversely, we could write the projectile disintegration amplitude (7.15) as a structure factor multiplied by the reciprocal of the propagator, which would in this case be expressed in the form

$$\Delta = \epsilon_x - \epsilon_y - \frac{\hbar^2 k_{zy}^2}{2\mu_{zy}}. \quad (7.47)$$

This quantity is equal to that given by eqn (7.18) which we have used for the target vertex (hence the same notation  $\Delta$ ), as can be proved by following the reasoning from eqns (7.30) to (7.35) with the nuclei  $B$  and  $A$  replaced with the nuclei  $x$  and  $y$ , respectively.

The formulation in terms of a transition amplitude is appropriate if the corresponding vertex interaction is of short range, as is often the case for the projectile vertex. On the other hand, the formulation in terms of a structure factor (i.e. in terms of a wave function overlap) is useful if the corresponding vertex involves nuclei which are large, which is usually true for the target nucleus. Thus the formula (7.14) which emerges naturally from the post form of the PWBA transfer amplitude, is automatically the most convenient one.

The physical transparency of formulae (7.14) and (7.37) may serve as a vindication of the use of the PWBA amplitude in the form (7.9), i.e. for neglecting the term  $V_{yA}$  in eqn (7.6): this rather intuitive approximation has turned out to provide us with the simplest description of the transfer mechanism. But clearly, the effect of the term  $V_{yA}$  has to be investigated, and this will be done in Section 7.3 via the introduction of the distorted waves.

The purpose of the preceding discussion has been merely to convey an idea of the physical content of the PWBA nucleon transfer amplitude; it is actually of no immediate use for the evaluation of the latter quantity. Whereas here it took some effort to rewrite the transfer amplitude (7.14) in the form of the Feynman amplitude (7.37), the description of direct reactions in terms of Feynman graphs arises naturally in the *dispersion theory of nuclear reactions* (cf. Shapiro 1961, 1962, 1963; Schnitzer 1965; Lipperheide 1970).

### 7.2.3 The target structure factor

The target structure factor (7.16) carries information on the structure of the target wave function. It contains the overlap integral

$$\phi_{AB:IA MA.IB MB}^z(\mathbf{r}_{zA}, s_z) = \int dA \Phi_{IB MB}^{B*}(\mathbf{r}_{zA}, s_z; A) \Phi_{IA MA}^A(A), \quad (7.48)$$

which is a function of the space and spin variables of the transferred nucleon.

In order to evaluate this function we expand the wave function of the residual nucleus  $B$  simultaneously in a complete set of wave functions  $\Phi_{\lambda:IA MA}^A(A)$  of the target nucleus  $A$  on one hand (here we use the label  $\lambda$  to denote the quantum numbers of the internal states of nucleus  $A$ ), and a complete set of single-particle shell-model wave functions  $\phi_{nlj M_j}(\mathbf{r}_{zA}, s_z)$ , on the other. The shell-model potential defining the latter should represent the average interaction exerted by the target nucleus  $A$  on the nucleon; with a judicious choice of this potential the expansion will then effectively reduce to a few terms only. The quantum numbers  $\{nlj\}$  are the radial, orbital angular momentum, and total spin quantum numbers of the shell-model orbit. One thus writes

$$\begin{aligned} \Phi_{IB MB}^B(B) &= \sum_{\lambda} \sum_{nlj M_j M_A} S_{nlj}^{1/2}(\lambda) (j M_j; IA MA | IB MB) \\ &\times \Phi_{\lambda:IA MA}^A(A) \phi_{nlj M_j}(\mathbf{r}_{zA}, s_z). \end{aligned} \quad (7.49)$$

The expansion coefficient  $S_{nlj}^{1/2}(\lambda)$  is called the *spectroscopic amplitude*; it is the square root of the *spectroscopic factor*  $S_{nlj}(\lambda)$ . Since the spectroscopic amplitude is a coefficient in an expansion in complete sets of target states  $\Phi_{\lambda:IA MA}^A(A)$  and shell-model states

$\phi_{nlj M_j}(\mathbf{r}_{zA}, s_z)$  which are orthonormal,

$$\int dA \Phi_{\lambda':IA' M'_A}^{A*}(A) \Phi_{\lambda:IA MA}^A(A) = \delta_{\lambda'\lambda} \delta_{I'A'I} \delta_{M'_A M_A}, \quad (7.50)$$

$$\sum_s \int d^3r \phi_{n'l'j'M'_j}^*(\mathbf{r}, s) \phi_{nlj M_j}(\mathbf{r}, s) = \delta_{n'n} \delta_{l'l} \delta_{j'j} \delta_{M'_j M_j}, \quad (7.51)$$

it represents the probability amplitude for the the nucleus  $B$  with spin  $\{IB MB\}$  to be describable as nucleus  $A$  in the state  $\lambda$  with spin  $\{IA MA\}$  plus a nucleon in the shell-model orbit  $\{nlj\}$  in the field of the nucleus  $A$ .

The wave function of the shell-model state has the explicit form

$$\phi_{nlj M_j}(\mathbf{r}, s_z) = R_{nlj}(r) \sum_{M_z m} (\frac{1}{2} M_z; lm | j M_j) \chi_{\frac{1}{2} M_z}(s_z) i^l Y_{lm}(\Omega), \quad (7.52)$$

where  $R_{nlj}(r)$  is the radial wave function. It is clear from eqn (7.49) that the function (7.52) must have the parity  $\pi_A \pi_B$ , and thus for given  $j$  only one of the possible values of  $l = j \pm \frac{1}{2}$ , namely the one with parity  $(-)^l = \pi_A \pi_B$ , is allowed to occur in the expansion (7.49). Using this expansion and relation (7.50), we find for the overlap integral (7.48)

$$\phi_{AB:IA MA.IB MB}^z(\mathbf{r}_{zA}, s_z) = \sum_{nlj M_j} S_{nlj}^{1/2}(0) (j M_j; IA MA | IB MB) \phi_{nlj M_j}^*(\mathbf{r}_{zA}, s_z). \quad (7.53)$$

Owing to the orthogonality of the nucleon spin states,

$$\sum_s \chi_{\frac{1}{2} M'}^*(s) \chi_{\frac{1}{2} M}(s) = \delta_{M'M}, \quad (7.54)$$

we can then write for the target structure factor (7.16), using eqn (7.52),

$$\begin{aligned} F_{M_z M_A, M_B}^{BA}(\mathbf{k}_{zA}) &= \sum_{nlj} \sum_{M_j m} S_{nlj}^{1/2} (\frac{1}{2} M_z; lm | j M_j) (j M_j; IA MA | IB MB) \\ &\times \frac{1}{(2\pi)^{3/2}} \int d^3r e^{i\mathbf{k}_{zA} \cdot \mathbf{r}} i^{-l} Y_{lm}^*(\Omega) R_{nlj}(r); \end{aligned} \quad (7.55)$$

here only the term with  $\lambda = 0$  corresponding to the target nucleus ground state remains, and we have introduced the abbreviated notation  $S_{nlj}^{1/2} = S_{nlj}^{1/2}(0)$  for the spectroscopic amplitude.

Using

$$e^{i\mathbf{k}_{zA} \cdot \mathbf{r}} = \sum_{l'm'} 4\pi i^{l'} j_{l'}(k_{zA} r) Y_{l'm'}^*(\hat{\mathbf{k}}_{zA}) Y_{l'm'}(\Omega) \quad (7.56)$$

and the orthogonality relation for the spherical harmonics, we find for the expression (7.55)

$$\begin{aligned} F_{M_z M_A, M_B}^{BA}(\mathbf{k}_{zA}) &= \sum_{nlj} \sum_{M_j m} S_{nlj}^{1/2} (\frac{1}{2} M_z; lm | j M_j) (j M_j; IA MA | IB MB) \\ &\times \left(\frac{2}{\pi}\right)^{1/2} Y_{lm}^*(\hat{\mathbf{k}}_{zA}) \int_0^\infty r^2 dr j_l(k_{zA} r) R_{nlj}(r). \end{aligned} \quad (7.57)$$

### 7.2.4 The (d,p) reaction in PWBA

Historically the most important application of PWBA has been to the neutron stripping reaction  $A(d,p)B$ . In the following we discuss this particular case, where  $x = d$ ,  $y = p$ , and  $z = n$ , since it will give us further insight into the direct reaction process.

#### The deuteron amplitude

In the projectile disintegration amplitude (7.15) the transferred particle is the neutron, and the internal state of particle  $y$  is simply the spin wave function of the proton,

$$\Phi_{I_y M_y}^y(y) = \chi_{\frac{1}{2} M_p}(s_p). \quad (7.58)$$

The projectile internal wave function is that of the deuteron, which is predominantly made up of an S-state, where proton and neutron move in an orbit with relative angular momentum zero (we neglect the small D-state admixture of the deuteron). On the other hand, the spins of proton and neutron in the deuteron add up to unity,  $I_d = 1$ , and we have therefore

$$\Phi_{I_x M_x}^x(x) = \phi^d(r_{np}) \chi_{1 M_d}(s_n, s_p). \quad (7.59)$$

The deuteron spin function is given by

$$\chi_{1 M_d}(s_n, s_p) = \sum_{M'_n M'_p} \left( \frac{1}{2}, M'_n; \frac{1}{2}, M'_p | 1 M_d \right) \chi_{\frac{1}{2} M'_n}(s_n) \chi_{\frac{1}{2} M'_p}(s_p), \quad (7.60)$$

and using the orthogonality relation for the spin functions (7.54), we can write the deuteron disintegration amplitude (7.15) as

$$\begin{aligned} T_{M_d \rightarrow M_n M_p}^{d,np}(\mathbf{k}_{np}) &= (\frac{1}{2} M_n; \frac{1}{2} M_p | 1 M_d) \frac{1}{(2\pi)^{3/2}} \\ &\times \int d^3 r_{np} e^{-i\mathbf{k}_{np} \cdot \mathbf{r}_{np}} V_{np}(\mathbf{r}_{np}) \phi^d(r_{np}). \end{aligned} \quad (7.61)$$

Since the radial wave function of the deuteron satisfies the Schrödinger equation (with  $\epsilon_d < 0$ )

$$\left( -\frac{\hbar^2}{2\mu_{np}} \nabla^2 + V_{np}(r) - \epsilon_d \right) \phi^d(r) = 0, \quad (7.62)$$

we find for the integral in eqn (7.61)

$$\int d^3 r_{np} e^{-i\mathbf{k}_{np} \cdot \mathbf{r}_{np}} V_{np}(\mathbf{r}_{np}) \phi^d(r_{np}) = \int d^3 r e^{-i\mathbf{k}_{np} \cdot \mathbf{r}} \left( \epsilon_d + \frac{\hbar^2}{2\mu_{np}} \nabla^2 \right) \phi^d(r).$$

After integrating by parts, where the surface terms vanish owing to the presence of the bound deuteron wave function  $\phi^d(r)$ , we let the operator  $\nabla^2$  operate on its eigenfunction  $\exp(-i\mathbf{k}_{np} \cdot \mathbf{r})$  to the left and replace it with  $-k_{np}^2$ . As a result we have

$$T_{M_d \rightarrow M_n M_p}^{d,np}(\mathbf{k}_{np}) = \Delta \cdot (\frac{1}{2} M_n; \frac{1}{2} M_p | 1 M_d) \frac{1}{(2\pi)^{3/2}} \int d^3 r e^{-i\mathbf{k}_{np} \cdot \mathbf{r}} \phi^d(r), \quad (7.63)$$

where

$$\Delta = \epsilon_d - \frac{\hbar^2 k_{np}^2}{2\mu_{np}} \quad (7.64)$$

is the quantity (7.47) evaluated for the present case. Comparing with eqn (7.24), we find that the expression multiplying  $\Delta$  on the right-hand side of eqn (7.63) represents the structure factor of the deuteron.

Instead of substituting the numerical value of the Clebsch–Gordan coefficient in eqn (7.63), we prefer to keep the coefficient in its present form in order to be able to make use of orthogonality relations later on. For the deuteron wave function we write

$$\phi^d(r) = D_0 \frac{e^{-\kappa_d r}}{r} \text{ with } \kappa_d = \sqrt{-2\mu_{np}\epsilon_d/\hbar^2}, \quad (7.65)$$

i.e. we assume that the internal wave function of the deuteron has its asymptotic form for all  $r > 0$ , corresponding to a solution for a potential with zero range. Evaluation of the integral in eqn (7.63) yields  $4\pi D_0/(\kappa_d^2 + k_{np}^2)$ , and we obtain for the deuteron amplitude the value

$$T_{M_d \rightarrow M_n M_p}^{d,np}(\mathbf{k}_{np}) = -(\frac{1}{2} M_n; \frac{1}{2} M_p | 1 M_d) \frac{\hbar^2}{(2\pi)^{1/2} \mu_{np}} D_0. \quad (7.66)$$

#### The (d,p) stripping cross section

The unpolarized (d,p) stripping cross section, i.e. the cross section averaged over the initial, and summed over the final spin projections is, using eqn (5.96) with  $I_d = 1$ , obtained as

$$\left( \frac{d\sigma}{d\Omega} \right)_{(d,p)}^{\text{PWBA}} = \left( \frac{2\pi}{\hbar} \right)^4 \mu_{dA} \mu_B \frac{k_{pB}}{k_{dA}} \frac{1}{3(2I_A + 1)} \sum_{M_d M_A} \sum_{M_p M_B} |T_{(d,p)}^{\text{PWBA}}|^2, \quad (7.67)$$

where the  $T$ -matrix is given by the target structure factor (7.57) multiplied by the deuteron amplitude (7.66) summed over  $M_n$ ,

$$\begin{aligned} T_{(d,p)}^{\text{PWBA}} &= - \sum_{M_n} \sum_{nlj} \sum_{M_j} S_{nlj}^{1/2} (\frac{1}{2} M_n; lm | j M_j)(j M_j; I_A M_A | I_B M_B) \\ &\times (\frac{1}{2} M_n; \frac{1}{2} M_p | 1 M_d) \frac{1}{\pi} \frac{\hbar^2}{\mu_{np}} D_0 Y_{lm}^*(\hat{\mathbf{k}}_{np}) \int_0^\infty r^2 dr j_l(k_{np} r) R_{nlj}(r). \end{aligned} \quad (7.68)$$

The right-hand side of expression (7.67) contains a product of six Clebsch–Gordan coefficients. For its evaluation one makes successive use of the following relations obtained from the unitarity and symmetry relations for the Clebsch–Gordan coefficients (cf. Edmonds 1957, Section 3.5),

$$\sum_{M_A M_B} (j' M'_j; I_A M_A | I_B M_B)(j M_j; I_A M_A | I_B M_B) = \frac{2I_B + 1}{2j + 1} \delta_{j'j} \delta_{M'_j M_j}, \quad (7.69)$$

$$\sum_{M_p M_d} (\frac{1}{2} M'_n; \frac{1}{2} M_p | 1 M_d)(\frac{1}{2} M_n; \frac{1}{2} M_p | 1 M_d) = \frac{3}{2} \delta_{M'_n M_n}, \quad (7.70)$$

$$\sum_{M_n M_j} \left( \frac{1}{2} M_n; l' m' | j M_j \right) \left( \frac{1}{2} M_n; l m | j M_j \right) = \frac{2j+1}{2l+1} \delta_{l'l} \delta_{m'm} \quad (7.71)$$

and (cf. Edmonds 1957, eqn (4.6.6))

$$\sum_m Y_{lm}^*(\hat{\mathbf{k}}_{nA}) Y_{lm}(\hat{\mathbf{k}}_{nA}) = \frac{2l+1}{4\pi} P_l(1) = \frac{2l+1}{4\pi}. \quad (7.72)$$

Under the assumption that only one major shell  $n$  contributes one arrives at

$$\begin{aligned} \left( \frac{d\sigma}{d\Omega} \right)_{(d,p)}^{\text{PWBA}} &= \frac{\mu_{dA}\mu_{pB}}{\mu_{np}^2} \frac{k_{pB}}{k_{dA}} \frac{2I_B + 1}{2I_A + 1} 2\pi D_0^2 \\ &\times \sum_{lj} S_{nlj} \left( \int_0^\infty r^2 dr j_l(k_{nA}r) R_{nlj}(r) \right)^2. \end{aligned} \quad (7.73)$$

If one shell-model state  $\{nlj\}$  is dominant only a single term of the sum is retained.

For the calculation of the radial integral one now introduces the *Butler radius*  $R$  as a lower cut-off (cf. Butler and Hittmair 1957). By thus excluding the region  $r < R$  one takes approximate account of the absorption of the channel wave functions inside the nucleus due to other, non-direct channels. It is further assumed that at distances larger than this radius the neutron is outside the region of interaction with the target nucleus. In this region the radial function  $R_{nlj}(r)$  is an eigenfunction of the free Schrödinger equation,

$$\left( \frac{d^2}{dr^2} - \frac{l(l+1)}{r^2} - \kappa_{nlj}^2 \right) r R_{nlj}(r) = 0 \quad \text{for } r > R, \quad (7.74)$$

where  $\kappa_{nlj}^2 = 2\mu_{nA}|\epsilon_{nlj}|/\hbar^2$ , and  $\epsilon_{nlj}$  is the energy of the shell-model state. The same equation with a different eigenvalue is satisfied by the free radial function  $r j_l(k_{nA}r)$ ,

$$\left( \frac{d^2}{dr^2} - \frac{l(l+1)}{r^2} + k_{nA}^2 \right) r j_l(k_{nA}r) = 0. \quad (7.75)$$

Multiplying eqn (7.75) by  $r R_{nlj}(r)$  and eqn (7.74) by  $r j_l(k_{nA}r)$ , taking the difference of these equations and integrating from  $R$  to  $\infty$ , we find for the radial integral

$$\begin{aligned} &\int_R^\infty r^2 dr j_l(k_{nA}r) R_{nlj}(r) \\ &= \frac{-1}{\kappa_{nlj}^2 + k_{nA}^2} \int_R^\infty dr \frac{d}{dr} \left( r R_{nlj}(r) \frac{d}{dr} [r j_l(k_{nA}r)] - r j_l(k_{nA}r) \frac{d}{dr} [r R_{nlj}(r)] \right) \\ &= \frac{R^2}{\kappa_{nlj}^2 + k_{nA}^2} \left( R_{nlj}(R) \frac{d}{dR} j_l(k_{nA}R) - j_l(k_{nA}R) \frac{d}{dR} R_{nlj}(R) \right), \end{aligned} \quad (7.76)$$

so that finally the stripping cross section for a single shell-model state  $\{nlj\}$  becomes

$$\begin{aligned} \left( \frac{d\sigma}{d\Omega} \right)_{(d,p)}^{\text{PWBA}} &= \frac{\mu_{dA}\mu_{pB}}{\mu_{np}^2} \frac{k_{pB}}{k_{dA}} \frac{2I_B + 1}{2I_A + 1} 2\pi D_0^2 S_{nlj} \left( \frac{R^2}{\kappa_{nlj}^2 + k_{nA}^2} \right)^2 \\ &\times \left( R_{nlj}(R) \frac{d}{dR} j_l(k_{nA}R) - j_l(k_{nA}R) \frac{d}{dR} R_{nlj}(R) \right)^2. \end{aligned} \quad (7.77)$$

Here  $k_{nA}$  is a function of the *stripping angle*  $\theta$ , i.e. the angle between the outgoing proton and the incoming deuteron; using eqn (7.12) with  $x = d$ ,  $y = p$ , and  $z = n$ , we find

$$\begin{aligned} k_{nA}^2 &= \left| \mathbf{k}_{dA} - \frac{m_A}{m_B} \mathbf{k}_{pB} \right|^2 \\ &= k_{dA}^2 + \left( \frac{m_A}{m_B} \right)^2 k_{pB}^2 - 2 \frac{m_A}{m_B} k_{dA} k_{pB} \cos \theta. \end{aligned} \quad (7.78)$$

Since the spherical Bessel function  $j_l(k_{nA}R)$  depends strongly on the parameter  $l$ , it is

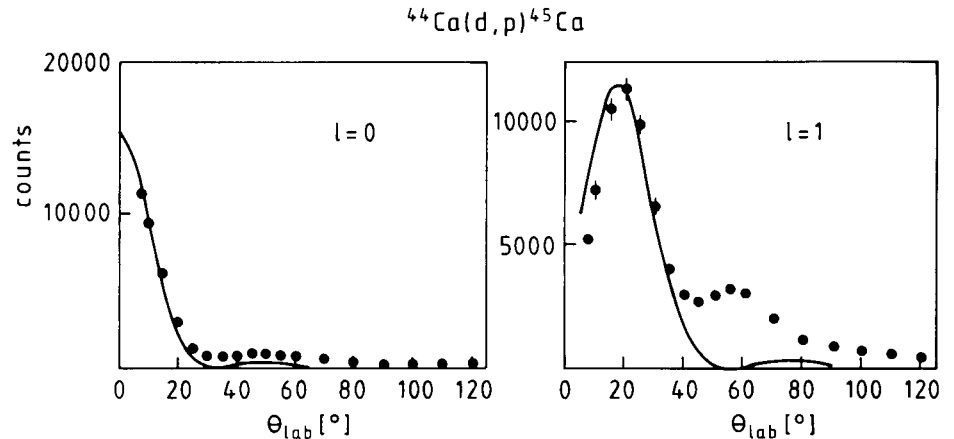


**Figure 7.5** PWBA angular distributions for neutron transfer into the states of  $^{45}\text{Ca}$  with  $l = 0$  at  $E = 2.394$  MeV and  $l = 1$  at  $E = 1.902$  MeV in the reaction  $^{44}\text{Ca}(d, p)^{45}\text{Ca}$  with  $E_{\text{lab}}(d) = 7.01$  MeV. The dots represent the data of Cobb and Guth (1957). The Butler radius has been chosen as  $R = 6$  fm, and the overall normalization of the distribution has been determined by a fit to the data.

seen from eqn (7.77) that the *angular distribution* of the final protons is determined by the angular momentum  $l$  of the shell-model state into which the neutron is transferred, whereas the *strength* of the cross section is governed by the spectroscopic factor  $S_{nlj}$ .

As an example for the application of formula (7.77), we show in Fig. 7.5 the angular distributions of the cross section for the reaction  $^{44}\text{Ca}(d, p)^{45}\text{Ca}$  leading to two different states in the final nucleus  $^{45}\text{Ca}$ . The absolute height of the angular distribution and the Butler radius  $R$  are used as free parameters. Comparison with the experimental data allows one to determine the angular momentum  $l$  of the neutron shell-model state. Apart

from this, the calculation does, unfortunately, not yield results which provide a very satisfactory fit. This means that one has to go beyond the PWBA.

## 7.3 DWBA for nucleon transfer

### 7.3.1 The general expression for the $T$ -matrix in DWBA

In the preceding section we have seen that the PWBA leads to formulae useful for comparison with experiment only when two *ad hoc* approximations are made which are inspired by ‘physical insight’: the neglect of the interaction  $V_{yA}$  when writing down eqn (7.9) and the cut-off at the radius  $R$  in the target structure factor integral in eqn (7.76). Now a more rigorous derivation of explicit cross section formulae is possible in the *distorted-wave Born approximation* (DWBA). To show this we follow the treatment of Austern (1970), Section 4.5 (cf. also Austern *et al.* 1964).

We consider again the reaction (7.1) together with (7.2), and as before, we use the post form of the  $T$ -matrix. The DWBA reaction amplitude for this case is given by the expression (5.146) (where the first term vanishes because  $\alpha$  and  $\beta$  are different),

$$T_{a \rightarrow b} = T_{ba}^{\text{DWBA}} = \langle b^{U^-} | W_\beta | a^{U^+} \rangle. \quad (7.79)$$

Here

$$W_\beta = V_\beta - U_\beta \quad (7.80)$$

denotes the residual interaction in the final channel, where

$$V_\beta = V_{yB} = \sum_{i \in y, j \in B} v(\mathbf{r}_i - \mathbf{r}_j) \quad (7.81)$$

is the sum of the two-particle interactions between the nucleons in nucleus  $y$  on one hand, and in the nucleus  $B$  on the other, while

$$U_\beta = U_\beta(\mathbf{r}_\beta) \quad (7.82)$$

is the distorting potential in arrangement channel  $\beta$ .

Referring back to Fig. 7.2, we have, in generalization of eqns (7.4) and (7.5), in the entrance channel

$$\langle a^{U^+} : \Phi_{I_x M_x}^x(x) \Phi_{I_A M_A}^A(A) \chi_\alpha^{(+)}(\mathbf{k}_\alpha, \mathbf{r}_\alpha), \quad (7.83)$$

and correspondingly in the exit channel

$$\langle b^{U^-} : \chi_\beta^{(-)*}(\mathbf{k}_\beta, \mathbf{r}_\beta) \Phi_{I_y M_y}^{y*}(y) \Phi_{I_B M_B}^{B*}(B). \quad (7.84)$$

The functions  $\chi_\alpha^{(+)}(\mathbf{k}_\alpha, \mathbf{r}_\alpha)$  and  $\chi_\beta^{(-)*}(\mathbf{k}_\beta, \mathbf{r}_\beta)$  are the distorted wave functions in the entrance and exit channels (cf. eqns (5.141) and (5.142)), calculated with the help of the distorting potentials  $U_\alpha(\mathbf{r}_\alpha)$  and  $U_\beta^*(\mathbf{r}_\beta)$ , respectively.

We now write down the matrix element (7.79) in more detail using as explicit variables of integration the relative coordinate  $\mathbf{r}_\beta = \mathbf{r}_{yB}$  in the exit channel  $\beta$ , and the internal coordinate  $\mathbf{r}_{zA}$  of the transferred particle with respect to the target nucleus  $A$  (cf. Fig. 7.2).

In PWBA we were able to separate the expression for the  $T$ -matrix into two integrals by going over to the variables of integration  $\mathbf{r}_{yz}$  and  $\mathbf{r}_{zA}$ . In the present case this is not

## 7.3 DWBA for nucleon transfer

possible. Since the distorted wave functions contain the coordinates  $\mathbf{r}_\alpha$  and  $\mathbf{r}_\beta$ , we now employ these variables in the explicit evaluation of the DWBA reaction amplitude. Using the relations (7.10) we find, by eliminating the variable  $\mathbf{r}_{zy}$ ,

$$\mathbf{r}_{zA} = \frac{m_x m_B}{m_x m_B - m_y m_A} \left( \mathbf{r}_\alpha - \frac{m_y}{m_x} \mathbf{r}_\beta \right); \quad (7.85)$$

then we have

$$\int d^3 r_\beta \int d^3 r_{zA} = \mathcal{J} \int d^3 r_\beta \int d^3 r_\alpha, \quad (7.86)$$

where the Jacobian  $\mathcal{J}$  is given by

$$\mathcal{J} = \left( \frac{m_x m_B}{m_x m_B - m_y m_A} \right)^3. \quad (7.87)$$

The interaction  $W_\beta$  depends on all nucleon coordinates, which we separate into a set containing the two variables  $\mathbf{r}_\alpha$  and  $\mathbf{r}_\beta$  and a set containing the remainder denoted by  $C$ ,

$$W_\beta = W_\beta(\mathbf{r}_\alpha, \mathbf{r}_\beta; C). \quad (7.88)$$

The DWBA reaction amplitude (7.79) thus becomes

$$\boxed{T_{xA \rightarrow yB}^{\text{DWBA}}(M_x M_A; \mathbf{k}_\alpha \rightarrow M_y M_B; \mathbf{k}_\beta) = \int d^3 r_\alpha \int d^3 r_\beta \chi_\beta^{(-)*}(\mathbf{k}_\beta, \mathbf{r}_\beta) \times \Gamma_{M_x M_A M_y M_B}(\mathbf{r}_\alpha, \mathbf{r}_\beta; xA \rightarrow yB) \chi_\alpha^{(+)}(\mathbf{k}_\alpha, \mathbf{r}_\alpha),} \quad (7.89)$$

where we have defined the interaction matrix

$$\boxed{\Gamma_{M_x M_A M_y M_B}(\mathbf{r}_\alpha, \mathbf{r}_\beta; xA \rightarrow yB) = \mathcal{J} \int dC \Phi_{I_y M_y}^{y*}(y) \Phi_{I_B M_B}^{B*}(B) \times W_\beta(\mathbf{r}_\alpha, \mathbf{r}_\beta; C) \Phi_{I_x M_x}^x(x) \Phi_{I_A M_A}^A(A);} \quad (7.90)$$

here the integration over the coordinates  $C$  implies also a summation over all spin variables in the nuclei  $x, y, A$ , and  $B$ .

For the further evaluation of the six-fold integral (7.89) one makes use of the transformation properties of the interaction matrix (7.90) under rotations of the variables  $\mathbf{r}_\alpha$  and  $\mathbf{r}_\beta$ . The rotation affects the internal wave functions  $\Phi_{I_y M_y}^{y*}(y)$ , etc. in the integral on the right-hand side of eqn (7.90) but it leaves the interaction  $W_\beta$  invariant. Therefore, the interaction matrix  $\Gamma$  transforms under rotations like the product of the four functions  $\Phi^{y*}, \Phi^{B*}, \Phi^x$ , and  $\Phi^A$  appearing under the integral. The four internal spins involved here can be coupled together to a single spin characterizing the interaction matrix. In doing this, one does not make use of the channel spins like  $\mathbf{S}_a = \mathbf{I}_x + \mathbf{I}_A$ , as might be suggested by the discussion in Section 5.3.1, but finds it more convenient to introduce the *spin transfers* and their projections,

$$\begin{aligned} \mathbf{s} &= \mathbf{I}_x - \mathbf{I}_y, & \mathbf{j} &= \mathbf{I}_B - \mathbf{I}_A, \\ M_s &= M_x - M_y, & M_j &= M_B - M_A, \end{aligned} \quad (7.91)$$

and the angular momentum  $\mathbf{l}$  with projection  $m$ ,

$$\begin{aligned} \mathbf{I} &= \mathbf{j} - \mathbf{s}, \\ m &= M_j - M_s. \end{aligned} \quad (7.92)$$

Substituting eqns (7.91) in eqn (7.92), we find

$$\mathbf{I} = \mathbf{I}_y + \mathbf{I}_B - \mathbf{I}_x - \mathbf{I}_A, \quad (7.93)$$

i.e. the angular momentum  $\mathbf{I}$  is the total change in internal nuclear spin (channel spin) from the initial to the final channel. Owing to the law of conservation of angular momentum the quantity  $-\mathbf{I}$  is therefore equal to the change in *orbital angular momentum* of the relative motion.

For the evaluation of the interaction matrix (7.90) we now observe that  $\Phi_{I_y M_y}^y(y)$  transforms like  $(-)^{I_y - M_y} \Phi_{I_y, -M_y}^y(y)$ , (cf. Edmonds 1957, eqn (5.5.3)), i.e. like a spin eigenfunction with an additional phase, and similarly for  $\Phi_{I_B M_B}^B(B)$ . We remove the phase factors by multiplying by  $(-)^{I_y - M_y + I_B - M_B}$ . Then we couple first  $\mathbf{I}_A$  and  $-\mathbf{I}_B$  to  $-\mathbf{j}$ , second  $\mathbf{I}_x$  and  $-\mathbf{I}_y$  to  $\mathbf{s}$  and finally  $-\mathbf{j}$  and  $\mathbf{s}$  to  $-\mathbf{I}$  (cf. Edmonds 1957, Section 3.5). This leads us to the spin-coupled *multipole coefficient*

$$\begin{aligned} \tilde{\Gamma}_{l(sj)m}(\mathbf{r}_\alpha, \mathbf{r}_\beta \rightarrow xA, yB) &= \sum_{M_j M_s} \sum_{M_x M_y} \sum_{M_A M_B} (j, -M_j; s M_s | l, -m) \\ &\times (I_x M_x; I_y, -M_y | s M_s) (I_A M_A; I_B, -M_B | j, -M_j) \\ &\times (-)^{I_y - M_y + I_B - M_B} \Gamma_{M_x M_A M_y M_B}(\mathbf{r}_\alpha, \mathbf{r}_\beta; xA \rightarrow yB). \end{aligned} \quad (7.94)$$

By construction this expression transforms like a tensor with spin  $l$  and spin projection  $-m$ , i.e. like the spherical harmonic  $Y_{l, -m}$  or  $(-)^m Y_{lm}^*$ .

The multipole coefficient determines the change of the parity via the interaction matrix (7.90). With  $\pi_x = \pm 1$  being the parity of the internal state of nucleus  $x$ , etc. the parity in the initial channel is  $\pi_x \pi_A$ , and in the final channel,  $\pi_y \pi_B$ . The change of parity in the reaction is therefore given by

$$\Delta\pi = \pi_x \pi_A \pi_y \pi_B. \quad (7.95)$$

The parity change takes the values  $\pm 1$ , where  $\Delta\pi = +1(-1)$  corresponds to a transition without (with) change of parity. Owing to the law of conservation of parity this change of internal parity must be compensated by an equal change of parity in the relative motion, that is, the latter is also given by  $\Delta\pi$ .

Multiplying the equation (7.94) on both sides by

$$(j, -M'_j; s M'_s | l, -m) (I_x M'_x; I_y, -M'_y | s M_s) (I_A M'_A; I_B, -M'_B | j, -M'_j)$$

and applying the orthogonality relation

$$\sum_{jm} (j_1 m_1; j_2, m_2 | jm) (j_1 m'_1; j_2, m'_2 | jm) = \delta_{m_1 m'_1} \delta_{m_2 m'_2} \quad (7.96)$$

to the first Clebsch–Gordan coefficient, then to the second and third, we obtain relation (7.94) in the inverted form

$$\begin{aligned} \Gamma_{M_x M_A M_y M_B}(\mathbf{r}_\alpha, \mathbf{r}_\beta; xA \rightarrow yB) &= (-)^{I_y - M_y + I_B - M_B} \\ &\times \sum_{lm} \sum_{s M_s} \sum_{j M_j} (j, -M_j; s M_s | l, -m) (I_x M_x; I_y, -M_y | s M_s) \\ &\times (I_A M_A; I_B, -M_B | j, -M_j) \tilde{\Gamma}_{l(sj)m}(\mathbf{r}_\alpha, \mathbf{r}_\beta; xA \rightarrow yB). \end{aligned} \quad (7.97)$$

Using the symmetry relations for the Clebsch–Gordan coefficients (cf. Edmonds 1957, Section 3.5) and the relations (7.91) and (7.92) for the angular-momentum projections we finally arrive at an expression which is consistent with the multipole expansion of Austern (1970, eqn (4.56)),

$$\begin{aligned} \Gamma_{M_x M_A M_y M_B}(\mathbf{r}_\alpha, \mathbf{r}_\beta; xA \rightarrow yB) &= \sum_{lsj} i^{-l} (-)^{I_y - M_y} \\ &\times (lm; s, M_x - M_y | j, M_B - M_A) (I_x M_x; I_y, -M_y | s, M_x - M_y) \\ &\times (I_A M_A; j, M_B - M_A | I_B, M_B) \Gamma_{l(sj)m}(\mathbf{r}_\alpha, \mathbf{r}_\beta; xA \rightarrow yB), \end{aligned} \quad (7.98)$$

where

$$\begin{aligned} \Gamma_{l(sj)m}(\mathbf{r}_\alpha, \mathbf{r}_\beta; xA \rightarrow yB) &= \\ \left( \frac{2l+1}{2I_B+1} \right)^{1/2} &(-)^{s+I_A+I_B-m} i^l \tilde{\Gamma}_{l(sj)m}(\mathbf{r}_\alpha, \mathbf{r}_\beta; xA \rightarrow yB). \end{aligned} \quad (7.99)$$

Since  $\tilde{\Gamma}_{l(sj)m}$  transforms like  $(-)^m Y_{lm}^*$  (cf. the remark after eqn (7.94)), the quantity  $\Gamma_{l(sj)m}$  transforms like  $Y_{lm}^*$ .

The multipole coefficient  $\Gamma_{l(sj)m}$  is usually written as the product of a *spectroscopic coefficient*  $A_{lsj}$ , which contains the spectroscopic information on the nuclei and is independent of  $m$ , and a *form factor*  $f_{l(sj)m}(\mathbf{r}_\alpha, \mathbf{r}_\beta)$ , which depends on the relative coordinates. It is the latter which determines the angular distribution. We thus write

$$\Gamma_{l(sj)m}(\mathbf{r}_\alpha, \mathbf{r}_\beta) = A_{lsj} f_{l(sj)m}(\mathbf{r}_\alpha, \mathbf{r}_\beta), \quad (7.100)$$

and obtain for the transfer amplitude (7.89), using eqn (7.98),

$$\begin{aligned} T_{xA \rightarrow yB}^{\text{DWBA}}(M_x M_A; \mathbf{k}_\alpha \rightarrow M_y M_B; \mathbf{k}_\beta) &= \sum_{lsj} \sum_m (2l+1)^{1/2} i^l (-)^{I_y - M_y} \\ &\times (lm; s, M_x - M_y | j, M_B - M_A) (I_x M_x; I_y, -M_y | s, M_x - M_y) \\ &\times (I_A M_A; j, M_B - M_A | I_B M_B) A_{lsj} \beta_{sj}^{lm}(\mathbf{k}_\alpha, \mathbf{k}_\beta), \end{aligned} \quad (7.101)$$

where the spatial integrals of the form factor  $f_{l(sj)m}(\mathbf{r}_\alpha, \mathbf{r}_\beta)$  are collected in the *reduced amplitude*

$$\begin{aligned} \beta_{sj}^{lm}(\mathbf{k}_\alpha, \mathbf{k}_\beta) &= \frac{i^{-l}}{(2l+1)^{1/2}} \int d^3 r_\alpha \int d^3 r_\beta \chi_\beta^{(-)*}(\mathbf{k}_\beta, \mathbf{r}_\beta) \\ &\times f_{l(sj)m}(\mathbf{r}_\alpha, \mathbf{r}_\beta) \chi_\alpha^{(+)}(\mathbf{k}_\alpha, \mathbf{r}_\alpha). \end{aligned} \quad (7.102)$$

As mentioned before, the spectroscopic coefficient  $A_{lsj}$  contains the *spectroscopic information*. The reduced amplitude  $\beta_{sj}^{lm}(\mathbf{k}_\alpha, \mathbf{k}_\beta)$ , on the other hand, determines the shape of the *angular distribution*.

For the unpolarized nucleon transfer cross section we find, evaluating eqn (5.96) in a similar manner as for the PWBA deuteron stripping cross section in Section 7.2.4,

$$\left(\frac{d\sigma}{d\Omega}\right)_{xA \rightarrow yB}^{\text{DWBA}} = \left(\frac{2\pi}{\hbar}\right)^4 \mu_\alpha \mu_\beta \frac{k_\beta}{k_\alpha} \frac{2I_B + 1}{(2I_x + 1)(2I_A + 1)} \times \sum_{lsj} |A_{lsj}|^2 \sum_m |\beta_{sj}^{lm}(\mathbf{k}_\alpha, \mathbf{k}_\beta)|^2. \quad (7.103)$$

The sum over multipoles  $\{lsj\}$  is incoherent, i.e. different multipoles make non-interfering additive contributions to the differential cross section.

### 7.3.2 The (d,p) reaction in DWBA

For a comparison with Section 7.2.4, we specialize the expressions of the preceding subsection to the reaction  $A(d, p)B$ . The residual interaction (7.80) in the exit channel is now given by

$$W_\beta = V_\beta - U_\beta = V_{np} + V_{pA} - U_\beta. \quad (7.104)$$

The set of implicit coordinates  $C$  introduced in eqn (7.88) here comprises the spin variables of the neutron and the proton,  $s_n$  and  $s_p$ , respectively, and the set of internal coordinates of the target nucleus  $A$ . In the present instance we assume that the residual interaction  $W_\beta$  is independent of spin, so that it depends only on the coordinates  $\mathbf{r}_\alpha$  and  $\mathbf{r}_\beta$  and on the internal coordinates  $A$ ,  $W_\beta = W_\beta(\mathbf{r}_\alpha, \mathbf{r}_\beta; A)$ . The interaction matrix (7.90) then reads

$$\begin{aligned} \Gamma_{M_d M_A M_p M_B}(\mathbf{r}_\alpha, \mathbf{r}_\beta; dA \rightarrow pB) &= \mathcal{J} \sum_{s_n s_p} \int dA \chi_{\frac{1}{2} M_p}^{p^*}(s_p) \Phi_{I_B M_B}^{B^*}(B) \\ &\quad \times W_\beta(\mathbf{r}_\alpha, \mathbf{r}_\beta; A) \phi^d(r_{np}) \chi_{1 M_d}(s_n, s_p) \Phi_{I_A M_A}^A(A) \\ &= \sum_{s_n s_p} \sum_{nlj M_j} (j M_j; I_A M_A | I_B M_B) S_{nlj}^{1/2} \chi_{\frac{1}{2} M_p}^{p^*}(s_p) \phi_{nlj M_j}^*(\mathbf{r}_{nA}, s_n) \\ &\quad \times \mathcal{J} \int dA \Phi_{I_A M_A}^{A^*}(A) W_\beta(\mathbf{r}_\alpha, \mathbf{r}_\beta; A) \Phi_{I_A M_A}^A(A) \\ &\quad \times \phi^d(r_{np}) \chi_{1 M_d}(s_n, s_p), \end{aligned} \quad (7.105)$$

where we have made use of the expansion (7.49), keeping only the ground-state term with  $\lambda = 0$ .

The interaction matrix (7.105) contains the expectation value of the interaction  $W_\beta$  in the internal state of the target nucleus  $A$ , which, using eqn (7.104), can be decomposed as

$$\begin{aligned} \int dA \Phi_{I_A M_A}^{A^*}(A) W_\beta(\mathbf{r}_\alpha, \mathbf{r}_\beta; A) \Phi_{I_A M_A}^A(A) &= V_{np}(r_{np}) \\ &\quad + \int dA \Phi_{I_A M_A}^{A^*}(A) V_{pA} \Phi_{I_A M_A}^A(A) - U_\beta(r_\beta). \end{aligned} \quad (7.106)$$

The second term on the right-hand side is the average interaction of the final proton with the nucleons in the nucleus  $A$ , while the distorting potential  $U_\beta(\mathbf{r}_\beta)$  represents an elastic interaction of the proton with the final nucleus  $B$ . In order to take realistic

account of the elastic scattering in channel  $\beta$ , one usually chooses a complex optical potential for  $U_\beta$ . The main part of this potential is the average interaction of the proton with the nucleons in the nucleus  $B$  (cf. Section 6.2.4). Although the nucleus  $B$  contains one neutron more than the nucleus  $A$ , and although the optical potential is complex while the average interaction of the proton in the field of the target nucleus  $A$  is real, one nevertheless assumes that these two quantities effectively cancel each other in the integral which gives the DWBA  $T$ -matrix (7.89). The error committed should lie within the uncertainties of the DWBA approximation in general (cf. Austern 1970, Section 5.8). On the right-hand side of eqn (7.106) we thus keep only the term  $V_{np}(\mathbf{r}_{np})$ .

The internal radial wave function of the deuteron in the entrance channel is given by eqn (7.65), which is the solution of the Schrödinger equation (7.62) with a potential  $V_{np}$  of zero range. From this equation we find, with  $\nabla^2(1/r) = -(1/r^2)\delta(r) = -4\pi\delta(\mathbf{r})$ ,

$$V_{np}(r)\phi^d(r) = \frac{\hbar^2}{2\mu_{pn}}(\nabla^2 - k_d^2)D_0 \frac{e^{-k_d r}}{r} = -\frac{2\pi\hbar^2 D_0}{\mu_{np}}\delta(\mathbf{r}). \quad (7.107)$$

Collecting these results, using eqns (7.52) and (7.60), and taking into account only one major shell  $n$ , we arrive at the interaction matrix (7.105) in the form

$$\begin{aligned} \Gamma_{M_d M_A M_p M_B}(\mathbf{r}_\alpha, \mathbf{r}_\beta; dA \rightarrow pB) &= -\frac{2\pi\hbar^2 D_0}{\mu_{np}} \sum_{lsj} i^{-l} S_{nlj}^{1/2} \delta_{s\frac{1}{2}} \\ &\quad \times (j, M_B - M_A; I_A M_A | I_B M_B)(\frac{1}{2}, M_d - M_p; lm|j, M_B - M_A) \\ &\quad \times (\frac{1}{2}, M_d - M_p; \frac{1}{2}, M_p | 1 M_d) \mathcal{J} Y_{lm}^*(\hat{\mathbf{r}}_{nA}) R_{nlj}(r_{nA}) \delta(\mathbf{r}_{np}). \end{aligned} \quad (7.108)$$

With the help of the symmetry relations for the Clebsch–Gordan coefficients (cf. Edmonds 1957, Section 3.5)

$$(j, M_B - M_A; I_A M_A | I_B M_B) = (-)^{j+I_A-I_B} (I_A M_A; j, M_B - M_A | I_B, M_B), \quad (7.109)$$

$$(\frac{1}{2}, M_d - M_p; lm|j, M_B - M_A) = (-)^{\frac{1}{2}+l-j} (lm; s, M_d - M_p | j, M_B - M_A), \quad (7.110)$$

and

$$(\frac{1}{2}, M_d - M_p; \frac{1}{2} M_p | 1 M_d) = (-)^{\frac{1}{2}-M_p} \sqrt{\frac{3}{2}} (1 M_d; \frac{1}{2}, -M_p | \frac{1}{2}, M_d - M_p), \quad (7.111)$$

we can write for expression (7.108)

$$\begin{aligned} \Gamma_{M_d M_A M_p M_B}(\mathbf{r}_\alpha, \mathbf{r}_\beta; dA \rightarrow pB) &= \sum_{lsj} i^{-l} (-)^{\frac{1}{2}-M_p} \\ &\quad \times (I_A M_A; j, M_B - M_A | I_B M_B)(1 M_d; \frac{1}{2}, -M_p | \frac{1}{2}, M_d - M_p) \\ &\quad \times (lm; \frac{1}{2}, M_d - M_p | j, M_B - M_A) \sqrt{\frac{3}{2}} (-)^{I_A - I_B + \frac{1}{2} + l} \left( -\frac{2\pi\hbar^2 D_0}{\mu_{np}} \right) S_{nlj}^{1/2} \delta_{s\frac{1}{2}} \\ &\quad \times \mathcal{J} Y_{lm}^*(\hat{\mathbf{r}}_{nA}) R_{nlj}(r_{nA}) \delta(\mathbf{r}_{np}). \end{aligned} \quad (7.112)$$

This expression is the interaction matrix (7.98) specialized to the (d,p) reaction. Comparing the two, we can identify the quantity  $\Gamma_{l(sj)m}$  as

$$\begin{aligned} \Gamma_{l(sj)m}(\mathbf{r}_\alpha, \mathbf{r}_\beta) &= (-)^{I_A - I_B + \frac{1}{2} + l} \left( -\frac{2\pi\hbar^2 D_0}{\mu_{np}} \right) \sqrt{\frac{3}{2}} S_{nlj}^{1/2} \delta_{s\frac{1}{2}} \\ &\times \mathcal{J} Y_{lm}^*(\hat{\mathbf{r}}_{nA}) R_{nlj}(r_{nA}) \delta(\mathbf{r}_{np}). \end{aligned} \quad (7.113)$$

The factorization (7.100) is now made in the form

$$A_{jsl} = (-)^{I_A - I_B + \frac{1}{2} + l} \left( -\frac{2\pi\hbar^2 D_0}{\mu_{np}} \right) \sqrt{\frac{3}{2}} S_{nlj}^{1/2} \delta_{s\frac{1}{2}}, \quad (7.114)$$

$$f_{j(\frac{1}{2}l)m}(\mathbf{r}_\alpha, \mathbf{r}_\beta) = \mathcal{J} Y_{lm}^*(\hat{\mathbf{r}}_{nA}) R_{nlj}(r_{nA}) \delta(\mathbf{r}_{np}). \quad (7.115)$$

We further rewrite the integral in the reduced amplitude (7.102) in terms of the variables of integration  $\{\mathbf{r}_{np}, \mathbf{r}_{nA}\}$  (cf. eqn (7.10)),

$$\int d^3 r_\alpha \int d^3 r_\beta = \mathcal{J}^{-1} \int d^3 r_{np} \int d^3 r_{nA},$$

and because of the appearance of the function  $\delta(\mathbf{r}_{np})$  in the integrand, where  $\mathbf{r}_{np} = -\mathbf{r}_\beta - (m_A/m_B)\mathbf{r}_{nA}$ , (cf. Fig. 7.2 with  $x = d$ ,  $y = p$ , and  $z = n$ ), we are left with the single integral

$$\begin{aligned} \beta_{\frac{1}{2}j}^{lm}(\mathbf{k}_\alpha, \mathbf{k}_\beta) &= \frac{i^{-l}}{(2l+1)^{1/2}} \int d^3 r_{nA} \chi_\beta^{(-)*}(\mathbf{k}_\beta, \frac{m_A}{m_B}\mathbf{r}_{nA}) \\ &\times Y_{lm}^*(\hat{\mathbf{r}}_{nA}) R_{nlj}(r_{nA}) \chi_\alpha^{(+)}(\mathbf{k}_\alpha, \mathbf{r}_{nA}). \end{aligned} \quad (7.116)$$

The DWBA cross section for the reaction  $A(d, p)B$  is then found from eqn (7.103) as

$$\begin{aligned} \left( \frac{d\sigma}{d\Omega} \right)_{(d,p)}^{\text{DWBA}} &= \left( \frac{2\pi}{\hbar} \right)^4 \mu_{dA} \mu_{pB} \frac{k_{pB}}{k_{dA}} \frac{2I_B + 1}{3(2I_A + 1)} \sum_{lj} \frac{6\pi^2 \hbar^4 D_0^2}{\mu_{np}^2} S_{nlj} \frac{1}{2l + 1} \\ &\times \sum_m \left| \int d^3 r \chi_\beta^{(-)*}(\mathbf{k}_\beta, \frac{m_A}{m_B}\mathbf{r}) Y_{lm}^*(\hat{\mathbf{r}}) R_{nlj}(r) \chi_\alpha^{(+)}(\mathbf{k}_\alpha, \mathbf{r}) \right|^2. \end{aligned} \quad (7.117)$$

Formula (7.117) becomes equal to the PWBA cross section (7.73) if one assumes that the main effect of the complex optical potentials  $\mathcal{U}_\alpha$  and  $\mathcal{U}_\beta$  on the wave functions  $\chi_\alpha^{(+)}$  and  $\chi_\beta^{(-)}$  is to reduce the latter to zero for  $r < R$ , where  $R$  is the Butler radius, and to leave them otherwise undistorted, i.e. to leave them plane waves for  $r > R$ . In this case we have for  $r > R$

$$\begin{aligned} \chi_\beta^{(-)*} \left( \mathbf{k}_\beta, \frac{m_A}{m_B} \mathbf{r} \right) \chi_\alpha^{(+)}(\mathbf{k}_\alpha, \mathbf{r}) &= \frac{1}{(2\pi)^3} \exp \left[ i \left( \mathbf{k}_{dA} - \frac{m_A}{m_B} \mathbf{k}_{pB} \right) \cdot \mathbf{r} \right] \\ &= \frac{1}{(2\pi)^3} \exp(i \mathbf{k}_{nA} \cdot \mathbf{r}), \end{aligned}$$

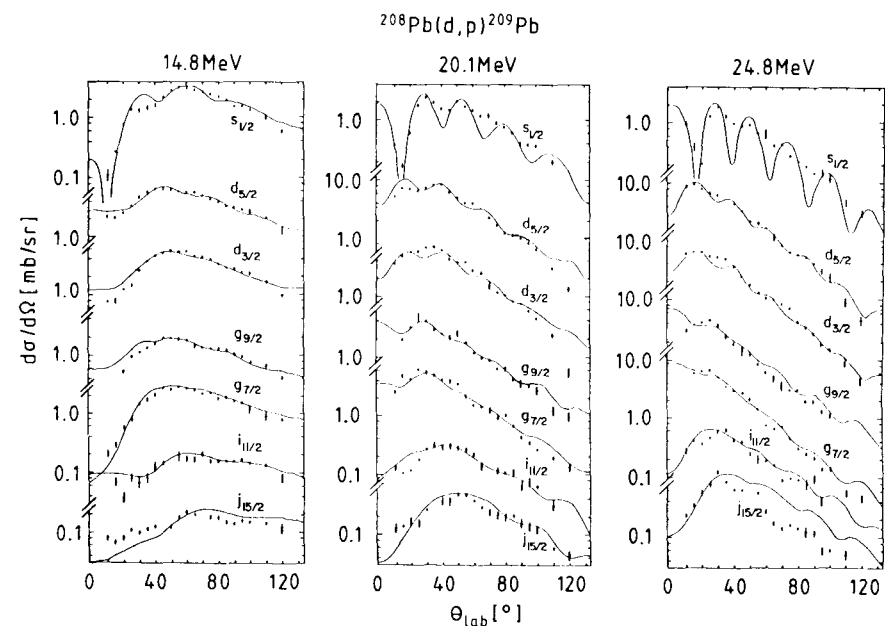


**Figure 7.6** Angle-differential cross section for the reaction  $^{208}\text{Pb}(d,p)^{209}\text{Pb}$  to the states  $s_{1/2}$ ,  $d_{5/2}$  etc. for  $E_{\text{lab}}(d) = 14.8, 20.4$ , and  $24.8$  MeV. The solid curves represent the results calculated in DWBA. The experimental data are taken from Muehlener *et al.* (1967).

where the last equation follows from eqn (7.12). Expanding the plane wave as in eqn (7.56) and using eqn (7.72), we recover the PWBA cross section (7.73) with the lower limit of the integral replaced with  $R$ .

The DWBA yields (d,p) reaction cross sections which are generally in good agreement with the experimental data. For an example we show in Fig. 7.6 the result of a zero-range DWBA calculation for the reaction  $^{208}\text{Pb}(d,p)^{209}\text{Pb}$ .

### 7.3.3 The zero-range approximation

The evaluation of the six-dimensional integral (7.102) for the general reduced transfer amplitude is rather laborious. A great simplification of the formalism results if one assumes that the projectile  $y$  is emitted at the same point at which the projectile  $x$  disintegrates. The previous case of deuteron stripping with a zero-range interaction between the proton and the neutron serves as the prototype of such an approximate formalism. The triangle in Fig. 7.2, which describes the relations between the coordinates in the integrand, then reduces to the straight line of Fig. 7.7, and the relative coordinate vectors appearing in the distorted wave functions become parallel,

$$\mathbf{r}_\beta = \frac{m_A}{m_B} \mathbf{r}_\alpha. \quad (7.118)$$

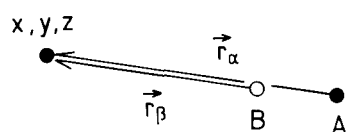


**Figure 7.7** Coordinates used in the description of the nucleon transfer reaction in the zero-range approximation.

The condition (7.118) is implemented in the formalism by writing the form factor  $f_{l(sj)m}$  in eqn (7.102) as

$$f_{l(sj)m}(\mathbf{r}_\alpha, \mathbf{r}_\beta) = \delta\left(\mathbf{r}_\beta - \frac{m_A}{m_B}\mathbf{r}_\alpha\right) F_{lsj}(r_\alpha) Y_{lm}^*(\hat{\mathbf{r}}_\alpha). \quad (7.119)$$

where  $F_{lsj}(r_\alpha)$  is some function of  $r_\alpha$  and the angular function  $Y_{lm}^*(\hat{\mathbf{r}}_\alpha)$  embodies the transformation properties of  $f_{l(sj)m}(\mathbf{r}_\alpha, \mathbf{r}_\beta)$  under rotations (cf. eqn (7.115)). The ansatz (7.119) is called the *zero-range approximation*.

We then obtain for the reduced amplitude (7.102) the single integral

$$\begin{aligned} \beta_{sj}^{lm}(\mathbf{k}_\alpha, \mathbf{k}_\beta) &= \frac{i^{-l}}{(2l+1)^{1/2}} \int d^3r \chi_\beta^{(-)*}\left(\mathbf{k}_\beta, \frac{m_A}{m_B}\mathbf{r}\right) \\ &\quad \times F_{lsj}(r) Y_{lm}^*(\hat{\mathbf{r}}) \chi_\alpha^{(+)}(\mathbf{k}_\alpha, \mathbf{r}). \end{aligned} \quad (7.120)$$

Here the function  $F_{lsj}(r)$  takes the place of the radial shell-model wave function  $R_{nlj}(r)$  in eqn (7.116), to which it reduces, for example, in the zero-range approximation for the (d,p) reaction.

For an explicit evaluation of the integral (7.120) we expand the distorted wave functions in partial waves as in eqn (1.119), using

$$P_l(\hat{\mathbf{r}} \cdot \hat{\mathbf{k}}) = \frac{4\pi}{2l+1} \sum_m Y_{lm}(\hat{\mathbf{r}}) Y_{lm}^*(\hat{\mathbf{k}}). \quad (7.121)$$

Thus we write

$$\chi_\alpha^{(+)}(\mathbf{k}_\alpha, \mathbf{r}; [U_\alpha]) = \frac{4\pi}{k_\alpha r} \sum_{l_\alpha m_\alpha} i^{l_\alpha} e^{i\sigma_{l_\alpha}} y_{l_\alpha}(k_\alpha, r) Y_{l_\alpha m_\alpha}(\hat{\mathbf{r}}) Y_{l_\alpha m_\alpha}^*(\hat{\mathbf{k}}_\alpha), \quad (7.122)$$

$$\chi_\beta^{(-)*}(\mathbf{k}_\beta, \mathbf{r}; [U_\beta^\dagger]) = \frac{4\pi}{k_\beta r} \sum_{l_\beta m_\beta} i^{-l_\beta} e^{i\sigma_{l_\beta}} y_{l_\beta}(k_\beta, r) Y_{l_\beta m_\beta}^*(\hat{\mathbf{r}}) Y_{l_\beta m_\beta}(\hat{\mathbf{k}}_\beta), \quad (7.123)$$

where the phases  $\sigma_l$  are the Coulomb phase shifts, and where in the second equation we have used  $\chi_\beta^{(-)*}(\mathbf{k}_\beta, \mathbf{r}) = \chi_\beta^{(+)}(-\mathbf{k}_\beta, \mathbf{r})$  in analogy to eqn (4.61). After substitution of the distorted wave function  $\chi_\beta^{(-)*}(\mathbf{k}_\beta, \mathbf{r})$  in the integral (7.120) the coordinate  $\mathbf{r}$  is replaced with  $(m_A/m_B)\mathbf{r}$ . The integration over the angular part of the variable of integration  $\mathbf{r}$  involves three spherical harmonics and yields a product of two Clebsch–Gordan coefficients (cf. Edmonds 1957, eqn (4.6.3)), while the radial integral cannot be

reduced further and has to be calculated numerically. We finally arrive at

$$\begin{aligned} \beta_{sj}^{lm}(\mathbf{k}_\alpha, \mathbf{k}_\beta) &= \sum_{l_\alpha m_\alpha} \sum_{l_\beta m_\beta} i^{l_\alpha - l_\beta - l} e^{i(\sigma_{l_\alpha} + \sigma_{l_\beta})} \left( \frac{4\pi(2l_\beta + 1)}{2l_\alpha + 1} \right)^{1/2} I_{l_\beta l_\alpha}^{lsj} \\ &\quad \times (l_\beta 0; l 0 | l_\alpha 0) (l_\beta m_\beta; lm | l_\alpha m_\alpha) Y_{l_\beta m_\beta}(\hat{\mathbf{k}}_\beta) Y_{l_\alpha m_\alpha}^*(\hat{\mathbf{k}}_\alpha), \end{aligned} \quad (7.124)$$

where

$$I_{l_\beta l_\alpha}^{lsj} = \frac{4\pi}{k_\alpha k_\beta m_A} \int_0^\infty dr y_{l_\beta}(k_\beta, \frac{m_A}{m_B}r) F_{lsj}(r) y_{l_\alpha}(k_\alpha, r). \quad (7.125)$$

The Clebsch–Gordan coefficient  $(l_\beta m_\beta; lm | l_\alpha m_\alpha)$  in the reduced amplitude (7.124) expresses the coupling between the angular momentum  $\mathbf{l}$  of eqn (7.93) and the orbital angular momenta  $\mathbf{l}_\alpha$  and  $\mathbf{l}_\beta$  in the initial and final distorted wave functions (7.122) and (7.123), respectively. The transferred spin  $\mathbf{l}$  is the negative of the transfer of orbital angular momentum in the relative motion.

In order to exhibit the dependence of the reduced amplitude (7.124) on the reaction angle  $\theta$ , we choose the  $z$ -axis in the direction of  $\mathbf{k}_\alpha$ , and the  $y$ -axis perpendicular to  $\mathbf{k}_\alpha$  and  $\mathbf{k}_\beta$ , i.e. perpendicular to the reaction plane. Then we have (cf. Edmonds 1957, Section 2.5)

$$Y_{l_\alpha m_\alpha}(\hat{\mathbf{z}}) = Y_{l_\alpha m_\alpha}(0, 0) = \delta_{m_\alpha 0} \sqrt{\frac{2l_\alpha + 1}{4\pi}}.$$

Thus the only remaining spherical harmonic in expression (7.124),  $Y_{l_\beta m_\beta}(\hat{\mathbf{k}}_\beta) = Y_{l_\beta m_\beta}(\Omega_\beta)$ , determines the angular distribution in terms of the reaction angle  $\Omega_\beta$  relative to the incident direction.

The Clebsch–Gordan coefficient  $(l_\beta 0 0 | l_\alpha 0)$  in eqn (7.124) is non-vanishing only if  $l_\beta + l + l_\alpha = \text{even}$ . Owing to conservation of parity, the change of parity  $\Delta\pi$  defined in eqn (7.95) is equal to the change of parity in the relative motion. For the orbitals  $l_\alpha$  and  $l_\beta$  in the distorted wave functions (7.122) and (7.123) this change of parity is equal to  $(-)^{l_\alpha + l_\beta}$ ; therefore

$$\Delta\pi = (-)^{l_\alpha + l_\beta}. \quad (7.126)$$

Since in the present instance  $l_\alpha + l_\beta$  is even (odd) if  $l$  is even (odd), we have here

$$\Delta\pi = (-)^l, \quad (7.127)$$

corresponding to a *normal change of parity*. It is here due to the zero-range approximation; when the interaction is of finite range, the rule of normal change of parity no longer holds, as will be shown in Section 7.3.4.

The values of the linear and angular momenta in the entrance and exit channels have a large effect on the magnitude of the radial integral (7.125). This accounts for the strong dependence of the transfer cross section on the  $Q$ -value and on the angular momentum transfer. The magnitude of this cross section is determined by the overlap of the distorted waves  $y_{l_\beta}$  and  $y_{l_\alpha}$ . In order to have maximum overlap, both functions must oscillate at the same rate, which means one must have  $k_\alpha \simeq k_\beta$ . This condition allows large cross sections only for particular ranges of  $Q$ -values, called *Q-windows*. Taking also account of angular momentum, one finds that good overlap for the first maxima of the radial wave

functions in eqn (7.125) requires  $l_\alpha/k_\alpha \simeq l_\beta/k_\beta$ . Therefore, if  $k_\alpha \simeq k_\beta$  in a particular reaction then  $l_\alpha \simeq l_\beta$  is favoured; if  $k_\alpha \neq k_\beta$  one must also have  $l_\alpha \neq l_\beta$ .

### 7.3.4 Finite-range calculations

*The exact treatment*

If all reaction partners involved in the transfer process are of appreciable size, the zero-range approximation is not valid. The integral (7.102) then has to be evaluated in its six-dimensional form.

To this end one begins by expanding the form factor  $f_{l(sj)m}(\mathbf{r}_\alpha, \mathbf{r}_\beta)$  in spherical harmonics with respect to the angular coordinates  $\hat{\mathbf{r}}_\alpha$  and  $\hat{\mathbf{r}}_\beta$ . As we have noted after eqn (7.99), the quantity  $\Gamma_{l(sj)m}$  and according to eqn (7.100),  $f_{l(sj)m}(\mathbf{r}_\alpha, \mathbf{r}_\beta)$  as well, must transform like  $Y_{lm}^*$ . We therefore write

$$f_{l(sj)m}(\mathbf{r}_\alpha, \mathbf{r}_\beta) = \sum_{l_\alpha l_\beta m_\beta} F_{l_\beta l_\alpha}^{lsj}(r_\alpha, r_\beta) (l_\beta m_\beta; l_\alpha, m - m_\beta | l m) \times Y_{l_\beta m_\beta}^*(\hat{\mathbf{r}}_\beta) Y_{l_\alpha m - m_\beta}^*(\hat{\mathbf{r}}_\alpha). \quad (7.128)$$

The distorted wave functions  $\chi_\alpha^{(+)}$  and  $\chi_\beta^{(-)}$  are expanded in partial waves (cf. eqns (7.122) and (7.123)) and the angular integrations are performed as before. One then arrives at the reduced amplitude

$$\beta_{sj}^{lm}(k_\alpha \hat{\mathbf{z}}, \mathbf{k}_\beta) = \frac{(4\pi)^{3/2}}{k_\alpha k_\beta} \sum_{l_\beta l_\alpha} i^{l_\alpha + l_\beta - l} e^{i\sigma_{l_\beta} + i\sigma_{l_\alpha}} I_{l_\beta l_\alpha}^{lsj} \times (l_\beta m; l, -m | l_\alpha 0) Y_{l_\beta, -m}(\theta, 0). \quad (7.129)$$

Here we have adopted the same coordinate system as after eqn (7.125). The radial integral  $I_{l_\beta l_\alpha}^{lsj}$  is a double integral of the form

$$I_{l_\beta l_\alpha}^{lsj} = \int_0^\infty r_\alpha dr_\alpha \int_0^\infty r_\beta dr_\beta y_{l_\beta}(k_\beta, r_\beta) F_{l_\beta l_\alpha}^{jsl}(r_\alpha, r_\beta) y_{l_\alpha}(k_\alpha, r_\alpha), \quad (7.130)$$

where the form factor  $F_{l_\beta l_\alpha}^{lsj}(r_\alpha, r_\beta)$  contains the finite-range potential and the radial wave function of the transferred particle. The integrals in eqn (7.130) have to be evaluated numerically.

Because now two spatial coordinates are involved, the parity selection rule (7.127) corresponding to a normal change of parity is not operative, and transitions with a ‘non-normal’ change of parity are no longer forbidden. In line with this, the Clebsch–Gordan coefficient  $(l_\beta 0; l 0 | l_\alpha 0)$  appearing in the zero-range expression (7.124), is absent in formula (7.129). Therefore, we may have both

$$\Delta\pi = (-)^l \text{ and } \Delta\pi = (-)^{l+1},$$

where  $l$  is the transferred nuclear spin (7.93). As noted before, this spin is equal to the magnitude of the change of orbital angular momentum in the relative motion.

Let us consider as an example the reaction  ${}^{12}\text{C}({}^{14}\text{N}, {}^{13}\text{C}){}^{13}\text{N}$  (cf. DeVries 1973), where both reaction partners are heavy ions. In this collision a neutron in the shell-model state  $1p_{1/2}$  is transferred from the nucleus  $x = {}^{14}\text{N}$  with spin  $I_x = 1$  and parity

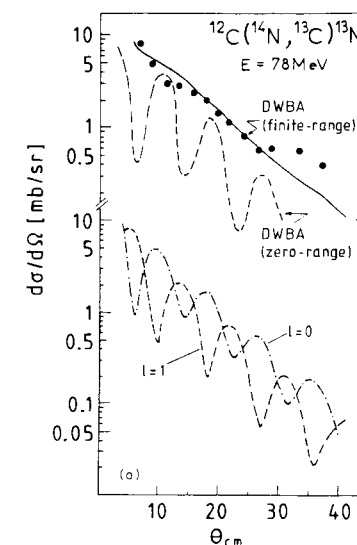


**Figure 7.8** Differential cross section for the reaction  ${}^{12}\text{C}({}^{14}\text{N}, {}^{13}\text{C}){}^{13}\text{N}(\text{g.s.})$  at  $E_{\text{lab}}(\text{N}) = 78$  MeV. In the upper part of the figure the data (represented by dots) are compared with the results of a DWBA calculation in the zero-range (dashed curve) and finite-range version (solid curve). In the lower part the contributions for  $l = 0$  and  $l = 1$  of the finite-range calculation are shown separately (cf. DeVries 1973).

$\pi_x = 1$  to the nucleus  $A = {}^{12}\text{C}$  with spin  $I_A = 0$  and parity  $\pi_A = 1$ . In the final channel we have the nucleus  $y = {}^{13}\text{C}$ , whose least bound nucleon is in the state  $1p_{1/2}$ , so that  $I_y = \frac{1}{2}$  and  $\pi_y = -1$ , and the nucleus  $B = {}^{13}\text{C}$ , which contains the neutron in the shell-model state  $1p_{1/2}$  and thus has  $I_B = \frac{1}{2}$  and  $\pi_B = -1$ . The change of parity (7.95) is equal to  $\Delta\pi = \pi_x \pi_A \pi_y \pi_B = 1$ . According to the angular momentum couplings implied by relations (7.91) and (7.92) we find  $l = 0, 1$  as possible values for  $l$ . Normal change of parity corresponds to  $l = 0$ . Therefore, if one performs the calculation in the zero-range approximation, the allowed contribution is that with  $l = 0$ .

It is seen from Fig. 7.8 that only the results of a finite-range calculation, which provides for normal and non-normal parity transfer, fit the data in a satisfactory way. In particular, they reproduce the smooth trend of the observed angular distribution, which is explained as superposition of the contributions for  $l = 0$  and  $l = 1$ ; taken separately, the latter display strong oscillations.

#### Recoil effects

The formalism just presented holds for any range of the transfer interaction and for any masses of the nuclei involved. With modern computers it is nowadays not difficult to calculate cross sections in this formalism. On the other hand, historically one has

been interested in casting the general formula into a form which resembles the zero-range expression, since that is easier to evaluate. Moreover, the latter is convenient for studying the effect of recoil in a transparent manner. We briefly indicate what is involved here.

The main purpose is to write the integral in the expression (7.102) for the reduced amplitude  $\beta_{sj}^{lm}(\mathbf{k}_\alpha, \mathbf{k}_\beta)$  in a form similar to the zero-range expression (7.120), where the variables appearing in the distorted wave functions are proportional to each other, as in eqn (7.118). This is achieved in the following way. We first write the variables  $\mathbf{r}_\alpha$  and  $\mathbf{r}_\beta$  in terms of the distance between the cores  $\mathbf{r}_{yA}$  (cf. Fig. 7.2),

$$\begin{aligned}\mathbf{r}_\alpha &= \mathbf{r}_{yA} + \frac{m_z}{m_x} \mathbf{r}_{zy}, \\ \mathbf{r}_\beta &= \frac{m_A}{m_B} \mathbf{r}_{yA} - \frac{m_z}{m_B} \mathbf{r}_{zy},\end{aligned}\quad (7.131)$$

where we have used  $\mathbf{r}_{zA} = \mathbf{r}_{zy} + \mathbf{r}_{yA}$  in eqns (7.10). Now we shift the arguments in the distorted waves with the help of *shift operators*,

$$\begin{aligned}\chi_\alpha^{(+)}(\mathbf{k}_\alpha, \mathbf{r}_\alpha) &= \chi_\alpha^{(+)}\left(\mathbf{k}_\alpha, \mathbf{r}_{yA} + \frac{m_z}{m_x} \mathbf{r}_{zy}\right) \\ &= \exp\left(\frac{m_z}{m_x} \mathbf{r}_{zy} \cdot \nabla\right) \chi_\alpha^{(+)}(\mathbf{k}_\alpha, \mathbf{r}_{yA}),\end{aligned}\quad (7.132)$$

$$\begin{aligned}\chi_\beta^{(-)*}(\mathbf{k}_\beta, \mathbf{r}_\beta) &= \chi_\beta^{(-)*}\left(\mathbf{k}_\beta, \frac{m_A}{m_B} \mathbf{r}_{yA} - \frac{m_z}{m_B} \mathbf{r}_{zy}\right) \\ &= \exp\left(-\frac{m_z}{m_A} \mathbf{r}_{zy} \cdot \nabla\right) \chi_\beta^{(-)*}\left(\mathbf{k}_\beta, \frac{m_A}{m_B} \mathbf{r}_{yA}\right),\end{aligned}\quad (7.133)$$

where the gradient  $\nabla$  operates on the coordinate  $\mathbf{r}_{yA}$ . We then rewrite expression (7.102) in the form

$$\begin{aligned}i^l (2l+1)^{1/2} \beta_{sj}^{lm}(\mathbf{k}_\alpha, \mathbf{k}_\beta) &= \mathcal{J} \int d^3 r_{yA} \int d^3 r_{zy} \chi_\beta^{(-)*}\left(\mathbf{k}_\beta, \frac{m_A}{m_B} \mathbf{r}_{yA}\right) \\ &\quad \times \exp\left(-\frac{m_z}{m_A} \mathbf{r}_{zy} \cdot \nabla\right) f_{l(sj)m}(\mathbf{r}_\alpha, \mathbf{r}_\beta) \\ &\quad \times \exp\left(\frac{m_z}{m_x} \mathbf{r}_{zy} \cdot \nabla\right) \chi_\alpha^{(+)}(\mathbf{k}_\alpha, \mathbf{r}_{yA}),\end{aligned}\quad (7.134)$$

where  $\overleftarrow{\nabla}$  operates to the left, and  $\mathcal{J}$  is the Jacobian of the transformation (7.131). From expression (7.134) we go over to

$$\begin{aligned}\beta_{sj}^{lm}(\mathbf{k}_\alpha, \mathbf{k}_\beta) &= \mathcal{J} \frac{i^{-l}}{(2l+1)^{1/2}} \int d^3 r_{yA} \chi_\beta^{(-)*}\left(\mathbf{k}_\beta, \frac{m_A}{m_B} \mathbf{r}_{yA}\right) \\ &\quad \times \mathcal{F}_{l(sj)m}(\mathbf{r}_{yA}) \chi_\alpha^{(+)}(\mathbf{k}_\alpha, \mathbf{r}_{yA}),\end{aligned}\quad (7.135)$$

where

$$\mathcal{F}_{l(sj)m}(\mathbf{r}_{yA}) = \int d^3 r_{zy} \exp\left(-\frac{\overleftarrow{\nabla} \cdot \frac{m_z}{m_A} \mathbf{r}_{zy}}{m_A}\right) f_{l(sj)m}(\mathbf{r}_\alpha, \mathbf{r}_\beta) \exp\left(\frac{m_z}{m_x} \mathbf{r}_{zy} \cdot \nabla\right), \quad (7.136)$$

and find that the finite-range reduced amplitude has attained a form similar to that of the zero-range expression (7.120), with all finite-range effects incorporated in the operator function  $\mathcal{F}_{l(sj)m}(\mathbf{r}_{yA})$ .

In heavy-ion reactions (cf. Buttle and Goldfarb 1966, 1968), one may approximately replace the operator  $-i\nabla$  acting on  $\chi_\alpha^{(+)}(\mathbf{k}_\alpha, \mathbf{r}_{yA})$  with the local momentum  $\mathbf{K}_\alpha(\mathbf{r}_{yA})$  in the optical potential  $U_\alpha$  in channel  $\alpha$ . Similarly, the operator  $-i\overleftarrow{\nabla}$  acting on  $\chi_\beta^{(-)*}(\mathbf{k}_\beta, (m_A/m_B)\mathbf{r}_{yA})$  may be replaced with the local momentum  $-\mathbf{K}_\beta(\mathbf{r}_{yA})$ . The arguments in the distorted wave functions in eqn (7.134) are now proportional to one another as in the zero-range approximation (cf. eqn (7.118)), but the product  $F_{nlj}(r)Y_{lm}^*(\hat{\mathbf{r}})$  in expression (7.120) becomes the more complicated function (7.136) evaluated in the manner just explained. If the mass of the transferred particle is small compared to the masses of the projectile and the target nucleus,

$$m_z \ll m_x, m_A, \quad (7.137)$$

we may replace the exponential shift operators with unity. This is called the *no-recoil approximation*, because when the mass  $m_z$  of the transferred nucleon  $z$  is neglected, the core nuclei experience no recoil.

When finite range and recoil are duly taken into account, the DWBA results are generally in good agreement with the data. However, it must be realized that one is neglecting multistep and Pauli antisymmetrization effects. Furthermore, one is not always certain of the correct choice of the optical potential for the distorted waves (it must sometimes be corrected for its non-locality), or of the shell-model potential to be used for the calculation of the radial single-particle function  $R_{nlj}(r)$ . Moreover, the strength of the interaction causing the transfer is not known very well, since it is generally determined by effective nucleon–nucleon forces inside the nuclei which may differ from those acting between free nucleons. Fortunately, these uncertainties appear to affect mainly the over-all normalization of the cross section, so that spins and *relative spectroscopic factors* can still be determined quite reliably.

## 7.4 Classical selection rules

Before embarking on a detailed calculation of the cross section for a particular transfer reaction, one may wish to obtain an approximate idea of which results to expect. This can be done by considering some simple selection rules. In order to see the operation of such rules we go over to the classical picture (cf. Brink 1972). We must then restrict the discussion to reactions at higher energies, where the classical approximation is valid.

We consider the transfer process (7.1) and (7.2) illustrated in classical terms in Fig. 7.9. In the reaction plane the projectile  $x$  moves in the horizontal direction with a velocity  $v$  which we assume to be so large that it remains unaffected by the transfer of the particle  $z$  with the small mass  $m$ ,  $\Delta v = 0$ . The target nucleus  $A$  is at rest. The particle  $z$  in the projectile  $x$  moves in an orbit around the core  $y$  with radius  $R_y$ , while in the final

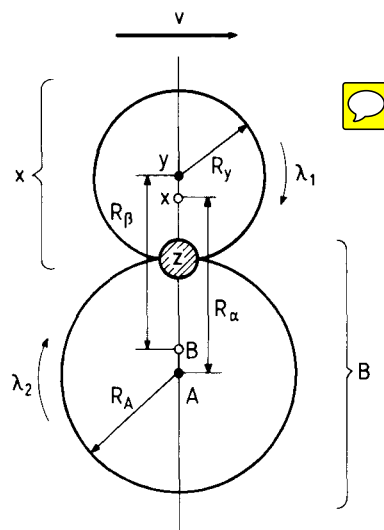


**Figure 7.9** Classical description of one-particle transfer.

nucleus  $B$  it moves in an orbit around the core  $A$  with radius  $R_A$ . The figure refers to the moment of transfer. The particle  $z$  is transferred at the point where the cores touch. Let the initial orbital angular momentum of the particle  $z$  and its projection be  $l_1\lambda_1$ , and the final angular momentum  $l_2\lambda_2$ . The corresponding angular wave functions are  $Y_{l_1\lambda_1}(\theta_1, \phi_1)$  and  $Y_{l_2\lambda_2}(\theta_2, \phi_2)$ , respectively. Classical conservation laws now lead to a number of selection rules which spell out the conditions under which the transfer cross section is expected to be large.

#### Spins of the final states

For an unhindered transfer the horizontal components of the momentum of the transferred particle  $z$  in nucleus  $x$ ,  $p^{(1)}$ , and in the nucleus  $B$ ,  $p^{(2)}$ , must be equal immediately before and after the collision,  $p^{(2)} = p^{(1)}$ . In Fig. 7.9 we read off

$$p^{(1)} = mv - \frac{\hbar\lambda_1}{R_y} \quad \text{and} \quad p^{(2)} = \frac{\hbar\lambda_2}{R_A}, \quad (7.138)$$

and therefore,

$$\frac{\lambda_2}{R_A} + \frac{\lambda_1}{R_y} = \frac{mv}{\hbar}. \quad (7.139)$$

Because the momentum  $mv$  is assumed to be large and  $\lambda_1$  is usually small, the angular momentum of the final state  $\lambda_2$  must be large. Therefore transfer into states with high spins is preferred.

#### The $Q$ -window

The change of the total angular momentum perpendicular to the plane can be decomposed into an intrinsic part  $\hbar\Delta\lambda$  and a change in the angular momentum of the relative motion,  $\Delta(\mu v R)$ , where  $\mu$  is the reduced mass and  $R$  the relative distance of the two nuclei. Owing to conservation of angular momentum, one requires

$$\hbar\Delta\lambda + \Delta(\mu v R) = 0, \quad (7.140)$$

where

$$\Delta\lambda = \lambda_2 - \lambda_1; \quad (7.141)$$

since we assume  $\Delta v = 0$ , we have

$$\Delta(\mu v R) = vR\Delta\mu + v\mu\Delta R. \quad (7.142)$$

The last relation can be rewritten by first noting that

$$\begin{aligned} \Delta\mu &= \mu_\beta - \mu_\alpha = \frac{1}{m_T}(m_y m_B - m_x m_A) \\ &= \frac{1}{m_T}[m_y(m_A + m) - (m_y + m)m_A] \\ &= \frac{m}{m_T}(m_y - m_A), \end{aligned} \quad (7.143)$$

where  $m_T = m_x + m_A = m_y + m_B$  is the total mass.

The change in relative distance is given by

$$\Delta R = R_\beta - R_\alpha, \quad (7.144)$$

where

$$R_\alpha = \frac{m_y}{m_x}R_y + R_A \quad (7.145)$$

is the distance between the centre of mass of the projectile nucleus  $x$  and that of the target nucleus  $A$ , and correspondingly,

$$R_\beta = \frac{m_A}{m_B}R_A + R_y \quad (7.146)$$

is the distance between the ejectile nucleus  $y$  and the centre of mass of the final nucleus  $B$  (cf. Fig. 7.9). Therefore we find

$$\begin{aligned} \Delta R &= \left(1 - \frac{m_y}{m_x}\right)R_y - \left(1 - \frac{m_A}{m_B}\right)R_A \\ &= \frac{1}{2}(R_y - R_A)m\frac{m_x + m_B}{m_x m_B} - \frac{1}{2}(R_y + R_A)\Delta\mu\frac{m_T}{m_x m_B} \\ &\approx \frac{1}{2\mu}[m(R_y - R_A) - R\Delta\mu], \end{aligned} \quad (7.147)$$

where we have used  $m_x m_B / (m_x + m_B) \approx m_x m_B / m_T \approx \mu$ , and have set  $R_y + R_A = R$ . Thus we obtain from eqn (7.142) (recall that  $\Delta v = 0$ )

$$\begin{aligned}\Delta(\mu v R) &\approx v R \Delta\mu + \frac{v}{2} [m(R_y - R_A) - R \Delta\mu] \\ &= \frac{vm}{2}(R_y - R_A) + \frac{R}{v} \Delta(\frac{1}{2}\mu v^2).\end{aligned}\quad (7.148)$$

On the right-hand side of this relation we recognize the change of kinetic energy at the transfer point, which we may call an effective  $Q$ -value,

$$\Delta(\frac{1}{2}\mu v^2) = Q_{\text{eff}}.\quad (7.149)$$

Taking into account the change in Coulomb energy caused by the transfer of a charged particle, the effective  $Q$ -value is related to the true  $Q$ -value of the reaction by

$$Q_{\text{eff}} = \begin{cases} Q & \text{for neutrons,} \\ Q - (Z_y Z_B - Z_x Z_A)e^2/R & \text{for protons.} \end{cases}\quad (7.150)$$

Going back to the condition (7.140), we can write it now in the form

$$\hbar(\lambda_2 - \lambda_1) + \frac{1}{2}mv(R_y - R_A) + \frac{R}{v}Q_{\text{eff}} = 0.\quad (7.151)$$

We thus find that only transfer reactions whose  $Q$ -value satisfies relations (7.150) and (7.151) are expected to have a large cross section. These relations define the  **$Q$ -window**.

### Parity

Assuming that the particles are transferred within the reaction plane we have  $\theta_1 = \theta_2 = \frac{\pi}{2}$ . Since  $Y_{l\lambda}(\frac{\pi}{2}, \phi)$  is non-vanishing only if  $l + \lambda$  is even (cf. Edmonds 1957, Section 2.5), we obtain the **parity selection rule**

$$\begin{aligned}l_1 + \lambda_1 &= \text{even,} \\ l_2 + \lambda_2 &= \text{even.}\end{aligned}\quad (7.152)$$

### Spin flip

A rule for spin-flip processes can be derived classically from Fig. 7.10. In this figure the target nucleus  $A$  is at rest, while the projectile  $x$  passes with velocity  $v$ . We consider the orbital angular momentum and spin of the nucleon  $z$  perpendicular to the reaction plane. In Fig. 7.10a the initial orbital angular momentum  $\lambda_1$  of particle  $z$  relative to the centre of the core  $y$  is such that at the moment of transfer the velocity  $v_1$  of  $z$  is opposite to  $v$ , so that its velocity  $v_2$  relative to the centre of core  $A$  after transfer is small. The nucleon  $z$  is easily absorbed by  $A$  with relative angular momentum  $\lambda_2$ , and the process is *allowed*. Now, the initial total spin of  $z$  perpendicular to the reaction plane is  $j_1^\perp = \lambda_1 \pm \frac{1}{2}$  and the corresponding final total spin is  $j_2^\perp = \lambda_2 \pm \frac{1}{2}$ . Since  $\lambda_1$  and  $\lambda_2$  are in the same direction (have the same sign) and the nucleon spin  $\frac{1}{2}$  does not change its direction (assuming that the interactions do not depend on spin), the spin  $\frac{1}{2}$  does not flip relative to the orbital angular momentum during this process; therefore ***an allowed process proceeds without spin flip***.

In Fig. 7.10b the initial angular momentum of the nucleon is reversed as compared with the previous situation. Now the nucleon is transferred to the core  $A$  with a large relative velocity  $v_2$ . The nucleon is less easily absorbed by  $A$  than before, and the

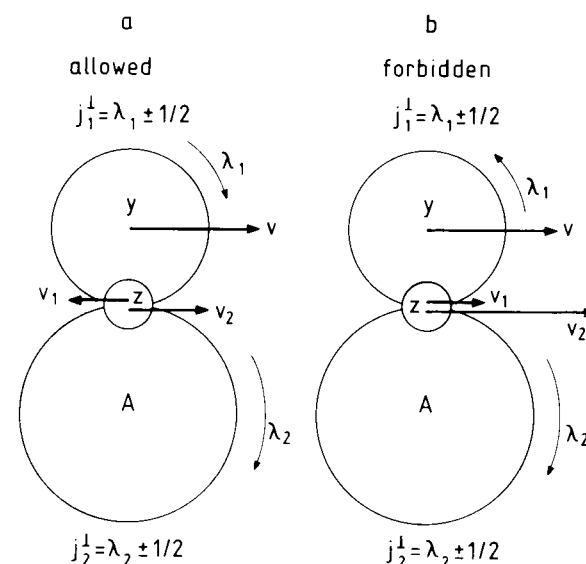


**Figure 7.10** Illustration of the spin-flip selection rule. (a) Allowed transfer (without spin flip), (b) forbidden transfer (with spin flip).

process is forbidden. Since the perpendicular component of the relative orbital angular momentum of the nucleon changes sign during the transfer whereas the nucleon spin  $\frac{1}{2}$  does not, the spin  $\frac{1}{2}$  flips relative to the orbital angular momentum. ***It follows that transitions with spin flip are suppressed as compared to transitions without spin flip***.

In the next subsection we shall discuss an example of a transfer reaction in order to illustrate how well these selection rules are obeyed, and how accurately the details of the measured cross section are reproduced by a finite-range DWBA calculation.

## 7.5 An example of single-nucleon transfer between heavy ions

Let us consider one-nucleon transfer in the collision  $^{16}\text{O} + ^{208}\text{Pb}$  at the rather high energy  $E_{\text{lab}}(^{16}\text{O}) = 793$  MeV (cf. Mermaz *et al.* 1987). We discuss both the one-proton transfer reaction  $^{208}\text{Pb}(^{16}\text{O}, ^{15}\text{N})^{209}\text{Bi}$  and the one-neutron transfer reaction  $^{208}\text{Pb}(^{16}\text{O}, ^{15}\text{O})^{209}\text{Pb}$ .

The proton levels available in the target nucleus  $^{208}\text{Pb}$  are the states  $1\text{h}_{9/2}^-, 2\text{f}_{7/2}^-, 1\text{i}_{13/2}^+, 3\text{p}_{3/2}^-, 2\text{f}_{5/2}^-$ , and  $3\text{p}_{1/2}^-$  (cf. Fig. 7.11a). Figure 7.12a shows that all these states are populated in proton transfer, except the states  $3\text{p}_{3/2}^-$  and  $3\text{p}_{1/2}^-$ . These are the states with the lowest spins, and we therefore find that the first selection rule of Section 7.4 is operating here: ***transfer to high-spin states is preferred***.

The situation is similar for neutron transfer; here the states  $2\text{g}_{9/2}^+, 1\text{i}_{11/2}^+, 3\text{d}_{5/2}^+$ ,  $1\text{j}_{15/2}^-, 4\text{s}_{1/2}^+, 2\text{g}_{7/2}^+$ , and  $3\text{d}_{3/2}^+$  are available (cf. Fig. 7.11b), and again the transfer to the

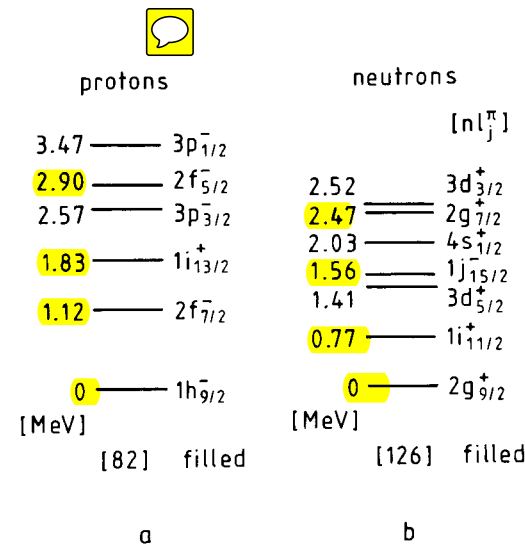


Figure 7.11 The low-lying proton states in  $^{209}\text{Bi}$  (a) and neutron states in  $^{209}\text{Pb}$  (b).

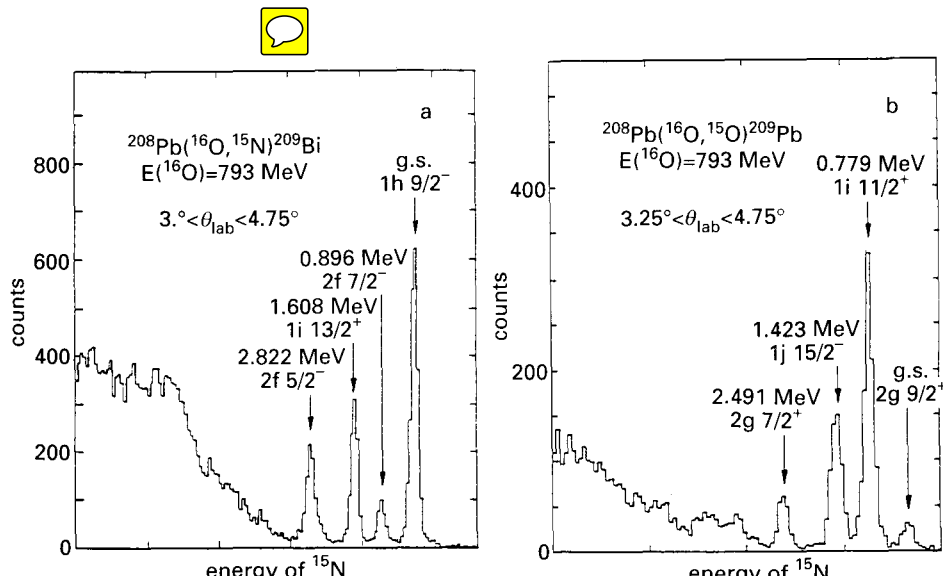


Figure 7.12 Energy spectra of the reactions (a)  $^{208}\text{Pb}(^{16}\text{O}, ^{15}\text{N})^{209}\text{Bi}$  and (b)  $^{208}\text{Pb}(^{16}\text{O}, ^{15}\text{O})^{209}\text{Pb}$ .

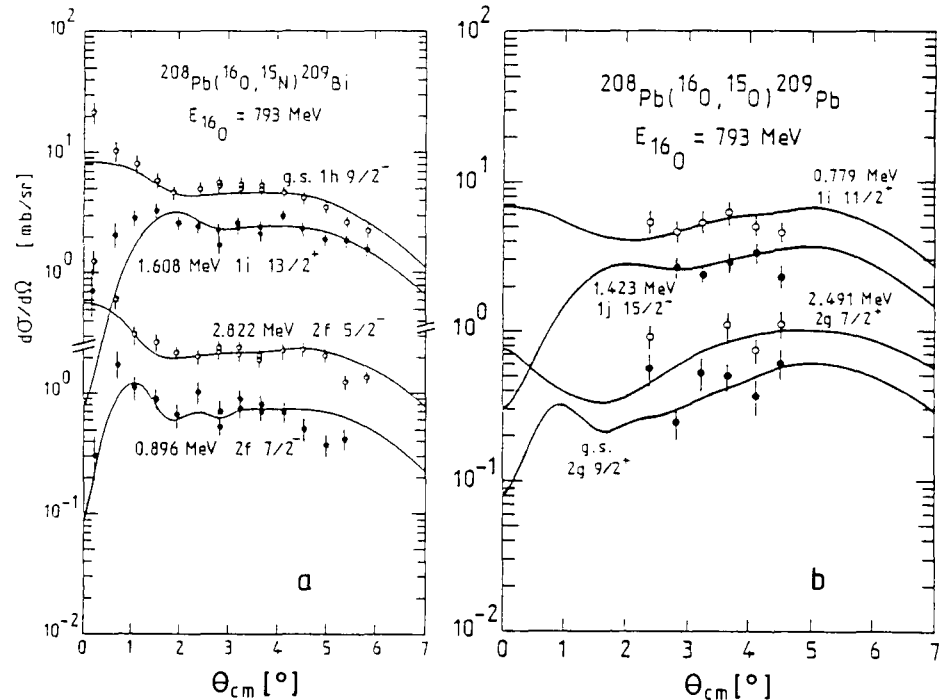


Figure 7.13 Comparison of experimental angular distributions for the reactions (a)  $^{208}\text{Pb}(^{16}\text{O}, ^{15}\text{N})^{209}\text{Bi}$  and (b)  $^{208}\text{Pb}(^{16}\text{O}, ^{15}\text{O})^{209}\text{Pb}$  with the results of finite-range DWBA calculations.

low-spin states  $3d_{5/2}^+$ ,  $4s_{1/2}^+$ , and  $3d_{3/2}^+$  is not seen in experiment in accordance with the first selection rule (cf. Fig. 7.12b).

The relative intensities of the observed lines can be explained with the help of the no-spin-flip selection rule. Because the initial state of the proton or neutron in the nucleus  $^{16}\text{O}$  is  $1p_{1/2}$ , we have  $j_1 = l_1 - \frac{1}{2}$ , and the final states with  $j_2 = l_2 - \frac{1}{2}$  should be more strongly excited than those with  $j_2 = l_2 + \frac{1}{2}$ , because the former can be reached without spin flip while the latter cannot. This is true for proton transfer: the  $2f_{7/2}$  state is excited more weakly than the  $2f_{5/2}$  state, and the  $1h_{9/2}$  state shows up particularly strongly (cf. Fig. 7.12a). It is true for neutrons as well: the ground state  $2g_{9/2}$  is excited more weakly than the state  $2g_{7/2}$ , while the  $1i_{11/2}$  state comes in very strongly (cf. Fig. 7.12b).

All these features are reproduced in the results of a finite-range DWBA analysis of the data (cf. Fig. 7.13). The relative intensities are well fitted. However, one is not able to reproduce the overall magnitude of the measured cross section by the calculation, and one therefore has to resign oneself to renormalizing the calculated cross section to fit the data. This appears to be a general problem in the analysis of single-particle transfer

data. At different collision energies, different normalization factors have to be used.

## 7.6 Notes and references

One of the early papers in the field of direct nuclear reactions is that of Oppenheimer and Phillips (1935) on deuteron stripping. Because of the extreme usefulness of direct reactions for the investigation of nuclear structure, a vast literature both on their theoretical foundations and on their application has come into existence. We refer to a number of monographs which have appeared in the course of time, Butler and Hittmair (1957), Tobocman (1961), Austern (1970), Satchler (1983), and Glendenning (1983).

In the present chapter we have only treated one-nucleon transfer. The DWBA formalism can, however, be extended to the treatment of two-nucleon and multi-nucleon transfer. **Besides in the monographs quoted above, various aspects concerning the transfer of more than one particle are discussed in the review articles by Goldfarb and von Oertzen (1979) and by Asciutto and Seglie (1984), in particular with respect to heavy-ion collisions.**

We have mainly discussed the reaction mechanism of direct reactions, and not the information one can obtain from them on the nuclear wave functions via the spectroscopic factor. The literature on this aspect is extensive; it is mainly concerned with tests of the single-particle and collective models. We mention as particular examples the extraction of the coefficients of the Bardeen–Cooper–Schrieffer (BCS) wave functions by single-particle transfer to quasi-particle states (cf. Yoshida 1961) and the determination of the coefficients of pairing-vibrational states by using (t,p) reactions (cf. Broglia and Riedel 1967).

**Direct reactions to unbound states** require a slight extension of the formalism developed in the present chapter. This subject has been discussed, for example, by Huby and Mines (1965), Vincent and Fortune (1970), Lipperheide (1970), and Fuchs *et al.* (1972) for stripping, and by Jacob and Maris (1966), Gross and Lipperheide (1970), Wille and Lipperheide (1972), and Fritsch *et al.* (1975) for knock-out reactions like (p,2p).

An approach to the theory of direct reactions based on Feynman graphs is that of dispersion theory (cf. Shapiro 1961, 1962, 1963; Schnitzer 1965).

## References

- Asciutto, R. J. and Seglie, E. A. (1984). In *Treatise on heavy-ion science*, ed. Bromley, D. A., vol. 1, Plenum, New York.
- Austern, N. (1970). *Direct nuclear reaction theories*, Wiley, New York.
- Austern, N., Drisko, R. M., Halbert, E. C. and Satchler, G. R. (1964). *Phys. Rev.* **133** B3.
- Brink, D. (1972). *Phys. Lett.* **40B** 37.
- Broglia, R.A. and Riedel, C. (1967). *Nucl. Phys.* **A92** 145.
- Butler, S. T. and Hittmair, O. H. (1957). *Nuclear stripping reactions*, Horwitz, Sydney.
- Buttle, P. J. A. and Goldfarb, L. J. B. (1966). *Nucl. Phys.* **78** 409.
- Buttle, P. J. A. and Goldfarb, L. J. B. (1968). *Nucl. Phys.* **A115** 461.
- Cobb, W.R., and Guth, D.B. (1957). *Phys. Rev.* **107** 181.
- DeVries, R.M. (1973). *Phys. Rev.* **C8** 951.

## 7.6 Notes and references

- Edmonds, A. R. (1957). *Angular momentum in quantum mechanics*, Princeton University Press, Princeton.
- Fritsch, W., Lipperheide, R. and Wille, U. (1975). *Nucl. Phys.* **A241** 79.
- Fuchs, H., Homeyer, H., Lipperheide, R., Möhring, K. and Oeschler, H. (1972). *Nucl. Phys.* **A196** 286.
- Glendenning, N. K. (1983). *Direct nuclear reactions*, Academic Press, New York.
- Goldfarb, L. J. B. and von Oertzen, W. (1979). In *Heavy ion collisions*, ed. Bock, R. vol. 1, Chapter 2, North-Holland, Amsterdam, p. 215 .
- Gross, D. H. E. and Lipperheide, R. (1970). *Nucl. Phys.* **A150** 449.
- Huby, R. and Mines, J. R. (1965). *Rev. Mod. Phys.* **37** 406.
- Jacob, G. and Maris, T. A. M. (1966). *Rev. Mod. Phys.* **38** 121.
- Lipperheide, R. (1970). *Phys. Lett.* **32B** 555.
- Mermaz, M. C., Berthier, B., Barette, J., Gastebois, J., Gillibert, A., Lucas, R., Matuszek, J., Miczaika, A., Van Renterghem, E., Suomijärvi, T., Boucenna, A., Disdier, D., Gorodetzky, P., Kraus, L., Linck, I., Lott, B., Rauch, V., Rebmeister, R., Scheibling, F., Schulz, N., Sens, J. C., Grunberg, C. and Mittig, W. (1987). *Z. Physik* **A326** 353.
- Muehlener, G., Poltorak, A. S., Parkinson, W. C. and Bassel, R.H. (1967). *Phys. Rev.* **159** 1039.
- Oppenheimer, J. R. and Phillips, M. (1935). *Phys. Rev.* **48** 500.
- Satchler, R. G. (1983). *Direct nuclear reactions*, Clarendon Press, Oxford.
- Schnitzer, H. J. (1965). *Rev. Mod. Phys.* **37** 666.
- Shapiro, I. S. (1961). *Nucl. Phys.* **28** 244.
- Shapiro, I. S. (1962). *Sov. Phys. JETP* **14** 1148.
- Shapiro, I. S. (1963). In *Selected topics in nuclear theory*, ed. Janouch, F., IAEA, Vienna, p. 85.
- Tobocman, W. (1961). *Theory of direct nuclear reactions*, Oxford University Press, London
- Vincent, C. M. and Fortune, H. T. (1970). *Phys. Rev.* **C2** 782.
- Wille, U. and Lipperheide, R. (1972). *Nucl. Phys.* **A189** 113.
- Yoshida, S. (1961). *Phys. Rev.* **123** 2122.

## THE COUPLED-CHANNEL DESCRIPTION OF DIRECT REACTIONS

### 8.1 Introduction

In the single-step approximation introduced in Section 5.4 and discussed in detail in Chapter 7, one assumes the reaction to proceed directly from the initial to the final state, and thus ignores the existence of any other than the entrance and exit channels. It was shown formally in Section 5.5 how the coupled-channel description allows one to go beyond this approximation. We shall now turn to the *practical implementation* of the coupled-channel method.

In Section 8.2 we develop an explicit *coupled-channel scheme* for the calculation of inelastic cross sections. We introduce the partial-wave decomposition in analogy to the procedure of Section 1.2.2 for single-channel scattering. Thereby we obtain a system of one-dimensional differential equations for the elastic and inelastic partial wave functions which are amenable to a numerical treatment. The asymptotic forms of these wave functions yield the scattering amplitudes, and hence the elastic and inelastic cross sections, as functions of the scattering angle. As a trivial application we discuss briefly the case of spin-orbit coupling.

We consider *inelastic scattering to collective states* in Section 8.3. The spin-coupled matrix elements for collective excitations are established in general form, and the coupled equations are derived explicitly for rotational and vibrational excitations. Cross sections for inelastic scattering to rotational states are calculated and compared with the experimental data.

The elastic-channel wave function resulting from a coupled-channel calculation can also be conceived as a solution of a single-particle Schrödinger equation with an optical potential. In Section 8.4 we present a microscopic derivation of such a potential by making explicit use of the coupled-channel formalism for Coulomb excitation. **It is found that the Coulomb coupling between the channels gives rise to a long-range Coulomb polarization potential which must be added to the usual phenomenological nuclear optical potential for an accurate description of the elastic scattering of heavy ions.**

As has been discussed in Section 5.5.2, the coupled-channel scheme for inelastic scattering may also be incorporated in improved procedures for the calculation of the *T*-matrix for rearrangement reactions. In Section 8.5 we present results of the *coupled-channel Born approximation* (CCBA), where the distorted-wave states in the DWBA *T*-matrix are replaced with inelastic scattering states taken from a coupled-channel calculation. Finally, in Section 8.6 we discuss results of the *coupled-reaction-channel method* (CRC), in which different arrangement channels are coupled with account of their non-orthogonality.

### 8.2 The coupled-channel (CC) formalism for inelastic scattering

#### 8.2.1 The CC equations in the partial-wave decomposition

In inelastic scattering processes the colliding nuclei do not transfer particles, but change only with regard to their internal structure and excitation energy. The initial and final states are therefore in the *same* arrangement channel. Following Section 5.5.1, we decompose the total Hamiltonian  $H$  in the form

$$H = T + h + V(\mathbf{r}, \xi), \quad (8.1)$$

where we have omitted the index labelling the arrangement channel. The kinetic energy operator

$$T = -\frac{\hbar^2}{2\mu} \nabla^2 \quad (8.2)$$

acts on the relative coordinate  $\mathbf{r}$  of the two nuclei, where  $\mu$  is their reduced mass. The operator  $h$  is the sum of the two internal Hamiltonians acting on the internal coordinates  $\xi$ . Finally, the term  $V(\mathbf{r}, \xi)$  is the internuclear interaction which depends on the relative as well as on the internal coordinates.

The main effect of the internuclear interaction can be represented as a sum of the static nuclear and Coulomb potentials between the collision partners. We represent this sum by a spherical term  $V_0(r)$  which does not couple different inelastic channels. It is convenient to subtract this potential from the internuclear interaction  $V(\mathbf{r}, \xi)$ , and to introduce in the place of the latter the residual coupling potential

$$V_{\text{coup}}(\mathbf{r}, \xi) = V(\mathbf{r}, \xi) - V_0(r). \quad (8.3)$$

We thus decompose the total Hamiltonian in the form

$$H = H_0 + V_{\text{coup}}(\mathbf{r}, \xi), \quad (8.4)$$

where

$$H_0 = T + h + V_0(r) \quad (8.5)$$

is a distorted-channel Hamiltonian in the sense of eqn (5.18) with  $V_0(r)$  assuming the role of the distorting potential.

**We restrict ourselves to the case where the projectile is spherical with spin zero, and is not excited during the collision.** We may then ignore the internal degrees of freedom of the projectile nucleus altogether. The internal Hamiltonian  $h$  and the internal coordinates  $\xi$  then refer only to the target nucleus, and the channel spin in a channel  $b$  is given by the target spin  $\{I_b M_b\}$  alone.

As discussed in Section 5.5.1, the inelastic scattering wave function of a system with initial quantum numbers  $a = \{\underline{a}; I_a M_a; \mathbf{k}_a\}$ ,  $\Psi_a^{\text{inel}} = \Psi_{\underline{a}; I_a M_a; \mathbf{k}_a}^{\text{inel}}(\mathbf{r}, \xi)$ , is restricted to a space of a finite number  $N$  of selected channels in the arrangement channel of the incident nuclei; these channels are labelled by the set of internal quantum numbers  $b = \{\underline{b}; I_b M_b\}$ . The label  $\underline{a}$  denotes the internal quantum numbers of the target nucleus besides its spin  $\{I_a M_a\}$ , and similarly for  $\underline{b}$ . **We thus assume that we can also neglect the indirect effect of all rearrangement channels on the inelastic scattering.** We note, however, that in some applications a phenomenological optical potential is taken for the potential  $V_0(r)$ , whose imaginary part would then include the effect of such channels.

The inelastic wave function is represented by the expansion (5.153), which we repeat here for convenience,

$$\Psi_a^{(+)\text{inel}}(\mathbf{r}, \xi) = \sum_{b=1}^N \psi_{ab}^{(+)}(\mathbf{r}) \phi_b(\xi). \quad (8.6)$$

The functions  $\phi_b(\xi)$  are the internal wave functions in the channels  $b$  satisfying

$$h\phi_b(\xi) = \epsilon_b \phi_b(\xi), \quad (8.7)$$

where the  $\epsilon_b$  are the energies of the internal states of the target. The functions  $\psi_{ab}^{(+)}(\mathbf{r})$  must have the asymptotic form (5.159), which we write more explicitly as

$$\begin{aligned} \psi_{\{\underline{a}; I_a M_a; \mathbf{k}_a\} \{\underline{b}; I_b M_b\}}^{(+)}(\mathbf{r}) &\rightarrow \psi_C(\eta_a, k_a; \mathbf{r}) \delta_{\{\underline{a}; I_a M_a\} \{\underline{b}; I_b M_b\}} \\ &+ f_{\{\underline{b}; I_b M_b\} \{\underline{a}; I_a M_a\}}^{+}(\Omega) \frac{e^{i[k_b r - \eta_b \ln(2k_b r)]}}{r} \quad \text{for } r \rightarrow \infty, b = 1, \dots, N, \end{aligned} \quad (8.8)$$

where  $\psi_C(\eta_a, k_a; \mathbf{r})$  is the incident Coulomb wave function. We have chosen the  $z$ -axis for the variable  $\mathbf{r}$  in the direction of the incoming momentum  $\mathbf{k}_a$ ; the angle  $\Omega$  defines the direction of the outgoing momentum  $\mathbf{k}_b$ .

The functions  $\psi_{ab}^{(+)}(\mathbf{r})$  satisfy the system of coupled equations (cf. eqn (5.156))

$$\left( -\frac{\hbar^2}{2\mu} \nabla^2 + V_0(r) + V_{bb}(\mathbf{r}) - \mathcal{E}_b \right) \psi_{ab}^{(+)}(\mathbf{r}) = - \sum_{c(c \neq b)}^N V_{bc}(\mathbf{r}) \psi_{ac}^{(+)}(\mathbf{r}), \quad (8.9)$$

where  $\mathcal{E}_b = E - \epsilon_b$  is the channel energy (5.157), and

$$V_{bc}(\mathbf{r}) = \int d\xi \phi_b^*(\xi) V_{\text{coupl}}(\mathbf{r}, \xi) \phi_c(\xi) \quad (8.10)$$

is the channel coupling matrix (5.158), with  $V_0$  subtracted from the internuclear interaction  $V(r, \xi)$ .

### The partial-wave decomposition

The inelastic scattering function  $\Psi_a^{(+)\text{inel}}(\mathbf{r}, \xi) = \Psi_{\{\underline{a}; I_a M_a; \mathbf{k}_a\}}^{(+)\text{inel}}(\mathbf{r}, \xi)$  is an eigenfunction of the Hamiltonian (8.4) in the restricted space of  $N$  inelastic channels. The Hamiltonian is invariant under rotations and the parity operation. It is, therefore, expedient to express the inelastic scattering function in terms of eigenfunctions of the total angular momentum  $JM$  and the parity  $\pi$ ,  $\Psi_{\{\underline{a}; I_a M_a\}}^{JM\pi}(\mathbf{r}, \xi)$ . (In the following we shall not refer to parity explicitly, counting it as one of the internal quantum numbers.) We are thus looking for a generalization of the partial-wave expansion (1.119) in the form

$$\Psi_{\{\underline{a}; I_a M_a; \mathbf{k}_a\}}^{(+)\text{inel}}(\mathbf{r}, \xi) = \sum_{J M l_a} c_{J M l_a}^{I_a M_a} \Psi_{\{\underline{a}; I_a M_a\}}^{JM}(\mathbf{r}, \xi). \quad (8.11)$$

In addition to expanding in angular momenta we must also expand in a finite number of channels in line with eqn (8.6). Combining the internal wave functions  $\phi_{\{\underline{b}; I_b M_b\}}(\xi)$  with the orbital angular momentum eigenfunctions  $Y_{l_b m_b}(\Omega)$ , we define the *spin-coupled*

### channel wave functions

$$\mathcal{Y}_{\{\underline{b}; I_b M_b\} JM}(\Omega, \xi) = \sum_{m_b M_b} (l_b m_b; I_b M_b | JM) Y_{l_b m_b}(\Omega) \phi_{\{\underline{b}; I_b M_b\}}(\xi), \quad (8.12)$$

which are eigenfunctions of the angular momentum operators  $\mathbf{l}^2$ ,  $\mathbf{I}^2$ ,  $\mathbf{J}^2$ , and  $J_z$ . These functions are coordinate representations of channel states of the type (5.104) in which the orbital angular momentum  $\mathbf{l}_b$  and the channel spin  $\mathbf{S}_b$  (here equal to the target spin  $\mathbf{I}_b$ ) are coupled to the total spin  $\mathbf{J}$ . In the remainder of this subsection we shall use the label  **$b$**  as a comprehensive index which replaces the set of indices  $\{\underline{b}; I_b M_b; JM\}$  labelling a channel wave function (8.12), or a part of them; it should always be clear which particular quantum numbers are included in  $b$ . Since all inelastic channels belong to the same arrangement channel, the channel wave functions (8.12) satisfy the orthogonality relation

$$\int d\Omega \int d\xi \mathcal{Y}_b^*(\Omega, \xi) \mathcal{Y}_c(\Omega, \xi) = \delta_{bc} \quad (8.13)$$

and the completeness relation

$$\sum_b \mathcal{Y}_b^*(\Omega', \xi') \mathcal{Y}_b(\Omega, \xi) = \delta(\Omega' - \Omega) \delta(\xi' - \xi), \quad (8.14)$$

as is clear from the orthogonality and completeness relations for the functions  $Y_{l_b m_b}(\Omega)$  and  $\phi_{\{\underline{b}; I_b M_b\}}(\xi)$ , and for the Clebsch–Gordan coefficients.

The spin-coupled inelastic scattering wave function  $\Psi_a^{JM}(\mathbf{r}, \xi)$  can now be expanded in terms of spin-coupled channel wave functions (8.12) with the same total angular momentum  $\{JM\}$  but different values of the quantum numbers  $b = \{\underline{b}; I_b M_b\}$ ,

$$\Psi_a^{JM}(\mathbf{r}, \xi) = \frac{1}{k_a r} \sum_{b=1}^N g_{ab}^J(r) \mathcal{Y}_b(\Omega, \xi). \quad (8.15)$$

Since only a finite number of values  $l_b$  can couple with  $I_b$  to the total angular momentum  $J$ , the sum in eqn (8.15) goes only over a finite number  $\mathcal{N}$  of terms. The number  $\mathcal{N}$  is in general larger than the number  $N$  in eqn (8.6). The expansion coefficients  $g_{ab}^J(r)$  are the radial wave functions in the spin-coupled channels  $b$ . Owing to rotational invariance they depend on the total spin  $J$  but not on its component  $M$ .

Just like the original inelastic wave function (8.11), each of its spin-coupled component wave functions (8.15) is an eigenfunction of the total Hamiltonian  $H$  in a restricted space, here the space of the  $\mathcal{N}$  selected channels. In other words, we have

$$\int d\Omega \int d\xi \mathcal{Y}_b^*(\Omega, \xi) (H - E) \Psi_a^{JM}(\mathbf{r}, \xi) = 0 \quad \text{with } b = 1, \dots, \mathcal{N}. \quad (8.16)$$

Substituting the expansion (8.15) in this equation and using the orthogonality relation (8.13), we obtain the set of coupled-channel equations (with  $b = 1, \dots, \mathcal{N}$ )

$$[T_b + V_0(r) + V_{bb}^J(r) - \mathcal{E}_b] g_{ab}^J(r) = - \sum_{c(c \neq b)}^N V_{bc}^J(r) g_{ac}^J(r), \quad (8.17)$$

which is the partial-wave analogue of eqns (8.9). In this set of equations the total angular momentum  $J$  is fixed, and the coupling occurs between states with different quantum

numbers  $b = \{\underline{b}; l_b I_b\}$  and  $c = \{\underline{c}; l_c I_c\}$ . The term

$$T_b = \frac{\hbar^2}{2\mu} \left( -\frac{d^2}{dr^2} + \frac{l_b(l_b+1)}{r^2} \right) \quad (8.18)$$

is the kinetic energy in the partial-wave channel with orbital angular momentum  $l_b$ , and

$$V_{bc}^J(r) = \int d\Omega \int d\xi \mathcal{Y}_b^*(\Omega, \xi) V_{\text{coupl}}(\mathbf{r}, \xi) \mathcal{Y}_c(\Omega, \xi) \quad (8.19)$$

is the coupling matrix element between channels  $b$  and  $c$ . The system (8.17) is a set of coupled differential equations for the radial wave functions  $g_{ab}^J(r)$ , which must be supplemented with appropriate boundary conditions.

### 8.2.2 The calculation of the inelastic cross section

The boundary conditions for the functions  $g_{ab}^J(r)$  have to be chosen in conformance with the asymptotic form (8.8). The Coulomb wave function  $\psi_C(\eta_a, k_a; \mathbf{r})$  appearing in this expression has the partial-wave expansion

$$\psi_C(\eta_a, k_a; \mathbf{r}) = \frac{1}{k_a r} \sum_{l_a} \sqrt{4\pi(2l_a+1)} i^{l_a} e^{i\sigma_a} F_{l_a}(\eta_a, k_a r) Y_{l_a 0}(\Omega), \quad (8.20)$$

where we have used eqn (1.108) and  $P_l(\cos\theta) = \sqrt{4\pi/(2l+1)} Y_{l 0}(\Omega)$ . Then we have

$$\begin{aligned} \psi_C(\eta_a, k_a; \mathbf{r}) \phi_{\underline{a}; I_a M_a}(\xi) &= \sum_{JM l_a} (l_a 0; I_a M_a | JM) \sqrt{4\pi(2l_a+1)} i^{l_a} e^{i\sigma_a} \\ &\quad \times \frac{F_{l_a}(\eta_a, k_a r)}{k_a r} \mathcal{Y}_{a; l_a I_a; JM}(\Omega, \xi), \end{aligned} \quad (8.21)$$

which is proved by inserting expression (8.12) and using the orthogonality relation for the Clebsch–Gordan coefficients,

$$\sum_{JM} (l_a 0; I_a M_a | JM) (l_a m'_a; I_a M'_a | JM) = \delta_{0m'_a} \delta_{M_a M'_a}. \quad (8.22)$$

For values of  $r$  larger than the range  $R$  of the interactions  $V_0(r)$  and  $V(\mathbf{r}, \xi)$  the eqns (8.17) decouple, and are separately solved by combinations of Coulomb wave functions. Now in all channels except the entrance channel the probability current is flowing *out*. The solutions  $g_{ab}^J(r)$  in the region  $r > R$  are therefore outgoing Coulomb functions  $H_{l_b}^{(+)}(\eta_b, k_b r)$  (cf. eqn (1.125)) in all spin-coupled channels except the entrance channel  $a = \{\underline{a}; l_a I_a; JM\}$ , which in addition contains the incident regular Coulomb function  $F_{l_a}(\eta_a, k_a r)$  (cf. eqn (1.110)); we therefore write

$$g_{ab}^J(r) = \delta_{ab} F_{l_a}(\eta_a, k_a r) + \frac{k_a}{4\pi} f_{ba}^J H_{l_b}^{(+)}(\eta_b, k_b r) \quad \text{for } r > R, \quad (8.23)$$

where we have introduced the factor  $k_a/4\pi$  in order to be able later to identify the coefficient  $f_{ba}^J$  with the scattering amplitude as it appears in (5.80). The coupled system (8.17), together with the boundary conditions (8.23), allows one to calculate the set of functions  $g_{ab}^J(r)$  for all values of  $r$ . From their asymptotic form one obtains the spin-coupled partial-wave scattering amplitude  $f_{ba}^J = f_{\{\underline{b}; l_b I_b\} \{\underline{a}; l_a I_a\}}$ .

## 8.2 The coupled-channel (CC) formalism for inelastic scattering

Comparing eqns (8.11), (8.15), (8.21), and (8.23), we find that we must set

$$c_{JM l_a}^{I_a M_a} = (l_a 0; I_a M_a | JM) \sqrt{4\pi(2l_a+1)} i^{l_a} e^{i\sigma_a}. \quad (8.24)$$

Similarly we see from eqns (8.8) and (8.23) and the asymptotic form of the outgoing Coulomb function (1.125) that the angle-dependent inelastic scattering amplitude  $f_{ba}^+ = f_{\{\underline{b}; l_b I_b\} \{\underline{a}; l_a M_a\}}^+(\Omega)$  is given by

$$\begin{aligned} f_{\{\underline{b}; l_b M_b\} \{\underline{a}; l_a M_a\}}^+(\Omega) &= \sum_{JM l_a} \sum_{l_b m_b} (l_a 0; I_a M_a | JM) (l_b m_b; I_b M_b | JM) \\ &\quad \times i^{l_a - l_b} e^{i(\sigma_a + \sigma_b)} \sqrt{(2l_a + 1)/4\pi} Y_{l_b m_b}(\Omega) f_{\{\underline{b}; l_b I_b\} \{\underline{a}; l_a I_a\}}^J. \end{aligned} \quad (8.25)$$

According to eqn (5.83) we then have for the inelastic scattering cross section

$$\frac{d\sigma_{\{\underline{a}; l_a M_a\} \rightarrow \{\underline{b}; l_b M_b\}}}{d\Omega} = \frac{k_b}{k_a} \left| f_{\{\underline{b}; l_b M_b\} \{\underline{a}; l_a M_a\}}^+(\Omega) \right|^2. \quad (8.26)$$

Averaging over the initial and summing over the final spin projections, we find for the unpolarized inelastic cross section

$$\begin{aligned} \frac{d\sigma_{\{\underline{a}; l_a\} \rightarrow \{\underline{b}; l_b\}}}{d\Omega_b} &= \frac{1}{2l_a + 1} \frac{k_b}{k_a} \sum_{M_a M_b} \left| \sum_{JM l_a} \sum_{l_b m_b} i^{l_a - l_b} e^{i(\sigma_a + \sigma_b)} \sqrt{(2l_a + 1)/4\pi} \right. \\ &\quad \times (l_a 0; I_a M_a | JM) (l_b m_b; I_b M_b | JM) Y_{l_b m_b}(\Omega) f_{\{\underline{b}; l_b I_b\} \{\underline{a}; l_a I_a\}}^J \left. \right|^2 \end{aligned} \quad (8.27)$$

We may convince ourselves that this result is in agreement (except for the Coulomb phases; in Chapter 5 the Coulomb interaction was not treated explicitly) with the general formulae (5.118) and (5.119) by making the identification

$$f_{ba}^J = -\mu \left( \frac{2\pi}{\hbar} \right)^2 T_{a \rightarrow b}^J, \quad (8.28)$$

which is the spin-coupled version of eqn (5.81). Using the relation between the  $T$ -matrix and the  $S$ -matrix (5.113) one can also express  $f_{ba}^J$  in terms of the spin-coupled  $S$ -matrix  $S_{ba}^J$ ,

$$f_{ba}^J = -\frac{2\pi i}{\sqrt{k_a k_b}} (S_{ba}^J - \delta_{ba}). \quad (8.29)$$

### Algorithms for the solution of the CC equations

The coupled equations (8.17) are to be solved for a set of  $\mathcal{N}$  functions  $g_{ab}^J(r)$  ( $b = 1, \dots, \mathcal{N}$ ) which are regular everywhere and subject to the boundary conditions (8.23). The traditional procedure (cf. Buck *et al.* 1963) for achieving this is the following.

Consider a set of solutions  $g_b(r)$  of eqns (8.17). At the origin all functions  $g_b(r)$  are regular and thus behave like  $C_b r^{l_b+1}$ . When starting the integration at some small finite distance  $\epsilon$  from the origin, we must specify the coefficients  $C_b$ . For example, we may choose  $\mathcal{N}$  different sets of  $C_b$ , labelled by  $n$ , such that  $C_b^n = \epsilon^{-l_b} \delta_{bn}$  ( $n = 1, \dots, \mathcal{N}$ ), which implies

$$\begin{aligned} g_b^n(\epsilon) &= \epsilon \delta_{bn}, \\ g_b^{n'}(\epsilon) &= (l_b + 1) \delta_{bn} \text{ for } n = 1, \dots, \mathcal{N}, \end{aligned} \quad (8.30)$$

where the prime denotes the derivative. In calculating a particular solution  $g_b^n(r)$ , one thus starts at  $r = \epsilon$  with a set of wave functions which vanish in all channels  $b$  except the one with  $b = n$ . As one proceeds to larger values of  $r$ , the channel coupling gradually admixes the channels with  $b \neq n$ .

The set of functions  $g_b^n(r)$  is, for a given  $n$ , a vector which satisfies the system of equations (8.17). One has  $\mathcal{N}$  such linearly independent vectors. For  $r \geq R$  they are certain linear combinations of the Coulomb functions  $F_{l_a}(\eta_a, k_a r)$  and  $H_{l_b}^{(+)}(\eta_b, k_b r)$ . They must now be superimposed in such a way that the physical boundary condition (8.23) is satisfied. That is, the physical solution is given by a superposition

$$g_{ab}^J(r) = \sum_{n=1}^{\mathcal{N}} c_n^{aJ} g_b^n(r) \quad (8.31)$$

whose coefficients  $c_n^{aJ}$ , together with the scattering functions  $f_{ba}^J$  (cf. eqn (8.23)), must be determined by matching the function (8.31) (and its derivative) to the physical wave function (8.23) at the matching radius  $R$ . This leads to the set of equations

$$\sum_{n=1}^{\mathcal{N}} c_n^{aJ} g_b^n(R) = \delta_{ab} F_{l_a}(\eta_a, k_a R) + \frac{k_a}{4\pi} f_{ba}^J H_{l_b}^{(+)}(\eta_b, k_b R) \quad (8.32)$$

and an analogous one for the radial derivatives. We therefore have altogether  $2\mathcal{N}$  linear equations for the computation of the  $\mathcal{N}$  coefficients  $c_n^{aJ}$  ( $n = 1, \dots, \mathcal{N}$ ) and the  $\mathcal{N}$  scattering functions  $f_{ba}^J$  ( $b = 1, \dots, \mathcal{N}$ ).

For a large number  $\mathcal{N}$  of coupled channels this procedure is not very efficient, and more appropriate iterative techniques have been developed (cf. Satchler 1983, Section 5.8, and references therein).

### 8.2.3 Spin-orbit coupling

An almost trivial example for the usefulness of the partial-wave formulation of the coupled-channel equations is the *spin-orbit coupling*. We consider the case of a spin- $\frac{1}{2}$  projectile impinging on a target nucleus with spin zero. Here the spin-orbit interaction

$$V_{\text{coupl}} = V_{ls}(r) (\mathbf{l} \cdot \mathbf{s}). \quad (8.33)$$

couples the spin of the projectile  $\mathbf{s}$  to the orbital angular momentum  $\mathbf{l}$  of the relative motion. The spin quantum number of the projectile  $\{\frac{1}{2}M_x\}$  is the only internal quantum number involved in the coupling. Interchanging the role of projectile and target, we have for internal wave functions the spin functions  $\chi_{\frac{1}{2}M}(s)$  with  $M = \pm \frac{1}{2}$ , and the expansion of the inelastic wave function (8.6) contains only two terms,

$$\Psi_M^{\text{inel}}(\mathbf{r}, s) = \psi_{M=\frac{1}{2}}^{(+)}(\mathbf{r}) \chi_{\frac{1}{2}\frac{1}{2}}(s) + \psi_{M=-\frac{1}{2}}^{(+)}(\mathbf{r}) \chi_{\frac{1}{2}-\frac{1}{2}}(s). \quad (8.34)$$

The two internal states are degenerate: besides the incident wave, the wave function (8.34) contains only a spin-flip, rather than a truly inelastic, component. The channel

coupling matrix (8.10) is given by

$$V_{bc}(\mathbf{r}) : V_{\{\frac{1}{2}M\}\{\frac{1}{2}M'\}} = V_{ls}(r) \sum_{s=\pm\frac{1}{2}} \chi_{\frac{1}{2}M}^*(s) (\mathbf{l} \cdot \mathbf{s}) \chi_{\frac{1}{2}M'}(s). \quad (8.35)$$

Writing  $\mathbf{s} = \frac{1}{2}\sigma$ , where  $\sigma$  is the set of Pauli matrices, we find

$$V_{\{\frac{1}{2}M\}\{\frac{1}{2}M'\}} = \frac{1}{2} V_{ls}(r) \begin{pmatrix} l_z & l_x - il_y \\ l_x + il_y & -l_z \end{pmatrix}. \quad (8.36)$$

This is a non-diagonal interaction matrix which couples states with different spin projections.

In the partial-wave formulation the system of spin-orbit equations is decoupled. Here the spin-coupled matrix (8.19) has the form

$$V_{bc}^J(r) : V_{\{\frac{1}{2}l\}\{\frac{1}{2}l'\}}^J = V_{ls}(r) \int d\Omega \sum_s \mathcal{Y}_{\frac{1}{2}l:JM}^*(\Omega, s) (\mathbf{l} \cdot \mathbf{s}) \mathcal{Y}_{\frac{1}{2}l':JM}(\Omega, s). \quad (8.37)$$

We introduce the total spin  $\mathbf{J} = \mathbf{l} + \mathbf{s}$  and write

$$\mathbf{l} \cdot \mathbf{s} = \frac{1}{2} (\mathbf{J}^2 - \mathbf{l}^2 - \mathbf{s}^2). \quad (8.38)$$

Since the spin-coupled channel functions  $\mathcal{Y}_{\frac{1}{2}l:JM}(\Omega, s)$  are eigenfunctions of  $\mathbf{J}^2$ ,  $\mathbf{l}^2$ , and  $\mathbf{s}^2$  with eigenvalues  $J(J+1)$ ,  $l(l+1)$ , and  $\frac{3}{4}$ , respectively, the matrix (8.37) takes the form

$$V_{\{\frac{1}{2}l\}\{\frac{1}{2}l'\}}^J = \frac{1}{2} V_{ls}(r) [J(J+1) - l(l+1) - \frac{3}{4}] \delta_{ll'}, \quad (8.39)$$

which is *diagonal*. For given  $J$  the values of  $l$  are restricted to  $l = J \pm \frac{1}{2}$ , so that

$$V_{\{\frac{1}{2}l\}\{\frac{1}{2}l'\}}^J = \frac{1}{2} V_{ls}(r) \begin{pmatrix} -l-1 & 0 \\ 0 & l \end{pmatrix}. \quad (8.40)$$

Solving the radial Schrödinger equation with the potential (8.40) for each spin  $J$  and partial wave  $l = J \mp \frac{1}{2}$ , one calculates the spin-coupled  $T$ -matrices  $T_{\{\frac{1}{2}l\}\{\frac{1}{2}l\}}^J$  and substitutes them in expression (5.111) for the  $T$ -matrix  $T_{\{\frac{1}{2}M:\mathbf{k}\}\{\frac{1}{2}M':\mathbf{k}'\}}^J$  with spin-flip ( $M' \neq M$ ) and without ( $M' = M$ ).

### 8.3 Inelastic excitation of collective states

When applying the preceding formalism to particular inelastic excitations, we must specify the internal coordinates  $\xi$  as well as the internal Hamiltonian  $h$  and the internal nuclear states  $\phi_b(\xi)$ . An explicit expression for the coupling interaction  $V_{\text{coupl}}(\mathbf{r}, \xi)$  must also be given, so that the matrix elements  $V_{bc}^J(r)$  of eqn (8.19) can be calculated. In the following we restrict ourselves to the description of collective, i.e. rotational and vibrational, excitations.

#### 8.3.1 The general form of the matrix elements

The kind of collective excitations which we are going to consider have to do with the deformations of the nuclear shape. We discuss the situation where the projectile

is spherical and remains unchanged during the scattering process. We are thus only concerned with the deformations of the target nucleus.

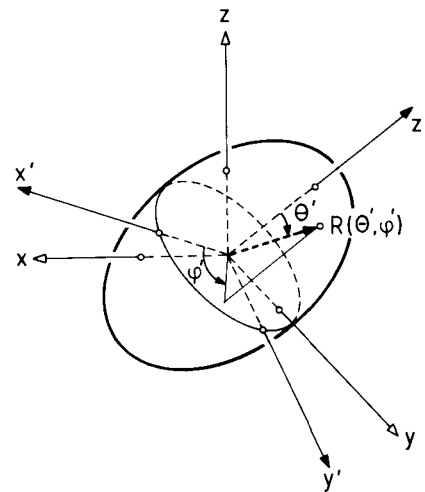


**Figure 8.1** Shape deformation of a nucleus. The axes  $\{x', y', z'\}$  define the body-fixed, and the axes  $\{x, y, z\}$  the space-fixed coordinate system. The orientation of the two coordinate systems relative to each other is determined by the Euler angles (see text).

For spherical targets the nuclear shape, and therefore also the shape of the potential between projectile and target, are characterized by a constant radius parameter  $R$ , which defines the distance of the centre of the nucleus from the surface, and which enters, for example, in the expressions for the nuclear Woods–Saxon potential (cf. eqn (1.146)); the parameter  $R_C$  plays the same role for the charge distribution (cf. eqn (1.115)). In a deformed nucleus, on the other hand, the radius parameter is no longer constant but depends on the location of the point on the surface from which this distance is taken. More precisely, it depends on the solid angle  $\Omega' = \{\theta', \varphi'\}$  of the point with respect to the body-fixed axes  $\{x', y', z'\}$  of the nucleus (cf. Fig. 8.1). This dependence can be expressed in general form in terms of spherical harmonics,

$$R = R_a(\Omega') = R_0 \left( 1 + \sum_{\lambda\mu} a_{\lambda\mu} Y_{\lambda\mu}(\Omega') \right), \quad (8.41)$$

where the *deformation parameters*  $a_{\lambda\mu}$  describe the type and size of the surface deformation in the body-fixed system. Since  $Y_{\lambda\mu}^* = (-)^{\mu} Y_{\lambda,-\mu}$ , we require

$$a_{\lambda\mu}^* = (-)^{\mu} a_{\lambda,-\mu} \quad (8.42)$$

in order to make the radius real. The mode  $\lambda = 0$  corresponds simply to an angle-independent change of the radius, which implies a change of volume of the nucleus ('breathing mode'); it will not be considered here. The mode  $\lambda = 1$  will also be disregarded, since it represents a translation of the nucleus as a whole. This is so

because the relation (8.41) for  $\lambda = 1$  can be written as  $R_a(\Omega') = R_0 (1 + \sqrt{3/4\pi} \mathbf{a} \cdot \hat{\mathbf{r}}')$ , where  $\hat{\mathbf{r}}'$  is a unit vector in the radial direction; in this form it describes a translation of the nucleus in the direction  $\hat{\mathbf{a}}$ . We thus consider only modes with  $\lambda \geq 2$ .

The radius function (8.41) can also be defined with respect to the space-fixed system  $\{x, y, z\}$  (cf. Fig. 8.1),

$$R = R_\alpha(\Omega) = R_0 \left( 1 + \sum_{\lambda\mu} \alpha_{\lambda\mu} Y_{\lambda\mu}(\Omega) \right), \quad (8.43)$$

where the parameters  $\alpha_{\lambda\mu}$  are the deformation parameters of the nucleus with respect to the space-fixed axes.

The orientation of the body-fixed system of axes relative to the space-fixed systems is determined by the Euler angles  $\omega = \{\alpha, \beta, \gamma\}$  (cf. Edmonds 1957, Section 1.3, in particular, Fig. 1.1). Under a rotation of the reference system from the body-fixed to the space-fixed axes, the spherical harmonics transform according to (cf. Edmonds 1957, eqn (4.1.4))

$$Y_{\lambda\mu}(\Omega') = \sum_{\mu'} D_{\mu'\mu}^\lambda(\omega) Y_{\lambda\mu'}(\Omega), \quad (8.44)$$

where  $D_{\mu'\mu}^\lambda(\omega)$  is the rotation matrix (cf. Edmonds 1957, Section 4.1). It then follows from a comparison of eqns (8.41) and (8.43) that the deformation parameters must transform according to

$$\alpha_{\lambda\mu} = \sum_{\mu'} D_{\mu'\mu}^\lambda(\omega) a_{\lambda\mu'}. \quad (8.45)$$

The inverse transformations are

$$Y_{\lambda\mu}(\Omega) = \sum_{\mu'} D_{\mu\mu'}^{\lambda*}(\omega) Y_{\lambda\mu'}(\Omega'), \quad (8.46)$$

$$a_{\lambda\mu} = \sum_{\mu'} D_{\mu'\mu}^{\lambda*}(\omega) \alpha_{\lambda\mu'}, \quad (8.47)$$

where use has been made of the relation

$$\sum_{\mu} D_{\mu\mu'}^{\lambda*}(\omega) D_{\mu''\mu}^{\lambda}(\omega) = \delta_{\mu'\mu''}. \quad (8.48)$$

The deformation parameters  $\alpha = \{\alpha_{\lambda\mu}\}$  play the role of the internal variables  $\xi$ .

#### The deformed nuclear potential

For a real nuclear potential, for example, of Woods–Saxon shape,

$$V_N(r - R) = \frac{V}{1 + \exp[(r - R)/a]}, \quad (8.49)$$

the introduction of the angle-dependent radius (8.43) leads to the deformed potential

$$V_N(\mathbf{r}, \alpha) = V_N[r - R_\alpha(\Omega)]. \quad (8.50)$$

We expand this potential in a Taylor series about the spherical shape, i.e. about the radius  $R_0$ . Assuming the deformations to be small, we restrict ourselves to the lowest

order in the deformation parameters  $\alpha_{\lambda\mu}$  and find

$$V_N(\mathbf{r}, \alpha) = V_N(r - R_0) + V_{\text{coupl}}^N(\mathbf{r}, \alpha), \quad (8.51)$$

where

$$V_{\text{coupl}}^N(\mathbf{r}, \alpha) = v^N(r) \sum_{\lambda\mu} \alpha_{\lambda\mu} Y_{\lambda\mu}(\Omega) \quad (8.52)$$

is the non-spherical part of the nuclear potential with

$$v^N(r) = -\left(\frac{\partial}{\partial r} V_N(r - R_0)\right) R_0. \quad (8.53)$$

### The deformed Coulomb potential

The Coulomb potential  $V_C(\mathbf{r}, \alpha)$  of a deformed nucleus is generally assumed to be given by the potential of a charge distribution with uniform density  $\rho_C = 3Z_t e / 4\pi R_C^3$ ,

$$\rho(\mathbf{r}) = \begin{cases} \rho_C & \text{for } r < R_\alpha(\Omega), \\ 0 & \text{for } r > R_\alpha(\Omega), \end{cases} \quad (8.54)$$

where  $Z_t e$  is the charge of the target nucleus, and the Coulomb radius  $R_C$  is the radius of the equivalent sphere. This charge distribution extends out to the surface described by the angle-dependent radius  $R_\alpha(\Omega)$ . Thus we write for the potential

$$V_C(\mathbf{r}, \alpha) = Z_p e \int d\Omega_s \int_0^{R_\alpha(\Omega_s)} s^2 ds \frac{\rho_C}{|\mathbf{r} - \mathbf{s}|}, \quad (8.55)$$

where  $Z_p e$  is the charge of the projectile. Using the formula (cf. Jackson 1975, eqn (3.70))

$$\frac{1}{|\mathbf{r} - \mathbf{s}|} = \sum_{LK} \frac{4\pi}{2L + 1} \frac{r_-^L}{r_+^{L+1}} Y_{LK}^*(\Omega_s) Y_{LK}(\Omega), \quad (8.56)$$

with  $r_{<(>)}$  the smaller (larger) of the distances  $r$  and  $s$ , we find

$$V_C(\mathbf{r}, \alpha) = Z_p e \sum_{LK} \frac{4\pi}{2L + 1} q_{LK}(r, \alpha) Y_{LK}(\Omega), \quad (8.57)$$

where we have introduced the multipole function

$$q_{LK}(r, \alpha) = \rho_C \int d\Omega_s Y_{LK}^*(\Omega_s) \int_0^{R_\alpha(\Omega_s)} s^2 ds \frac{r_-^L}{r_+^{L+1}}. \quad (8.58)$$

If  $r < R_{\min}$ , where  $R_{\min}$  is the minimum value of  $R_\alpha(\Omega_s)$ , we find for the radial integral up to first order in the deformation parameters, with  $R_0 = R_C$  and  $L \neq 2$ ,

$$\begin{aligned} \int_0^{R_\alpha(\Omega_s)} s^2 ds \frac{r_-^L}{r_+^{L+1}} &= \frac{1}{r^{L+1}} \int_0^r ds s^{L+2} + r^L \int_r^{R_\alpha} ds s^{-L-1} \\ &= \frac{2L + 1}{(L - 2)(L + 3)} r^2 - \frac{1}{L - 2} \frac{r^L}{R_\alpha^{L-2}} \\ &\approx \frac{2L + 1}{(L - 2)(L + 3)} r^2 - \frac{1}{L - 2} \frac{r^L}{R_C^{L-2}} + \frac{r^L}{R_C^{L-2}} \sum_{\lambda\mu} \alpha_{\lambda\mu} Y_{\lambda\mu}(\Omega_s), \end{aligned} \quad (8.59)$$

### 8.3 Inelastic excitation of collective states

and for  $L = 2$ ,

$$\begin{aligned} \int_0^{R_\alpha(\Omega_s)} s^2 ds \frac{r_-^L}{r_+^{L+1}} &= r^2 \left[ \frac{1}{5} + \ln\left(\frac{R_\alpha}{r}\right) \right] \\ &\approx r^2 \left[ \frac{1}{5} + \ln\left(\frac{R_C}{r}\right) + \sum_{\lambda\mu} \alpha_{\lambda\mu} Y_{\lambda\mu}(\Omega_s) \right]. \end{aligned} \quad (8.60)$$

The factor  $r^2$  multiplying the sum over the parameters  $\alpha$  is consistent with that appearing in expression (8.59).

For  $r > R_{\max}$ , where  $R_{\max}$  is the maximum value of  $R_\alpha(\Omega_s)$ , we find

$$\begin{aligned} \frac{1}{r^{L+1}} \int_0^{R_\alpha} ds s^{L+2} &= \frac{1}{L + 3} \frac{R_\alpha^{L+3}}{r^{L+1}} \\ &\approx \frac{1}{L + 3} \frac{R_C^{L+3}}{r^{L+1}} + \frac{R_C^{L+3}}{r^{L+1}} \sum_{\lambda\mu} \alpha_{\lambda\mu} Y_{\lambda\mu}(\Omega_s). \end{aligned} \quad (8.61)$$

Using the orthogonality relation for the spherical harmonics, we obtain from eqn (8.58), for  $L = 0$ ,

$$q_{00}(r, \alpha) = \begin{cases} \rho_C \sqrt{4\pi} R_C^2 \frac{1}{6} [3 - (r/R_C)^2] & \text{for } r < R_C, \\ \rho_C \sqrt{4\pi} R_C^3 \frac{1}{3} 1/r & \text{for } r > R_C, \end{cases} \quad (8.62)$$

and for  $L \geq 2$ ,

$$q_{LK}(r, \alpha) = \alpha_{LK} \rho_C R_C^2 \begin{cases} (r/R_C)^L & \text{for } r < R_C, \\ (R_C/r)^{L+1} & \text{for } r > R_C. \end{cases} \quad (8.63)$$

In defining the limits of the two regions of  $r$  we have replaced  $R_{\min}$  and  $R_{\max}$  with  $R_C$ , which is allowed in lowest-order approximation in the deformation parameters.

For the spherical part of the Coulomb interaction (8.57) we find, using eqn (8.62)

$$V_C(r) = \begin{cases} (Z_p Z_t e^2 / 2R_C) [3 - (r/R_C)^2] & \text{for } r < R_C, \\ Z_p Z_t e^2 / r & \text{for } r > R_C \end{cases} \quad (8.64)$$

(cf. eqn (1.115)), while the non-spherical, coupling part is of the form

$$V_{\text{coupl}}^C(\mathbf{r}, \alpha) = \sum_{LK} v_L^C(r) \alpha_{LK} Y_{LK}(\Omega), \quad (8.65)$$

where

$$v_L^C(r) = \frac{3Z_p Z_t e^2}{R_C} \frac{1}{2L + 1} \begin{cases} (r/R_C)^L & \text{for } r < R_C, \\ (R_C/r)^{L+1} & \text{for } r > R_C; \end{cases} \quad (8.66)$$

here we have used eqn (8.63) and  $\rho_C = 3Z_t e / 4\pi R_C^3$ .

The total Coulomb potential is given by

$$V_C(\mathbf{r}, \alpha) = V_C(r) + V_{\text{coupl}}^C(\mathbf{r}, \alpha). \quad (8.67)$$

Finally, adding the nuclear contribution, eqns (8.51) and (8.52), we have for the total, Coulomb-plus-nuclear potential

$$V(\mathbf{r}, \alpha) = V_C(r) + V_N(r) + V_{\text{coupl}}(\mathbf{r}, \alpha), \quad (8.68)$$

where

$$V_{\text{coupl}}(\mathbf{r}, \alpha) = V_{\text{coupl}}^C(\mathbf{r}, \alpha) + V_{\text{coupl}}^N(\mathbf{r}, \alpha) = \sum_{LK} v_L(r) \alpha_{LK} Y_{LK}(\Omega) \quad (8.69)$$

with

$$v_L(r) = v_L^C(r) + v_L^N(r). \quad (8.70)$$

The expression (8.69) represents the multipole expansion of the coupling potential.

#### Reduction of the coupling matrix elements in the spin-coupled basis

The matrix element of the coupling potential (8.69) between spin-coupled states of the form (cf. eqn (8.12))

$$|II; JM\rangle = \sum_{M_I m} (lm; IM_I | JM) Y_{lm}(\Omega) |IM_I\rangle \quad (8.71)$$

becomes, with  $b = \{l_b I_b\}$  and  $c = \{l_c I_c\}$  (cf. Edmonds 1957, eqn (7.1.6)),

$$\begin{aligned} V_{bc}^J(r) &= \langle l_b I_b; JM | V_{\text{coupl}} | l_c I_c; JM \rangle \\ &= \sum_L (-)^{l_c + I_b + J} \left\{ \begin{matrix} J & l_b & l_b \\ L & l_c & I_c \end{matrix} \right\} \langle I_b \| \alpha_L \| I_c \rangle \langle l_b \| Y_L \| l_c \rangle v_L(r), \end{aligned} \quad (8.72)$$

where the expression in curly brackets is a 6-j symbol (cf. Edmonds 1957, eqn (6.1.5)), and the quantities  $\langle \dots \| \dots \| \dots \rangle$  are *reduced matrix elements* (cf. Edmonds 1957, eqn (5.4.1)).

For  $\langle l_b \| Y_L \| l_c \rangle$  we have (cf. Edmonds 1957, eqn (5.4.5))

$$\langle l_b \| Y_L \| l_c \rangle = (-)^{l_b} \left( \frac{(2l_b + 1)(2L + 1)(2l_c + 1)}{4\pi} \right)^{1/2} \left( \begin{matrix} l_b & L & l_c \\ 0 & 0 & 0 \end{matrix} \right), \quad (8.73)$$

where the expression in the second large parentheses is a 3-j symbol which is related to the Clebsch-Gordan coefficient (cf. Edmonds 1957, eqn (3.7.3)) by

$$\left( \begin{matrix} j_1 & j_2 & j_3 \\ m_1 & m_2 & m_3 \end{matrix} \right) = (-)^{j_1 - j_2 - m_3} (2j_3 + 1)^{-1/2} \langle j_1 m_1; j_2 m_2 | j_3, -m_3 \rangle. \quad (8.74)$$

We then obtain

$$\begin{aligned} V_{bc}^J(r) &= \sum_L (-)^{l_c + I_b + J + l_b} \left( \frac{(2l_b + 1)(2L + 1)(2l_c + 1)}{4\pi} \right)^{1/2} \\ &\times \left( \begin{matrix} l_b & L & l_c \\ 0 & 0 & 0 \end{matrix} \right) \left\{ \begin{matrix} J & l_b & l_b \\ L & l_c & I_c \end{matrix} \right\} \langle I_b \| \alpha_L \| I_c \rangle v_L(r). \end{aligned} \quad (8.75)$$

This formula exhibits the general spin-coupled structure of the matrix elements in the coupled-channel equations. For actual applications it remains to evaluate the reduced matrix element  $\langle I_b \| \alpha_L \| I_c \rangle v_L(r)$  in any particular case. This will be done in the following for rotational and vibrational excitations.

#### 8.3.2 Rotational excitations

##### The rotational Hamiltonian and the rotational states

We consider a permanently deformed nucleus with axial symmetry about a body-fixed axis which defines the  $z'$ -direction. In this case the deformation parameters  $a_{\lambda\mu}$  in the body-fixed system have the form

$$a_{\lambda\mu} = \beta_\lambda \delta_{\mu 0}, \quad (8.76)$$

where the parameters  $\beta_\lambda$  are constants describing the static deformation of the nucleus. In the space-fixed system we have, using eqn (8.45),

$$\alpha_{\lambda\mu} = \beta_\lambda D_{\mu 0}^\lambda(\omega). \quad (8.77)$$

Thus the internal variables for rotations, i.e. the deformation parameters  $\alpha = \{\alpha_{\lambda\mu}\}$  in the space-fixed system, are divided into a set of body-fixed deformation parameters  $\beta_\lambda$  and the set of Euler angles  $\omega$  through which the body-fixed system of axes is rotated into the space-fixed system.

We consider an axially symmetric nucleus which rotates about a space-fixed axis with total spin  $I$  and spin projection  $M$ . In this case the spin projection on the body-fixed symmetry axis is also a conserved quantum number called  $K$ ; it characterizes the intrinsic state of the deformed nucleus (cf. Preston and Bhaduri 1975, Section 9.5) and is equal, for example, to the  $z'$ -component of the total angular momentum of a Nilsson single-particle state. The spin configuration of such a rotating state is shown in Fig. 8.2. This state is described by the state vector  $|IMK\rangle$  and is, in the nomenclature of Section 5.2.1, an *internal state*.

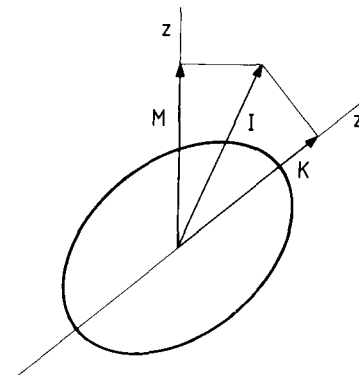


Figure 8.2 The rotational state of a deformed nucleus.

We treat only the simplest case and consider a structureless axially symmetric nucleus with moment of inertia  $J$  rotating about an axis perpendicular to the symmetry axis. This corresponds to setting  $K = 0$ , which implies  $I = \text{even}$  (cf. Preston and Bhaduri

1975, Section 9.4). The state  $|IM0\rangle$  satisfies the equations

$$\frac{\hbar^2}{2\mathcal{J}} \mathbf{I}^2 |IM0\rangle = \frac{\hbar^2}{2\mathcal{J}} I(I+1) |IM0\rangle, \\ \mathbf{I}_z |IM0\rangle = M |IM0\rangle, \quad (8.78)$$

where  $\hbar\mathbf{I}$  is the angular momentum operator. The first equation (8.78) is the Schrödinger equation for the rotational state, and  $\hbar^2\mathbf{I}^2/2\mathcal{J}$  is the rotational Hamiltonian.

In the coordinate representation the state  $|IM0\rangle$  is given by a function of the Euler angles  $\omega = \{\alpha, \beta, \gamma\}$  which has the form (cf. Edmonds 1957, eqn (4.1.25))

$$\langle \alpha, \beta, \gamma = 0 | IM0 \rangle = \left( \frac{2I+1}{4\pi} \right)^{1/2} D_M^I(\alpha, \beta, 0) = (-)^M Y_{IM}(\beta, \alpha). \quad (8.79)$$

#### The coupling matrix element for rotations

The coupling matrix element (8.75) contains as essential dynamical quantity the reduced matrix element  $\langle I_b \| \alpha_L \| I_c \rangle$ . For rotations we have, using eqn (8.77),

$$\langle I_b \| \alpha_L \| I_c \rangle = \beta_L \langle I_b \| D_{00}^L \| I_c \rangle = \beta_L (-)^{I_b} \langle I_b 0 | D_{00}^L | I_c 0 \rangle \begin{pmatrix} I_b & L & I_c \\ 0 & 0 & 0 \end{pmatrix}^{-1}, \quad (8.80)$$

where we have employed the Wigner–Eckart theorem (cf. Edmonds 1957, eqn (5.4.1)). With the help of eqn (8.79) and formula (4.6.3) of Edmonds (1957) we obtain

$$\langle I_b 0 | D_{00}^L | I_c 0 \rangle = \left( \frac{4\pi}{2L+1} \right)^{1/2} \int d(\cos \beta) d\alpha Y_{I_b 0}(\beta, \alpha) Y_{L 0}(\beta, \alpha) Y_{I_c 0}(\beta, \alpha) \\ = \sqrt{(2I_b+1)(2I_c+1)} \begin{pmatrix} I_b & L & I_c \\ 0 & 0 & 0 \end{pmatrix}^2, \quad (8.81)$$

so that

$$\langle I_b \| \alpha_L \| I_c \rangle = \beta_L (-)^{I_b} \sqrt{(2I_b+1)(2I_c+1)} \begin{pmatrix} I_b & L & I_c \\ 0 & 0 & 0 \end{pmatrix}. \quad (8.82)$$

Let us consider explicitly the case  $I_b = 0$ ,  $I_c = I$ , where the reduced matrix element (8.82) is non-vanishing only if  $L = I$ ; we find, using

$$\begin{pmatrix} 0 & L & I \\ 0 & 0 & 0 \end{pmatrix} = \delta_{IL} \frac{(-)^I}{\sqrt{2I+1}} \quad (8.83)$$

(cf. Edmonds 1957, Appendix 2, Table 2),

$$\langle 0 \| \alpha_L \| I \rangle = \beta_I (-)^I \delta_{IL}. \quad (8.84)$$

The nuclear and Coulomb potentials do not in general have identical deformations, i.e. the nuclear and the Coulomb deformation parameters  $\beta_I^N$  and  $\beta_I^C$  are different. The matrix element (8.75) then has the form, for  $I_b = 0$ ,  $I_c = I = L$ ,

$$V_{bc}^J = (-)^{I_c + J + I_b} \left( \frac{(2I_b+1)(2I+1)(2I_c+1)}{4\pi} \right)^{1/2} \begin{pmatrix} I_b & I & I_c \\ 0 & 0 & 0 \end{pmatrix} \\ \times \begin{Bmatrix} J & 0 & I_b \\ I & I_c & I \end{Bmatrix} (-)^I [\beta_I^N v^N(r) + \beta_I^C v_I^C(r)]. \quad (8.85)$$

The Coulomb deformation parameter  $\beta_I^C$  can be measured directly in electric multipole transitions. Here the reduced electric multipole transition probability, i.e. the  $B(EI, 0 \rightarrow I)$  value which determines the strength of  $\gamma$ -transitions of multipolarity  $I$  between two nuclear states with spin 0 and  $I$  (cf. Preston and Bhaduri 1975, eqn (9.95)), is related to  $\beta_I^C$  by

$$\beta_I^C = \frac{4\pi}{3Z_t e R_C^I} [B(EI, 0 \rightarrow I)]^{1/2}. \quad (8.86)$$

#### First example: multiple Coulomb rotational excitations

As a first application we consider the scattering of  $^{84}\text{Kr}$  by  $^{238}\text{U}$  at  $E_{\text{lab}} = 385$  MeV (cf. Tolsma 1979). For these very heavy ions the collision energy is so low that the partners remain outside the region of nuclear interaction. We can, therefore, neglect the nuclear part of the interaction, and consider Coulomb excitation only. We restrict ourselves to electric quadrupole transitions; for the reduced transition probability the value  $B(E2, 0 \rightarrow 2) = 12.25 e^2 b^2$  is used. Solving the coupled-channel equations and calculating the differential cross sections  $d\sigma_{0 \rightarrow I}(\theta)/d\Omega$  for the inelastic scattering to a state with spin  $I$  according to eqn (8.27), we obtain the excitation probabilities  $P_I(\theta)$  defined as

$$P_I(\theta) = \frac{k_I}{k_0} \frac{d\sigma_{0 \rightarrow I}(\theta)}{d\Omega} \Bigg/ \frac{d\sigma_C(\theta)}{d\Omega}, \quad (8.87)$$

where  $k_I$  is the wave number in channel  $I$ , and  $d\sigma_C(\theta)/d\Omega$  the Rutherford cross section. The results are shown in Fig. 8.3. This example gives an idea of the size of the excitation probabilities as functions of the scattering angle  $\theta$  and the spin transfer  $I$ . A comparison with experiment will be made in the second example.

#### Second example: multiple nuclear and Coulomb rotational excitations

For a second example we consider the inelastic scattering of  $^{16}\text{O}$  by  $^{152}\text{Sm}$  at the energy  $E_{\text{lab}} = 72$  MeV, as measured by Weber *et al.* (1976) and analyzed by Kim (1979). This energy lies slightly above the Coulomb barrier, and both the Coulomb and nuclear interactions have to be taken into account. The results of the coupled-channel calculations are compared with those of single-step DWBA calculations. Figure 8.4a illustrates the difference of the coupling schemes in the two calculations. Whereas in DWBA only the direct couplings  $0^+ \rightarrow 2^+$  and  $0^+ \rightarrow 4^+$  are taken into account, the coupled-channel calculation also includes the recoupling between these states as well as the coupling between the magnetic substates of the  $2^+$  and  $4^+$  states (reorientation effect).

A deformed complex Woods–Saxon optical potential with the parameters  $V = 13.0$  MeV,  $r_{0V} = 1.37$  fm,  $a_V = 0.5$  fm,  $W = 2.8$  MeV,  $r_{0W} = 1.40$  fm,  $a_W = 0.55$  fm has been used, and the nuclear form factors have the strength parameters  $\beta_2^N R_N = 1.65$  fm and  $\beta_4^N R_N = 0.29$  fm. The electric quadrupole and hexadecapole interactions are determined from the experimental values  $B(E2) = 3.45 e^2 b^2$  and  $B(E4) = 0.21 e^2 b^4$ ; for the Coulomb radius  $R_C = 1.25 (A_p^{1/3} + A_T^{1/3})$  fm was taken. The calculated cross sections are shown in Fig. 8.4b together with the measured ones. It is seen that only the multistep coupled-channel results reproduce the experimental data, whereas the single-step DWBA cross sections fail to do so.

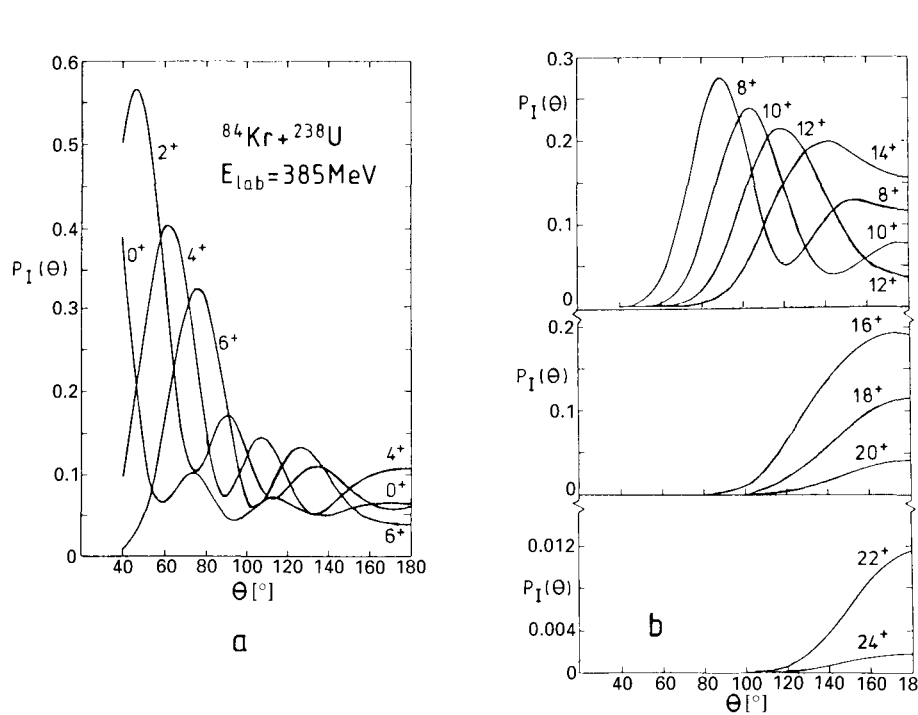


**Figure 8.3** Calculated Coulomb excitation probabilities  $P_I(\theta)$  as functions of the scattering angle  $\theta$  for the excitation of rotational states  $I^\pi$  of the target nucleus  $^{238}\text{U}$  in the scattering of  $^{84}\text{Kr}$  by  $^{238}\text{U}$  at  $E_{\text{lab}} = 385$  MeV. (a)  $I^\pi = 0^+, \dots, 6^+$ ; (b)  $I^\pi = 8^+, \dots, 24^+$ .

### 8.3.3 Vibrational excitations

#### The vibrational Hamiltonian and the vibrational states

If the deformation is not permanent but dynamical, i.e. time-dependent, the deformation parameters  $\alpha_{\lambda\mu}$  become dynamical variables representing surface modes, which for small deformations may be described as *vibrations* (cf. Preston and Bhaduri 1975, Section 9.2). These vibrations are quantized. As in the case of rotations, we work in the space-fixed system, since the channel wave functions used in the interaction matrix elements are also defined in this system. The parameters  $\alpha_{\lambda\mu}$  are interpreted as elongation operators in the mode  $\{\lambda\mu\}$ , which together with the canonically conjugate momentum operators  $\pi_{\lambda\mu}$  form a set of self-adjoint operators satisfying

$$\alpha_{\lambda\mu}^\dagger = (-)^\mu \alpha_{\lambda,-\mu} \quad \text{and} \quad \pi_{\lambda\mu}^\dagger = (-)^\mu \pi_{\lambda,-\mu}. \quad (8.88)$$

They obey the commutation rules

$$\begin{aligned} [\alpha_{\lambda\mu}, \pi_{\lambda'\mu'}] &= i\hbar \delta_{\lambda\lambda'} \delta_{\mu\mu'}, \\ [\alpha_{\lambda\mu}, \alpha_{\lambda'\mu'}] &= [\pi_{\lambda\mu}, \pi_{\lambda'\mu'}] = 0. \end{aligned} \quad (8.89)$$

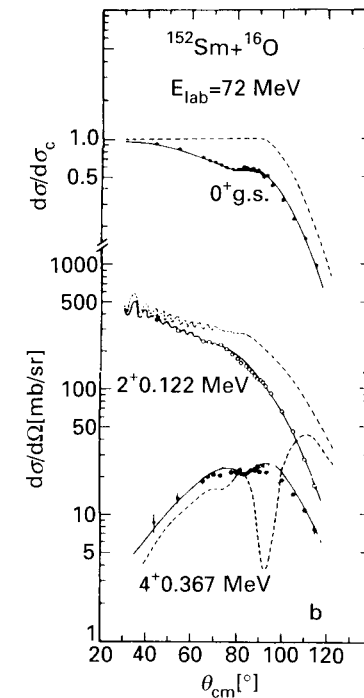
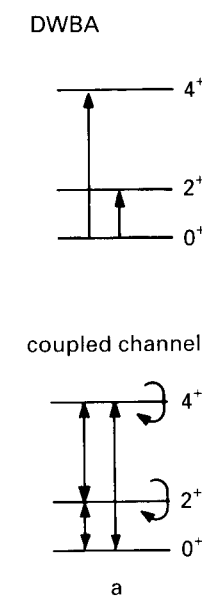


**Figure 8.4** Inelastic scattering of  $^{16}\text{O}$  by  $^{152}\text{Sm}$ . (a) Coupling schemes for the target excitations in DWBA and in the coupled-channel calculation. (b) The elastic and inelastic cross sections resulting from DWBA (dashed curves) and coupled-channel calculations (solid curves) in comparison with the experimental data (dots).

The vibrational Hamiltonian has the form

$$h = \sum_{\lambda\mu} \left( \frac{1}{2B_\lambda} \pi_{\lambda\mu}^\dagger \pi_{\lambda\mu} + \frac{C_\lambda}{2} \alpha_{\lambda\mu}^\dagger \alpha_{\lambda\mu} \right), \quad (8.90)$$

where the constants  $B_\lambda$  and  $C_\lambda$  are the inertial parameter and the spring constant, respectively, for the vibrational mode  $\lambda$ .

It is convenient to go over to operators  $c_{\lambda\mu}$  and  $c_{\lambda\mu}^\dagger$  which annihilate and create vibrational excitations of the nuclear surface (phonons). These operators are linearly related to the operators  $\alpha_{\lambda\mu}$  and  $\pi_{\lambda\mu}$ ,

$$\begin{aligned} c_{\lambda\mu} &= \left( \frac{B_\lambda \omega_\lambda}{2\hbar} \right)^{1/2} \alpha_{\lambda\mu} + i(-)^\mu \left( \frac{1}{2\hbar B_\lambda \omega_\lambda} \right)^{1/2} \pi_{\lambda,-\mu}, \\ c_{\lambda\mu}^\dagger &= (-)^\mu \left( \frac{B_\lambda \omega_\lambda}{2\hbar} \right)^{1/2} \alpha_{\lambda,-\mu} - i \left( \frac{1}{2\hbar B_\lambda \omega_\lambda} \right)^{1/2} \pi_{\lambda\mu}, \end{aligned} \quad (8.91)$$

where

$$\omega_\lambda = \left( \frac{C_\lambda}{B_\lambda} \right)^{1/2} \quad (8.92)$$

is the eigenfrequency of the vibrational mode  $\lambda$ . We have conversely

$$\begin{aligned} a_{\lambda\mu} &= \left( \frac{\hbar}{2B_\lambda\omega_\lambda} \right)^{1/2} (c_{\lambda\mu} + (-)^\mu c_{\lambda,-\mu}^\dagger), \\ \pi_{\lambda\mu} &= i \left( \frac{\hbar B_\lambda \omega_\lambda}{2} \right)^{1/2} (c_{\lambda\mu}^\dagger - (-)^\mu c_{\lambda,-\mu}). \end{aligned} \quad (8.93)$$

Using eqns (8.89) and (8.91) we find that the phonon annihilation and creation operators satisfy the commutation relations

$$\begin{aligned} [c_{\lambda\mu}, c_{\lambda'\mu'}^\dagger] &= \delta_{\lambda\lambda'} \delta_{\mu\mu'}, \\ [c_{\lambda\mu}, c_{\lambda'\mu'}] &= [c_{\lambda\mu}^\dagger, c_{\lambda'\mu'}^\dagger] = 0. \end{aligned} \quad (8.94)$$

In terms of these operators the Hamiltonian (8.90) now takes the form

$$h = \sum_{\lambda\mu} \hbar\omega_\lambda (c_{\lambda\mu}^\dagger c_{\lambda\mu} + \frac{1}{2}), \quad (8.95)$$

which is a sum over the phonon modes  $\{\lambda\mu\}$ , each contributing an energy  $\hbar\omega_\lambda$ .

The vibrational, or phonon, states are eigenstates of the Hamiltonian (8.95). They are generated in the following way. We introduce the ground state  $|0\rangle$  as the state which contains no vibrational quanta in any mode. Since no phonons can be annihilated in it, the application of the phonon annihilation operator  $c_{\lambda\mu}$  on it yields zero,

$$c_{\lambda\mu}|0\rangle = 0. \quad (8.96)$$

A one-phonon state with angular momentum  $\{IM_I\}$  is generated by applying the creation operator  $c_{IM_I}^\dagger$  to the ground-state vector

$$|n=1; IM_I\rangle = c_{IM_I}^\dagger |0\rangle; \quad (8.97)$$

a two-phonon state with angular momentum  $\{IM_I\}$  is generated by applying two spin-coupled creation operators to the ground state,

$$|n=2; IM_I\rangle = \frac{1}{\sqrt{1 + \delta_{\lambda_1\lambda_2}}} \sum_{\mu_1\mu_2} (\lambda_1\mu_1; \lambda_2\mu_2 | IM_I) c_{\lambda_1\mu_1}^\dagger c_{\lambda_2\mu_2}^\dagger |0\rangle, \quad (8.98)$$

and so on. The vibrational states are thus characterized by the phonon number  $n$  and the spin  $\{IM_I\}$ .

#### *The coupling matrix element for vibrations*

A spin-coupled vibrational channel state is described by the vector  $|n_b; l_b I_b; JM\rangle$ , where  $I_b$  is the spin of the phonon state and  $l_b$  the orbital angular momentum of the relative motion. The spin-coupled matrix element (8.72) has the form

$$V_{bc}^J(r) = \langle n_b; l_b I_b; JM | V_{\text{coupl}} | n_c; l_c I_c; JM \rangle; \quad (8.99)$$

it contains the reduced matrix element  $\langle n_b; I_b \| \alpha_L \| n_c; I_c \rangle$ , which reads, using eqn (8.93) and the Wigner–Eckart theorem (cf. Edmonds 1957, eqn (5.4.1)),

$$\begin{aligned} \langle n_b; I_b \| \alpha_L \| n_c; I_c \rangle &= \left( \frac{\hbar}{2B_L\omega_L} \right)^{1/2} (-)^{I_b} \begin{pmatrix} I_b & L & I_c \\ 0 & 0 & 0 \end{pmatrix}^{-1} \\ &\times \langle n_b; I_b 0 | (c_{L0} + c_{L0}^\dagger) | n_c; I_c 0 \rangle. \end{aligned} \quad (8.100)$$

For the transition from the ground state  $|n_b = 0; I_b = 0, M_b = 0\rangle$  to a one-phonon state  $|n_c = 1; I_c = I, M_c = 0\rangle = c_{I0}^\dagger |0; 00\rangle$  we find, employing eqns (8.94) and relation (8.96) in the adjoint form  $\langle 0 | c_{\lambda\mu}^\dagger = 0$ ,

$$\begin{aligned} \langle 0; 0 \| \alpha_L \| 1; I \rangle &= \left( \frac{\hbar}{2B_L\omega_L} \right)^{1/2} \begin{pmatrix} 0 & L & I \\ 0 & 0 & 0 \end{pmatrix}^{-1} \langle 0; 00 | c_{L0} c_{I0}^\dagger | 0; 00 \rangle \\ &= \left( \frac{\hbar}{2B_I\omega_I} \right)^{1/2} (-)^I (2I+1)^{1/2} \delta_{LI}. \end{aligned} \quad (8.101)$$

In the last line of this equation we have used eqn (8.83).

As in the case of rotations, it is convenient to replace the quantity  $\hbar/2B_I\omega_I$  in the Coulomb part of the interaction with the  $B(EI)$  value for the one-phonon transition, which here is given by (cf. Preston and Bhaduri 1975, eqn (9.24))

$$B(EI, 1 \rightarrow 0) = \left( \frac{3}{4\pi} Z_1 e R_C^I \right)^2 \left( \frac{\hbar}{2B_I\omega_I} \right). \quad (8.102)$$

We then have

$$\langle 0; 0 \| \alpha_L \| 1; I \rangle = (-)^I (2I+1)^{1/2} \delta_{LI} \frac{4\pi}{3Z_1 e R_C^I} [B(EI, 1 \rightarrow 0)]^{1/2}. \quad (8.103)$$

Since the interaction potential is linear in the phonon creation and annihilation operators (cf. eqn (8.100)), it gives rise to matrix elements which couple states which differ by one phonon. If we had gone to higher orders in  $\alpha_{\lambda\mu}$  when evaluating expressions (8.52) or (8.65), we would have obtained terms in the interaction which connect states which differ by more than one phonon. However, even with the linear interaction potential the multistep nature of the coupled-channel solution will allow one to describe transitions between states differing in *any* number of phonons. A more general discussion of the coupled-channel scheme for vibrational excitations can be found in Tamura (1965), where the phonon operators are defined in a slightly different way.

## 8.4 The Coulomb polarization potential

### 8.4.1 The generalized Coulomb polarization potential

In the coupled-channel framework it is straightforward to derive an approximate explicit form of the optical potential along the lines discussed in Chapter 6, which can then be used for the calculation of elastic cross sections.

We shall do this for a system of two heavy ions, following Love *et al.* (1977). We assume the projectile to remain in its ground state, and take into account only the single-step Coulomb excitation to a few excited states of the target nucleus with spin  $\{IM\}$ .

This approximation is expected to be valid for scattering at rather low energies, where the nuclei stay outside the range of nuclear interaction, and where only the lowest-lying states are excited. For simplicity we consider the case of a single excited state, so that we are dealing only with two channels whose internal states are the ground and first-excited states of the target nucleus, and which we denote by  $|0\rangle = |00\rangle$  and the multiplet  $|IM\rangle$ ,  $M = -I, \dots, I$ , respectively. A generalization to the direct excitation of other excited states of the target and projectile is immediately possible by summing over the separate contributions of these states.

Using eqn (6.12) for the generalized optical potential  $\mathcal{V}$  with the notation  $|a\rangle = |0\rangle$ ,  $Q = \sum_n |n\rangle\langle n|$  with  $|n\rangle = |IM\rangle$ ,  $V_\alpha = V_0 + (V_\alpha - V_0) = V_0 + V$ , and  $\langle n|V_\alpha|n'\rangle = \langle n|V|n'\rangle = V_{nn'}$  for  $n \neq n'$ , we obtain

$$\mathcal{V} = V_0 + \langle 0|V|0\rangle + \langle 0|VQ\frac{1}{E + i\eta - T - h - V}QV|0\rangle. \quad (8.104)$$

Here  $V_0 = V_C + V_N$  is the real static Coulomb-plus-nuclear potential between the collision partners in their ground states. It is corrected by the diagonal coupling matrix element  $\langle 0|V|0\rangle$ , which, however, turns out to be small compared with the former and will be neglected.

We are interested in the second term of expression (8.104). This is the dynamical or polarization potential,

$$V_{\text{pol}} = \langle 0|VQ\frac{1}{E + i\eta - T - h - V}QV|0\rangle. \quad (8.105)$$

Since we only consider Coulomb excitation, we call this potential the *Coulomb polarization potential*. The expression (8.105) is complex, energy dependent, non-local, and rather formal. However, we shall derive from it an explicit equivalent local potential, which can then be used as input in an optical-model calculation of the elastic scattering amplitude. (We remark that the polarization potential discussed in Section 6.5.1 corresponds only to the real part of the Coulomb polarization potential).

We simplify the discussion by omitting the interaction  $V$  in the denominator of expression (8.105), thus neglecting a term  $QVQ = V_{11}$  representing the Coulomb interaction between excited states, which is of minor importance. In the coordinate representation we then have for the Coulomb polarization potential generated by the coupling to a state with spin  $I$

$$\begin{aligned} V_{\text{pol}}(\mathbf{r}, \mathbf{r}') &= \sum_M \langle 00|V(\mathbf{r})|IM\rangle \langle IM|\frac{1}{E + i\eta - T - (\epsilon_I - \epsilon_0)}|IM\rangle \langle IM|V(\mathbf{r}')|00\rangle \\ &= V_{IM}^*(\mathbf{r}) G_I(\mathbf{r}, \mathbf{r}') V_{IM}(\mathbf{r}), \end{aligned} \quad (8.106)$$

where the coupling potential  $V_{IM}(\mathbf{r})$  is given by the matrix element

$$V_{IM}(\mathbf{r}) = \langle IM|V(\mathbf{r})|00\rangle. \quad (8.107)$$

We further neglect the excitation energy  $\epsilon_I$  and normalize the ground-state energy  $\epsilon_0$  of the target nucleus to zero, so that  $E$  is the incident energy. Then the Green function

$G_I(\mathbf{r}, \mathbf{r}')$  becomes the free Green function (4.59),

$$G_I(\mathbf{r}, \mathbf{r}') \approx G(\mathbf{r}, \mathbf{r}') = -\frac{\mu}{2\pi\hbar^2} \frac{e^{ik|\mathbf{r}-\mathbf{r}'|}}{|\mathbf{r}-\mathbf{r}'|} \text{ with } k = \sqrt{2\mu E/\hbar^2}. \quad (8.108)$$

#### The matrix elements

The coupling interaction for Coulomb excitation is given by eqn (8.65). We then have for the coupling matrix element

$$V_{IM}(\mathbf{r}) = \langle IM|V(\mathbf{r})|00\rangle = v_I^C(r) \langle IM|\alpha_{IM}|00\rangle Y_{IM}(\Omega). \quad (8.109)$$

Employing the form factor  $v_I^C(r)$  of eqn (8.66), we then find

$$V_{IM}(\mathbf{r}) = V_I(r) Y_{IM}(\Omega) \quad (8.110)$$

with

$$V_I(r) = C_I \begin{cases} r^I/R_C^{I+1} & \text{for } r < R_C, \\ R_C^I/r^{I+1} & \text{for } r > R_C, \end{cases} \quad (8.111)$$

where the coefficient  $C_I$  is given by

$$C_I = \frac{4\pi Z_p e}{R_C^I(2I+1)} \langle IM|q_{IM}|00\rangle, \quad (8.112)$$

and the multipole operator  $q_{IM}$  is related to  $\alpha_{IM}$  via

$$q_{IM} = \frac{3Z_t e R_C^I}{4\pi} \alpha_{IM}. \quad (8.113)$$

Applying the Wigner–Eckart theorem (cf. Edmonds 1957, eqn (5.4.1)) we find

$$\langle IM|q_{IM}|00\rangle = \frac{\langle I||q_I||0\rangle}{(2I+1)^{1/2}} = \frac{[B(EI, 0 \rightarrow I)]^{1/2}}{(2I+1)^{1/2}}, \quad (8.114)$$

where we have replaced the reduced matrix element  $\langle I||q_I||0\rangle$  with the square root of the  $B(EI, 0 \rightarrow I)$  value (cf. Bohr and Mottelson 1969, Section 1A-5). Thus the coefficient  $C_I$  becomes

$$C_I = \frac{4\pi Z_p e}{R_C^I(2I+1)^{3/2}} [B(EI, 0 \rightarrow I)]^{1/2}. \quad (8.115)$$

#### 8.4.2 The equivalent local Coulomb polarization potential

The polarization potential (8.106) is non-local. We now proceed to calculate the equivalent local potential. For simplicity we take it in the form of the trivially equivalent local potential (cf. eqn (6.138)),

$$V_{\text{pol}}(\mathbf{r}) = \left( \int d^3r' V_{\text{pol}}(\mathbf{r}, \mathbf{r}') \psi(\mathbf{r}') \right) / \psi(\mathbf{r}), \quad (8.116)$$

where  $\psi(\mathbf{r})$  is the solution to the Schrödinger equation with the non-local potential (8.106). We approximate this wave function by a plane wave  $\exp(i\mathbf{k} \cdot \mathbf{r})$ , so that the equivalent local Coulomb polarization potential is given by

$$V_{\text{pol}}(\mathbf{r}) = \int d^3r' V_{\text{pol}}(\mathbf{r}, \mathbf{r}') e^{i\mathbf{k} \cdot (\mathbf{r}' - \mathbf{r})}. \quad (8.117)$$

The non-local potential (8.106) is invariant under the simultaneous rotation of the vectors  $\mathbf{r}$  and  $\mathbf{r}'$ . In other words, when operating on an eigenfunction of angular momentum, it reproduces it except for an angle-independent factor. This implies that the equivalent local potential must depend on the radius  $r$  only (we ignore a possible dependence on the scalar product  $\mathbf{k} \cdot \mathbf{r}$ ). This property is not in general possessed by the approximate expression (8.117), but we may restore it by replacing the latter with its spherical part, which we obtain by averaging over the angle  $\Omega$ ,

$$V_{\text{pol}}(r) = \frac{1}{4\pi} \int d\Omega \int d^3 r' V_{\text{pol}}(\mathbf{r}, \mathbf{r}') e^{i\mathbf{k} \cdot (\mathbf{r}' - \mathbf{r})}. \quad (8.118)$$

To proceed further, we write the matrix element  $V_{IM}(\mathbf{r})$  as a Fourier transform,

$$V_{IM}(\mathbf{r}) = \int d^3 q e^{i\mathbf{q} \cdot \mathbf{r}} \tilde{V}_{IM}(\mathbf{q}), \quad (8.119)$$

where the function  $\tilde{V}_{IM}(\mathbf{q})$  is given by the inverse Fourier transform

$$\begin{aligned} \tilde{V}_{IM}(\mathbf{q}) &= \frac{1}{(2\pi)^3} \int d^3 r e^{-i\mathbf{q} \cdot \mathbf{r}} V_{IM}(\mathbf{r}) \\ &= \frac{(-i)^I}{2\pi^2} \int_0^\infty r^2 dr j_I(qr) Y_{IM}(\Omega_q) V_I(r) \\ &= (-i)^I \tilde{V}_I(q) Y_{IM}(\Omega_q). \end{aligned} \quad (8.120)$$

Here we have used eqn (8.110), and the quantity  $\tilde{V}_I(q)$  is the Fourier–Bessel transform of the form factor  $V_I(r)$ ,

$$\tilde{V}_I(q) = \frac{1}{2\pi^2} \int_0^\infty r^2 dr j_I(qr) V_I(r) \quad (8.121)$$

whose inverse gives back the form factor,

$$V_I(r) = 4\pi \int_0^\infty q^2 dq j_I(qr) \tilde{V}_I(q). \quad (8.122)$$

Introducing the new variable  $\mathbf{x} = \mathbf{r} - \mathbf{r}'$  and using eqn (8.119), we find for the local Coulomb polarization potential (8.118),

$$\begin{aligned} V_{\text{pol}}(r) &= -(-i)^I \frac{1}{4\pi} \frac{\mu}{2\pi\hbar^2} V_I(r) \int d\Omega \int q^2 dq d\Omega_q \int x^2 dx d\Omega_x \\ &\quad \times \sum_M Y_{IM}^*(\Omega) \frac{e^{ikx}}{x} Y_{IM}(\Omega_q) \tilde{V}_I(q) e^{i\mathbf{q} \cdot \mathbf{r}} e^{-i\mathbf{q} \cdot \mathbf{x}} e^{-i\mathbf{k} \cdot \mathbf{x}}. \end{aligned} \quad (8.123)$$

The integration over the angle  $\Omega$  produces a term  $i^I j_I(qr) 4\pi Y_{IM}^*(\Omega_q)$ ; summing the two spherical harmonics which depend on the angle  $\Omega_q$  over  $M$  we obtain the constant  $(2I+1)/4\pi$ . The integration over  $\Omega_q$  then introduces a term  $4\pi j_0(qx)$ , and the integration over  $\Omega_x$  a term  $4\pi j_0(kx)$ . As a result we are left with

#### 8.4 The Coulomb polarization potential

$$\begin{aligned} V_{\text{pol}}(r) &= -\frac{2\mu(2I+1)}{\hbar^2} V_I(r) \int_0^\infty q^2 dq j_I(qr) \tilde{V}_I(q) \\ &\quad \times \int_0^\infty x^2 dx \frac{e^{ikx}}{x} j_0(kx) j_0(qx). \end{aligned} \quad (8.124)$$

The small values of  $q$  determine the asymptotic behaviour of the form factor  $V_I(r)$ . Since we are interested primarily in the potential at large values of  $r$ , we therefore evaluate the expression (8.124) in the limit of small  $q$ . The last integral in this expression can now be calculated. Using  $j_0(z) = \sin z/z$  and

$$e^{ikx} \sin(kx) = \frac{1}{2} \{\sin(2kx) + i[1 - \cos(2kx)]\}, \quad (8.125)$$

we find

$$\begin{aligned} \int_0^\infty x^2 dx \frac{e^{ikx}}{x} j_0(kx) j_0(qx) &= \frac{1}{2kq} \left( \int_0^\infty \frac{dx}{x} \sin(2kx) \sin(qx) \right. \\ &\quad \left. + i \int_0^\infty \frac{dx}{x} \sin(qx) - i \int_0^\infty \frac{dx}{x} \cos(2kx) \sin(qx) \right). \end{aligned} \quad (8.126)$$

Here the first integral becomes  $\ln \sqrt{(2k+q)/(2k-q)} \simeq q/2k$  (cf. Gradshteyn and Ryzhik 1965, eqn (3.741.1)), the second has the value  $\pi/2$ , and the third integral vanishes (cf. Gradshteyn and Ryzhik 1965, eqn (3.741.2)); therefore

$$\int_0^\infty x^2 dx \frac{e^{ikx}}{x} j_0(kx) j_0(qx) = \frac{1}{4k^2} \left( 1 + i\pi \frac{k}{q} \right). \quad (8.127)$$

The Coulomb polarization potential (8.124) thus becomes, with  $E = \hbar^2 k^2 / 2\mu$ ,

$$V_{\text{pol}}(r) = -\frac{2I+1}{16\pi E} V_I(r) [V_I(r) + 2ikF_I(r)]. \quad (8.128)$$

The quantity  $V_I(r)$  is the original form factor (8.111). The function  $F_I(r)$  appearing in the imaginary part is given by

$$F_I(r) = 2\pi^2 \int_0^\infty q dq j_I(qr) \tilde{V}_I(q), \quad (8.129)$$

where the integrand contains one power less of the variable  $q$  than the Fourier–Bessel integral (8.122) for the form factor  $V_I(r)$ . In order to evaluate the integral (8.129), we first calculate

$$\tilde{V}_I(q) = C_I \int_0^\infty r^2 dr j_I(qr) \frac{r_-^I}{r_+^{I+1}}, \quad (8.130)$$

where  $r_{<(>)}$  is the smaller (larger) of the radii  $r$  and  $R_C$ . Now we have

$$\frac{r_-^I}{r_+^{I+1}} = \frac{2I+1}{2\pi^2} \int_0^\infty k^2 dk j_I(kr) \frac{4\pi}{k^2} j_I(kR_C) \quad (8.131)$$

and

$$\frac{2}{\pi} \int_0^\infty r^2 dr j_I(qr) j_I(kr) = \frac{1}{q^2} \delta(q - k). \quad (8.132)$$

Using these two relations in the integral (8.130), we arrive at the simple expression

$$\tilde{V}_I(q) = \frac{2I+1}{2\pi^2 q^2} C_I j_I(qR_C). \quad (8.133)$$

We then obtain, with  $j_I(qr) = (\pi/2qr)^{1/2} J_{I+\frac{1}{2}}(r)$  and eqn (6.574) of Gradshteyn and Ryzhik (1965),

$$\begin{aligned} F_I(r) &= (2I+1)C_I \int_0^\infty \frac{dq}{q} j_I(qr) j_I(qR_C) \\ &= \frac{\pi}{8} C_I (2I+1) \frac{R_C^I}{r^I} \frac{2^{2I+1}(I-1)!}{(2I+1)!!\pi} F(I, -\frac{1}{2}; I + \frac{3}{2}; (R_C/r)^2), \end{aligned} \quad (8.134)$$

where  $F(a, b; c; z)$  is the hypergeometric function.

The Coulomb polarization potential consists, in general, of a sum over  $I$  of the terms given on the right-hand side of eqn (8.128). Collecting the previous results, we see that the leading term in the real part of the Coulomb polarization potential is the quadrupole contribution with  $I = 2$ . This term is proportional to  $[V_2(r)]^2 \sim r^{-6}$  for large  $r$ ,

$$\text{Re } V_{\text{pol}}(r) = -\frac{\pi}{25} \frac{B(E2, 0 \rightarrow 2)}{E} \frac{Z_p^2 e^2}{r^6}. \quad (8.135)$$

It is the well-known quadrupole–quadrupole polarization term, which, for example, in molecular physics, yields the tail of the van der Waals potential. It is in our case dominated by the large static potential  $V_0(r)$ , and therefore does not play an important role.

More interesting in our context is the imaginary part of the Coulomb polarization potential, whose leading term is obtained by evaluating the hypergeometric function in eqn (8.134) for  $I = 2$  as (cf. Abramowitz and Stegun 1965, eqn (15.1.1))

$$F(2, -\frac{1}{2}; \frac{7}{2}; z^2) \simeq 1 - \frac{2}{7}z^2 - \frac{1}{21}z^4 - \dots \quad (8.136)$$

We find

$$\text{Im } V_{\text{pol}}(r) = \begin{cases} -\frac{2}{3}(w_{\text{pol}}/R_C^9)r^4 & \text{for } r < R_C \\ -[1 - \frac{2}{7}(R_C/r)^2 - \frac{1}{21}(R_C/r)^4]w_{\text{pol}}r^{-5} & \text{for } r > R_C, \end{cases} \quad (8.137)$$

where the strength factor  $w_{\text{pol}}$  is given by

$$w_{\text{pol}} = \frac{4\pi}{75} \frac{2\mu}{\hbar^2 k} Z_p^2 e^2 B(E2, 0 \rightarrow 2). \quad (8.138)$$

It turns out that the neglect of the Coulomb effects in the Green function (8.108) is not a satisfactory approximation. This can be mended by replacing the wave number  $k$  in eqn (8.138) with the local Coulomb wave number

$$k_C(r) = k \left(1 - \frac{Z_p Z_t e^2}{Er}\right)^{1/2}. \quad (8.139)$$

Furthermore, we have neglected the excitation energy  $\epsilon_I$  when setting  $\epsilon_I - \epsilon_0 = 0$  (cf. the discussion after eqn (8.106)). In order to correct for this, one may introduce an

adiabaticity factor  $g_I(\xi) = f_{EI}(\xi)/f_{EI}(0)$ , where  $\xi = \eta\epsilon_I/2E$ , and where the function  $f_{EI}(\xi)$  is defined in Alder *et al.* (1956).

The expression (8.137) then becomes

$$\text{Im } V_{\text{pol}}(r) = \begin{cases} -\frac{2}{3} K_C(R_C)(W_{\text{pol}}/R_C^9)r^4 & \text{for } r < R_C, \\ -[1 - \frac{2}{7}(R_C/r)^2 - \frac{1}{21}(R_C/r)^4]K_C(r)W_{\text{pol}}r^{-5} & \text{for } r > R_C, \end{cases} \quad (8.140)$$

where

$$K_C(r) = k/k_C(r) = \left(1 - \frac{Z_p Z_t e^2}{Er}\right)^{-1/2} \quad (8.141)$$

and

$$W_{\text{pol}} = \frac{4\pi}{75} \frac{2\mu}{\hbar^2 k} Z_p^2 e^2 B(E2, 0 \rightarrow 2) g_2(\xi). \quad (8.142)$$

The imaginary part of the Coulomb polarization potential behaves like  $r^{-5}$  for large  $r$ . Thus it has a longer tail than the real part, which vanishes like  $r^{-6}$ . It extends appreciably beyond the nuclear imaginary part of the optical potential, which for example, in its Woods–Saxon form, vanishes exponentially at large distances. The long range of the Coulomb polarization potential has its origin in the long range of the interaction causing the Coulomb excitations.

#### Other approaches for the calculation of the Coulomb polarization potential

The most severe approximation made above has been the replacement of the scattering states in the Green function with plane waves (cf. eqn (8.108)), which is only imperfectly remedied by the corrections just discussed. One can improve on this by considering the Coulomb polarization potential in each partial wave separately using the appropriate Coulomb Green function. This, however, leads to a Coulomb polarization potential which depends on the angular momentum  $l$  (cf. Baltz *et al.* 1978).

Another approximation has been the restriction to second-order couplings of the inelastic channels. In order to calculate the Coulomb polarization potential with account of higher-order inelastic processes, one may make use of inverse scattering methods, where the polarization potential is determined from the elastic  $S$ -matrix elements obtained in a coupled-channel scheme (cf. Fröbrich *et al.* 1979).

#### 8.4.3 Examples

The first application of the Coulomb polarization potential to elastic scattering data has been to the system  $^{18}\text{O} + ^{184}\text{W}$  (cf. Love *et al.* 1977). For another example, we consider the system  $^{40}\text{Ar} + ^{208}\text{Pb}$  at  $E_{\text{lab}}(\text{Ar}) = 236$  MeV (cf. Fig. 8.5), which is taken from the work of Arlt *et al.* (1980). Here the excitation of several projectile and target states with different multipolarities must be taken into account. The level scheme for these states is shown in Fig. 8.5a.

#### Elastic scattering

The elastic scattering cross section is determined by the total potential between the collision partners. To the Coulomb polarization potential, which describes only the

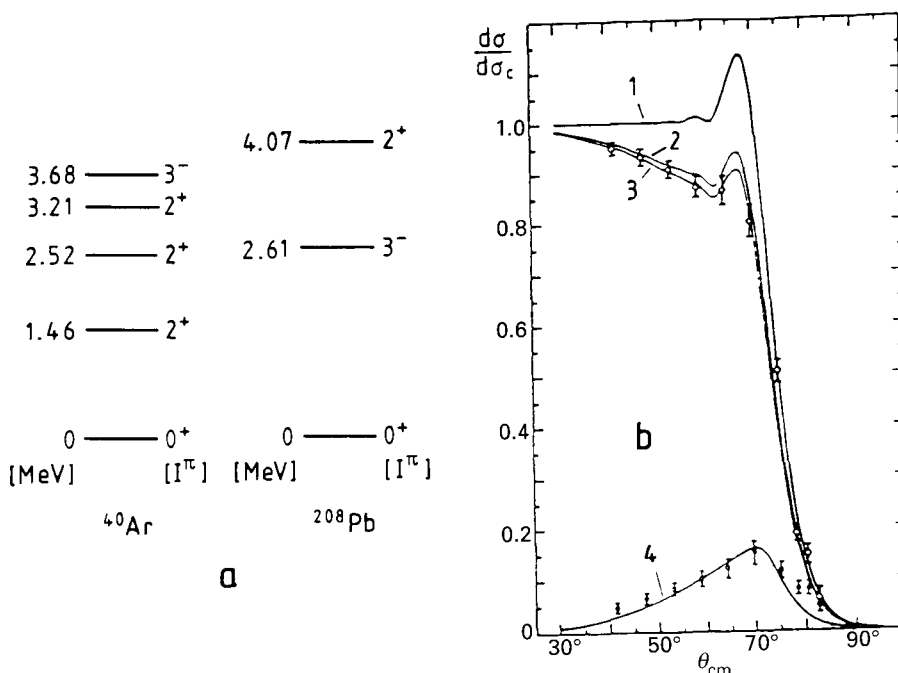


**Figure 8.5** Elastic and inelastic scattering in the presence of projectile and target excitations in the system  $^{40}\text{Ar} + ^{208}\text{Pb}$ . (a) The low-lying states in the nuclei  $^{40}\text{Ar}$  and  $^{208}\text{Pb}$ . (b) curves 1–3: the elastic cross section (divided by the Rutherford cross section) calculated with and without inclusion of the Coulomb polarization potential (see text); curve 4: the inelastic cross section for the excitation of the first  $2^+$  state in  $^{40}\text{Ar}$ . The dots represent the experimental data (cf. Arlt *et al.* 1980).

long-range part of the total optical potential, we must therefore add a phenomenological nuclear optical potential. Figure 8.5b shows various calculated elastic cross sections in comparison with the data. Curve 1 represents the result of an optical-model calculation without Coulomb polarization potential, using a Woods-Saxon potential with the parameters  $V = 21.5 \text{ MeV}$ ,  $r_{0V} = 1.34 \text{ fm}$ ,  $a_V = 0.49 \text{ fm}$ ,  $W = 7.0 \text{ MeV}$ ,  $r_{0W} = 1.43 \text{ fm}$ , and  $a_W = 0.30 \text{ fm}$ . Curve 2 corresponds to a calculation including the Coulomb polarization potential, in which the latter takes account only of projectile excitations. When the target excitations are included as well, one obtains curve 3. It is seen from the figure that the data require the use of the full Coulomb polarization potential.

### Inelastic scattering

The inelastic cross section for exciting the first  $2^+$  state in  $^{40}\text{Ar}$  has also been calculated. This was done by factorizing the inelastic cross section in the form

$$\left( \frac{d\sigma}{d\Omega} \right)_{2^+} = P_{2^+}(\theta) \left( \frac{d\sigma}{d\Omega} \right)_{\text{el}}, \quad (8.143)$$

which is a good approximation at energies close to the Coulomb barrier, where Coulomb-nuclear interference is not important. Here  $P_{2^+}(\theta)$  is the Coulomb excitation probability for the  $2^+$  state of  $^{40}\text{Ar}$ , and  $(d\sigma/d\Omega)_{\text{el}}$  is the elastic cross section calculated using the optical potential with omission of the Coulomb polarization potential. Curve 4 of Fig. 8.5b represents the inelastic cross section for the first excited  $2^+$  state in  $^{40}\text{Ar}$  calculated with the help of eqn (8.143).

### Quasi-elastic scattering and the reaction cross section

In the example just discussed the elastic and inelastic channels were resolved experimentally. However, in many reactions, in particular in heavy-ion collisions, this is not possible. Instead of the true elastic cross section, one measures the so-called *quasi-elastic cross section* which contains contributions from non-elastic channels with channel energies close to that of the elastic channel. The quasi-elastic cross section is therefore larger than the true elastic cross section (cf. Fig. 8.6). The role of the Coulomb polarization potential in this connection is illustrated in Fig. 8.6, which shows the elastic cross section for the system  $^{86}\text{Kr} + ^{88}\text{Sr}$  at  $E_{\text{lab}}(\text{Kr}) = 400 \text{ MeV}$  obtained in an optical-model calculation. When the Coulomb polarization potential is omitted, the Coulomb-excited channels are not regarded as contributors to the absorption in the elastic channel. The current which they remove from the elastic channel is not counted as a loss, and they are thus implicitly included in the calculated elastic cross section. Therefore, the elastic cross section is in this case to be identified with the quasi-elastic cross section (curve 1 in Fig. 8.6). The true elastic cross section is obtained if the calculation includes a Coulomb polarization potential which takes account of all important excited channels (curve 4). If only a part of the inelastic channels is included, we have an intermediate situation (curves 2 and 3). These considerations also have relevance for the reaction cross section. The reaction cross section calculated via eqn (1.69) using an *S*-matrix obtained from an optical-model fit to the quasi-elastic scattering (without Coulomb polarization potential) is smaller than the true reaction cross section. The difference between the two is equal to the inelastic cross section contained in the quasi-elastic one. Examples are given in Table 8.1 (compiled from the results of Siekmann *et al.* 1982). Here  $\sigma_r^{(1)}$  is the reaction cross section obtained from an optical-model fit (without Coulomb polarization potential) of quasi-elastic scattering data. When the calculated Coulomb polarization potential is added to the optical potential (whereby the absorption is increased), the reaction cross section becomes the true one,  $\sigma_r^{(2)}$ . The difference between the two reaction cross sections yields the unresolved inelastic part of the quasi-elastic cross section.

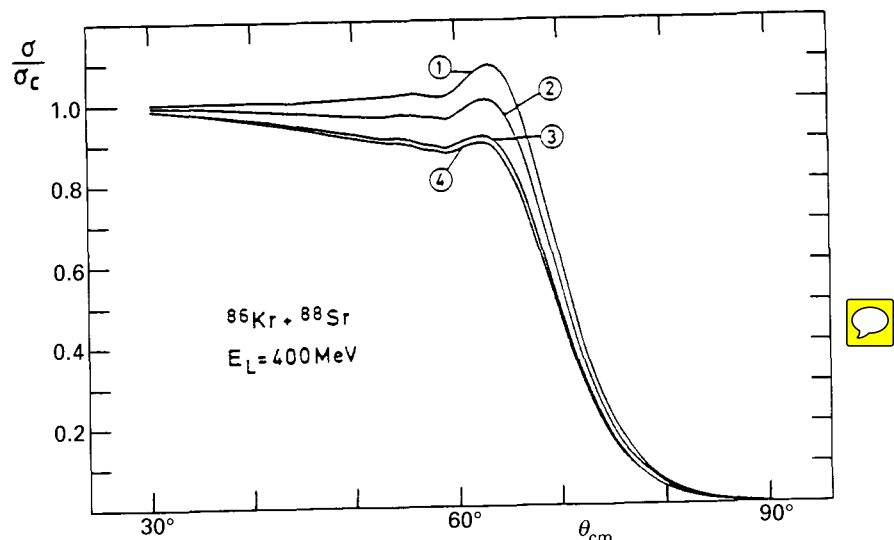


**Figure 8.6** The elastic cross section for the system  $^{86}\text{Kr} + ^{88}\text{Sr}$  at  $E_{\text{lab}}(\text{Kr}) = 400$  MeV, obtained by an optical-model calculation. Curve 1: without Coulomb polarization potential (quasi-elastic scattering); curve 2: with account of the  $2^+$  state in the target  $^{88}\text{Sr}$ ; curve 3: with account of the  $2^+$  state in the target and the  $2^+$  state in the projectile; curve 4: with account of the  $2^+$  and  $3^-$  states in the target and the  $2_1^+$  and  $2_2^+$  states in the projectile.

**Table 8.1** Reaction cross sections derived from the quasi-elastic and true elastic scattering.

$E_{\text{lab}}$ (MeV)	system	$\sigma_r^{(1)}$ (mb)	$\sigma_r^{(2)}$ (mb)	$\sigma_{\text{inelastic}}$ (mb)
380	$\text{Sr}^{88}$	1095	1791	697
380	$\text{Zr}^{90}$	946	1514	569
400	$\text{Sr}^{88}$	1399	2111	712
400	$\text{Sr}^{90}$	1257	1833	576

## 8.5 The coupled-channel Born approximation (CCBA) for transfer

The coupled-channel Born approximation (CCBA) for the description of transfer reactions is an extension of the DWBA (cf. Tamura 1974). It includes multistep inelastic

excitations in the arrangement channels before and after the actual transfer, which latter is only treated as a single-step process. The CCBA is applicable in situations where the effect of inelastic excitations in the entrance and exit arrangement channels is important and the transfer process itself is weak.

In Section 5.5.2 we have derived the CCBA  $T$ -matrix (cf. eqn (5.166)), which has the form

$$\begin{aligned} T_{ba} &= \langle b^-(\text{inel}) | W_\beta | a^+(\text{inel}) \rangle \\ &= \sum_{b'a'} \int d^3 r_\beta \int d^3 r_\alpha \psi_{bb'}^{(-)}(\mathbf{r}_\beta) \langle b | W_\beta(\mathbf{r}_\alpha, \mathbf{r}_\beta) | a \rangle \psi_{aa'}^{(+)}(\mathbf{r}_\alpha). \end{aligned} \quad (8.144)$$

Here the summation goes over the intermediate inelastic channels  $a'$  in the arrangement channel  $\alpha$  before, and the channels  $b'$  in the arrangement channel  $\beta$  after the transfer. The inelastic wave functions  $\psi_{aa'}^{(+)}$  and  $\psi_{bb'}^{(-)}$  are obtained from coupled-channel calculations in the entrance and exit arrangement channels, respectively.

We do not derive explicit formulae for the transfer cross section. They are similar to the expressions obtained for the CC and DWBA cross sections. Rather, we quote the results of some calculations.

### One-nucleon transfer

For an example we discuss the system  $^{19}\text{F}(^{16}\text{O}, ^{15}\text{N})^{20}\text{Ne}$  (cf. Low *et al.* 1976). The coupling scheme is shown in Fig. 8.7a. Proton transfer from the ground state of  $^{19}\text{F}$  to the  $0^+$ ,  $2^+$ , and  $4^+$  states of  $^{20}\text{Ne}$  is considered, and the inelastic excitations in  $^{19}\text{F}$  and  $^{20}\text{Ne}$  are taken into account. Figure 8.7b shows the results of CCBA calculations for two cases: with only the excitations in  $^{20}\text{Ne}$  included, and with account of the excitations in both  $^{20}\text{Ne}$  and  $^{19}\text{F}$ . These are compared with finite-range DWBA results and with the experimental data.

The CCBA provides a reasonable description of the one-nucleon transfer process. The most important difference with regard to DWBA is the change of phase in the oscillations of the differential cross sections.

### Two-nucleon transfer

We close the section with some remarks on two-nucleon transfer, and quote an example of a CCBA calculation for such a process. We assume that both nucleons are transferred simultaneously as a cluster. The Born approximation is applicable because the two-nucleon transfer interaction is weak, and the cross sections are generally smaller than those for one-nucleon transfer by a factor of about five. Taking finite-range effects into account raises the cross section by a factor of about 4 as compared to a zero-range calculation. We consider a case where target and projectile excitations are important, as for example, in the two-neutron transfer reaction  $^{18}\text{O}(^{74}\text{Ge}, ^{76}\text{Ge})^{16}\text{O}$  (cf. Lemaire and Low 1977). The corresponding coupling scheme is shown in Fig. 8.8a. The  $2^+$  excitations in the target  $^{74}\text{Ge}$  and the projectile  $^{18}\text{O}$  both contribute to the reaction cross section. The arrows (1–5) indicate the different transfer interactions which are taken into account in first order (g.s. = ground state): (1)  $^{74}\text{Ge}$  (g.s.)– $^{76}\text{Ge}$  (g.s.); (2)  $^{74}\text{Ge}$  (g.s.)– $^{76}\text{Ge}$  ( $2_1^+$ ); (3)  $^{74}\text{Ge}$  ( $2_1^+$ )– $^{76}\text{Ge}$  (g.s.); (4)  $^{74}\text{Ge}$  ( $2_1^+$ )– $^{76}\text{Ge}$  ( $2_1^+$ ); (5)  $^{16}\text{O}$  (g.s.)–

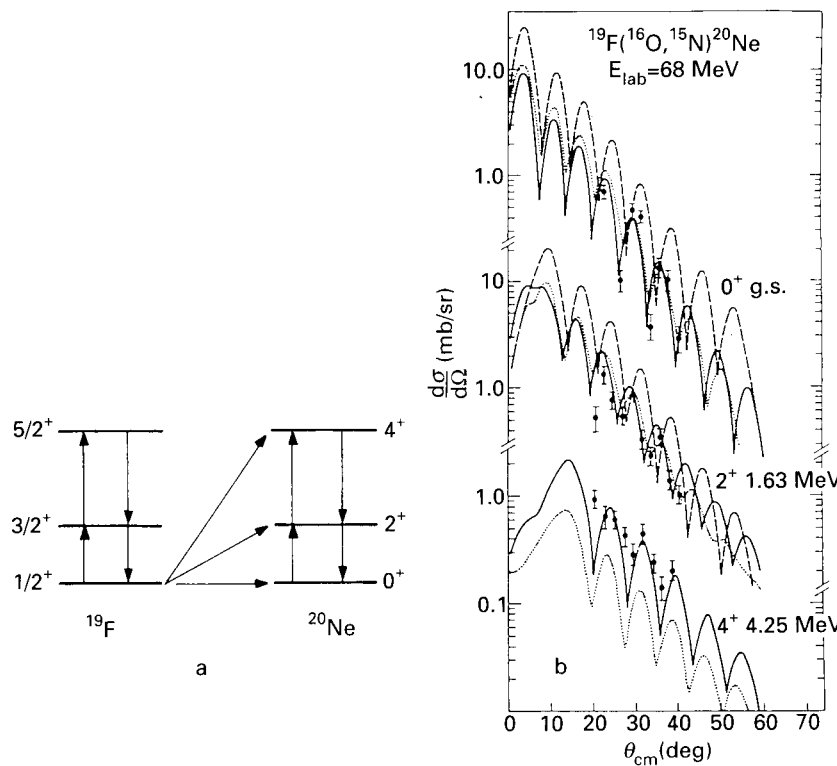


**Figure 8.7** The reaction  $^{19}\text{F} + ^{16}\text{O} \rightarrow ^{20}\text{Ne} + ^{15}\text{N}$ . (a) CCBA coupling scheme. (b) CCBA transfer cross sections in comparison with the DWBA results. Dotted curves: CCBA( $^{20}\text{Ne} - ^{20}\text{Ne}^*$ ); solid curves: CCBA( $^{20}\text{Ne} - ^{20}\text{Ne}^* + ^{19}\text{F} - ^{19}\text{F}^*$ ); dashed curves: DWBA. The experimental data are represented by dots.

$^{18}\text{O}(2^+_1)$ . The angular distributions are described reasonably well by the CCBA (cf. Fig. 8.8b), but the absolute cross sections come out too small. This may be due to the fact that sequential transfer processes have been neglected. For further details we refer to Glendenning (1983) and Satchler (1983), and references therein.

## 8.6 Coupled-reaction-channel calculations (CRC)

In the coupled-reaction-channel (CRC) method one takes approximate account of the recoupling between the exit and entrance channels of a transfer reaction. The general formalism has been derived in Section 5.5.3. Again we only quote the results of some calculations. As an example we consider the system  $^{16}\text{O} + ^{48}\text{Ca}$  at  $E_{\text{lab}}(\text{O}) = 56 \text{ MeV}$  (cf. Low 1976). Here a large number of final channels can be reached, such as the elastic channel, inelastic channels with projectile and target excitation, single-nucleon

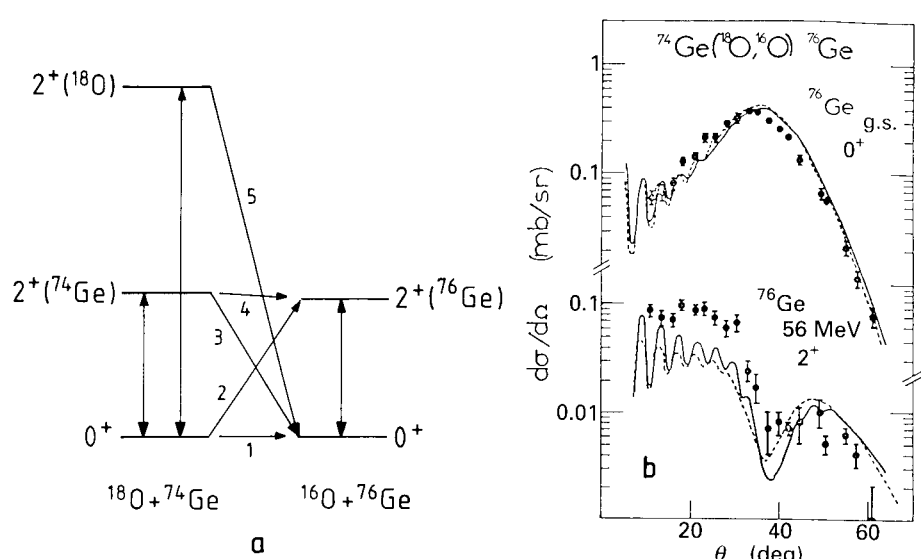


**Figure 8.8** The two-nucleon transfer reaction  $^{74}\text{Ge}(^{18}\text{O}, ^{16}\text{O})^{76}\text{Ge}$ . (a) Coupling scheme for target and projectile excitations. (b) Results of CCBA calculations for the two-neutron transfer reaction  $^{74}\text{Ge}(^{18}\text{O}, ^{16}\text{O})^{76}\text{Ge}$  in comparison with the data of Bond *et al.* (1977). The solid and dashed curves are fits with two different optical potentials in the coupled-channel equations.

transfer channels (pick-up or stripping of protons and neutrons), as well as two-nucleon and multi-nucleon transfer channels. We restrict our attention to inelastic scattering

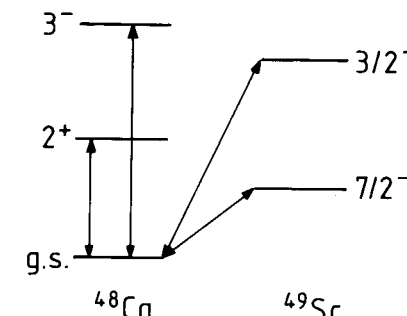


**Figure 8.9** Coupling scheme for the states involved in the processes  $^{48}\text{Ca}(^{16}\text{O}, ^{16}\text{O}')^{48}\text{Ca}^*$  (inelastic scattering) and  $^{48}\text{Ca}(^{16}\text{O}, ^{15}\text{N})^{49}\text{Sc}$  (one-proton transfer).

and single-nucleon transfer. Figure 8.9 shows the coupling scheme for the channels involved in the two processes  $^{48}\text{Ca}(^{16}\text{O}, ^{16}\text{O}')^{48}\text{Ca}^*$  (inelastic) and  $^{48}\text{Ca}(^{16}\text{O}, ^{15}\text{N})^{49}\text{Sc}$  (one-proton transfer).

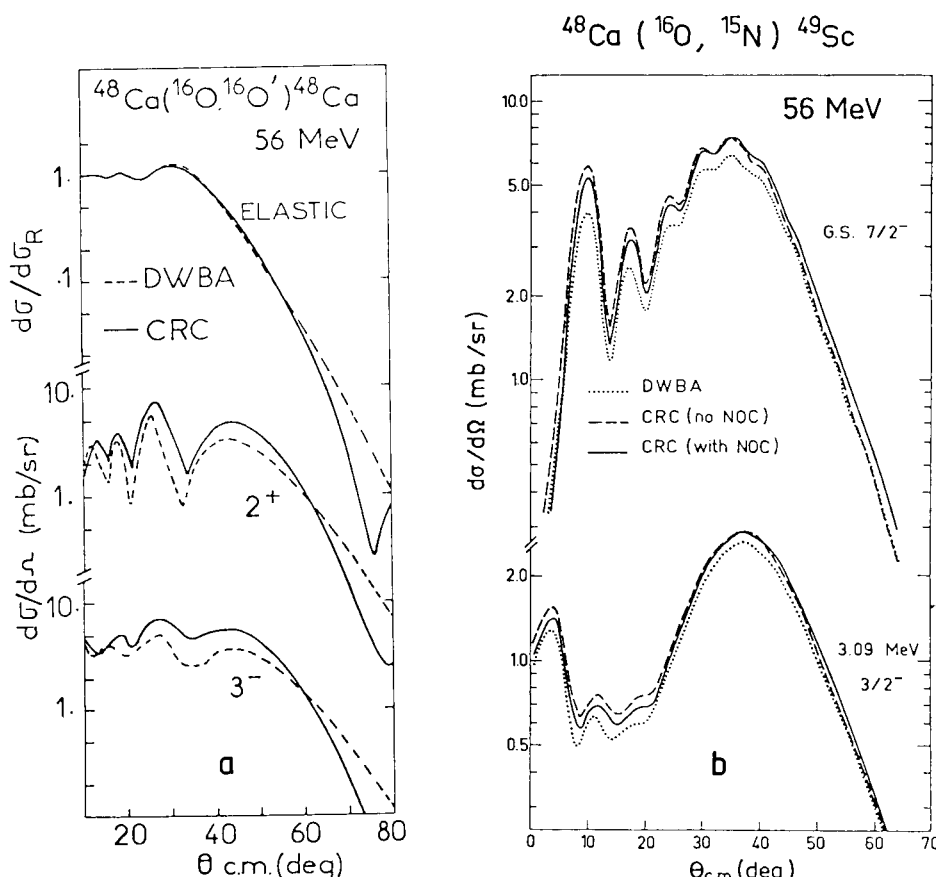


**Figure 8.10** Comparison of the results of CRC and DWBA calculations. (a) The inelastic cross section for the process  $^{48}\text{Ca}(^{16}\text{O}, ^{16}\text{O}')^{48}\text{Ca}^*$ . (b) The one-proton transfer cross section for the process  $^{48}\text{Ca}(^{16}\text{O}, ^{15}\text{N})^{49}\text{Sc}$ .

### Inelastic scattering

The results of a CRC calculation are compared with those of a DWBA calculation (where the recoupling between the transfer channels is neglected) in Fig. 8.10a. It is seen that the inelastic scattering cross sections are influenced by the recoupling.

### One-proton transfer

A typical one-proton transfer cross section is shown in Fig. 8.10b. This figure contains, besides the experimental data, the results of CRC calculations with and without non-orthogonality corrections (NOC), as well as those of the single-step DWBA. Here it is particularly important to include the Coulomb interaction in the terms  $V_\alpha - U_\alpha$  and

$V_\beta - U_\beta$  occurring in the CRC equations (5.174) and (5.175). For a good reproduction of the data it is necessary to treat finite-range effects properly. It is seen that the CRC calculations give rise to some modifications of the DWBA results, more so in the inelastic scattering than in the transfer process.

### One-neutron transfer

As a final example we consider the reaction  $^{208}\text{Pb}(^{17}\text{O}, ^{16}\text{O})^{209}\text{Pb}$  at  $E_{\text{lab}}(^{17}\text{O}) = 78$  MeV leading to different final states in  $^{209}\text{Pb}$ . The coupling scheme is shown in Fig. 8.11. It involves the coupling to the inelastic  $2s_{1/2}^+$  state in  $^{17}\text{O}$ , and to the neutron stripping and pick-up channels  $(^{17}\text{O}, ^{16}\text{O})^{209}\text{Pb}$  and  $(^{17}\text{O}, ^{18}\text{O})^{207}\text{Pb}$ , respectively. Figure 8.12 shows the experimental differential cross sections for neutron transfer  $^{208}\text{Pb}(^{17}\text{O}, ^{16}\text{O})^{209}\text{Pb}$  at  $E_{\text{lab}} = 78$  MeV to different final states in  $^{209}\text{Pb}$  in comparison with the results of finite-range CRC and DWBA calculations. It can be seen that CRC is superior to DWBA, in particular for transitions to low-spin states at backward angles.

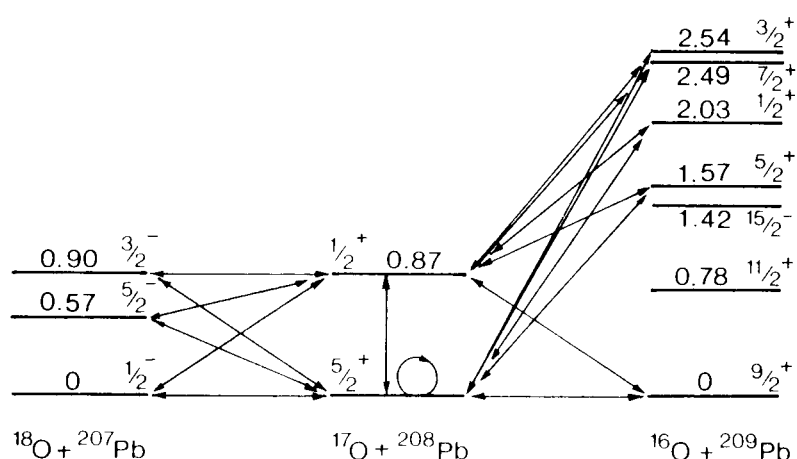


**Figure 8.11** Channel couplings in the CRC calculations for the system  $^{17}\text{O} + ^{208}\text{Pb}$ ; the states shown are those in the nuclei  $^{207}\text{Pb}$ ,  $^{17}\text{O}$  and  $^{209}\text{Pb}$  (cf. Lilley *et al.* 1987).

## 8.7 Notes and references

The quantal coupled-channel formalism provides an adequate description of inelastic and transfer scattering processes as long as only a restricted number of channels are important. However, it is not always clear which are the ‘important channels’ which must be included in the calculation. Another difficulty arises from the fact that the limits of computer capacities are quickly reached when a large number of channels have to be taken into account.

Various approximate schemes are available as alternatives to the numerical solution of the exact quantal coupled-channel equations. For example, for heavy-ion systems one may apply the semiclassical time-dependent method used in Coulomb excitation (cf.

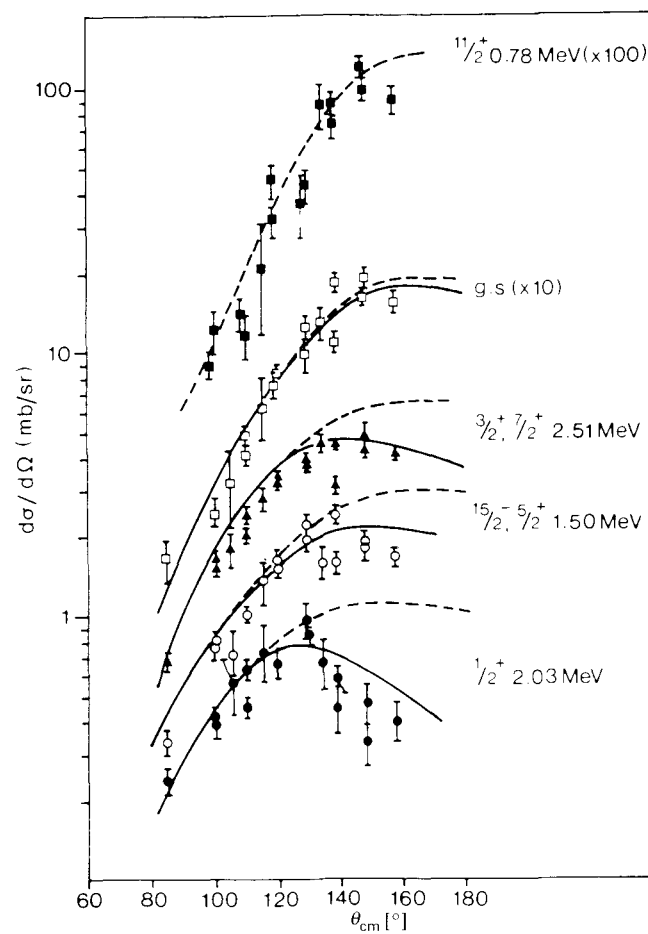


**Figure 8.12** Comparison of the experimental differential cross section for  $^{208}\text{Pb}(^{17}\text{O}, ^{16}\text{O})^{209}\text{Pb}$  at  $E_{\text{lab}}(^{17}\text{O}) = 78 \text{ MeV}$  with CRC (solid curves) and DWBA (dashed curves) calculations (cf. Thompson *et al.* 1988).

Winther and de Boer 1970; Alder and Winther 1975). Another approximate procedure for the description of inelastic scattering is the angle-dependent phase shift method (cf. Massmann and Lipperheide 1979; Lipperheide *et al.* 1981), which can be used when the excitation energies are small.

Multiple-step processes play an increasingly important role in coupling inelastic scattering and transfer channels as one goes over to heavier ions and to somewhat higher energies. Collective states are easily excited, and generally many complicated internal states have to be taken into account for a meaningful interpretation of the measured

cross sections. Although attempts have been made (e.g., by Lenske and Wolter 1992) to extend coupled-channel methods to the description of such *deep-inelastic collisions*, it is more adequate to use more global approaches, as discussed in Chapters 11 and 12.

### References

- Abramowitz, M. and Stegun, I. A. (1965). *Handbook of mathematical functions*, Dover, New York.
- Alder, K. and Winther, A. (1975). *Electromagnetic excitation. Theory of Coulomb excitation with heavy ions*, North-Holland, Amsterdam.
- Alder, K., Bohr, A., Huus, T., Mottelson, B. and Winther, A. (1956). *Rev. Mod. Phys.* **28** 432.
- Arlt, U., Bass, R., Hartmann, V., Renfordt, R., Sapotta, K., Fröbrich, P. and Schäfer, W. (1980). *Phys. Rev.* **C22** 1790.
- Baltz, A. J., Kauffmann, S. K., Glendenning, N. K. and Pruess, K. (1978). *Phys. Rev. Lett.* **40** 20.
- Bohr, A. and Mottelson, B. R. (1969). *Nuclear structure*, vol. 1, Benjamin, New York.
- Bond, P. D., Körner, H. J., Lemaire, M.-C., Pisano, D. J. and Thorn, C. E. (1977). *Phys. Rev.* **C16** 177.
- Buck, B., Stamp, A. P. and Hodgson, P. E. (1963). *Phil. Mag.* **8** 1805.
- Edmonds, A. R. (1957). *Angular momentum in quantum mechanics*, Princeton University Press, Princeton.
- Fröbrich, P., Lipperheide, R. and Fiedeldey, H. (1979). *Phys. Rev. Lett.* **43** 1147.
- Glendenning, N. K. (1983). *Direct nuclear reactions*, Academic Press, New York.
- Gradshteyn, I. S. and Ryzhik, I. M. (1965). *Tables of integrals, series, and products*, Academic Press, New York.
- Jackson, J. D. (1975). *Classical electrodynamics*, 2nd edn, Wiley, New York.
- Kim, B. T. (1979). *Phys. Lett.* **B80** 353.
- Lemaire, M. C. and Low, K. S. (1977). *Phys. Rev.* **C16** 183.
- Lenske, H. and Wolter, H. (1992). *Nucl. Phys.* **A538** 483c.
- Lilley, J. S., Nagarajan, M. A., Banes, D. W., Fulton, B. R. and Thompson, I. J. (1987). *Nucl. Phys.* **A463** 710.
- Lipperheide, R., Massmann, H. and Rossner, H. (1981). *Nucl. Phys.* **A366** 119.
- Love, W. G., Terasawa, T. and Satchler, G. R. (1977). *Nucl. Phys.* **A291** 183.
- Low, K. S. (1976). *J. de Physique Colloque* **C5**, suppl. 11, vol. 37, 15.
- Low, K. S., Tamura, T. and Udagawa, T. (1976). *Phys. Rev.* **C13** 2579.
- Massmann, H. and Lipperheide, R. (1979). *Ann. Phys.* **123** 120.
- Preston, M. A. and Bhaduri, R. K. (1975). *The structure of the nucleus*, Addison-Wesley, New York.
- Satchler, G. R. (1983). *Direct nuclear reactions*, Oxford University Press, Oxford.
- Siekmann, H., Gebauer, B., Bohlen, H. G., Kluge, H., von Oertzen, W., Fröbrich, P., Strack, B., Hildenbrand, K. D., Sann, H. and Lynen, U. (1982). *Z. Physik* **A307** 113.
- Tamura, T. (1965). *Rev. Mod. Phys.* **37** 679.
- Tamura, T. (1974). *Phys. Rep.* **14C** 59.
- Thompson, I. J., Nagarajan, M. A., Lilley, J. S. and Fulton, B. R. (1988). *Nucl. Phys.* **A487** 141.

- Tolsma, L. D. (1979). *Phys. Rev.* **C20** 592.  
Weber, D. J., Franey, M. A., Dehnhard, D., Artz, J. L., Shkolnik, V. and Hintz, N. M. (1976). *Bull. Am. Phys. Soc.* **21** 304.  
Winther, A. and de Boer, J. (1966). In *Coulomb excitation*, eds. Alder, K. and Winther, A., Academic Press, New York.

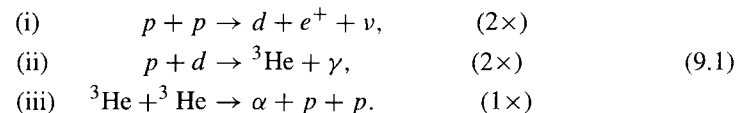
## Part D

### The compound nucleus

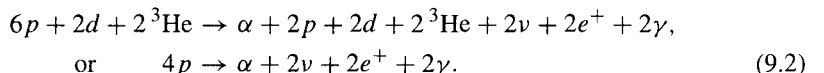
## FUSION

## 9.1 Introduction

Fusion is, in the general sense of the term, a process in which two or more nuclei join to form a new, heavier nucleus. An example is the fusion of hydrogen nuclei into  $^4\text{He}$  ( $\alpha$ -particles). One of the routes of this process is the following (cf. Clayton 1968, Chapter 5.2)

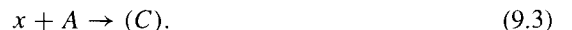


Adding up the left- and right-hand sides we obtain



The net effect of the sequence of reactions (i) to (iii) is to combine four protons to form an  $\alpha$ -particle together with two neutrinos, two positrons, and two  $\gamma$ -quanta. The two positrons will eventually annihilate with electrons to produce additional  $\gamma$ -quanta. In all these reactions the entrance and exit channels contain more than one stable particle, of which some are non-nuclear, namely positrons,  $\gamma$ -rays, or neutrinos.

The fusion process (9.1) occurs in stars, and is therefore of great significance for the evolution of the universe. From the viewpoint of reaction theory it is a succession of elementary rearrangement reactions; it is not fusion in the sense which we shall be concerned with, namely the fusion of *two* nuclei, light or heavy, into a *single* system,



Such a process is not a reaction of the kind discussed in Chapter 5. Instead, the nuclei  $x$  and  $A$  in the entrance channel join to form a **compound nucleus (C)**, which is not stable on a macroscopic time scale, as required in the definition of a reaction channel, but which stays together for a time which is long on a *nuclear* time scale, so that it can be introduced as an intermediate system into which probability current is fed. Fusion of this type appears as absorption from the entrance channel, though it may occur with various elastic or non-elastic steps interposed.

Thus we identify fusion with the *formation of a compound nucleus*. It occurs as the initial stage of a compound reaction, i.e. a reaction proceeding via the formation of a compound nucleus which later decays into true final channels. Indeed, the probability for the formation of a compound nucleus, which we call the **fusion cross section**, is

determined experimentally by measuring the total rate of decay into the final products. When registering these products one must verify that the reaction has indeed proceeded via a compound nucleus. The details of compound-nucleus decay will be discussed in Chapter 10. In the present chapter our main concern are the conditions for the formation of the compound nucleus.

The cross section for compound-nucleus formation or fusion,  $\sigma_F$ , has already been introduced in Section 6.3.3. It is equal to the absorption cross section in the optical model if all reactions proceed via the compound nucleus; in this case it is determined by the imaginary part of the optical potential. However, reaction channels may also be excited via direct couplings (cf. Section 9.5) or in a deep-inelastic process (cf. Chapters 11 and 12). In order to take these effects into account, simple models for the fusion mechanism have been introduced. These have gradually been refined in order to include more and more aspects of the processes accompanying fusion.

We shall not obtain the fusion cross section by deriving it in a deductive way using the formal reaction theory of Chapter 5. Rather, we proceed phenomenologically. Some basic results of formal reaction theory will necessarily have to be used; but we shall often rely on classical or semiclassical approximations, on the phenomenological optical model and, in the parts of Chapters 11 and 12 devoted to fusion, on classical equilibrium and non-equilibrium thermodynamics.

In Section 9.2 we explain more precisely the notion of a *compound nucleus*. The main topic will be its stability, that is, we shall discuss the conditions under which it stays together long enough to appear as stable on a nuclear time scale.

Section 9.3 is devoted to *classically allowed* fusion, where the energy in the initial channel is high enough to allow the collision partners to overcome the potential barrier generated by the repulsive Coulomb field between them. This is *fusion above the barrier*. A classical formula for the fusion cross section is derived, and the effects of the stability of the compound nucleus on this cross section are investigated.

The subject of Section 9.4 is *sub-barrier fusion*. Here the initial energy is so low that in a classical description, the Coulomb barrier prevents the nuclei from approaching close enough to be able to fuse. Therefore, quantal tunnelling must come into play. We first study one-dimensional barrier penetration in the semiclassical or WKB approximation. Then the quantal penetrability of a parabolic barrier is derived, and generalised to the Hill–Wheeler formula for barriers with more general shapes. These results are used in the derivation of the explicit Wong formula for the fusion cross section. Finally, the numerical calculation of exact quantal barrier penetrabilities is briefly discussed.

In Section 9.5 we consider the *effect of direct nuclear reaction processes* both on sub-barrier fusion and on fusion above the barrier. This will be done in the coupled-channel formalism. The essential physics is explained first in a schematic two-channel model. This model is then extended so as to take into account all inelastic channels in the sudden approximation, leading to a closed expression for the fusion cross section, the *zero-point fluctuation formula*. Finally, some full coupled-channel calculations are discussed, where the main approximation consists in the restriction to a finite number of channels. The coupled-channel approach has only a limited range of application; when the number of channels becomes very large, as in the description of heavier systems, the reaction mechanism requires a different treatment (cf. Chapters 11 and 12).

Finally, in Section 9.6, we describe a *phenomenological quantal fusion model*, where an absorptive fusion potential is introduced as an extension of the optical model.

## 9.2 The compound nucleus

### 9.2.1 The compound nucleus and its decay

When projectile and target come into close contact during a nuclear reaction they form a combined system in which the nucleons interact strongly with each other. Except when this intermediate system is light, the energy carried in from the entrance channel is usually not invested in one or a few degrees of freedom, i.e. in single-particle or collective excitations (this would correspond to direct processes) but is shared more or less stochastically among many complicated configurations. Once this has happened, it takes a long time on a nuclear scale until the energy is concentrated again in some configuration of nucleons from which a transition to an open final channel can take place. In general many configurations are so strongly coupled among each other that none stands out in any particular way. A description in terms of phase-coherent reaction states as defined in Section 5 then becomes impossible. It was Niels Bohr (1936) who found a suitable approach to the theory of such reactions by introducing the concept of a *compound nucleus*.

The term compound nucleus describes a nuclear system composed of the nucleons from the two collision partners which is not defined as an eigenstate of the total Hamiltonian of the reaction, but as a mixture of transitory configurations which may be visualized as quasi-bound many-particle–many-hole ‘compound states’ of the type introduced in the schematic model of Section 6.2 (cf. in particular, the discussion in the last part of Section 6.2.3). Generally these have a very complicated structure, and are assumed to be in statistical equilibrium with each other. The equilibrated system exists for a time which is long compared with the time it would take the projectile to pass by the target in the absence of interactions. The lifetime of a compound nucleus generally lies between  $10^{-19}$  s and  $10^{-16}$  s; it is appreciably longer than the ‘flying-by time’ of the projectile (which is of the order of  $10^{-21}$  s), but it is of course still short on a macroscopic scale.

The compound nucleus is highly excited and has a temperature; it is ‘hot’. It also carries an angular momentum equal to the sum of the angular momentum of the relative motion in the entrance channel and the spins of the initial collision partners. The excitation energy and the angular momentum of the compound nucleus are eventually released via a decay into smaller fragments. For compound nuclei at energies corresponding to incident laboratory energies  $E < 10$  MeV per nucleon of the fusing projectile (these are the energies in which we are mainly interested in the following discussion) we distinguish two main decay schemes:

(i) *Evaporation*, i.e. emission of light particles like neutrons, protons,  $\alpha$ -particles, and so on. There remains a bound residual nucleus called *evaporation residue* of a slightly lower mass than the compound nucleus. The particle evaporation process is generally accompanied by  $\gamma$ -emission, which has to be taken into account in the energy and angular momentum balance. The evaporation residue contains all the nucleons originally present in the compound nucleus except the few evaporated ones, and is therefore the nucleus in the final channel into which projectile and target have fused in the literal sense.

(ii) **Fission**, where the compound nucleus splits up into two halves of more or less equal size. This process is accompanied by evaporation of light particles out of the fissioning nucleus, and similarly the fission fragments will generally decay further by evaporation. The emitted particles are called *pre-scission* and *post-scission* particles, respectively.

For lighter systems evaporation predominates. The rate of production of evaporation residues is then a measure of the fusion cross section (*fusion-evaporation*). For medium-heavy systems evaporation competes with the fission process. For heavy systems fission is the dominant mode of decay of the compound nucleus. In this case the fusion cross section is essentially determined by the fission cross section (*fusion-fission*).

In general it is the sum of the measured cross sections for these two main modes of decay which yields the magnitude of the fusion cross section. In order to verify that a compound nucleus has indeed been formed in the process, further evidence (relating to the momenta of the evaporation residues, the angular distribution of the emitted particles, or to the angle between the fission fragments) must be adduced to identify a given reaction as a compound reaction. At projectile energies  $E > 10$  MeV per nucleon *incomplete fusion* starts to compete with *complete fusion*, i.e. processes like pre-equilibrium particle emission and projectile break-up occur which lead to an incomplete transfer of linear momentum. At still higher energies the compound nucleus can also break up into several heavy pieces. This process is called *multiplication*. It will not be discussed in this book.

Although the compound nucleus will eventually decay, it is stable on a nuclear time scale. Its very existence is tantamount to its stability in this sense. The latter is mainly influenced by the values of the mass and the angular momentum. For a semi-quantitative description of the effect of these two parameters we make use of the macroscopic liquid-drop model of the nucleus.

### 9.2.2 Stability in the mass

The most important quantity determining the stability of a nucleus is its energy as compared to the energies of any two component nuclei into which it may be subdivided (we consider only the decomposition into *two* fragments; the stability against disintegration into more than two fragments is generally greater).

Figure 9.1 shows schematically a nucleus  $A$  and its decomposition into two fragments  $A_1$  and  $A_2$  at contact. Because of the short range of the nuclear forces, we may assume that there is Coulomb repulsion but no nuclear attraction between the fragments in this configuration. If all systems are in their ground state, we have for the difference  $\tilde{B}$  between the energy of the separated fragments (equal to the sum of the internal energies of the fragments  $(A_1, Z_1)$  and  $(A_2, Z_2)$ ) plus the Coulomb energy  $V_C$  at contact and the energy of the nucleus  $(A, Z)$  (cf. Fig. 9.2),

$$\begin{aligned}\tilde{B} &= \tilde{B}(A_1, Z_1; A_2, Z_2) \\ &= \epsilon(A_1, Z_1) + \epsilon(A_2, Z_2) + V_C(A_1, Z_1; A_2, Z_2) - \epsilon(A, Z),\end{aligned}\quad (9.4)$$

where  $A = A_1 + A_2$ ,  $Z = Z_1 + Z_2$ ,  $\epsilon(A_i, Z_i)$  is the internal energy of the nucleus  $(A_i, Z_i)$ , and the Coulomb energy of the two fragments in contact at the radius  $R_C$  =

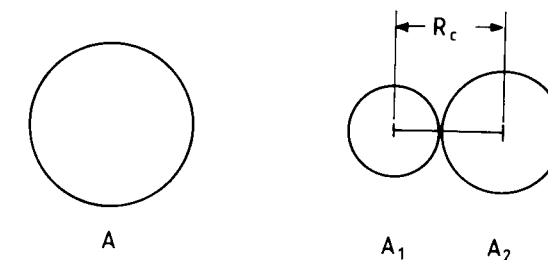


Figure 9.1 A nucleus  $A$  and its decomposition into two fragments  $A_1$  and  $A_2$  at contact.

$[0.5 + 1.36(A_1^{1/3} + A_2^{1/3})]$  fm is given by  $V_C(A_1, Z_1; A_2, Z_2) = Z_1 Z_2 e^2 / R_C$ . The quantity  $\tilde{B}$  is the energy released when the two fragments in contact form the nucleus  $(A, Z)$ , which we call the compound nucleus. Conversely, it is the internal energy above the ground-state level which the compound nucleus must have in order to ascend the height  $\tilde{B}$  defined by the energy of the two decay products at contact. For  $\tilde{B} > 0$  the compound nucleus is stable, and for  $\tilde{B} < 0$  it is unstable.

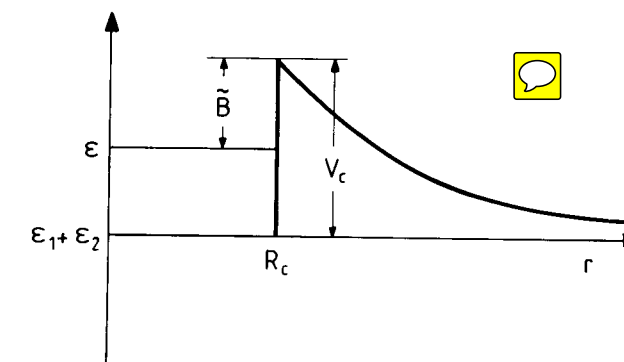


Figure 9.2 The definition of the energy release  $\tilde{B}$  on formation of a nucleus with energy  $\epsilon = \epsilon(A, Z)$  from two fragments with energies  $\epsilon_1 = \epsilon(A_1, Z_1)$  and  $\epsilon_2 = \epsilon(A_2, Z_2)$ .  $V_C$  denotes the height of the Coulomb barrier at contact,  $r = R_C$ .

For the calculation of the ground-state energy  $\epsilon(A, Z)$  we make use of the Bethe-Weizsäcker liquid-drop formula (cf. Bohr and Mottelson 1969) in the form proposed by Myers and Swiatecki (1966),

$$\epsilon(A, Z) = \epsilon_V(A, Z) + \epsilon_S(A, Z) + \epsilon_C(A, Z). \quad (9.5)$$

Here we have introduced the volume energy

$$\epsilon_V(A, Z) = - \left[ 1 - \kappa \left( \frac{N - Z}{A} \right)^2 \right] a_V A, \quad (9.6)$$

the surface energy

$$\epsilon_S(A, Z) = \left[ 1 - \kappa \left( \frac{N - Z}{A} \right)^2 \right] a_S A^{2/3}, \quad (9.7)$$

(both modified by the symmetry correction  $-\kappa[(N - Z)/A]^2$  with  $N = A - Z$ ), and the Coulomb energy

$$\epsilon_C(A, Z) = \frac{3}{5} \frac{e^2 Z^2}{r_0 A^{1/3}} \left( 1 - \frac{5}{6} \frac{\pi^2 a^2}{r_0^2 A^{2/3}} \right), \quad (9.8)$$

corrected for the diffuseness  $a$  of the surface. The coefficients in eqns (9.6) to (9.8) have the values  $a_V = 15.677$  MeV,  $a_S = 18.56$  MeV,  $\kappa = 1.79$ ,  $r_0 = 1.2049$  fm, and  $a = 0.546$  fm.

The energy release  $\tilde{B} = \tilde{B}(A, Z, \alpha)$ , or equivalently, the energy needed for a split-up into a system of fragments  $(A_1, A - A_1)$  (calculated from eqns (9.4) to (9.8) for different compound nuclei, i.e. different values of  $A$ ) is shown in Fig. 9.3 as a function of the asymmetry parameter  $\alpha = A_1/A$ . **Here  $Z$  has been chosen along the bottom of the valley of  $\beta$ -stability, where  $Z = \frac{1}{2}(A - 0.006A^{5/3})$ .**

Three regions of stability of the compound nucleus can be distinguished (because of the symmetry of the figure, we only discuss the left side):

(i) **If  $A < 120$** , the value of  $\tilde{B}(\alpha)$  is large for  $\alpha = \frac{1}{2}$  and low for  $\alpha \approx 0$ : the decays to fragments with very different masses ( $\alpha \ll 1$ ) are energetically favoured. The daughter nuclei are a light nucleus ( $n, p, \alpha, \dots$ ) and a heavy one with a mass slightly less than that of the mother nucleus. The light nucleus is called the ‘evaporated’ particle and the heavy fragment, the *evaporation residue*. A compound reaction in which the compound nucleus decays in this very asymmetric fashion is called a *fusion–evaporation* reaction.

(ii) **For  $120 < A < 300$**  symmetric final configurations are favoured. A compound reaction terminating in a near-symmetric decay is called a *fusion–fission* reaction.

(iii) **For  $A > 300$  the compound nucleus is unstable even in its ground state.** In reactions where the value of total mass lies in this region the compound nucleus does not have the time to equilibrate so as to decay afterwards by the energetically favoured symmetric fission. Instead, the di-nuclear complex in the entrance channel immediately goes over into the final two-body configuration. One speaks here of a *capture or fast fission* process because the projectile is only captured briefly without forming a compound nucleus, and the intermediary system decays more rapidly than in normal fission.

The curves  $\tilde{B} = \tilde{B}(\alpha)$  in Fig. 9.3 represent, for fixed total mass  $A$ , the change in energy of a configuration of two spherical fragments at the contact radius  $R_C$  as the asymmetry parameter  $\alpha$  is varied. They can be interpreted as the *driving potential* in the dynamical evolution of the di-nuclear intermediary system at contact as a function of the parameter  $\alpha$  (cf. eqn (11.105)). The system is driven to a more symmetric or asymmetric configuration if the slope of the potential  $\tilde{B}(\alpha)$  (on the left side of the figure)

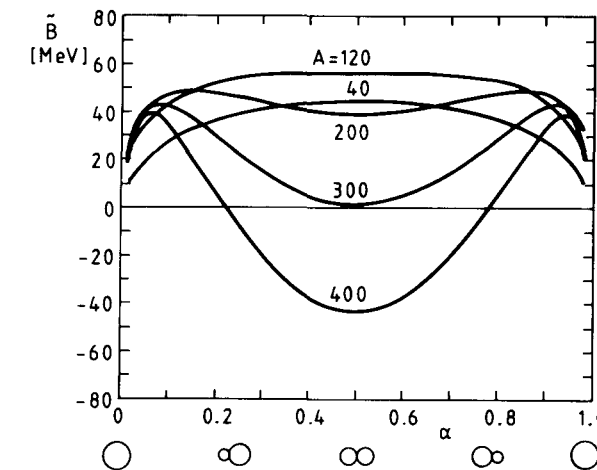


**Figure 9.3** The energy release  $\tilde{B}(A, Z, \alpha)$  on formation of a compound nucleus  $(A, Z)$  from its component nuclei  $A_1$  and  $(A - A_1)$  as a function of the asymmetry parameter  $\alpha = A_1/A$  (cf. Swiatecki 1972). The two-fragment configurations for a few values of the asymmetry parameter are shown below the abscissa.

is negative or positive, respectively. This interpretation is useful for the description of deep-inelastic collisions in which the nuclei stay in close contact for some time but do not penetrate each other as in a compound reaction (cf. Section 11.4.4 and Nörenberg 1980).

The preceding discussion can only give a crude idea of the dependence of the stability of a compound nucleus on its mass, charge, and energy. We add two remarks.

First, in actual fission processes the compound nucleus does not split up into two spherical nuclei, as suggested by Fig. 9.1. At the point of separation, called the scission point, the two fragments are in general strongly deformed, which results in less stability for the compound nucleus.

Second, for an estimate of the *true stability* of the compound system (i.e. its survival over macroscopic times) one should consider an energy difference analogous to the *Q*-value introduced in Section 5.2.1 and compare the energy of the compound nucleus with the energies of the final fragments at a large distance from each other, where the Coulomb term does not appear. The curves in Fig. 9.3 would then be moved downward by the amount  $V_C(A_1, Z_1; A_2, Z_2)$  with the result that all nuclides above iron would become unstable. However, it is seen from Fig. 9.2 that now the term  $V_C$  plays the role of the height of a *barrier* through which the two fragments have to tunnel if  $\tilde{B} > 0$ . This makes the lifetime of the compound nucleus so long that it is still the height of the barrier  $B$  which determines the stability of the compound nucleus, and not the *Q*-value. In general this barrier is a function not only of the distance between the fragments but also of their deformation.

### 9.2.3 Stability in angular momentum

After the mass, the second important parameter determining the stability of the compound nucleus is the angular momentum. Its effect on the energy of a nuclear system is connected with the non-spherical deformations of the latter.

A nucleus with non-vanishing angular momentum is subject to the action of centrifugal forces. It has higher energy, and is therefore less stable, than a nucleus without angular momentum. Above a certain critical value of the angular momentum the nucleus will not hold together at all. A compound nucleus can then not be formed, since it would immediately fission. This *critical angular momentum*  $l_{\text{crit}}^f$  can be estimated in the following way (cf. Cohen *et al.* 1974). The compound nucleus is generally non-spherical. Its shape is defined in terms of a set of deformation parameters  $\{\delta\}$ . In order to take account of the effects of deformation and angular momentum, the liquid-drop energy of a spherical nucleus is supplemented with a term which depends on the parameters  $\{\delta\}$  and on the angular momentum  $l$ ,

$$\Delta\epsilon(A, Z, l; \delta) = \epsilon_{\text{def}}(\delta) + \epsilon_{\text{rot}}(l, \delta). \quad (9.9)$$

Here

$$\epsilon_{\text{def}}(\delta) = \epsilon_S(\delta) - \epsilon_S(0) + \epsilon_C(\delta) - \epsilon_C(0) \quad (9.10)$$

is the deformation part of the surface and Coulomb energies as functions of the deformation parameters, and

$$\epsilon_{\text{rot}}(l, \delta) = \frac{\hbar^2}{2J(\delta)} l(l+1) \quad (9.11)$$

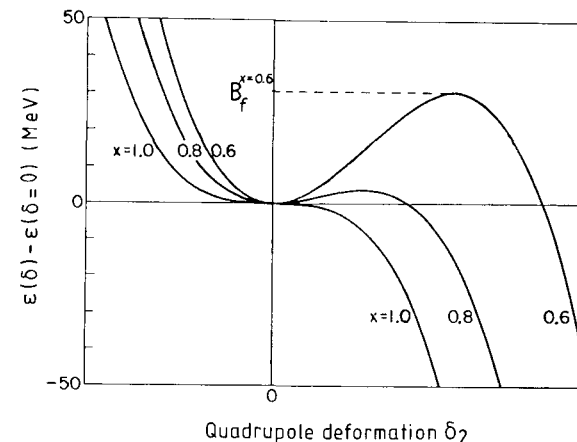
is the rotational energy of the nucleus with a moment of inertia  $J(\delta)$ . The most stable shape of the nucleus is found by minimizing the energy with respect to the deformation at fixed angular momentum  $l$ . The deformation parameters corresponding to the minimum are functions of the angular momentum,  $\delta = \delta(l)$ .

Figure 9.4 shows the deformation energy for angular momentum  $l = 0$  as a function of the quadrupole deformation  $\delta_2$ ; the other deformation parameters have the values which minimize the energy for a given  $\delta_2$ . The different curves refer to nuclei with different values of the *fissility parameter*  $x$ , which is defined as the ratio of the Coulomb energy over twice the surface energy at zero deformation (cf. eqns (9.7) and (9.8)), and is a measure of the instability against fission,

$$x = \frac{\epsilon_C}{2\epsilon_S} = \frac{Z^2}{A} \frac{3e^2(1 - 5\pi^2 a^2 / 6r_0^2 A^{2/3})}{10 r_0 a_S [1 - \kappa(N - Z)^2 / A^2]} \approx \frac{1}{50} \frac{Z^2}{A} \approx \frac{Z}{120}. \quad (9.12)$$

In nuclei with  $x < 1$  the deformation energy develops a *fission barrier* of height  $B_f$ , which delays the decay of the compound nucleus. On the other hand, nuclei with  $x > 1$  have no barrier and are therefore unstable. According to eqn (9.12) this applies to all nuclei with  $Z > 120$ , which therefore undergo prompt fission.

Figure 9.4 further shows that the deformation energy for  $l = 0$  has a minimum at zero deformation,  $\delta_2^{\min}(0) = 0$ , if it has a minimum at all. However, if  $l \neq 0$  the most stable shape is in general no longer spherical,  $\delta_2^{\min}(l) \neq 0$ . With increasing  $l$  the fission barrier moves inward and its height  $B_f(l)$  is lowered, until it vanishes at the critical



**Figure 9.4** The deformation energy  $\epsilon_{\text{def}}(\delta) = \epsilon(\delta) - \epsilon(\delta = 0)$  of a nucleus with angular momentum  $l = 0$  as a function of the quadrupole deformation parameter  $\delta_2$ . The curves correspond to three different values of the fissility parameter  $x$ .  $B_f^x$  is the height of the barrier for given  $x$  (cf. Nix 1972a).

angular momentum  $l_{\text{crit}}^f$ ; for angular momenta above this value the compound nucleus is unstable against prompt fission.

In Fig. 9.5 the upper curve represents the value of  $l_{\text{crit}}^f$  as function of the mass number  $A$  of the compound nucleus. Above this curve a compound nucleus cannot be formed because it fissions promptly. The figure also contains a hatched area labelled  $l_{\text{crit}}^n$ , which is the region of angular momenta for which the fission barrier height  $B_f(l)$  is about equal to the separation energy  $B_n$  of the least-bound neutron,  $B_f(l_{\text{crit}}^n) = B_n > 0$ . In the region between the upper curve and the hatched area fission dominates over neutron emission, but is delayed because of the presence of a fission barrier. Below the hatched area we have  $B_f(l) > B_n$ , so that the energy needed to surmount the fission barrier is higher than that needed to emit a neutron: in the competition between fission and neutron evaporation the latter is favoured. In the hatched area particle emission and fission occur with comparable probability.

These results are not expected to be in quantitative agreement with experimental data, because shell effects have not been considered, the moment of inertia may not have been correctly estimated, and the fission dynamics, especially at high angular momenta, has not been taken into account in an adequate manner.

## 9.3 Fusion above the barrier

### 9.3.1 The classical fusion cross section

Having discussed the conditions for the stability of the compound nucleus, that is, for its very existence, we now turn to the derivation of the cross sections for fusion. We use

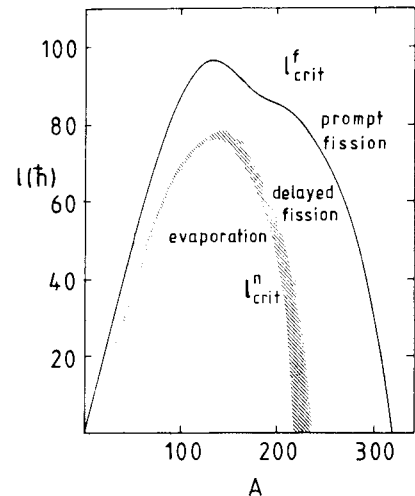


**Figure 9.5** The critical angular momentum as function of the mass number. The curve labelled  $l_f^{\text{crit}}$  indicates the limit of stability against prompt fission. The hatched area labelled  $l_n^{\text{crit}}$  separates the regions of evaporation and delayed fission.

the classical picture.

For a first estimate of the fusion cross section we assume that projectile and target can interact in only two ways: the projectile either scatters elastically off the target or fuses with it into a compound nucleus, i.e. is absorbed. The projectile moves in the field of the Coulomb-plus-nuclear scattering potential  $V(r)$ . For a given impact parameter  $b$  the radial motion is governed by the effective potential (cf. eqn (2.23))

$$V_b(r) = V(r) + E \frac{b^2}{r^2}, \quad (9.13)$$

which is shown in Fig. 9.6 for various impact parameters  $b$ . Except when the impact parameter  $b$  is very large, the effective potential contains a barrier. It is repulsive on the outer flank of the barrier and becomes attractive on the inner flank of it. As discussed in the final part of Section 9.2.2, such a barrier is necessary for the formation of a compound nucleus, i.e. for fusion.

Let us consider a trajectory with an energy  $E$  low enough that an impact parameter exists for which the effective potential has a barrier whose height coincides with  $E$ . This impact parameter is called the *grazing impact parameter*,  $b_{\text{gr}}$ . The corresponding radial distance defines the *barrier radius*  $R_B$ . If the projectile has an impact parameter  $b > b_{\text{gr}}$ , it will be reflected by the barrier. If  $b < b_{\text{gr}}$ , the projectile surmounts the barrier and proceeds towards the interior, where it is absorbed by the action of the nuclear forces: it fuses with the target.

The definition of the grazing impact parameter  $b_{\text{gr}}$  as a limiting parameter for the onset

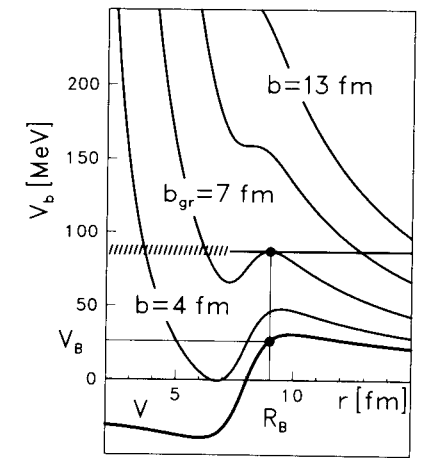


**Figure 9.6** Scattering potential  $V(r)$  and effective potential  $V_b(r)$  for the system  $^{18}\text{O} + ^{58}\text{Ni}$  for various values of the impact parameter  $b$ . The heavy horizontal line represents a trajectory with energy  $E$ . The grazing impact parameter  $b_{\text{gr}}$ , the barrier radius  $R_B$ , and the barrier height  $V_B$  for the energy  $E$  are indicated.

of fusion applies only to the simple situation where the system either undergoes elastic scattering or fuses. If, however, direct or deep-inelastic collisions become important, which happens at higher energies and for heavier collision partners, the name grazing impact parameter is used for that impact parameter which separates the region of quasi-elastic from that of deep-inelastic processes. In this case the onset of fusion is determined by an impact parameter  $b_F$  which separates the deep-inelastic from the fusion events (cf. Section 11.2.1).

The barrier radius  $R_B$  as well as the corresponding value of the scattering potential,  $V_B = V(R_B) = V_{b=0}(R_B)$ , depend weakly on the fusion impact parameter  $b_{\text{gr}}$ , i.e. on the energy  $E$ . Usually one replaces them with energy-independent quantities and takes for  $R_B$  the s-wave barrier radius and for  $V_B$  the s-wave barrier height. In Fig. 9.6 we read off the following relation, using eqn (9.13),

$$V_B + E \frac{b_{\text{gr}}^2}{R_B^2} = E, \quad (9.14)$$

so that

$$b_{\text{gr}} = R_B \sqrt{1 - \frac{V_B}{E}}. \quad (9.15)$$

Going back to Fig. 2.3, we consider the set of trajectories entering on the left through the ring area  $2\pi b db$ . If their impact parameters satisfy  $b < b_{\text{gr}}$  they reach the interior of the nucleus and are terminated there, i.e. they fuse. The fusion cross section for them is equal to  $2\pi b db$ ; integrating these contributions from  $b = 0$  to  $b_{\text{gr}}$  we obtain the total

*fusion cross section*

$$\sigma_F = \pi b_{\text{gr}}^2. \quad (9.16)$$

Substituting here the expression (9.15) we find

$$\sigma_F(E) = \pi R_B^2 \left( 1 - \frac{V_B}{E} \right). \quad (9.17)$$

Figure 9.7 shows the fusion cross section (9.17) for the system  $^{20}\text{Ne} + ^{27}\text{Al}$  in comparison with the data of Morgenstern *et al.* (1983) (which will be discussed also in connection with Figs. 9.9 and 9.10). It rises from zero at a threshold energy equal to the barrier height  $V_B$  and goes over into the ‘geometric cross section’  $\pi R_B^2$  for large energies. However, it must be realized that beyond the energy at which the barrier of the effective potential disappears (cf. the discussion above), formula (9.17) with an energy-independent barrier radius  $R_B$  is no longer valid. It is therefore not surprising that the theoretical curve does not reproduce the data at higher energies.

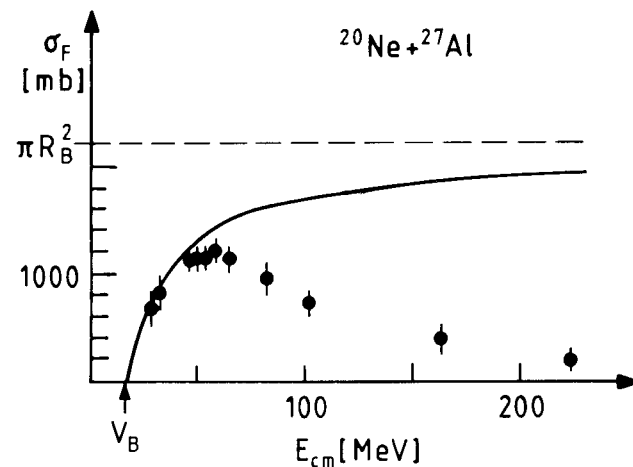


**Figure 9.7** The classical fusion cross section for the system  $^{20}\text{Ne} + ^{27}\text{Al}$  as a function of energy. The data are from Morgenstern *et al.* (1983).

The classical picture of fusion has its quantal counterpart in the sharp-cut-off approximation (3.24) for the transmission coefficient in wave optics, here written as ( $l_{\text{gr}} = kb_{\text{gr}}$ )

$$T_l = \begin{cases} 1 & \text{for } l < l_{\text{gr}}, \\ 0 & \text{for } l > l_{\text{gr}}. \end{cases} \quad (9.18)$$

In the present situation formula (1.73) for the reaction cross section is identified with the fusion cross section,

$$\sigma_F(E) = \frac{\pi}{k^2} \sum_{l=0}^{\infty} (2l+1) T_l, \quad (9.19)$$

and we obtain

$$\sigma_F(E) = \frac{\pi}{k^2} \sum_{l=0}^{l_{\text{gr}}} (2l+1) = \frac{\pi}{k^2} (l_{\text{gr}} + 1)^2. \quad (9.20)$$

In the classical limit  $l_{\text{gr}} \gg 1$  this becomes

$$\sigma_F(E) = \frac{\pi}{k^2} l_{\text{gr}}^2 = \pi b_{\text{gr}}^2, \quad (9.21)$$

which agrees with eqn (9.16).

For an estimate of the grazing angular momentum as a function of mass number we go back to eqn (9.15). We introduce the ‘above-barrier energy’  $\tilde{E} = E - V_B$  and write for the reduced mass  $\mu = (A_1 A_2 / A) m_N$ , where  $m_N$  is the nucleon mass. We then find

$$l_{\text{gr}} = kb_{\text{gr}} = R_B \sqrt{\frac{2\mu\tilde{E}}{\hbar^2}} = R_B \sqrt{\frac{2m_N\tilde{E}}{\hbar^2}} \sqrt{\frac{A_1(A-A_1)}{A}} \quad (9.22)$$

where  $R_B$  is approximately equal to the sum of the radii of target and projectile. Figure 9.8 shows the grazing angular momentum as a function of projectile mass for different energies. We see that one can bring considerably more angular momentum into the compound system in collisions with heavy ions than with light ions. This is one of the features which makes collisions with heavy ions so interesting, for example, for the observation of high spin states.

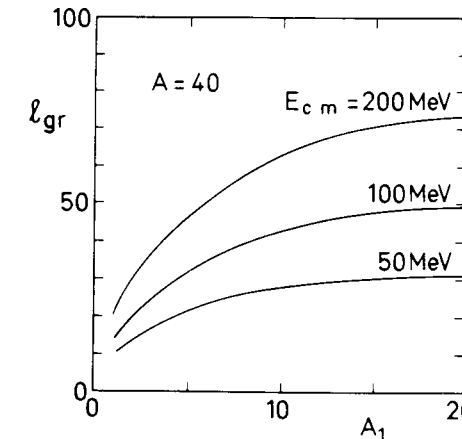


**Figure 9.8** The grazing angular momentum as a function of the projectile mass  $A_1$  for different centre-of-mass energies.

One often plots the measured fusion cross section as a function of the inverse energy  $1/E$ , because then the classical fusion cross section (9.17) is represented by a straight line. Such a plot is shown in Fig. 9.9 again for the fusion of  $^{20}\text{Ne}$  and  $^{27}\text{Al}$ . The point of intersection of the straight line with the abscissa yields the barrier height  $V_B$ . The straight line in the high-energy region does not represent the fusion cross section (cf. the

discussion after eqn (9.17)). However, by extrapolation, its point of intersection with the ordinate may be used to estimate the barrier radius  $R_B$ .

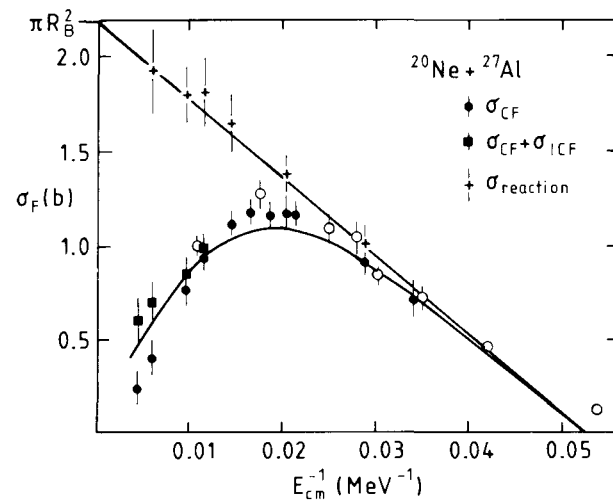


**Figure 9.9** The classical fusion cross section for the system  $^{20}\text{Ne} + ^{27}\text{Al}$  as a function of  $1/E$  (straight line) in comparison with the data of Morgenstern *et al.* (1983) (black dots) and Ngyen Van Sen *et al.* (1983) (open circles). Data are shown for the total reaction cross section  $\sigma_{\text{reaction}}$  as well as for the complete fusion cross section  $\sigma_{\text{CF}}$  and the complete-plus-incomplete fusion cross section  $\sigma_{\text{CF}} + \sigma_{\text{ICF}}$  (cf. Section 9.3.6). The solid curve represents the results of a calculation in the surface-friction model discussed in Chapter 12.

Looking at the experimental points in Fig. 9.9, we see that for low energies, to the right, there is a data point above the classical curve, while for high energies, to the left, the data points lie below it. The first effect, the rise above the classical fusion cross section at energies near the barrier, is due to quantum tunnelling, which will be discussed in Section 9.4. The second effect, the drop of the fusion cross section, has to do with the fact that at high energies other non-elastic channels besides fusion begin to be important. If the energy-independent radius  $R_B$  is interpreted simply as a radius inside of which any non-elastic process may take place (not only fusion), then the straight line represents the total reaction cross section, and therefore overestimates the cross section for fusion. The additional processes may be direct processes, like the excitation of collective modes or transfer, which will be discussed in Section 9.5. They may also be of a more complicated nature, like the deep-inelastic processes; we shall come back to this topic in Chapters 11 and 12.

### 9.3.2 Compound nucleus stability and the fusion cross section

In the previous subsection we have derived the fusion cross section under the assumption that compound-nucleus formation (fusion) occurs whenever the collision partners overlap. However, we have seen in Section 9.2 that certain conditions must be satisfied

in order that the system of overlapping nuclei is stable enough to represent a compound nucleus. The limitation of compound nucleus stability generally leads to a reduction of the fusion cross section.

#### Limitation by mass

According to Fig. 9.3 an absolute limit for the existence of a nucleus is given by the condition  $A > 300$  (cf. Section 9.2.2). This means that projectile and target cannot fuse into a compound nucleus when the latter has mass number  $A > 300$ .

It should be borne in mind, however, that this mass limitation is not very precise. On one hand, the stability criterion in Section 9.2.2 refers to spherical nuclei; deformation effects may lower the stability, especially for heavy nuclei. The heaviest naturally occurring nuclides have a mass number much smaller than 300. On the other hand, the liquid-drop model of the nucleus used in Section 9.2.2 has to be refined by taking shell effects into account (cf. Strutinsky 1967). The shell structure of the compound nucleus has a stabilizing effect, so that one cannot rigorously exclude stable nuclei with mass number  $A \gtrsim 300$ . Indeed, attempts have been made (so far without success) to produce *superheavy* nuclei with such large masses (cf. also Section 12.3.5).

#### Limitation by angular momentum

A further limitation of the formation of a compound nucleus comes from angular momentum considerations. It was shown in Section 9.2.3 that the compound nucleus becomes unstable against prompt fission for angular momenta above the critical value  $l_{\text{crit}} = l_{\text{crit}}^f$ .

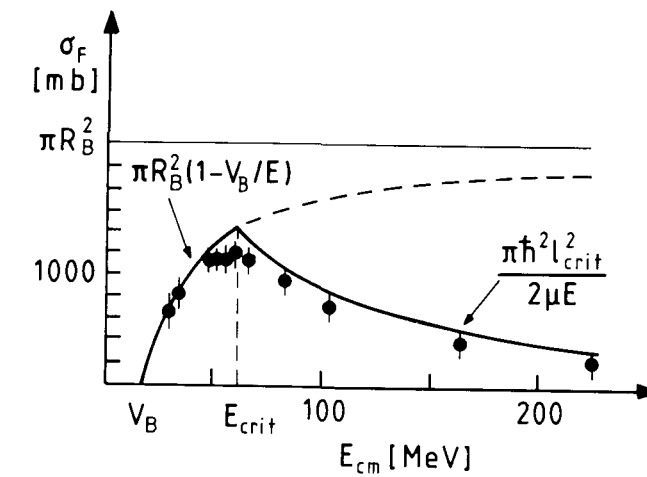


**Figure 9.10** The effect of the critical angular momentum  $l_{\text{crit}}$  on the fusion cross section. The data refer to the system  $^{20}\text{Ne} + ^{27}\text{Al}$  (cf. Morgenstern *et al.* 1983).

Therefore, only those of the trajectories reaching the interior of the nucleus actually lead to fusion whose impact parameter  $b$  is smaller than the critical value  $b_{\text{crit}} = l_{\text{crit}}/k$ . If  $b_{\text{gr}} < b_{\text{crit}}$  the cut-off of the impact parameters contributing to fusion is given by  $b_{\text{gr}}$  as

before, but if  $b_{\text{gr}} > b_{\text{crit}}$  the cut-off is provided by  $b_{\text{crit}}$ . Therefore we have

$$\sigma_F = \begin{cases} \pi b_{\text{gr}}^2 & \text{for } b_{\text{gr}} < b_{\text{crit}}, \\ \pi b_{\text{crit}}^2 & \text{for } b_{\text{gr}} > b_{\text{crit}}. \end{cases} \quad (9.23)$$

The change in regime occurs at the energy  $E_{\text{crit}}$  at which  $b_{\text{gr}} = b_{\text{crit}}$ . Instead of eqn (9.23) we can therefore write, using eqn (9.15) and  $b_{\text{crit}}^2 = l_{\text{crit}}^2/k^2 = \hbar^2 l_{\text{crit}}^2/2\mu E$ ,

$$\sigma_F = \begin{cases} \pi R_B^2(1 - V_B/E) & \text{for } E < E_{\text{crit}}, \\ \pi \hbar^2 l_{\text{crit}}^2/2\mu E & \text{for } E > E_{\text{crit}}. \end{cases} \quad (9.24)$$

This fusion cross section is plotted in Fig. 9.10 for the system  $^{20}\text{Ne} + ^{27}\text{Al}$  measured by Morgenstern *et al.* (1983). We find reasonable agreement with the data.

### 9.3.3 The yrast-line limitation

If one looks at the position of the levels of a medium-heavy or heavy nucleus in an energy-versus-spin plot (cf. Fig. 9.11), one finds that they generally lie above a line called the *yrast line* (cf. Thomas 1968; Johnson and Szymanski 1973). This is a reflection of the fact that the excitation of angular momentum is accompanied by excitation in energy, for example rotational energy, so that for a given spin  $l$  the energy cannot be lower than a minimal energy. Viewed differently, for a given energy the spin cannot be larger than a maximal spin, corresponding to a state which is *yrast* (Swedish) = ‘the most whirling’.

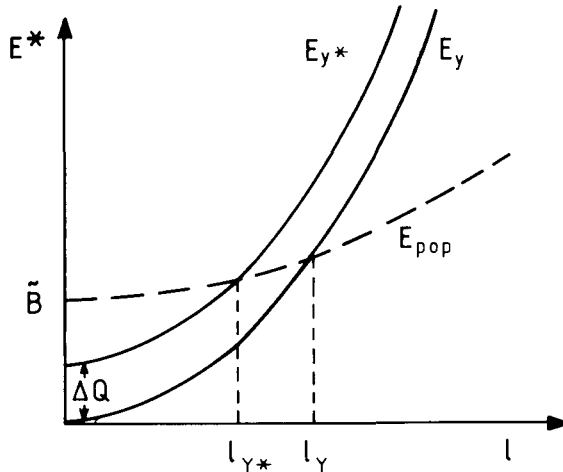


Figure 9.11 Yrast line  $E_y$ , statistical yrast line  $E_{y*}$ , and population line  $E_{\text{pop}}$ .

The yrast line is approximately described by the formula

$$E_y(l) = \frac{\hbar^2}{2\mathcal{J}} l^2, \quad (9.25)$$

where  $\mathcal{J}$  is an effective moment of inertia.

### 9.3 Fusion above the barrier

On the other hand, a compound nucleus formed from two spinless nuclei with orbital angular momentum  $l$  is excited to the *population energy*

$$E_{\text{pop}}(l) = \tilde{B} + \frac{\hbar^2}{2\mu R_C^2} l^2, \quad (9.26)$$

where  $\tilde{B}$  is the energy release defined in Section 9.2.2, and where it is assumed that the radial kinetic energy at the point of contact  $r = R_C$  is equal to zero. Since in general the latter is non-vanishing the excitation energy  $E^*$  deposited in the compound nucleus lies above the population line defined by eqn (9.26).

For a given excitation energy  $E^*$  only the angular momenta  $l$  which lie to the left of both the population and the yrast curves contribute to fusion. The fusion cross section is determined by the highest angular momentum absorbed by the compound nucleus. We have seen earlier that this is the grazing angular momentum  $l_{\text{gr}}$  or the critical angular momentum  $l_{\text{crit}}$ , whichever is lower. It now emerges that if both are larger than the angular momentum  $l_y(E^*)$  on the yrast line, it is the latter which determines the value of the fusion cross section,

$$\sigma_F = \frac{\pi \hbar^2}{2\mu E} l_y^2(E^*) = \frac{\pi \mathcal{J}}{\mu E} E^* = \frac{\pi \mathcal{J}}{\mu} \left(1 + \frac{Q}{E}\right); \quad (9.27)$$

here we have set  $E^* = E + Q$ , where  $Q$  is the  $Q$ -value for fusion.

Lee *et al.* (1980) have modified this picture somewhat by introducing the concept of a ‘statistical yrast line’ (cf. Fig. 9.11). They take account of the fact that fusion is not determined by the yrast line for ground-state nuclei, but by a curve which runs parallel to the yrast line and corresponds to compound nuclei excited to an energy  $\Delta Q$ , i.e. having a non-vanishing temperature. This is the statistical yrast line. It is described by the formula

$$E_{y*}(l) = \frac{\hbar^2}{2\mathcal{J}} l^2 + \Delta Q. \quad (9.28)$$

A new critical angular momentum  $l_{y*}$  is now defined by the crossing point of the curves  $E_{\text{pop}}(l)$  and  $E_{y*}(l)$ , and if  $\min(l_{\text{gr}}, l_{\text{crit}}) > l_{y*}$ , the value of  $l_{y*}$  determines the fusion cross section  $\sigma_F$ . We then find for the fusion cross section

$$\sigma_F = \frac{\pi \hbar^2}{2\mu E} l_{y*}^2(E^*) = \frac{\pi \mathcal{J}}{\mu} \left(1 + \frac{Q - \Delta Q}{E}\right). \quad (9.29)$$

### 9.3.4 The critical distance

There are further effects which influence the behaviour of the fusion cross section. These have to do with direct and deep-inelastic collision processes which take place during the approach phase before the actual compound-nucleus formation. They are called *entrance channel effects*. A simple phenomenological recipe for taking these into account will now be discussed.

We have so far assumed that all trajectories which are able to pass over the effective barrier lead to fusion as long as their impact parameter  $b$  satisfies  $b < \min(b_{\text{gr}}, b_{\text{crit}}, b_{y*})$  and as long as the associated effective potential has a barrier in the first place. However, it is plausible that one should regard fusion as a process which sets in only when the nuclei

have sufficient overlap, i.e. when their relative distance is smaller than some *critical distance*  $d$ , which may be appreciably smaller than the barrier radius. Trajectories which pass over the barrier but do not penetrate more closely than this critical distance would then not lead to fusion. They could, however, induce direct or deep-inelastic processes, where the collision partners are excited but keep their identity except for the possible exchange of a few nucleons.

The critical distance for fusion has been introduced as a phenomenological parameter which is assumed to be independent of energy and angular momentum (cf. Galin *et al.* 1974; Glas and Mosel 1974, 1975). Its effect on the fusion cross section can be understood from Fig. 9.12. This figure is similar to Fig. 9.6; it shows three trajectories at different energies  $E$ , and the effective potentials  $V_b(r)$  for the corresponding three

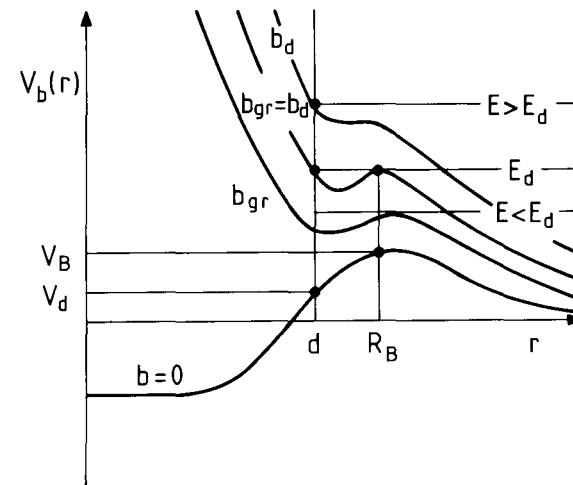


**Figure 9.12** The critical distance  $d$  and the occurrence of fusion along trajectories with three different energies.

maximum impact parameters below which fusion is possible. The energy denoted by  $E_d$  is the energy for which the effective potential  $V_b(d)$  at the critical distance  $d$  and the effective barrier height  $V_b(R_B)$  are equal. For  $E < E_d$  the former lies below the latter, and for  $E > E_d$  it lies above. In the first case the fusion cross section is determined by the grazing angular momentum  $b_{gr}$ , as in the classical model of Section 9.3.2. In the second case, the projectile overcomes the outer barrier, but fusion occurs only for impact parameters up to the value  $b_d$  for which the effective potential equals the energy  $E$  at the critical distance  $d$ ,  $V_b(d) = E$ . The value of  $b_d$  is here determined by the condition  $b_d^2 = d^2(1 - V_d/E)$ , where we have introduced the abbreviated notation  $V_d = V(d) = V_{b=0}(d)$ . The change of regime occurs at the energy  $E_d$  for which  $b_d = b_{gr}$ , or  $d^2(1 - V_d/E_d) = R_B^2(1 - V_B/E_d)$ . The fusion cross section as a function

of energy thus has the form

$$\sigma_F = \begin{cases} \pi R_B^2(1 - V_B/E) & \text{for } E < E_d, \\ \pi d^2(1 - V_d/E) & \text{for } E > E_d. \end{cases} \quad (9.30)$$

This formula is valid in the low- and intermediate-energy region. At high energies the stability or yrast-line criteria generally take over. Figure 9.13 shows the experimental fusion cross section for the system  $^{40}\text{Ar} + ^{121}\text{Sb}$  and its fit by formula (9.30).

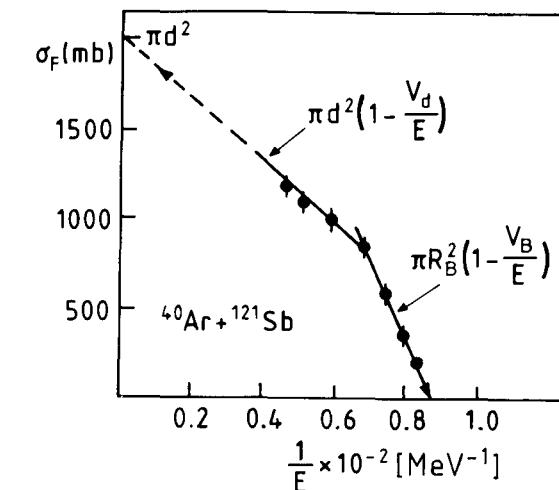


**Figure 9.13** The effect of the critical distance on the fusion cross section for the system  $^{40}\text{Ar} + ^{121}\text{Sb}$  (from Lefort and Ngô 1978).

The introduction of the critical distance is the simplest phenomenological means of taking account of the non-compound processes accompanying fusion in the entrance channel. It causes a reduction of the part of the reaction cross section leading to fusion, as the example of Fig. 9.13 shows. A more refined way of including these processes in the classical description, using trajectory models with frictional forces, will be discussed in Chapter 12.

### 9.3.5 Summary of the classical description of fusion

From the preceding discussion a few general conclusions can be drawn on the behaviour of the fusion cross section and on the type of reactions induced by two heavy ions colliding at given energy and impact parameter.

#### Energy dependence of the fusion cross section

In general, one must distinguish three regions of energy when considering the behaviour of the fusion cross section. Let us again choose  $1/E$  as the variable on the abscissa (cf. Fig. 9.14 showing the fusion cross section for the system  $^{32}\text{S} + ^{27}\text{Al}$ ).

At low energies,  $E < E_d$  (region I), we identify the fusion cross section with the total reaction cross section, which is determined by the grazing impact parameter  $b_{\text{gr}}$ ,

$$\sigma_F(E) = \pi R_B^2 \left(1 - \frac{V_B}{E}\right) \text{ for } E < E_d. \quad (9.31)$$

At higher energies,  $E_d < E < E_{\text{crit}}$  (region II), other non-elastic processes besides fusion begin to take place in the region between the barrier and the nuclear interior, with the consequence that the radius inside of which fusion alone takes place is no longer the barrier radius  $R_B$  but the smaller critical distance  $d$ . In formula (9.31) the quantities  $R_B$  and  $V_B$  must then be replaced with  $d$  and  $V_d$ ,

$$\sigma_F(E) = \pi d^2 \left(1 - \frac{V_d}{E}\right) \text{ for } E_d < E < E_{\text{crit}}. \quad (9.32)$$

At still higher energies,  $E > E_{\text{crit}}$  (region III), the fusion is limited by the critical angular momentum  $l_{\text{crit}}$  for stability against prompt fission, i.e. the fusion cross section is determined by

$$\sigma_F(E) = \frac{\pi \hbar^2}{2\mu E} l_{\text{crit}}^2 \text{ for } E > E_{\text{crit}} \quad (9.33)$$

(for some examples the yrast line limitation might be more appropriate).

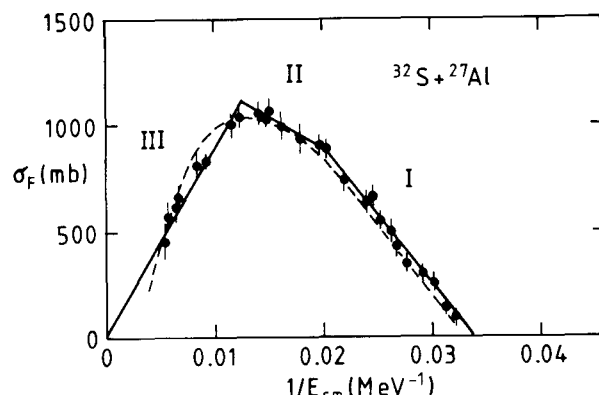


**Figure 9.14** Energy dependence of the fusion cross section for the system  ${}^{32}\text{S} + {}^{27}\text{Al}$  (after Doukellis 1988). The data are from Rosner *et al.* (1985). The dashed curve represents the results of calculations using the dynamical surface-friction model (cf. Fröbrich 1989).

The limitations of fusion discussed above derive from the properties of the compound nucleus itself (limitations of its stability by mass and angular momentum) and from the effects of the critical distance (entrance channel effects). The latter will always accompany the stability effects, and may even override them. As noted before, they have to do with the excitation of direct non-elastic and deep-inelastic processes undergone by the collision partners along their trajectories. The effect of the direct reactions will be discussed later in this chapter, while the treatment of the deep-inelastic collisions

is postponed until Chapter 12. In anticipation of the results of that chapter we remark that the dynamical friction model employed there, which is an entrance-channel model, allows for a unified description of the energy dependence of the fusion cross section in regions I–III. The result of a calculation in this model is also shown in Fig. 9.14.

### 9.3.6 A classification of nuclear reactions

In the light of the preceding discussion we can undertake a general classification of nuclear reactions (fusion reactions and others) for a system with given total mass number  $A = A_1 + A_2$  in the (impact-parameter)<sup>2</sup>-versus-energy plot shown in Fig. 9.15.

At low and medium-high energies one distinguishes three types of collisions which differ by impact parameter (or the corresponding angular momentum). The range  $b > b_{\text{gr}}$  is the region of *distant collisions* (elastic scattering and Coulomb excitation). For  $b \approx b_{\text{gr}}$  one has *grazing collisions* (direct inelastic excitations and transfer). Both the distant and the grazing collisions belong to the group of *quasi-elastic collisions*. When  $b < b_{\text{gr}}$  one observes *close collisions* (deep-inelastic scattering and fusion).

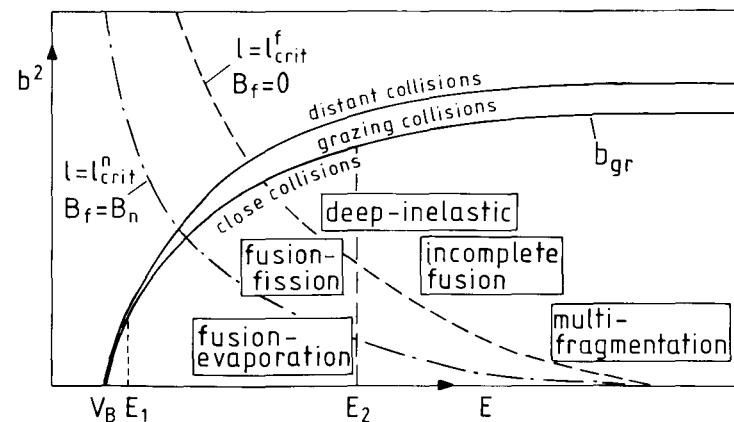


**Figure 9.15** Classification of nuclear reactions by impact parameter and energy. The dashed and dash-dotted curves represent the critical angular momenta limiting the compound nucleus stability via fission and neutron evaporation, respectively. The solid curves rising from left to right represent the limiting impact parameters for reactions (upper curve) and for fusion (lower curve) at low and intermediate energies.

Since  $b^2 = l^2/k^2 \propto l^2/E$ , a fixed angular momentum  $l$  defines a hyperbola. The two hyperbolas in the figure correspond to the two critical angular momenta  $l_{\text{crit}}^n$  and  $l_{\text{crit}}^f$  discussed in connection with Fig. 9.5. There is no restriction on fusion by angular momentum below the lower hyperbola defined by the condition  $B_f = B_n$ . The compound nuclei formed in this region will mostly decay by evaporation, resulting in the production of evaporation residues (fusion in the literal sense). Just above the lower hyperbola evaporation and fission compete, but on the way to the upper hyperbola (defined by  $B_f = 0$ ) fission quickly takes over. Above both hyperbolas the angular momentum brought in from the entrance channel is too high for producing a stable compound nucleus,

and fusion is no longer possible. Instead, deep-inelastic and (for heavy systems) fast fission processes become predominant.

The two curves rising from left to right enclose the region of grazing collisions. The upper curve (multiplied by  $\pi$ ) represents the reaction cross section  $\sigma_r$ , and the lower curve, up to energies where deep-inelastic collisions set in, represents the fusion cross section  $\sigma_F$ . The difference  $\sigma_r - \sigma_F$  is small for low energies (e.g. at  $E = E_1$ ), and therefore the fusion cross section is here well approximated by the reaction cross section. For higher energies the grazing collisions become more and more important.

At the energies exemplified by the vertical line  $E = E_2$  the trajectories with impact parameter below the curve separating the regions of close and grazing collisions lead either to fusion (if they have an impact parameter below the critical value  $l_{\text{crit}}^f/k$ ) or to deep-inelastic collisions (if not).

Up to now we have been dealing with *complete fusion*, in which the momentum of the relative motion is completely transferred to the fused system. However, at high energies (and small impact parameters), pre-compound emission of light particles and projectile break-up before fusion are observed. In these processes a compound nucleus is formed with less than the full available momentum and mass. The missing momentum is carried away by the emitted particles. We have to do with *incomplete fusion*. The contributions from these processes are identified in the data shown in Fig. 9.9. The light particles emitted in incomplete fusion have a pronounced angular distribution, in contrast to those evaporated from the completely fused compound nucleus; this is one of the features by which they can be identified. We do not discuss incomplete fusion further, but refer to a review article on this subject by Fuchs and Möhring (1994). At even higher energies multifragmentation, i.e. fragmentation into more than two heavy nuclei occurs. For review articles on this subject, cf. Gross (1990) and Moretto and Wozniak (1994).

The quasi-elastic, direct processes have been discussed in detail in previous chapters. Here and in the next chapter we treat compound-nucleus reactions, i.e. reactions proceeding via fusion. Deep-inelastic collisions are the subject of Chapters 11 and 12.

#### *The spin distribution of fusion*

It is seen from eqn (9.19) that the partial fusion cross section, i.e. the probability for compound nucleus formation as a function of the orbital angular momentum  $\hbar l$ , is given by

$$\sigma_F(l) = \frac{\pi}{k^2} (2l + 1) T_l, \quad (9.34)$$

which is called the *spin distribution* of fusion. Indeed, if the intrinsic spins of the nuclei in the entrance channel are neglected, the quantity  $\hbar l$  is the total angular momentum of the reaction, and is equal to the spin of the compound nucleus.

The sharp-cut-off model (9.18) for the transmission coefficient as a function of  $l$  implies a triangular form for the spin distribution. Figure 9.16 shows such distributions for the two energies  $E_1$  and  $E_2$  appearing in Fig. 9.15. Following the vertical lines  $E = E_1$  and  $E = E_2$  in Fig. 9.15 we see that in the first case fusion exhausts the lower part of the spin distribution up to the point of intersection with the curve representing the grazing impact parameter  $b_{\text{gr}} = b_{\text{gr}}(E)$  ( $l_{\text{gr}} = kb_{\text{gr}}$ ), and in the second case, up to

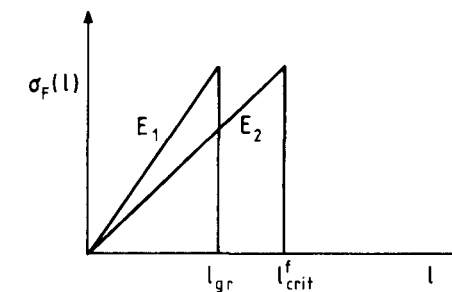


**Figure 9.16** The spin distribution of fusion in the sharp-cut-off approximation for the energies  $E_1$  and  $E_2$  indicated in Fig. 9.15. The limitation of fusion is given by the grazing angular momentum  $l_{\text{gr}}$  and the critical angular momentum  $l_{\text{crit}}^f$ , respectively.

the point of intersection with the curve labelled by the limiting angular momentum  $l_{\text{crit}}^f$ .

Realistic spin distributions are smoothed out by the quantal tunnelling effect and by the coupling to internal degrees of freedom (or by thermal fluctuations in friction models, cf. Chapter 12).

## 9.4 Sub-barrier fusion

We have so far employed purely classical concepts in order to explain the main features of the fusion cross section. In the classical picture particles approach the barrier on trajectories which either lead to fusion or do not. In terms of the transmission coefficients  $T_l$  we therefore have  $T_l = 1$  (complete transmission, i.e. fusion) or  $T_l = 0$  (no transmission, and therefore no fusion). However, at low energies quantum effects come into play and influence the behaviour of the fusion cross section. In particular, quantal tunnelling allows for *partial transmission*. In the following we treat barrier transmission as a quantum phenomenon. In order to arrive at simple explicit formulae, we work in the semiclassical approximation. We are then in a position to describe *sub-barrier fusion*, i.e. fusion at energies lower than the effective fusion barrier, which is forbidden in the purely classical picture.

### 9.4.1 The transmission coefficient in the WKB approximation

We consider one-dimensional scattering by a potential barrier at an energy lower than the barrier top (cf. Fig. 9.17). The incoming plane wave on the right (region I) is partially reflected at the turning point a; the remainder penetrates into the barrier region (II), which it leaves again at the turning point b to become the transmitted wave in region III. We neglect multiple reflections under the barrier.

The complete WKB solution is constructed by connecting the solutions in the three regions. We begin with the WKB wave function in region I and its analytic continuation into region II across the turning point a. We use the results of Section 2.3.1 and set  $l = 0$

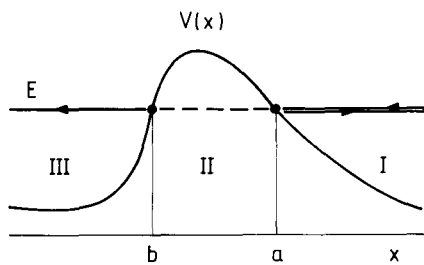


Figure 9.17 Semiclassical sub-barrier scattering.

for the present one-dimensional example. Introducing the local momentum

$$p(x) = \sqrt{2\mu[E - V(x)]}, \quad (9.35)$$

we see from eqn (2.72) that a real WKB solution in region I of the form

$$\psi_1(x) = \frac{1}{[p(x)]^{1/2}} \cos\left(\frac{1}{\hbar} \int_a^x p(x') dx' - \frac{\pi}{4}\right) \quad (\text{I}) \quad (9.36)$$

continues into region II as (cf. eqn (2.64))

$$\psi_1(x) = \frac{1}{2|p(x)|^{1/2}} e^{\frac{1}{\hbar} \int_a^x |p(x')| dx'} \quad (\text{II}) \quad (9.37)$$

The linearly independent partner to the solution (9.36) in region I is the real function

$$\psi_2(x) = \frac{1}{[p(x)]^{1/2}} \sin\left(\frac{1}{\hbar} \int_a^x p(x') dx' - \frac{\pi}{4}\right). \quad (\text{I}) \quad (9.38)$$

For this solution we have so far no analytic continuation into region II. However, we know that the general solution in region II must have the form of a real sum of the function (9.37) and its linearly independent partner

$$\psi_2(x) = \frac{C}{2|p(x)|^{1/2}} e^{-\frac{1}{\hbar} \int_a^x |p(x')| dx'}, \quad (\text{II}) \quad (9.39)$$

where the real constant  $C$  remains to be determined. Since the function (9.37) is already the continuation of the function (9.36), the continuation of the function (9.38) into region II must be the function (9.39) itself.

In order to determine the constant  $C$ , we make use of the fact (cf. Landau and Lifshitz 1965, §50) that the Wronskian

$$W[\psi_1, \psi_2] = \psi_1 \psi'_2 - \psi'_1 \psi_2 \quad (9.40)$$

of two solutions  $\psi_1$  and  $\psi_2$  of the same Schrödinger equation at the same energy is a constant. This follows from

$$W'[\psi_1, \psi_2] = \psi_1 \psi''_2 - \psi''_1 \psi_2 = 0,$$

which is proved by expressing the second derivatives of the wave functions in terms of the wave functions themselves with the help of the Schrödinger equation. Thus the Wronskians of the wave functions  $\psi_1$  and  $\psi_2$  in the regions I and II are the same (and constant),

$$W[\psi_1, \psi_2]_{\text{I}} = W[\psi_1, \psi_2]_{\text{II}}. \quad (9.41)$$

Substituting the expressions (9.36) to (9.39) in this relation, we find for the constant  $C$  the value

$$C = -2. \quad (9.42)$$

Let us now consider the continuation across the other turning point,  $b$ . Here the barrier region lies to the right, whereas it was situated to the left in the previous discussion. The wave functions to the left and right of such a turning point are obtained by reflecting the previous results in the turning point,  $(x - a) \rightarrow (a - x)$ . This reverses the barrier, and the only change in the wave functions is the reversal of the limits of the integrals. Renaming the turning point, we obtain the desired connections across the turning point  $b$ . Thus we find from eqns (9.37) and (9.36), respectively,

$$\psi_3(x) = \frac{1}{2|p(x)|^{1/2}} e^{\frac{1}{\hbar} \int_x^b |p(x')| dx'}, \quad (\text{II}) \quad (9.43)$$

$$\psi_3(x) = \frac{1}{[p(x)]^{1/2}} \cos\left(\frac{1}{\hbar} \int_x^b p(x') dx' - \frac{\pi}{4}\right), \quad (\text{III}) \quad (9.44)$$

and from eqns (9.39), (9.42), and (9.38)

$$\psi_4(x) = \frac{-1}{|p(x)|^{1/2}} e^{-\frac{1}{\hbar} \int_x^b |p(x')| dx'}, \quad (\text{II}) \quad (9.45)$$

$$\psi_4(x) = \frac{1}{[p(x)]^{1/2}} \sin\left(\frac{1}{\hbar} \int_x^b p(x') dx' - \frac{\pi}{4}\right). \quad (\text{III}) \quad (9.46)$$

For the scattering situation in Fig. 9.17 the wave function in region III must be purely outgoing. This is achieved by writing it as the following linear combination of solutions  $\psi_3$  and  $\psi_4$ ,

$$\begin{aligned} \psi_{\text{III}}^{(\text{out})}(x) &= \psi_3 + i\psi_4 \\ &= \frac{1}{[p(x)]^{1/2}} e^{i[\frac{1}{\hbar} \int_x^b p(x') dx' - \frac{\pi}{4}]}. \end{aligned} \quad (\text{III}) \quad (9.47)$$

Asymptotically this is an outgoing wave

$$\psi_{\text{III}}^{(\text{out})}(x) \rightarrow \frac{1}{(\hbar k)^{1/2}} e^{-ikx+i\beta} \quad \text{for } x \rightarrow -\infty, \quad (\text{III}) \quad (9.48)$$

where  $\beta$  is some constant real phase.

For the continuation of the function (9.47) into the region II we find, using eqns (9.43) and (9.45),

$$\begin{aligned} \psi_{\text{II}}(x) &= \psi_3(x) + i\psi_4 \\ &= \frac{1}{|p(x)|^{1/2}} \left( \frac{1}{2} e^{\frac{1}{\hbar} \int_x^b |p(x')| dx'} - i e^{-\frac{1}{\hbar} \int_x^b |p(x')| dx'} \right). \end{aligned} \quad (\text{II}) \quad (9.49)$$

In order to proceed further toward the region I, we express this function as a linear combination of the functions  $\psi_1(x)$  and  $\psi_2(x)$ . To this end we first rewrite the exponentials on the right-hand side of eqn (9.49),

$$e^{\pm\frac{1}{\hbar}\int_x^b|p(x')|dx'} = e^{\mp\frac{1}{\hbar}\int_b^a|p(x')|dx'} e^{\mp\frac{1}{\hbar}\int_a^x|p(x')|dx'}. \quad (9.50)$$

Then it is seen from eqns (9.37), (9.39), (9.42), and (9.49) that the expression

$$\psi_{II}(x) = -2ie^{\frac{1}{\hbar}\int_b^a|p(x')|dx'}\psi_1(x) - \frac{1}{2}e^{-\frac{1}{\hbar}\int_b^a|p(x')|dx'}\psi_2(x) \quad (\text{II}) \quad (9.51)$$

is the desired combination. The continuation of the function (9.51) into the region I is now effected via the functions  $\psi_1(x)$  and  $\psi_2(x)$  using eqns (9.36) and (9.38), and yields

$$\begin{aligned} \psi_1(x) &= \frac{1}{[p(x)]^{1/2}} \left[ -2ie^{\frac{1}{\hbar}\int_b^a|p(x')|dx'} \cos\left(\frac{1}{\hbar}\int_a^x p(x')dx' - \frac{\pi}{4}\right) \right. \\ &\quad \left. - \frac{1}{2}e^{-\frac{1}{\hbar}\int_b^a|p(x')|dx'} \sin\left(\frac{1}{\hbar}\int_a^x p(x')dx' - \frac{\pi}{4}\right) \right]. \quad (\text{I}) \end{aligned} \quad (9.52)$$

In this expression the cosine term with the positive exponent in the coefficient predominates over the sine term; we therefore keep only the former. Decomposing this term into incoming and outgoing parts, we find that the incoming part propagating from right to left has the form

$$\psi_1^{(\text{in})} = \frac{1}{i[p(x)]^{1/2}} e^{\frac{1}{\hbar}\int_b^a|p(x')|dx'} e^{-i[\frac{1}{\hbar}\int_a^x p(x')dx' - \frac{\pi}{4}]}. \quad (\text{I}) \quad (9.53)$$

The transmission coefficient is given by the ratio of the absolute squares of the outgoing wave (9.47) in region III and the ingoing wave (9.53) in region I,

$$T = \frac{|\psi_{III}^{(\text{out})}|^2}{|\psi_1^{(\text{in})}|^2}, \quad (9.54)$$

which yields for the *transmission coefficient in the WKB approximation*

$$T = \exp\left(-\frac{2}{\hbar}\int_b^a|p(x')|dx'\right), \quad (9.55)$$

where the function  $p(x)$  is given by eqn (9.35).

Expression (9.55) is only valid at energies well below the barrier top, since only then are the two turning points far apart from each other so that one can treat them separately, as we have done. On the other hand, for energies above the barrier top there are no (real) turning points; the WKB transmission coefficient is therefore set equal to unity,  $T = 1$ .

The transmission near the barrier top has been treated semiclassically by Brink and Smilansky (1983), who sum up the contributions of the multiple reflections of the trajectories under the barrier with proper account of the phases. Alternatively, one can apply the full quantum theory. We shall do this in the following, simplifying the barrier to a parabola.

#### 9.4.2 Tunnelling through a parabolic barrier

We consider a potential barrier of the form of an inverted parabola (cf. Kemble 1935; Hill and Wheeler 1953; Landau and Lifshitz 1965, §50),

$$V(x) = V_B - \frac{1}{2}\mu\omega^2x^2, \quad (9.56)$$

for which the Schrödinger equation reads

$$\left(-\frac{\hbar^2}{2\mu}\frac{d^2}{dx^2} + V_B - \frac{1}{2}\mu\omega^2x^2\right)\psi = E\psi. \quad (9.57)$$

With  $\xi = x(\mu\omega/\hbar)^{1/2}$  and  $\epsilon = (E - V_B)/\hbar\omega$  this equation can be written as

$$\left(-\frac{d^2}{d\xi^2} - \xi^2\right)\psi = 2\epsilon\psi. \quad (9.58)$$

We are interested in the asymptotic behaviour of the wave function for which we may use an ansatz of the WKB form (2.62), which in the present variable is given by

$$\psi_{\pm}(\xi) = \frac{1}{[\pi(\xi)]^{1/2}} e^{\pm i\int^{\xi}\pi(\xi')d\xi'}, \quad (9.59)$$

where

$$\pi(\xi) = \sqrt{2\epsilon + \xi^2} \rightarrow \xi + \frac{\epsilon}{\xi} \quad \text{for } |\xi| \rightarrow \infty. \quad (9.60)$$

Substituting this expression in the asymptotic wave function (9.59), we find for the latter

$$\psi_{\pm}(\xi) = e^{\pm i\xi^2/2}\xi^{\pm i\epsilon - 1/2} \quad \text{for } |\xi| \rightarrow \infty. \quad (9.61)$$

Since the potential (9.56) does not vanish in the asymptotic region (it becomes arbitrarily large negative), the asymptotic wave functions (9.61) are not plane waves. However, their probability current densities are constant, and are given by

$$j_{\pm}(\xi) = \frac{\hbar}{2\mu i}(\psi_{\pm}^*\psi'_{\pm} - \psi_{\pm}^{*\prime}\psi_{\pm}) \rightarrow \pm \frac{\hbar}{\mu} \frac{\xi}{|\xi|} \quad \text{for } |\xi| \rightarrow \infty. \quad (9.62)$$

Let us consider the signs of  $j_{\pm}(\xi)$ . For  $\xi > 0$  as well as for  $\xi < 0$ , the plus sign corresponds to waves which leave the barrier region either to the right or the left, whereas the minus sign characterizes waves which enter the barrier region, again from either side. The scattering situation of Fig. 9.17 is therefore described by the wave function

$$\psi(\xi) = e^{-i\xi^2/2}\xi^{-i\epsilon - 1/2} + \mathcal{R}e^{i\xi^2/2}\xi^{i\epsilon - 1/2} \quad \text{for } \xi \rightarrow \infty \quad (9.63)$$

on the right, and by the wave function

$$\psi(\xi) = \mathcal{T}e^{i\xi^2/2}|\xi|^{i\epsilon - 1/2} \quad \text{for } \xi \rightarrow -\infty \quad (9.64)$$

on the left. The coefficients  $\mathcal{R}$  and  $\mathcal{T}$  are the reflection and transmission factors. They are determined by connecting the functions (9.63) and (9.64) via analytic continuation in the complex  $\xi$ -plane (cf. Fig. 9.18).

First we continue the function (9.63) along the large circle on the right down to a point P in the lower-right quadrant ( $\xi = Re^{-i\pi/4}$  with  $R \rightarrow \infty$ ), as indicated in the

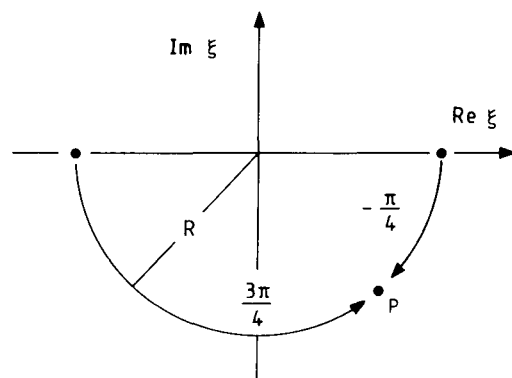


**Figure 9.18** Analytic continuation of the transmitted wave function in the complex  $\xi$ -plane.

figure. The second term predominates over the first term, which is exponentially damped in the lower half-plane, so that at this point we can set the function (9.63) equal to the second term alone.

We also continue the solution (9.64) to the point P along the circle on the left ( $\xi = Re^{i3\pi/4}$ ) and set the functions (9.63) and (9.64) equal to each other,

$$\mathcal{R} e^{R^2/2} (Re^{-i\pi/4})^{i\epsilon-1/2} = T e^{R^2/2} (Re^{i3\pi/4})^{i\epsilon-1/2}, \quad (9.65)$$

or

$$\mathcal{R} = -ie^{-\pi\epsilon} T. \quad (9.66)$$

By flux conservation we have

$$|\mathcal{T}|^2 + |\mathcal{R}|^2 = 1, \quad (9.67)$$

which, together with eqn (9.66), yields the transmission coefficient

$$T = |\mathcal{T}|^2 = \frac{1}{1 + \exp(-2\pi\epsilon)} \quad (9.68)$$

or

$$T = T(E) = \frac{1}{1 + \exp[2\pi(V_B - E)/\hbar\omega]}. \quad (9.69)$$

This formula is an exact quantum result and holds for all energies, and thus also for  $E = V_B$ , i.e. at the barrier top.

#### The Hill–Wheeler formula

The WKB approximation of the transmission coefficient for the parabolic barrier is obtained by noting that well below the barrier top, where  $T \ll 1$ , the exact solution goes over into its WKB form. Thus we find

$$T^{\text{WKB}}(E) = e^{-2\pi(V_B-E)/\hbar\omega}, \quad (9.70)$$

and the exact transmission coefficient can be written as

$$T = \frac{T^{\text{WKB}}}{1 + T^{\text{WKB}}}. \quad (9.71)$$

This formula has been derived for the special case of a parabolic barrier. We note that precisely at the barrier top, where  $E = V_B$ , the WKB transmission coefficient is equal to unity, whereas the exact value given by eqn (9.71) is  $\frac{1}{2}$ .

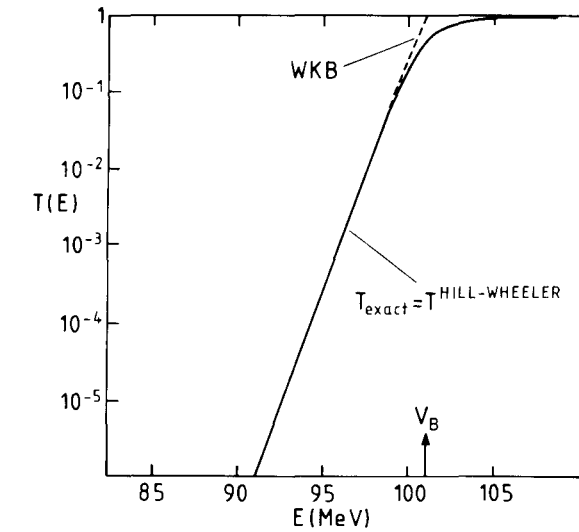


**Figure 9.19** The exact quantal transmission coefficient  $T(E)$  for the Eckart potential in comparison with the WKB and Hill–Wheeler results for the system  $^{58}\text{Ni} + ^{58}\text{Ni}$  (cf. Fröbrich *et al.* 1990).

Near the barrier top any physically reasonable potential can be approximated by a parabola,

$$V(x) \approx V_B + \frac{1}{2} \left. \frac{d^2 V}{dx^2} \right|_{x_B} (x - x_B)^2, \quad (9.72)$$

where  $V_B$  is the height of the barrier, and  $x_B$  its position. Comparison with eqn (9.56) shows that near the barrier the potential can be replaced with a parabolic potential with the curvature (oscillator frequency)

$$\omega_B^2 = - \left. \frac{1}{\mu} \frac{d^2 V}{dx^2} \right|_{x_B} > 0. \quad (9.73)$$

Then one may apply formula (9.71) also to general barriers. It extrapolates the WKB transmission coefficient, which is valid only well below the barrier top, into the region around and above the barrier top. The explicit expression (9.69) for the transmission coefficient, with  $\omega$  replaced by  $\omega_B$  of formula (9.73), thus becomes the *Hill–Wheeler*

formula (cf. Hill and Wheeler 1953)

$$T(E) = \frac{1}{1 + \exp[2\pi(V_B - E)/\hbar\omega_B]}. \quad (9.74)$$

Figure 9.19 shows the exact quantal transmission coefficient for the Eckart potential (cf. Landau and Lifshitz 1965, §25)

$$V(x) = \frac{V_B}{\cosh^2(ax)} \quad (9.75)$$

with  $V_B = 101$  MeV and  $a = 3.4$  fm (these parameters are appropriate for the fusion of  $^{58}\text{Ni} + ^{58}\text{Ni}$ ) in comparison with the WKB and Hill–Wheeler results. It is seen that the Hill–Wheeler formula reproduces the exact curve within the line thickness, whereas the WKB is a good solution only well below the barrier. The barrier (9.75) is symmetric; for unsymmetric barriers the agreement between the Hill–Wheeler and the exact results is not as good.

#### 9.4.3 Semiclassical transmission in nuclear fusion

##### Partial-wave transmission coefficients

The preceding results have been derived for transmission in *one* dimension. Actual nuclear fusion takes place in three-dimensional space; however, since the fusion cross section is given by the sum (9.19) over the *partial-wave transmission coefficients*  $T_l$ , the one-dimensional results can be made use of by applying them to the barrier transmission in the radial variable  $r$ .

The transmission coefficient  $T_l$  is associated with the effective potential  $V_l(r)$  of eqn (2.47). The Hill–Wheeler formula (9.74) for this potential yields

$$T_l(E) = \frac{1}{1 + \exp[2\pi[V_B + \hbar^2 l(l+1)/2\mu R_B^2 - E]/\hbar\omega_B]}, \quad (9.76)$$

where

$$\omega_B^2 = \left| \frac{1}{\mu} \frac{d^2}{dr^2} \left( V(r) + \frac{\hbar^2 l(l+1)}{2\mu r^2} \right) \right|_{R_B}. \quad (9.77)$$

The parameters  $R_B$ ,  $V_B$ , and  $\omega_B$  depend only weakly on  $E$  and  $l$ , in particular for heavy systems.

##### The Wong formula

Substituting the transmission coefficients (9.76) in the partial-wave expansion (9.19) of the fusion cross section we can derive an analytic formula for the latter. We assume that only the  $l$ -dependence displayed explicitly in expression (9.76) has to be taken into account, and write

$$\begin{aligned} \sigma_F(E) &= \frac{\pi}{k^2} \sum_{l=0}^{\infty} (2l+1) T_l(E) \\ &\approx \frac{2\pi}{k^2} \int_0^{\infty} \frac{l dl}{1 + \exp[2\pi[V_B + \hbar^2 l^2/2\mu R_B^2 - E]/\hbar\omega_B]}. \end{aligned} \quad (9.78)$$

With the substitutions  $y = l^2$ ,  $a = \exp[2\pi(V_B - E)/\hbar\omega_B]$  and  $b = \pi\hbar/\mu R_B^2 \omega_B$  we obtain

$$\sigma_F(E) = \frac{\pi}{k^2} \int_0^{\infty} \frac{dy}{1 + a \exp(by)} = \frac{\pi}{k^2 b} \ln\left(1 + \frac{1}{a}\right). \quad (9.79)$$

Going back to the original parameters, we arrive at the *Wong formula* for the fusion cross section (cf. Wong 1973),

$$\sigma_F(E) = \frac{\hbar\omega_B R_B^2}{2E} \ln\{1 + \exp[2\pi(E - V_B)/\hbar\omega_B]\}. \quad (9.80)$$

The fusion cross section is determined by three parameters, the barrier height  $V_B$ , the barrier radius  $R_B$ , and the curvature  $\hbar\omega_B = \hbar\sqrt{|V''_B|}/\mu$ .

At high energies the exponential in the argument of the logarithm in expression (9.80) is much larger than unity, and the formula reverts to the classical result (9.31). At low energies, appreciably below the barrier height  $V_B$ , the exponential term is small; one can expand the logarithm and obtains an exponential energy dependence. Thus we have

$$\sigma_F(E) = \begin{cases} \pi R_B^2 [1 - (V_B/E)] & \text{for } E > V_B, \\ (\hbar\omega_B R_B^2/2E) \exp[-2\pi(V_B - E)/\hbar\omega_B] & \text{for } E < V_B. \end{cases} \quad (9.81)$$

Fusion cross sections calculated with the help of the Wong formula are shown in Fig. 9.20.

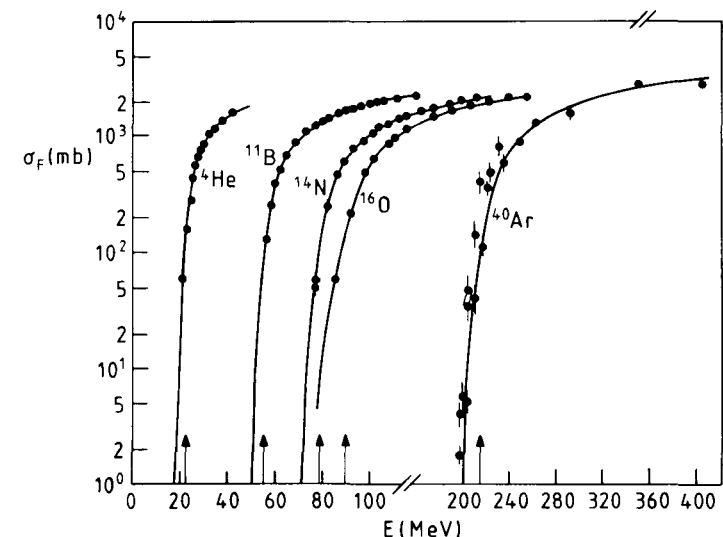


**Figure 9.20** Cross sections for the fusion of  $^4\text{He}$ ,  $^{11}\text{B}$ ,  $^{14}\text{N}$ ,  $^{16}\text{O}$ , and  $^{40}\text{Ar}$  with  $^{238}\text{U}$  calculated with the help of the Wong formula in comparison with experimental data (cf. Wong 1973). The arrows indicate the barrier energies  $V_B$ .

#### 9.4.4 Quantal barrier penetration

##### The ingoing-wave boundary condition

In the preceding section we have derived the semiclassical partial-wave transmission coefficients  $T_l$  in analytic form. For a truly quantal calculation of these quantities one must take recourse to numerical methods. One solves the Schrödinger equation for the effective potential  $V_l(r)$  with the boundary condition that on the inner (left-hand) flank of the effective barrier the wave moves away from the barrier toward the centre of the nucleus (cf. Fig. 9.17). This is the method of the *ingoing-wave boundary condition* (cf. Rawitscher 1963 and references therein). On the outer (right-hand) flank the wave has ingoing as well as reflected components. The absolute square of the ratio of the amplitude of the inner-flank wave over that of the outer-flank ingoing wave yields the transmission coefficient  $T_l$ .

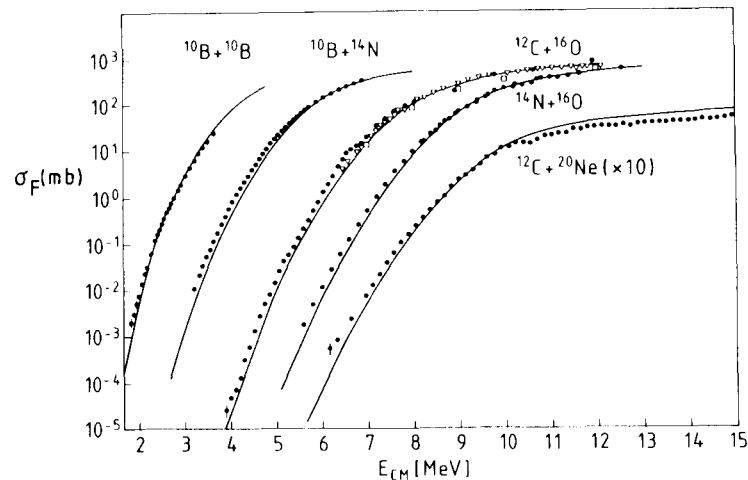


**Figure 9.21** Fusion cross sections for light nuclei calculated in the barrier-penetration model in comparison with experimental data (cf. Krappe *et al.* 1983).

Calculating the transmission coefficient with the help of the ingoing-wave boundary condition amounts to solving the one-dimensional potential scattering problem of quantum mechanics (cf. Messiah 1972, Chapter III, §11). In the latter problem the boundary condition for the transmitted wave is actually applied ‘at  $-\infty$ ’, whereas in the ingoing-wave boundary condition model the matching occurs inside the nucleus just after the barrier has been passed. However, since the shape of the barrier in the region of the transmitted wave has practically no effect on the transmission probability, any reasonable extrapolation of it can be used to extend the transmission problem to  $-\infty$ . Fusion cross sections calculated in such a quantal barrier penetration model are shown in Figs. 9.21 for light nuclei (cf. Krappe *et al.* 1983). It is seen that the data are well reproduced.

The requirement of a purely ingoing wave on the inner flank of the effective barrier can also be fulfilled by introducing a strongly absorptive, imaginary potential in the interior region of the nucleus, which extends out to a radius about equal to the critical distance  $d$  introduced in Section 9.3.4. Such a potential absorbs all the current transmitted across the barrier, and thus effectively converts the wave on the inside of the barrier into a purely ingoing one.

##### Transmission coefficients and barrier penetrability

The possibility of using an absorptive potential in the description of transmission through a barrier leads us to a more general discussion of the meaning of the transmission coefficients.

In Section 1.2.3 we have discussed quantal absorption in terms of the transmission coefficients  $T_l$ . They were introduced as the ratio of the absorbed over the incoming current in the  $l$ -th partial wave, and were calculated by taking the integral of the imaginary part of the optical potential multiplied by the partial-wave density (cf. eqn (1.65)). A classical trajectory absorbed in the nuclear interior corresponds quantally to a situation where the wave function reaches into the region inside the nucleus behind the barrier and ‘feels’ an imaginary potential there which is so strong that the current is completely absorbed. In this case the value of the coefficient  $T_l$  depends only on the extent to which the barrier, i.e. the *real* potential, allows the wave function to reach the interior. Here the coefficient  $T_l$  is indeed a *transmission* coefficient in the sense that it represents the *barrier penetrability*. In the classical picture this penetrability is equal either to one or zero. But in the semiclassical approximation or in rigorous quantum theory, partial transmission (tunnelling) is possible below the barrier top, while the above-barrier transmission is reduced, corresponding to the smooth-cut-off model discussed in Section 3.4. The coefficient  $T_l$  then still describes transmission alone. This is the *barrier penetration model* for sub-barrier fusion.

The situation is different when the absorption inside the nucleus behind the barrier is *not* complete. Then the coefficient  $T_l$  depends on both the barrier penetrability and the strength of the absorption. If transmission and absorption are spatially separated because the imaginary part of the optical potential lies outside the barrier, i.e. in region III of Fig. 9.17, the coefficient  $T_l$  is the product of the barrier penetrability  $P_l(\text{II})$  across region II and a factor  $A_l(\text{III})$  describing absorption in region III,

$$T_l = P_l(\text{II}) A_l(\text{III}). \quad (9.82)$$

When the imaginary part of the optical potential reaches over into the region II below the barrier, transmission and absorption overlap. In this case the coefficient  $T_l$  as we define it in this book yields correctly the probability for the overall *absorption* of the partial wave with angular momentum  $l$ , but ceases to describe the transmission (= penetrability) alone, although the traditional notation  $T_l$  for it may suggest this.

##### Failure of one-dimensional barrier penetration models

We have assumed so far that fusion, that is absorption, occurs in the elastic channel. In this case the only dynamical variable in the problem is the distance between the two fusing nuclei, for which reason this is sometimes called the *one-dimensional description*.

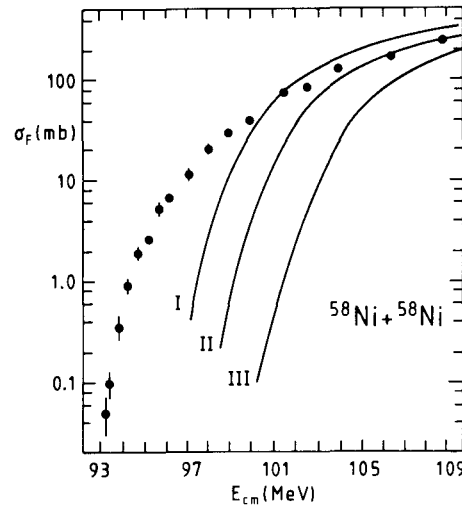


**Figure 9.22** Fusion cross section for the system  $^{58}\text{Ni} + ^{58}\text{Ni}$  calculated in the one-dimensional barrier-penetration model. Different potentials were used: (I) Bass (1980), (II) Krappe *et al.* (1979), and (III) the proximity potential of Blocki *et al.* (1977). The dots represent the experimental data of Beckerman (1985).

The one-dimensional barrier penetration model, semiclassical or quantal, is adequate for light systems. However, this is no longer so in the case of heavier systems. Figure 9.22 shows the results of ‘one-dimensional’ barrier penetration calculations for the system  $^{58}\text{Ni} + ^{58}\text{Ni}$ . Here the experimental data cannot be fitted no matter which potential is used. The reason for this failure is that an increasing number of non-elastic channels have to be taken into account for heavier systems, giving rise to a behaviour of the fusion cross section which cannot be reproduced by the one-dimensional model. This will be discussed in the next section.

## 9.5 Fusion in the presence of nuclear excitations

As two fusing nuclei approach each other, they will in general undergo transitions from the ground state to excited states and transfer particles between themselves, before coming close enough to form a compound nucleus. The elastic channel couples to non-elastic channels, and the transmission across the barrier takes place in each of these channels as well. The situation for two channels is illustrated in Fig. 9.23. The incoming wave splits up into various inelastic waves with different transmission probabilities  $T_n$ , which have to be combined in order to obtain the total transmission into the interior of the compound system.

Since the channel energy in the non-elastic channels is lower than in the elastic channel, implying smaller transmission coefficients, one expects to find a lower total

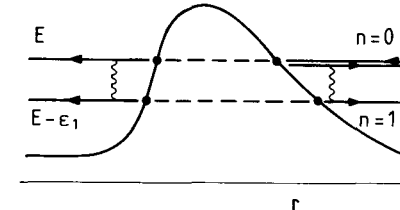


**Figure 9.23** Schematic illustration of fusion in two channels. The interior of the nucleus is to the left.

transmission for the coupled system. On the other hand, the interactions which are responsible for the coupling also contribute to the effective barriers in the various channels, with the net effect of lowering them, as we shall see. This would lead to an enhancement of the transmission coefficient. Only a detailed calculation can establish definitely which effect is stronger.

In the present chapter we consider only fusion at energies below and slightly above the barrier. At energies high above the barrier so many channels become involved that it is no longer possible to treat them individually. Here the energy loss and not the coupling interaction is the determining factor, and will be treated in a friction model in Chapter 12.

For simplicity we consider only the coupling to inelastic channels, that is, we ignore rearrangement processes such as transfer. Recalling the discussion of coupled channels in Section 8.2, we supplement the barrier potential  $V_0(r)$  in the relative distance  $r$  with an internal Hamiltonian  $h(\xi)$  for the target nucleus (it is straightforward to include projectile excitations as well), where  $\xi$  stands for the internal dynamical variables. We further add a term  $V_{\text{coup}}(\mathbf{r}, \xi)$  coupling the relative motion and the internal degrees of freedom. Then the total Hamiltonian is

$$H = -\frac{\hbar^2}{2\mu} \nabla^2 + h(\xi) + V_0(r) + V_{\text{coup}}(\mathbf{r}, \xi). \quad (9.83)$$

The Schrödinger equation for the total wave function  $\Psi_a(\mathbf{r}, \xi)$  has the form

$$\left( -\frac{\hbar^2}{2\mu} \nabla^2 + h(\xi) + V_0(r) + V_{\text{coup}}(\mathbf{r}, \xi) \right) \Psi_a(\mathbf{r}, \xi) = E \Psi_a(\mathbf{r}, \xi). \quad (9.84)$$

As in Section 8.2.1 we introduce the internal eigenstates  $\phi_b(\xi)$  with eigenenergies  $\epsilon_b$  and the coupling matrix elements

$$V_{bc}(\mathbf{r}) = \int d\xi \phi_b^*(\xi) V_{\text{coup}}(\mathbf{r}, \xi) \phi_c(\xi). \quad (9.85)$$

The total wave function  $\Psi_a(\mathbf{r}, \xi)$  is expanded in the form

$$\Psi_a(\mathbf{r}, \xi) = \sum_b \psi_{ab}(\mathbf{r}) \phi_b(\xi). \quad (9.86)$$

From the Schrödinger equation (9.84) we derive coupled-channel equations (cf. eqn (8.9))

$$\left( -\frac{\hbar^2}{2\mu} \nabla^2 + V_0(r) + V_{bb}(r) + \epsilon_b - E \right) \psi_b(\mathbf{r}) = - \sum_{c(c \neq b)} V_{bc}(\mathbf{r}) \psi_c(\mathbf{r}) \quad (9.87)$$

for the channel wave functions  $\psi_b(\mathbf{r}) = \psi_{ab}(\mathbf{r})$  (we leave out the index of the incoming channel  $a$ ). This system of coupled Schrödinger equations is to be solved subject to the boundary condition that the solution in the incident channel is composed of an ingoing and an outgoing wave, while all other channels contain only outgoing waves.

As in the case of one-dimensional fusion, the absorption in the interior of the nucleus is either effected by an ingoing-wave boundary condition in all channels, or by a strong imaginary potential.

### 9.5.1 A schematic two-channel model

The essential physical features of channel coupling can be studied in the model of two s-wave channels ( $l=0$ ) discussed by Dasso *et al.* (1983). The channel energies are  $\mathcal{E}_b = E - \epsilon_b$  for  $b = 0$  (the elastic channel) and  $b = 1$  (the inelastic channel). We further set  $V_{11}(r) = V_{00}(r)$ ,  $V_{01}(r) = V_{10}(r) = F(r)$ , and  $V_0(r) + V_{00}(r) = V(r)$ . The coupled-channel system (9.87) then reduces to the two equations

$$\begin{aligned} \left( -\frac{\hbar^2}{2\mu} \frac{d^2}{dr^2} + V(r) - \mathcal{E}_0 \right) \psi_0(r) &= -F(r) \psi_1(r), \\ \left( -\frac{\hbar^2}{2\mu} \frac{d^2}{dr^2} + V(r) - \mathcal{E}_1 \right) \psi_1(r) &= -F(r) \psi_0(r). \end{aligned} \quad (9.88)$$

The incoming wave function in the elastic channel gives rise to reflected and transmitted waves in the elastic and inelastic channels with wave numbers  $k_0^2 = 2\mu\mathcal{E}_0/\hbar^2$  and  $k_1^2 = 2\mu\mathcal{E}_1/\hbar^2$ , respectively (cf. Fig. 9.23). The asymptotic form of the solution is, in accordance with eqns (8.23) and (8.29), for  $b = 0, 1$  (we disregard Coulomb effects),

$$\psi_b(r) \rightarrow \delta_{b0} \sin(k_b r) + \sqrt{\frac{k_0}{k_b}} \frac{1}{2i} (S_{b0} - \delta_{b0}) e^{ik_b r} \quad \text{for } r \rightarrow \infty. \quad (9.89)$$

Here  $S_{b0}$  is the S-matrix element for the transition from the elastic channel 0 to channel  $b$ , in terms of which the total transmission coefficient is given by

$$T = 1 - \sum_b |S_{b0}|^2. \quad (9.90)$$

We now take recourse to the *sudden approximation*, where one assumes that the relative motion is much faster than the internal one. This implies that one may set the internal energies equal to zero,  $\epsilon_b = 0$  so that  $\mathcal{E}_0 = \mathcal{E}_1 = E$  and  $k_0 = k_b = k$ .

Adding and subtracting the equations (9.88) we obtain the decoupled *eigenchannel* equations

$$\left( -\frac{\hbar^2}{2\mu} \frac{d^2}{dr^2} + V(r) \pm F(r) - E \right) \psi^{[\pm]}(r) = 0. \quad (9.91)$$

for the eigenchannel wave functions

$$\psi^{[\pm]}(r) = \psi_0(r) \pm \psi_1(r). \quad (9.92)$$

These have the asymptotic behaviour

$$\psi^{[\pm]}(r) \rightarrow \delta_{b0} \sin(kr) + \frac{1}{2i} (S_{\pm} - 1) e^{ikr} \quad \text{for } r \rightarrow \infty, \quad (9.93)$$

and the corresponding transmission coefficients are

$$T_{\pm} = 1 - |S_{\pm}|^2. \quad (9.94)$$

Transforming back to the physical channel wave functions  $\psi_{0,1}$  we find

$$\begin{aligned} S_{00} &= \frac{1}{2} (S_+ + S_-), \\ S_{10} &= \frac{1}{2} (S_+ - S_-). \end{aligned} \quad (9.95)$$

The total transmission coefficient is then given by

$$T = 1 - |S_{00}|^2 - |S_{10}|^2 = 1 - \frac{1}{2} (|S_+|^2 + |S_-|^2), \quad (9.96)$$

or

$$T = \frac{1}{2} (T_+ + T_-). \quad (9.97)$$

It is seen from eqn (9.91) that for  $F(r) > 0$  the transmission coefficient  $T_{\pm}$  is associated with a barrier  $V(r) \pm F(r)$  which is higher (lower) than the bare barrier  $V(r)$  in the uncoupled elastic channel (if  $F(r) < 0$ , the roles of  $T_+$  and  $T_-$  are interchanged). The transmission coefficients  $T_{\pm}$  thus have the behaviour shown in Fig. 9.24 together with that of the bare transmission coefficient  $T^{\text{bare}}$ , for which  $F(r) = 0$ . We see that

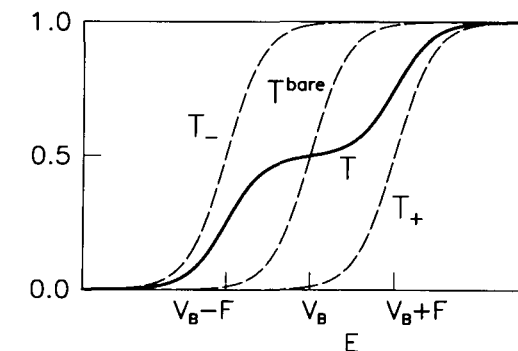


**Figure 9.24** Transmission coefficients in the two-channel model. The coefficients  $T_{\pm}$  and  $T^{\text{bare}}$  are represented by dashed curves and the total transmission coefficient  $T$  by the solid curve.

due to the coupling the fusion cross section

$$\sigma_F(E) = \frac{\pi}{k^2} T(E) \quad (9.98)$$

is enhanced at energies below the barrier, and reduced above the barrier.

### 9.5.2 The zero-point fluctuation formula

The previous schematic model can be generalized to include the orbital angular momentum. Moreover, in the sudden limit one may couple not only two but the complete set of states of the internal Hamiltonian, i.e. all inelastic channels. This results in the simple and intuitively pleasing *zero-point fluctuation formula*.

Let us assume that the internal variables  $\xi$  describe a collective surface motion (vibration or rotation) of the target nucleus as discussed in Section 8.3. We consider the potential (8.68) which we write in the form

$$V(\mathbf{r}, \alpha) = V(r, [R_\alpha(\Omega)]), \quad (9.99)$$

where

$$R_\alpha(\Omega) = R_0 \left( 1 + \sum_{\lambda\mu} \alpha_{\lambda\mu} Y_{\lambda\mu}(\Omega) \right) \quad (9.100)$$

is the angle-dependent radius function introduced in eqn (8.43). We regard the potential (9.99) as a spherical potential which contains a parameter  $R$ . For deformed potentials this parameter is replaced with the function  $R_\alpha(\Omega)$ , which makes the potential non-spherical.

Following Section 8.2.1, we consider the total wave function (8.11), here denoted by  $\Psi(\mathbf{r}, \alpha)$ , together with eqns (8.15) and (8.24), where we have replaced  $\xi$  with  $\alpha$  and introduced the abbreviated notation  $\alpha = \{\alpha_{\lambda\mu}\}$ . In the initial channel  $a$  with incident momentum  $k_a = k$  we have  $I_a = M_a = 0$ , so that  $l_a = J$ , and in the final channel  $b$  we set  $I_b = I$ ,  $l_b = l$ . The radial wave functions  $g_{b;II}^J(r)$  in the expansion (8.15) are obtained by projection on the orthogonal channel states  $\mathcal{Y}_{b;II;J0}(\Omega, \alpha)$ ,

$$g_{b;II}^J(r) = \frac{kr i^{-J} e^{-i\sigma_I}}{\sqrt{4\pi(2J+1)}} \int d\Omega \int d\alpha \mathcal{Y}_{b;II;J0}^*(\Omega, \alpha) \Psi(\mathbf{r}, \alpha). \quad (9.101)$$

According to eqns (8.23) and (8.29), the solutions  $g_{b;II}^J(r)$  must have the asymptotic form (taking into account the Coulomb interaction)

$$\begin{aligned} g_{b;II}^J(r) &\rightarrow \delta_{b0} \delta_{IJ} \delta_{I0} \sin[kr - \eta \ln(2kr) - \frac{\pi}{2}l + \sigma_I] \\ &- \frac{i}{2} \sqrt{\frac{k}{k_b}} (S_{b;II}^J - \delta_{b0} \delta_{IJ} \delta_{I0}) e^{i[k_b r - \eta \ln(2k_b r) - \frac{\pi}{2}l + \sigma_I]} \quad \text{for } r \rightarrow \infty. \end{aligned} \quad (9.102)$$

The fusion cross section  $\sigma_F$  in the sudden limit is then given by

$$\sigma_F = \frac{\pi}{k^2} \sum_J (2J+1) \left( 1 - \sum_{bII} |S_{b;II}^J|^2 \right). \quad (9.103)$$

The neglect of the excitation energies of the internal states in the sudden approximation is equivalent to discarding the internal Hamiltonian  $h(\alpha)$  in the Hamiltonian  $H_0$  of eqn (8.5) (we normalize the ground-state energy to zero,  $\epsilon_0 = 0$ ). The total Hamiltonian (8.4) then becomes

$$H = T + V(r, [R_\alpha(\Omega)]). \quad (9.104)$$

### 9.5 Fusion in the presence of nuclear excitations

In the absence of the Hamiltonian  $h_\alpha$  the internal coordinates  $\alpha$  now change their role from dynamical variables to parameters. The Schrödinger equation for the wave function  $\Psi(\mathbf{r}, \alpha)$  is

$$\left( -\frac{\hbar^2}{2\mu} \nabla^2 + V(r, [R_\alpha(\Omega)]) \right) \Psi(\mathbf{r}, \alpha) = E \Psi(\mathbf{r}, \alpha). \quad (9.105)$$

We now assume that the angular dependence of the radius function  $R_\alpha(\Omega)$  is much weaker than that of the wave function  $\Psi(\mathbf{r}, \alpha)$  itself. More precisely, we assume that the latter can be identified with a solution for a *spherical* potential  $V(r, [R])$  containing the parameter  $R$ ,

$$\left( -\frac{\hbar^2}{2\mu} \nabla^2 + V(r, [R]) \right) \Psi(\mathbf{r}, [R]) = E \Psi(\mathbf{r}, [R]), \quad (9.106)$$

where in the end the parameter  $R$  will be replaced with the radius function  $R_\alpha(\Omega)$ . In making this identification it is convenient for later purposes to introduce the ground-state wave function of the internal motion  $\phi_{0;00}(\alpha)$  as a coefficient,

$$\Psi(\mathbf{r}, [R]) = \phi_{0;00}(\alpha) \tilde{\Psi}(\mathbf{r}, [R]). \quad (9.107)$$

The Schrödinger equation (9.106) is solved by writing the solution  $\tilde{\Psi}(\mathbf{r}, [R])$  as a partial-wave expansion as in eqn (1.119),

$$\tilde{\Psi}(\mathbf{r}, [R]) = \frac{1}{kr} \sum_l \sqrt{4\pi(2l+1)} i^l e^{i\sigma_l} y_l(r, [R]) Y_{l0}(\Omega), \quad (9.108)$$

where the partial wave functions  $y_l(r, [R])$  are solutions of the radial wave equations

$$\left( -\frac{\hbar^2}{2\mu} \frac{d^2}{dr^2} + \frac{\hbar^2 l(l+1)}{2\mu r^2} + V(r, [R]) \right) y_l(r, [R]) = E y_l(r, [R]). \quad (9.109)$$

For these solutions we require the asymptotic behaviour appropriate for single-channel potential scattering,

$$\begin{aligned} y_l(r, [R]) &\rightarrow \sin[kr - \eta \ln(2kr) - \frac{\pi}{2}l + \sigma_l] \\ &- \frac{i}{2} (S_l([R]) - 1) e^{i[kr - \eta \ln(2kr) - \frac{\pi}{2}l + \sigma_l]} \quad \text{for } r \rightarrow \infty. \end{aligned} \quad (9.110)$$

The solution  $y_l(r, [R])$  is the generalization of the eigenchannel wave function (9.92) in the two-channel model of Section 9.5.1, with the continuous parameter  $R$  replacing the index  $\pm$ . The corresponding fusion cross section is

$$\sigma_F([R]) = \frac{\pi}{k^2} \sum_l (2l+1) (1 - |S_l([R])|^2). \quad (9.111)$$

According to eqn (9.101) we then find for the *incident wave* in the physical channel  $\{b; IIJ\}$  at  $r \rightarrow \infty$

$$\begin{aligned} &\frac{i^{-J} e^{-i\sigma_I}}{\sqrt{2J+1}} \int d\Omega \int d\alpha \mathcal{Y}_{b;II;J0}^*(\Omega, \alpha) \phi_{0;00}(\alpha) \\ &\times \sum_{l'} \sqrt{2l'+1} Y_{l'0}(\Omega) \sin[kr - \eta \ln(2kr) - \frac{\pi}{2}l' + \sigma_{l'}] \\ &= \delta_{b0} \delta_{IJ} \sin[kr - \eta \ln(2kr) - \frac{\pi}{2}l + \sigma_l]. \end{aligned} \quad (9.112)$$

Thus the correct boundary condition (9.102) for the incident physical partial wave is obtained; the ansatz (9.107) has been chosen precisely for this purpose.

For the physical  $S$ -matrix elements  $S_{b:II}^J$  we find in a similar fashion

$$\begin{aligned} S_{b:II}^J &= \frac{i^{-J} e^{-i\sigma_J}}{\sqrt{2J+1}} \int d\Omega \int d\alpha Y_{b:II;J0}^*(\Omega, \alpha) \phi_{0:00}(\alpha) \\ &\quad \times \sum_{l'} \sqrt{2l'+1} i^{l'} e^{i\sigma_{l'}} S_{l'}([R_\alpha(\Omega)]) Y_{l'0}(\Omega). \end{aligned} \quad (9.113)$$

The fusion cross section then becomes, with the help of eqn (9.103),

$$\begin{aligned} \sigma_F &= \frac{\pi}{k^2} \sum_J (2J+1) \left( 1 - \sum_{bII} |S_{b:II}^J|^2 \right) \\ &= \frac{\pi}{k^2} \sum_{l'l''} \sqrt{(2l'+1)(2l''+1)} \left[ \delta_{l'l''} - i^{l'-l''} e^{i(\sigma_{l'}-\sigma_{l''})} \int d\Omega' \int d\alpha' \right. \\ &\quad \left. \int d\Omega \int d\alpha S_{l'}^*([R_{\alpha'}(\Omega')]) \phi_{0:00}^*(\alpha') Y_{l''0}^*(\Omega') \right. \\ &\quad \left. \times \left( \sum_{bIIJ} Y_{b:II;J0}(\Omega', \alpha') Y_{b:II;J0}^*(\Omega, \alpha) \right) Y_{l'0}(\Omega) \phi_{0:00}(\alpha) S_{l'}([R_\alpha(\Omega)]) \right] \\ &= \frac{\pi}{k^2} \sum_{l'l''} \sqrt{(2l'+1)(2l''+1)} \left( \delta_{l'l''} - i^{l'-l''} e^{i(\sigma_{l'}-\sigma_{l''})} \int d\Omega Y_{l''0}^*(\Omega) Y_{l'0}(\Omega) \right. \\ &\quad \left. \int d\alpha |\phi_{0:00}(\alpha)|^2 S_{l'}^*([R_\alpha(\Omega)]) S_{l'}([R_\alpha(\Omega)]) \right); \end{aligned} \quad (9.114)$$

here we have made use of the completeness relation (8.14) for the spin-coupled channel wave functions  $\mathcal{Y}_b(\Omega, \alpha)$ .

The spinless ground-state wave function  $\phi_{0:00}(\alpha)$  is independent of the orientation of the system of axes with respect to which the deformations are defined. If this system is chosen such that the  $z$ -axis is oriented along the vector  $\mathbf{r}$ , the angle  $\Omega$  in the radius function  $R_\alpha(\Omega)$  is zero,

$$\begin{aligned} R_\alpha &= R_\alpha(\Omega = 0) = R_0 \left( 1 + \sum_\lambda \alpha_{\lambda 0} Y_{\lambda 0}(0) \right) \\ &= R_0 \left( 1 + \sum_\lambda \alpha_{\lambda 0} \sqrt{\frac{2\lambda+1}{4\pi}} \right), \end{aligned} \quad (9.115)$$

and the integral over  $\alpha$  in the last line of expression (9.114) is independent of  $\Omega$ . The integration over  $\Omega$  then involves only the orthogonal spherical harmonics, yielding  $\delta_{l'l''}$ , and we are left, finally, with

$$\sigma_F = \frac{\pi}{k^2} \sum_l (2l+1) \int d\alpha |\phi_{0:00}(\alpha)|^2 (1 - |S_l([R_\alpha])|^2), \quad (9.116)$$

or, using eqn (9.111),

$$\sigma_F = \int d\alpha |\phi_{0:00}(\alpha)|^2 \sigma_F([R_\alpha]). \quad (9.117)$$

This is the *zero-point fluctuation formula* (cf. Esbensen 1981; Jacobs and Smilansky 1983). It expresses the fusion cross section as an average of the fusion cross sections for an ensemble of spherical barrier potentials in which the radius fluctuates as a function of the surface deformation parameters  $\alpha = \{\alpha_{\lambda\mu}\}$ . The average is taken over the distribution of these fluctuations in the ground state of the deformation modes.

#### Rotational excitations

For rotations the collective variables  $\alpha = \{\alpha_{\lambda\mu}\}$  are the constant deformation parameters  $\beta_\lambda$  and the set of Euler angles  $\omega = \{\alpha, \beta, \gamma\}$  (cf. Section 8.3.1). According to eqns (8.77) and (9.115), the radius function has the form

$$\begin{aligned} R_\alpha(\Omega = 0) &= R_0 \left( 1 + \sum_\lambda \beta_\lambda \sqrt{\frac{2\lambda+1}{4\pi}} D_{00}^\lambda(0, \beta, 0) \right) \\ &= R_0 \left( 1 + \sum_\lambda \beta_\lambda Y_{\lambda 0}(\beta, 0) \right) = R(\beta). \end{aligned} \quad (9.118)$$

The ground-state wave function is equal to (cf. eqn (8.79))

$$\phi_{0:00}(\alpha) = Y_{00}(\beta, \alpha) = \frac{1}{\sqrt{4\pi}}. \quad (9.119)$$

The expression (9.117) for the fusion cross section then takes the form of an integral over the Euler angles  $\alpha$  and  $\beta$

$$\sigma_F = \int_0^{2\pi} d\alpha \int_{-1}^1 d(\cos \beta) \frac{1}{4\pi} \sigma_F([R(\beta)]) = \frac{1}{2} \int_{-1}^1 d(\cos \beta) \sigma_F([R(\beta)]). \quad (9.120)$$

The fusion cross section is given by an ensemble of fusion cross sections for deformed nuclei (with fixed internal deformation parameters  $\beta_\lambda$ ) oriented in the directions  $\beta$ , averaged over the angles  $\beta$ .

#### Vibrational excitations

For vibrations we replace formula (9.117), which is written in the coordinate space representation for the oscillator variables  $\alpha$ , with its equivalent in terms of the operator form of these variables, eqn (8.93),

$$\sigma_F = \langle 0 | \sigma_F([R_\alpha]) | 0 \rangle. \quad (9.121)$$

In order to evaluate the ground-state expectation value on the right-hand side of this equation, we first write

$$\begin{aligned} \langle 0 | \sigma_F([R_\alpha]) | 0 \rangle &= \int dR \langle 0 | \delta(R_\alpha - R) | 0 \rangle \sigma_F([R]) \\ &= \frac{1}{2\pi} \int dR \int_{-\infty}^{\infty} dq \langle 0 | e^{iq(R_\alpha - R)} | 0 \rangle \sigma_F([R]). \end{aligned} \quad (9.122)$$

For the ground-state expectation value of the exponential in eqn (9.122) we find

$$\begin{aligned}\langle 0 | e^{iq(R_\alpha - R)} | 0 \rangle &= e^{iq(R_0 - R)} \langle 0 | \exp\left(iqR_0 \sum_\lambda \alpha_{\lambda 0} Y_{\lambda 0}(\Omega = 0)\right) | 0 \rangle \\ &= e^{iq(R_0 - R)} \langle 0 | e^{A+B} | 0 \rangle,\end{aligned}\quad (9.123)$$

where we have used eqn (8.93) for  $\mu = 0$ ,

$$\alpha_{\lambda 0} = \left(\frac{\hbar}{2B_\lambda \omega_\lambda}\right)^{1/2} (c_{\lambda 0} + c_{\lambda 0}^\dagger), \quad (9.124)$$

and defined

$$\begin{aligned}A &= iqR_0 \sum_\lambda \left(\frac{\hbar}{2B_\lambda \omega_\lambda}\right)^{1/2} c_{\lambda 0}^\dagger Y_{\lambda 0}(0) \\ B &= iqR_0 \sum_\lambda \left(\frac{\hbar}{2B_\lambda \omega_\lambda}\right)^{1/2} c_{\lambda 0} Y_{\lambda 0}(0).\end{aligned}\quad (9.125)$$

We now apply the Baker–Campbell–Hausdorff formula for two operators  $A$  and  $B$  whose commutator is a c-number (cf. Messiah 1972, eqn (XII.29); Wilcox 1967),

$$e^{A+B} = e^A e^{-\frac{1}{2}[A,B]} e^B; \quad (9.126)$$

in the present case we have

$$\begin{aligned}-\frac{1}{2}[A, B] &= -\sum_\lambda \frac{\hbar}{4B_\lambda \omega_\lambda} q^2 R_0^2 Y_{\lambda 0}(0) Y_{\lambda 0}(0) \\ &= -\frac{1}{2} q^2 \sum_\lambda \frac{(2\lambda + 1)\hbar}{8\pi B_\lambda \omega_\lambda} R_0^2.\end{aligned}\quad (9.127)$$

The exponential  $\exp(A)$  operating on the ground-state bra on the left can be replaced with unity since

$$\langle 0 | e^A = \langle 0 | \left[ 1 + iqR_0 \sum_\lambda \left(\frac{\hbar}{2B_\lambda \omega_\lambda}\right)^{1/2} c_{\lambda 0}^\dagger Y_{\lambda 0}(0) + \dots \right] = \langle 0 | \quad (9.128)$$

because of eqn (8.96). The same holds for the exponential  $\exp(B)$  operating on the ground-state ket on the right. We thus find

$$\langle 0 | e^{A+B} | 0 \rangle = e^{-\sigma^2 q^2 / 2}, \quad (9.129)$$

where we have introduced the total mean square fluctuation of the oscillator modes with multipole moment  $\lambda$  in their ground state,

$$\sigma^2 = \sum_\lambda \frac{(2\lambda + 1)\hbar}{8\pi B_\lambda \omega_\lambda} R_0^2. \quad (9.130)$$

Integration over  $q$  in eqn (9.122) yields

$$\frac{1}{2\pi} \int_{-\infty}^{\infty} dq e^{iq(R_0 - R)} e^{-\sigma^2 q^2 / 2} = \frac{1}{\sqrt{2\pi\sigma^2}} e^{-(R - R_0)^2 / 2\sigma^2}. \quad (9.131)$$

This is the distribution of the nuclear radius  $R$  in the ground state of all surface oscillator modes  $\lambda$ . From eqns (9.121) and (9.122) we then obtain for the fusion cross section

$$\sigma_F = \int dR \frac{1}{\sqrt{2\pi\sigma^2}} e^{-(R - R_0)^2 / 2\sigma^2} \sigma_F([R]). \quad (9.132)$$

Thus the fusion cross section is given by an ensemble of fusion cross sections for spherical nuclei with radius  $R$ , averaged over the distribution of this radius in the ground state of all surface oscillator modes.

The zero-point fluctuation formula (9.132) has been derived under the condition that the excitation energies  $\hbar\omega_\lambda$  are negligibly small, corresponding to the sudden limit. In the spirit of this approximation one also assumes that the inertial parameters  $B_\lambda$  are very large, so that the products  $B_\lambda \omega_\lambda$  appearing in the mean square fluctuation (9.130) are finite and can be evaluated using the empirical values of the parameters  $B_\lambda$  and  $\omega_\lambda$  (which, it is true, are neither very large nor very small, respectively).

### 9.5.3 The full coupled-channel description

In a full coupled-channel treatment we must go back to the original set of equations (9.87). Describing the fusion as an absorption effected by an imaginary potential, we have

$$\left(-\frac{\hbar^2}{2\mu} \frac{d^2}{dr^2} + V(r) + iW^{(F)}(r) + \epsilon_b - E\right) \psi_b(r) = -\sum_{c \neq b}^N V_{bc}(r) \psi_c(r), \quad (9.133)$$

where the diagonal coupling term is absorbed in the real part of the potential  $V(r) = V_0(r) + V_{bb}(r)$  and the term  $iW^{(F)}(r)$  is the imaginary *fusion potential*. This potential is introduced to take account of fusion from each channel.

The total fusion cross section is the sum of contributions from the various channels,

$$\sigma_F = \sum_b^N \sigma_F^{(b)} = \frac{\pi}{k^2} \sum_l (2l + 1) \left(1 - \sum_{b=0}^N |S_{b0}^l|^2\right), \quad (9.134)$$

where  $S_{b0}^l$  is the  $l$ -th partial S-matrix element for the transition from the elastic channel to the channels  $b$  with  $b = 0, \dots, N$ . We may separate out the term referring to the incident channel and write

$$\sigma_F = \frac{\pi}{k^2} \sum_l (2l + 1) (1 - |S_{00}^l|^2) - \frac{\pi}{k^2} \sum_l (2l + 1) \sum_{b=1}^N |S_{b0}^l|^2. \quad (9.135)$$

We then see, using eqns (1.72) and (1.73), that the fusion cross section is equal to the reaction cross section minus the sum of the direct non-elastic cross sections,

$$\sigma_F = \sigma_r - \sum \sigma(\text{direct non-elastic}). \quad (9.136)$$

#### Examples and comparison with experiment

The qualitative effects of the channel coupling discussed in Section 9.5.1 show up in the results of quantitative coupled-channel calculations. Such calculations have been performed, for example, by Stockstad and Gross (1981), Krappe *et al.* (1983), and others.

In the following we give examples of sub-barrier fusion cross sections obtained by quantal coupled-channel calculations, and compare them with experimental data. Figure 9.25 shows that the fusion of *light* systems is reasonably well described. As the systems

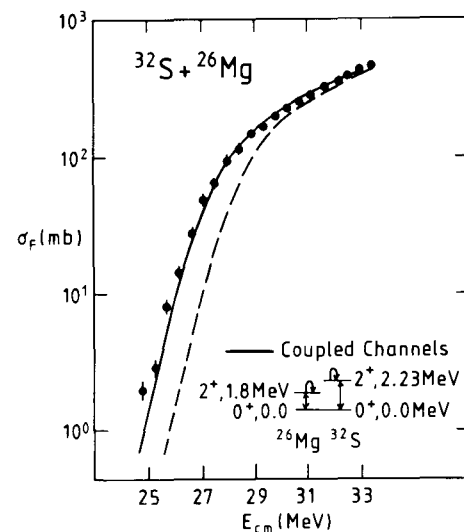


**Figure 9.25** The fusion cross section resulting from a coupled-channel calculation (solid curve) for the light system  $^{32}\text{S} + ^{26}\text{Mg}$  in comparison with experiment (dots) (cf. Rhoades-Brown and Braun-Munzinger 1984). The couplings used in the calculation of the theoretical curve are shown in the inset. The dashed curve represents the fusion cross section calculated with the couplings turned off.

get heavier, the coupled-channel description becomes less accurate, even when transfer channels are included. A recent example for somewhat heavier systems is shown in Fig. 9.26, from which it is seen that no quantitative agreement with the data is achieved. Coupling to only a few low-lying non-elastic channels is not at all sufficient to reproduce the data (cf. Fig. 9.27) for *heavy* systems.

A further problem arising in the coupled-channel description has to do with the expansion of the nuclear potential in terms of the deformation parameters in order to obtain the coupling potential. Usually only the terms linear in the deformation parameters are taken into account (cf. eqn (8.52)). It was, however, shown by Esbensen and Landowne (1987) that second-order terms play a non-negligible role in describing the fusion excitation function. This raises the question of the convergence of this expansion.

When more and more channels have to be included in the calculation, at least two additional difficulties come up. First, one does not know which channels are the important ones, because these are difficult to identify experimentally. Second, even if one did know the channels and their form factors, it is technically impossible to solve numerically the large number of coupled differential equations which would then be involved.

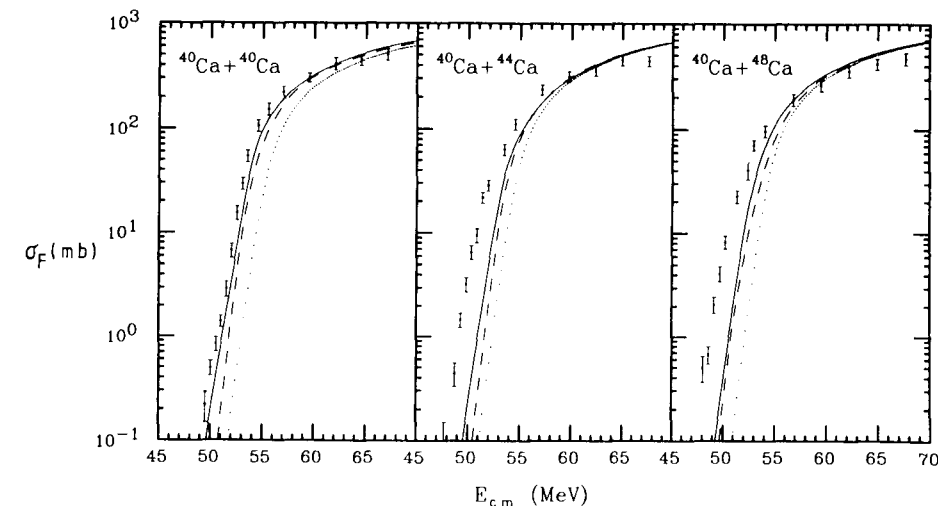


**Figure 9.26** Results of coupled-channel calculations of the fusion cross section for the systems  $^{40}\text{Ca} + ^{40,44,48}\text{Ca}$  in comparison with experiment (cf. Esbensen *et al.* 1989). Dotted curve: no coupling to non-elastic channels; dashed curve: with coupling to single-nucleon transfer channels only; solid curve: with inclusion of the vibrational and single-nucleon transfer channels.

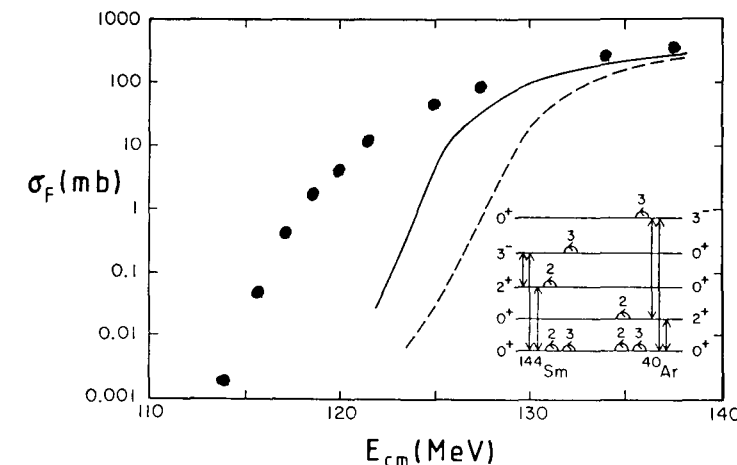


**Figure 9.27** Results of coupled-channel calculations (solid curve) of the fusion cross section for the heavy system  $^{40}\text{Ar} + ^{144}\text{Sm}$  in comparison with experiment (cf. Rhoades-Brown *et al.* 1985). The couplings used in the calculation of the theoretical curve are shown in the inset. The dashed curve represents the fusion cross section calculated with the couplings turned off.

Therefore, one is forced to go over to more global descriptions. One possibility is to simulate the effect of the many non-elastic channels by a classical friction model, as we shall do in Chapter 12. Another is a single-channel description which introduces an absorptive potential for fusion as distinct from the absorptive potential for other non-elastic processes. Such a model will be discussed in the next section.

## 9.6 Description of fusion in the optical model

When it is no longer possible to couple all open channels explicitly, one may take recourse to a description in terms of a complex potential  $\mathcal{V}(r) = V(r) + iW(r)$  in the elastic channel alone, where the effect of the non-elastic channels is taken into account in the form of absorption. The absorption responsible for the fusion has to be distinguished from that for the loss of current into non-compound channels. We mention here without a derivation, for which we refer to Hussein (1984) and Udagawa *et al.* (1985), that this can be done approximately by separating the imaginary part of the optical potential into the *fusion-absorption potential*  $W^F$  responsible for fusion, and another part  $W^D$  responsible for non-compound, i.e. direct and deep-inelastic, reactions,

$$W(r) = W^F(r) + W^D(r). \quad (9.137)$$

The total transmission (absorption) coefficient is then given by eqn (1.65) as

$$T_l = -\frac{8}{\hbar v} \int_0^\infty dr |y_l(r)|^2 W(r), \quad (9.138)$$

while the absorption coefficient for fusion alone is

$$T_l^F = -\frac{8}{\hbar v} \int_0^\infty dr |y_l(r)|^2 W^F(r), \quad (9.139)$$

and that for the direct reactions alone

$$T_l^D = -\frac{8}{\hbar v} \int_0^\infty dr |y_l(r)|^2 W^D(r). \quad (9.140)$$

The solution  $y_l(r)$  corresponding to the *full* optical potential  $\mathcal{V}(r)$  appears in the expressions (9.139) and (9.140), so that both add up to the total transmission coefficient (9.138),

$$T_l = T_l^F + T_l^D. \quad (9.141)$$

The spin distribution of fusion is then given by

$$\sigma_F(l) = \frac{\pi}{k^2} (2l+1) T_l^F, \quad (9.142)$$

and the fusion cross section itself by

$$\sigma_F = \sum_l \sigma_F(l). \quad (9.143)$$

A simple model for the fusion-absorption potential  $W^F(r)$  has been proposed by Udagawa and Tamura (1984) and by Kim *et al.* (1986). The imaginary part of the optical

potential  $W(r)$ , which is typically of the Woods–Saxon shape (1.146) and is given for all  $r > 0$ , is divided up spatially into a fusion part,

$$W^F(r) = \begin{cases} W(r) & \text{for } r < d, \\ 0 & \text{for } r > d, \end{cases} \quad (9.144)$$

and a direct part,

$$W^D(r) = \begin{cases} 0 & \text{for } r < d, \\ W(r) & \text{for } r > d; \end{cases} \quad (9.145)$$

here  $d = r_F(A_P^{1/3} + A_T^{1/3})$ .

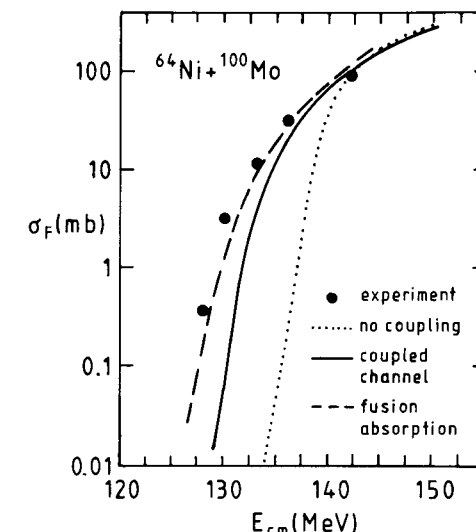


**Figure 9.28** The fusion cross section for the system  $^{64}\text{Ni} + ^{100}\text{Mo}$  calculated in a one-dimensional approach (no coupling, dotted curve), in a coupled-channel approach (solid curve) and with the help of the fusion-absorption potential (dashed curve). The dots represent the data of Halbert *et al.* (1989).

The fusion cross section for the system  $^{64}\text{Ni} + ^{100}\text{Mo}$  calculated with the help of this model is shown in Fig. 9.28 together with experimental data (cf. Halbert *et al.* 1989). The optical-model parameters used in the calculation are  $V = 178$  MeV,  $W = 80$  MeV,  $r_0 = 1.087$  fm, and  $a = 0.707$  fm for both the real and imaginary parts, and  $d = r_F(A_P^{1/3} + A_T^{1/3})$  with  $r_F = 1.44$  fm. The necessity of introducing such a relatively large radius is an indication that fusion already sets in in the region of the fusion barrier, and depends on the conditions there.

### The spin distribution of fusion

The spin distribution of fusion is calculated with the help of eqn (9.142). Its first and second moments are given by

$$\langle l \rangle = \frac{1}{\sigma_F} \sum_l \sigma_F(l) l$$

$$\langle l^2 \rangle = \frac{1}{\sigma_F} \sum_l \sigma_F(l) l^2. \quad (9.146)$$

The moments calculated with the help of these formulae are compared with the data for the  $^{64}\text{Ni} + ^{100}\text{Mo}$  system in Fig. 9.29. It is seen that the fusion-absorption model approach allows one to reproduce the experimental data rather well, compared to what is achieved with a coupled-channel scheme, let alone with a one-dimensional barrier penetration model where the effect of the non-elastic channels is neglected altogether. The present

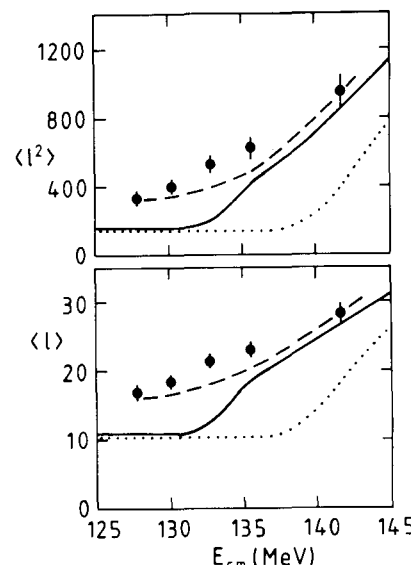


**Figure 9.29** First,  $\langle l \rangle$ , and second moments,  $\langle l^2 \rangle$ , of the fusion spin distribution for the system  $^{64}\text{Ni} + ^{100}\text{Mo}$  calculated in the fusion-absorption model (dashed curves), in the coupled-channel scheme (solid curve) and with the help of a one-dimensional barrier-penetration model (dotted curve). The dots represent the data of Halbert *et al.* (1989).

single-channel approach in the optical model allows for a unified phenomenological description of elastic scattering and fusion. The real part of the complex potential, i.e. the barrier, is the same for both processes, and the imaginary part is divided up between them in a physically reasonable way. It appears from Figs. 9.28 and 9.29 that this description yields better results than the coupled-channel approach when applied to heavier systems, and leads to a surprisingly good reproduction of the experimental data also for other systems (cf. Teneiro *et al.* 1994).

### 9.7 Notes and references

The fusion of heavy ions has been described extensively in the reviews by Nörenberg and Weidenmüller (1976), Lefort (1980), Mosel (1980, 1984), and Birkelund and Huizenga (1983). Sub-barrier fusion is reviewed by Beckerman (1985), and with particular attention to the spin distributions by Vandenbosch (1992). Three international conferences have been held to discuss topics connected with sub-barrier fusion; the corresponding proceedings (cf. Steadman 1985; Signorini *et al.* 1988; Stefanini *et al.* 1994) provide a survey of the relevant literature.

The investigation of nuclear fusion has been stimulated in part by the search for super-heavy elements (cf. Nix 1972*b*). These have so far not been found, but meanwhile a number of new trans-uranium elements have been produced in heavy-ion fusion collisions (cf. Armbruster 1985; Hofmann *et al.* 1995).

A microscopic theory of fusion can be formulated in the time-dependent Hartree-Fock approximation (TDHF), where the system of colliding nuclei is described by a time-dependent Slater determinant of nucleon wave functions, and the initial state is given by two separate nucleon clusters moving towards each other (cf. Davies *et al.* 1984).

We also mention the barrier fluctuation scheme developed by Rowley (1992), where one can obtain information on the barrier distributions from an analysis of precisely measured fusion excitation functions.

We emphasize that fusion in competition with deep-inelastic processes has *not* been discussed in this chapter. This topic will be taken up in Chapter 12, where the relevant references will also be given.

### References

- Armbruster, P. (1985). *Ann. Rev. Nucl. Part. Sci.* **35** 135.
- Bass, R. (1980). *Lecture notes in physics*, vol. 117, Springer, Berlin, p. 281.
- Beckerman, M. (1985). *Phys. Rep.* **C129** 145.
- Birkelund, J. R. and Huizenga, J. R. (1983). *Ann. Rev. Nucl. Part. Sci.* **33** 265.
- Blocki, J., Randrup, J., Swiatecki, W. J. and Tsang, G. F. (1977). *Ann. Phys. (N.Y.)* **105** 427.
- Bohr, A. and Mottelson, B. R. (1969). *Nuclear structure*, vol. 1, Benjamin, New York.
- Bohr, N. (1936). *Nature* **137** 344.
- Brink, D. M. and Smilansky, U. (1983). *Nucl. Phys.* **A405** 301.
- Clayton, D. D. (1968). *Principles of stellar evolution and nucleosynthesis*, McGraw-Hill, New York.
- Cohen, S., Plasil, F. and Swiatecki, W. J. (1974). *Ann. Phys. (N.Y.)* **82** 557.
- Dasso, C. H., Landowne, S. and Winther, Aa. (1983). *Nucl. Phys.* **A405** 381.
- Davies, K. T. R., Devi, K. R. S., Koonin, S. E. and Strayer, M. R. (1984). *Treatise on heavy-ion science*, ed. Bromley, D. A., vol. 3, Plenum Press, New York, p. 3.
- Doukellis, G. (1988). *Phys. Rev.* **C37** 2233.
- Esbensen, H. (1981). *Nucl. Phys.* **A352** 147.
- Esbensen, H. and Landowne, S. (1987). *Phys. Rev.* **C35** 2090.
- Esbensen, H., Fricke, S. H. and Landowne, S. (1989). *Phys. Rev.* **C40** 2046.

- Fröbrich, P. (1989). *Phys. Rev.* **C39** 2085.
- Fröbrich, P., Lipperheide, R. and Möhring, K. (1990). *Z. Physik* **B78** 325.
- Fuchs, H. and Möhring, K. (1994). *Rep. Prog. Phys.* **57** 231.
- Galin, J., Guerreau, D., Lefort, M. and Tarrago, X. (1974). *Phys. Rev.* **C9** 1018.
- Glas, D. and Mosel, U. (1974). *Phys. Rev.* **C10** 2620.
- Glas, D. and Mosel, U. (1975). *Nucl. Phys.* **A237** 429.
- Gross, D. H. E. (1990). *Rep. Prog. Phys.* **53** 605.
- Halbert, M. L., Beene, J. R., Hensley, D. C., Honkanen, K., Semkow, T. M., Abenante, V., Sarantites, D. G. and Li, Z. (1989). *Phys. Rev.* **C40** 2558.
- Hill, D. L. and Wheeler, J. A. (1953). *Phys. Rev.* **89** 1102.
- Hofmann, S., Ninov, V., Hessberger, F. P., Armbruster, P., Folger, H., Münzenberg, G., Schött, H., Popeko, A., Yeremin, A. V., Andreyev, A. N., Saro, S., Janik, R. and Leino, M. (1995). *Z. Physik* **A350** 277, 281.
- Hussein, M. S. (1984). *Phys. Rev.* **C30** 1962.
- Jacobs, P. M. and Smilansky, U. (1983). *Phys. Lett.* **127B** 313.
- Johnson, A. and Szymanski, Z. (1973). *Phys. Rep.* **C7** 181.
- Kemble, E. (1935). *Phys. Rev.* **48** 549.
- Kim, B. T., Udagawa, T. and Tamura, T. (1986). *Phys. Rev.* **C33** 370.
- Krappe, H. J., Nix, J. R. and Sierk, A. J. (1979). *Phys. Rev.* **C20** 992.
- Krappe, H. J., Möhring, K., Nemes, M. C. and Rossner, H. (1983). *Z. Physik* **A314** 23.
- Landau, L. D. and Lifshitz, E. M. (1965). *Quantum mechanics*, Pergamon, Oxford.
- Lee, S. M., Matsuse, T. and Arima, A. (1980). *Phys. Rev. Lett.* **45** 165.
- Lefort, M. (1980). *Heavy-ion collisions*, ed. Bock, R., vol. 2, North-Holland, Amsterdam, p. 45.
- Lefort, M. and Ngô, Ch. (1978). *Ann. Phys.* **3** 5.
- Messiah, A. (1972). *Quantum mechanics*, vol. 1, North-Holland, Amsterdam.
- Moretto, L. G. and Wozniak, G. J. (1994). *Ann. Rev. Nucl. Part. Sci.* **43** 379.
- Morgenstern, H., Bohne, W., Grabisch, K., Lehr, H. and Stöffler, W. (1983). *Z. Physik* **A 313** 39.
- Mosel, U. (1980). *Heavy-ion collisions*, ed. Bock, R., vol. 2, North-Holland, Amsterdam, p. 275.
- Mosel, U. (1984). *Treatise on heavy-ion science*, ed. Bromley, D. A., vol. 2, Plenum Press, New York, p. 3.
- Myers, W. and Swiatecki, W. J. (1966). *Nucl. Phys.* **81** 1.
- Ngyen Van Sen, Darves-Blanc, R., Goudrand, J. C. and Merchez, F. (1983). *Phys. Rev.* **C27** 194.
- Nix, J. R. (1972a). *Los Alamos preprint*, LA-DC-72-769.
- Nix, J. R. (1972b). *Physics Today*, **25**, no. 4, p. 30.
- Nörenberg, W. (1980). *Heavy-ion collisions*, ed. Bock, R., vol. 2, North-Holland, Amsterdam, p. 1.
- Nörenberg, W. and Weidenmüller, H. A. (1976). *Introduction to the theory of heavy-ion collisions*, Springer, Berlin.
- Rawitscher, G. H. (1963). *Nucl. Phys.* **A85** 337.
- Rhoades-Brown, M. J. and Braun-Munzinger, P. (1984). *Phys. Lett.* **B136** 19.

## 9.7 Notes and references

- Rhoades-Brown, M. J., Braun-Munzinger, P., Prakash, M. and Sen, S. (1985). *Lecture notes in physics*, vol. 219, Springer, Berlin, p. 162.
- Rosner, G., Pochodzalla, J., Heck, B., Hlawatsch, G., Miczaika, A., Rabe, H.J., Butsch, R., Kolb, B. and Sedlmeyer, B. (1985). *Phys. Lett.* **B150** 87.
- Rowley, N. (1992). *Nucl. Phys.* **A538** 205c.
- Signorini, C., Skorka, S., Spolaore, P. and Vitturi, A., eds. (1988). *Lecture notes in physics*, vol. 317, Springer, Berlin.
- Steadman, S. G., ed. (1985). *Lecture notes in physics*, vol. 219, Springer, Berlin.
- Stefanini, A.M., Nebbia, G., Lunardi, S., Montagnoli, G. and Vitturi, A., eds. (1994). *Heavy-ion fusion: exploring the variety of nuclear properties*, World Scientific, Singapore.
- Stockstad, R. G. and Gross, E. E. (1981). *Phys. Rev.* **C23** 281.
- Strutinsky, V. M. (1967). *Nucl. Phys.* **A95** 420.
- Swiatecki, W. J. (1972). *J. de Physique* **33** C5-45.
- Teneiro, C., Gomes, P. R. S., Penna, T. J. P., Liguori Neto, R., Acquadro, J. C., Freitas, P. A. B. and Crema, E. (1994). *Phys. Rev.* **C49** 1218.
- Thomas, T. D. (1968). *Ann. Rev. Nucl. Sci.* **18** 343.
- Udagawa, T. and Tamura, T. (1984). *Phys. Rev.* **C29** 1922.
- Udagawa, T., Kim, B. T. and Tamura, T. (1985). *Phys. Rev.* **C32** 124.
- Vandenbosch, R. (1992). *Ann. Rev. Nucl. Part. Sci.* **42** 447.
- Wilcox, R. M. (1967). *J. Math. Phys.* **8** 962.
- Wong, C. Y. (1973). *Phys. Rev. Lett.* **31** 766.

# 10

## COMPOUND-NUCLEUS REACTIONS

### 10.1 Introduction

In the preceding chapter we discussed fusion, that is, the formation of a compound nucleus. It was noted there that this compound nucleus occurs as an intermediate transitory system in a *compound-nucleus reaction*. Thus fusion is only the initial phase of such a reaction. In a second step the compound nucleus decays by evaporation or fission. Combining the cross section for fusion from an entrance channel  $a$  with the probability for compound-nucleus decay to a final channel  $b$ , one arrives at the cross section for the compound-nucleus reaction from channel  $a$  to channel  $b$ ,  $\sigma_{a \rightarrow b}^C$ . It follows that the fusion cross section is equal to the *total* compound reaction cross section, i.e. it is given by the compound reaction cross section summed over all final channels,

$$\sigma_F(a) = \sum_b \sigma_{a \rightarrow b}^C. \quad (10.1)$$

In fact this can be regarded as the *definition* of the fusion cross section.

Compound-nucleus reactions occur whenever the reaction mechanism involves many degrees of freedom in the combined projectile-target system at close contact. This is not the case if the collision partners are both light nuclei. But when a light, low-energy projectile combines with a nucleus which is heavy, a large number of different transitory configurations may be formed, as discussed in Section 9.2.1. They give rise to narrow isolated resonances in the reaction cross section as a function of the incident energy. When energy and mass of the projectile increase, the number of these transitory states increases as well, their structure becomes more complicated, and the resonances begin to overlap. Eventually, and this is generally the case in collisions where both partners are heavy ions, the complexity of the compound nucleus becomes so high that the latter can no longer be described in terms of individual compound states but must be treated by statistical methods. This leads us to the statistical picture of the compound nucleus introduced by Niels Bohr (1936), which has already been invoked in the previous chapter.

In Section 10.2 we incorporate Bohr's compound-nucleus idea in the derivation of the reaction cross section. In doing so we derive the final cross section formulae directly from the results of the general reaction theory of Chapter 5, and avoid thereby the establishment of a detailed theoretical framework of its own kind, like the '*R*-matrix' theory (cf. Lane and Thomas 1958) or the shell-model theory of nuclear reactions (cf. Mahaux and Weidenmüller 1969).

In line with Section 6.3.2, which, however, was restricted to elastic scattering, we define the compound-nucleus reaction as that part of the reaction which is associated

with the *fluctuating part* of the *S*-matrix. The energy average of the absolute square of the fluctuating part of the reaction amplitude determines the *compound reaction cross section*. The latter is factorized into a formation cross section and a decay probability in accordance with Bohr's independence hypothesis. Together with the principle of detailed balance this hypothesis allows one to establish the *Hauser-Feshbach formula* which expresses the compound reaction cross section solely in terms of a set of fusion cross sections, or transmission coefficients. The general compound reaction cross section thus derived applies to compound reactions in which the final channels contain two nuclei,  $b = y + B$ , an 'evaporated' light one,  $y$ , like a neutron, proton, or  $\alpha$ -particle, and a heavy one,  $B$ , the residual nucleus or evaporation residue. The description of fission requires special considerations.

Compound nuclei are in general highly excited, and so are the final nuclei. Therefore, a large number of different final states are accessible in the exit channel. These are not treated individually; instead one considers a small interval of final energies and replaces the sum of the cross sections to all accessible final states in this interval with an average of the cross section multiplied by the number of these states. The number of states per unit energy interval is the *level density*, which will be derived in Section 10.3.

Finally, in Section 10.4, we discuss the different *decay modes* of the compound nucleus in detail. We begin by writing down explicit formulae for the evaporation cross section. We then proceed to the discussion of *transition rates*, which enter in the description of the emission of more than one light particle via an evaporation cascade. Rate formulae will be derived for evaporation as well as for fission, the other important mode of decay of the compound nucleus. The rate of the accompanying process of  $\gamma$ -radiation will also be given. Last, we describe an example of a calculation of evaporation cascades.

### 10.2 The compound reaction cross section

#### 10.2.1 The fluctuation cross section

In analogy to what was found in Section 6.3.2 on compound-elastic scattering the contribution of the compound-nucleus mechanism in a general nuclear reaction gives rise to a fluctuating part of the reaction *S*-matrix. The energy average of the square of this fluctuating part determines the fluctuation cross section, which is identified with the compound reaction cross section.

In order to obtain the fluctuation cross section, we make use of the general formalism of Section 5.3, and consider the spin-coupled *S*-matrix  $S_{a \rightarrow b}^J$ . In analogy to eqn (6.101) we separate this *S*-matrix into an energy-averaged and a fluctuating term,

$$S_{a \rightarrow b}^J = \overline{S_{a \rightarrow b}^J} + S_{a \rightarrow b}^{J(f1)}, \quad (10.2)$$

where we have introduced the abbreviated channel index  $a = \{\underline{a}; l_a S_a\}$ , and similarly for  $b$ . The energy average of the fluctuating part  $S_{a \rightarrow b}^{J(f1)}$  vanishes by definition,

$$\overline{S_{a \rightarrow b}^{J(f1)}} = 0. \quad (10.3)$$

The fluctuations of the *S*-matrix cause similar fluctuations of the reaction cross section. Since these are generally not resolved in experiment, one considers the energy

average of the general unpolarized differential cross section (5.120) in conjunction with (5.122). This involves taking the average of a product of  $S$ -matrices which, in view of eqns (10.2) and (10.3), can be written as

$$\overline{(S_{a \rightarrow b}^{J*} - \delta_{ab})(S_{a' \rightarrow b'}^{J'} - \delta_{a'b'})} = \overline{(S_{a \rightarrow b}^{J*} - \delta_{ab})(S_{a' \rightarrow b'}^{J'} - \delta_{a'b'})} + \overline{S_{a \rightarrow b}^{J(f)} S_{a' \rightarrow b'}^{J'(f)}}. \quad (10.4)$$

We require that the fluctuating parts of  $S$ -matrices with different quantum numbers  $\{Jl_a l_b\}$  are uncorrelated random functions of the energy, so that the energy average of a product of two  $S$ -matrix elements satisfies the relation

$$\overline{S_{\{\underline{a}; l_a S_a\} \rightarrow \{\underline{b}; l_b S_b\}}^{J(f)} S_{\{\underline{a}; l'_a S_a\} \rightarrow \{\underline{b}; l'_b S_b\}}^{J'(f)}} = |S_{\{\underline{a}; l_a S_a\} \rightarrow \{\underline{b}; l_b S_b\}}^{J(f)}|^2 \delta_{JJ'} \delta_{l_a l'_a} \delta_{l_b l'_b}. \quad (10.5)$$

This is a basic assumption of the statistical theory of the compound-nucleus reaction.

The energy average of the differential cross section (5.120) is now decomposed into two terms

$$\frac{d\sigma_{\{\underline{a}; l_a S_a\} \rightarrow \{\underline{b}; l_b S_b\}}}{d\Omega_b} = \frac{d\sigma_{\{\underline{a}; l_a S_a\} \rightarrow \{\underline{b}; l_b S_b\}}^{\text{direct}}}{d\Omega_b} + \frac{d\sigma_{\{\underline{a}; l_a S_a\} \rightarrow \{\underline{b}; l_b S_b\}}^{\text{fl}}}{d\Omega_b}, \quad (10.6)$$

where the direct reaction cross section  $d\sigma_{a \rightarrow b}^{\text{direct}}/d\Omega_b$  and the fluctuation cross section  $d\sigma_{a \rightarrow b}^{\text{fl}}/d\Omega_b$  are each given by formula (5.120) in conjunction with eqn (5.122), in which  $(S_{a \rightarrow b}^{J*} - \delta_{ab})(S_{a' \rightarrow b'}^{J'} - \delta_{a'b'})$  is replaced with the first and second terms on the right-hand side of eqn (10.4), respectively.

In conformance with Section 6.3.2 we identify the fluctuation cross section with the compound reaction cross section (both are *average* quantities). This is most conveniently done for the partial reaction cross section (5.130). Taking the average of this quantity and using eqn (5.73) together with eqns (10.5) and (10.6), we find for the partial compound reaction cross section at total angular momentum  $J$  for the transition from the channel  $\{\underline{a}; l_a S_a\}$  to the channel  $\{\underline{b}; l_b S_b\}$

$$\sigma_{\{\underline{a}; l_a S_a\} \rightarrow \{\underline{b}; l_b S_b\}}^{J(C)} = \frac{\pi}{k_a^2} (2J+1) \overline{|S_{\{\underline{a}; l_a S_a\} \rightarrow \{\underline{b}; l_b S_b\}}^{J(f)}|^2}. \quad (10.7)$$

We employ this relation to replace the quantity  $|S_{a \rightarrow b}^{J(f)}|^2$  in the fluctuation cross section  $d\sigma_{a \rightarrow b}^{\text{fl}}/d\Omega_b$  with  $\sigma_{a \rightarrow b}^{J(C)}$ , and go over to the *angle-differential compound reaction cross section*  $d\sigma_{\{\underline{a}; I_x I_A\} \rightarrow \{\underline{b}; I_y I_B\}}^C/d\Omega_b$  using (5.116), (5.120), and (5.122). We find for this quantity

$$\begin{aligned} \frac{d\sigma_{\{\underline{a}; I_x I_A\} \rightarrow \{\underline{b}; I_y I_B\}}^C}{d\Omega_b} &= \frac{1}{(2I_x+1)(2I_A+1)} \frac{1}{4\pi} \sum_{L=0}^{\infty} P_L(\cos\theta) \sum_J \sum_{S_a l_a} \sum_{S_b l_b} \\ &(-)^{S_b - S_a} \tilde{Z}(l_a J l_a J, S_a L) \tilde{Z}(l_b J l_b J, S_b L) \frac{1}{2J+1} \sigma_{\{\underline{a}; l_a S_a\} \rightarrow \{\underline{b}; l_b S_b\}}^{J(C)}. \end{aligned} \quad (10.8)$$

In accordance with eqns (5.116) and (5.129), we obtain the integrated compound reaction cross section by integrating over the angle  $\Omega$ ,

$$\sigma_{\{\underline{a}; I_x I_A\} \rightarrow \{\underline{b}; I_y I_B\}}^C = \frac{1}{(2I_x+1)(2I_A+1)} \sum_{J=0}^{\infty} \sum_{S_a=|I_x-I_A|}^{I_x+I_A} \sum_{l_a=|J-S_a|}^{J+S_a} \sum_{S_b=|I_y-I_B|}^{I_y+I_B} \sum_{l_b=|J-S_b|}^{J+S_b} \sigma_{\{\underline{a}; l_a S_a\} \rightarrow \{\underline{b}; l_b S_b\}}^{J(C)}. \quad (10.9)$$

Both the differential and the integrated compound reaction cross sections consist of an incoherent sum over the total angular momentum  $J$ , whose individual terms contain as the essential physical quantity the partial compound reaction cross section  $\sigma_{a \rightarrow b}^{J(C)}$ .

### 10.2.2 The Hauser–Feshbach formula

#### Bohr's independence hypothesis

In the statistical picture the compound nucleus is regarded as a system which lives long enough to reach equilibrium between its modes of excitation. It has ‘forgotten’ all characteristics of the entrance channel except the conserved quantities such as particle number, energy, spin, and parity. Out of this state of equilibrium it decays into the open final channels. The decay of the compound nucleus depends only on its equilibrium properties, not on the way in which it was formed. This is the basis for the fundamental hypothesis of Bohr's compound reaction description, which postulates that *formation and decay of the compound nucleus are independent of each other*. Accordingly, the partial compound reaction cross section is factorized into the partial cross section for fusion from the entrance channel  $a$ ,  $\sigma_F^J(a)$ , and the probability  $G^J(b)$  for the decay of the compound nucleus to the final channel  $b$ ,

$$\sigma_{a \rightarrow b}^{J(C)} = \sigma_F^J(a) G^J(b), \quad (10.10)$$

where  $a = \{\underline{a}; l_a S_a\}$  and  $b = \{\underline{b}; l_b S_b\}$ . Of all the conserved quantities we have specified only the total spin  $J$  explicitly.

The definition of the fusion cross section as the compound reaction cross section summed over all final channels (cf. eqn (10.1)) carries over to the partial cross sections, and we have

$$\sigma_F^J(a) = \sum_b \sigma_{a \rightarrow b}^{J(C)}. \quad (10.11)$$

Therefore, the decay probabilities  $G^J(b)$  must satisfy

$$\sum_b G^J(b) = 1. \quad (10.12)$$

#### Application of the principle of detailed balance

In Section 5.3.3 we have derived the principle of detailed balance (5.131),

$$k_a^2 \sigma_{a \rightarrow b}^J = k_b^2 \sigma_{b \rightarrow a}^J, \quad (10.13)$$

which relates the unpolarized partial cross section of a reaction at total angular momentum  $J$  to that of its time-reverse.

The principle of detailed balance also holds for compound reaction cross sections, since a compound reaction is determined by a many-nucleon Hamiltonian  $H$  of the type (5.25) just like any other nuclear reaction. This Hamiltonian satisfies the relation of time-reversal invariance (5.91). A compound reaction is special only in that a large number of degrees of freedom is involved in its intermediate stage, and rather than following through the details of the reaction mechanism and keeping track of all phases, we prefer to simplify the calculation of the cross section by introducing the statistical picture of the compound nucleus.

From the cross section (10.10) for the reaction  $a \rightarrow b$  we obtain the cross section for the time-reversed reaction  $b \rightarrow a$  by interchanging the indices  $a$  and  $b$ ,

$$\sigma_{b \rightarrow a}^{J(C)} = \sigma_F^J(b) G^J(a). \quad (10.14)$$

Substituting both expressions in the detailed-balance relation (10.13), we find

$$\frac{k_a^2 \sigma_F^J(a)}{G^J(a)} = \frac{k_b^2 \sigma_F^J(b)}{G^J(b)}. \quad (10.15)$$

The left-hand side of this equation depends only on channel  $a$ , and the right-hand side only on channel  $b$ . Since  $a$  and  $b$  are arbitrary channels, both sides must be equal to a channel-independent quantity, which we call  $U$ . We then find that the probability for the decay of the compound nucleus to a channel  $b$  is given by

$$G^J(b) = \frac{k_b^2 \sigma_F^J(b)}{U}. \quad (10.16)$$

Equation (10.12) yields

$$U = \sum_b k_b^2 \sigma_F^J(b), \quad (10.17)$$

and we obtain from eqn (10.10) for the partial compound reaction cross section

$$\sigma_{a \rightarrow b}^{J(C)} = k_b \frac{\sigma_F^J(a) \sigma_F^J(b)}{\sum_c k_c^2 \sigma_F^J(c)}. \quad (10.18)$$

Thus the partial cross section for the compound reaction  $a \rightarrow b$  is exclusively determined by the partial fusion cross sections in all channels.

#### Partial fusion cross sections and transmission coefficients

Summing the compound reaction cross section (10.18) over the final states  $b$  and using eqns (10.7) and (10.11), we obtain the partial fusion cross section in the form

$$\sigma_F^J(a) = \frac{\pi}{k_a^2} (2J+1) \sum_b \overline{|S_{a \rightarrow b}^{J(\text{fl})}|^2}. \quad (10.19)$$

We now go back to the unitarity relation (5.114) and take the average over energy,

$$\sum_b \overline{|S_{a \rightarrow b}^J|^2} = 1, \quad (10.20)$$

or, with the decomposition (10.2),

$$\sum_b \overline{|S_{a \rightarrow b}^J|^2} + \sum_b \overline{|S_{a \rightarrow b}^{J(\text{fl})}|^2} = 1. \quad (10.21)$$

For simplicity we disregard the contribution of the direct reactions ( $a \neq b$ ) to the averaged  $S$ -matrix; however, we do take account of the shape-elastic scattering in the elastic channel,  $b = a$ . We thus set  $\overline{S_{a \rightarrow b}^J} \approx \delta_{ab} \overline{S_{a \rightarrow a}^J}$ , and use eqn (10.21) in expression (10.19) to obtain

$$\sigma_F^J(a) = \frac{\pi}{k_a^2} (2J+1) (1 - \overline{|S_{a \rightarrow a}^J|^2}). \quad (10.22)$$

Recalling the definition (6.120) we introduce the (optical) transmission coefficient

$$T_a^J = 1 - \overline{|S_{a \rightarrow a}^J|^2} \quad (10.23)$$

and have

$$\sigma_F^J(a) = \frac{\pi}{k_a^2} (2J+1) T_a^J. \quad (10.24)$$

For the compound reaction cross section (10.18) we can now write

$$\sigma_{a \rightarrow b}^{J(C)} = \frac{\pi}{k_a^2} (2J+1) \frac{T_a^J T_b^J}{\sum_c T_c^J}. \quad (10.25)$$

This is the *Hauser–Feshbach formula* (cf. Hauser and Feshbach 1952; Wolfenstein 1951). It expresses the partial compound reaction cross section purely in terms of transmission coefficients.

The neglect of the direct reaction contributions is a matter of convenience, allowing one to express the fusion cross section in terms of the shape-elastic  $S$ -function  $\overline{S_{a \rightarrow a}^J}$  which can be readily calculated with the help of an optical potential. However, it is clear from eqns (10.19) and (10.21) how the Hauser–Feshbach formula can be extended to include the effect of direct reactions: one simply writes for the transmission coefficients, instead of eqn (10.23),

$$T_a^J = 1 - \overline{|S_{a \rightarrow a}^J|^2} - \sum_{b \neq a} \overline{|S_{a \rightarrow b}^J|^2}, \quad (10.26)$$

where the sum goes over all the direct non-elastic channels  $b$  which one wishes to include. The corresponding  $S$ -matrix elements  $\overline{S_{a \rightarrow b}^J}$  can be obtained from coupled-channel calculations (cf. Section 9.5.3).

#### 10.2.3 The angle-differential cross section

In order to derive an explicit formula for the angle-differential compound reaction cross section, we substitute the Hauser–Feshbach expression (10.25) with  $a = \{\underline{a}; l_a S_a\}$  and  $b = \{\underline{b}; l_b S_b\}$  in the general formula (10.8). This yields

$$\begin{aligned} \frac{d\sigma_{\{\underline{a}; I_x I_A\} \rightarrow \{\underline{b}; I_y I_B\}}^C}{d\Omega_b} &= \frac{1}{(2I_x + 1)(2I_A + 1)} \frac{1}{4k_a^2} \sum_{L=0}^{\infty} P_L(\cos \theta) \\ &\times \sum_J \sum_{S_a l_a} \sum_{S_b l_b} (-)^{S_b - S_a} \tilde{Z}(l_a J l_a J, S_a L) \tilde{Z}(l_b J l_b J, S_b L) \\ &\times \frac{T_{l_a S_a}^J(\underline{a}) T_{l_b S_b}^J(\underline{b})}{\sum_c \sum_{I_z I_C} \sum_{S_c=|I_z-I_C|}^{I_z+I_C} \sum_{l_c=|J-S_c|}^{J-S_c} T_{l_c S_c}^J(\underline{c})}, \end{aligned} \quad (10.27)$$

where the channel  $c$  contains the nuclei  $z$  and  $C$ ,  $c = z + C$ , and  $\theta = \theta_b$  is the reaction angle (one should not confuse the nucleus  $C$  in channel  $c$  with the compound nucleus  $C$ ).

The  $\tilde{Z}$ -coefficients are, according to eqn (5.123), proportional to the Clebsch–Gordan coefficients  $(l_a 0; l_a 0 | L 0)$  and  $(l_b 0; l_b 0 | L 0)$ , respectively. These are non-vanishing only if  $2l_a + L = \text{even}$  or  $2l_b + L = \text{even}$ , i.e. if  $L = \text{even}$ . Since the Legendre polynomials  $P_L(\cos \theta)$  are even functions of  $\cos \theta$  for  $L = \text{even}$  and since  $|\cos \theta| = |\cos(\pi - \theta)|$ , the angular distribution of the products of a compound-nucleus reaction is *symmetric about 90°*. This feature of the differential cross section is a consequence of the randomness assumption (10.5) and provides an important test of the compound nature of a nuclear reaction.

Similarly, substituting eqn (10.25) in (10.9), one obtains for the integrated compound reaction cross section

$$\begin{aligned} \sigma_{\{\underline{a}; I_x I_A\} \rightarrow \{\underline{b}; I_y I_B\}}^C &= \frac{1}{(2I_x + 1)(2I_A + 1)} \frac{\pi}{k_a^2} \sum_{J=0}^{\infty} \sum_{S_a=|I_x-I_A|}^{I_x+I_A} \sum_{l_a=|J-S_a|}^{J+S_a} \\ &(2J+1) T_{l_a S_a}^J(\underline{a}) \frac{\sum_{S_b=|I_y-I_B|}^{I_y+I_B} \sum_{l_b=|J-S_b|}^{J+S_b} T_{l_b S_b}^J(\underline{b})}{\sum_c \sum_{I_z I_C} \sum_{S_c=|I_z-I_C|}^{I_z+I_C} \sum_{l_c=|J-S_c|}^{J-S_c} T_{l_c S_c}^J(\underline{c})}. \end{aligned} \quad (10.28)$$

#### The fusion cross section

The (unpolarized) fusion cross section is obtained from formula (10.28) by summing over all final channels  $b = \{\underline{b}; I_y I_B\}$ ,

$$\sigma_F(\underline{a}; I_x I_A) = \sum_{\underline{b}} \sum_{I_y I_B} \sigma_{\{\underline{a}; I_x I_A\} \rightarrow \{\underline{b}; I_y I_B\}}^C. \quad (10.29)$$

The denominator on the right-hand side of eqn (10.28) then cancels against a similar term in the numerator, and we find

$$\sigma_F(\underline{a}; I_x I_A) = \sum_{J=0}^{\infty} \sigma_F^J(\underline{a}; I_x I_A), \quad (10.30)$$

where the partial fusion cross section  $\sigma_F^J(\underline{a}; I_x I_A)$  is defined by

$$\sigma_F^J(\underline{a}; I_x I_A) = \frac{1}{(2I_x + 1)(2I_A + 1)} \sum_{S_a=|I_x-I_A|}^{I_x+I_A} \sum_{l_a=|J-S_a|}^{J+S_a} \sigma_F^J(\underline{a}; l_a S_a); \quad (10.31)$$

here

$$\sigma_F^J(\underline{a}; l_a S_a) = \frac{\pi}{k_a^2} (2J+1) T_{l_a S_a}^J(\underline{a}) \quad (10.32)$$

is the partial fusion cross section with specified orbital angular momentum  $l_a$  and channel spin  $S_a$ .

Expression (10.31) together with eqn (10.32) is the generalization of formula (9.19) for the fusion cross section for spinless particles, to which it reduces for  $I_x = I_A = 0$  (implying  $S_a = 0$  and  $J = l_a$ ) if we introduce the notation  $T_{l_a 0}^J = T_{l_a}$ .

The integrated compound reaction cross section (10.28) can now be written in the form

$$\begin{aligned} \sigma_{\{\underline{a}; I_x I_A\} \rightarrow \{\underline{b}; I_y I_B\}}^C &= \sum_{J=0}^{\infty} \sigma_F^J(\underline{a}; I_x I_A) \\ &\times \frac{\sum_{S_b=|I_y-I_B|}^{I_y+I_B} \sum_{l_b=|J-S_b|}^{J+S_b} T_{l_b S_b}^J(\underline{b})}{\sum_c \sum_{I_z I_C} \sum_{S_c=|I_z-I_C|}^{I_z+I_C} \sum_{l_c=|J-S_c|}^{J-S_c} T_{l_c S_c}^J(\underline{c})}. \end{aligned} \quad (10.33)$$

#### 10.2.4 The energy-differential cross section

Formula (10.28) gives the integrated compound reaction cross section for the transition from a spin-averaged initial state  $a$  to a final state  $b$  summed over spin projections. Usually a large number of final channels are open, so that many final states  $b$  are accessible in an energy interval  $d\epsilon_b$  of the order of magnitude of the experimental resolution. To describe experimental cross sections one must, therefore, sum over all final-channel states  $b$  with internal energies in the interval  $(\epsilon_b, \epsilon_b + d\epsilon_b)$ . Since we have two nuclei in channel  $b$ ,  $y$  and  $B$ , we must actually consider the two intervals  $(\epsilon_y, \epsilon_y + d\epsilon_y)$  and  $(\epsilon_B, \epsilon_B + d\epsilon_B)$  with  $\epsilon_b = \epsilon_y + \epsilon_B$ . We then write the cross section in the form

$$d^2\sigma_{a \rightarrow b}^C = \sigma_{a \rightarrow b}^C \rho_y(\epsilon_y^*; I_y) d\epsilon_y \rho_B(\epsilon_B^*; I_B) d\epsilon_B, \quad (10.34)$$

where  $\sigma_{a \rightarrow b}^C$  is the average cross section for the transition from the initial state  $a$  to any one of the final states  $b$  with energies in the interval specified above. The quantities  $\rho_B(\epsilon_B^*; I_B)$  and  $\rho_y(\epsilon_y^*; I_y)$  are the *level densities* of the nuclei  $B$  and  $y$ , respectively.

The level density  $\rho_B(\epsilon_B^*; I_B)$  is defined as *the number of states per unit energy* of the nucleus  $B$  with spin  $I_B$  at the internal excitation energy  $\epsilon_B^* = \epsilon_B - \epsilon_B^0$  ( $\epsilon_B^0$  is its ground-state energy). If several states have the same excitation energy, so that the corresponding energy level is degenerate, this degeneracy is taken into account. The only exception is the trivial spin degeneracy  $2I_B + 1$  which is *not* included in counting the number of states. The definition of the level density  $\rho_y(\epsilon_y^*; I_y)$  is analogous.

We now introduce the excitation energy  $E_C^*$  of the compound nucleus,

$$E_C^* = E_C - E_C^0, \quad (10.35)$$

where  $E_C^0$  is the ground-state energy of the compound nucleus, and its *binding energy*  $B_b$  with respect to the channel  $b = y + B$  (cf. Section 9.2.2)

$$B_b = \epsilon_b^0 - E_C^0 = \epsilon_y^0 + \epsilon_B^0 - E_C^0. \quad (10.36)$$

The total available energy in a final channel  $b$ ,  $\epsilon_y + \epsilon_B + \mathcal{E}_b$ , where  $\mathcal{E}_b$  is the (kinetic) channel energy, is equal to the energy of the compound nucleus,  $\epsilon_y + \epsilon_B + \mathcal{E}_b = E_C$ . Then the internal excitation energy in the final nucleus  $B$  can be written in the form

$$\epsilon_B^* = \epsilon_B - \epsilon_B^0 = E_C - \epsilon_y - \mathcal{E}_b - \epsilon_B^0 = E_C^* - \epsilon_y^* - B_b - \mathcal{E}_b, \quad (10.37)$$

where we have used eqns (10.35) and (10.36). Since it is the channel energy  $\mathcal{E}_b$  in channel  $b$  which is directly measured, we employ eqn (10.37) to introduce it in the argument of the level density  $\rho_B(\epsilon_B^*)$ , replacing  $\epsilon_B^*$  as the variable. Equation (10.34) then yields the energy-differential compound reaction cross section for the transition to all final nuclear states in the energy interval  $(\mathcal{E}_b, \mathcal{E}_b + d\mathcal{E}_b)$  with spins  $I_y$  and  $I_B$ , respectively,

$$\frac{d\sigma_{a \rightarrow b}^C}{d\mathcal{E}_b} = \int d\epsilon_y \sigma_{a \rightarrow b}^C \rho_y(\epsilon_y^*; I_y) \rho_B(E_C^* - \epsilon_y^* - B_b - \mathcal{E}_b; I_B). \quad (10.38)$$

More explicitly, the energy-differential cross section has the form (cf. eqn (10.33))

$$\begin{aligned} \frac{d\sigma_{\{\underline{a}; I_x I_A\} \rightarrow \{\underline{b}; I_y I_B\}}^C}{d\mathcal{E}_b} &= \sum_{J=0}^{\infty} \sigma_F^J(\underline{a}; I_x I_A; \mathcal{E}_b) \\ &\times \frac{T^J(\underline{b}; I_y I_B; \mathcal{E}_b)}{\sum_{\underline{c}} \sum_{I_z I_C} \int_0^{E_C^* - B_c} d\mathcal{E}_c T^J(\underline{c}; I_z I_C; \mathcal{E}_c)}, \end{aligned} \quad (10.39)$$

where the partial fusion cross section  $\sigma_F^J(\underline{a}; I_x I_A; \mathcal{E}_b)$  is given by eqn (10.31), and where we have introduced the notation

$$\begin{aligned} T^J(\underline{b}; I_y I_B; \mathcal{E}_b) &= \sum_{S_b=|I_y - I_B|}^{I_y + I_B} \sum_{l_b=|J - S_b|}^{J+S_b} \int d\epsilon_y \rho_y(\epsilon_y^*; I_y) \\ &\times \rho_B(E_C^* - \epsilon_y^* - B_b - \mathcal{E}_b; I_B) T_{l_b, S_b}^J(\underline{b}; \mathcal{E}_b) \end{aligned} \quad (10.40)$$

in the numerator, and correspondingly in the denominator. In these formulae we have made explicit the dependence of the transmission coefficients on the channel energy,  $T_{l_b, S_b}^J(b) = T_{l_b, S_b}^J(\underline{b}; \mathcal{E}_b)$ . They are regarded as averages over the interval  $(\mathcal{E}_b, \mathcal{E}_b + d\mathcal{E}_b)$ .

#### *The transmission coefficients in the Hauser–Feshbach formula*

The expression for the compound reaction cross section contains transmission coefficients and level densities. The calculation of the latter is a topic requiring a separate discussion, which we defer to the following section. As to the transmission coefficients, these have already been discussed in Section 9.4. There we considered the fusion of nuclei in their ground states. However, in the Hauser–Feshbach formula we are dealing with transmission coefficients  $T(b)$  for final channels  $b$  in which the nuclei are in general highly excited. Two methods for obtaining the transmission coefficients for excited nuclei are usually employed: (i) one simply assumes complete absorption for them and uses the model of a black nucleus as in eqn (9.18), or (ii) one calculates, somewhat more realistically, the transmission coefficients with the help of optical-model formulae of

the type (10.23), where the optical potentials are determined by fitting elastic scattering cross sections at an energy equal to the channel energy  $\mathcal{E}_b$ .

Furthermore, transmission coefficients have meaning only for two-body channels, whereas compound nuclei generally can also decay to channels containing more than two nuclei. Particular examples of such processes are break-up and multifragmentation, which occur at high compound-nucleus energies. However, at the energies which we are considering here the final nuclei, if they are not bound, are at least quasi-stable in the compound-nucleus sense, and decay afterwards in a sequential process. Transmission coefficients can then be defined for each stage of such a *cascade* of decays. These processes will be discussed in Section 10.4.

## 10.3 The nuclear level density

The level density of a nucleus with nucleon number  $A$  and energy  $\epsilon$  is defined as the number of nuclear states in the range  $(\epsilon, \epsilon + d\epsilon)$  divided by the energy interval  $d\epsilon$ . In order to calculate the level density one must, strictly speaking, determine all eigenvalues (and their degeneracy) of the nuclear Hamiltonian  $h_A$  and count how many of these fall into the interval  $(\epsilon_A, \epsilon_A + d\epsilon_A)$ . This can be done only in very simple models, as for example independent-particle models. Even then, the explicit counting of levels is onerous, and one usually takes recourse to more indirect methods. In the present section we shall first derive the level density of an ideal Fermi gas in a thermodynamical approach, which will lead to the Bethe formula. Next we apply a somewhat different method for a more realistic calculation using the nuclear shell model.

### 10.3.1 The level density in the Fermi gas model

In the Fermi gas model the nucleus is regarded as an ideal gas of  $A$  fermions enclosed in the fixed nuclear volume

$$V = \frac{4\pi}{3} R^3 \quad \text{with} \quad R = r_0 A^{1/3}. \quad (10.41)$$

We are thus dealing with a system of  $A$  independent nucleons each moving in a spherical, infinite square-well potential, as shown in Fig. 10.1. This ‘spherical box’ is assumed to be generated by the average field of the nucleons, and represents an idealization of the more realistic single-particle Coulomb-plus-nuclear potential employed in the shell model.

The most convenient way of describing the thermodynamics of the ideal Fermi gas is to introduce the notion of the *grand-canonical ensemble*, where the system is assumed to have a fixed temperature  $T$  and a fixed chemical potential  $\mu$ . The latter is defined as the energy required to add an extra particle to the system. This approach is justified for large systems. How well it applies to nuclei will be discussed in Section 10.3.3. The Fermi gas is treated in books on statistical thermodynamics (cf. Becker 1964, §53). We repeat the derivations here in order to use them as a reference in the rather similar shell-model approach of Section 10.3.2.

In the grand-canonical ensemble with temperature  $T$  and chemical potential  $\mu$  the many-particle states  $i$  with energy  $E_i$  and particle number  $N_i$  are distributed according

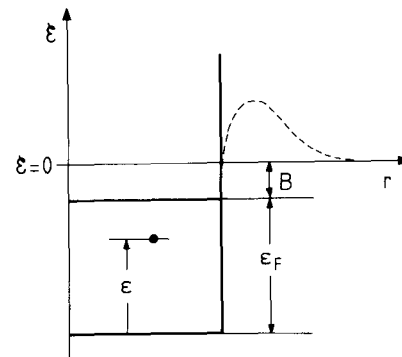


**Figure 10.1** A nucleon in a spherical infinite square well. The dashed curve represents schematically the Coulomb-plus-nuclear potential. The energy  $\epsilon$  is reckoned from the bottom of the well, and the energy  $\mathcal{E}$  from the continuum threshold  $\mathcal{E} = 0$ . The Fermi energy  $\epsilon_F$  and the binding energy  $B$  of the least-bound fermion in the ground state of the system ( $T = 0$ ) are indicated.

to the law

$$w_i = w_i(\mu, \beta) = \frac{1}{Z(\mu, \beta)} e^{-\beta(E_i - \mu N_i)}, \quad (10.42)$$

where  $Z(\mu, \beta)$  is the *grand partition sum* over all states  $i$  of the system,

$$Z(\mu, \beta) = \sum_i e^{-\beta(E_i - \mu N_i)}; \quad (10.43)$$

here  $\beta = 1/k_B T$  is the (inverse) temperature, and  $k_B$  is the Boltzmann constant. We use the letter  $E_i$  to denote the energy of the system (nucleus) as a whole, in contrast to the notation  $\epsilon_A$  we have employed so far. We do this in order to adhere to the customary notation for the description of the Fermi gas, where the letter  $\epsilon$  denotes the energy of a *single fermion*.

The procedure for calculating the level density is to derive expressions for the average particle number in the grand-canonical ensemble

$$\overline{N(\mu, \beta)} = \sum_i w_i N_i \quad (10.44)$$

and for the average energy

$$\overline{E(\mu, \beta)} = \sum_i w_i E_i, \quad (10.45)$$

which are functions of the parameters  $\mu$  and  $\beta$ . These average quantities are then set equal to the actual number of fermions  $A$  and the actual energy  $E$  of the system,

$$\overline{N(\mu, \beta)} = A, \quad (10.46)$$

$$\overline{E(\mu, \beta)} = E. \quad (10.47)$$

By inverting these relations one obtains the chemical potential and the temperature as functions of  $A$  and  $E$ ,  $\mu = \mu(A, E)$  and  $(k_B T)^{-1} = \beta = \beta(A, E)$ . One then calculates the entropy  $S = S(\mu, \beta) = S(A, E)$  with the help of the thermodynamical relation

$$S(A, E) = \int_{E_0}^E \frac{dE'}{T(A, E')}, \quad (10.48)$$

where  $E_0$ , the energy at zero temperature, is identified with the energy of the ground state of the system. The density of states  $\rho(A, E)$  for given particle number  $A$  and total energy  $E$  in terms of the entropy  $S(A, E)$  is finally obtained with the help of the fundamental relation (cf. Becker 1964, §45; Reif 1965, eqn (3.3.12))

$$\rho(A, E) = \rho(A, E_0) e^{S(A, E)/k_B}. \quad (10.49)$$

We now go through this procedure for a gas of independent fermions. We label the single-particle states by  $v$  and denote their energies by  $\epsilon(v)$ . The many-particle states  $i$  of the system are then determined by specifying the sets of occupation numbers  $n_i(v)$  for each  $i$ . Since each single-particle state can be occupied by at most one fermion we have  $n_i(v) = 0$  or  $1$ . The particle number of a state  $i$  is given by

$$N_i = \sum_v n_i(v), \quad (10.50)$$

and the energy by

$$E_i = \sum_v n_i(v) \epsilon(v). \quad (10.51)$$

The grand partition sum (10.43) then becomes

$$Z(\mu, \beta) = \sum_i e^{-\beta \sum_v n_i(v)[\epsilon(v) - \mu]} = \sum_i \prod_v e^{-\beta n_i(v)[\epsilon(v) - \mu]}. \quad (10.52)$$

Each state  $i$  is associated with a different assignment of the values 0 and 1 to the occupation numbers  $n_i(v)$  of the complete set of single-particle states  $v$ . Therefore, the right-hand side of eqn (10.52) can be rewritten as a product over  $v$  of a sum of two terms, one with  $n_i(v) = 0$ , the other with  $n_i(v) = 1$ ,

$$Z(\mu, \beta) = \prod_v \left( 1 + e^{-\beta[\epsilon(v) - \mu]} \right). \quad (10.53)$$

Using first the left-hand part of eqn (10.52) and then eqn (10.53), we now find for the average occupation number  $\bar{n}(v)$  of the level  $v$ ,

$$\bar{n}(v) = \sum_i w_i n_i(v) = -\frac{1}{\beta} \frac{\partial}{\partial \epsilon(v)} \ln Z(\mu, \beta) \Big|_{\mu, \beta = \text{const}} = \frac{1}{1 + e^{\beta[\epsilon(v) - \mu]}}. \quad (10.54)$$

According to eqns (10.44), (10.46), and (10.50), we find for the fermion number  $A$ ,

$$A = \overline{N(\mu, \beta)} = \sum_v \bar{n}(v), \quad (10.55)$$

and for the energy  $E$ , employing eqns (10.45), (10.47), and (10.51),

$$E = \overline{E(\mu, \beta)} = \sum_v \bar{n}(v) \epsilon(v). \quad (10.56)$$

Alternatively, using eqns (10.42) to (10.44) and eqn (10.46), we have for the fermion number  $A$

$$A = \frac{1}{\beta} \frac{\partial}{\partial \mu} \ln Z(\mu, \beta) \Big|_{\beta=\text{const}}, \quad (10.57)$$

and for the energy  $E$ , using eqns (10.45) and (10.47),

$$E = \mu A - \frac{\partial}{\partial \beta} \ln Z(\mu, \beta) \Big|_{\mu=\text{const}}. \quad (10.58)$$

Equations (10.55) and (10.56) will be employed presently for the calculation of the ground-state properties of the system, when  $T = 0$  or  $\beta \rightarrow \infty$ , while eqns (10.57) and (10.58) will be considered later in the discussion of the excited system for  $T > 0$ .

We now derive analytic expressions for the functions  $A = A(\mu, \beta)$  and  $E = E(\mu, \beta)$ . To this end we go over to the continuum limit for the single-particle spectrum, and consider the number of single-particle states of fermions with momentum  $p(v) = p$  in the interval  $(p, p + dp)$  and the volume  $V$

$$g(p)dp = 4 \frac{V 4\pi}{(2\pi\hbar)^3} p^2 dp. \quad (10.59)$$

In terms of the single-particle energy  $\epsilon = \epsilon(p) = p^2/2m$  this takes the form

$$g(\epsilon)d\epsilon = 4 \frac{V 4\pi 2^{1/2} m^{3/2}}{(2\pi\hbar)^3} \epsilon^{1/2} d\epsilon, \quad (10.60)$$

where  $m$  is the nucleon mass, and the factor 4 has been introduced, in anticipation of nuclear applications, to take account of the spin-isospin degeneracy. Instead of eqns (10.55) and (10.56) we then write

$$A = \int_0^\infty d\epsilon g(\epsilon) \bar{n}(\epsilon), \quad (10.61)$$

$$E = \int_0^\infty d\epsilon g(\epsilon) \bar{n}(\epsilon) \epsilon. \quad (10.62)$$

### The ground state ( $T = 0$ )

Let us calculate the integrals (10.61) and (10.62) first for zero temperature,  $T = 0$ , i.e. for the ground state of the system with particle number  $A$  and energy  $E = E_0$ . The value of the chemical potential in the ground state  $\mu_0 = \mu(A, E_0)$  is the *Fermi energy*,

$$\mu_0 = \epsilon_F. \quad (10.63)$$

For  $T = 0$  ( $\beta \rightarrow \infty$ ) the average occupation number (10.54) as a function of the fermion energy  $\epsilon$  becomes

$$\bar{n}(\epsilon) = \begin{cases} 1 & \text{for } \epsilon < \epsilon_F, \\ 0 & \text{for } \epsilon > \epsilon_F. \end{cases} \quad (10.64)$$

Then we find from eqns (10.60) and (10.61)

$$A = \int_0^{\epsilon_F} d\epsilon g(\epsilon) = \frac{16\pi}{3} \frac{(2m\epsilon_F)^{3/2}}{(2\pi\hbar)^3} V. \quad (10.65)$$

This relation together with eqn (10.41) implies that the Fermi energy  $\epsilon_F$  is determined by the radius parameter  $r_0$ ,

$$\epsilon_F = \frac{(9\pi)^{2/3}}{2mc^2} \left( \frac{\hbar c}{2r_0} \right)^2. \quad (10.66)$$

The single-particle density of states (10.60) can now be written, by eliminating  $V$  with the help of eqn (10.65),

$$g(\epsilon) = \frac{3}{2} \frac{A}{\epsilon_F^{3/2}} \epsilon^{1/2}. \quad (10.67)$$

Substituting this result in eqn (10.62) and using eqn (10.64), we obtain for the ground-state energy of the system

$$E_0 = \int_0^{\epsilon_F} d\epsilon \epsilon g(\epsilon) = \frac{3}{5} \epsilon_F A. \quad (10.68)$$

### The excited state ( $T > 0$ )

In order to calculate the average energy at finite temperature we shall make use of relations (10.57) and (10.58), and therefore begin by considering the logarithm of the grand partition sum (10.53),

$$\ln Z(\mu, \beta) = \sum_v \ln \left( 1 + e^{-\beta(\epsilon(v) - \mu)} \right) = \int_0^\infty d\epsilon g(\epsilon) \ln \left( 1 + e^{-\beta(\epsilon - \mu)} \right). \quad (10.69)$$

We subdivide the integral from 0 to  $\infty$  into an integral from 0 to  $\mu$ , at the same time changing to the variable  $x = \mu - \epsilon$ , and an integral from  $\mu$  to  $\infty$ , with the new variable  $x = \epsilon - \mu$ . We then find

$$\ln Z(\mu, \beta) = \int_0^\mu dx g(\mu - x) \ln(1 + e^{\beta x}) + \int_0^\infty dx g(\mu + x) \ln(1 + e^{-\beta x}). \quad (10.70)$$

In the first integral we set  $(1 + e^{\beta x}) = e^{\beta x}(1 + e^{-\beta x})$  and obtain

$$\begin{aligned} \ln Z(\mu, \beta) = & \int_0^\mu dx g(\mu - x) \beta x + \int_0^\mu dx g(\mu - x) \ln(1 + e^{-\beta x}) \\ & + \int_0^\infty dx g(\mu + x) \ln(1 + e^{-\beta x}). \end{aligned} \quad (10.71)$$

The integrands in the last two integrals contribute appreciably only for  $x < 1/\beta = k_B T$ . For small temperatures we have  $\mu \gg 1/\beta$ . Therefore we can replace the upper limit  $\mu$  in the second integral with  $\infty$ , combine the second and third integrals, and expand  $g(\mu - x) + g(\mu + x)$  in powers of  $x$ ,

$$g(\mu - x) + g(\mu + x) = 2g(\mu) + g''(\mu)x^2 + \dots \quad (10.72)$$

Integrating by parts and using formula (3.411.4) of Gradshteyn and Ryzhik (1965),

$$\begin{aligned} \int_0^\infty dx \ln(1 + e^{-\beta x}) &= \frac{1}{\beta} \int_0^\infty \frac{y dy}{1 + e^y} = \frac{\pi^2}{12\beta}, \\ \int_0^\infty dx x^2 \ln(1 + e^{-\beta x}) &= \frac{1}{3\beta^3} \int_0^\infty \frac{y^3 dy}{1 + e^y} = \frac{7\pi^4}{360\beta^3}, \end{aligned}$$

we obtain

$$\ln Z(\mu, \beta) = \beta \int_0^\mu d\epsilon g(\epsilon)(\mu - \epsilon) + g(\mu) \frac{\pi^2}{6\beta} + g''(\mu) \frac{7\pi^4}{360\beta^3} + \dots \quad (10.73)$$

The last term is negligible for large values of  $\beta$ , i.e. for small temperatures, and for slow variations of  $g(\mu)$ .

Using the expansion (10.73) of the grand partition sum we now derive the particle number  $A$  from eqn (10.57) and the energy  $E$  from eqn (10.58). To lowest non-vanishing order in  $T = 1/k_B\beta$  we find

$$A = \int_0^\mu d\epsilon g(\epsilon) + g'(\mu) \frac{\pi^2}{6\beta^2}, \quad (10.74)$$

$$E = \int_0^\mu d\epsilon g(\epsilon)\epsilon + g(\mu) \frac{\pi^2}{6\beta^2} + \mu g'(\mu) \frac{\pi^2}{6\beta^2}. \quad (10.75)$$

For low temperatures the parameter  $\mu$  is close to  $\mu_0 = \epsilon_F$ , and we may write

$$\begin{aligned} \int_0^\mu d\epsilon g(\epsilon) &= \int_0^{\epsilon_F} d\epsilon g(\epsilon) + g(\epsilon_F)(\mu - \epsilon_F) + \dots \\ &= A + g(\epsilon_F)(\mu - \epsilon_F) + \dots, \end{aligned} \quad (10.76)$$

$$\begin{aligned} \int_0^\mu d\epsilon g(\epsilon)\epsilon &= \int_0^{\epsilon_F} d\epsilon g(\epsilon)\epsilon + g(\epsilon_F)\epsilon_F(\mu - \epsilon_F) + \dots \\ &= E_0 + g(\epsilon_F)\epsilon_F(\mu - \epsilon_F) + \dots, \end{aligned} \quad (10.77)$$

where we have used eqns (10.65) and (10.68). Substituting the integral (10.76) in eqn (10.74) we obtain

$$g'(\mu) \frac{\pi^2}{6\beta^2} \approx -g(\epsilon_F)(\mu - \epsilon_F). \quad (10.78)$$

We therefore find with the help of eqns (10.75) and (10.77),

$$E = E_0 - g(\epsilon_F)(\mu - \epsilon_F)^2 + g(\mu) \frac{\pi^2}{6\beta^2}. \quad (10.79)$$

Equation (10.78) implies that  $\mu - \epsilon_F = \mathcal{O}(\beta^{-2})$ . Up to second order we may therefore neglect the second term on the right-hand side of eqn (10.79), and replace  $\mu$  with  $\epsilon_F$  in the function  $g(\mu)$  in the third term. We then obtain

$$E = E_0 + g(\epsilon_F) \frac{\pi^2}{6\beta^2}, \quad (10.80)$$

and the excitation energy  $E^* = E - E_0$  becomes, with  $\beta = 1/k_B T$ ,

$$E^* = a(k_B T)^2. \quad (10.81)$$

Here we have introduced the *level density parameter*

$$a = \frac{\pi^2}{6} g(\epsilon_F), \quad (10.82)$$

which is determined by the single-particle level density at the Fermi energy  $g(\epsilon_F)$ . Equation (10.81) is a basic result of the thermodynamics of fermions. It states that the excitation energy of an ideal Fermi gas is proportional to the square of the temperature.

Let us now determine the values of the parameters of the Fermi gas model in its application to the nucleus. Substituting in formula (10.66) the nucleon mass  $mc^2 = 940$  MeV and the nuclear radius parameter  $r_0 = 1.1$  fm, we find for the Fermi energy in nuclei

$$\epsilon_F \approx 40 \text{ MeV}. \quad (10.83)$$

This is the energy of the highest level occupied by the nucleons in the nucleus at zero temperature (i.e. in the ground state). The nucleons are here regarded as being enclosed in a spherical box of the volume of the nucleus, that is, the nucleons move in a square well with infinitely high walls (cf. Fig. 10.1). In a realistic nucleus these walls cannot be infinitely high, because the nucleons must be allowed to leave the nucleus at sufficiently high excitation energies. Moreover, the potential well will not be square, but is rather expected to have the shape of the shell-model or Woods–Saxon potentials. However, one is interested only in the states below and slightly above the Fermi level, i.e. the states filling the levels in the lower part of the well. For these, we may, for the moment, retain the picture of the infinite square well.

The Fermi energy is reckoned from the bottom of this well (cf. Fig. 10.1). The position of the latter relative to the threshold energy  $\mathcal{E} = 0$  of a particle outside the well is determined as follows. According to the definition of the chemical potential, the Fermi energy is the energy which one has to supply when adding another fermion to the system of  $A$  fermions in the ground state. We now recall that one actually gains the binding energy  $B \approx 8$  MeV by adding a nucleon at rest to a nucleus in the ground state; therefore, the bottom of the well must be placed at the energy  $-\epsilon_F - B \approx -48$  MeV below the continuum threshold energy  $\mathcal{E} = 0$ .

The value of the level density parameter  $a$  is obtained from eqns (10.67), (10.82), and (10.83) as

$$a \approx \frac{A}{16} \text{ MeV}^{-1}. \quad (10.84)$$

This value is about a factor of two too small compared to the empirical value of  $a \approx A/8$  (cf. Section 10.3.4 and Fig. 10.2), because the single-particle level density at the Fermi energy is smaller for a Fermi gas in a spherical box than for a realistic nucleus, in which the well widens toward the top. The temperature is proportional to the square root of the excitation energy, and we find, using eqn (10.81), that for example the nucleus  $^{208}\text{Pb}$  at an excitation energy of 100 MeV has the temperature  $k_B T = \sqrt{E^*/a} \approx \sqrt{8E^*/A} \approx 2$  MeV. Comparison of this value with the value of  $\mu \approx \epsilon_F = 40$  MeV shows that the condition  $\mu \gg 1/\beta$ , necessary for our derivations, is well satisfied.

### The Bethe formula

The change of entropy for constant volume  $V$  and particle number  $A$  is connected with the change of energy by the relation

$$dS = \frac{dE}{T}, \quad (10.85)$$

so that according to the inverse of eqn (10.81)

$$S(E) = \int_{E_0}^E \frac{dE'}{T} = k_B \int_0^{E^*} dE'^* \sqrt{\frac{a}{E'^*}} = 2k_B \sqrt{a E^*}. \quad (10.86)$$

Introducing the new notation  $\rho(A, E) = \rho_A(E^*)$ , we now employ the relation (10.49) and find for the level density

$$\rho_A(E^*) = \rho_A(0) e^{2\sqrt{a E^*}}. \quad (10.87)$$

This is the *Bethe formula* (cf. Bethe 1937), in which the level density depends exponentially on the excitation energy  $E^*$ . The dependence on the nucleon number  $A$  is mainly contained in the level density parameter  $a$  (cf. eqn (10.84)).

### 10.3.2 The level density in the nuclear shell model

We now proceed from the Fermi gas model to the more realistic nuclear shell model (cf. Ericson 1959, 1960; Bohr and Mottelson 1969, Appendix 2B). In doing this we shall calculate the level density by a method which is somewhat different from the thermodynamical one used above.

In the nuclear shell model the single-nucleon states  $v$  are eigenstates of the phenomenological shell-model potential. A many-nucleon shell-model state  $i$  is again specified in terms of the occupation numbers  $n_i(v)$ . These determine the nucleon number  $N_i$  via formula (10.50), and the nuclear energy  $E_i$  via formula (10.51). The exact shell-model level density for a nucleus with particle number  $A$  and energy  $E$  is given by

$$\rho(A, E) = \sum_i \delta(A - N_i) \delta(E - E_i). \quad (10.88)$$

This expression consists of a sum of many close-lying  $\delta$ -peaks. Our aim is to arrive at a ‘smoothed’ analytic expression for this level density.

To this end we introduce the Laplace transform of the level density,

$$Z(\alpha, \beta) = \int_0^\infty dA \int_0^\infty dE \rho(A, E) e^{-(\beta E - \alpha A)} = \sum_i e^{-(\beta E_i - \alpha N_i)}. \quad (10.89)$$

Evaluating the sum on the right-hand side using appropriate approximations, one arrives at a smooth function  $Z(\alpha, \beta)$  whose inverse Laplace transform yields a continuous level density function  $\rho(A, E)$ . Although here the parameter  $\beta$  is not the temperature, and the parameter  $\alpha/\beta$  not the chemical potential, the Laplace transform (10.89) evidently has the same structure as the grand partition sum (10.43). The present approach is therefore essentially equivalent to the thermodynamical one.

As in eqn (10.53) we can again write

$$Z(\alpha, \beta) = \prod_v \left\{ 1 + e^{\alpha - \beta \epsilon(v)} \right\}. \quad (10.90)$$

We define a *single-particle density* of shell-model states

$$g(\epsilon) = \sum_v \delta[\epsilon - \epsilon(v)] \quad (10.91)$$

with the energy scale shifted such that  $\epsilon(v) \geq 0$  for all  $v$ . We then take the logarithm of expression (10.90) and write it as

$$\ln Z(\alpha, \beta) = \int_0^\infty d\epsilon g(\epsilon) \ln(1 + e^{\alpha - \beta \epsilon}). \quad (10.92)$$

We may replace the single-particle density  $g(\epsilon)$  of eqn (10.91) with a smooth function equal to its average if the interval  $1/\beta$  inside of which the logarithm in the integrand of eqn (10.92) gives the main contribution is large compared to the spacing of the single-particle levels  $\epsilon(v)$ ,  $g^{-1}(\epsilon_F)$ , i.e. if

$$\frac{g(\epsilon_F)}{\beta} \gg 1. \quad (10.93)$$

Then we employ again the expansion (10.73), replacing  $\mu$  with  $\alpha/\beta$ ,

$$\ln Z(\alpha, \beta) = \int_0^{\alpha/\beta} d\epsilon g(\epsilon)(\alpha - \beta\epsilon) + g(\alpha/\beta) \frac{\pi^2}{6\beta} + g''(\alpha/\beta) \frac{7\pi^4}{360\beta^3} + \dots \quad (10.94)$$

Finally, the level density is obtained by applying the inverse Laplace transform,

$$\begin{aligned} \rho(A, E) &= \frac{1}{(2\pi i)^2} \iint_{-i\infty}^{i\infty} d\alpha d\beta Z(\alpha, \beta) e^{-\alpha A + \beta E} \\ &= -\frac{1}{(2\pi)^2} \iint_{-i\infty}^{i\infty} d\alpha d\beta \exp \Phi(\alpha, \beta), \end{aligned} \quad (10.95)$$

where

$$\Phi(\alpha, \beta) = \ln Z(\alpha, \beta) - \alpha A + \beta E. \quad (10.96)$$

For the explicit evaluation of the integral (10.95) we use the two-dimensional saddle-point method. The saddle point  $(\alpha_s, \beta_s)$  is determined by the conditions

$$\begin{aligned} \frac{\partial \Phi}{\partial \alpha} &= \frac{\partial \ln Z}{\partial \alpha} - A = 0, \\ \frac{\partial \Phi}{\partial \beta} &= \frac{\partial \ln Z}{\partial \beta} + E = 0. \end{aligned} \quad (10.97)$$

Substituting expression (10.94) in these equations and neglecting all derivatives of  $g(\mu)$ , we find

$$\int_0^{\mu_s} d\epsilon g(\epsilon) = A, \quad (10.98)$$

$$\int_0^{\mu_s} d\epsilon g(\epsilon) \epsilon + \frac{\pi^2}{6\beta_s^2} g(\mu_s) = E, \quad (10.99)$$

where  $\mu_s = \alpha_s/\beta_s$ .

Equations (10.50) and (10.51) imply for the shell-model ground state with energy  $E_0$

$$A = \int_0^{\epsilon_F} d\epsilon g(\epsilon), \quad (10.100)$$

$$E_0 = \int_0^{\epsilon_F} d\epsilon g(\epsilon) \epsilon, \quad (10.101)$$

where  $\epsilon_F$  is the Fermi energy in the shell model. Comparing eqns (10.98) and (10.99) with eqns (10.100) and (10.101), we see that, to lowest order in  $1/\beta$ , the stationary point  $(\alpha_s, \beta_s)$  is determined by the Fermi energy and the excitation energy:

$$\frac{\alpha_s}{\beta_s} = \mu_s = \epsilon_F, \quad (10.102)$$

$$\frac{\pi^2}{6\beta_s^2} g(\epsilon_F) = E - E_0 = E^*. \quad (10.103)$$

The integral (10.95) becomes

$$\rho(A, E) = \frac{1}{2\pi\sqrt{\det D}} \exp [\ln Z(\alpha_s, \beta_s) - \alpha_s A + \beta_s E], \quad (10.104)$$

where the determinant  $\det D$  is given by

$$\det D = \left[ \frac{\partial^2 \ln Z}{\partial \alpha^2} \frac{\partial^2 \ln Z}{\partial \beta^2} - \left( \frac{\partial^2 \ln Z}{\partial \alpha \partial \beta} \right)^2 \right]_{\alpha_s, \beta_s} = \frac{12}{\pi^2} (E^*)^2. \quad (10.105)$$

An explicit expression for the exponent is obtained by using eqns (10.94), (10.98), (10.99), (10.102), and (10.103), and we arrive finally at the following expression for the level density,

$$\rho_A(E^*) = \frac{1}{\sqrt{48} E^*} \exp \left( 2\sqrt{\frac{\pi^2}{6} g(\epsilon_F) E^*} \right). \quad (10.106)$$

This formula agrees with the Bethe formula (10.87) except for the pre-factor and the definition of the single-particle level density  $g(\epsilon_F)$ , which here has to be obtained from the single-particle spectrum in the shell model. The formula has to be modified if more than one kind of particle (protons and neutrons) is considered, and if collective states are involved. For a further discussion we refer to Section 10.3.4.

### 10.3.3 On the derivation of the level density formulae

The level density of a nucleus with nucleon number  $A$  and energy  $E$  was defined at the beginning of Section 10.3 as the number of nuclear states in the range  $(E, E + dE)$  divided by the energy interval  $dE$ . We have calculated this quantity for the Fermi gas by thermodynamics, and for the nuclear shell model by the saddle-point method.

In the thermodynamical approach we have represented the system of nucleons by a grand-canonical ensemble at fixed chemical potential and temperature, rather than by a micro-canonical ensemble at fixed particle number and energy, as would be the correct procedure. We did this in order to avoid having to implement the cumbersome conditions of fixed  $A$  and  $E$  when counting the levels. The replacement of the micro- with the grand-canonical ensemble is allowed if the identification of the particle number and the energy with their ensemble averages is justified, i.e. if the fluctuations of these quantities about their mean values are small,

$$\left( \frac{\Delta N}{N} \right)^2 \ll 1, \quad (10.107)$$

$$\left( \frac{\Delta E}{E - E_0} \right)^2 \ll 1. \quad (10.108)$$

Let us consider these quantities in the Fermi gas model. We first discuss the variance of the particle number

$$(\Delta N)^2 = (N - \bar{N})^2 = \bar{N^2} - \bar{N}^2, \quad (10.109)$$

which is given by the expression

$$(\Delta N)^2 = \frac{1}{\beta^2} \frac{\partial^2}{\partial \mu^2} \ln Z(\mu, \beta) = \frac{g(\epsilon_F)}{\beta}, \quad (10.110)$$

where we have replaced  $Z(\alpha, \beta)$  with the leading term in eqn (10.73). Using the empirical value  $a = A/8$  for the level density parameter, we find from eqn (10.82) that

$$g(\epsilon_F) = \frac{3A}{4\pi^2}, \quad (10.111)$$

and therefore

$$\left( \frac{\Delta N}{N} \right)^2 = \frac{g(\epsilon_F)}{\beta A^2} = \frac{3k_B T}{4\pi^2 A}. \quad (10.112)$$

The condition (10.107) then requires

$$k_B T \ll \frac{4\pi^2}{3} A \approx 13 A \text{ MeV}. \quad (10.113)$$

This inequality is generally well satisfied, in particular for the nuclei produced in heavy-ion collisions. For example, a nucleus with  $A = 200$  and excitation energy  $E^* = 100$  MeV has, according to eqn (10.81), a temperature of  $k_B T = \sqrt{8E^*/A} \approx 2$  MeV, which complies with the condition (10.113).

Turning now to the variance of the energy, we find similarly

$$\begin{aligned} (\Delta E)^2 &= \bar{E^2} - \bar{E}^2 = \left[ \frac{\partial^2}{\partial \beta^2} - 2 \frac{\mu}{\beta} \frac{\partial^2}{\partial \beta \partial \mu} + \left( \frac{\mu}{\beta} \right)^2 \frac{\partial^2}{\partial \mu^2} \right] \ln Z(\alpha, \beta) \\ &= \frac{\pi^2}{3\beta^3} g(\epsilon_F) - \frac{2\mu}{\beta} A + \left( \frac{\mu}{\beta} \right)^2 \beta g(\mu). \end{aligned} \quad (10.114)$$

Keeping only the leading term, we find for the left-hand side of condition (10.108)

$$\left( \frac{\Delta E}{E - E_0} \right)^2 = \frac{12\beta}{\pi^2 g(\epsilon_F)}, \quad (10.115)$$

and the condition of small energy fluctuations becomes, using eqn (10.111),

$$k_B T \gg \frac{16}{A}. \quad (10.116)$$

This inequality holds for heavy nuclei at not too low temperatures. For example, it applies for a nucleus with  $A = 200$  and  $E^* = 100$  MeV, in which case  $k_B T = 2$  MeV.

But for lighter nuclei at low excitation energies condition (10.116) is not satisfied, and we find that the condition of small energy fluctuations is not so well fulfilled as that of small particle-number fluctuations. Thus the grand-canonical approach is not strictly valid.

The arguments we have used here apply to the Fermi gas model. However, the situation is similar in the shell model, and it is no accident that the condition of smoothness of the shell-model level density (10.93) is nearly identical with the condition

$$\frac{g(\epsilon_F) \pi^2}{\beta} \frac{\pi^2}{12} \gg 1 \quad (10.117)$$

following from eqns (10.108) and (10.115).

### 10.3.4 A practical level density formula

So far we have considered the level density as a function of excitation energy only. However, for practical applications its dependence on other parameters must also be included. Here we present, without derivation, a frequently used level density formula which takes account of the spin  $I$  and of the fact that nuclei are composed of two types of fermions, neutrons and protons (cf. Dilg *et al.* 1973; Huizenga and Moretto 1972),

$$\rho_A(E^*; I) = \frac{e^{2\sqrt{a(E^* - \Delta)}}}{12\sqrt{2}\sigma a^{1/4}(E^* - \Delta + t)^{5/4}} (2I + 1) \frac{e^{-I(I+1)/2\sigma^2}}{2\sigma^2}. \quad (10.118)$$

This is the level density of a nucleus with spin  $I$  at the excitation energy  $E^*$ . In spite of what the appearance of the factor  $2I + 1$  may suggest, the trivial degeneracy of the state with spin  $I$  is *not* included (cf. Ericson 1960, eqn (3.26)). The *spin cut-off parameter*  $\sigma^2$  is given by

$$\sigma^2 = \frac{I_{\text{rigid}}}{\hbar^2} t, \quad (10.119)$$

where  $I_{\text{rigid}}$  is the rigid moment of inertia, and the temperature parameter  $t$  (measured in MeV) is related to the excitation energy  $E^*$  via

$$E^* - \Delta = at^2 - t. \quad (10.120)$$

The excitation energy  $E^*$  is shifted by the parameter  $\Delta$  which is contributed by pairing effects. The values of the parameters  $\Delta$  and  $a$  have been determined empirically for a large number of nuclei (cf. Dilg *et al.* 1973). Figure 10.2 displays the values of the parameter  $a$ ; the average trend of the level density parameter is well fitted by the straight line  $a = A/8$ .

Formula (10.118) applies to nuclei at higher excitation energies. For low excitation energies ( $E^* \leq 5$  MeV) a ‘constant-temperature formula’ of the type

$$\rho_A(E^*) = C e^{E^*/k_B T} \quad (10.121)$$

(with  $C$  and  $T$  as parameters) generally provides a better fit to the data. A combination of a formula similar to eqn (10.118) with formula (10.121) has been proposed by Gilbert and Cameron (1965).

There are other important effects which lead to corrections of the level density formulae derived in the single-particle model, such as the superfluidity of nuclei and

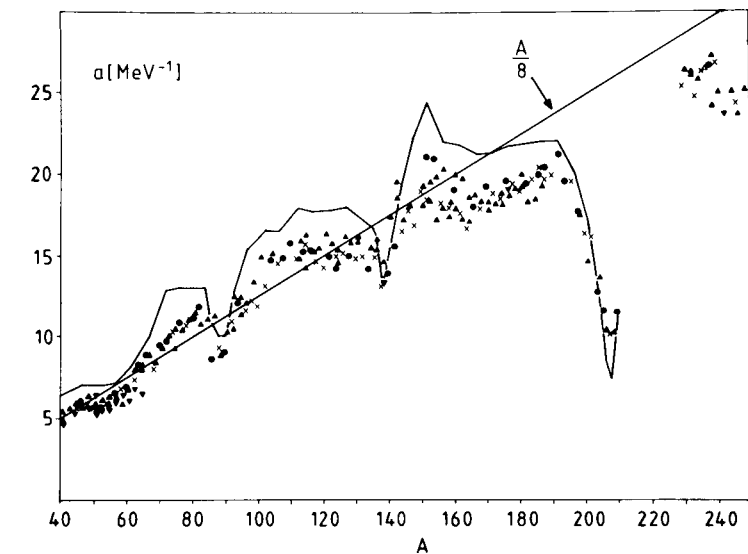


**Figure 10.2** Empirical values of the level density parameter  $a$  versus the mass number  $A$  according to Dilg *et al.* (1973). Crosses: even-even; circles: odd-odd; triangles: odd-mass nuclei. The solid curve results from an analysis of Faccini *et al.* (1968). The straight line  $a = A/8$  reproduces the average trend of the empirical values of  $a$ .

the presence of collective states (collective rotational or vibrational enhancement of the level density). The dependence of the level density parameter on deformation is also important, in particular for the description of fission (cf. Sections 10.4.2 and 12.4). A comprehensive review on level densities can be found in the book by Ignatyuk (1983).

## 10.4 Decay modes of the compound nucleus

In Section 10.2.4 we derived an explicit formula for the energy-differential compound reaction cross section, which for each total angular momentum  $J$  factorizes into a fusion cross section and a probability for the decay of the compound nucleus via different modes (cf. eqn (10.39)). The former has been treated in Chapter 9; the decay modes will be discussed in the following.

We begin with the derivation of the evaporation cross section, i.e. the cross section for emission of a single light particle. Evaporation is the main decay mode for not too heavy compound nuclei at low excitation energies. We then introduce the *rate* of evaporation, and also of other processes, namely, fusion, fission, and  $\gamma$ -decay. Such rates are the main ingredients in the formulation of a theory of the sequential decay of a compound nucleus.

### 10.4.1 The evaporation cross section

Let us first consider compound-nucleus reactions in which all final channels are made up of a structureless light particle (neutron, proton, or  $\alpha$ -particle) and a residual nucleus. In the numerator of expression (10.39) we take for the light particle the particle  $y$ . Its level density is given by a  $\delta$ -function,

$$\rho_y(\epsilon_y^*; I_y) = \delta(\epsilon_y^*). \quad (10.122)$$

The integration in expression (10.40) is then trivial. The same holds for the particle  $z$  in the denominator of formula (10.39). Summing over the spin  $I_B$  of the residual nucleus, we find for the cross section for the evaporation of a particle  $y$  with channel energy  $\mathcal{E}_b$  and spin  $I_y$ ,

$$\begin{aligned} \frac{d\sigma_{\{\underline{a}; I_x I_A\} \rightarrow \{\underline{b}; I_y\}}^C}{d\mathcal{E}_b} &= \sum_{J=0}^{\infty} \sigma_F^J(\underline{a}; I_x I_A; \mathcal{E}_a) \\ &\times \frac{\sum_{I_B} \sum_{S_b=|I_y-I_B|}^{I_y+I_B} \sum_{l_b=|J-S_b|}^{J+S_b} \rho_B(E_C^* - B_b - \mathcal{E}_b; I_B) T_{l_b S_b}^J(\underline{b}; \mathcal{E}_b)}{\sum_{c I_c} \int_0^{E_C^*-B_c} d\mathcal{E}_c \rho_C(E_C^* - B_c - \mathcal{E}_c; I_c) T_{l_c S_c}^J(\underline{c}; \mathcal{E}_c)}. \end{aligned} \quad (10.123)$$

Rather than applying this formula as it stands, it is convenient to introduce certain approximations which simplify it considerably.

The first approximation is to omit the spin cut-off factor in the level density (10.118); that is, one writes

$$\rho_B(\epsilon_B^*; I_B) \approx (2I_B + 1)\rho_B(\epsilon_B^*). \quad (10.124)$$

This amounts to neglecting the quantity  $I_B(I_B + 1)$  in comparison with the parameter  $\sigma^2$ , which is justified for not too low excitation energies, i.e. for high values of the temperature parameter  $t$ . When summing over the final spins  $I_B$  in expression (10.123), we first change the order of summation,

$$\sum_{I_B} \sum_{S_b=|I_y-I_B|}^{I_y+I_B} \sum_{l_b=|J-S_b|}^{J+S_b} = \sum_{l_b} \sum_{S_b=|J-l_b|}^{J+l_b} \sum_{I_B=|S_b-I_y|}^{S_b+I_y}, \quad (10.125)$$

and use the relation

$$\sum_{I_B=|S_b-I_y|}^{S_b+I_y} (2I_B + 1) = (2S_b + 1)(2I_y + 1) \quad (10.126)$$

in the numerator. Proceeding analogously in the denominator, one obtains a term  $(2S_c + 1)(2I_z + 1)$  there.

The second approximation consists in assuming that the transmission coefficient depends on no angular momentum other than the orbital one,

$$T_{l_b S_b}^J(\underline{b}; \mathcal{E}_b) \approx T_{l_b}(\underline{b}; \mathcal{E}_b). \quad (10.127)$$

This assumption implies that the potential barrier parameters  $V_B$ ,  $R_B$ , and  $\omega_B$ , which determine the dependence of the transmission coefficient on the orbital angular momen-

tum  $l$  (cf., e.g. formula (9.76)), can be regarded as independent of the channel spin  $S$  and the total spin  $J$ .

The summation over the final channel spin  $S_b$  in the numerator is now carried out easily and introduces a factor

$$\sum_{S_b=|J-l_b|}^{J+l_b} (2S_b + 1) = (2J + 1)(2l_b + 1)$$

in the numerator, and analogously in the denominator. The factor  $(2J + 1)$  cancels, and we are left with

$$\begin{aligned} \frac{d\sigma_{\{\underline{a}; I_x I_A\} \rightarrow \{\underline{b}; I_y\}}^C}{d\mathcal{E}_b} &= \sum_{J=0}^{\infty} \sigma_F^J(\underline{a}; \mathcal{E}_a) \\ &\times \frac{(2I_y + 1)\rho_B(E_C^* - B_b - \mathcal{E}_b) \sum_{l_b} (2l_b + 1) T_{l_b}(\underline{b}; \mathcal{E}_b)}{\sum_{c I_c} (2I_z + 1) \int_0^{E_C^*-B_c} d\mathcal{E}_c \rho_C(E_C^* - B_c - \mathcal{E}_c) \sum_{l_c} (2l_c + 1) T_{l_c}(\underline{c}; \mathcal{E}_c)}. \end{aligned} \quad (10.128)$$

Introducing the fusion cross sections  $\sigma_F(\underline{b}; \mathcal{E}_b)$  of eqn (9.19) in the final channels, we find

$$\begin{aligned} \frac{d\sigma_{\{\underline{a}; I_x I_A\} \rightarrow \{\underline{b}; I_y\}}^C}{d\mathcal{E}_b} &= \sigma_F(\underline{a}; \mathcal{E}_a) \\ &\times \frac{(2I_y + 1)\rho_B(E_C^* - B_b - \mathcal{E}_b) k_b^2 \sigma_F(\underline{b}; \mathcal{E}_b)}{\sum_{c I_c} (2I_z + 1) \int_0^{E_C^*-B_c} d\mathcal{E}_c \rho_C(E_C^* - B_c - \mathcal{E}_c) k_c^2 \sigma_F(\underline{c}; \mathcal{E}_c)}. \end{aligned} \quad (10.129)$$

From this formula we see that the energy distribution of the particles  $y$  in the final channel  $b$  is described by the following function of the channel energy  $\mathcal{E}_b$  (with  $k_b^2 = 2\mu_b \mathcal{E}_b / \hbar^2$ ),

$$\frac{d\sigma_{\{\underline{a}; I_x I_A\} \rightarrow \{\underline{b}; I_y\}}^C}{d\mathcal{E}_b} = \text{const } \mathcal{E}_b \sigma_F(\underline{b}; \mathcal{E}_b) \rho_B(E_C^* - B_b - \mathcal{E}_b). \quad (10.130)$$

We now write the level density of the residual nucleus in the form (cf. formula (10.49))

$$\rho_B(E_C^* - B_b - \mathcal{E}_b) = \rho_B(0) e^{S_B(E_C^* - B_b - \mathcal{E}_b)/k_B}. \quad (10.131)$$

Assuming that the channel energy  $\mathcal{E}_b$  is small compared to the total available energy  $E_C^* - B_b$ , we expand the entropy up to the term linear in  $\mathcal{E}_b$ ,

$$S_B(E_C^* - B_b - \mathcal{E}_b) = S_B(E_C^* - B_b) - \mathcal{E}_b \left. \frac{\partial S_B(E)}{\partial E} \right|_{E_C^* - B_b} + \dots \quad (10.132)$$

The derivative  $(\partial S_B / \partial E)|_{E_C^* - B_b}$  is equal to the inverse temperature  $1/T$  of the residual nucleus  $B$  at the energy  $E_C^* - B_b$ ,

$$\frac{1}{T} = \left. \frac{\partial S_B}{\partial E} \right|_{E_C^* - B_b}. \quad (10.133)$$

With  $S_B(E_C^* - B_b) = 2k_B\sqrt{a(E_C^* - B_b)}$  (cf. eqn (10.86)) we then obtain for the level density

$$\rho_B(E_C^* - B_b - \mathcal{E}_b) = \rho_B(0)e^{2\sqrt{a(E_C^* - B_b)}}e^{-\mathcal{E}_b/k_B T}. \quad (10.134)$$

The energy spectrum of the emitted particles is thus given by the *Weisskopf–Ewing formula* (cf. Weisskopf and Ewing 1940)

$$\frac{d\sigma_{\{g; I_x I_A\} \rightarrow \{b; I_y\}}^C}{d\mathcal{E}_b} = \text{const } \mathcal{E}_b \sigma_F(b; \mathcal{E}_b) e^{-\mathcal{E}_b/k_B T}. \quad (10.135)$$

For neutrons the fusion cross section can approximately be replaced with the energy-independent geometrical cross section, and formula (10.135) yields a Maxwell distribution for the energy of the emitted neutrons. The spectrum described by this distribution is called the *evaporation spectrum* since it resembles the energy spectrum of the molecules evaporated from the surface of a liquid. It is seen from formula (10.135) that one may deduce the temperature of the residual nucleus from the slope of the straight line representing the evaporation spectrum in a logarithmic plot of the quantity  $(d\sigma^C/d\mathcal{E}_b)/\mathcal{E}_b$ .

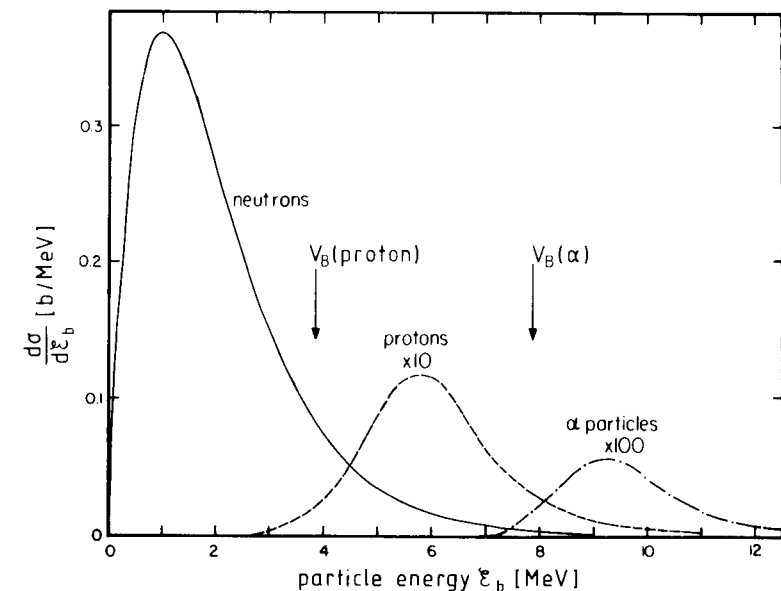
The temperature  $T$  of the residual nucleus differs from that of the compound nucleus before the emission of the light particle, because the emitted particle carries off the energy  $\mathcal{E}_b$ . However, this difference is small for heavy nuclei at higher excitation energies.

Figure 10.3 shows the energy spectra of neutrons, protons, and  $\alpha$ -particles obtained from formula (10.135), where the fusion cross sections have been calculated with the help of optical potentials. The threshold energy for charged particles is shifted away from that of the neutron by the Coulomb-barrier energy  $V_B(b)$ .

The observed energy distribution of the emitted light particles is often more complicated than that shown in Fig. 10.3. The structures which deviate from the evaporation shape of the spectrum are due to direct reactions and ‘pre-compound processes’. In the latter, particles are emitted from the compound system before it has reached complete equilibrium. They contribute to the high-energy tail of the energy distribution.

#### 10.4.2 Rates of fusion, evaporation, fission, and $\gamma$ -decay

If the excitation energy of a compound nucleus is high, as in the case of heavy-ion induced reactions, a large amount of energy is left over after one light particle has been emitted. The residual nucleus is so highly excited that it is unstable and decays again: it plays the role of a compound nucleus for the emission of a second light particle, and so on until a truly particle-stable evaporation residue is reached, whose only decay mode is  $\gamma$ -decay. In describing such a *cascade*, we treat the compound nucleus as a system existing in compound states (cf. Section 6.2.2) distributed with a level density  $\rho_C(E_C^*; J)$ . These states are then regarded as initial or final states of the individual processes making up the cascade. The transitions to or from such a compound state cannot be described by cross sections, which are ratios of asymptotic currents of stable particles. Instead, one introduces *transition rates*  $R_{a \rightarrow b}$ ; these are defined as the number of transitions per unit time from a state  $a$  to a state  $b$ . In the definition of a rate, the states do not necessarily have to be bound; they may be quasi-bound like the compound states or the ‘transition states’ to be defined below.



**Figure 10.3** Typical calculated energy spectra of neutrons, protons, and  $\alpha$ -particles. The proton spectrum is multiplied by the factor 10, that of the  $\alpha$ -particles by the factor 100 (cf. Vogt 1968).

In the following we derive an expression for the general reaction rate starting from the reaction cross section. We then introduce the fusion rate, i.e. the rate of compound-nucleus formation, from which the rates of compound-nucleus decay by emission of neutrons, protons, or  $\alpha$ -particles can be obtained by invoking time-reversal invariance (cf. Thomas 1964, 1968). Thereafter, we define a fission rate, which allows us to discuss fission as the other important mode of decay of the compound nucleus. Finally, rates for the emission of  $\gamma$ -quanta are introduced, since the inclusion of  $\gamma$ -radiation is important for a proper accounting in the energy and angular momentum balance. We close with a brief description of a cascade calculation for evaporation.

#### The reaction rate

In Section 5.2.5 we derived a formula giving the differential cross section for the transition from a two-body channel state  $a$  of the initial system  $x + A$  to another two-body channel state  $b$  of the final system  $y + B$  which has the form (cf. eqn (5.84))

$$d\sigma_{a \rightarrow b} = \left(\frac{2\pi}{\hbar}\right)^4 \mu_\alpha \mu_\beta \frac{k_b}{k_a} |T_{a \rightarrow b}|^2 d\Omega_b. \quad (10.136)$$

This cross section is defined as the number of particles  $y$  emitted per unit time in the final channel state  $b = \{y + B; b_y, b_B; \mathcal{E}_b, (\Omega_b, \Omega_b + d\Omega_b)\}$  if the current density of particles  $x$  impinging on the target nucleus  $A$  in the initial channel state  $a$  is equal to unity.

Let us consider a volume  $V$ , which may be visualized as given by the cross section area of the incident beam of particles  $x$  times the thickness of the target made up of the target nuclei  $A$ . In the stationary description this volume contains permanently a constant number  $N_x$  of projectile nuclei and  $N_A$  of target nuclei. All projectile and target nuclei give identical, independent contributions to the total number of reaction events in the volume  $V$ . The reaction cross section represents the reaction probability per unit time for unit projectile current density and a single target nucleus. The total number of such events is therefore given by the incident current density  $j_a = N_x v_a / V$  times the number  $N_A$  of target nuclei in  $V$  times the cross section for an individual scattering event  $\sigma_{a \rightarrow b}$ ,

$$N_x \frac{v_a}{V} N_A \sigma_{a \rightarrow b}.$$

This is the number of transitions (per unit time) in the volume  $V$  from an initial state  $a$  where all projectiles  $N_x$  have the momentum  $\mathbf{k}_a$ , to a corresponding final state  $b$  with momentum  $\mathbf{k}_b$ . It is called the *rate* of this process. The numbers  $N_x$  and  $N_A$  are generally very large. Our considerations apply to a large ensemble of identical, independent reaction events, not to a single one.

The quantity  $T_{a \rightarrow b}$  is the matrix element (5.67) of the  $T$ -operator taken between plane-wave states normalized to  $(2\pi)^{-3}$  particles per unit volume (cf. eqn (4.4)). Going over to states which are normalized to one particle in the volume  $V$ , we introduce the corresponding  $T$ -matrix  $\tilde{T}_{a \rightarrow b}$ , which is related to the quantity  $T_{a \rightarrow b}$  appearing in formula (10.136) by

$$\tilde{T}_{a \rightarrow b} = \frac{(2\pi)^3}{V} T_{a \rightarrow b}. \quad (10.137)$$

The current density in an initial state  $a$  normalized in this way is equal to  $v_a / V$ . Therefore, the number of transitions per unit time from the initial channel state  $a$  containing *one* particle  $x$  impinging on *one* target nucleus  $A$  in the volume  $V$  ( $N_x = N_A = 1$ ), to the final channel state  $b$  containing the particle  $y$  and the residual nucleus  $B$ , integrated over the scattering angle  $\Omega_b$ , is given by the *reaction rate*

$$R_{a \rightarrow b} = \frac{v_a}{V} \int d\sigma_{a \rightarrow b}, \quad (10.138)$$

or more explicitly,

$$\begin{aligned} R_{\{a; \mathbf{k}_a\} \rightarrow \{b; \mathcal{E}_b\}} &= \frac{v_a}{V} \left( \frac{2\pi}{\hbar} \right)^4 \mu_\alpha \mu_\beta \frac{k_b}{k_a} \int d\Omega_b |T_{\{a; \mathbf{k}_a\} \rightarrow \{b; \mathbf{k}_b\}}|^2 \\ &= \frac{2\pi}{\hbar} \int \frac{d\Omega_b}{4\pi} |\tilde{T}_{\{a; \mathbf{k}_a\} \rightarrow \{b; \mathbf{k}_b\}}|^2 \frac{V 4\pi \mu_\beta p_b}{(2\pi\hbar)^3}. \end{aligned} \quad (10.139)$$

In this expression we recognize the level density, or phase-space volume per unit energy in units of  $(2\pi\hbar)^3$ , of the relative-motion states in the final channel with energy  $\mathcal{E}_b$

$$\rho(\mathcal{E}_b) = \frac{V 4\pi p_b^2}{(2\pi\hbar)^3} \frac{dp_b}{d\mathcal{E}_b} = \frac{V 4\pi \mu_\beta p_b}{(2\pi\hbar)^3}. \quad (10.140)$$

We can now write for the reaction rate

$$R_{\{a; \mathbf{k}_a\} \rightarrow \{b; \mathcal{E}_b\}} = \frac{2\pi}{\hbar} P_{\{a; \mathbf{k}_a\} \rightarrow \{b; \mathcal{E}_b\}} \rho(\mathcal{E}_b), \quad (10.141)$$

where

$$P_{\{a; \mathbf{k}_a\} \rightarrow \{b; \mathcal{E}_b\}} = \int \frac{d\Omega_b}{4\pi} |\tilde{T}_{\{a; \mathbf{k}_a\} \rightarrow \{b; \mathbf{k}_b\}}|^2 \quad (10.142)$$

is the absolute square of the  $T$ -matrix for the transition of the system from a single state  $\{a; \mathbf{k}_a\}$  to the single state  $\{b; \mathbf{k}_b\}$  (averaged over the scattering angle  $\Omega_b$ ). Equation (10.141) is the exact, non-perturbative form of *Fermi's golden rule* for the rate of a transition from the two-body channel state  $a$  to another two-body channel state  $b$ .

#### The fusion rate

After having discussed the reaction rate, we define the *fusion rate*  $R_{\{b; I_y I_B; \mathcal{E}_b\} \rightarrow F}^J$  as the number of compound nuclei with spin  $J$  formed per unit time from an initial two-particle channel state with quantum numbers  $b = \{b; I_y I_B; \mathcal{E}_b\}$  (averaged over the spin projections). By the same arguments which led to eqn (10.138), this rate is connected with the partial fusion cross section  $\sigma_F^J(b; I_y I_B; \mathcal{E}_b)$  of eqn (10.31) via the relation

$$R_{\{b; I_y I_B; \mathcal{E}_b\} \rightarrow F}^J = \frac{v_b}{V} \sigma_F^J(b; I_y I_B; \mathcal{E}_b). \quad (10.143)$$

We now regard the compound nucleus as a system of nucleons confined to a volume of nuclear dimensions which is described by the compound states  $\{\underline{C}; J; E_C\}$ . These states have a distribution in energy determined by the compound-nucleus level density  $\rho_C(E_C^*; J)$ . In this picture Fermi's golden rule yields for the rate of compound-nucleus formation (10.143) the alternative formula

$$R_{\{b; I_y I_B; \mathcal{E}_b\} \rightarrow F}^J = \frac{2\pi}{\hbar} P_{\{b; I_y I_B; \mathcal{E}_b\} \rightarrow \{\underline{C}; J; E_C\}}^J (2J+1) \rho_C(E_C^*; J), \quad (10.144)$$

where  $P_{\{b; I_y I_B; \mathcal{E}_b\} \rightarrow \{\underline{C}; J; E_C\}}^J$  is the  $T$ -matrix squared for the two-particle channel state  $\{b; I_y I_B; \mathcal{E}_b\}$  to the compound state  $\{\underline{C}; J; E_C\}$ ; the factor  $2J+1$  accounts for the spin degeneracy not included in the level density  $\rho_C(E_C^*; J)$ .

#### The evaporation rate

Let us consider the decay of a compound nucleus in a compound state  $C$  with energy  $E_C$  and spin  $J$  by emission of a light particle  $y$  with spin  $I_y$  and channel energy in the range  $(\mathcal{E}_b, \mathcal{E}_b + d\mathcal{E}_b)$ , leaving a residual nucleus with spin  $I_B$ . Its differential rate is given by Fermi's golden rule,

$$\begin{aligned} dR_{\{\underline{C}; J; E_C\} \rightarrow \{b; I_y I_B; \mathcal{E}_b\}}^J &= \frac{2\pi}{\hbar} P_{\{\underline{C}; J; E_C\} \rightarrow \{b; I_y I_B; \mathcal{E}_b\}}^J \\ &\times \rho_B(E_C^* - B_b - \mathcal{E}_b; I_B) (2I_B + 1) (2I_y + 1) \frac{V 4\pi \mu_\beta p_b}{(2\pi\hbar)^3} d\mathcal{E}_b. \end{aligned} \quad (10.145)$$

Here  $P_{\{\underline{C}; J; E_C\} \rightarrow \{b; I_y I_B; \mathcal{E}_b\}}^J$  is the  $T$ -matrix squared for the transition from the compound state  $\{\underline{C}; J; E_C\}$  to the final evaporation-channel state  $\{b; I_y I_B; \mathcal{E}_b\}$ . It is multiplied by

the level density  $\rho_B$  of the residual nucleus  $B$ , the spin degeneracies of the two final nuclei, and the level density of the relative-motion states.

Because of time-reversal invariance (cf. Section 5.2.6) the  $T$ -matrix for a transition from a state  $a$  to a state  $b$  is the same as for the reverse transition, so that in the present instance,

$$P_{\{\underline{C}; J; E_C\} \rightarrow \{\underline{b}; I_y I_B; \mathcal{E}_b\}}^J = P_{\{\underline{b}; I_y I_B; \mathcal{E}_b\} \rightarrow \{\underline{C}; J; E_C\}}^J. \quad (10.146)$$

The quantity  $P_{\{\underline{b}; I_y I_B; \mathcal{E}_b\} \rightarrow \{\underline{C}; J; E_C\}}^J$  occurs in the formula (10.144) for the fusion rate. Then eqns (10.143) to (10.146) yield for the *differential evaporation rate* for a particle  $y$  with spin  $I_y$  and energy  $E_b$ , with the residual nucleus  $B$  left in a state with spin  $I_B$ ,

$$\begin{aligned} dR_{\{\underline{C}; J; E_C\} \rightarrow \{\underline{b}; I_y I_B; \mathcal{E}_b\}}^J &= \frac{(2I_y + 1)(2I_B + 1)}{(2J + 1)\rho_C(E_C^*; J)} \\ &\times \frac{4\pi p_b^2}{(2\pi\hbar)^3} \rho_B(E_C^* - B_b - \mathcal{E}_b; I_B) \sigma_F^J(\underline{b}; I_y I_B; \mathcal{E}_b) d\mathcal{E}_b. \end{aligned} \quad (10.147)$$

The *evaporation rate* for particle  $y$  with spin  $I_y$  is obtained by summing over the spins  $I_B$  of the residual nucleus  $B$  and integrating over the energy of the emitted particle  $\mathcal{E}_b$ . With  $p_b^2 = 2\mu_B\mathcal{E}_b$  we find

$$\begin{aligned} R_{\{\underline{C}; J; E_C\} \rightarrow \{\underline{b}; I_y\}}^J &= \frac{2I_y + 1}{(2J + 1)\rho_C(E_C^*; J)} \frac{\mu_B}{\pi^2\hbar^3} \sum_{I_B} (2I_B + 1) \\ &\times \int_0^{E_C^* - B_b} d\mathcal{E}_b \mathcal{E}_b \rho_B(E_C^* - B_b - \mathcal{E}_b; I_B) \sigma_F^J(\underline{b}; I_y I_B; \mathcal{E}_b). \end{aligned} \quad (10.148)$$

Substituting here expressions (10.31) together with (10.32), we find an alternative formula for the evaporation rate

$$\begin{aligned} R_{\{\underline{C}; J; E_C\} \rightarrow \{\underline{b}; I_y\}}^J &= \frac{1}{2\pi\hbar\rho(E_C^*; J)} \frac{1}{(2I_x + 1)(2I_A + 1)} \sum_{I_B} (2I_y + 1)(2I_B + 1) \\ &\times \int_0^{E_C^* - B_b} d\mathcal{E}_b \rho_B(E_C^* - B_b - \mathcal{E}_b; I_B) \sum_{S_b=|I_B-I_y|}^{I_B+I_y} \sum_{l_b=|J-S_b|}^{J+S_b} T_{l_b S_b}^J(\underline{b}; \mathcal{E}_b). \end{aligned} \quad (10.149)$$

In order to understand the physical meaning of the quantities entering in formula (10.149) we look at Fig. 10.4. Here the evaporation of a light particle with orbital angular momentum  $l_b$  (we do not indicate the spins  $I_y$  and  $S_b$ ) from a compound nucleus with excitation energy  $E_C^*$  and spin  $J$  and level density  $\rho_C(E^*, J)$  is illustrated schematically. The potential curve  $V_{l_b}(r)$  represents the effective potential  $V(r) + \hbar^2 l_b(l_b + 1)/2\mu_B r^2$  in which the particle  $y$  moves as it escapes from the compound nucleus. The figure makes clear how the compound-nucleus excitation energy  $E_C^*$  is divided up between the excitation energy of  $\epsilon_B^*$  of the residual nucleus and the final kinetic energy  $\mathcal{E}_b$  of the evaporated particle, taking into account the binding energy  $B_b$  of the particle  $y$ . The transmission coefficients  $T_{l_b S_b}^J(\underline{b}; \mathcal{E}_b)$  describe the probability of transmission of the

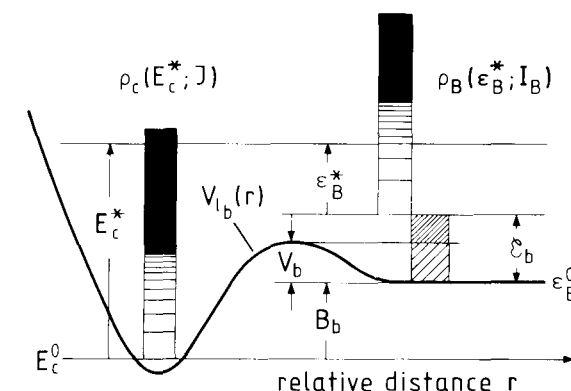


**Figure 10.4** Schematic illustration of the evaporation mode of compound-nucleus decay. See text for a description.

particle across the barrier  $V_b$  (this barrier is the fusion barrier for the inverse process  $y + B \rightarrow C$ ). In the classical limit the transmission coefficients vanish for subbarrier energies  $\mathcal{E}_b < V_b$  and are equal to unity otherwise.

In applications formula (10.149) is usually simplified by using transmission coefficients which depend only on the orbital angular momentum  $l_b$ ,  $T_{l_b S_b}^J \approx T_{l_b}$  (cf. eqn (10.127)). These can be calculated either with the help of an optical potential (cf., e.g. Blann and Komoto 1981), or in the sharp cut-off model (cf. Blann 1980).

#### The fission rate

Having introduced the concept of a rate in order to describe transitions between states which need only be quasi-stable and do not have to be asymptotic and directly observable, we can now include the fission process as a decay mode of the compound nucleus. We describe the mechanism of this mode with the help of Fig. 10.5.

In neutron-induced fission the compound nucleus formed in the initial stage of the fusion-fission process is an excited system whose deformation is essentially that of the target nucleus in the ground state (spherical for light, and deformed for heavy targets). Analogously, one assumes in fission induced by heavy ions that the excited compound nucleus has the same shape as in its ground state, which for simplicity is assumed to be undeformed. Fission then proceeds via continuous dynamical deformations away from the initial spherical compound-nucleus state  $\{\underline{C}; J; E_C\}$ , leading to a necking-in between two ‘halves’ which separate at the *scission point*. The energy of deformation is taken out of the excitation energy vested in the statistical degrees of freedom of the compound nucleus. It is eventually recovered after scission when it reappears as kinetic or internal excitation energy of the fission fragments.

The compound system follows a one-parameter (called the ‘fission coordinate’  $q$ ) fission path in the multi-dimensional space of an appropriate set of geometrical parameters

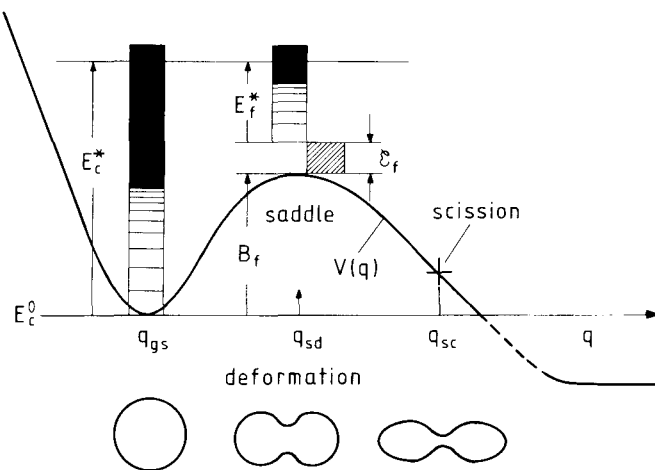


**Figure 10.5** Schematic illustration of the fission mode of compound-nucleus decay. See text for a description.

describing the dynamical process of continuous nuclear deformations. Along this path the static deformation energy is given by the *fission potential*  $V(q)$ , which is normalized to zero at the point  $q = q_{\text{gs}}$  corresponding to the spherical initial compound nucleus as it has been formed in the fusion process (the compound nucleus in its deformation ground state). During fission the system starts from the initial value  $q = q_{\text{gs}}$  and passes over the maximum  $B_f = V(q_{\text{sd}})$  of the fission potential at the saddle point  $q = q_{\text{sd}}$ . The deformation at this point determines the final fission configuration. In analogy to the initial (spherical) compound-nucleus states  $\{\underline{C}; J; E_C\}$  we define *transition states*  $\{\underline{f}; J; E_f\}$  of the compound system at the saddle point, which all have the deformation corresponding to the value  $q_{\text{sd}}$  of the fission coordinate  $q$ . The *fission rate* can then be defined as the rate of the transition from the state  $\{\underline{C}; J; E_C\}$  to all accessible transition states  $\{\underline{f}; J; E_f\}$ . The latter define the ‘fission channels’, which, however, are not channels in the strict sense defined in Section 5.2.1 since a nucleus in a transition state is not stable. It is a quasi-stable nucleus which differs from the initial compound nucleus by having an energy which is diminished by the part of the energy vested in the deformation degrees of freedom at the saddle-point.

An expression for the fission rate can now be obtained using similar arguments as in the derivation of the evaporation rate. We regard the fission coordinate  $q$ , usually taken as half the distance between the centres of the future fission fragments, as a dynamical variable. Its time derivative, i.e. the ‘fission velocity’  $\dot{q}$ , is related to its momentum  $p$  via  $p = m(q)\dot{q}$ , where  $m(q)$  is a mass parameter representing the inertia against changes in the deformation; it becomes the reduced mass of the fission fragments after scission. The kinetic energy of the deformation is given by  $\mathcal{E} = p^2/2m(q)$ .

We may treat the dynamics of the deformation during fission as if it were that of a

particle with coordinate  $q$ , velocity  $\dot{q}$ , etc. We first consider the inverse process of fission, that is, the formation of a compound system out of its fission fragments. The velocity of this process at the saddle point is  $\dot{q}_{\text{sd}} = -p_f/m_{\text{sd}}$ . We recall that in the derivation of rate formulae we have in mind an ensemble of a large number of identical nuclei all going through the same deformation process. Normalizing the transition state to one ‘particle’ in a one-dimensional ‘volume’  $s$ , we have  $\dot{q}/s$  particles disappearing from this volume per unit time (which are replaced with new ones in the stationary regime). We now adopt the hypothesis that a nucleus evolving from a transition state, i.e. from the top of the fission barrier, in the direction of decreasing fission coordinate  $q$  will always end up as a compound nucleus in its initial, undeformed state, in the same manner as we argued in Section 9.3.1 that two fusing nuclei will always form a compound nucleus once they have passed the fusion barrier. The rates of compound-nucleus formation from the different transition states  $\{\underline{f}; J; E_f\}$  are, then, all given by one and the same value

$$R_{\{\underline{f}; J; E_f\} \rightarrow \{\underline{C}; J; E_C\}} = \frac{\dot{q}_{\text{sd}}}{s}. \quad (10.150)$$

On the other hand, Fermi’s golden rule yields for this rate, in analogy to formula (10.144),

$$R_{\{\underline{f}; J; E_f\} \rightarrow \{\underline{C}; J; E_C\}} = \frac{2\pi}{\hbar} P_{\{\underline{f}; J; E_f\} \rightarrow \{\underline{C}; J; E_C\}} (2J+1) \rho_C(E_C^*; J). \quad (10.151)$$

We now turn to the fission process, which is the reverse of the process just discussed, namely, the transition from an initial compound-nucleus state to a transition state. In order to write down a formula for the fission rate, we must specify the level density of the compound nucleus at the saddle point. It consists of two parts. The first part is the level density for the deformation states at the saddle point, i.e. the phase-space volume per unit energy for the dynamical variables  $q_{\text{sd}}$  and  $p_f$ . Having introduced the ‘volume’  $s$ , we obtain for this level density the expression  $sdp_f/2\pi\hbar$ . The other part is the level density of the statistical compound states at the saddle point  $\rho_{\text{sd}}(E_f^*; J)$  multiplied by the spin degeneracy  $2J+1$ . The level density at the saddle point is not that of the initial compound nucleus, because (i) the energy available for filling the compound levels at the saddle point is lowered by an amount equal to the difference in deformation energy between the saddle and the spherical state (this difference is equal to the deformation energy, which has a kinetic part  $\mathcal{E}_f$  and a static part  $B_f$ ; the latter is the *fission barrier*), and (ii) the compound levels are distributed differently because of the change in geometrical shape of the compound nucleus.

As a result we have for the fission rate

$$\begin{aligned} dR_{\{\underline{C}; J; E_C\} \rightarrow \{\underline{f}; J; E_f\}} &= \frac{2\pi}{\hbar} P_{\{\underline{C}; J; E_C\} \rightarrow \{\underline{f}; J; E_f\}} \\ &\times (2J+1) \rho_{\text{sd}}(E_f^*; J) \frac{s}{2\pi\hbar} dp_f. \end{aligned} \quad (10.152)$$

Owing to the micro-reversibility relation (5.95) the quantities  $P$  (squared  $T$ -matrices) in eqns (10.151) and (10.152), are equal. This leads us to the principle of detailed balance for fission, which states that the compound-nucleus formation and

fission rates are related by

$$\rho_C(E_C^*; J) dR_{\{\underline{C}; J; E_C\} \rightarrow \{\underline{f}; J; E_f\}} = \rho_{sd}(E_f^*; J) \frac{s}{2\pi\hbar} dp_f R_{\{\underline{f}; J; E_f\} \rightarrow \{\underline{C}; J; E_C\}}. \quad (10.153)$$

Since  $dp_f = (dp_f/dE_f)dE_f = (m_f/p_f)dE_f = dE_f/\dot{q}_{sd}$ , we obtain, using eqn (10.150), the Bohr–Wheeler formula for the total fission rate (cf. Bohr and Wheeler 1939).

$$R_{\{\underline{C}; J; E_C\} \rightarrow \{\underline{f}; J; E_f\}} = \frac{1}{2\pi\hbar\rho_C(E_C^*; J)} \int_0^{E_C^*-B_f} dE_f \rho_{sd}(E_C^* - B_f - E_f; J). \quad (10.154)$$

Here account is taken of the fact that the total available excitation energy  $E_C^*$  is divided up between the deformation energy at the saddle point  $B_f$ , the kinetic energy associated with the fission coordinate at the saddle point  $E_f$ , and the internal excitation energy  $E_f^*$ , so that

$$E_f^* = E_C^* - B_f - E_f. \quad (10.155)$$

occurs in the argument of the level density  $\rho_{sd}(E_f^*; J)$ .

The accuracy of formula (10.154) may be improved slightly by taking into account tunnelling via insertion of the transmission coefficient  $T_f(E_f)$  of the fission barrier, which in its Hill–Wheeler form is given by (cf. eqn (9.74))

$$T_f(E_f) = \left[ 1 + \exp\left(-\frac{2\pi E_f}{\hbar\omega_{sd}}\right) \right]^{-1}, \quad (10.156)$$

where the quantity  $\omega_{sd}$  is the related to the curvature of the fission potential at the barrier top. The fission rate then becomes (cf., e.g. Vandenbosch and Huizenga 1973).

$$R_{\{\underline{C}; J; E_C\} \rightarrow \{\underline{f}; J; E_f\}} = \frac{1}{2\pi\hbar\rho_C(E_C^*; J)} \times \int_{-B_f}^{E_C^*-B_f} dE_f \rho_{sd}(E_C^* - B_f - E_f; J) T_f(E_f). \quad (10.157)$$

◇ We may obtain the Bohr–Wheeler formula (10.157) from the evaporation rate formula (10.149) summed over  $I_y$ , taking due account of the differences between the evaporation and fission processes. The main distinction is that evaporation is a three-dimensional process (formula (10.149) contains a sum over orbital angular momenta), whereas the relative motion of the fission fragments is one-dimensional ('head on' in the fission coordinate  $q$ ). In order to make the connection between the two formulae, we therefore set  $l_b = 0$  in expression (10.149), which implies  $S_b = J$ , replace the level density  $\rho_B$  summed over the spins  $I_B$  and  $I_y$  with the level density  $\rho_{sd}$  of the compound system at the saddle point, and omit the factor containing the spins  $I_A$  and  $I_x$ . Changing the asymptotic energies  $B_b$  and  $\mathcal{E}_b$  (cf. Fig. 10.4) into the energies  $B_f$  and  $E_f$  at the saddle (cf. Fig. 10.5), and the transmission coefficient  $T_{l_b S_b}^J(b; \mathcal{E}_b)$  into  $T_f(E_f)$ , we arrive at the Bohr–Wheeler formula (10.157). ◇

#### The competition between fission and neutron evaporation

An estimate of the relative importance of the two main competing modes of compound-nucleus decay, fission and neutron evaporation, can be obtained in the following way.

The ratio of the fission rate  $R_{C \rightarrow f}$  and the neutron emission rate  $R_{C \rightarrow n}$  (cf. eqns (10.154) and (10.149), respectively) is governed by the level densities. For a rough estimate we replace these level densities with their values at threshold,  $\mathcal{E}_f = 0$  for fission and  $\mathcal{E}_n = 0$  for neutron emission. We find, using the Bethe formula (10.87),

$$\frac{R_{C \rightarrow f}}{R_{C \rightarrow n}} \approx \frac{\rho_f(E_C^* - B_f)}{\rho_n(E_C^* - B_n)} \approx \frac{\exp[2\sqrt{a_f(E_C^* - B_f)}]}{\exp[2\sqrt{a_n(E_C^* - B_n)}]}. \quad (10.158)$$

We consider excitation energies much larger than the fission barrier and the neutron binding energy,  $E_C^* \gg B_f, B_n$ , and set the two level density parameters equal,  $a_f = a_n = a$ . Then we obtain, keeping only terms of first order in  $B_f/E_C^*$  and  $B_n/E_C^*$ ,

$$\frac{R_f}{R_n} \approx \exp\left(\sqrt{\frac{a}{E_C^*}}(B_n - B_f)\right). \quad (10.159)$$

It follows that (i) fission dominates over neutron evaporation,  $R_f > R_n$ , if the fission barrier is lower than the binding energy of the neutron,  $B_f \leq B_n$ , and vice versa; (ii) the ratio  $R_f/R_n$  increases with rising excitation energy  $E_C^*$  if  $B_f > B_n$  and decreases if  $B_f < B_n$ . The competition between fission and neutron evaporation has already been discussed qualitatively in Section 9.3.6 in connection with the classification of reaction mechanisms (cf. also Fig. 9.15).

For several decades the statistical model of the compound nucleus has been reasonably successful in the description of the data on fission and particle emission. However, discrepancies have become observable in recent years as the analyses became more refined. In particular the measured pre-scission neutron multiplicities at higher energies cannot be explained by the statistical model (cf. Hilscher and Rossner 1992), and dynamical effects such as friction have to be included. This will be discussed in Section 12.4.

#### The $\gamma$ -radiation rate

A further competing mode in compound-nucleus decay is  $\gamma$ -emission. This is a non-nuclear process which has to be considered here since it affects the energy and angular momentum balance. The emission of  $\gamma$ -radiation does not change the particle number of the compound system but carries off energy and angular momentum. The  $\gamma$ -emission rate is given by the formula (cf. Grover and Gilat 1967; Ruddy *et al.* 1969).

$$R_{\{\underline{C}; J; E_C\} \rightarrow \gamma} = \frac{1}{2\pi\hbar\rho_C(E_C^*, J)} \sum_L \sum_{I=|J-L|}^{J+L} \int d\epsilon_\gamma \rho_C(E_C^* - \epsilon_\gamma, I) \xi_L \epsilon_\gamma^{2L+1}, \quad (10.160)$$

where  $\epsilon_\gamma$  is the energy of the  $\gamma$ -particle and the parameters  $\xi_L$  are connected with the Weisskopf single-particle estimate of the strength of a  $\gamma$ -transition with multipolarity  $L$ . The arguments leading to formula (10.160) are given in Blatt and Weisskopf (1952, Section XII.7) and in Stokstad (1984). One usually takes only  $E1, M1$ , and  $E2$  transitions into account. The special case of giant-dipole  $\gamma$ -emission will be discussed in Section 12.4.1.

*Lifetime and widths*

The rates of the various modes of decay of the compound nucleus determine its lifetime. Consider a number  $N$  of compound nuclei decaying via the modes  $b$  with the rates  $R_{C \rightarrow b}$ . In the course of these decay processes the original number  $N$  of compound nuclei will be depleted. This was not the case in the previous, stationary discussion, where the number of compound nuclei was kept constant via fusion with constant incident flux. However, in the absence of such replenishment the number of nuclei must decrease at a rate  $R_C$  which is given by the sum of the partial rates  $R_{C \rightarrow b}$ ,

$$R_C = \sum_b R_{C \rightarrow b}. \quad (10.161)$$

We thus have for the number of nuclei decaying per unit time

$$\frac{dN}{dt} = -R_C N. \quad (10.162)$$

The solution of this equation yields an exponential law for the depletion of the number of compound nuclei,

$$N(t) = N(0)e^{-R_C t}. \quad (10.163)$$

It is customary to introduce the *width*

$$\Gamma = \hbar R_C \quad (10.164)$$

in place of the rate  $R_C$ . Historically, this derives from the fact that isolated compound-nucleus states decaying at a rate  $R_C$  give rise to resonances in the energy-differential compound reaction cross section which have this width (cf. the discussion below eqn (6.60)). The exponential decay law (10.163) then becomes

$$N(t) = N(0)e^{-\Gamma t/\hbar}. \quad (10.165)$$

The time  $\tau$  during which the number of compound nuclei has decreased by the factor  $1/e$  is called the *mean lifetime* of a compound nucleus; it is given by

$$\tau = \frac{\hbar}{\Gamma}. \quad (10.166)$$

One also defines the partial widths for the various decay modes  $b$

$$\Gamma(b) = \hbar R_{C \rightarrow b}, \quad (10.167)$$

which according to eqn (10.161) satisfy

$$\Gamma = \sum_b \Gamma(b). \quad (10.168)$$

Going back to Section 10.2.2, we note that the decay probabilities  $G(b)$  introduced there can be expressed in terms of the partial widths via

$$G(b) = \frac{\Gamma(b)}{\Gamma}. \quad (10.169)$$

Multiplying this expression by the fusion cross section in channel  $a$  yields the cross section  $\sigma_{a \rightarrow b}^C$  for the compound reaction  $a \rightarrow b$  (cf. eqn (10.10)). This line of reasoning

is the one followed by Ericson (1960) in the derivation of the compound reaction cross section.

**10.4.3 Evaporation cascades in light systems**

We have discussed the various modes of compound-nucleus decay and derived expressions for the corresponding rates. A compound nucleus may decay by any one of these modes, and such decays may follow one another if sufficient energy is available. For example, we have already mentioned the possibility of sequential emission of light particles if the final nucleus after the evaporation of the first particle retains enough excitation energy to emit another one. Similarly, the fission fragments emerging in the decay via the fission mode generally have again all the characteristics of a compound nucleus of about half the size of the original one, and therefore decay further by evaporation. Fission, or more precisely, scission may also be preceded by the emission of neutrons, protons,  $\alpha$ -particles, or  $\gamma$ -quanta (pre-scission particle emission). Such processes will be discussed in Section 12.4. In the present section we restrict ourselves to the sequential emission of light particles (*evaporation cascades*).

A *cascade* of decays by evaporation may be viewed as a ‘family tree’ in which the top is the initial compound nucleus formed as a result of fusion. This compound nucleus has a large excitation energy and a certain spin distribution. Each step from one generation to the next below involves a compound nucleus decaying into a light particle (or  $\gamma$ -quantum) and a residual nucleus. These processes occur with rates given by the rate formulae discussed above. The aim of a cascade calculation is to determine the number of the residual nuclei in the various daughter generations (characterized by different mass,  $A$ , and charge numbers,  $Z$ ) whose internal energy is insufficient for further emission of particles. These nuclei are the final evaporation residues.

Two main methods of calculation have been employed. In the first method one calculates the rates of all evaporation modes from the initial compound nucleus to the nuclei in the first daughter generation. Then the rates of all possible decays from the first to the second generation are determined and combined with the former rates. In this fashion one goes down the family tree from one complete generation to the next until stable evaporation residues are reached in all generations. The relative rates with which these residual nuclei are produced determine the evaporation residue distribution. Figure 10.6 displays the mass distribution of the evaporation residues resulting from the decay of the light compound system  $F + Al$ , calculated in this way for various excitation energies with the use of the code CASCADE (cf. Pühlhofer 1977). Since it has been found that in such a light system fission is strongly suppressed, a cascade calculation including only evaporation processes is justified.

The second method is ‘vertical’, in that one follows a decay chain from the initial compound nucleus to one particular nucleus in the first daughter generation, then to another particular nucleus in the second generation, and so on. There are many different chains of this type. They are taken into account by a Monte Carlo sampling over all possible chains, where the relative weight of each chain is determined by the rates of the decay modes participating in the chain. One collects the final nuclei at the end of all chains in bins of mass and charge and in this way obtains the element distribution of the evaporation residues. This procedure has been employed, for example, by Hillman

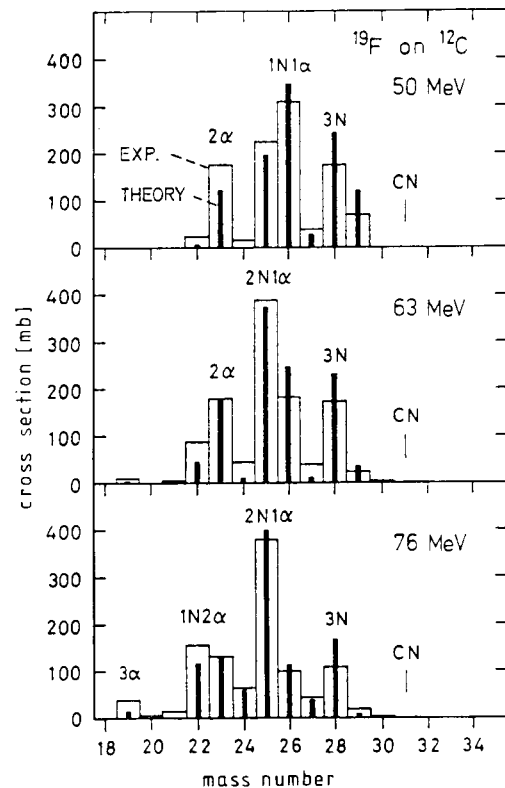


**Figure 10.6** Experimental (histograms) and calculated evaporation-residue mass distributions (heavy vertical lines) resulting from the decay of compound system F + Al at 50, 63, and 76 MeV (the data are from Pühlhofer *et al.* 1975).

and Eyal (1976) in the code JULIAN, of which improved versions are now available at many laboratories. A Monte Carlo cascade calculation of this type will also be discussed in Section 12.4 in the context of a dynamical description of compound-nucleus decay including fission, particle emission, and  $\gamma$ -radiation.

## 10.5 Notes and references

In this chapter we have made use of Bohr's independence hypothesis for an expeditious derivation of reaction cross sections and rates. In order to obtain a more detailed understanding of the reaction mechanism in terms of the nuclear interactions it is necessary to develop a proper theory of compound reactions. The best-known and historically the first such theory is the *R*-matrix theory (cf. Kapur and Peierls 1938; Wigner and Eisenbud 1947; Teichmann and Wigner 1952; Lane and Thomas 1958). In this theory

the compound states are virtual states of the compound nuclear system defined inside a sphere with an '*R*-matrix radius' slightly larger than the nuclear radius. A discrete spectrum of compound levels is generated by applying appropriate boundary conditions. The compound states are matched to the free scattering solutions at the *R*-matrix radius, which leads to reaction amplitudes whose energy dependence is given by a sum of Breit-Wigner resonance terms of the type appearing in the compound-elastic amplitude (6.85) discussed in Section 6.3. In heavier nuclei and at higher energies the number of compound states becomes enormous. A statistical treatment then leads to the same cross section formulae as we obtained in the present chapter. Another approach to the description of compound processes makes use of the shell-model theory of nuclear reactions (cf. Mahaux and Weidenmüller 1969). It was in this framework that we derived the schematic optical potential in Section 6.2.2, together with the compound-elastic scattering amplitude. The shell-model theory of nuclear reactions leads to similar results as the *R*-matrix theory.

On the basis of such formalisms one can further investigate not only the compound reaction cross section, which we have identified with the fluctuation cross section, but also correlations between cross sections at neighbouring energies (*Ericson fluctuations*; cf. Ericson 1963; Ericson and Mayer-Kuckuk 1966).

We have not discussed the pre-compound reactions, in which intermediate states of a simpler structure than that of the true compound states are involved, like, for example, the doorway states briefly mentioned in Section 6.2.3. Pre-compound reactions are reviewed, for example, by Blann (1975).

The fission treated in this chapter is *induced*, not spontaneous, fission. For recent reviews of fission see, for example, Hilscher *et al.* (1989) and Wagemans (1991).

## References

- Becker, R. (1964). *Theorie der Wärme*, Springer, Berlin.
- Bethe, H. A. (1937). *Rev. Mod. Phys.* **9** 69.
- Blann, M. (1975). *Ann. Rev. Nucl. Sci.* **25** 123.
- Blann, M. (1980). *Phys. Rev.* **C21** 1770.
- Blann, M. and Komoto, T. T. (1981). *Phys. Rev.* **C24** 426.
- Blatt, J. M. and Weisskopf, V. F. (1952). *Theoretical nuclear physics*, Wiley, New York.
- Bohr, A. and Mottelson, B. R. (1969). *Nuclear structure*, vol. 1, Benjamin, New York.
- Bohr, N. (1936). *Nature* **137** 344.
- Bohr, N. and Wheeler, J. A. (1939). *Phys. Rev.* **56** 426.
- Dilg, W., Schantl, W., Vonach, H. and Uhl, M. (1973). *Nucl. Phys.* **A217** 269.
- Ericson, T. (1959). *Nucl. Phys.* **11** 481.
- Ericson, T. (1960). *Adv. Phys.* **9** 425.
- Ericson, T. (1963). *Ann. Phys. (N. Y.)* **23** 390.
- Ericson, T. and Mayer-Kuckuk, T. (1966). *Ann. Rev. Nucl. Sci.* **16** 183.
- Facchini, U. and Saetta-Menichella, E. (1968). *Energia Nucleare* **15** 54.
- Gilbert, A. and Cameron, A. (1965). *Can. J. Phys.* **43** 1446.
- Gradshteyn, I. S. and Ryzhik, I. M. (1965). *Tables of integrals, series, and products*, Academic Press, New York.

- Grover, J. R. and Gilat, J. (1967). *Phys. Rev.* **157** 802, 814, 823.  
Hauser, W. and Feshbach, H. (1952). *Phys. Rev.* **87** 366.  
Hillman, M. and Eyal, Y. (1976). *Proc. European conf. on nuclear physics with heavy ions*, vol. 1: Contributions, Caen, Sept. 1976, eds, Fernandez, B. et al., p.109.  
Hilscher, D. and Rossner, H. (1992). *Ann. Phys. (Paris)* **17** 471.  
Hilscher, D., Krappe, H.-J. and von Oertzen, W., eds (1989). *Proc. int. conf. on fifty years research in nuclear fission, Nucl. Phys.* **A502**.  
Huizenga, J. R. and Moretto, L. G. (1972). *Ann. Rev. Nucl. Sci.* **22** 427.  
Ignatyuk, A. V. (1983). *Statistical properties of excited atomic nuclei*, Energomizdat, Moscow (in Russian); translated as IAEA report, INDC(CCP)-233/L, Vienna, 1985.  
Kapur, P. L. and Peierls, R. E. (1938). *Proc. Roy. Soc. (London)* **A166** 277.  
Lane, A. M. and Thomas, R. G. (1958). *Rev. Mod. Phys.* **30** 257.  
Mahaux, C. and Weidenmüller, H. A. (1969). *Shell-model approach to nuclear reactions*, North-Holland, Amsterdam.  
Pühlhofer, F., Pfeffer, W., Kohlmeyer, B. and Schneider, W. F. W. (1975). *Nucl. Phys.* **A244** 329.  
Pühlhofer, F. (1977). *Nucl. Phys.* **A280** 267.  
Reif, F. (1965). *Fundamentals of statistical and thermal physics*, McGraw-Hill, New York.  
Ruddy, F. H., Pate, B. D. and Vogt, E. W. (1969). *Nucl. Phys.* **A127** 323.  
Stokstad, R. G. (1984). In *Treatise on heavy-ion science*, ed. Bromley, D. A., vol. 3, Plenum, New York, p. 83.  
Teichmann, T. and Wigner, E. P. (1952). *Phys. Rev.* **87** 123.  
Thomas, T. D. (1964). *Nucl. Phys.* **53** 558.  
Thomas, T. D. (1968). *Ann. Rev. Nucl. Sci.* **18** 343.  
Vandenbosch, R. and Huizenga, J. R. (1973). *Nuclear fission*, Academic Press, New York.  
Vogt, E. (1968). *Adv. Nucl. Phys.* **1** 261.  
Wagemans, C., ed. (1991). *The nuclear fission process*, CRC Press, Boca Raton, FL.  
Weisskopf, V. F. and Ewing, D. H. (1940). *Phys. Rev.* **57** 472.  
Wigner, E. P. and Eisenbud, L. (1947). *Phys. Rev.* **72** 29.  
Wolfenstein, L. (1951) *Phys. Rev.* **82** 690.

## Part E

### Dissipation and fluctuations

## DEEP-INELASTIC COLLISIONS. PHENOMENA AND THEORY

### 11.1 Introduction

So far we have been concerned with direct and compound-nucleus reactions. We shall now consider another type of reaction, the dissipative or *deep-inelastic collisions* (DIC), which display features of both of the former. Deep-inelastic collisions are special to heavy ions, and are the more pronounced the heavier the collision partners. They can be described in classical terms, and generally take place at intermediate impact parameters. For large impact parameters they go over into the direct or quasi-elastic reactions, and for small impact parameters into fusion.

The DIC are not direct reactions because the nuclei come so close that they interact violently. Many degrees of freedom in both collision partners are excited, and nucleons are transferred back and forth. The excitations absorb a large amount of energy and may be viewed as a ‘heating-up’ of the nuclei, as in a compound-nucleus reaction. However, the DIC are not compound-nucleus reactions either. The collision partners do not overlap completely; they do not stay together for the long times characteristic of compound-nucleus reactions, and they retain their identity except for the net exchange of a few nucleons.

In Section 11.2 we describe the place of the DIC in a general classification of nuclear reactions by energy and impact parameter. We then list the *phenomena characterizing deep-inelastic collisions*, that is, the specific features of the DIC cross sections in regard to energy loss, particle transfer, and scattering angle. This will provide the basis for the development of a theory of these collisions, to which the remainder of this chapter is devoted.

For a theoretical description of the dissipative collisions one could, in principle, use the formal theory of reactions as a starting point for a microscopic derivation of the DIC cross sections. But the formalism is quite cumbersome, and in order to arrive at tractable formulae one has to make approximations which are difficult to control. At the present stage of development no ‘final’ microscopic theory exists. We therefore take recourse to a more *heuristic, phenomenological model*, of which we require only that it is rich enough to contain the relevant features, and that it allows us to reproduce the large variety of available experimental data reasonably well. In restricting the theoretical discussion to this model we do not wish to convey the impression that this is the only way of treating the DIC. The literature contains other descriptions, and in the notes and references at the end of the chapter we refer to different microscopic attempts to arrive at more rigorous and general theories, and quote other phenomenological approaches.

In the present chapter we introduce only the theoretical framework for our interpretation of the DIC; details of the application of the formalism will be discussed in Chapter 12. We regard the relative motion of the heavy ions as classical. During the collision the internal degrees of freedom of the collision partners are excited. They are assumed to equilibrate rapidly, and their effect on the relative motion is simulated by the action of a ‘heat bath’ as in the theory of Brownian motion. The relative motion of the colliding nuclei is described by *Langevin equations*. These are set up in Section 11.3. They contain frictional and fluctuating forces, whose common origin finds expression in the fluctuation-dissipation theorem.

In Section 11.4 we derive the *Fokker–Planck equation* for the classical distribution function of the dynamical variables describing the relative motion, and establish its relation with the Langevin equations.

Numerical methods for solving the Fokker–Planck and Langevin equations are discussed in Section 11.5.

## 11.2 Dissipative phenomena

### 11.2.1 The spin distribution of nuclear reactions

In order to define deep-inelastic collisions we refer to Section 9.3.6. In Fig. 9.15 a general classification of nuclear reactions was given in terms of energy and impact parameter. Let us go back to this figure. Classically, each impact parameter determines a unique trajectory, and therefore the different reaction mechanisms can be classified by this parameter. Consider a vertical line corresponding to some fixed energy. The cross section for a certain reaction type evaluated along such a line yields the corresponding reaction cross section as a function of the impact parameter. In quantal language it is the partial reaction cross section as a function of the orbital angular momentum  $l$ , or *spin distribution of the reaction*. It will be discussed in the following with particular attention to the region of higher incident energies, i.e. energies near  $E_2$  in the right part of Fig. 9.15.

Figure 11.1 illustrates this classification of reactions in the scattering plane. Small impact parameters ( $b_F$ ) lead to compound-nucleus formation or fusion. At intermediate impact parameters ( $b_{DIC}$ ) we have the deep-inelastic collisions to be discussed in the present chapter. At larger impact parameters ( $b_{gr}$ ) grazing collisions occur, giving rise to quasi-elastic scattering or direct reactions. Finally, very large impact parameters correspond to distant collisions and are associated with elastic scattering or at most Coulomb excitation.

The different impact parameters  $b = l/k$  make additive contributions to the reaction cross section  $\sigma_r$  (cf. eqns (1.63) and (1.64)),

$$\sigma_r = \sum_l \sigma_r(l), \quad (11.1)$$

where the partial reaction cross section

$$\sigma_r(l) = \frac{\pi}{k^2} (2l + 1) T_l \quad (11.2)$$

is determined by the transmission coefficient  $T_l$  (cf. eqn (1.72) and Section 9.4). Since

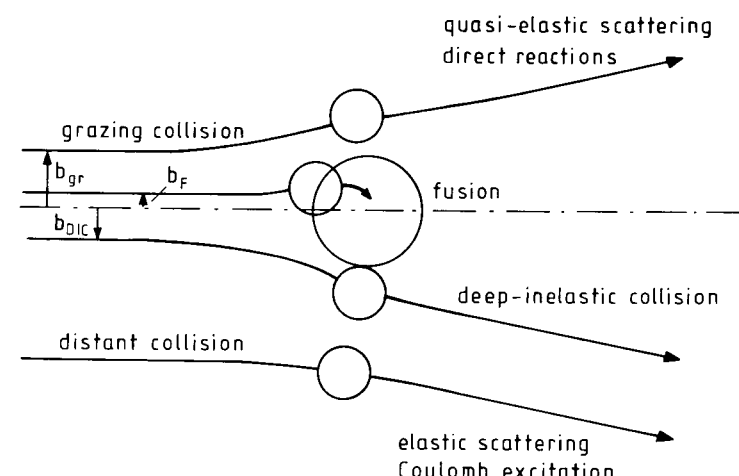


Figure 11.1 Classification of reactions by impact parameter.

we are dealing with large angular momenta, it is convenient to go over to a continuous description in which eqn (11.1) becomes

$$\sigma_r = \int_0^\infty dl \sigma_r(l) \quad (11.3)$$

with

$$\sigma_r(l) = \frac{2\pi}{k^2} l T(l). \quad (11.4)$$

The spin distribution is shown schematically in Fig. 11.2. In the classical picture we assume that all trajectories which pass over the barrier lead to a reaction, which implies

$$T(l) = \begin{cases} 1 & \text{for } l < l_{gr}, \\ 0 & \text{for } l > l_{gr}, \end{cases} \quad (11.5)$$

where  $l_{gr} = kb_{gr}$  is the grazing angular momentum (cf. eqn (9.18)). The reaction cross section is then given by the triangular area below the straight line

$$\sigma_r(l) = \frac{2\pi}{k^2} l \quad (11.6)$$

between the values  $l = 0$  and  $l = l_{gr}$ .

We distinguish three regions of angular momentum  $l$ , each associated with one of the types of reaction mentioned in connection with Fig. 11.1,

$$\begin{aligned} 0 < l < l_F & \text{fusion,} \\ l_F < l < l_{DIC} & \text{deep-inelastic collisions,} \\ l_{DIC} < l < l_{gr} & \text{quasi-elastic collisions.} \end{aligned} \quad (11.7)$$

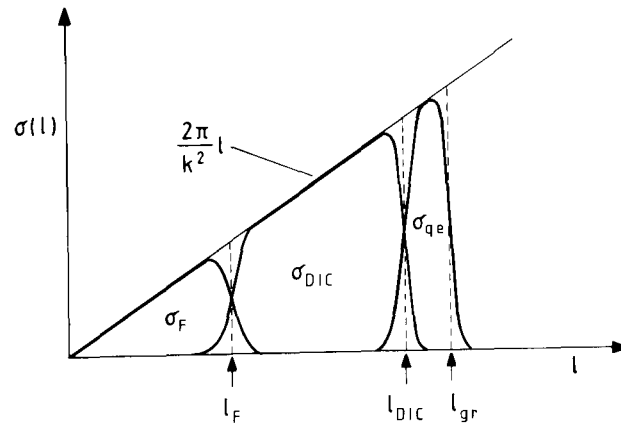


**Figure 11.2** The spin distribution of a heavy-ion reaction. The regions for fusion ( $\sigma_F$ ), deep-inelastic ( $\sigma_{DIC}$ ), and quasi-elastic collisions ( $\sigma_{qe}$ ) are indicated.

Classically, each angular-momentum range contributes to a single reaction type. However, one expects that the mechanisms ‘overlap’ in the border regions due to quantal and statistical (thermal) effects, as indicated in the figure.

The partitioning of the spin distribution into the various types of reactions is different for different energies, as can be seen from Fig. 9.15. It is also different for light and heavy systems. For light heavy ions deep-inelastic scattering is very weak, because there are not so many degrees of freedom available which can be excited; therefore one has mainly quasi-elastic scattering besides fusion. As one goes over to heavier collision partners the DIC become increasingly important, while fusion is more and more suppressed because of the increasing Coulomb repulsion. For very heavy nuclei, formation of an equilibrated compound system, i.e. fusion, no longer occurs. Nevertheless, the system passes through an intermediate di-nuclear complex where the reaction partners excite each other and exchange particles. This mechanism is called *capture*. Energy dissipation and mass exchange take longer than in a typical DIC, but the process is faster than ordinary fission, so that the name *fast fission* is also in use. We shall not discuss it further.

In view of Fig. 11.2 we can write down simple formulae for the total cross sections for fusion, DIC, and quasi-elastic scattering. For the fusion cross section we have, using eqn (11.6),

$$\sigma_F = \frac{2\pi}{k^2} \int_0^{l_F} l dl = \frac{\pi}{k^2} l_F^2, \quad (11.8)$$

for the total deep-inelastic cross section

$$\sigma_{DIC} = \frac{2\pi}{k^2} \int_{l_F}^{l_{DIC}} l dl = \frac{\pi}{k^2} (l_{DIC}^2 - l_F^2) \quad (11.9)$$

and for the quasi-elastic cross section

$$\sigma_{qe} = \frac{2\pi}{k^2} \int_{l_{DIC}}^{l_{gr}} l dl = \frac{\pi}{k^2} (l_{gr}^2 - l_{DIC}^2). \quad (11.10)$$

We see that the calculation of these cross sections reduces to the determination of the limiting  $l$ -values for fusion,  $l_F$ , deep-inelastic collisions,  $l_{DIC}$ , and quasi-elastic scattering,  $l_{gr}$ .

### 11.2.2 Characteristic features of deep-inelastic collisions (DIC)

So far we have circumscribed the deep-inelastic collisions by what they are not, i.e. we have distinguished them from fusion and quasi-elastic scattering. Let us now discuss in greater detail the characteristic features of the DIC as reviewed, for example, by Gobbi and Nörenberg (1980) or Huizenga and Schröder (1984).

As a typical example for a DIC we consider the collision of  $^{136}\text{Xe}$  with  $^{209}\text{Bi}$  at  $E_{\text{lab}}(\text{Xe}) = 1422$  MeV (cf. Wollersheim *et al.* 1981). Figure 11.3 shows the contour plot of the double differential cross section  $d^2\sigma/dEdZ$  as a function of the final centre-of-mass energy  $E$  and the charge  $Z$  of the emitted projectile-like fragments. From this figure we read off:

(i) Projectile and target remain essentially unchanged except for a net exchange of a few nucleons, that is, deep-inelastic collisions are essentially binary and involve little rearrangement.

(ii) The figure contains many events with small final energies. Therefore, a large part of the kinetic energy (several hundred MeV) of the collision partners is used up for internal excitations. This is the effect which has given rise to the name *deep-inelastic collisions*. The large energies deposited in the nuclei will cause a ‘heating’ of the latter. Model calculations have shown that this occurs within rather short times, of the order of a few  $10^{-22}$  s.

(iii) Although the net mass and charge transfer between the fragments is small on the average, the figure shows that the charge transfer for a given energy loss (and scattering angle) is not unique, but scatters over a considerable range of values. Similarly, the angular distribution for given energy loss is not sharp, but is spread over a wide range of angles, as is seen in the double differential cross sections  $d^2\sigma/dEd\theta$  of Figs. 11.4 to 11.6 to be discussed in detail below. The same holds for the mass transfer and the energy loss. Thus large fluctuations occur in the charge and in the mass, as well as in the energy and in the scattering angle.

(iv) Measurements of  $\gamma$ -multiplicities show that the  $\gamma$ -rays emitted after a DIC carry angular momentum, which is taken out of the relative motion of the collision partners. This shows that there is considerable transfer of angular momentum from the relative motion to the internal system.

(v) The limiting angular momentum for DIC,  $l_{DIC}$ , increases with mass and energy, and at the same time the fusion angular momentum  $l_F$  decreases. For heavy systems there is less fusion because of the increasing Coulomb repulsion, and the DIC are the dominant process: the DIC cross sections increase with increasing mass and energy of the heavy ions.

(vi) A particular feature of the deep-inelastic collisions is, finally, that the DIC

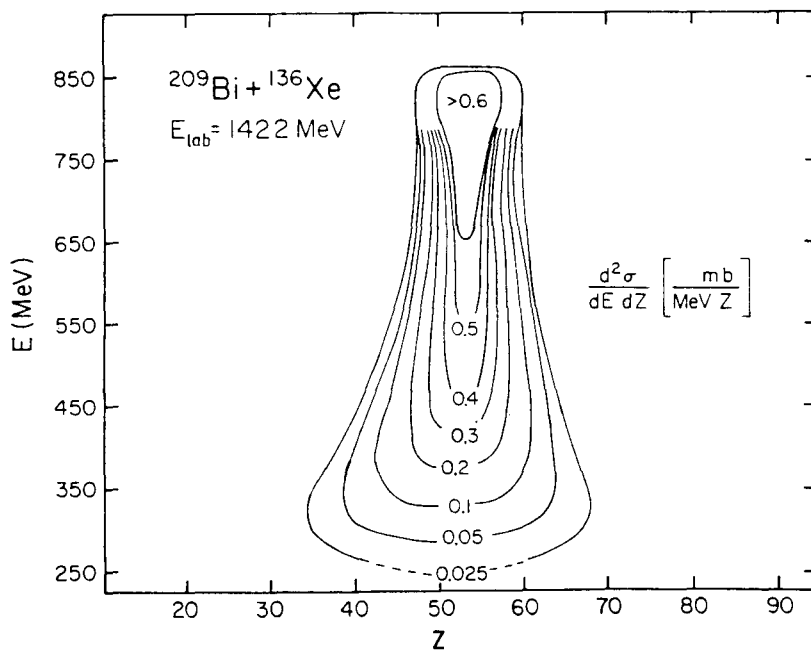


**Figure 11.3** The experimental double differential cross section  $d^2\sigma/dEdZ$  as a function of the final centre-of-mass energy  $E$  and charge  $Z$  of the emitted projectile-like fragments for the system  $^{136}\text{Xe} + ^{209}\text{Bi}$  at  $E_{\text{lab}}(\text{Xe}) = 1422$  MeV.

angular distributions are highly anisotropic. This is a property which the DIC have in common with the direct reactions. Three different types of angular distributions can be distinguished; they arise from a competition between the action of the Coulomb-plus-nuclear forces and the energy-loss mechanism under different kinematical conditions:

— Coulomb-like collisions. If the collision partners are highly charged and the incident energy is relatively low, the Coulomb repulsion dominates. The projectile is strongly reflected to large, backward scattering angles. Figure 11.4, taken from Hildenbrand *et al.* (1983), shows a contour plot in the energy-angle plane of the double differential cross section  $d^2\sigma/dEd\theta$  for the system  $^{154}\text{Sm} + ^{154}\text{Sm}$  at 970 MeV (this type of plot is called a *Wilczynski plot*, cf. Wilczynski 1973). Since in this case the collision partners are identical the angular distribution is symmetric about  $90^\circ$ .

— Focusing collisions. For higher energies or lighter nuclei the Coulomb forces are balanced by the conservative and dissipative nuclear forces. This results in scattering into a narrow angular region, called ‘focusing’. Figure 11.5 shows a Wilczynski plot for the system  $^{136}\text{Xe} + ^{209}\text{Bi}$  at  $E_{\text{lab}}(\text{Xe}) = 1422$  MeV (cf. Wollersheim *et al.* 1981) where, over a large range of final energies, the scattering goes essentially into a narrow range of angles around  $35^\circ$ .

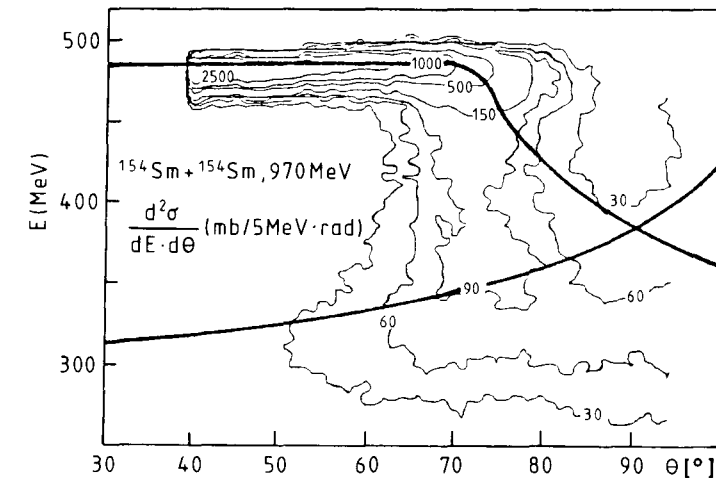


**Figure 11.4** Experimental Wilczynski plot of Coulomb-like deep-inelastic scattering for the system  $^{154}\text{Sm} + ^{154}\text{Sm}$  at  $E_{\text{lab}} = 970$  MeV (cf. Hildenbrand *et al.* 1983). The solid curves represent the energy–angle correlation calculated in the surface-friction model (cf. Section 12.2.3).

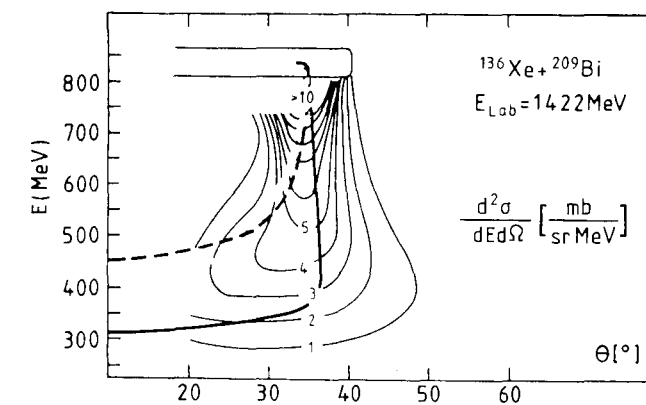


**Figure 11.5** Experimental Wilczynski plot showing the focusing behaviour of the angular distribution for the system  $^{136}\text{Xe} + ^{209}\text{Bi}$  at  $E_{\text{lab}}(\text{Xe}) = 1422$  MeV (cf. Wollersheim *et al.* 1981). The solid and dashed curves represent the energy–angle correlations calculated in the surface-friction model (cf. Section 12.2) with and without dynamical deformation of the collision partners, respectively.

— Orbiting collisions. If the attractive nuclear force dominates over the Coulomb force it pulls the trajectory of the projectile around the target into the region of negative scattering angles. In Section 2.2.3 we have discussed orbiting where the trajectory turns around the target several times. In the present instance the loss of kinetic energy will generally bring the particle to a halt before it actually can orbit around the target; nevertheless, we associate the name ‘orbiting’ with any trajectory leading to a negative deflection angle. An example is provided by the system  $^{86}\text{Kr} + ^{139}\text{La}$  at  $E_{\text{lab}}(\text{Kr}) = 710$  MeV (cf. Fig. 11.6 taken from Vandenbosch *et al.* 1978). We recall that negative deflection angles are counted as positive scattering angles; thus the lower contours are reflections about the ordinate of the negative-deflection-angle branch of the plot.

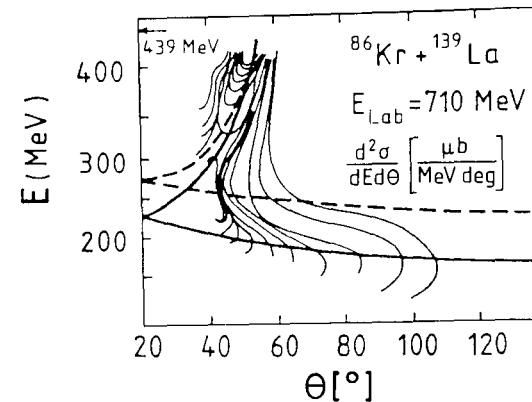


**Figure 11.6** Experimental Wilczynski plot displaying orbiting in the system  $^{86}\text{Kr} + ^{139}\text{La}$  at  $E_{\text{lab}}(\text{Kr}) = 710$  MeV (cf. Vandenbosch *et al.* 1978). The solid and dashed curves represent the energy–angle correlations calculated in the surface-friction model (cf. Section 12.2) with and without dynamical deformation of the collision partners, respectively.

### 11.2.3 The friction hypothesis

We have observed that deep-inelastic collisions occur mainly in heavier systems, for which the local de Broglie wavelength

$$\lambda(r) = \frac{2\pi\hbar}{p(r)} = \frac{2\pi\hbar}{\sqrt{2\mu[E - V(r)]}} \quad (11.11)$$

is generally small compared with typical nuclear dimensions. Taking as an example the system  $^{40}\text{Ar} + ^{238}\text{Th}$ , one finds  $\lambda \leq 0.5$  fm for a typical energy of  $\geq 100$  MeV above the barrier top, which is much smaller than the nuclear radius  $R \approx 10$  fm. Because of the small wavelength a *classical description* of deep-inelastic collisions appears to be adequate.

Furthermore, we have seen that a specific feature of the deep-inelastic collisions is the high loss of kinetic energy of the collision partners. This means that the latter become highly excited during the collision. Since the number of states increases rapidly with excitation energy, a multitude of reaction channels open up, and there will be strong coupling between these. Quantal coupled-channel calculations are then impossible.

Since in any case one measures only quantities averaged over many channels, a *statistical approach* is called for.

With these observations in mind, we present in the remainder of this chapter an idealized theoretical framework for the interpretation and calculation of the measured DIC cross sections. The mechanism of the energy loss of the colliding particles is described as *classical friction* due to the coupling of the nuclear trajectory to the internal nuclear degrees of freedom, which are represented schematically by a ‘heat bath’ of harmonic oscillators. The internal degrees of freedom are treated as random variables. They introduce *fluctuations* in the relative motion, which are responsible for the widths in the angular, energy, mass, and charge distributions of the DIC cross section.

The description is modelled on the theory of *Brownian motion*, only that there the bath surrounds the Brownian particle, whereas in the nuclear case the bath is ‘inside’ the collision partners. The approach advocated here is certainly too simplified for a realistic description of the *detailed* mechanism of the actual deep-inelastic collisions, but it appears to contain the main physical features necessary for the interpretation of the experimental data. The comparison of the calculated results with experiment will be deferred to Chapter 12.

## 11.3 The Langevin description

### 11.3.1 A model Lagrangian and its equations of motion

The following model has been used by Gross (1980) to explain the appearance of friction in scattering, and by Fröbrich (1991) to elucidate the connection between Langevin equations and the Fokker–Planck equation. Two colliding nuclei with reduced mass  $M$  move in the field of an interaction potential  $V(R)$ , where  $R$  is the collective coordinate of the relative motion of the collision partners (for simplicity we regard the problem as one-dimensional). The Lagrangian for the relative motion is

$$\mathcal{L}_0(R, \dot{R}) = \frac{1}{2}M\dot{R}^2 - V(R). \quad (11.12)$$

The internal motion of the particles is described by a set of harmonic oscillators of mass  $m_i$  and frequency  $\omega_i$  with internal coordinate  $q_i$ . The corresponding internal Lagrangian has the form

$$\mathcal{L}_{\text{intl}}(q_i, \dot{q}_i) = \sum_i \frac{m_i}{2}(\dot{q}_i^2 - \omega_i^2 q_i^2). \quad (11.13)$$

The interaction between the relative motion and the oscillators is assumed to be separable and linear in the oscillator coordinates. These are drastic assumptions. They are made here to enable us to derive explicit formulae for the forces governing the relative motion. The full Lagrangian is thus given by

$$\mathcal{L}(R, \dot{R}; q_i, \dot{q}_i) = \mathcal{L}_0(R, \dot{R}) + \mathcal{L}_{\text{intl}}(q_i, \dot{q}_i) + \sum_i f_i(R)q_i, \quad (11.14)$$

where  $f_i(R)$  is the form factor of the coupling; it must vanish at distances  $R$  beyond which the reaction partners cease to interact, and therefore has about the same range as the scattering potential  $V(R)$ .

The equations of motion derived from the Lagrangian (11.14) are

$$M\ddot{R} = -\frac{dV(R)}{dR} + \sum_i q_i \frac{df_i(R)}{dR}, \quad (11.15)$$

$$m_i \ddot{q}_i = -m_i \omega_i^2 q_i + f_i(R). \quad (11.16)$$

#### Elimination of the internal motion

In order to arrive at an effective equation of motion in the collective coordinate  $R$  alone, we must eliminate the internal coordinates. To this end we first solve eqns (11.16) for the variables  $q_i$  in terms of the coordinate  $R = R(t)$ . We find

$$q_i(t) = q_i^0(t) + \int_{t_0}^t ds \frac{f_i(R(s))}{m_i \omega_i} \sin \omega_i(t-s), \quad (11.17)$$

where the first term is the solution of the homogeneous part of eqn (11.16) with  $f_i(R) = 0$ , and has the form

$$q_i^0(t) = q_{i0} \cos \omega_i(t-t_0) + \frac{p_{i0}}{m_i \omega_i} \sin \omega_i(t-t_0); \quad (11.18)$$

the quantities  $q_{i0}$  and  $p_{i0}$  are the values of the coordinates and momenta of the oscillators of the bath at an initial time  $t_0$ . The second term on the right-hand side of eqn (11.17) is contributed by the inhomogeneity  $f_i(R)$ , and incorporates the effect of the relative motion on the internal system.

Substituting the internal coordinates (11.17) in eqn (11.15), we obtain a differential equation for the coordinate  $R$  alone,

$$\begin{aligned} M\ddot{R} = & -\frac{dV(R)}{dR} + \sum_i \frac{1}{m_i \omega_i} \int_{t_0}^t ds f_i(R(s)) \sin \omega_i(t-s) \frac{df_i(R)}{dR} \\ & + \sum_i q_i^0(t) \frac{df_i(R)}{dR}; \end{aligned} \quad (11.19)$$

here the time argument of the coordinate  $R$  is  $t$ , unless indicated otherwise.

Integrating by parts in the second term on the right-hand side of eqn (11.19), we find

$$\begin{aligned} \int_{t_0}^t ds f_i(R(s)) \sin \omega_i(t-s) = & \frac{f_i(R(s))}{\omega_i} \cos \omega_i(t-s) \Big|_{s=t_0}^{s=t} \\ & - \int_{t_0}^t ds \frac{df_i(R(s))}{dR} \dot{R}(s) \frac{1}{\omega_i} \cos \omega_i(t-s), \end{aligned} \quad (11.20)$$

where the dot denotes the time derivative,  $\dot{R}(s) = dR(s)/ds$ . The surface term contributes only at the upper limit  $s = t$ ,

$$\frac{f_i(R(s))}{\omega_i} \cos \omega_i(t-s) \Big|_{s=t_0}^{s=t} = \frac{f_i(R)}{\omega_i},$$

since we assume that  $R(t)$  is very large at the initial time, so that the form factor vanishes there,  $f_i(R(t_0)) = 0$ .

As a result eqn (11.19) takes the form

$$M\ddot{R} = \tilde{F}(R) + F_{\text{frict}}(R, \dot{R}) + F_{\text{L}}(R, t). \quad (11.21)$$

Here we have introduced the *renormalized conservative force*

$$\tilde{F}(R) = -\frac{d\tilde{V}(R)}{dR} \quad (11.22)$$

as the derivative of the *renormalized conservative potential*

$$\tilde{V}(R) = V(R) - \sum_i \frac{1}{2m_i \omega_i^2} [f_i(R)]^2. \quad (11.23)$$

We have further defined the *frictional force*

$$F_{\text{frict}}(R, \dot{R}) = -\sum_i \frac{1}{m_i \omega_i^2} \int_{t_0}^t ds \frac{df_i(R(s))}{dR} \cos \omega_i(t-s) \frac{df_i(R(s))}{dR} \dot{R}(s) \quad (11.24)$$

and the *Langevin force*

$$F_{\text{L}}(R, t) = \sum_i q_i^0(t) \frac{df_i(R)}{dR}. \quad (11.25)$$

#### 11.3.2 The renormalized potential

The renormalized potential (11.23) is equal to the original potential  $V(R)$  plus another conservative term (i.e. a term depending only on the coordinate  $R$ ), which arises from the coupling to the internal system.

The renormalization term can actually be ‘defined away’ by writing the full Lagrangian in the form (cf. Caldeira and Leggett 1983)

$$\mathcal{L}(R, \dot{R}; q_i, \dot{q}_i) = \mathcal{L}_0(R, \dot{R}) + \sum_i \frac{m_i}{2} \dot{q}_i^2 - \sum_i \frac{m_i \omega_i^2}{2} \left( q_i - \frac{f_i(R)}{m_i \omega_i^2} \right)^2; \quad (11.26)$$

here the coupling is introduced by replacing the coordinate  $q_i$  in the undisturbed oscillator potential with  $q_i - f_i(R)/m_i \omega_i^2$ . The effective equation of motion for  $R$  derived from such a Lagrangian contains only the original potential  $V(R)$ .

The different ways of writing the coupling term affect only the conservative potential, not the frictional force. In many applications the renormalization term is not calculated explicitly but assumed to be contained in the phenomenological potential used for trajectory calculations. However, in heavy-ion collisions the driving potential  $\tilde{V}(R)$  is influenced by the heating-up of the nuclei. This effect is generally disregarded in the description of deep-inelastic collisions; but it will be accounted for in the treatment of heavy-ion induced fission (cf. Section 12.4.1).

#### 11.3.3 The frictional force

The frictional force (11.24) is a rather complicated object as it stands. Its value at the time  $t$  is given by an integral over all previous times  $s$  in the interval  $t_0 < s < t$ , i.e. it

is a retarded, or *non-Markovian*, force. We write it as

$$F_{\text{frict}}(R, \dot{R}) = - \int_{t_0}^t ds \gamma(t, s) \dot{R}(s). \quad (11.27)$$

Here we have introduced the friction kernel (for simplicity we assume all oscillator masses to be equal,  $m_i = m$ , and similarly for the form factors,  $f_i(R) = f(R)$ )

$$\gamma(t, s) = f'(R(t)) f'(R(s)) \sum_i \frac{1}{m\omega_i^2} \cos \omega_i(t - s), \quad (11.28)$$

where  $f'(R)$  stands for the derivative with respect to the argument,  $f'(R) = df(R)/dR$ . The sum over the oscillators  $i$  is a sum of many terms with varying signs which effectively vanishes except when all the cosine functions have nearly vanishing arguments, i.e. in the region  $|t - s| \leq \epsilon$ ; the small time interval  $\epsilon$  is the *memory time* which determines the retardation of the frictional force, i.e. its ‘length of memory’. We can therefore write approximately

$$\sum_i \frac{1}{m\omega_i^2} \cos \omega_i(t - s) \approx 2\gamma_0 \delta_\epsilon(t - s), \quad (11.29)$$

where  $\delta_\epsilon(t - s)$  is a ‘smeared-out  $\delta$ -function’ with a range  $\epsilon$ . Integrating eqn (11.29) over  $t$  on both sides, we find for the *frictional strength*  $\gamma_0$

$$2\gamma_0 = \int_{-\infty}^{\infty} dt \sum_i \frac{1}{m\omega_i^2} \cos \omega_i t, \quad (11.30)$$

where the factor 2 is introduced for later convenience. The frictional kernel  $\gamma(t, s)$  then becomes

$$\gamma(t, s) = 2\gamma(R) \delta_\epsilon(t - s) \quad (11.31)$$

with the *friction coefficient*

$$\gamma(R) = \gamma_0 [f'(R)]^2. \quad (11.32)$$

Here we have assumed that the dependence of the coordinate  $R(t)$  on the time  $t$  is weak, so that we can set  $R(s) = R(t)$  for  $|s - t| \leq \epsilon$ .

It is convenient to introduce the spectral density  $g(\omega)$  of the intrinsic excitations, which allows us to replace the sum over the different oscillators  $i$  with an integral over their frequencies,

$$\sum_i \dots \rightarrow \int_0^\infty d\omega g(\omega) \dots$$

Equation (11.29) is then replaced with

$$\int_0^\infty d\omega g(\omega) \frac{1}{m\omega^2} \cos \omega(t - s) \approx 2\gamma_0 \delta_\epsilon(t - s), \quad (11.33)$$

where (cf. eqn (11.30))

$$2\gamma_0 = \int_{-\infty}^{\infty} dt \int_0^\infty d\omega g(\omega) \frac{1}{m\omega^2} \cos \omega t. \quad (11.34)$$

Substituting expression (11.31) in the right-hand side of eqn (11.27) (we gain a factor  $\frac{1}{2}$  because the smeared-out  $\delta$ -function is integrated only up to the position of its peak,

i.e. only over half its area) and assuming again that the time-dependent coordinate  $R(t)$  varies smoothly over the time interval  $\epsilon$ , we obtain a ‘time-local’ *frictional force*

$$F_{\text{frict}}(R, \dot{R}) = -\gamma(R) \dot{R} \quad (11.35)$$

with the friction coefficient  $\gamma(R)$  given by eqn (11.32) together with eqns (11.30) or (11.34).

◊ In the particular case of a quadratic spectral density  $g(\omega) = g_0 \omega^2$  the friction coefficient becomes strictly local in time (Markovian), since

$$\int_0^\infty d\omega g(\omega) \frac{1}{m\omega^2} \cos \omega(t - s) = \frac{g_0 \pi}{m} \delta(t - s), \quad (11.36)$$

where we have used

$$\int_0^\infty d\omega \cos \omega(t - s) = \frac{1}{2} \int_{-\infty}^\infty d\omega e^{i\omega(t-s)} = \pi \delta(t - s). \quad (11.37)$$

Equation (11.34) then becomes

$$2\gamma_0 = \frac{g_0 \pi}{m}. \quad (11.38)$$

In solid-state physics one often assumes linear coupling also in the collective coordinate,  $f_i(R) \propto R$ , which according to eqn (11.32) leads to a constant, so-called ohmic friction coefficient.

If the spectral density is quadratic the second term in the conservative potential (11.23), the renormalisation term, diverges unless it is ‘defined away’. Otherwise one must introduce a high-frequency cut-off in the intrinsic spectrum. ◊

The frictional force induces an *energy loss* in the relative motion: multiplying eqn (11.35) by the velocity  $\dot{R}$ , we find that the energy change per unit time due to the action of the frictional force is given by

$$\dot{E}(t) = F_{\text{frict}}(R, \dot{R}) \dot{R} = -\gamma(R) \dot{R}^2, \quad (11.39)$$

which is always negative. The friction removes energy from the relative motion and transfers it to internal excitations of the collision partners.

#### 11.3.4 The Langevin force

Next we discuss the Langevin force (11.25), which depends separately on the coordinate  $R$  and on the time  $t$ . For simplicity we assume again that the form factors are the same for all oscillators, and write eqn (11.25) as

$$F_L(R, t) = f'(R) \xi(t), \quad (11.40)$$

where the variable

$$\xi(t) = \sum_i q_i^0(t) \quad (11.41)$$

describes the motion of the set of oscillators as a whole. The time dependence of the oscillator variables  $q_i^0(t)$  has the harmonic form (11.18).

These oscillators are assumed to represent a ‘heat bath’. Like the molecules in *Brownian motion*, they must be assumed to influence each other and to excite other

possible internal degrees of freedom which are not coupled directly to the relative motion. When writing down the Lagrangian (11.13) for the internal motion we did not include these interactions explicitly. They must, however, be taken into account implicitly; these interactions are responsible for the equilibration of the heat bath.

In order to explain the nature of the Langevin force, we first discuss the familiar Brownian motion of a small but ‘macroscopic’ particle in an emulsion. We shall come back to the nuclear case of deep-inelastic collisions in Section 11.3.6.

In Brownian motion the bath as a whole is much larger than the Brownian particle, and can be regarded as unaffected by the latter. Owing to the implicit interactions of the oscillators of the bath, the coordinates  $q_{i0}$  and momenta  $p_{i0}$  are treated as *random variables* whose distribution has mean value zero,

$$\langle q_{i0} \rangle = 0, \quad \langle p_{i0} \rangle = 0, \quad (11.42)$$

where  $\langle \dots \rangle$  denotes the average over the ensemble of these variables. They are regarded as uncorrelated,

$$\begin{aligned} \langle q_{i0} q_{j0} \rangle &= \delta_{ij} \langle q_{i0}^2 \rangle, \\ \langle p_{i0} p_{j0} \rangle &= \delta_{ij} \langle p_{i0}^2 \rangle, \\ \langle q_{i0} p_{j0} \rangle &= 0, \end{aligned} \quad (11.43)$$

where the quantities  $\langle q_{i0}^2 \rangle$  and  $\langle p_{i0}^2 \rangle$  are the mean-square elongation and momentum of the  $i$ -th oscillator, respectively.

The variable  $\xi(t)$  in eqn (11.41) is a sum over random variables and is, therefore, itself a time-dependent random variable. By virtue of the central-limit theorem (cf. Reif 1965, Chapter 1) it has a Gaussian distribution. We find, using eqn (11.42),

$$\langle \xi(t) \rangle = 0, \quad (11.44)$$

and using eqns (11.18), (11.42), and (11.43),

$$\begin{aligned} \langle \xi(t) \xi(t') \rangle &= \sum_i \langle q_{i0}^2 \rangle \cos \omega_i(t - t_0) \cos \omega_i(t' - t_0) \\ &\quad + \sum_i \frac{1}{m_i^2 \omega_i^2} \langle p_{i0}^2 \rangle \sin \omega_i(t - t_0) \sin \omega_i(t' - t_0). \end{aligned} \quad (11.45)$$

We write

$$\begin{aligned} 2 \cos \omega_i(t - t_0) \cos \omega_i(t' - t_0) &= \cos \omega_i(t - t') + \cos \omega_i(t + t' + 2t_0), \\ 2 \sin \omega_i(t - t_0) \sin \omega_i(t' - t_0) &= \cos \omega_i(t - t') - \cos \omega_i(t + t' + 2t_0), \end{aligned}$$

and observe, as in formula (11.28), that the sums in eqn (11.45) effectively vanish except when the arguments of the cosine terms are near zero, which can happen only for the terms containing  $\cos \omega_i(t - t')$ . Thus we obtain

$$\langle \xi(t) \xi(t') \rangle \approx \sum_i \frac{\langle \epsilon_{i0} \rangle}{m_i \omega_i^2} \cos \omega_i(t - t'), \quad (11.46)$$

where  $\langle \epsilon_{i0} \rangle$  is the mean energy of the  $i$ -th oscillator,

$$\langle \epsilon_{i0} \rangle = \frac{\langle p_{i0}^2 \rangle}{2m_i} + \frac{1}{2} m_i \omega_i^2 \langle q_{i0}^2 \rangle. \quad (11.47)$$

We assume that the heat bath is in equilibrium and can be characterized by a temperature  $T$ . Applying the equipartition theorem for the one-dimensional oscillator (with two degrees of freedom), we have

$$\langle \epsilon_{i0} \rangle = k_B T, \quad (11.48)$$

where  $k_B$  is the Boltzmann constant. Then eqn (11.46) becomes

$$\langle \xi(t) \xi(t') \rangle \approx k_B T \sum_i \frac{1}{m_i \omega_i^2} \cos \omega_i(t - t'). \quad (11.49)$$

Referring back to eqn (11.29), we see that with all oscillator masses set equal,  $m_i = m$ , the sum on the right-hand side of eqn (11.49) can be replaced with  $2\gamma_0 \delta_\epsilon(t - t')$ , so that we obtain the correlation function

$$\langle \xi(t) \xi(t') \rangle = 2d_0 \delta_\epsilon(t - t'), \quad (11.50)$$

where the *correlation strength*  $d_0$  is given by

$$d_0 = \gamma_0 k_B T. \quad (11.51)$$

Equation (11.50) states that the fluctuations of the random variable  $\xi(t + \epsilon)$  at time  $t + \epsilon$  or later are not affected by those of  $\xi(t)$  at the earlier time  $t$ . Thus the memory time  $\epsilon$  assumes the role of a *correlation time*, i.e. of the time interval within which the random variable  $\xi(t')$  at time  $t'$  influences the variable  $\xi(t)$  at time  $t$ .

Since the fluctuations of  $\xi(t)$  at time  $t$  are independent of those at all earlier times  $t' < t - \epsilon$  we must regard the temperature  $T$  appearing in eqn (11.49) as the actual temperature at time  $t$ , not that at the initial time  $t_0$  as it appears from eqn (11.48). For Brownian motion in an emulsion the temperature is constant, so the last remark is irrelevant. However, we shall see below that in deep-inelastic collisions the ‘bath’ is affected by the nuclear motion. Therefore the mean energy of the oscillators rises as time progresses, and with it the temperature.

◊ For a quadratic spectral density we have according to eqns (11.36) to (11.38),

$$\langle \xi(t) \xi(t') \rangle = 2d_0 \delta(t - t') = 2 \frac{\gamma_0 \pi}{m} k_B T \delta(t - t'). \quad (11.52)$$

In this case the correlation time vanishes, and the variable  $\xi(t)$  is said to be ‘ $\delta$ -correlated’ or *Markovian*. ◊

It is convenient to introduce the normalized variable

$$\Gamma(t) = \frac{1}{\sqrt{d_0}} \xi(t), \quad (11.53)$$

which like the variable  $\xi(t)$  is a time-dependent random variable with a Gaussian distribution. Its average and its correlation function are

$$\begin{aligned}\langle \Gamma(t) \rangle &= 0, \\ \langle \Gamma(t)\Gamma(t') \rangle &= 2\delta_\epsilon(t-t'),\end{aligned}\quad (11.54)$$

where eqns (11.44) and (11.50) have been used.

The Langevin force (11.40) itself is equal to the random variable  $\xi(t)$  multiplied by the derivative of the form factor,  $f'(R)$ . Assuming that the latter is a smooth function of  $R$  which is insensitive to variations of the argument due to the fluctuations in  $\xi(t)$  (recall that  $R(t)$  is also a random variable owing to its coupling to  $\xi(t)$  via eqn (11.21)), we find that the average of the Langevin force is (cf. eqn (11.40))

$$\langle F_L(R(t), t) \rangle = 0. \quad (11.55)$$

Its correlation function is

$$\langle F_L(R(t), t)F_L(R(t'), t') \rangle = 2D(R)\delta_\epsilon(t-t'), \quad (11.56)$$

where we have introduced the *fluctuation strength coefficient*

$$D(R) = d_0[f'(R)]^2, \quad (11.57)$$

which will later turn out to have the physical meaning of a diffusion coefficient in the momentum (cf. eqn (11.91)). Combining eqns (11.40), (11.53), and (11.57), we obtain the Langevin force in the form

$$F_L(R, t) = \sqrt{D(R)}\Gamma(t). \quad (11.58)$$

### 11.3.5 The fluctuation-dissipation theorem

Comparing eqn (11.32) with eqns (11.51) and (11.57), we obtain the relation

$$D(R) = \gamma(R)k_B T, \quad (11.59)$$

which connects the fluctuation strength coefficient  $D(R)$  of the Langevin force with the friction coefficient  $\gamma(R)$ . It is a simple consequence of the fact that the frictional and Langevin forces both have their origin in the coupling between the relative motion and the bath, represented by the second term on the right-hand side of eqn (11.15).

The relation (11.59) is a special case of the *fluctuation-dissipation theorem*. In the present model it comes as no surprise. But in statistical theory it can be shown that such a relation exists quite generally and is, therefore, called a theorem (cf. Kubo 1957). The relation (11.59) is often given the name ‘Einstein relation’, which is unfortunate, for we shall see that the original Einstein relation has a different meaning (cf. eqn (11.130)).

Formula (11.48), which has been used in deriving eqn (11.59), is a classical relation. It holds only for temperatures high enough that the bath can be treated by classical Boltzmann statistics. At low temperatures, which in the nuclear case means near the ground state of the colliding nuclei, the quantal expression (cf. Messiah 1972, eqn (XII.52))

$$\langle \epsilon_i \rangle = \frac{1}{2}\hbar\omega_i \coth\left(\frac{\hbar\omega_i}{2k_B T}\right) \quad (11.60)$$

must replace eqn (11.48). For  $T \rightarrow 0$  it goes over into  $\langle \epsilon_i \rangle = \hbar\omega_i/2$ : the mean energy of the oscillator at zero temperature does not vanish but is determined by the quantal

*zero-point fluctuations* of the oscillator in the ground state. For large temperatures  $T$  the limit (11.48) is attained.

### 11.3.6 The Langevin equations; their applicability to DIC

#### The Langevin equations

After the preceding manipulations we write down the equation of motion (11.21) in its previous form

$$M\ddot{R} = \tilde{F}(R) + F_{\text{frict}}(R, \dot{R}) + F_L(R, t) \quad (11.61)$$

but with the simplified version (11.35) of the frictional force,

$$F_{\text{frict}}(R, \dot{R}) = -\gamma(R)\dot{R}, \quad (11.62)$$

and of the Langevin force (cf. eqn (11.58)),

$$F_L(R, t) = \sqrt{D(R)}\Gamma(t), \quad (11.63)$$

where the fluctuation strength coefficient  $D(R)$  is connected with the friction coefficient  $\gamma(R)$  by the fluctuation-dissipation theorem (11.59). Introducing the momentum of the relative motion  $P = M\dot{R}$ , we finally obtain from eqn (11.61) the *Langevin equations*

$$\begin{aligned}\dot{R} &= \frac{P}{M}, \\ \dot{P} &= \tilde{F}(R) - \gamma(R)\frac{P}{M} + \sqrt{D(R)}\Gamma(t).\end{aligned}\quad (11.64)$$

The variables  $R$  and  $P$  are themselves random variables, since they are solutions of the coupled equations (11.64) which contain the random variable  $\Gamma(t)$ .

It is convenient for later discussions to write the Langevin equations (11.64) in a more general multidimensional form, replacing the variables  $\{R, P\}$  with the general set of dynamical variables  $x = \{x_i\}$  (cf., e.g. Stratonovich 1967; Risken 1989),

$$\dot{x}_i = h_i(x) + \sum_j g_{ij}(x)\Gamma_j(t), \quad i = 1, \dots, N, \quad (11.65)$$

where

$$\langle \Gamma_i(t) \rangle = 0 \quad (11.66)$$

and

$$\langle \Gamma_i(t)\Gamma_j(t') \rangle = 2\delta_{ij}\delta_\epsilon(t-t'). \quad (11.67)$$

The functions  $h_i(x)$  contain the conservative and frictional forces, and the functions  $g_{ij}(x)$  the fluctuation strength coefficients.

#### Applicability of the Langevin equations to deep-inelastic collisions

So far we have discussed Brownian motion, where the large bath of oscillators influences the motion of the Brownian particle, while the bath itself is *not* affected by its coupling to the particle motion. In particular, its temperature remains constant. In deep-inelastic collisions, on the other hand, we assume that the bath represents the internal degrees of freedom in the interior of the colliding nuclei (cf. Section 11.2.3). The average properties of this kind of bath are surely influenced by the coupling to the relative motion of the

nuclei. One of the obvious effects of this coupling is that the energy loss (11.39) due to friction reappears as an energy gain in the bath, so that the temperature of the bath rises as its energy increases during the course of the collision. Therefore, we must allow that the fluctuation strength coefficient  $D(R)$  (cf. (11.59)) which determines the strength of the fluctuations of the Langevin force via eqns (11.21) and (11.51) is not constant, but is continually readjusted as the bath ‘heats up’. The assumption underlying this scheme is that the internal system equilibrates quickly, i.e. that its ‘equilibration time’ is smaller than the correlation time  $\epsilon$ , and also smaller than the time scale of the macroscopic relative motion.

Whether these conditions are fulfilled in actual deep-inelastic collisions may be doubted seriously. Nevertheless, we shall assume that Langevin equations with a phenomenological Markovian friction term and a Gaussian-distributed random force can be used to describe such processes. It is thus understood from now on that a temperature  $T$  of the excited nuclei can be defined at each stage of the collision process. This temperature, and therefore also the fluctuation strength of the Langevin force, change with time, but at a rate which is slow on the scale of the equilibration and correlation times.

We have derived the Langevin equations with the help of a particular model, which allows us to understand their structure and their physical meaning. We now forget the particulars of this derivation and take the equations (11.65) as they stand, with the random forces  $\Gamma_i(t)$  defined by eqns (11.66) and (11.67). The conservative forces and the frictional form factors are regarded as phenomenological quantities which have to be specified within an appropriate nuclear model. If the strength coefficients of the random forces are determined by the fluctuation-dissipation theorem, the ‘internal bath’ enters in the description via the temperature  $T$ , which is calculated along each trajectory. The ensemble average over these temperatures is the physical temperature of the bath.

### 11.3.7 Discretization of the Langevin equations

For the further development we discretize the Langevin equations. This will be particularly helpful for establishing the connection with the Fokker–Planck equation. The discretization is also necessary for performing numerical calculations.

We introduce the time interval  $\tau$  and consider the times  $t_n = n\tau$ . The interval  $\tau$  is chosen larger than the correlation time  $\epsilon$  of the random process  $\Gamma(t)$ , but smaller than the times over which the forces and form factors in the Langevin equation vary appreciably as functions of the coordinate  $R = R(t)$ . We now integrate eqns (11.64) from  $t_n$  to  $t_{n+1} = t_n + \tau$ . We regard the functions  $\tilde{F}(R)$ ,  $\gamma(R)$ , and  $D(R)$  as constant in this interval and replace them with their values at time  $t_n$ . Thus we have, with  $R_n = R(t_n)$  and  $P_n = P(t_n)$ ,

$$\begin{aligned} R_{n+1} &= R_n + \frac{P_n}{M}\tau, \\ P_{n+1} &= P_n + \left( \tilde{F}(R_n) - \gamma(R_n)\frac{P_n}{M} \right) \tau + \sqrt{D(R_n)} W_n, \end{aligned} \quad (11.68)$$

where the random variable

$$W_n = W(t_n) = \int_{t_n}^{t_{n+1}} dt' \Gamma(t') \quad (11.69)$$

is a sum of Gaussian-distributed random numbers and is therefore again Gaussian-distributed. It can be written as  $W_n = a_n w(t_n)$ , where  $w(t_n)$  is a normalized random variable which satisfies

$$\langle w(t_n) \rangle = 0 \quad (11.70)$$

and

$$\langle w(t_n) w(t_{n'}) \rangle = 2\delta_{nn'}. \quad (11.71)$$

The last equation is consistent with the assumption that  $\tau$  is larger than the correlation time  $\epsilon$  of the random process  $\Gamma(t)$  (cf. eqn (11.54)), so that there is no correlation between the values of the function  $\Gamma(t)$  in the intervals  $t_n < t < t_{n+1}$  and  $t_{n'} < t < t_{n'+1}$  if  $n \neq n'$ .

The coefficient  $a_n$  is determined by comparing (cf. eqn (11.54))

$$\begin{aligned} \langle W_n^2 \rangle &= \int_{t_n}^{t_{n+1}} dt' \int_{t_n}^{t_{n+1}} dt'' \langle \Gamma(t') \Gamma(t'') \rangle \\ &= 2 \int_{t_n}^{t_{n+1}} dt' \int_{t_n}^{t_{n+1}} dt'' \delta_\epsilon(t' - t'') = 2\tau \end{aligned} \quad (11.72)$$

with

$$\langle W_n^2 \rangle = a_n^2 \langle [w(t_n)]^2 \rangle = 2a_n^2. \quad (11.73)$$

This yields  $a_n = \sqrt{\tau}$ .

The discretized form of the Langevin equations is now

$$\begin{aligned} R_{n+1} &= R_n + \frac{P_n}{M}\tau, \\ P_{n+1} &= P_n + \left( \tilde{F}(R_n) - \gamma(R_n)\frac{P_n}{M} \right) \tau + \sqrt{D(R_n)}\sqrt{\tau} w(t_n). \end{aligned} \quad (11.74)$$

In the general formulation we then have

$$x_i(t_{n+1}) = x_i(t_n) + h_i[x(t_n)]\tau + \sum_j g_{ij}[x(t_n)]\sqrt{\tau} w_j(t_n). \quad (11.75)$$

◊ The discretization method we have used here is due to Itô (1944). Other methods of discretization have also been proposed, for example, that of Stratonovich (1967), in which the functions on the right-hand side of eqn (11.68) are evaluated not at  $R_n$ ,  $P_n$  but at  $(R_n + R_{n+1})/2$ ,  $(P_n + P_{n+1})/2$ . The Stratonovich method leads to a Fokker–Planck equation which is in general different from that obtained with the Itô discretization, and may not describe precisely the same physics. Therefore, when applying the Langevin method to actual cases one must be aware of the fact that the choice of a discretization of the Langevin equation implies a particular physical interpretation. For a discussion of these problems cf., for example, van Kampen (1981, in particular Sections VIII.8 and 9). ◊

## 11.4 The Fokker–Planck description

We are not interested in each single random solution  $\{x_i(t)\}$  of the Langevin equations (11.65). Rather, we require the distribution of these solutions, i.e. the *distribution function* or *probability density*  $d(x; t)$  of the set of variables  $x$  as a function of the time  $t$ . This distribution function can be obtained by sampling a sufficiently large number of Langevin trajectories. However, it is possible to convert the Langevin equations into an equation whose solution yields the distribution function directly. This equation is the *Fokker–Planck equation*. It will be derived in the following.

### 11.4.1 The Kramers–Moyal expansion

The distribution function  $d(x; t + \tau)$  at time  $t + \tau$  is connected with the distribution function  $d(x; t)$  at the time  $t$  by the relation

$$d(x; t + \tau) = \int dx' P(x, t + \tau; x', t) d(x'; t), \quad (11.76)$$

where  $P(x, t + \tau; x', t)$  is the *transition probability*. It is defined as the conditional probability density of the variable  $x$  at time  $t + \tau$  when it is known that this variable has had the sharp value  $x'$  at the earlier time  $t$ . Equation (11.76) expresses the law of composition of the two probability densities on the right-hand side into the one on the left-hand side.

The conditional probability density could in principle depend on more than one earlier time. If, as in the present case, it depends only on *one* previous time it is called *Markovian*. This is the simplest way of correlating distributions at different times. The conditional probability density contains all the dynamics, that is the physics, of the underlying process.

We now introduce the identity

$$P(x, t + \tau; x', t) = \int dy \delta(y - x) P(y, t + \tau; x', t) \quad (11.77)$$

and consider the formal expansion of the  $\delta$ -function into a Taylor series

$$\delta(y - x) = \delta(x' - x + y - x') = \sum_{n=0}^{\infty} \frac{(y - x')^n}{n!} \left( -\frac{\partial}{\partial x} \right)^n \delta(x' - x). \quad (11.78)$$

For the moment we treat the set of variables  $x = \{x_i\}$  as if it were a single variable  $x$ ; the correct many-variable formulation resumes with eqn (11.84). We then can rewrite the transition probability in the form of a moment expansion

$$P(x, t + \tau; x', t) = \sum_{n=0}^{\infty} \frac{1}{n!} \left( -\frac{\partial}{\partial x} \right)^n [M_n(x'; t, \tau) \delta(x' - x)] \quad (11.79)$$

with the moments

$$\begin{aligned} M_n(x'; t, \tau) &= \int dy (y - x')^n P(y, t + \tau; x', t) \\ &= \langle [x'(t + \tau) - x'(t)]^n \rangle. \end{aligned} \quad (11.80)$$

## 11.4 The Fokker–Planck description

The last line of this equation follows from the observation that by the definition of the transition probability  $P(y, t + \tau; x', t)$ , the variable  $y$  appearing in it represents the time-dependent random variable  $x'(t + \tau)$  at the time  $t + \tau$ , which has had the definite value  $x'(t) = x'$  at the time  $t$ ; the integral over  $y$  is an average over the random values  $x'(t + \tau)$  at time  $t + \tau$  with  $x'(t)$  fixed.

Substituting the expansion (11.79) in equation (11.76) and integrating over the  $\delta$ -function we obtain

$$d(x; t + \tau) - d(x; t) = \sum_{n=1}^{\infty} \left( -\frac{\partial}{\partial x} \right)^n \left( \frac{M_n(x; t, \tau)}{n!} d(x; t) \right). \quad (11.81)$$

Dividing this equation on each side by the time step  $\tau$  and going to the limit  $\tau \rightarrow 0$ , we obtain the *Kramers–Moyal expansion*

$$\frac{\partial}{\partial t} d(x; t) = \sum_{n=1}^{\infty} \left( -\frac{\partial}{\partial x} \right)^n [D^{(n)}(x; t) d(x; t)], \quad (11.82)$$

where

$$D^{(n)}(x; t) = \frac{1}{n!} \lim_{\tau \rightarrow 0} \frac{M_n(x; t, \tau)}{\tau} = \frac{1}{n!} \lim_{\tau \rightarrow 0} \frac{\langle [x(t + \tau) - x(t)]^n \rangle}{\tau}. \quad (11.83)$$

Written explicitly in the  $N$  variables  $x_i$ , eqn (11.82) becomes

$$\frac{\partial}{\partial t} d(x; t) = - \sum_i \frac{\partial}{\partial x_i} [D_i^{(1)}(x; t) d(x; t)] + \sum_{ij} \frac{\partial^2}{\partial x_i \partial x_j} [D_{ij}^{(2)}(x; t) d(x; t)] + \dots, \quad (11.84)$$

where the coefficients  $D^{(n)}(x; t)$  take the form

$$\begin{aligned} D_i^{(1)}(x; t) &= \lim_{\tau \rightarrow 0} \frac{1}{\tau} \langle [x_i(t + \tau) - x_i(t)] \rangle, \\ D_{ij}^{(2)}(x; t) &= \frac{1}{2} \lim_{\tau \rightarrow 0} \frac{1}{\tau} \langle [x_i(t + \tau) - x_i(t)][x_j(t + \tau) - x_j(t)] \rangle, \\ D_{ijk}^{(3)}(x; t) &= \dots; \end{aligned} \quad (11.85)$$

here the third coefficient is defined in analogy to the second, and so on.

### 11.4.2 The connection with the Langevin equations

The coefficients  $D^{(n)}(x; t)$  of eqn (11.85) can be evaluated with the help of the discretized Langevin equations (11.75), which we write in the form

$$x_i(t + \tau) - x_i(t) = \sqrt{\tau} \left( h_i(x) \sqrt{\tau} + \sum_j g_{ij}(x) w_j(t) \right). \quad (11.86)$$

Substituting these expressions in the right-hand sides of eqn (11.85) and using eqns (11.70) and (11.71), we find

$$\begin{aligned}
D_i^{(1)}(x; t) &= \lim_{\tau \rightarrow 0} \frac{1}{\tau} \sqrt{\tau} \left( h_i(x) \sqrt{\tau} + \sum_j g_{ij}(x) \langle w_j(t) \rangle \right) = h_i(x), \\
D_{ij}^{(2)}(x; t) &= \frac{1}{2} \lim_{\tau \rightarrow 0} \frac{1}{\tau} \tau \left( h_i(x) h_j(x) \tau + h_i(x) \sum_k g_{jk}(x) \sqrt{\tau} \langle w_k(t) \rangle \right. \\
&\quad \left. + h_j(x) \sum_l g_{il}(x) \sqrt{\tau} \langle w_l(t) \rangle + \sum_{kl} g_{il}(x) g_{jk}(x) \langle w_k(t) w_l(t) \rangle \right) \\
&= \sum_k g_{ik}(x) g_{jk}(x), \\
D_{ijk}^{(3)}(x; t) &= \frac{1}{6} \lim_{\tau \rightarrow 0} \frac{1}{\tau} \tau^{3/2} (\dots) = 0, \\
D_{ij\dots}^{(n)}(x; t) &= 0 \text{ for } n > 3.
\end{aligned} \tag{11.87}$$

Only the first two coefficients are non-vanishing, and they are independent of the time. The first is called the *drift coefficient*

$$v_i(x) = D_i^{(1)}(x), \tag{11.88}$$

and the second the *diffusion coefficient*

$$D_{ij}(x) = D_{ij}^{(2)}(x). \tag{11.89}$$

◇ In the preceding discretization scheme the Kramers–Moyal expansion is cut off automatically after the second term. One may suspect that this is not generally so. In this connection a lemma of Pawula (1967) is of interest, which states that if the expansion does not terminate after the first or second terms it does not terminate at all (cf. Risken 1989, Section 4.3). ◇

### 11.4.3 The Fokker–Planck equation

Owing to eqns (11.87) to (11.89), the Kramers–Moyal expansion (11.84) reduces to the *Fokker–Planck equation*

$$\frac{\partial}{\partial t} d(x; t) = - \sum_i \frac{\partial}{\partial x_i} v_i(x) d(x; t) + \sum_{ij} \frac{\partial^2}{\partial x_i \partial x_j} D_{ij}(x) d(x; t), \tag{11.90}$$

where here and in the following the derivatives act on all terms to the right.

In the particular case of the Langevin equations (11.64), i.e. for  $x_1 = R$  and  $x_2 = P$ , we find from eqns (11.87) to (11.89)

$$\begin{aligned}
v_R &= \frac{P}{M}, \\
v_P &= \tilde{F}(R) - \gamma(R) \frac{P}{M}, \\
D_{RR} &= 0, \\
D_{PP} &= D(R), \\
D_{RP} &= 0.
\end{aligned} \tag{11.91}$$

Only *one* diffusion coefficient is non-vanishing, namely  $D_{PP}$ , the diffusion coefficient in the momentum. It is equal to the fluctuation strength function  $D(R)$ . However, this does not mean that the variable  $R$  does not fluctuate, because owing to its coupling to  $P$  it is random as well.

The Fokker–Planck equation associated with the Langevin equations (11.64) reads

$$\begin{aligned}
\frac{\partial}{\partial t} d(R, P; t) &= \left[ -\frac{\partial}{\partial R} \frac{P}{M} - \frac{\partial}{\partial P} \left( \tilde{F}(R) - \gamma(R) \frac{P}{M} \right) \right. \\
&\quad \left. + \frac{\partial^2}{\partial P^2} D(R) \right] d(R, P; t).
\end{aligned} \tag{11.92}$$

#### 11.4.4 Simple examples

In order to become acquainted with the Fokker–Planck equation and its solution we consider some analytically solvable examples.

##### One-dimensional Fokker–Planck equation with constant coefficients

The one-dimensional Fokker–Planck equation with constant coefficients reads

$$\frac{\partial}{\partial t} d(Z; t) = \left( -v \frac{\partial}{\partial Z} + D \frac{\partial^2}{\partial Z^2} \right) d(Z; t). \tag{11.93}$$

Such an equation has been used by Nörenberg (1974) to treat charge transfer in deep-inelastic collisions. The variable  $Z$  denotes the charge of the projectile-like fragment, so that the distribution function  $d(Z; t)$  describes how the charge of the projectile changes with time.

Introducing the new variable  $X = Z - vt$  in the place of  $Z$ , we obtain the equation

$$\frac{\partial}{\partial t} d(X; t) = D \frac{\partial^2}{\partial X^2} d(X; t). \tag{11.94}$$

This equation has the form of a *diffusion equation*. With the initial condition  $d(X; 0) = \delta(X)$  it has the solution

$$d(X; t) = \frac{1}{\sqrt{4\pi D t}} e^{-X^2/4Dt}, \tag{11.95}$$

or

$$d(Z; t) = \frac{1}{\sqrt{4\pi D t}} e^{-(Z-vt)^2/4Dt}. \tag{11.96}$$

The distribution function is normalized,

$$\langle 1 \rangle = \int dZ d(Z; t) = 1. \tag{11.97}$$

The mean value  $\bar{Z}(t)$  and the variance  $\sigma_{ZZ}^2$  are found from the first and second moments of the distribution function,

$$\begin{aligned}
\bar{Z}(t) &= \langle Z \rangle = \int dZ Z d(Z; t) = vt, \\
\sigma_{ZZ}^2 &= \langle [Z - \bar{Z}(t)]^2 \rangle = \int dZ (Z - vt)^2 d(Z; t) = 2Dt.
\end{aligned} \tag{11.98}$$

The distribution function (11.96) is shown in Fig. 11.7 for different times. The mean value and the variance increase linearly with time. The constant  $D$  which determines

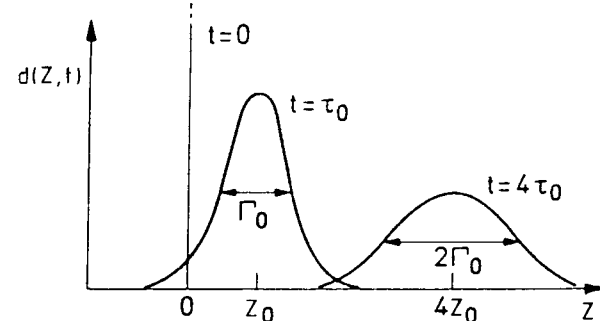


**Figure 11.7** The solution (11.96) of the one-dimensional Fokker–Planck equation with constant coefficients at different times. The charge  $Z$  and the widths  $\Gamma_Z$  are indicated for two times differing by a factor of four;  $Z_0 = Z(\tau_0)$  and  $\Gamma_0 = \Gamma_Z(\tau_0)$ .

the rate of increase of the variance is called the *diffusion constant*.

The spreading of the distribution function is characterized by the full width at half-maximum  $\Gamma_Z$  which according to eqn (11.96) is defined by

$$\exp[-(\Gamma_Z/2)^2/4Dt] = \frac{1}{2};$$

this yields a width which increases in proportion to the square root of time,

$$\Gamma_Z = \Gamma_Z(t) = 4\sqrt{(\ln 2)Dt}. \quad (11.99)$$

The charge transfer described by the Fokker–Planck equation occurs only in the time interval during which the collision partners are in close contact, which begins at  $t = 0$  and ends at the *interaction time*  $\tau_{\text{int}}$ . Thereafter, the charge variable  $Z$  is no longer subject to stochastic interactions and is equal to the charge of the projectile-like fragment after the collision. The distribution function for this last quantity is therefore equal to  $d(Z; \tau_{\text{int}})$ . If the interaction time can be calculated in some model, it is then possible to extract values of the drift and diffusion coefficients from the measured charge distribution. In DIC the interaction time is generally proportional to the deflection angle, so that one can use the latter as a measure of the former.

For an illustration we consider the system  $^{232}\text{Th} + ^{40}\text{Ar}$  at 388 MeV (cf. Nörenberg 1974). Figure 11.8a shows the distribution functions for the projectile-like charge  $Z$  at different deflection angles  $\Theta_{\text{lab}}$  (or interaction times  $\tau_{\text{int}}$ ); in Fig. 11.8b we plot the square of the widths  $\Gamma_Z^2$ . According to eqn (11.99) these are proportional to the interaction time. From Fig. 11.8a it is seen that  $v \approx 0$ . This means that there is no drift in the charge distribution, it stays centered around the initial mean value at all times: the mean charge of the projectile remains constant. The diffusion coefficients for the two energies indicated in Fig. 11.8b can be read off from the slopes of the two straight lines.

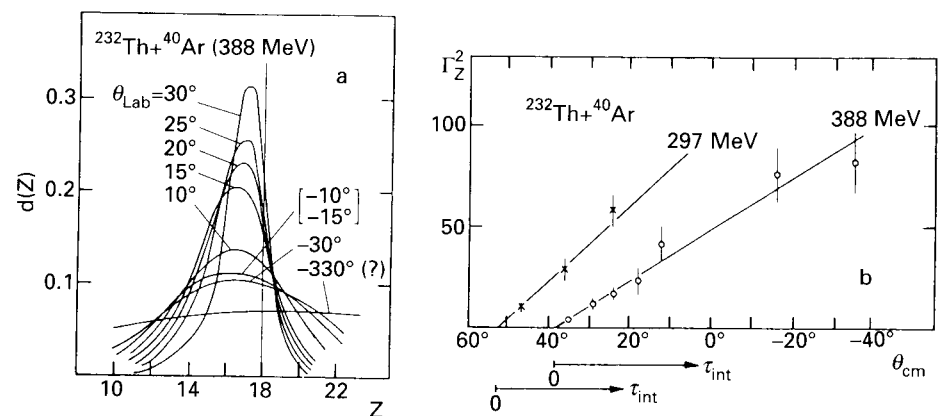


**Figure 11.8** Charge transfer in the system  $^{232}\text{Th} + ^{40}\text{Ar}$  at 388 MeV. (a) Charge distribution  $d(Z)$  of the projectile-like fragments ( $Z_{\text{proj}} = 18$ ) for different deflection angles  $\Theta_{\text{lab}}$ . (b) The square of the width  $\Gamma_Z^2$  of the charge distribution as function of the deflection angle (or interaction time  $\tau_{\text{int}}$ ) for the same system at the two energies 297 and 388 MeV.

#### One-dimensional Fokker–Planck equation with a linear drift coefficient

We generalize the preceding Fokker–Planck equation with constant coefficients to an equation with a variable drift coefficient  $v(Z)$ . The latter is determined by the potential energy surface  $U(Z)$  of the collision partners as a function of the charge  $Z$  of the projectile-like fragments. This surface is a driving potential in the variable  $Z$ , which is given by the energy release  $\tilde{B}(A, Z, \alpha)$  introduced in Section 9.2.2. In the present case the Fokker–Planck equation has the form

$$\frac{\partial}{\partial t} d(Z, t) = \left( -\frac{\partial}{\partial Z} v(Z) + D \frac{\partial^2}{\partial Z^2} \right) d(Z, t). \quad (11.100)$$

We require that the equilibrium solution, i.e. the stationary solution of eqn (11.100) to which the full solution reduces for  $t \rightarrow \infty$ , has the form of a Boltzmann distribution

$$d(Z) \propto e^{-U(Z)/k_B T}, \quad (11.101)$$

where  $T$  is the temperature of the system. This requirement relates the drift term  $v(Z)$  to the diffusion coefficient  $D$ : in the stationary regime, where  $\partial d(Z, t)/\partial t = 0$ , eqn (11.100) becomes

$$\frac{\partial}{\partial Z} \left( -v(Z) + D \frac{\partial}{\partial Z} \right) d(Z, t) = 0, \quad (11.102)$$

so that

$$v(Z) = \frac{1}{d(Z)} \frac{d}{dZ} D d(Z), \quad (11.103)$$

where the constant of integration has been incorporated in the drift term. Substituting here eqn (11.101), we find

$$v(Z) = -\frac{D}{k_B T} \frac{\partial U(Z)}{\partial Z}. \quad (11.104)$$

This relation connects the drift term with the diffusion term, and is a special form of the fluctuation-dissipation theorem (11.59).

In first approximation (neglecting shell effects in the binding energy) the driving potential  $U(Z)$  can be calculated within the framework of the liquid-drop model, where it is assumed to be quadratic in  $Z$ ,

$$U(Z) = \frac{C}{Z_{\text{tot}}^2} (Z - Z_s)^2. \quad (11.105)$$

Here  $Z_{\text{tot}}$  is the total charge of projectile and target, and  $Z_s = Z_{\text{tot}}/2$ . The factor  $C$  is the stiffness of the driving potential.

For the harmonic driving potential (11.105) the Fokker–Planck equation (11.100) becomes

$$\frac{\partial}{\partial t} d(Z, t) = \left( \frac{\partial}{\partial Z} \frac{2CD}{k_B T Z_{\text{tot}}^2} (Z - Z_s) + D \frac{\partial^2}{\partial Z^2} \right) d(Z, t). \quad (11.106)$$

It contains a linear drift coefficient and a constant diffusion coefficient. The solution of this equation has again a Gaussian form,

$$d(Z, t) = \frac{1}{\sqrt{2\pi\sigma_{ZZ}^2(t)}} \exp\left(-\frac{[Z - \bar{Z}(t)]^2}{2\sigma_{ZZ}^2(t)}\right), \quad (11.107)$$

where, for an initial projectile charge  $Z(0) = Z_{\text{proj}}$ ,

$$\begin{aligned} \bar{Z}(t) &= Z_s - (Z_{\text{proj}} - Z_s) \exp\left(-\frac{2CD}{k_B T Z_{\text{tot}}^2} t\right), \\ \sigma_{ZZ}^2(t) &= \frac{k_B T Z_{\text{tot}}^2}{2C} \left[ 1 - \exp\left(-\frac{4CD}{k_B T Z_{\text{tot}}^2} t\right) \right]. \end{aligned} \quad (11.108)$$

For large interaction times the system evolves towards symmetry,

$$\bar{Z}(t) \rightarrow Z_s = \frac{Z_{\text{tot}}}{2} \quad \text{for } t \rightarrow \infty. \quad (11.109)$$

The width of the distribution does not go to infinity as in the case of a constant drift term (cf. eqn (11.98)), but converges to a constant value which is determined by the stiffness  $C$  of the driving potential and the temperature  $T$ ,

$$\sigma_{ZZ}^2(t) \rightarrow \frac{k_B T Z_{\text{tot}}^2}{2C} \quad \text{for } t \rightarrow \infty. \quad (11.110)$$

Further examples for charge transfer in DIC will be given in Section 12.3.1.

*Two-dimensional Fokker–Planck equation with constant coefficients: Brownian motion*

For a further example we consider a two-dimensional Fokker–Planck equation with constant coefficients. We assume that the force  $\tilde{F}$ , the friction strength  $\gamma$ , and the diffusion

coefficient  $D$  in the two-dimensional Fokker–Planck equation (11.92) are constant, as for a Brownian particle which is subject to gravitation. In this case the Fokker–Planck equation for the distribution function  $d = d(R, P; t)$  reads

$$\frac{\partial}{\partial t} d(R, P; t) = \left( -\frac{P}{M} \frac{\partial}{\partial R} - \tilde{F} \frac{\partial}{\partial P} + \frac{\gamma}{M} \frac{\partial}{\partial P} P + D \frac{\partial^2}{\partial P^2} \right) d(R, P; t). \quad (11.111)$$

The distribution function  $d = d(R, P; t)$  is normalized to unity in phase space at any time  $t$ ,

$$\iint dR dP d(R, P; t) = 1. \quad (11.112)$$

It vanishes for large values of  $R$  or  $P$ , i.e. ‘at the surface’.

As in the foregoing examples, the solution of eqn (11.111) is again of Gaussian form, but this time in two variables,

$$\begin{aligned} d(R, P; t) &= \frac{1}{(2\pi)^2 (\sigma_{RR}^2 \sigma_{PP}^2 - \sigma_{RP}^2 \sigma_{PR}^2)^{1/2}} \exp \left\{ -\frac{1}{2} [(\sigma^2)_{RR}^{-1} (R - \bar{R}(t))^2 \right. \\ &\quad \left. + 2(\sigma^2)_{RP}^{-1} (R - \bar{R}(t))(P - \bar{P}(t)) + (\sigma^2)_{PP}^{-1} (P - \bar{P}(t))^2] \right\}. \end{aligned} \quad (11.113)$$

Here the time-dependent *mean values*  $\bar{R}(t)$  and  $\bar{P}(t)$  are given by

$$\begin{aligned} \bar{R}(t) &= \langle R(t) \rangle = \iint dR dP R d(R, P; t), \\ \bar{P}(t) &= \langle P(t) \rangle = \iint dR dP P d(R, P; t), \end{aligned} \quad (11.114)$$

and the functions  $(\sigma^2)_{RR}^{-1}$ , etc. are the elements of the inverse of the  $2 \times 2$  matrix made up of the *variances*  $\sigma_{RR}^2(t)$ ,  $\sigma_{PP}^2(t)$  and the *covariance*  $\sigma_{RP}^2(t) = \sigma_{PR}^2(t)$ ,

$$\begin{aligned} \sigma_{RR}^2(t) &= \langle [R - \bar{R}(t)]^2 \rangle = \langle R^2 \rangle - \bar{R}^2(t), \\ \sigma_{PP}^2(t) &= \langle [P - \bar{P}(t)]^2 \rangle = \langle P^2 \rangle - \bar{P}^2(t), \\ \sigma_{RP}^2(t) &= \langle [R - \bar{R}(t)][P - \bar{P}(t)] \rangle = \langle RP \rangle - \bar{R}(t)\bar{P}(t). \end{aligned} \quad (11.115)$$

In order to determinate these functions we return to the Fokker–Planck equation (11.111) and derive differential equations for them which can be solved in analytic form.

For example, for the mean value  $\bar{P}(t)$  we multiply eqn (11.111) by  $P$  on both sides and integrate over the variables  $R$  and  $P$ . On the left-hand side we have

$$\iint dR dP P \frac{\partial}{\partial t} d(R, P; t) = \frac{d}{dt} \iint dR dP P d(R, P; t) = \frac{d}{dt} \bar{P}(t).$$

Integrating by parts on the right-hand side of eqn (11.111), we find that the term containing the derivative with respect to  $R$  vanishes, because all surface terms do so. The same is true for the term containing the second derivative with respect to  $P$ . Only the terms containing  $\partial/\partial P$  contribute,

$$\begin{aligned} & \iint dR dP P \left( -\tilde{F} \frac{\partial}{\partial P} + \frac{\gamma}{M} \frac{\partial}{\partial P} P \right) d(R, P; t) \\ &= \iint dR dP \left( \tilde{F} - \gamma \frac{P}{M} \right) d(R, P, t) = \tilde{F} - \gamma \frac{\bar{P}(t)}{M}. \end{aligned}$$

We therefore find

$$\frac{d\bar{P}}{dt} = \tilde{F} - \gamma \frac{\bar{P}}{M}. \quad (11.116)$$

In a similar fashion one obtains

$$\frac{d\bar{R}}{dt} = \frac{\bar{P}}{M}. \quad (11.117)$$

These are the classical equations of motion for the mean values of the spatial coordinate  $R$  and the momentum  $P$ .

The diffusive properties of the system are determined by the variances. We obtain a differential equation for the variance  $\sigma_{PP}^2$  in the momentum by multiplying the Fokker–Planck equation (11.111) on both sides by the factor  $(P - \bar{P})^2$  and observing that again the surface terms vanish after integration by parts. On the left-hand side we have

$$\iint dR dP (P - \bar{P})^2 \frac{\partial}{\partial t} d(R, P; t) = \frac{d}{dt} \sigma_{PP}^2, \quad (11.118)$$

and on the right-hand side,

$$\begin{aligned} & \iint dR dP (P - \bar{P})^2 \left( -\frac{P}{M} \frac{\partial}{\partial R} - \tilde{F} \frac{\gamma}{M} \frac{\partial}{\partial P} + \frac{\gamma}{M} \frac{\partial}{\partial P} P + D \frac{\partial^2}{\partial P^2} \right) d(R, P; t) \\ &= -\frac{2\gamma}{M} \sigma_{PP}^2 + 2D. \end{aligned} \quad (11.119)$$

Therefore,

$$\frac{d}{dt} \sigma_{PP}^2 + \frac{2\gamma}{M} \sigma_{PP}^2 = 2D. \quad (11.120)$$

Analogously, we derive an equation for the covariance  $\sigma_{RP}^2$ ,

$$\frac{d}{dt} \sigma_{RP}^2 + \frac{\gamma}{M} \sigma_{RP}^2 = \frac{1}{M} \sigma_{PP}^2, \quad (11.121)$$

and for the variance  $\sigma_{RR}^2$ ,

$$\frac{d}{dt} \sigma_{RR}^2 = \frac{2}{M} \sigma_{RP}^2. \quad (11.122)$$

We solve eqn (11.116) with the initial conditions  $\bar{P}(0) = P_0$ , and eqns (11.120) to (11.122) with the initial conditions  $\sigma_{PP}^2(0) = \sigma_{RR}^2(0) = \sigma_{RP}^2(0) = 0$  for  $t = 0$ . Using the method of variation of the constant, we find

$$\begin{aligned} \bar{P}(t) &= \frac{M\tilde{F}}{\gamma} + \left( P_0 - \frac{M\tilde{F}}{\gamma} \right) e^{-\gamma t/M}, \\ \sigma_{PP}^2(t) &= \frac{MD}{\gamma} \left( 1 - e^{-2\gamma t/M} \right), \\ \sigma_{RR}^2(t) &= \frac{2D}{\gamma^2} t + \frac{DM}{\gamma^3} \left( 4e^{-\gamma t/M} - e^{-2\gamma t/M} - 3 \right). \end{aligned} \quad (11.123)$$

From these equations we obtain the limits

$$\sigma_{PP}^2(t) \rightarrow \begin{cases} 2Dt & \text{for } t \rightarrow 0, \\ MD/\gamma & \text{for } t \rightarrow \infty, \end{cases} \quad (11.124)$$

and analogously

$$\sigma_{RR}^2(t) \rightarrow \begin{cases} (4D/3M^2)t^3 & \text{for } t \rightarrow 0, \\ (2D/\gamma^2)t & \text{for } t \rightarrow \infty. \end{cases} \quad (11.125)$$

Thus the spread in momentum  $\sigma_{PP}^2$  initially increases linearly with time, and becomes constant for large times. In contrast to this, the spatial spread  $\sigma_{RR}^2$  initially increases more slowly, like the third power of time; however, for large times it becomes proportional to the time.

#### The Einstein relation

The Fokker–Planck equation (11.111) contains a diffusion coefficient  $D$  in the momentum  $P$ , but none in the coordinate  $R$ . Nevertheless, owing to the coupling between the two variables, there is diffusion also in the spatial coordinate  $R$  with a variance which at large times increases linearly with time. This type of behaviour was studied earlier in connection with the diffusion equation (11.94). Thus the coordinate  $R$  at large times appears to be governed by a diffusion equation (cf. also Becker 1964, §76)

$$\frac{\partial}{\partial t} d(R, t) = D_R^{\text{diff}} \frac{\partial^2}{\partial R^2} d(R, t) \quad (11.126)$$

with the variance (cf. eqn (11.98))

$$\sigma_{RR}^2 = 2D_R^{\text{diff}} t. \quad (11.127)$$

Comparison with eqn (11.125) yields for the asymptotic spatial diffusion constant  $D_R^{\text{diff}}$  the value

$$D_R^{\text{diff}} = \frac{D}{\gamma^2}, \quad (11.128)$$

although the actual spatial diffusion coefficient  $D_{RR}$  is equal to zero.

For Brownian motion in a medium in thermal equilibrium we have (cf. eqn (11.59))

$$D = D_{PP} = \gamma k_B T. \quad (11.129)$$

The last two relations yield

$$D_R^{\text{diff}} = \frac{k_B T}{\gamma}. \quad (11.130)$$

This is the famous *Einstein relation* (cf. Einstein 1905) which states that the spatial diffusion constant  $D_R^{\text{diff}}$  is proportional to the inverse of the friction constant  $\gamma$ . In Section 11.3.5 we obtained the relation (11.129) in more general form as the fluctuation-dissipation theorem (cf. eqn (11.59)). We mentioned there that it is sometimes also called ‘Einstein relation’, but it should not be confused with the original Einstein relation (11.130).

## 11.5 Methods of solving for the distribution function

The Fokker–Planck equation (11.90) is a partial differential equation in the time  $t$  and the set of variables  $x$ . In applications to deep-inelastic collisions these variables are generally the radial coordinate, the radial momentum, the orbital angular momentum and the conjugate angle, charges, masses, deformation degrees of freedom, and others. For so many variables it is hopeless to attempt a direct numerical solution, for example, by using grid methods.

A widely used approximate way for solving Fokker–Planck equations in many dimensions is the *Gaussian approximation*, where the solution is sought in a multi-dimensional Gaussian form. The positions and widths of this Gaussian in the different variables are calculated from equations for the first and second moments, as has been done in Section 11.4. The method takes explicit account only of these two moments; it is therefore also called the ‘moment expansion method’. It is exact if the diffusion coefficients are constant and the drift terms are at most linear in the dynamical variables, as in the second example of Section 11.4.4. However, this is not generally the case in actual physical situations. In order to make use of a Gaussian ansatz one linearizes the drift terms as far as the fluctuations are concerned. One speaks in this case of the ‘quasi-linear approximation’.

Another method of solving the Fokker–Planck equation is based on the observation that we have introduced it as the equation which determines the distribution function of random variables satisfying Langevin equations. Therefore, instead of finding the distribution function as a solution of the Fokker–Planck partial differential equation, it can also be determined directly by *computer simulation* of the random process described by the corresponding stochastic Langevin equations. In this method a large number of sample trajectories are produced by solving the Langevin equations with computer-generated random Langevin forces. By way of this ‘Monte Carlo sampling’ of the trajectories the distribution function of the dynamical variables can be built up for all times. The method is exact within the statistical error, which depends on the number of trajectories one includes in the calculation. It provides a practicable calculational procedure also in multidimensional cases.

### 11.5.1 The Gaussian solution of the Fokker–Planck equation

The Gaussian approach is suggested by the results of the preceding section, where it was found that the solution has a Gaussian form if the coefficients of the Fokker–Planck equation are constant (cf. eqn (11.93)), or if the drift coefficient is linear (cf. eqn (11.106), or eqn (11.111) for the two-dimensional case). One thus makes the following multidimensional Gaussian *ansatz* for the solution of the general Fokker–Planck equation (11.90) with non-linear coefficients,

$$d(x; t) = A \exp \left( -\frac{1}{2} \sum_{i,j=1}^N [\sigma^2(t)]_{ij}^{-1} [x_i - \bar{x}_i(t)][x_j - \bar{x}_j(t)] \right), \quad (11.131)$$

where  $N$  is the number of variables, and

$$A = \frac{1}{\sqrt{(2\pi)^N \det(\sigma_{ij}^2)}}. \quad (11.132)$$

The function (11.131) depends on the time-dependent parameters  $\bar{x}_i(t)$  and  $[\sigma^2(t)]_{ij}^{-1}$ ,  $i, j = 1, \dots, N$ . These have the following meaning. The parameter  $\bar{x}_i$  is the mean value of the variable  $x_i$ , which is given by the first moment

$$\bar{x}_i(t) = \int dx x_i d(x, t), \quad (11.133)$$

where  $dx$  denotes the integration over the set of all variables  $x$ , i.e. over all phase space. The quantity  $[\sigma^2(t)]_{ij}^{-1}$  is the inverse of the variance matrix  $\sigma_{ij}^2(t)$  which is defined as

$$\sigma_{ij}^2(t) = \int dx [x_i - \bar{x}_i(t)][x_j - \bar{x}_j(t)] d(x; t). \quad (11.134)$$

Equations (11.133) and (11.134) are proved by substituting the density function (11.131) on the right-hand side and making an appropriate transformation of the variables of integration.

The mean values  $\bar{x}_i(t)$  and the variances  $\sigma_{ij}^2(t)$  are (so far) unknown parameters in the Gaussian distribution function  $d(x_i; t)$  of eqn (11.131). Equations for these quantities can be derived from the Fokker–Planck equation (11.90) in the same manner as in Section 11.4.4.

The present approach is similar to that in the two-dimensional case with constant coefficients (cf. eqns (11.111) and (11.113)). However, there the Gaussian form was exact, and the mean values and variances satisfied exact equations, whereas here the solution is only approximate, and the equations for the mean values and variances cannot be written down in closed form but must be truncated by linearization.

We illustrate the method by the example of a deep-inelastic collision. Consider the collision of two heavy ions under the influence of a Coulomb-plus-nuclear potential  $V(r)$  and an additional centrifugal potential, giving rise to a conservative force  $F(r) = -dV(r)/dr + L^2/\mu r^3$ . In addition, the heavy ions are subject to frictional forces in the radial and tangential directions with friction form factors  $K_r(r)$  and  $K_\phi(r)$ , which in turn give rise to diffusion coefficients  $D_r(r) = k_B T K_r(r)$  and  $D_\phi(r) = k_B T K_\phi(r)$  (here the fluctuation-dissipation theorem (11.59) has been applied). The physical content of the model will be discussed in more detail in Section 12.2.1.

The dynamical variables are  $x = r, p_r, L$ , and  $\phi$  (relative distance, radial momentum, orbital angular momentum perpendicular to the scattering plane, and conjugate angle), and the Fokker–Planck equation reads

$$\begin{aligned} \frac{\partial}{\partial t} d(r, p_r, \phi, L; t) = & - \left[ \frac{p_r}{\mu} \frac{\partial}{\partial r} + \frac{L}{\mu r^2} \frac{\partial}{\partial \phi} \right. \\ & + \left( -\frac{dV(r)}{dr} + \frac{L^2}{\mu r^3} \right) \frac{\partial}{\partial p_r} + \frac{\partial}{\partial p_r} \frac{p_r}{\mu} K_r(r) + D_r(r) \frac{\partial^2}{\partial p_r^2} \\ & \left. + \frac{\partial}{\partial L} K_\phi(r) \frac{L}{\mu} + D_\phi(r) r^2 \frac{\partial^2}{\partial L^2} \right] d(r, p_r, \phi, L; t). \end{aligned} \quad (11.135)$$

The equations for the mean values and variances are obtained by the same methods as in Section 11.4.4 (making use of integration by parts and the vanishing of the surface terms). We find, for example, for the variable  $\bar{p}(t)$  (cf. eqn (11.116)),

$$\begin{aligned} \frac{d}{dt}\bar{p}_r &= \int dr dp_r d\phi dL p_r \frac{\partial}{\partial t} d(r, p_r, \phi, L; t) \\ &= \int dr dp_r d\phi dL p_r \left[ \left( \frac{dV(r)}{dr} - \frac{L^2}{\mu r^3} \right) \frac{\partial}{\partial p_r} + \frac{\partial}{\partial p_r} \frac{p_r}{\mu} K_r(r) \right] d(r, p_r, \phi, L; t) \\ &= -\frac{\overline{dV(r)}}{dr} + \frac{\overline{L^2}}{\mu r^3} - \frac{\overline{p_r}}{\mu} K_r(r). \end{aligned} \quad (11.136)$$

This equation for the mean value  $\bar{p}_r$  (the first moment in the variable  $p_r$ ) contains mean values of the nonlinear and multidimensional functions  $dV(r)/dr$ ,  $L^2/r^3$  and  $p_r K_r(r)$ . The situation is similar for the other dynamical equations derived from the Fokker–Planck equation (11.135). Thus they do not form a closed system of equations. We are forced to introduce a further approximation, which consists in replacing the mean values of the functions of the dynamical variables with functions of the mean values of these variables,

$$\overline{G(x)} \approx G(\bar{x}). \quad (11.137)$$

This amounts to assuming that the functions in question do not fluctuate appreciably, or that in the expansion

$$\begin{aligned} \overline{G(x)} &= G(\bar{x}) + G'(\bar{x})\overline{(x - \bar{x})} + \frac{1}{2}G''(\bar{x})\overline{(x - \bar{x})^2} + \dots \\ &= G(\bar{x}) + \frac{1}{2}G''(\bar{x})\sigma_x^2 + \dots \end{aligned} \quad (11.138)$$

all terms on the right-hand side but the first can be neglected. This approximation is called the *quasi-linear approximation*. It is exact for linear functions.

Applying the quasi-linear approximation to eqn (11.136) and to the equations for the other dynamical variables as well, we arrive at equations which are identical with the classical equations of motion involving conservative and friction forces (cf. Gross and Kalinowski 1978),

$$\begin{aligned} \dot{\bar{r}} &= \frac{\bar{p}_r}{\mu}, \\ \dot{\bar{p}}_r &= -\frac{dV(\bar{r})}{d\bar{r}} + \frac{\bar{L}^2}{\mu\bar{r}^3} - \frac{K_r(\bar{r})}{\mu} \bar{p}_r, \\ \dot{\bar{\phi}} &= \frac{\bar{L}}{\mu\bar{r}^2}, \\ \dot{\bar{L}} &= -\frac{K_\phi(\bar{r})}{\mu} \bar{L}. \end{aligned} \quad (11.139)$$

The equations for the variances are derived in a similar way. We write down only those which we need to determine the angle-differential cross section,

$$\begin{aligned} \frac{d}{dt}\sigma_{\phi\phi}^2 &= \frac{2}{\mu\bar{r}^2}\sigma_{\phi L}^2, \\ \frac{d}{dt}\sigma_{\phi L}^2 &= \frac{\sigma_{LL}^2}{\mu\bar{r}^2} - \sigma_{\phi L}^2 \frac{K_\phi(\bar{r})}{\mu}, \\ \frac{d}{dt}\sigma_{LL}^2 &= -2\sigma_{LL}^2 \frac{K_\phi(\bar{r})}{\mu} + 2D_\phi(\bar{r})\bar{r}^2. \end{aligned} \quad (11.140)$$

The fact that the equations for the mean values (11.139) are decoupled from those for the variances implies that regardless of the presence of fluctuations, the usual classical equations of motion can be used for the description of the deep-inelastic collisions; their solutions are to be interpreted as the mean values of the dynamical variables.

The initial condition for the solution  $d(r, p_r, \phi, L; t)$  is applied outside the region of interaction at a time  $t_0$ . Here the dynamical variables have prescribed values  $r_0, p_{r0}, \phi_0$ , and  $L_0$ , so that the distribution function has the form

$$d(r, p_r, \phi, L; t_0) = \delta(r - r_0)\delta(p_r - p_{r0})\delta(\phi - \phi_0)\delta(L - L_0). \quad (11.141)$$

If there were no diffusion terms, the solution of the Fokker–Planck equation would be, for all times  $t$ ,

$$d(r, p_r, \phi, L; t) = \delta(r - \bar{r}(t))\delta(p_r - \bar{p}_r(t))\delta(\phi - \bar{\phi}(t))\delta(L - \bar{L}(t)), \quad (11.142)$$

where the functions  $\bar{r}(t)$ , etc. are the solutions of the classical equations of motion (11.139) (this can be verified by direct substitution in the Fokker–Planck equation (11.135) with the coefficients  $D$  set equal to zero).

The distribution function (11.142) describes classical motion along a trajectory. If the diffusion terms are taken into account as well, this trajectory is ‘smeared out’ into a distribution of trajectories described by the Gaussian distribution function (11.131). The mean values and variances appearing in this function are determined with the help of the ordinary differential equations (11.139) and (11.140). These have to be supplemented with the initial conditions  $\bar{r}(t_0) = r_0 = R$  (outside the nuclear range),  $\bar{L}(t_0) = L_0 = bkh$ , etc. and  $\sigma_{ij}^2(t_0) = 0$ . Substituting the solutions for the mean values and the variances for each value of  $b$  in expression (11.131), one arrives at the four-dimensional time-dependent distribution function  $d_b(r, p_r, \phi, L; t)$  as a function of the impact parameter  $b$ .

#### *The differential cross section for DIC*

From the distribution functions  $d_b(r, p_r, \phi, L; t)$  one can derive expressions for the DIC cross sections by going to the limit  $t \rightarrow \infty$ . Here we consider only the angle-differential cross section. It is obtained by integrating the distribution function over the variables  $r, p_r$ , and  $L$ . This results in a distribution for the angle  $\phi$  with mean value  $\bar{\phi}(\infty)$ , which is equivalent to a distribution of the deflection angle  $\theta$  with mean value  $\bar{\theta} = \Theta_b$ , defined for each impact parameter  $b$ . The quantity  $\Theta_b$  as a function of  $b$  is the deflection function associated with the mean trajectory. Writing  $\sigma_b^2$  for the variance  $\sigma_{\theta\theta}^2$ , we obtain

$$d_b(\theta) = \frac{1}{\sqrt{2\pi\sigma_b^2}} \exp\left(-\frac{(\theta - \Theta_b)^2}{2\sigma_b^2}\right). \quad (11.143)$$

Finally, the differential cross section for DIC is found by integrating over the impact parameter from the fusion value  $b_F$  to the value  $b_{\text{DIC}}$ , which separates the DIC from quasi-elastic scattering (cf. eqn (11.7)),

$$\left(\frac{d\sigma}{d\theta}\right)_{\text{DIC}} = 2\pi \int_{b_F}^{b_{\text{DIC}}} b db d_b(\theta). \quad (11.144)$$

If the diffusive effects vanish, i.e. if  $\sigma_b^2 = 0$ , the distribution function (11.143) reduces to a  $\delta$ -function, and eqn (11.144) reverts to the classical cross section (2.25),

$$\left(\frac{d\sigma}{d\theta}\right)_{\text{DIC}} = 2\pi \int_{b_F}^{b_{\text{DIC}}} b db \delta(\theta - \Theta_b) = 2\pi \sum_i \frac{b_i}{|d\Theta_b/db|_i}, \quad (11.145)$$

where  $\{b_i\}$  is the set of solutions (in the range  $b_F < b < b_{\text{DIC}}$ ) of the equation  $\theta - \Theta_b = 0$  for a given angle  $\theta$ . Here we have used the formula

$$\delta(f(x)) = \sum_i (|df(x)/dx|_i)^{-1} \delta(x - x_i),$$

where the parameters  $x_i$  are the zeros of the function  $f(x)$ ,  $f(x_i) = 0$ . We have written the cross section in terms of the deflection angle instead of the scattering angle. The relation between these two angles is given in eqn (2.11).

We postpone the discussion of multiple differential cross sections and their comparison with actual heavy-ion collision experiments until Section 12.3.1 where we generalize the present model to include deformation modes and charge and mass transfer. Before doing so we discuss the method of computer simulation in the next section.

### 11.5.2 Computer simulation of the Langevin process

If the drift terms in the Fokker–Planck equation are strongly nonlinear the Fokker–Planck solution is not of Gaussian form, and the quasi-linear approximation breaks down. An alternative method of solution is to go back to the Langevin equations themselves and to solve them as stochastic differential equations by computer simulation (cf. Risken 1989, Section 3.6; Honerkamp 1990). The distribution function for the dynamical variables is then obtained by *Monte Carlo sampling* of the Langevin trajectories.

We illustrate this method by a simple example which is one-dimensional in the variable  $x$ , and in which the accuracy of the procedure can be checked against the results of a direct numerical solution of the Fokker–Planck equation on a grid.

The example is a model of mass transfer for the system  $^{238}\text{U} + ^{238}\text{U}$  (cf. Grossmann 1980), described by the Fokker–Planck equation

$$\frac{\partial}{\partial t} d(x; t) = \left( -\frac{\partial}{\partial x} v(x) + D \frac{\partial^2}{\partial x^2} \right) d(x; t) \quad (11.146)$$

in the dimensionless variables for the time,  $t$ , and the mass,  $x$ . The initial condition is  $d(x, 0) = \delta(x)$ .

The drift coefficient  $v(x)$  is nonlinear owing to shell effects in the underlying driving potential which, in contrast to the second example of Section 11.4.4, are taken into account here. We use as mass variable the asymmetry parameter  $x = (A_1 - 238)/30$  (here  $A_1$  is the mass number of the projectile which changes during the transfer process;

the normalization 1/30 has been introduced so that  $x = -1$  at shell closure  $A_1 = 208$ ) in terms of which the drift term is given by

$$v(x) = \frac{d\Phi(x)}{dx}, \quad (11.147)$$

where the function  $\Phi(x)$  represents the driving potential parametrized as

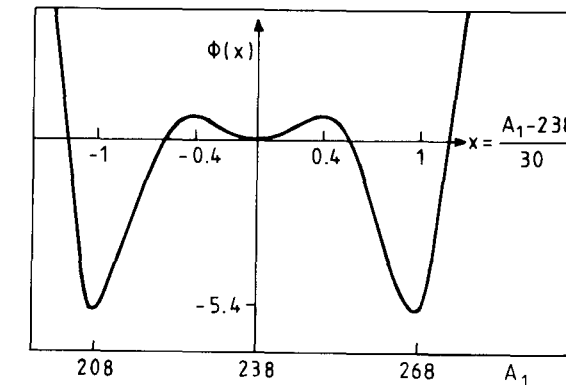


**Figure 11.9** The driving potential  $\Phi(x)$  for mass transfer as function of the mass parameter  $x = (A_1 - 238)/30$ .

$$\Phi(x) = 10x^2 - \frac{145}{4}x^4 + \frac{125}{6}x^6 \quad (11.148)$$

(cf. Fig. 11.9). The minima in this potential are caused by the shell closure in the nucleus  $^{208}\text{Pb}$ .

The diffusion coefficient is assumed to be constant and takes the value  $D = \frac{1}{2}$  if the dimensionless time  $t$  is connected with the physical interaction time  $\tau_{\text{int}}$  via  $t = (2\tilde{D}/30^2)\tau_{\text{int}}$ , where  $\tilde{D} = 7.5 \times 10^{-22} \text{ s}^{-1}$  is the physical diffusion coefficient. The physical solution of eqn (11.146) is found from  $d(x, t)$  by going over to the physical parameters,  $d(x, t) = d(A_1, \tau_{\text{int}})$ .

The Fokker–Planck equation (11.146) has been solved directly on a grid (cf. Brosa 1980), and also by Fröbrich and Xu (1988), who use the program package for partial differential equations of Raith *et al.* (1982). The resulting solution  $d(A_1, \tau_{\text{int}})$  is shown in Fig. 11.10 for the three interaction times  $\tau_{\text{int}} = 0.3, 1.2$ , and  $2.4 \times 10^{-21} \text{ s}$ .

We now turn to the solution via computer simulation of the Langevin equation associated with eqn (11.146), which according to Section 11.4.2, is given by

$$\frac{dx}{dt} = v(x) + \sqrt{D} \Gamma(t). \quad (11.149)$$

In its discretized form it reads (cf. eqn (11.75))

$$x_{n+1} = x_n + v(x_n) \tau + \sqrt{D} \sqrt{\tau} w(t_n). \quad (11.150)$$

It has the form of a recursion relation in which at each time step one inserts a random number  $w(t_n) = w$  taken from a Gaussian distribution with mean value zero and variance equal to 2.

#### Generation of the random number $w$

Random number generators usually produce *uniformly distributed* random numbers  $r$  in the range  $0 \leq r \leq 1$ . One can generate Gaussian-distributed random numbers  $w$  from a set of uniformly distributed random numbers  $\{r_v\}$  by defining (cf. Risken 1989, Section 3.6)

$$w = \sqrt{\frac{24}{M}} \sum_{v=1}^M (r_v - \frac{1}{2}), \quad (11.151)$$

where an appropriate value for  $M$  is  $M = 10$ . The random numbers  $w$  have mean value zero. By virtue of the central-limit theorem (cf. Reif 1965, Chapter 1), the random numbers  $w$ , being sums of random numbers, are Gaussian-distributed with mean value zero. Their distribution has a variance equal to 2,

$$\begin{aligned} \langle w^2 \rangle &= \frac{24}{M} \sum_{v=1}^M \sum_{\mu=1}^M \langle (r_v - \frac{1}{2})(r_\mu - \frac{1}{2}) \rangle \\ &= \frac{24}{M} \sum_{v=1}^M \langle (r_v - \frac{1}{2})^2 \rangle \approx \frac{24}{M} M \int_{-1/2}^{1/2} dx x^2 = 2. \end{aligned} \quad (11.152)$$

Another method of generating a Gaussian distribution of random numbers is to use the fact that a distribution  $p_1(r)$  of a set of random variables  $r$  in an interval  $a_1 \leq r \leq b_1$  is transformed into a distribution  $p_2(w)$  of another set of random variables  $w$  in the interval  $a_2 \leq w \leq b_2$  if in these regions the two variables are related by the equation

$$p_1(r)dr = p_2(w)dw. \quad (11.153)$$

With the uniform distribution  $p_1(r) = 1$  in the interval  $0 \leq r \leq 1$  we obtain a distribution  $p_2(w)$  for  $w$  in another interval  $a \leq w \leq b$  by solving  $dr/dw = p_2(w)$  for  $w$ , which yields  $w(r)$  as the inverse of

$$r = r(w) = \int_a^w p_2(w')dw'. \quad (11.154)$$

Choosing for  $p_2(w)$  a normalized Gaussian function, we obtain

$$r(w) = \frac{1}{\sqrt{2\pi}} \int_{-\infty}^w e^{-t^2/2} dt, \quad (11.155)$$

whose inverse produces the Gaussian-distributed numbers  $w$  in the interval  $-\infty < w < \infty$  from the uniformly distributed numbers  $r$  in the interval  $0 \leq r \leq 1$ .

#### The solution of the Langevin equations

With the random number  $w(t_n)$  provided by the random number generator, the difference equation (11.150) is used to calculate the value  $x = x_{n+1}$  a time step  $\tau$  away from the initial time  $t_n$  where the variable  $x$  had the value  $x_n$ . Choosing a new random number

$w(t_{n+1})$  at the time  $t_n + \tau$ , this process is repeated in order to determine the value of  $x$  in the next time step, and so on. The process is terminated when the interaction time  $\tau_{\text{int}}$  is reached. The distribution function  $d(x, \tau_{\text{int}})$  is obtained by counting the number of trajectories ending in particular bins of the variable  $x$ .

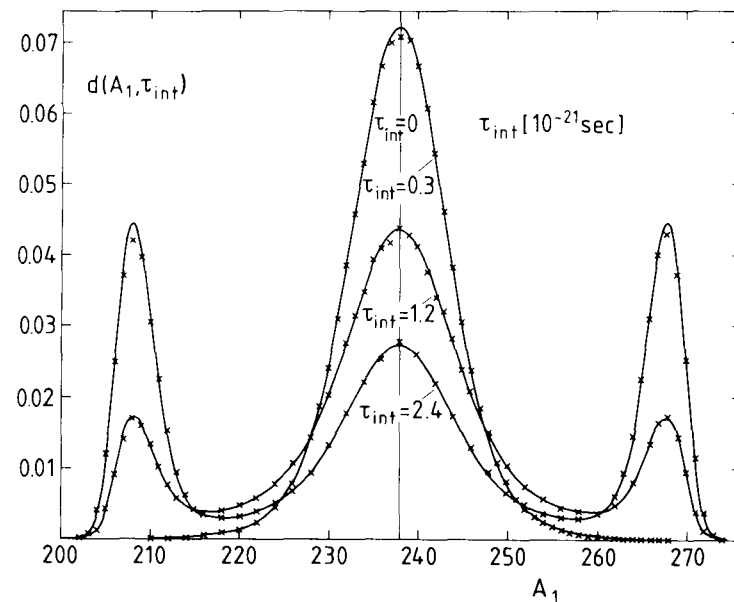


**Figure 11.10** The distribution function  $d(A_1, \tau_{\text{int}})$  for different interaction times  $\tau_{\text{int}}$  calculated by solving the Fokker–Planck equation on a grid (solid curves) and by computer simulation of the Langevin process (crosses).

The results of such a calculation (crosses) are superimposed on those of the Fokker–Planck calculation (curves) in Fig. 11.10 (cf. Fröbrich and Xu 1988). Here  $10^5$  trajectories have been sampled, ending in bins of size  $\Delta A_1 = 1$  in the range  $200 < A_1 < 280$ . The time step in the Langevin calculation was chosen as  $\tau = 10^{-4}$ . The relative error in each bin is of the order of  $1/\sqrt{n}$ , where  $n$  is the number of trajectories in the bin; one can improve the accuracy of the method by increasing the number of trajectories sampled.

The distribution function  $d(A_1, \tau_{\text{int}})$  calculated by computer simulation of the Langevin process agrees with the grid solution of the Fokker–Planck equation to the extent shown in Fig. 11.10. It is clearly not of Gaussian form, and can therefore not be obtained in the Gaussian approximation. As time develops, a bifurcation sets in, and for large times two pronounced peaks appear at the positions of the minima of the driving potential.

Whereas in this simple one-dimensional example it is a matter of taste which method of calculation one prefers, the situation is different in the multidimensional case. Here the Monte Carlo sampling of Langevin trajectories is at present the only feasible method.

◇ Higher-order algorithms for solving the Langevin equations have been developed by Mil'shtein (1974), Abe *et al.* (1986), Honerkamp (1990), and Marten and Fröbrich (1992), but the experience from the present example shows that one does not necessarily have any profit from going to higher-order because the gain in computing time due to the larger time steps is less than the time needed for the calculation of the additional terms which occur in the higher-order equations. ◇

## 11.6 Notes and references

Deep-inelastic collisions were first identified by Kaufmann and Wolfgang (1959), but their importance as a new kind of reaction came to be recognized only after the work of Galin *et al.* (1969) and of Volkov and collaborators (cf. Artukh *et al.* 1973). Reviews of the extensive experimental material and theoretical interpretations can be found in Huizenga and Schröder (1984) and Gobbi and Nörenberg (1980).

Classical trajectories with frictional forces have been introduced for the description of deep-inelastic heavy-ion scattering by Gross and collaborators (cf. Gross *et al.* 1973), Tsang (1974), and Bondorf *et al.* (1974). The classical friction model discussed in the present chapter has as the starting point the paper of Gross and Kalinowski (1978). The treatment of the fluctuations follows the work of Fröbrich and collaborators (for recent reviews cf. Fröbrich 1991, 1992). Within the scope of this book it is not possible to discuss the attempts at a more fundamental, microscopic description of the deep-inelastic collisions, or to describe in detail alternative phenomenological approaches. However, we cite some of the pertinent literature. Rather than trying to be complete we quote selected papers in which further references can be found.

For later developments of the approach of Gross see Pal and Gross (1988). Krappe (1990) reviews calculations of the friction force using perturbation theory, and also discusses other models.

The *proximity theory* of friction (cf. Blocki *et al.* 1978) has enjoyed considerable popularity. Here friction in the entrance channel is explained by particle transfer through a window between the colliding nuclei (window friction, cf. Randrup 1979); for compact configurations it is the collisions of the nucleons with the nuclear walls which cause the friction (wall friction). For a transparent description of this model see Swiatecki (1981). A review and extensive applications of the proximity model are given by Feldmeier (1987).

We further mention the model by Broglia *et al.* (1981), where the coupling of damped collective states to the relative motion is considered as an important mechanism for the energy loss.

Of the microscopic theories of deep-inelastic collisions using a ‘first principles’ approach, we cite the following.

Weidenmüller and co-workers base their treatment on a *random matrix hypothesis* for the interaction between the collective and intrinsic excitations, and derive and solve (within the quasi-linear approximation) a multidimensional Fokker–Planck equation with microscopically determined transport coefficients. A review of this and other theoretical models is given by Weidenmüller (1980).

## 11.6 Notes and references

Hofmann and Siemens (1977) use the *linear response theory*, in which the statistical fluctuations play an important part. For later developments see, for example, Hofmann *et al.* (1989), Yamaji *et al.* (1988), and Hofmann (1992). In these papers temperature-dependent transport coefficients are derived, and modifications of the Einstein relation are discussed.

Nörenberg (1984) introduces the concept of *diabatic dissipative dynamics*. Here the diabatic coupling between the collective and intrinsic degrees of freedom induces a non-Markovian friction force. The coherence of the single-particle motion in the time-dependent mean field is destroyed by the two-body collisions. This theory has been applied, for example, for describing structure effects in the fusion of heavy ions (cf. Berdichevsky *et al.* 1989) and recently to the emission of high energy  $\delta$ -electrons in coincidence with DIC (cf. Rhein *et al.* 1994).

A different line of approach is taken by the *time-dependent Hartree–Fock theory* (TDHF), in which self-consistent equations for the mean field are solved (cf. Davies *et al.* 1985).

The cross sections of deep-inelastic collisions have also been interpreted as *inclusive* cross sections. The appropriate formalism for this approach is the *influence functional* formalism of Feynman and Vernon (1963), which has been applied to DIC by Möhring and Smilansky (1980) and Brink *et al.* (1979). This method can be employed to describe tunnelling processes accompanied by friction (for the decay of a metastable state cf. Caldeira and Leggett 1983; for the scattering situation cf. Fröbrich *et al.* 1990).

### References

- Abe, Y., Gregoire, C. and Delagrange, H. (1986). *J. de Physique* **C4** **47** 329.
- Artukh, A. G., Gridnev, G. F., Mikheev, V. L., Volkov, V. V. and Wilczynski, J. (1973). *Nucl. Phys.* **A215** 91.
- Becker, R. (1964). *Theorie der Wärme*, Springer, Berlin.
- Berdichevsky, D., Lukasiak, A., Nörenberg, W. and Rozmeij, P. (1989). *Nucl. Phys.* **A499** 609.
- Bondorf, J. P., Sobel, M. I. and Sperber, D. (1974). *Phys. Rep.* **C15** 83.
- Broglia, R. A., Dasso, C. H. and Winther, A. (1981). *Proc. int. school of physics ‘Enrico Fermi’, Varenna Course 1979*, North-Holland, Amsterdam, p. 327.
- Blocki, H., Boneh, Y., Nix, J., Randrup, J., Robel, M., Sierk, A. J. and Swiatecki, W. J. (1978). *Ann. Phys. (N.Y.)* **113** 330.
- Brink, D. M., Neto, J. and Weidenmüller, H. A. (1979). *Phys. Lett.* **B80** 170.
- Brosa, U. (1980). *Z. Physik* **A298** 77.
- Caldeira, A. O. and Leggett, A. J. (1983). *Ann. Phys. (N.Y.)* **149** 374.
- Davies, K. T. R., Devi, K. R. S., Koonin, S. E. and Strayer, M. R. (1985). In *Heavy-ion science*, ed. Bromley, D. A., vol. 3, Plenum Press, New York and London, p. 3.
- Einstein, A. (1905). *Ann. Phys.* **17** 549.
- Einstein, A. (1906). *Ann. Phys.* **19** 371.
- Feldmeier, H. (1987). *Rep. Prog. Phys.* **50** 915.
- Feynman, R. P. and Vernon, F. L. (1963). *Ann. Phys. (N.Y.)* **24** 118.
- Fröbrich, P. (1991). *Springer Proc. in Phys.* **58** 93.

- Fröbrich, P. (1992). *Nucl. Phys.* **A545** 87c.
- Fröbrich, P. and Xu, S. Y. (1988). *Nucl. Phys.* **A477** 143.
- Fröbrich, P., Lipperheide, R. and Möhring, K. (1990). *Z. Physik* **B78** 325.
- Galin, J., Guerreau, D., Lefort, M., Peter, J., Tarrago, X. and Basile, R. (1969). *Phys. Rev.* **182** 1267.
- Gobbi, A. and Nörenberg, W. (1980). In *Heavy ion collisions*, ed. Bock, R., vol. 2, North-Holland, Amsterdam, p. 128.
- Gross, D. H. E. (1980). *Lecture notes in physics*, vol. 117, Springer, Berlin, p. 81.
- Gross, D. H. E. and Kalinowski, H. (1978). *Phys. Rep.* **45C** 175.
- Gross, D. H. E., Kalinowski, H. and Beck, R. (1973). *Proc. int. conf. nucl. phys.*, Munich, eds De Boer, J. and Mang, H. J., North-Holland, Amsterdam, p. 383.
- Grossmann, S. (1980). *Z. Physik* **A296** 251.
- Hildenbrand, K. D., Freiesleben, H., Gobbi, A., Lynen, U., Olmi, A., Sann, H. and Wu, E. C. (1983). *Nucl. Phys.* **A405** 179.
- Hofmann, H. (1992). *Proc. int. conf. on nucl. structure and nucl. reactions at low and intermediate energies*, Dubna, p. 292.
- Hofmann, H. and Siemens, P. (1977). *Nucl. Phys.* **A275** 464.
- Hofmann, H., Samhammer, R. and Ockenfuss, G. (1989). *Nucl. Phys.* **A496** 269.
- Honerkamp, J. (1990). *Stochastische Dynamische Systeme*, VCH Verlagsgesellschaft, Weinheim.
- Huizinga J. R. and Schröder, U. (1984). In *Heavy-ion science*, ed. Bromley, D. A., vol. 2, Plenum Press, New York, p. 115.
- Itô, K. (1944). *Proc. Imp. Acad., Tokyo* **20** 519.
- Kaufmann, R. and Wolfgang, R. (1959). *Phys. Rev. Lett.* **3** 232.
- Krappe, H. J. (1990). *Proc. int. school seminar on heavy ion physics*, ed. Ivashkevich, E. V., Dubna, p. 602.
- Kubo, R. (1957). *J. Phys. Soc. Japan*, **12** 570.
- Marten, J. and Fröbrich, P. (1992). *Nucl. Phys.* **A545** 854.
- Messiah, A. (1972). *Quantum mechanics*, vol. I, North-Holland, Amsterdam.
- Mil'shtein, G. N. (1974). *Theory Probab. Appl.* **XIX** 557.
- Möhring, K. and Smilansky, U. (1980). *Nucl. Phys.* **A338** 227.
- Nörenberg, W. (1974). *Phys. Lett.* **52B** 289.
- Nörenberg, W. (1984). *Nucl. Phys.* **428** 177c.
- Pal, S. and Gross, D. H. E. (1988). *Z. Physik* **A329** 349.
- Pawula, R. F. (1967). *Phys. Rev.* **162** 186.
- Raith, K., Glotz, G. and Schönauer, W. (1982). *Interner Bericht Nr. 22/82*, Rechenzentrum, Universität Karlsruhe.
- Randrup, J. (1979). *Nucl. Phys.* **A327** 490.
- Reif, F. (1965). *Fundamentals of statistical and thermal physics*, McGraw-Hill, New York.
- Rhein, M., Barth, R., Ditzel, E., Feldmeier, H., Kankeleit, E., Lips, V., Müntz, C., Nörenberg, W., Oeschler, H., Piechaczek, A., Polai, W. and Schall, I. (1994). *Phys. Rev.* **C49** 250.
- Risken, H. (1989). *The Fokker-Planck equation*, 2nd ed., Springer, Berlin.
- Stratonovich, R. L. (1967). *Topics in the theory of random noise*, vols. I and II, Gordon and Breach, New York.
- Swiatecki, W. J. (1981). *Phys. Scr.* **24** 113.
- Tsang, C. F. (1974). *Phys. Scr.* **10A** 90.
- Vandenbosch, R., Webb, M. P., Dyer, P., Puigh, R. J. and Weisfield, R. (1978). *Phys. Rev.* **C17** 1672.
- Van Kampen, N. G. (1981). *Stochastic processes in physics and chemistry*, North-Holland, Amsterdam.
- Weidenmüller, H. A. (1980). *Progr. Part. Nucl. Phys.* **3** 49.
- Wilczynski, J. (1973). *Phys. Lett.* **47B** 484.
- Wollersheim, H. J., Wilcke, W. W., Birkeland, J. R., Huizenga, J. R., Schröder, W. U., Freiesleben, H. and Hilscher, D. (1981). *Phys. Rev.* **C24** 2114.
- Yamaji, S., Hofmann, H. and Samhammer, R. (1988). *Nucl. Phys.* **A475** 487.

# 12

## ANALYSIS OF DEEP-INELASTIC COLLISIONS, FUSION, AND HEAVY-ION INDUCED FISSION

### 12.1 Introduction

In Chapter 11 we introduced friction and fluctuations in order to describe the dissipative processes occurring in deep-inelastic collisions. For the calculation of these effects we derived the Langevin and Fokker-Planck equations. We studied these equations for several simple examples and discussed general methods of solving them.

In the present chapter we proceed to a detailed analysis of data taken in experiments on deep-inelastic collisions, fusion above the barrier, and heavy-ion induced fission. For the specification of the dynamics of the DIC and fusion we make use of a particular phenomenological model, the *surface-friction model*. It allows us to give a comprehensive and coherent account of the subject. We restrict ourselves almost exclusively to this model which brings order into the profusion of experimental data and describes them fairly well. It is beyond the scope of this book to go into the details of alternative microscopic or phenomenological treatments. Relevant literature is quoted in the notes and references of this and the preceding chapter.

In Section 12.2 we begin with a discussion of the surface-friction model for *rigid spherical nuclei* moving along classical trajectories, in terms of which one can understand typical features of fusion and DIC, at least qualitatively. The application of this model to the description of experiments requires the friction to set in strongly at distances larger than the sum of the half-density radii of the colliding nuclei, i.e. in their surfaces; this explains the name of the model. Next, we take into account the *deformability* of the nuclei during the collision, which is essential for a quantitative description of the observed energy loss in DIC and its effect on fusion. The radial frictional force is assumed to be proportional to the time derivative of the distance between the surfaces of the colliding deformable nuclei along the line connecting their centres of mass.

The effect of *statistical fluctuations* will be considered in Section 12.3. We first discuss the Gaussian (quasi-linear) approximation for solving the Fokker-Planck equation of the surface-friction model in the analysis of DIC data, in particular, of angular distributions and charge transfer. We then turn to the computer simulation of the Langevin process, i.e. to the method of Monte Carlo sampling of Langevin trajectories. This procedure is more practicable and flexible than the former, and represents in fact the only feasible general method of treating dissipative processes involving many collective degrees of freedom. It allows one to describe DIC cross sections, the bifurcation into fusion and DIC close to the fusion barrier, spin distributions for fusion and DIC, as well

as the emission of  $\delta$ -electrons serving as an atomic clock for DIC. In all these processes statistical fluctuations play a significant role.

Section 12.4 is devoted to an analysis of *dynamical effects in the fission of hot nuclei*, i.e. fission of compound nuclei produced by fusion of heavy ions. This process is treated by a dynamical (Langevin) description combined with a statistical model. The motion along the fission path is governed by a temperature-dependent driving force which is determined by the entropy of the nucleus, and is assumed to be overdamped owing to strong friction. Pre-scission evaporation of light particles (neutrons, protons,  $\alpha$ -particles) and  $\gamma$ -radiation are taken into account. For an illustration, the results of a calculation of fission probabilities and pre-scission neutron multiplicities are presented and compared with experiment.

### 12.2 Classical trajectories in the surface-friction model

In this section we analyse the deep-inelastic collisions and fusion processes in terms of classical trajectories. We establish the form and strength of the conservative and frictional forces, write down the equations of motion and discuss their solution. First, we consider the motion of rigid nuclei, and then include the surface vibrations of deformable nuclei. This is followed by the analysis of actual experiments on DIC and fusion. It will be seen that the model of rigid nuclei does not provide a satisfactory description of the data, while the inclusion of dynamical deformations allows one to reproduce the main features of the measured cross sections quantitatively.

#### 12.2.1 Rigid nuclei

The simplest description of deep-inelastic collisions and fusion is afforded by a model of classical scattering with nuclear friction (cf., e.g. Gross and Kalinowski 1978). Here the equations of motion (2.3) for a two-particle system with reduced mass  $\mu$  are extended to include phenomenological frictional forces in the coordinates  $r$  and  $\phi$ . In the presence of such non-conservative forces the energy  $E$  and the angular momentum  $L$  are no longer constants of motion. Therefore the trajectories and the deflection function cannot be given in the form of closed integrals as in eqns (2.6) and (2.9). They must, instead, be obtained by solving Newton's equations of motion numerically. These equations are derived from the Lagrangian  $\mathcal{L}$  which governs the conservative part of the motion, and the Rayleigh dissipation function  $\mathcal{R}$  which determines the frictional effects.

#### *The Lagrangian*

The Lagrangian  $\mathcal{L}$  has the following form,

$$\mathcal{L} = \mathcal{L}(r, \phi, \dot{r}, \dot{\phi}) = \frac{\mu}{2} \dot{r}^2 + \frac{\mu}{2} r^2 \dot{\phi}^2 - V(r), \quad (12.1)$$

where the central potential  $V(r)$  consists of a Coulomb part  $V_C(r)$  and a nuclear part  $V_N(r)$ ,

$$V(r) = V_C(r) + V_N(r); \quad (12.2)$$

the variable  $r$  is the distance between the centres of mass of the colliding nuclei.

For the Coulomb interaction we use a point-Coulomb potential,

$$V_C(r) = \frac{Z_1 Z_2 e^2}{r}. \quad (12.3)$$

This potential correctly describes the Coulomb interaction between two collision partners whose surfaces overlap only slightly, which is the case for the nuclei moving along DIC trajectories in the surface-friction model.

The nuclear potential is calculated as a symmetrized single-folding potential,

$$V_N(r) = \frac{1}{2} \int d^3 r' V_P(|\mathbf{r} - \mathbf{r}'|) \rho_T(r') + \frac{1}{2} \int d^3 r' V_T(|\mathbf{r} - \mathbf{r}'|) \rho_P(r'), \quad (12.4)$$

where the empirical potential  $V_P$  for the scattering of a nucleon by the projectile nucleus P and the potential  $V_T$  for the scattering of a nucleon by the target nucleus T are folded with the empirical nucleon densities  $\rho_T$  of the target and  $\rho_P$  of the projectile, respectively. The nucleon–nucleus potentials are chosen to have the phenomenological Woods–Saxon form

$$V_i(r) = \frac{V_0}{1 + e^{(r - R_{Vi})/a_V}} \quad \text{with } i = P, T, \quad (12.5)$$

where  $R_{Vi} = 1.25 A_i^{1/3}$  fm ( $A_i$  is the number of nucleons in the projectile and the target,  $i = P, T$ ),  $V_0 = -50$  MeV, and  $a_V = 0.65$  fm are universal empirical parameters. The mass density is also assumed to be of Woods–Saxon shape,

$$\rho_i(r) = \frac{\rho_0}{1 + e^{(r - R_{\rho i})/a_\rho}} \quad \text{with } i = P, T, \quad (12.6)$$

where  $\rho_0 = 0.170$  fm $^{-3}$ ,  $R_{\rho i} = 1.12 A_i^{1/3} - 0.86 A_i^{-1/3}$  fm, and  $a_\rho = 0.54$  fm.

The potential (12.4) is calculated numerically from these nucleon–nucleus potentials and densities, and is then fitted by the expression

$$V_N(r) = - \sum_{n=1}^5 A_n (r - R)^{n-1} \ln \left[ 1 + \exp \left( - \frac{r - R}{a} \right) \right]. \quad (12.7)$$

The coefficients  $A_1, \dots, A_5$  depend on the number of nucleons in the collision partners P and T. The quantity  $R$  is the sum of the radii of projectile and target,  $R = r_0(A_P^{1/3} + A_T^{1/3})$ , and the radius parameter  $r_0$  and the surface thickness  $a$  have the values  $r_0 = 1.3$  fm and  $a = 0.61$  fm for all systems.

#### The Rayleigh dissipation function

The Rayleigh dissipation function  $\mathcal{R}$  is written as

$$\mathcal{R} = -\frac{1}{2} K_r(r) \dot{r}^2 - \frac{1}{2} K_\phi(r) r^2 \dot{\phi}^2, \quad (12.8)$$

where  $K_r(r)$  and  $K_\phi(r)$  are the radial and tangential friction form factors, respectively. The Rayleigh function gives rise to frictional forces in the dynamical variables which are proportional to the corresponding velocities.

Since friction acts in the region of nuclear interaction, the friction form factors  $K_r(r)$  and  $K_\phi(r)$  must vanish at large distances together with the nuclear potentials. In order to establish the shape of these form factors one must have recourse to a model.

Unfortunately, we cannot apply verbatim the microscopic model of Section 11.3.3 with the friction coefficient (11.32) which is proportional to the square of the coupling form factor derivative,  $\propto [f'(R)]^2$ , since it is based on a factorized interaction between relative motion and internal degrees of freedom. This assumption has been introduced for ease of argumentation, but it is not very realistic. A perturbation-theoretical derivation which does not make use of such a factorization (cf. Gross and Kalinowski 1978, Section 7.2), yields a frictional force proportional to the square of the conservative nuclear force  $\propto [V'_N(R)]^2$ . We therefore write

$$K_r(r) = K_r^0 \left( \frac{dV_N(r)}{dr} \right)^2, \quad K_\phi(r) = K_\phi^0 \left( \frac{dV_N(r)}{dr} \right)^2, \quad (12.9)$$

where  $K_r^0$  and  $K_\phi^0$  are the strength coefficients of the radial and tangential friction forces, respectively. By fitting these coefficients to experiment one obtains for them the *universal* values

$$K_r^0 = 4.0 \times 10^{-23} \text{ s MeV}^{-1}, \quad K_\phi^0 = 0.01 \times 10^{-23} \text{ s MeV}^{-1}. \quad (12.10)$$

#### The equations of motion

As long as the potential  $V(r)$  and the friction form factors  $K_r(r)$  and  $K_\phi(r)$  are central, as we assume here, the motion is confined to the scattering plane and can be described in terms of the two coordinates  $q_1 = r$  and  $q_2 = \phi$ . The equations of motion are given by the Euler–Lagrange equations

$$\frac{d}{dt} \frac{\partial \mathcal{L}}{\partial \dot{q}_i} - \frac{\partial \mathcal{L}}{\partial q_i} = \frac{\partial \mathcal{R}}{\partial \dot{q}_i} \quad \text{for } i = 1, 2. \quad (12.11)$$

They read explicitly

$$\begin{aligned} \mu \ddot{r} - \mu r \dot{\phi}^2 + \frac{dV(r)}{dr} + K_r(r) \dot{r} &= 0, \\ \frac{d}{dt} (\mu r^2 \dot{\phi}) + K_\phi(r) r^2 \dot{\phi} &= 0, \end{aligned} \quad (12.12)$$

where the dot denotes the derivative with respect to time,  $\dot{r} = dr/dt$ , etc. Introducing the radial momentum  $p_r = \mu \dot{r}$  and the orbital angular momentum perpendicular to the scattering plane  $L = \mu r^2 \dot{\phi}$  we arrive at the equations of motion in Hamiltonian form,

$$\begin{aligned} \dot{r} &= \frac{p_r}{\mu}, \\ \dot{p}_r &= -\frac{dV(r)}{dr} + \frac{L^2}{\mu r^3} - \frac{K_r(r)}{\mu} p_r, \\ \dot{\phi} &= \frac{L}{\mu r^2}, \\ \dot{L} &= -\frac{K_\phi(r)}{\mu} L. \end{aligned} \quad (12.13)$$

The second equation contains the radial friction force which causes the damping of the radial motion, whereas the last equation describes angular momentum dissipation, i.e.

the irreversible transfer of orbital angular momentum from the relative to the internal motion of the collision partners. The same equations (cf. eqn (11.139)) have been derived in Section 11.5.1 for the mean values of the dynamical variables using a Fokker–Planck equation.

Tangential and radial friction together generate an energy loss in the relative motion which is used to heat up the collision partners. In order to find an expression for this energy loss we consider the time derivative of the energy of relative motion,  $\dot{E} = \dot{T} + \dot{V}$ , where  $T = (p_r^2/2\mu) + (L^2/2\mu r^2)$  is the kinetic energy, and  $\dot{V} = (dV/dr)\dot{r}$ . We find

$$\begin{aligned}\dot{E} &= \frac{p_r}{\mu} \dot{p}_r - \frac{L^2}{\mu r^3} \dot{r} + \frac{L}{\mu r^2} \dot{\phi} + \frac{dV}{dr} \dot{r} \\ &= \frac{p_r}{\mu} \left( -\frac{dV}{dr} + \frac{L^2}{\mu r^3} - \frac{K_r}{\mu} p_r \right) - \frac{L^2}{\mu r^3} \frac{p_r}{\mu} - \frac{L^2}{\mu^2 r^2} K_\phi + \frac{dV}{dr} \frac{p_r}{\mu} \\ &= -K_r r^2 - K_\phi r^2 \dot{\phi}^2,\end{aligned}\quad (12.14)$$

where in the second and third lines we have made use of the equations of motion (12.13). Thus the energy loss along the trajectory is given by twice the Rayleigh dissipation function (12.8),

$$\dot{E} = 2\mathcal{R}. \quad (12.15)$$

#### The solution of the equations of motion

At a given incident energy  $E_i$  the equations of motion (12.13) and (12.14) are solved numerically for each impact parameter  $b$  or initial angular momentum  $L_i = \hbar l_i = \hbar b k_i = b\sqrt{2\mu E_i}$ . Since the potential  $V(r)$  contains a Coulomb tail, the trajectories asymptotically start and end as Rutherford trajectories (cf. Fig. 12.1). The numerical integration of eqns (12.13) is initiated at the time  $t_i$  at a position  $r_i$  outside the range of the nuclear forces, where the radial momentum  $p_r$  and the angle  $\phi$  have their Rutherford values. The initial conditions are, therefore,

$$\begin{aligned}r(t_i) &= r_i, \\ p_r(r_i) &= \sqrt{2\mu E_i(1 - 2\eta_i/k_i r_i) - \hbar^2 l_i^2/r_i^2}, \\ \phi(r_i) &= \phi_i^C(r_i) = \frac{\pi}{2} - \arcsin\left(\frac{\eta_i + l_i^2/k_i r_i}{\sqrt{\eta_i^2 + l_i^2}}\right), \\ l(r_i) &= l_i\end{aligned}\quad (12.16)$$

(cf. eqn (2.16); here the angle  $\phi$  is referred to the symmetry axis of the initial Rutherford hyperbola). The integration proceeds through the region of nuclear interaction and is terminated at a time  $t_f$  when a position  $r_f$  outside this region has been reached. At this point the energy has its final value  $E_f$ . The angle  $\phi$  has progressed by an amount  $\Delta\phi$  (cf. Fig. 12.1). In order to determine the deflection angle  $\Theta$  we add to  $\Delta\phi$  the initial and final Rutherford angles  $\Delta\phi_i^C$  and  $\Delta\phi_f^C$ , which are given by

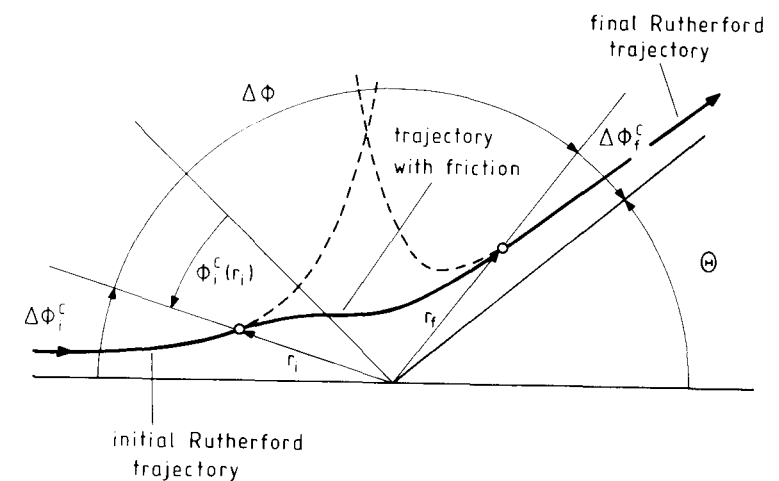


**Figure 12.1** Determination of the deflection angle  $\Theta$  for classical motion with friction. The two hyperbolas (dashed curves) represent the Rutherford trajectories along which the motion proceeds in the initial and final phases. The trajectory inside the region of nuclear interaction (from  $r_i$  to  $r_f$ ) is found by numerical integration.

$$\begin{aligned}\Delta\phi_i^C &= |\phi_i^C(\infty) - \phi_i^C(r_i)| \\ &= \left| \arcsin\left(\frac{\eta_i}{\sqrt{\eta_i^2 + l_i^2}}\right) - \arcsin\left(\frac{\eta_i + l_i^2/(k_i r_i)}{\sqrt{\eta_i^2 + l_i^2}}\right) \right|,\end{aligned}\quad (12.17)$$

and analogously for  $\Delta\phi_f^C$ . The deflection angle is then obtained as

$$\Theta = \pi - (\Delta\phi_i^C + \Delta\phi + \Delta\phi_f^C). \quad (12.18)$$

For given incident energy  $E_i$  the final energy  $E_f$  and the final angular momentum  $l_f$  depend on the initial angular momentum  $l_i$ , so that the deflection angle  $\Theta$  is itself a function of  $l_i$ . This function  $\Theta(l_i)$  is a deflection function in the same sense as the closed expression (2.9) for trajectories without friction, and therefore the cross section is given by formula (2.14), which reads, with  $b = l_i/k_i$ ,

$$\frac{d\sigma}{d\Omega} = \frac{l_i}{k_i^2 \sin \theta |d\Theta(l_i)/dl_i|}. \quad (12.19)$$

In addition to the angular distribution of the scattered particles one also finds for each initial angular momentum  $l_i$  the energy loss  $\Delta E = E_i - E_f$  and the angular-momentum loss  $\Delta L = \hbar\Delta\ell = \hbar(l_i - l_f)$  suffered along the trajectory deflected into the angle  $\Theta(l_i)$ .

For an illustration we consider the collision of  $^{40}\text{Ar}$  with  $^{232}\text{Th}$  at the energy  $E_i = 323$  MeV. Figure 12.2a shows the trajectory of the radial motion with initial angular

momentum  $l_i = 150$ . As the projectile approaches the effective potential barrier it loses energy, and therefore the trajectory bends down. At the same time the angular momentum decreases, so that the effective barrier is lowered as well; the final energy is  $E_f = 230$  MeV and the final angular momentum,  $l_f = 142$ . The deflection angle  $\Theta$  for this system, together with the energy loss  $\Delta E$  and angular momentum loss  $\Delta l$  as functions of the initial angular momentum  $l_i$ , are shown in Fig. 12.2b.

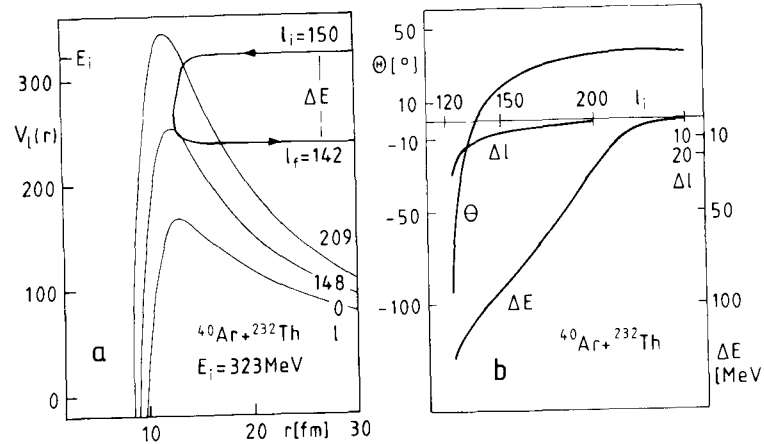


**Figure 12.2** Classical scattering with friction. (a) The trajectory of the radial motion for the system  $^{40}\text{Ar} + ^{232}\text{Th}$  with  $E_i = 323$  MeV and  $l_i = 150$ ; the effective potential  $V_l(r) = V(r) + \hbar^2 l(l+1)/2\mu r^2$  for the angular momenta  $l = 0, 148$ , and  $209$  is included in the figure. (b) Deflection angle  $\Theta$ , energy loss  $\Delta E$ , and angular momentum loss  $\Delta l$  as functions of the initial angular momentum  $l_i$ .

The experimental information on the scattering and on the energy loss is contained in the double differential cross sections  $d^2\sigma/dEd\theta$ , i.e. in the Wilczynski plots already shown in Section 11.2.2, which include the results of the present calculation. We postpone a detailed discussion of these cross sections until we have generalized the model by allowing the nuclei to deform dynamically.

### 12.2.2 Deformable nuclei

For a quantitative reproduction of the data it turns out to be necessary to extend the model of rigid nuclei by introducing dynamical deformations (cf., e.g. Gross *et al.* 1981). In the present treatment we follow Fröbrich *et al.* (1983) and Fröbrich (1984a) and consider only quadrupole vibrations of the colliding nuclei. We do not take explicit account of the formation of a neck between the touching nuclei, as it is done, for example, in the models of Swiatecki (1981) and Feldmeier (1987).

Figure 12.3 is a schematic drawing of the collision of two deformable nuclei in the centre-of-mass system. To the coordinates  $r$  and  $\phi$  of the relative motion we add the centre-of-mass system. To the coordinates  $r$  and  $\phi$  of the relative motion we add as dynamical variables the quadrupole deformation parameters  $a_i$  of the low-energy

surface-vibration modes  $i = P, T$  of projectile and target. For simplicity we restrict ourselves to a ‘nose-to-nose’ geometry of the colliding nuclei, i.e. we take the line connecting the centres of mass of the two colliding nuclei as the common symmetry axis for their deformation, and do not allow motion out of the scattering plane. It is then

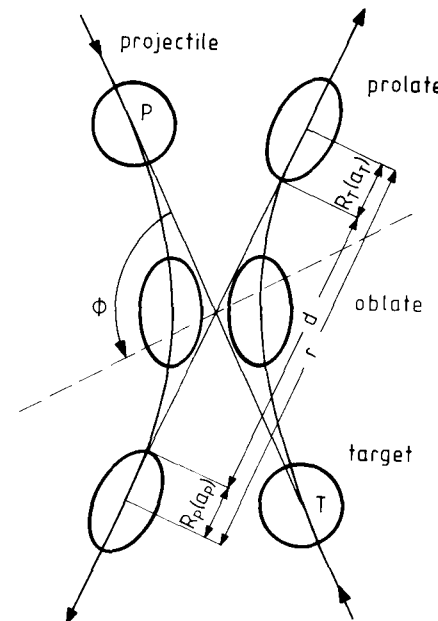


**Figure 12.3** Schematic drawing describing the collision of two deformable nuclei in the surface-friction model. The angle  $\phi$  is the relevant Euler angle describing the rotation of the projectile-target system (see text).

clear from the figure that in the transformation of the deformation parameters from the body-fixed to the space-fixed system (cf. eqn (8.45)) the relevant Euler angle is equal to the angular coordinate  $\phi$  describing the motion of the two nuclei in the centre-of-mass system. We assume again that the nuclear potential and the friction form factors depend only on the distance between the nuclear surfaces connecting the centres of mass of the nuclei.

The calculations show that the collision partners are deformed into oblate shapes in the approach phase, and into strongly prolate shapes as they separate. The oblate deformations at contact lead to enhanced dynamical barriers which hinder the fusion process, so that the fusion cross section is expected to be reduced in comparison with the case of rigid nuclei. The strongly prolate shapes in the exit channel, on the other hand, allow for enhanced energy losses, and the kinetic energy of the final nuclei can be reduced to values below the Coulomb-barrier energy of spherical nuclei. These features will turn out to be important for obtaining a quantitative agreement with the data (cf. Sections 12.2.3 and 12.2.4).

### The Lagrangian

The Lagrangian of the model has the form

$$\mathcal{L} = \frac{\mu}{2}\dot{r}^2 + \frac{\mu}{2}r^2\dot{\phi}^2 - V(r, \{a_i\}) + \mathcal{L}_{\text{vib}}. \quad (12.20)$$

Here

$$\mathcal{L}_{\text{vib}} = \sum_{i=\text{P,T}} \left( \frac{B_i}{2}\dot{a}_i^2 - \frac{C_i}{2}a_i^2 \right) \quad (12.21)$$

is the Lagrangian of the vibrational modes associated with the quadrupole-deformation variables  $a_{2\mu}^i = a_i \delta_{\mu 0}$  (cf. eqn (8.41)); the quantities  $B_i$  and  $C_i$  are the mass and stiffness parameters of projectile and target for quadrupole vibrations, which are taken from the liquid-drop model (cf. Preston and Bhaduri 1975, Section 9.2).

The expression (12.21) is the Lagrangian for quadrupole vibrations. For convenience we have written it in terms of the body-fixed deformation variables  $a_i$ , although its correct form would be in terms of the space-fixed variables  $\alpha_{2\mu}^i = D_{\mu 0}^2(0, \phi, 0)a_i$  (cf. eqns (8.45) and (8.90)). Thus we neglect the rotational energy  $\propto \dot{\phi}^2$  associated with the deformation modes (cf. Preston and Bhaduri 1975, Section 9.3) in comparison with the centrifugal potential of the relative motion.

The deformed potential  $V(r, \{a_i\})$  consists again of Coulomb and nuclear parts,

$$V(r, \{a_i\}) = V_C(r, \{a_i\}) + V_N(r, \{a_i\}). \quad (12.22)$$

The deformed Coulomb potential has the form

$$V_C(r, \{a_i\}) = \frac{Z_1 Z_2 e^2}{r} + \frac{3}{5} \frac{Z_1 Z_2 e^2}{r^3} \sum_{i=\text{P,T}} R_{0i}^2 a_i Y_{20}(0, 0), \quad (12.23)$$

where the monopole–quadrupole term (cf. eqn (8.65)) is written in the body-fixed system with nose-to-nose geometry.

The deformed nuclear potential is assumed to depend only on the distance between the nuclear surfaces along the line connecting the centres of mass of the nuclei (cf. Fig. 12.3). Instead of calculating a folding potential from deformed nucleon–nucleus potentials and nuclear densities in analogy to the procedure of Section 12.2.1, we determine the nuclear potential in a simpler fashion. We replace the argument  $r - R$  in the spherical potential (12.7) with the surface distance

$$d = d(\{a_i\}) = r - R_P(a_P) - R_T(a_T), \quad (12.24)$$

where

$$R_i(a_i) = R_{0i}[1 + a_i Y_{20}(0, 0)] \quad \text{with } i = \text{P, T} \quad (12.25)$$

are the radii of the deformed nuclei at their ‘noses’ (cf. eqn (8.41)); the quantities  $R_{0i}$  are the equivalent radii of the undeformed nuclei, and  $Y_{20}(0, 0) = \sqrt{5/4\pi}$ . In addition we introduce a factor which corrects for curvature effects in terms of the geometrical mean of the principal curvatures  $\kappa_{\text{P,T}}^{\parallel}$  and  $\kappa_{\text{P,T}}^{\perp}$  of the deformed projectile and target at contact (cf. Broglia *et al.* 1981),

$$G(\{a_i\}) = (R_{0P} + R_{0T}) \frac{1}{R_{0P} R_{0T} [(\kappa_{\text{P}}^{\parallel} + \kappa_{\text{T}}^{\parallel})(\kappa_{\text{P}}^{\perp} + \kappa_{\text{T}}^{\perp})]^{1/2}}. \quad (12.26)$$

For the shape (12.25) one obtains (cf. Fröbrich 1984a)

$$G = G(\{a_i\}) = (R_{0P} + R_{0T}) \left( \sum_{i=\text{P,T}} R_{0i} \frac{1 + 8a_i \sqrt{5/16\pi}}{(1 + 2a_i \sqrt{5/16\pi})^2} \right)^{-1}. \quad (12.27)$$

In generalization of formula (12.7) we therefore have for the deformed nuclear potential

$$V_N(r, \{a_i\}) = -G \sum_{n=1}^5 A_n d^{n-1} \ln \left[ 1 + \exp \left( -\frac{d}{a} \right) \right]. \quad (12.28)$$

### The Rayleigh dissipation function

We now turn to the frictional forces acting between the deformed nuclei. In the surface-friction model the radial frictional force is proportional to the velocity with which the nuclear surfaces move relative to one another. More precisely, the frictional force is assumed to be proportional to the time derivative of the distance  $d$  defined in eqn (12.24). Whereas for rigid spherical nuclei the distance between the surfaces of the nuclei is fixed by the distance between their centres of mass, this is not so in the case of deformed nuclei, where the surface distance depends also on the deformation variables.

We decompose the Rayleigh dissipation function into a sum of radial, tangential, and internal-vibrational terms,

$$\mathcal{R} = \mathcal{R}_r + \mathcal{R}_\phi + \mathcal{R}_{\text{vib}}. \quad (12.29)$$

The radial term is given by

$$\mathcal{R}_r = -\frac{1}{2} K_r d^2, \quad (12.30)$$

where the form factor  $K_r$  depends on the distance  $r$  between the centres of mass of the nuclei and on the deformation variables  $a_i$ ,

$$K_r = K_r(r, \{a_i\}). \quad (12.31)$$

We find, using eqns (12.24) and (12.25),

$$\begin{aligned} \mathcal{R}_r &= -\frac{1}{2} K_r \left( \dot{r} - \sum_{i=\text{P,T}} \frac{\partial R_i(a_i)}{\partial a_i} \dot{a}_i \right)^2 \\ &= -\frac{1}{2} K_r \left( \dot{r}^2 + \frac{5}{4\pi} \sum_{i,j=\text{P,T}} R_{0i} R_{0j} \dot{a}_i \dot{a}_j - 2\dot{r} \sqrt{\frac{5}{4\pi}} \sum_{i=\text{P,T}} R_{0i} \dot{a}_i \right). \end{aligned} \quad (12.32)$$

The radial part of the Rayleigh dissipation function contains diagonal terms for the damping of the radial motion and the vibrations, as well as non-diagonal terms. The latter describe the frictional coupling of the deformation variables to each other and to the relative motion.

The tangential term is assumed to be the same as for rigid nuclei,

$$\mathcal{R}_\phi = -\frac{1}{2} K_\phi r^2 \dot{\phi}^2, \quad (12.33)$$

where the form factor  $K_\phi$  again depends on the variables  $r$  and  $a_i$ ,

$$K_\phi = K_\phi(r, \{a_i\}). \quad (12.34)$$

Finally, we have introduced in the Rayleigh dissipation function a friction term

$$\mathcal{R}_{\text{vib}} = - \sum_{i=\text{P,T}} \frac{1}{2} K_i \dot{a}_i^2 \quad (12.35)$$

which accounts for the *internal* damping of the vibrations of the nuclei due to their coupling to more complicated excitation modes not included explicitly in the formalism. The presence of this term implies that the vibrations of the separated nuclei satisfy the damped-oscillator equation

$$B_i \ddot{a}_i + K_i \dot{a}_i + C_i a_i = 0. \quad (12.36)$$

Writing

$$K_i = K_i^0 \sqrt{B_i C_i}, \quad (12.37)$$

we find for eqn (12.36) the solution

$$a_i = e^{-\frac{1}{2}\sqrt{C_i/B_i} K_i^0 t} \left( b_i e^{-\frac{1}{2}\sqrt{C_i/B_i} \sqrt{K_i^{02}-4} t} + c_i e^{\frac{1}{2}\sqrt{C_i/B_i} \sqrt{K_i^{02}-4} t} \right). \quad (12.38)$$

For overdamped motion we have  $K_i^0 > 2$ , so that the solution (12.38) contains no oscillations. It will turn out that the measured energy losses in DIC require a strong overdamping of the vibrational modes. They are compatible with a universal value of the strength parameter  $K_i^0 = 20$ . The dependence on the mass of the colliding nuclei is then contained exclusively in the factor  $\sqrt{C_i/B_i}$ .

The complete Rayleigh dissipation function (12.29) can now be written in the form

$$\mathcal{R} = -\frac{1}{2} K_r \dot{r}^2 - \frac{1}{2} \sum_{i,j=\text{P,T}} K_{a_ia_j} \dot{a}_i \dot{a}_j - \frac{1}{2} \sum_{i=\text{P,T}} K_{ra_i} \dot{r} \dot{a}_i - \frac{1}{2} K_\phi r^2 \dot{\phi}^2 \quad (12.39)$$

with the coefficients ( $i, j = \text{P, T}$ )

$$\begin{aligned} K_{ra_i} &= -\sqrt{\frac{5}{4\pi}} 2 R_{0i} K_r, \\ K_{a_ia_j} &= \frac{5}{4\pi} R_{0i} R_{0j} K_r + \delta_{ij} K_i, \end{aligned} \quad (12.40)$$

For the frictional form factors  $K_r$  and  $K_\phi$  we write, in analogy to eqn (12.9),

$$\begin{aligned} K_r &= K_r(r, \{a_i\}) = K_r^0 \left( \frac{dV_N(r, \{a_i\})}{dr} \right)^2, \\ K_\phi &= K_\phi(r, \{a_i\}) = K_\phi^0 \left( \frac{dV_N(r, \{a_i\})}{dr} \right)^2, \end{aligned} \quad (12.41)$$

where the deformed nuclear potential  $V_N(r, \{a_i\})$  is given by formulae (12.24) and (12.28).

#### The equations of motion

The equations of motion of the surface-friction model for deformable nuclei are obtained from eqn (12.11) with the Lagrangian (12.20) together with eqns (12.21) to (12.28), and the Rayleigh function (12.39) together with eqns (12.37), (12.40), and (12.41).

Introducing the radial momentum  $p_r = \mu \dot{r}$ , the angular momentum  $L = \mu r^2 \dot{\phi}$  and the vibrational momentum  $\pi_i = B_i \dot{a}_i$ , we find

$$\begin{aligned} \dot{r} &= \frac{p_r}{\mu}, \\ \dot{p}_r &= -\frac{\partial V}{\partial r} + \frac{L^2}{\mu r^3} - \frac{K_r}{\mu} p_r - \sum_{i=\text{P,T}} \frac{1}{2} K_{ra_i} \frac{\pi_i}{B_i}, \\ \dot{\phi} &= \frac{L}{\mu r^2}, \\ \dot{L} &= -\frac{K_\phi}{\mu} L, \\ \dot{a}_i &= \frac{\pi_i}{B_i}, \\ \dot{\pi}_i &= -\frac{\partial V}{\partial a_i} - \sum_{j=\text{P,T}} K_{a_ia_j} \frac{\pi_j}{B_j} - \frac{1}{2} K_{ra_i} \frac{p_r}{\mu} - C_i a_i, \end{aligned} \quad (12.42)$$

where in the last two lines  $i = \text{P, T}$ .

#### The universal parameters of the surface-friction model

In the same way as in Section 12.2.1, the solution of the equations of motion (12.42) leads to angular distributions of the scattered particles as well as energy and angular-momentum losses. Fitting the calculated results to the experimental data for a large variety of systems yields for the frictional strength parameters the *universal* values

$$\begin{aligned} K_r^0 &= 3.5 \times 10^{-23} \text{ s MeV}^{-1}, \\ K_\phi^0 &= 0.01 \times 10^{-23} \text{ s MeV}^{-1}, \\ K_i^0 &= 20. \end{aligned} \quad (12.43)$$

Note that here the value of the radial strength parameter  $K_r^0$  is lower than the value  $K_r^0 = 4.0 \times 10^{-23} \text{ s MeV}^{-1}$  for rigid nuclei (cf. eqn (12.10)). This is so because the deformation modes are now taken into account explicitly, whereas earlier their effect was implicitly contained in the radial strength parameter.

With these three parameters fixed once and for all, and applying the general prescription for the calculation of the nuclear potential, one succeeds in a nearly quantitative description of deep-inelastic scattering and fusion for practically all systems throughout the periodic table. Examples will be discussed in this and the following section. This universality of the surface-friction model, besides its simplicity, provides the main motivation for discussing it here so extensively.

#### 12.2.3 DIC: The energy–angle correlation

We begin the analysis of DIC data with a qualitative explanation of the Wilczynski plot, which is a contour plot of the double differential cross section  $d^2\sigma/dEd\theta$  with respect to the final energy  $E$  and the scattering angle  $\theta$ . For an example we show in Fig. 12.4 the experimental Wilczynski plot for the scattering of Ar by Th at  $E_{\text{lab}}(\text{Ar}) = 388$  MeV with the nuclei K and Ac as final products (cf. Wilczynski 1973). The dashed

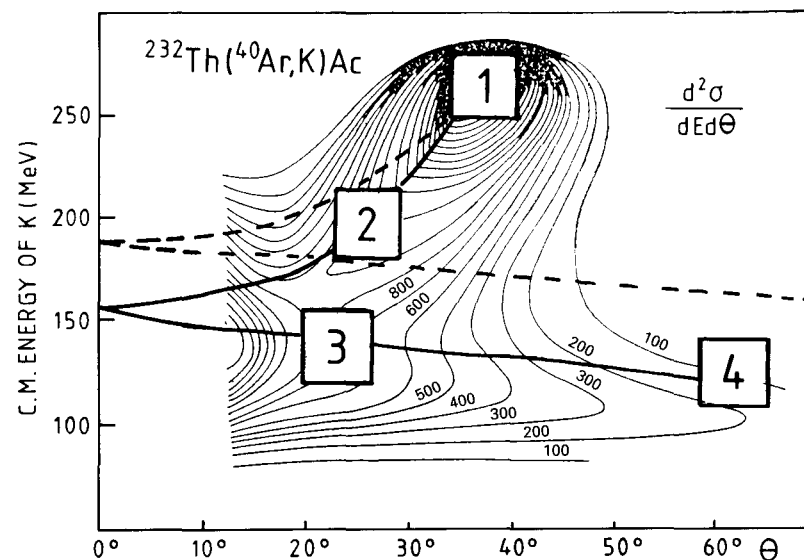


**Figure 12.4** Experimental Wilczynski plot for the system Ar + Th at  $E_{\text{lab}}(\text{Ar}) = 388$  MeV. Two theoretical ( $E - \theta$ ) correlation curves for rigid (dashed curve) and deformable nuclei (solid curve) are included. The regions 1, 2, 3, and 4 correspond to different types of trajectories (cf. Fig. 12.6 and the text).

curve is obtained as the result of calculations using the model of rigid spherical nuclei. A point on it represents the final energy  $E = E_f$  and the scattering angle  $\theta$  for the corresponding trajectory with initial angular momentum  $l_i$ . The curve thus reflects the correlation between the energy  $E$  and the angle  $\theta$  for all trajectories (( $E - \theta$ ) correlation), and should describe the ridge line of the Wilczynski plot. It is seen that the theoretical curve for rigid nuclei does not reproduce the data. In particular, it does not bend down sufficiently rapidly in order to be in agreement with the experimental energy losses. When the dynamical deformations are included one obtains the solid curve for the ( $E - \theta$ ) correlation. This curve agrees rather well with the ridge line of the experimental Wilczynski plot.

The deflection angle  $\Theta(l_i)$  and the energy loss  $\Delta E(l_i)$  associated with the ( $E - \theta$ ) correlation curve of Fig. 12.4 are shown separately in Fig. 12.5. In both of these figures four regions are distinguished, corresponding to the four types of trajectories of Fig. 12.6. Trajectory 1 is a grazing trajectory with initial angular momentum  $l_i = 220$  which only leads to very small energy loss (quasi-elastic scattering). Along trajectory 2 ( $l_i = 160$ ) an energy  $\Delta E \approx 80$  MeV is lost and the deflection angle has the positive value of  $\Theta = 25^\circ$ . Trajectory 3 ( $l_i = 126$ ) with energy loss  $\Delta E \approx 130$  MeV ends at a negative deflection angle  $\Theta = -22^\circ$  (measured as a positive scattering angle in the detector). Finally, for trajectory 4 ( $l_i = 122$ ) the energy loss is  $\Delta E \approx 120$  MeV, and the deflection

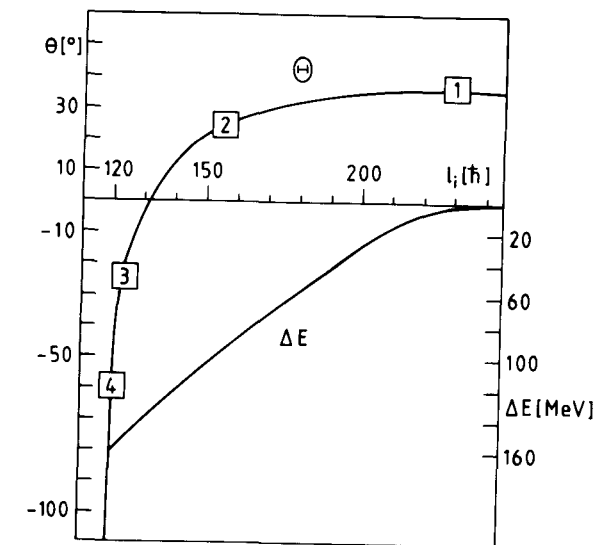


**Figure 12.5** Deflection angle  $\Theta$  and energy loss  $\Delta E$  as functions of the initial angular momentum  $l_i$  for the system Ar + Th at  $E_{\text{lab}}(\text{Ar}) = 388$  MeV. The regions regions 1, 2, 3, and 4 correspond to different types of trajectories (cf. Fig. 12.6 and the text).

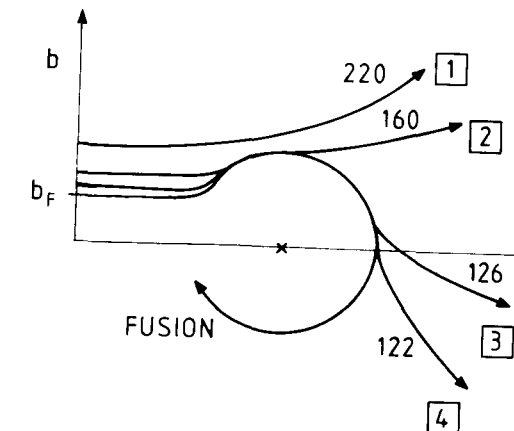


**Figure 12.6** Four types of trajectories corresponding to the four regions indicated in Figs. 12.4 and 12.5. The numbers give the value of the initial angular momentum of the trajectory in units of  $\hbar$ .

angle has the large negative value  $\Theta = -60^\circ$ . A typical orbiting trajectory leading to fusion is also included in Fig. 12.6.

Various calculated  $(E - \theta)$  correlation curves have already been shown in Section 11.2.2. It is seen there from a comparison with the ridge lines of the corresponding experimental Wilczynski plots that the surface-friction model for deformable nuclei reproduces the measured energy-angle correlations for rather different dynamical regimes, namely, for the Coulomb-like (Fig. 11.4), the focusing (Fig. 11.5), and the orbiting deep-inelastic collisions (Fig. 11.6). The considerable improvement over the results for rigid nuclei obtained by introducing the dynamical deformations derives from the large prolate deformations of the nuclei in the exit channel. These allow such large energy losses that the final kinetic energy drops below the energy of the Coulomb barrier of spherical nuclei. Such losses are observed in experiment; they cannot be attained with the model of rigid spherical nuclei (cf. Figs. 11.5, 11.6, and 12.4).

#### 12.2.4 Fusion above the barrier. The extra push

In Section 9.3.5 we discussed fusion above the barrier using classical trajectories. There we distinguished three regions in a classification of the energy dependence of the fusion cross section, exemplified by the light system  $^{32}\text{S} + ^{27}\text{Al}$  (cf. Fig. 9.14). In the low-energy region I the fusion cross section exhausts the entire reaction cross section. In the intermediate-energy region II non-elastic processes compete with fusion; they occur outside a certain critical distance. Finally, in the high-energy region III fusion is limited by a critical angular momentum for the stability against prompt fission, or by the yrast line.

The surface-friction model of classical trajectories allows for a unified description of fusion in all three energy regions. Those trajectories which are scattered by the potential and emerge again from the region of interaction contribute to DIC. Those which overcome the fusion barrier cause fusion. The model ceases to be applicable at energies where incomplete fusion sets in (cf. Section 9.3.6).

The details of the formation of the compound system inside the barrier do not enter in the description, that is, the surface-friction model is an entrance-channel model. The fusion is not determined by the properties of the compound nucleus itself but by features of the collision system outside and at the nuclear surface. In this respect the present model is similar to the quantal optical-model treatment of fusion discussed in Section 9.6, where the effect of the direct non-elastic and deep-inelastic channels is taken into account via an absorptive potential  $W^D(r)$  located rather far out.

We begin with a qualitative discussion of the influence of friction on fusion. In Section 9.3.1 we derived a classical formula for the fusion cross section in the sharp-cut-off model (cf. eqn (9.20)). In this description no friction is involved, and the limiting angular momentum for fusion is the grazing angular momentum  $l_{\text{gr}}$ , so that the fusion cross section is given by (cf. eqn (9.20))

$$\sigma_F^{\text{no fric}} = \frac{\pi}{k^2} (l_{\text{gr}} + 1)^2. \quad (12.44)$$

It is entirely determined by the Coulomb-plus-nuclear potential barrier (we set  $l_{\text{gr}} = kb_{\text{gr}}$  and use eqn (9.15)),

$$\sigma_F^{\text{no fric}} = \pi R_B^2 \left( 1 - \frac{V_B}{E} \right) \quad (12.45)$$

(cf. eqn (9.17)). Figure 12.7 shows a frictionless trajectory with an incident energy  $E$

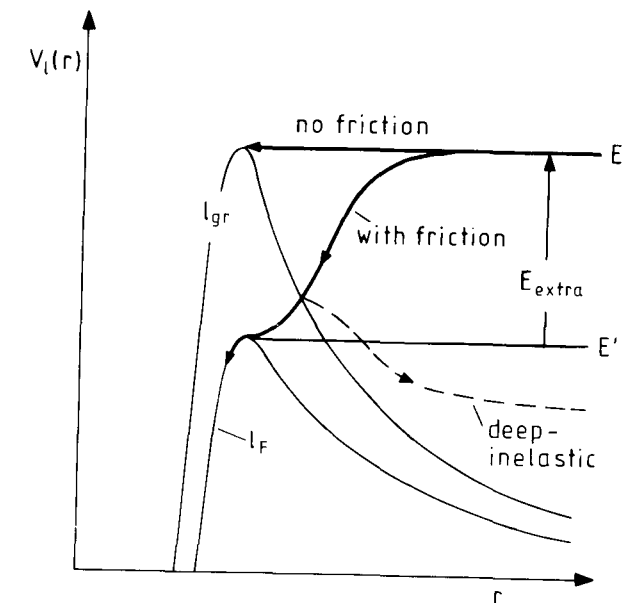


**Figure 12.7** Schematic plot illustrating the definition of the limiting angular momenta for fusion without ( $l_{\text{gr}}$ ) and with radial friction ( $l_F$ ). See text for explanation.

together with the effective barrier with angular momentum  $l = l_{\text{gr}}$  which has exactly the height  $E$ . Now let us include friction, for simplicity restricting ourselves to radial friction alone, so that the angular momentum  $l$  is conserved. Friction removes energy from the relative motion: the trajectory bends down and is reflected from the effective potential with  $l = l_{\text{gr}}$ , contributing to deep-inelastic scattering. The same happens to trajectories with lower angular momentum  $l < l_{\text{gr}}$  until a limiting angular momentum  $l_F$  is reached for which the effective barrier is low enough that the trajectory can pass over it. We thus have

$$l_F < l_{\text{gr}}. \quad (12.46)$$

The fusion cross section with account of friction is given by

$$\sigma_F^{\text{fric}} = \frac{\pi}{k^2} (l_F + 1)^2. \quad (12.47)$$

Comparing with eqn (12.44) we have  $\sigma_F^{\text{fric}} < \sigma_F^{\text{no fric}}$ , that is, friction reduces fusion.

Without friction, the energy  $E'$  needed to surmount the effective barrier with  $l = l_F$  would be equal to the height of this barrier, and thus smaller than the original energy

*E*. But with friction, a trajectory with the energy  $E'$  cannot pass over the barrier for the angular momentum  $l_F$ . The system has to be given an extra energy  $E_{\text{extra}} = E - E'$  in order to be able to fuse. This energy difference is called the *extra push*.

The actual fusion process is somewhat more complicated than just described. So far we have only taken account of the energy loss caused by radial friction, which is indeed the essential effect. However, because of angular-momentum dissipation the centrifugal barrier is reduced as the nuclei approach each other, which causes an increase of the fusion cross section. The dynamical deformations also have an effect on fusion. Owing to the presence of the monopole–quadrupole Coulomb interaction (12.23) and the non-diagonal frictional coupling terms between relative motion and the deformation modes (cf. eqns (12.42)), the colliding nuclei are deformed into oblate shapes in the entrance channel. These oblate deformations cause a dynamical enhancement of the fusion barrier which leads to a reduction of the fusion cross section.

The fusion angular momentum  $l_F$  is determined by all the effects just discussed, i.e. by the combined action of dissipation and dynamical deformations. It is found technically by solving the equations of motion (12.42) for a range of initial angular momenta  $l_i$  at a given energy. For large values of  $l_i$  the trajectories are reflected from the barrier, i.e. they contribute to the deep-inelastic collisions. Reducing the value of  $l_i$  one arrives at the critical value  $l_F$  at which the trajectory is no longer reflected, but surmounts the barrier and reaches the region of strong nuclear interaction; here the friction lowers the energy so much that it prevents the trajectory from leaving the interior again: the nuclei fuse.

In the following we compare the results of the calculations with measured fusion cross sections for typical cases throughout the periodic table (cf. Fröbrich 1984a, where also the references to the experimental data are given).

In Fig. 9.9 of Chapter 9 we considered the fusion of  $^{20}\text{Ne}$  with  $^{27}\text{Al}$  and compared the data with the classical fusion cross section  $\sigma_F^{\text{no fric}}$  (cf. eqn (12.45)) as well as with the result of a surface-friction model calculation in anticipation of the present chapter. It is seen from this figure that the reduction of the classical fusion cross section at higher energies is due to the effect of frictional forces in combination with dynamical deformations.

As a further example of a relatively light system we show in Fig. 12.8 the measured and calculated fusion cross section for the system  $^{32}\text{S} + ^{27}\text{Al}$ . Again we find agreement with experiment. In the figure we have included the result of the proximity-friction model (cf. Birkelund *et al.* 1979), where the nuclei are regarded as rigid and spherical.

Finally, we consider the results of surface-friction model calculations for the fusion of the system  $\alpha + ^{233}\text{U}$  and compare them with the experimental data of Meyer *et al.* (1979) (cf. Fig. 12.9). The fusion is complete for  $E^{-1} > 0.02 \text{ MeV}^{-1}$  (dots), but for higher energies only part of the total fusion cross section (dots) is associated with complete fusion (open triangles). The remainder is contributed by incomplete fusion processes (cf. Section 9.3.6). Even in this extremely asymmetric case with a projectile as light as an  $\alpha$ -particle the data on complete fusion are well reproduced.

#### The extra push at the barrier

As one goes to heavier collision systems, friction and dynamical deformation effects become increasingly important, and the fusion cross section drops more and more below the

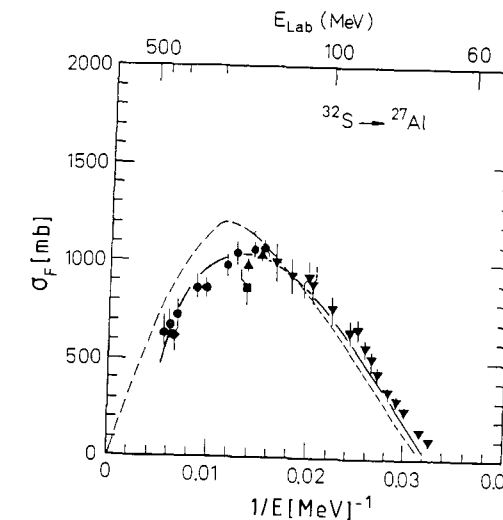


**Figure 12.8** The experimental fusion cross section for the system  $^{32}\text{S} + ^{27}\text{Al}$  in comparison with the results of calculations. Solid curve: results of the surface-friction model. Dashed curve: results of the proximity-friction model.

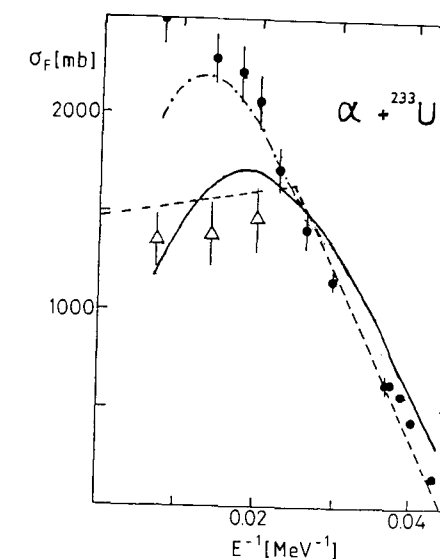


**Figure 12.9** The experimental fusion cross section for the system  $\alpha + ^{233}\text{U}$  (dots: complete + incomplete fusion; open triangles: complete fusion) in comparison with the results of the surface-friction model (solid curve). The results of calculations using the proximity model (dash-dotted curve) and the critical-distance model (dashed curve) are also shown.

value without friction  $\sigma_F^{\text{no fric}}$  (cf. Fig. 12.10). For very heavy systems even the threshold for fusion (i.e. the energy at which  $\sigma_F^{\text{fric}} = 0$ , or  $l_F = 0$ ) is shifted up from the value  $V_B$  of the static nuclear-plus-Coulomb barrier, or s-wave barrier. This is the extra-push effect at the barrier.

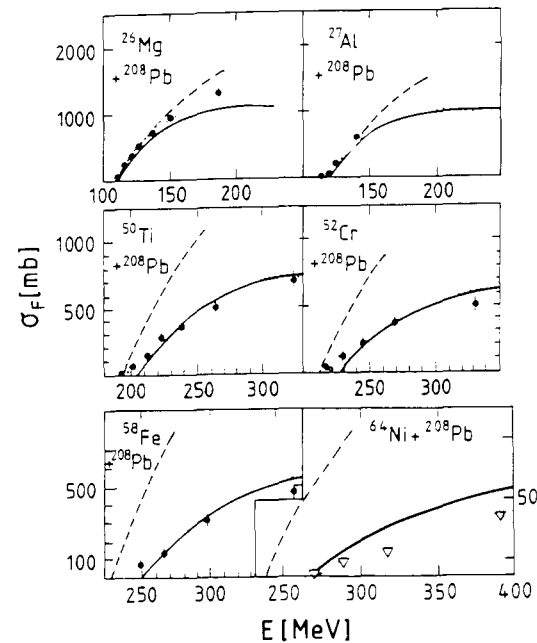


**Figure 12.10** Experimental fusion (capture) cross sections for a number of heavy systems in comparison with the frictionless fusion cross sections  $\sigma_F^{\text{no fric}}$  (dashed curves) and the results of surface-friction model calculations (solid curves).

The behaviour of the experimental data for heavy systems is reproduced by the results of surface-friction model calculations. The static fusion barrier  $V_B$  (the zero of the dashed curve in Fig. 12.10) is effectively replaced with the *dynamical fusion barrier*  $B_{\text{dyn}}$  (the zero of the solid curve). The difference between the two is the *extra push at the barrier*,

$$E_{\text{extra}} = B_{\text{dyn}} - V_B. \quad (12.48)$$

In the following the terms ‘above barrier’ or ‘below barrier’ refer to the dynamical barrier  $B_{\text{dyn}}$ . The experimental threshold energy for the onset of fusion is identified with this dynamical barrier.

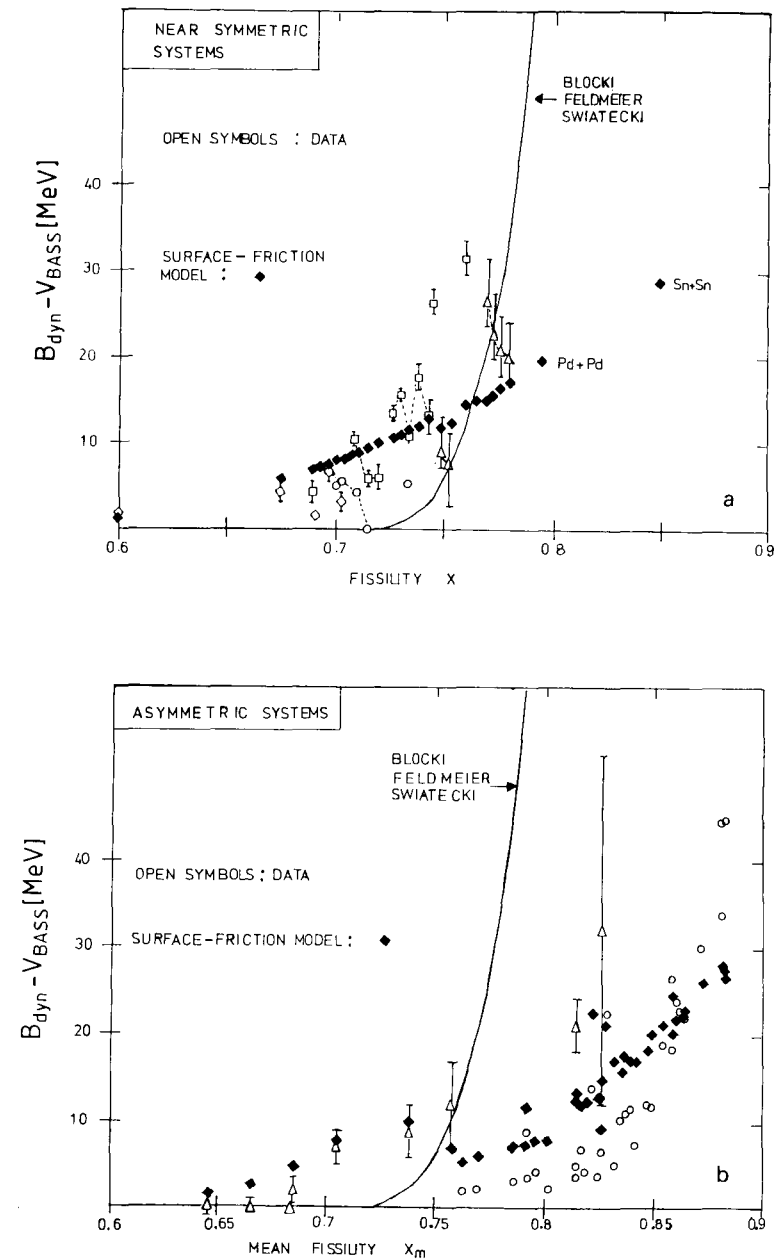


**Figure 12.11** Experimental extra-push energies  $E_{\text{extra}} = B_{\text{dyn}} - V_{\text{Bass}}$  (open symbols) for near-symmetric and asymmetric systems in comparison with the results of surface-friction model (black diamonds, cf. Fröbrich 1988, also for the references to the data) and proximity-model calculations (solid curves, cf. Blocki *et al.* 1986).

There is no extra-push effect at the barrier for asymmetric systems as, for example,  $^{26}\text{Mg} + ^{208}\text{Pb}$ , but the regime changes if one goes to more symmetric systems like  $^{64}\text{Ni} + ^{208}\text{Pb}$ , where the extra push at the barrier is about 30 MeV.

The extra-push energies  $E_{\text{extra}}$ , obtained from the experimental threshold energies  $B_{\text{dyn}}$  and the static barriers  $V_B = V_{\text{Bass}}$  calculated from a model without dynamical deformations (cf. Bass 1980), are plotted against the fissility  $x$  (cf. eqn (9.12)) in Fig. 12.11. The results of surface-friction model calculations (cf. Fröbrich 1988) are shown in the same figure.

The results obtained with the proximity model of Blocki *et al.* (1986) are also plotted in Fig. 12.11. In this model the authors extract a global curve from the results of their dynamical calculations which include the effects not only of the extra push (in which case the mass asymmetry between the collision partners is fixed, as in the surface-friction model) but also that of the ‘extra-extra push’ (which allows for changes in the mass asymmetry during the collision and generally produces an additional energy shift). The good reproduction of the data afforded by the surface-friction model suggests that this model is not in need of improvement via extra-extra push effects. It describes the average trend of the data, and in particular, the vanishing of the extra-push energy for lighter systems. On the other hand, in the proximity model the onset of the extra push with increasing fissility occurs too late, and its rise is too steep, especially for asymmetric systems. Both models are macroscopic and do not take account of specific shell-structure effects which are partly responsible for the scatter of the data around the average trend. These deviations can only be described in more microscopic models (cf., e.g. Berdichevsky *et al.* 1989).

The collision of very heavy systems actually does not produce a compound nucleus since the di-nuclear complex formed in the intermediary stage separates again before a fully equilibrated system is formed. Such a process is called *capture* rather than fusion. For example, as shown by Bock *et al.* (1982), the most asymmetric reaction in Fig. 12.10,  $^{26}\text{Mg} + ^{208}\text{Pb}$ , proceeds as a fusion collision whereas the more symmetric collisions clearly exhibit features of a capture process, i.e. they end in symmetric fragmentation without forming a compound nucleus. Since the surface-friction model is an entrance channel model it does not distinguish between fusion and capture. Capture is also called *fast fission*, because it is faster than normal fission (but slower than DIC).

## 12.3 Fluctuations in deep-inelastic collisions and fusion

In the last section we discussed those features of deep-inelastic collisions and fusion which could be explained in terms of classical trajectories with friction, leaving out the fluctuations. We now turn to phenomena in which the fluctuations play an essential role. Following Section 11.5 we first use the Gaussian approximation to the solution of the multidimensional Fokker–Planck equation in order to analyse the DIC differential cross sections with respect to energy loss, scattering angle and charge number. We then apply the method of Monte Carlo sampling of Langevin trajectories in a calculation of Wilczynski plots in DIC, as well as for the description of the bifurcation into fusion and DIC close to a barrier, of fusion spin distributions, and of the emission of  $\delta$ -electrons during DIC.

### 12.3.1 Gaussian solution of the Fokker–Planck equation

Multidimensional Fokker–Planck equations have been applied to DIC by Ngô and Hofmann (1977), Berlanger *et al.* (1978), Agassi *et al.* (1978), Yadav and Nörenberg (1982), and Feldmeier and Spangenberg (1985); all these authors use the Gaussian approximation. As a further example we discuss here the Fokker–Planck equation in the surface-friction model (cf. Fröbrich *et al.* 1983). It is a generalization of eqn (11.135) which includes deformation and charge-transfer variables, so that the distribution function  $d = d(x; t)$  now depends on the set of variables  $x = \{r, p_r, L, \phi, \pi_i, a_i, Z\}, i = P, T$ . This function satisfies the multidimensional Fokker–Planck equation

$$\begin{aligned} & \left[ \frac{\partial}{\partial t} + \frac{p_r}{\mu} \frac{\partial}{\partial r} + \frac{L}{\mu r^2} \frac{\partial}{\partial \phi} + \left( -\frac{\partial V}{\partial r} + \frac{L^2}{\mu r^3} \right) \frac{\partial}{\partial p_r} + \sum_i \frac{\pi_i}{B_i} \frac{\partial}{\partial a_i} - \sum_i \frac{\partial V}{\partial a_i} \frac{\partial}{\partial \pi_i} \right] d \\ &= \frac{\partial}{\partial p_r} \frac{p_r}{\mu} K_r d + D_r \frac{\partial^2}{\partial p_r^2} d + \frac{\partial}{\partial L} K_\phi \frac{L}{\mu} d + D_\phi r^2 \frac{\partial^2}{\partial L^2} d \\ &+ \sum_{i,j} \frac{\partial}{\partial \pi_i} K_{a_i a_j} \frac{\pi_j}{B_j} d + \sum_{i,j} D_{a_i a_j} \frac{\partial^2}{\partial \pi_i \partial \pi_j} d \\ &+ \sum_i \frac{\partial}{\partial \pi_i} K_{r a_i} \frac{p_r}{\mu} d + \sum_i D_{r a_i} \frac{\partial^2}{\partial \pi_i \partial p_r} d \\ &+ \sum_i \frac{\partial}{\partial p_r} \frac{\pi_i}{B_i} K_{r a_i} d + \sum_i D_{r a_i} \frac{\partial^2}{\partial p_r \partial \pi_i} d \\ &- \frac{\partial}{\partial Z} v_Z d + D_Z \frac{\partial^2}{\partial Z^2} d. \end{aligned} \quad (12.49)$$

The potential  $V = V(r, \{a_i\})$  and the friction coefficients  $K_r = K_r(r, \{a_i\})$ , etc. have been discussed in detail in Section 12.2.2.

As explained in Section 11.5.1, the Gaussian solution of the Fokker–Planck equation (12.49) reduces to the solution of a set of equations of motion for the mean trajectories and a set of equations for the variances of the dynamical variables. The mean values and variances determine the distribution function  $d(x; t)$  in its Gaussian form. From the distribution function at large times one obtains the cross sections by integrating over the impact parameter and the unobserved variables.

When solving for the mean trajectories one calculates the frictional energy loss at each point in time. It is equated to the excitation energy  $E^*$  of the collision partners along the trajectory. From the latter quantity a time-dependent temperature is obtained via the Fermi-gas formula (cf. eqn (10.81))

$$k_B T = \sqrt{\frac{E^*}{a}}, \quad (12.50)$$

where the level density parameter is taken as  $a = A/8$ , and  $A$  is the mass number of the joint projectile–target system.

The diffusion coefficients  $D_r$ , etc., which enter only in the equations for the variances but not in the equations of motion for the trajectories, are assumed to be related to the

friction coefficients  $K_r$ , etc. by the relations (cf. eqn (11.59))

$$D_r = K_r k_B T, \text{ etc.} \quad (12.51)$$

The last line of eqn (12.49) refers to charge transfer. It contains as variable the charge  $Z$  of the projectile-like fragment, for which a Fokker–Planck equation has already been established and solved in eqns (11.100) and (11.107). The driving term  $v_Z$  for the charge  $Z$  is determined from the liquid-drop potential energy surface (cf. eqn (11.104)), and the corresponding diffusion coefficient  $D_Z$  is taken from Ayik *et al.* (1978).

The solution of eqn (12.49) at large times,  $d(x; t \rightarrow \infty)$ , determines the DIC differential cross section with respect to energy, angle, and charge of the scattered heavy ion via

$$\frac{d^3\sigma}{dEd\theta dZ} = \sqrt{\frac{\mu}{2E}} \frac{d^3\sigma}{dpd\theta dZ} = \sqrt{\frac{\mu}{2E}} 2\pi \int db b \int dr dL \int \prod_i (d\pi_i da_i) d_b(x; t \rightarrow \infty), \quad (12.52)$$

where the integration goes over the impact parameters  $b$  (i.e. the initial angular momenta) and those variables  $\{r, L, a_i, \pi_i\}$  which are not observed.

In the Gaussian approximation a multidimensional Gaussian ansatz of the form (11.131) is made for the distribution function. The integrations in expression (12.52) can then be performed analytically, except that over the impact parameter  $b$ . We introduce the mean deflection angle  $\Theta_b = \pi - (\Delta\phi_i^C + \Delta\phi + \Delta\phi_f^C)_b$  (cf. eqn (12.18) and Fig. 12.1) and find after integrating  $d_b(x; t \rightarrow \infty) = d_b(r, p_r, L, \theta, \pi_i, a_i, Z; t \rightarrow \infty)$  over  $r, L, a_i$ , and  $\pi_i$  (and denoting  $p_r$  by  $p$ )

$$\begin{aligned} d_b(p, \theta, Z; t \rightarrow \infty) &= \frac{1}{2\pi \sqrt{\sigma_{pp}^2 \sigma_{\theta\theta}^2 - (\sigma_{p\theta}^2)^2}} \\ &\times \exp\left(-\frac{(\theta - \Theta_b)^2 \sigma_{pp}^2 - 2(\theta - \Theta_b)(p - \bar{p})\sigma_{p\theta}^2 + (p - \bar{p})^2 \sigma_{\theta\theta}^2}{2[\sigma_{pp}^2 \sigma_{\theta\theta}^2 - (\sigma_{p\theta}^2)^2]}\right) \\ &\times \frac{1}{\sqrt{2\pi \sigma_Z^2}} \exp\left(-\frac{(Z - \bar{Z})^2}{2\sigma_Z^2}\right). \end{aligned} \quad (12.53)$$

In separating out the Gaussian for the charge transfer variable  $Z$  we assume that the charge transfer does not couple back to the relative motion and therefore has no effect on it. This has been proved to be a good approximation by Schmidt and Teichert (1981) and Fröbrich *et al.* (1983). The parameters of the charge distribution itself,  $\bar{Z}$  and  $\sigma_Z^2$ , do, however, depend on the interaction time determined by the relative motion.

#### Wilczynski plot. Angular and charge distributions of DIC

In the following we discuss some results for DIC cross sections calculated in the Gaussian approximation.

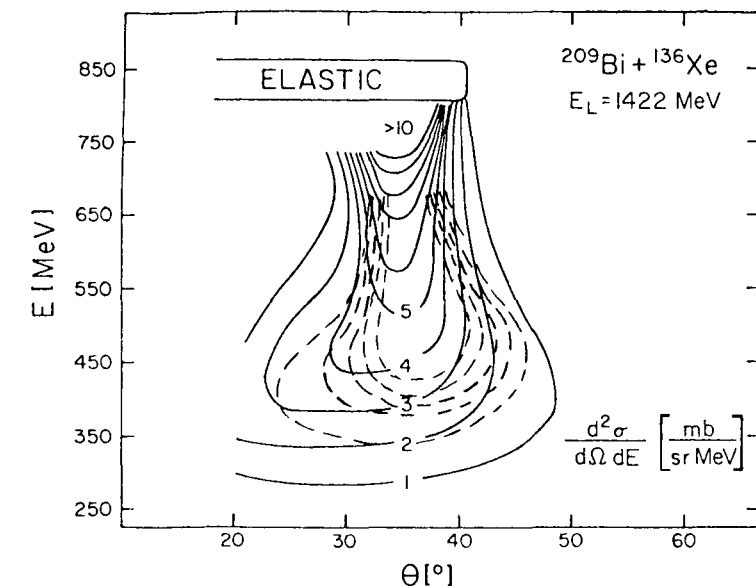


**Figure 12.12** Experimental Wilczynski plot for the system  $^{209}\text{Bi} + ^{136}\text{Xe}$  at  $E_{\text{lab}}(\text{Xe}) = 1422$  MeV (solid contour lines) in comparison with the results of a calculation in the Gaussian approximation (dashed contour lines). The numbers at the solid contour lines give the cross section  $d^2\sigma/dEd\Omega$  in the centre-of-mass system in the units  $\text{mb MeV}^{-1} \text{sr}^{-1}$ ; they also apply to the dashed contour lines in an analogous manner.

The double differential cross section with respect to the final energy  $E$  and the deflection angle  $\theta$  is obtained by integrating expression (12.52) over  $Z$ . We obtain

$$\frac{d^2\sigma}{dEd\theta} = \sqrt{\frac{\mu}{2E}} 2\pi \int_0^\infty bdb d_b(p, \theta; t \rightarrow \infty), \quad (12.54)$$

where  $d_b(p, \theta; t \rightarrow \infty)$  is given by the first two factors of formula (12.53). The contour plot of this double differential cross section is the Wilczynski plot.

The angular distribution follows in a second step by integrating also over the energy. We find (cf. also eqn (11.144)),

$$\frac{d\sigma}{d\theta} = \int dE \frac{d^2\sigma}{dEd\theta} = 2\pi \int_0^\infty bdb \frac{1}{\sqrt{2\pi \sigma_{\theta\theta}^2(b)}} \exp\left(-\frac{(\theta - \Theta_b)^2}{2\sigma_{\theta\theta}^2(b)}\right). \quad (12.55)$$

As an example we consider the system  $^{209}\text{Bi} + ^{136}\text{Xe}$ , where the incident  $^{136}\text{Xe}$  nucleus has the energy  $E_{\text{lab}} = 1422$  MeV. In Fig. 12.12 we show the experimental Wilczynski plot representing  $d^2\sigma/dEd\Omega = (1/2\pi \sin \theta)d^2\sigma/dEd\theta$  (cf. Wollersheim *et al.* 1981) in comparison with the calculated results (cf. Fröbrich 1984b). We see

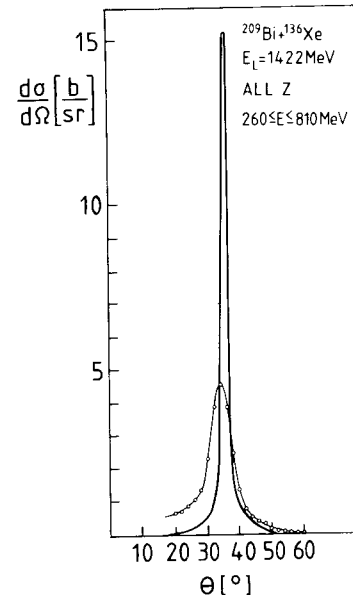


**Figure 12.13** The experimental differential scattering cross section for the system  $^{209}\text{Bi} + ^{136}\text{Xe}$  (circles) in comparison with the results of a calculation in the Gaussian approximation.

that although the experimental and calculated contour lines do not coincide precisely, the observed focusing behaviour is well reproduced. The calculated cross section is, however, too small for large energy losses, and it is too sharply peaked in angle. The latter shortcoming is more clearly revealed by the angular distribution shown in Fig. 12.13. The poor reproduction (cf. Fröbrich *et al.* 1983) of the experimental curve will be seen in Section 12.3.2 to be due to the use of the Gaussian approximation. Integrating the angular distribution over the angle yields the total deep-inelastic cross section; here theory and experiment agree.

In Fig. 12.14 we show the calculated cross section  $d^2\sigma/dEdZ$  for the same system obtained by integrating expression (12.52) over the angle, and compare it with the experimental data shown already in Fig. 11.3. Finally, Fig. 12.15 displays the corresponding experimental charge distribution in comparison with the theoretical results.

We note that, for high energy losses in particular, the energy widths of the cross section come out too small, and the mean values of the charge or mass of the projectile-like particles move in the direction of symmetry (i.e. nucleon transfer proceeds preferably from the heavier to the lighter collision partner), whereas the experimental mean values tend slightly toward asymmetric systems. These features are observed in many other systems, for example, in  $^{36.40}\text{Ar} + ^{92.100}\text{Mo}$  (cf. Bohne *et al.* 1983), for which not only the charge transfer is measured and analyzed but also the mass transfer. Changing the parameters in the Fokker-Planck equation does not improve the agreement between theory and experiment. For example, increasing the diffusion coefficient in order to obtain better agreement for the widths causes the system to tend even more rapidly

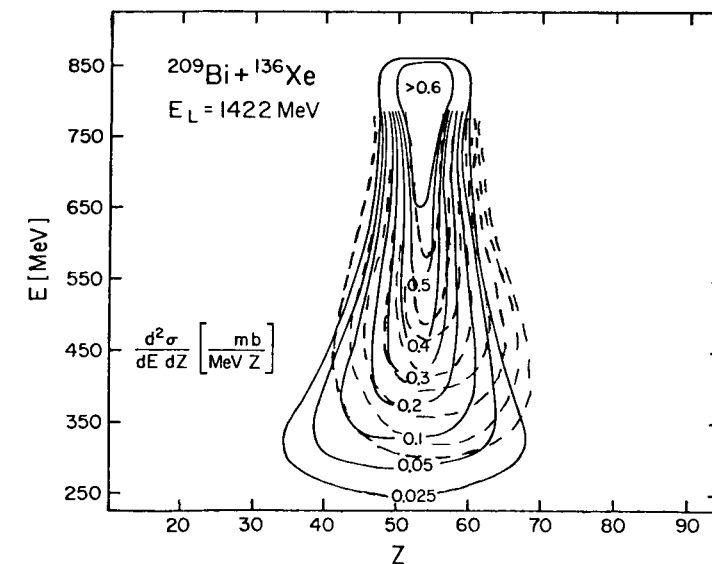


**Figure 12.14** The experimental cross section  $d^2\sigma/dEdZ$  for the system  $^{209}\text{Bi} + ^{136}\text{Xe}$  (solid contour lines) in comparison with the results of a calculation in the Gaussian approximation (dashed contour lines).

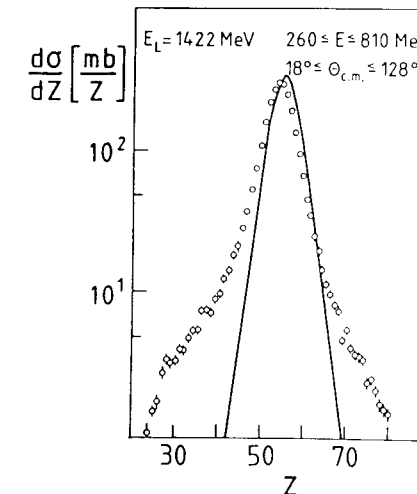


**Figure 12.15** The experimental charge distribution for the system  $^{209}\text{Bi} + ^{136}\text{Xe}$  (circles) in comparison with the results of a calculation in the Gaussian approximation.

toward symmetry, contrary to experiment. It has therefore been proposed that at large energy losses a different mechanism might be responsible for the observed mean values and widths, namely, the statistical rupture of the neck between the collision partners (cf. Brosa *et al.* 1990, and references therein).

For a more detailed discussion of charge and mass diffusion see the review articles by Freiesleben and Kratz (1984) and Adamyan *et al.* (1994).

### 12.3.2 Monte Carlo sampling of Langevin trajectories

#### The discretized Langevin equations of the surface-friction model

It has been shown in Section 11.4.2 how the Langevin and Fokker–Planck equations are related. We use these results to derive from the Fokker–Planck equation (12.49) (leaving out the charge transfer variable  $Z$ ) a set of Langevin equations which we write down in the following discretized form (cf. Marten and Fröbrich 1992),

$$\begin{aligned} p_{r(n+1)} &= p_{r(n)} - \left( \frac{\partial V}{\partial r} - \frac{L^2}{\mu r^3} + K_r \frac{p_r}{\mu} + \sum_i K_{ra_i} \frac{\pi_i}{B_i} \right)_n \tau + \sqrt{D_{r(n)} \tau} w_r(t_n), \\ r_{n+1} &= r_n + \frac{p_{r(n)} + p_{r(n+1)}}{2\mu} \tau, \\ L_{n+1} &= L_n - K_{\phi(n)} L_n \tau + \sqrt{D_{\phi(n)} \tau} w_{\phi}(t_n), \\ \phi_{n+1} &= \phi_n + \frac{L_n + L_{n+1}}{2\mu r_n^2} \tau, \end{aligned} \quad (12.56)$$

$$\begin{aligned} \pi_{i(n+1)} &= \pi_{i(n)} - \left( \frac{\partial V}{\partial a_i} + \sum_j K_{a_ia_j} \frac{\pi_j}{B_j} + K_{ra_i} \frac{p_r}{\mu} + C_i a_i \right)_n \tau + \sqrt{D_{a_i} \tau} w_{a_i}(t_n), \\ a_{i(n+1)} &= a_{i(n)} + \frac{\pi_{i(n)} + \pi_{i(n+1)}}{2B_i} \tau; \end{aligned}$$

here  $p_{r(n)} = p_r(t_n)$ , etc. The quantities  $w_r(t_n)$ ,  $w_{\phi}(t_n)$ , and  $w_{a_i}(t_n)$  are independent random variables of the form (11.151) or (11.155). Instead of employing the algorithm of Section 11.3.7 (cf. Fröbrich and Xu 1988) we here have discretized the equations by taking the *mean values* of the momenta in the equations for the corresponding co-ordinates. This procedure is known as the Heun method in the theory of ordinary differential equations (cf., e.g. Kelly 1967), and improves the numerical stability of the solution.

With the incident energy  $E_i$  and the initial angular momentum  $L_i = \hbar k b$  fixed at some initial time (and the other initial variables defined by eqns (12.16)), the stochastic equations of motion (12.56) are solved in the manner explained in Section 11.5.2.

This results in a distribution function  $d_b(E, \theta; t \rightarrow \infty)$  for the final energy  $E$  and the scattering angle  $\theta$ .

#### DIC: Wilczynski plot, angular distribution

Once the distribution function  $d_b(E, \theta; t \rightarrow \infty)$  has been determined, the double differential cross section  $d^2\sigma/dEd\theta$  with respect to the final energy  $E$  and scattering angle  $\theta$  (represented by the Wilczynski plot) can be calculated by integrating over the impact parameter  $b$  as in eqn (12.54). However, since the distribution function is found by

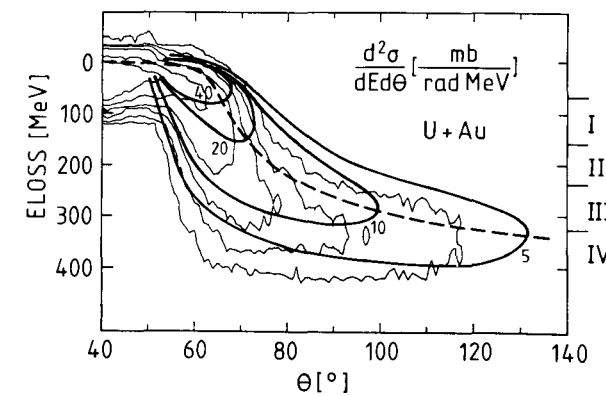


**Figure 12.16** Experimental Wilczynski plot (thin contour lines) for the system U + Au at  $E_{\text{lab(Au)}} = 8.65$  MeV/nucleon in comparison with the results of a Langevin calculation (heavy contour lines). The dashed curve represents the theoretical ( $E - \theta$ ) correlation without account of fluctuations. The numbers I to IV indicate the energy-loss windows in which  $\delta$ -electrons have been measured in coincidence with DIC (cf. Section 12.3.6).

Monte Carlo sampling of trajectories for each impact parameter  $b = l/k$ , it is natural to perform the subsequent integration over  $l$  as part of the sampling procedure. To this end we write the cross section (12.54) in the form ( $d_b = d_l$ )

$$\frac{d^2\sigma}{dEd\theta} = \frac{\pi}{k^2} \int_0^{l_s} 2ldl d_l(E, \theta; t \rightarrow \infty), \quad (12.57)$$

where  $l_s$  denotes the upper end of the range of initial angular momenta which contribute to the integral (it can be chosen as the grazing angular momentum  $l_{\text{gr}}$ ), and make the transformation of variables

$$l = l(x) = l_s \sqrt{x}. \quad (12.58)$$

The new variable  $x$  is regarded as a uniformly distributed random number in the range  $0 \leq x \leq 1$ . The double differential cross section is given by the number  $N(E, \theta)$  of Langevin trajectories, generated from the set of random numbers  $x$ , which end in the energy-loss and angle bins  $(E, E + \Delta E)$  and  $(\theta, \theta + \Delta\theta)$ , respectively, divided by the bin widths  $\Delta E$  and  $\Delta\theta$  and the total number of trajectories  $N$ ,

$$\frac{d^2\sigma}{dEd\theta} = \frac{\pi}{k^2} l_s^2 \int_0^1 dx d_{l(x)}(E, \theta; t \rightarrow \infty) = \frac{\pi}{k^2} l_s^2 \frac{1}{N} \frac{N(E, \theta)}{\Delta E \Delta\theta}. \quad (12.59)$$

For an example we show in Fig. 12.16 an experimental Wilczynski plot for the system U + Au at  $E_{\text{lab}}(\text{Au}) = 8.65$  MeV/nucleon in comparison with the results of a Langevin calculation (cf. Fröbrich and Stroth 1990).

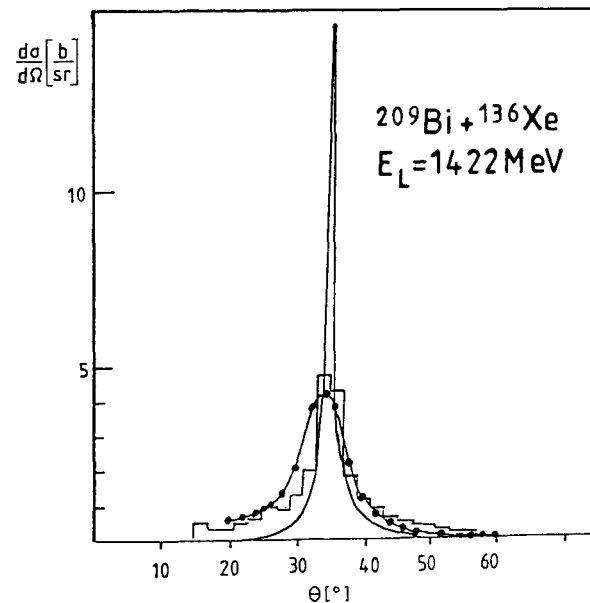


**Figure 12.17** The experimental angular distribution for the system  $^{209}\text{Bi} + ^{136}\text{Xe}$  at  $E_{\text{lab}}(\text{Xe}) = 1422$  MeV (dots) in comparison with the results of a calculation using the Gaussian approximation (solid curve) and of a Langevin calculation (histogram).

Together with the cross section (12.59) one can also calculate the angular distribution  $d\sigma/d\theta$  as the number of trajectories  $N(\theta)$  ending in the angle bin  $(\theta, \theta + \Delta\theta)$  divided by  $\Delta\theta$  and  $N$ ,

$$\frac{d\sigma}{d\theta} = \frac{\pi}{k^2} l^2 \frac{1}{N} \frac{N(\theta)}{\Delta\theta}. \quad (12.60)$$

In Fig. 12.17 we compare the measured angular distribution (cf. Wollersheim *et al.* 1981) for the system  $^{209}\text{Bi} + ^{136}\text{Xe}$  at  $E_{\text{lab}}(\text{Xe}) = 1422$  MeV with the calculated results using the Gaussian approximation (already shown in Fig. 12.13) on one hand, and with the results of a Langevin calculation on the other (cf. Fröbrich 1991). This example clearly demonstrates the superiority of the last method.

### 12.3.3 Bifurcation into fusion and DIC close to the barrier

For a better understanding of the Langevin mechanism we consider the scattering situation shown in Fig. 12.18 for the system  $^{58}\text{Ni} + ^{112}\text{Sn}$  at the incident energy 163 MeV in the centre-of-mass system. The barrier is that of the Coulomb-plus-nuclear potential (i.e. the effective potential for  $l = 0$ ). The incident energy and initial angular momentum

have been chosen such that in the surface-friction model the *mean trajectory* just hits the top of the static fusion barrier  $V_B$ . This energy therefore has the value of the dynamical fusion barrier  $B_{\text{dyn}}$  (cf. Section 12.2.4). The difference between the dynamical and static barriers is the extra push  $E_{\text{extra}}$ , which is also indicated in the figure.

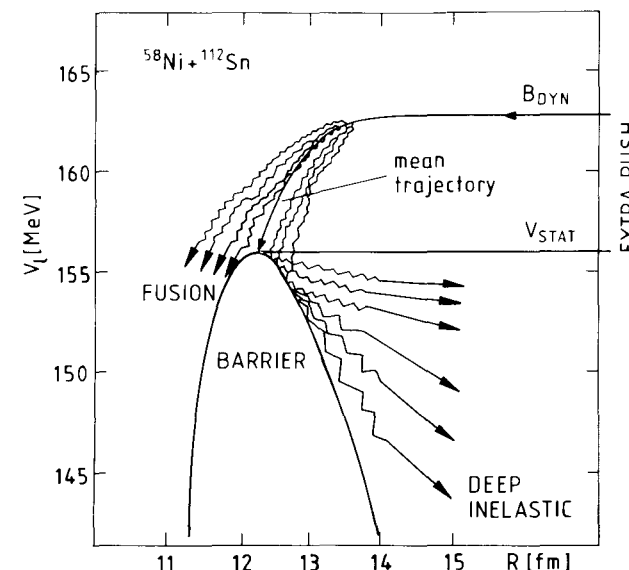


**Figure 12.18** Bifurcation into fusion and DIC in the system  $^{58}\text{Ni} + ^{112}\text{Sn}$  with  $l = 0$  and incident energy 163 MeV in the centre-of-mass system. A mean frictional trajectory with an incident energy equal to the dynamical barrier  $B_{\text{dyn}}$  is shown, illustrating the extra-push effect.

The trajectories produced by the Monte Carlo sampling for given incident energy and initial angular momentum are distributed on both sides of the mean trajectory, as shown schematically in the figure. Some of them have sufficient energy to surmount the barrier, while the others are reflected: the distribution function bifurcates into a fusion branch and a DIC branch. A Gaussian solution of the Fokker-Planck equation could not describe this effect because it yields only a single maximum, but the Langevin approach is ideally suited for this.

The DIC branch contains trajectories along which the energy loss is smaller than those generally occurring in deep-inelastic collisions (one commonly introduces a certain minimum energy loss  $\Delta E_{\text{DIC}}$  above which all energy losses are regarded as being caused by deep-inelastic processes). The classical friction model automatically includes such trajectories, but these should not be counted as DIC trajectories, since they correspond to direct processes (quasi-elastic scattering).

The bifurcation scheme displayed in Fig. 12.18 refers to a special incident energy chosen to be equal to the dynamical barrier  $B_{\text{dyn}}$ . However, the situation is similar for

other incident energies, above and below the dynamical barrier.

The trajectories of the fusion branch contribute to the fusion cross section, which is given by

$$\sigma_F = \frac{\pi}{k^2} \sum_l (2l+1) T_l^F = \frac{\pi}{k^2} \int_0^{l_{\text{max}}} 2ldl T_l^F, \quad (12.61)$$

where  $T_l^F$  is the transmission coefficient for fusion, i.e. the probability that the trajectory with angular momentum  $l$  reaches the inside of the nucleus. Using the transformation (12.58), we again calculate this cross section by Monte Carlo sampling,

$$\sigma_F = \frac{\pi}{k^2} l_{\text{max}}^2 \int_0^1 dx T_{l(x)}^F = \frac{\pi}{k^2} l_{\text{max}}^2 \frac{N_F}{N}, \quad (12.62)$$

where  $N_F$  is the number of trajectories leading to fusion, and  $N$  is the total number of trajectories.

Analogously one obtains the total cross section for deep-inelastic scattering in the form

$$\sigma_{\text{DIC}} = \frac{\pi}{k^2} l_{\text{max}}^2 \int_0^1 dx T_{l(x)}^{\text{DIC}} = \frac{\pi}{k^2} l_{\text{max}}^2 \frac{N_{\text{DIC}}}{N}. \quad (12.63)$$

where  $N_{\text{DIC}}$  is the number of reflected trajectories with energy loss larger than  $\Delta E_{\text{DIC}}$ .

Calculated fusion and deep-inelastic cross sections for the reaction  ${}^{58}\text{Ni} + {}^{112}\text{Sn}$  (cf. Marten and Fröbrich 1992) are compared with the experimental results of Wolfs *et al.* (1987) and Wolfs (1987) in Fig. 12.19. Here  $\Delta E_{\text{DIC}} = 20$  MeV has been chosen. The data for the highest energy are taken from van den Berg *et al.* (1988). Two theoretical curves are entered in the figures. The thin solid curves were calculated using the surface-friction model with the standard parameters. They do not reproduce the experimental curves too well. In order to improve on this, the same calculations have been repeated with a slightly increased (by 10%) radius of the potential (heavy solid curves). This yields the correct thresholds for fusion and DIC. The agreement between theory and experiment is quite reasonable for the fusion cross section, but the calculated DIC cross section is still somewhat too small at low energies.

Both the Langevin and Gaussian methods are classical schemes, and they cannot be used to describe fusion when the incident energy of the trajectories does not suffice to allow them to surmount the static fusion barrier. In this case a theory of dissipative tunnelling is needed (cf. the notes and references at the end of the chapter).

Dasso and Pollaro (1989) have obtained a similar agreement with the data as in Fig. 12.19, using a different friction model which includes fluctuations due to the quantal zero-point motion of the collective modes of the collision partners. The relative importance of statistical and quantal fluctuations in heavy-ion collisions still remains to be investigated more fully.

#### 12.3.4 The spin distributions of fusion and DIC

The cross sections for fusion and deep-inelastic collisions can be decomposed into partial cross sections  $\sigma_F(l)$  and  $\sigma_{\text{DIC}}(l)$ , respectively, which represent the contributions of the angular momenta  $l$  to the total fusion and DIC cross sections. In analogy to the spin distribution of a reaction (11.2) they are called the *spin distributions* of fusion and DIC.

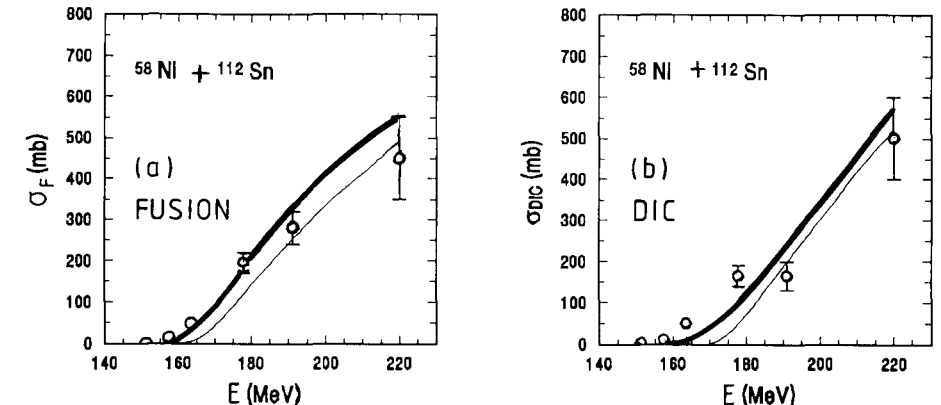


**Figure 12.19** The experimental total fusion (a) and deep-inelastic cross sections (b) (open circles) for the  ${}^{58}\text{Ni} + {}^{112}\text{Sn}$  system in comparison with the results of calculations in the surface-friction model with the standard parameters (thin solid curves). The heavy solid curves represent the calculated results with a potential radius increased by 10%.

They are given in terms of the transmission coefficients  $T_l^F$  and  $T_l^{\text{DIC}}$ ,

$$\begin{aligned} \sigma_F(l) &= \frac{\pi}{k^2} (2l+1) T_l^F, \\ \sigma_{\text{DIC}}(l) &= \frac{\pi}{k^2} (2l+1) T_l^{\text{DIC}}. \end{aligned} \quad (12.64)$$

The spin distributions can be calculated by Monte Carlo sampling simultaneously with the total cross sections,

$$\begin{aligned} [\sigma_F(l)]_j &= \frac{2\pi}{k^2} l_j \frac{N_j^F}{N_j}, \\ [\sigma_{\text{DIC}}(l)]_j &= \frac{2\pi}{k^2} l_j \frac{N_j^{\text{DIC}}}{N_j}; \end{aligned} \quad (12.65)$$

here  $l_j$  are the initial angular momenta,  $N_j^F$  the number of fusing,  $N_j^{\text{DIC}}$  the number of DIC, and  $N_j$  the total number of trajectories in the  $j$ -th angular momentum bin  $j$ .

If statistical fluctuations are not taken into account, fusion and deep-inelastic processes are clearly separated in the angular momentum  $l$ . This is shown in Fig. 12.20a, which is the result of a surface-friction model calculation without fluctuations for the system  ${}^{58}\text{Ni} + {}^{112}\text{Sn}$  at  $E = 177.9$  MeV. It is seen from Fig. 12.18, which refers to the same system, that this energy lies well above the dynamical barrier energy of 163 MeV. It has been believed for a long time that such a separation of reaction types by angular momentum occurs in reality, at least above the barrier; in fact the classification of reactions in Section 9.3.6 was based on this assumption. However, when the fluctuations

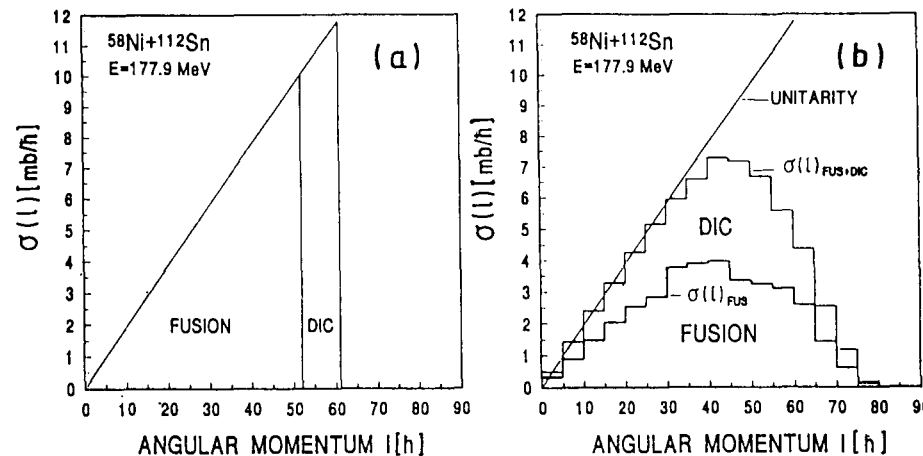


**Figure 12.20** Calculated fusion and DIC spin distributions for the system  $^{58}\text{Ni} + ^{112}\text{Sn}$  at  $E = 177.9$  MeV in the centre-of-mass system without (a) and with fluctuations (b). The unitarity limit is defined by the straight line  $\sigma(l) = 2\pi l/k^2$ .

are included in the model calculations, the spin distributions overlap (cf. Fig. 12.20b). Now even at energies above the barrier, fusion and DIC are not well separated in angular momentum  $l$ . The fusion spin distribution by itself does not reach the geometrical limit  $\sigma(l) = 2\pi l/k^2$  (often called the ‘unitarity limit’); when the DIC spin distribution is added, this limit is reached in the region of close collisions,  $l < l_{\text{gr}}$ .

The spin distributions discussed in connection with Fig. 12.20 have been calculated, not measured. There exist no data on the spin distributions of DIC in competition with fusion. However, fusion spin distributions have been measured for a variety of systems. In Fig. 12.21 we compare calculated (cf. Fröbrich 1991) with experimental fusion spin distributions (cf. Duchêne and Haas 1990) for the asymmetric system  $^{16}\text{O} + ^{144}\text{Nd}$  and the symmetric system  $^{80}\text{Se} + ^{80}\text{Se}$ , which fuse into a compound nucleus with the same mass, charge and excitation energy,  $E^* = 58$  MeV. This energy lies above the barrier. The fusion spin distributions for the two collision systems are very different. This is due to the difference in the amounts of angular momentum brought into the compound nucleus from the entrance channel in the asymmetric and symmetric systems. The calculated spin distributions reproduce the experimental data satisfactorily, for the symmetric as well as for the asymmetric system.

A systematic theoretical analysis of fusion data for heavier systems has been carried out within the surface-friction model by Marten and Fröbrich (1992). Among others, the systems  $^{64}\text{Ni} + ^{92,96}\text{Zr}$  studied by Kühn *et al.* (1989) and Stefanini *et al.* (1990) at energies slightly above the Coulomb barrier have been investigated. Here both the data and the calculated results stay below the unitarity limit; the difference is due to deep-inelastic scattering.

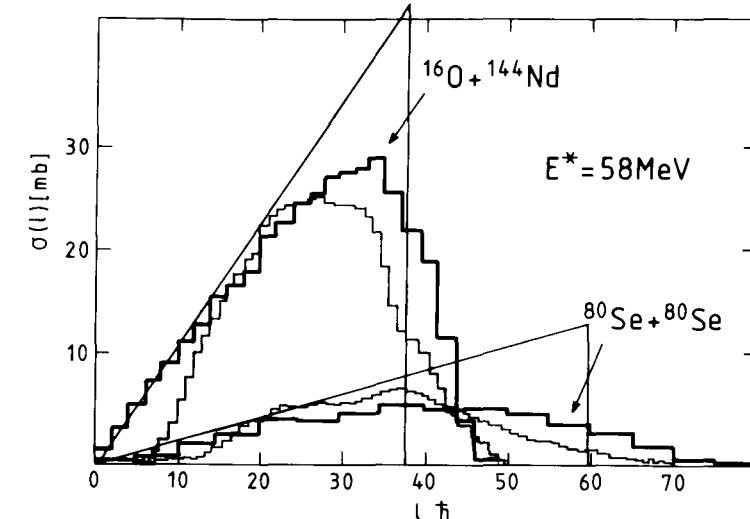


**Figure 12.21** Experimental fusion spin distributions (thin histograms) in comparison with the results of Langevin calculations (heavy histograms) for the systems  $^{80}\text{Se} + ^{80}\text{Se}$  and  $^{16}\text{O} + ^{144}\text{Nd}$  at the compound-nucleus excitation energy  $E^* = 58$  MeV. The straight lines represent the unitarity limit.

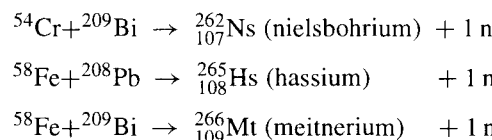
So far we have discussed calculations for systems in which the incident energy lies above the dynamical barrier  $B_{\text{dyn}}$ . For an adequate description below that barrier (but still above the static barrier  $V_B$ ) within the Langevin scheme the Einstein relation has been modified phenomenologically (cf. Fröbrich and Richert 1990). Theoretical arguments for such a modification have been advanced by Hofmann *et al.* (1989). It is intuitively clear that the fluctuations do not disappear as the temperature approaches zero (as is the case when the Einstein relation is used), because the quantal zero-point motion survives. Therefore the fluctuations have to be stronger than implied by the Einstein relation. For example, the data for  $^{64}\text{Ni} + ^{100}\text{Mo}$  (cf. Halbert *et al.* 1989) have been compared with the results of calculations without fluctuations, with fluctuations derived from the Einstein relation, and with fluctuations using increased diffusion coefficients. Above the dynamical barrier the fusion cross section, the first moments  $\langle l \rangle$ , and the second moments  $\langle l^2 \rangle$  are reproduced when the Einstein relation is used, whereas at sub-barrier energies a consistent description can only be achieved with the help of increased diffusion coefficients. With the same coefficients other fusion-evaporation systems are also reasonably well described. The enhanced diffusion does not, however, suffice to reproduce the large second moment  $\langle l^2 \rangle$  measured at sub-barrier energies for fusion-fission systems. More work is necessary to understand fusion excitation functions and spin distributions for heavy systems at sub-barrier energies.

At the present level of research one expects theories of fusion to describe simultaneously fusion excitation functions and spin distributions down to sub-barrier energies. For reviews on theoretical models in comparison with data, see, for example, Satchler (1989), Fröbrich (1990), and in particular, Vandenbosch (1992).

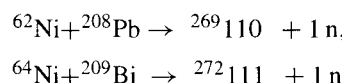
### 12.3.5 Superheavy elements

Heavy-ion fusion reactions provide the appropriate means to search for superheavy elements, i.e. nuclei much heavier than uranium. In order to have a chance to produce such new nuclei with an observable lifetime one usually tries to produce them in the lowest possible state of excitation. This means that the incident energy of the fusion reaction must be chosen well below the dynamical barrier. The fusion cross section will then be rather small (of the order of a few picobarn), but it must still be measurable.

The elements  $Z = 107$ , 108, and 109 have been produced as residual nuclei in compound-nucleus reactions in which one neutron is evaporated (cf. Armbruster 1985),



Recently the elements  $Z = 110$  and  $Z = 111$  have been found in the reactions



(cf. Hofmann *et al.* 1995). All these elements have been identified by their  $\alpha$ -decays to known decay products. Details on the physics of the synthesis of heavy elements by heavy-ion induced fusion with relevant references to the literature can be found, for example, in the article by Reisdorf and Schädel (1992).

The surface-friction model can help in finding the appropriate bombarding energy for experiments designed to produce superheavy elements (cf. Hofmann *et al.* 1992; Hofmann 1993). Since at sub-barrier energies the mean trajectory does not pass over the fusion barrier, statistical fluctuations must be included here. These allow for fusion events at incident energies well below the dynamical barrier. Take, for example, the reaction leading to  $Z = 110$ . Here the surface-friction model yields for the dynamical barrier the value  $B_{\text{dyn}} = 269.2$  MeV. This value is to be compared with the energy  $E = 239.8$  MeV in the centre-of-mass system at which the element  $Z = 110$  has been produced (cf. Hofmann *et al.* 1995). The difference of about 30 MeV between these two values must be bridged by the effect of the statistical fluctuations. The extra push is calculated as  $E_{\text{extra}} = 28.5$  MeV and therefore the static barrier has about the same value as the bombarding energy. The effects of extra push and fluctuations work in opposite directions, and the surface-friction model thus allows for the possibility of fusion events around the energy of the static barrier. Actual Langevin calculations of the fusion cross section, however, are not feasible in this case because the small cross section requires the sampling of an impossibly large number of trajectories.

Whereas the above-cited new elements have been detected in the (heavy ion, 1n)

channel at low excitation energies, another possibility to produce superheavy elements is via 'hot' fusion reactions using more asymmetric systems with a maximum cross section for the formation of evaporation residues in the (heavy ion, 5n) channel. The excitation energy in this case is about 50 MeV. The heaviest element produced in this way up to now is  ${}^{267}_{108}\text{Hs}$ , which has been detected in the reaction  ${}^{34}\text{S} + {}^{238}\text{U} \rightarrow {}^{267}_{108}\text{Hs} + 5\text{n}$  (cf. Oganessian 1994).

### 12.3.6 $\delta$ -electrons as an atomic clock for DIC

The heavy ions participating in a deep-inelastic collision temporarily form a short-lived quasi-molecule which can emit fast electrons, called  $\delta$ -electrons. These originate predominantly from the K-shell. They have been measured in coincidence with heavy ions in particular energy-loss bins. It is of special interest to investigate this correlation because it enables one (in principle) to use the  $\delta$ -electrons as an atomic clock for the DIC (cf. Reinhardt *et al.* 1979).

The  $\delta$ -electron emission probability per unit energy, i.e. the electron spectrum, can be obtained in adiabatic time-dependent perturbation theory (cf. Schiff 1968, Section 35) as

$$\frac{dP_{e^-}}{dE_{e^-}} = |a(\omega)|^2, \quad (12.66)$$

where

$$\begin{aligned} a(\omega) &= \frac{1}{\hbar\omega} \int_{-\infty}^{\infty} dt \left\langle e^{-\left| \frac{\partial H(R(t))}{\partial t} \right| b} \right\rangle e^{i\omega t} \\ &= \frac{1}{\hbar\omega} \int_{-\infty}^{\infty} dt \left\langle e^{-\left| \frac{\partial H(R)}{\partial R} \right| b} \right\rangle \dot{R}(t) e^{i\omega t}. \end{aligned} \quad (12.67)$$

Here the dot denotes the time derivative, and  $\hbar\omega = E_{e^-} + E_b$  is the energy transfer from the bound electron state in the K-shell with mean binding energy  $E_b$  to the final free electron state with kinetic energy  $E_{e^-}$ . The matrix element is taken between these initial and final Dirac states, and the Hamiltonian  $H(R)$  is the Coulomb potential generated by the nuclei moving along classical trajectories  $R = R(t)$ . It has been shown (cf., e.g. Backe 1984) that the matrix element  $\langle e^- | \partial H(R)/\partial R | b \rangle$  is approximately proportional to  $1/R$ , so that we can write

$$a(\omega) = \frac{N}{\omega} \int_{-\infty}^{\infty} dt \frac{\dot{R}(t)}{R(t)} e^{i\omega t}, \quad (12.68)$$

where  $N$  is an overall normalization factor. In the simplest approximation the quantities  $N$  and  $E_b$  are determined by a fit of the electron spectra in coincidence with elastic heavy-ion scattering, and are then also used for the inelastic events. It is the time variation of  $\dot{R}(t)/R(t)$  which determines the  $\delta$ -electron spectra.

For pure Coulomb trajectories the electron spectrum is a monotonically decreasing function of the energy of the emitted electrons. For trajectories along which the nuclei come into contact the amplitude  $a(\omega)$  can be decomposed into three terms. The first term corresponds to the incoming Coulomb trajectory until the onset of nuclear contact at time  $T_1$ ; the second term describes the period from  $T_1$  to  $T_2$  during which the nuclear surfaces are in contact; finally, the third term is connected with the outgoing Coulomb

trajectory from  $T_2$  to infinity. We thus write

$$a(\omega) = \frac{N}{\omega} \left( \int_{-\infty}^{T_1} dt + \int_{T_1}^{T_2} dt + \int_{T_2}^{\infty} dt \right) \frac{\dot{R}(t)}{R(t)} e^{i\omega t}. \quad (12.69)$$

If one assumes that during the time of nuclear contact the nuclei stick together at a fixed distance,  $\dot{R}(t) = 0$ , then the middle integral in formula (12.69) vanishes. Taking the absolute square of the amplitude  $a(\omega)$  then gives rise to an interference term which depends on the time of nuclear contact  $T_2 - T_1$ , and which leads to oscillations in the  $\delta$ -electron spectrum. From the period of these oscillations one can read off the nuclear contact time.

It is true that nuclear sticking cannot be expected to occur in this pure form, and various effects have been taken into account to make the description more realistic (for a recent review cf. Müller-Nehler and Soff 1994). Here we consider the  $\delta$ -electron emission from the point of view of the surface-friction model (cf. Fröblich and Stroth 1990). Figure 12.22 shows the electron spectrum for the system U + Au at  $E_{\text{lab}}(\text{Au}) = 8.65 \text{ MeV/nucleon}$  in coincidence with DIC in the energy-loss window  $E_{\text{loss}} = 280 \pm 45 \text{ MeV}$ , i.e. in the region III in Fig. 12.16. It is found that (i) the trajectories do not exhibit sticking, i.e. the distance between the nuclei is never strictly constant during a finite period of time; (ii) it is not sufficient to use a single trajectory with a mean impact parameter for each energy loss window; rather one has to integrate over a distribution of impact parameters; (iii) in comparing with the data the experimental energy-loss resolution must be taken into account, and finally, (iv) the fluctuations of the trajectories have to be included. The last point is the most important one. The fluctuations lead to *interaction-time distributions* instead of a single interaction time.

These effects are made visible in Fig. 12.22. The solid curve represents the complete calculation, which involves integration over the impact parameter distribution, folding over the experimental energy resolution and sampling of fluctuating trajectories. The figure also contains the results of a calculation with a single non-fluctuating trajectory corresponding to an energy loss of 280 MeV (dashed curve), and of a calculation without fluctuations but with integrations over the impact parameters and the experimental energy resolution (dash-dotted curve).

Although the original hope of measuring directly the interaction times for DIC has not been fulfilled, because in conformance with the calculations no pronounced oscillations have been found in the energy spectra of the  $\delta$ -electrons, one can nevertheless extract not only mean interaction times but also interaction-time distributions from the surface-friction model calculations. The results can be expected to be rather reliable because the model not only reproduces the  $\delta$ -ray spectra but also, as we have seen, many features of DIC and fusion. The mean DIC interaction times for the system Au+U corresponding to the four energy-loss windows in Fig. 12.16 have been calculated as (in units of  $10^{-21} \text{ s}$ ): 1.13 in region I ( $100 \pm 45 \text{ MeV}$ ), 1.22 in region II ( $190 \pm 45 \text{ MeV}$ ), 1.81 in region III ( $280 \pm 45 \text{ MeV}$ ), and 2.50 in region IV ( $> 325 \text{ MeV}$ ).

Rhein *et al.* (1994) have recently analysed  $\delta$ -electron data at higher energies. Their results indicate that at these energies the description of deep-inelastic collisions in terms of a Markovian friction model might be too simplified, and that non-Markovian (memory) effects may play a role.

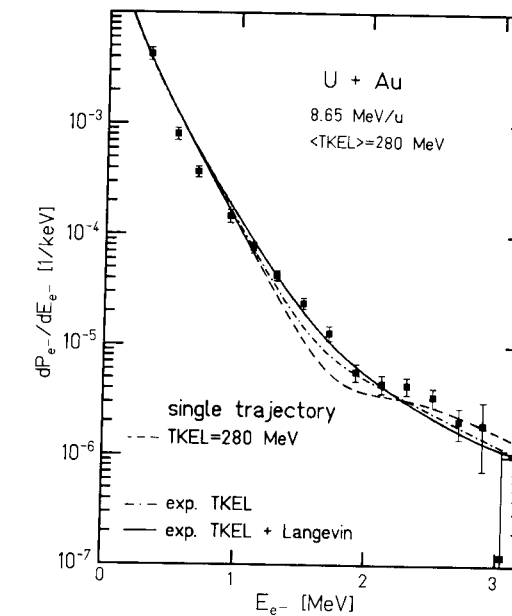


**Figure 12.22** The experimental  $\delta$ -electron spectrum in comparison with the results of surface-friction model calculations. The total kinetic energy loss is denoted by TKEL. See text for details.

## 12.4 Dynamical effects in heavy-ion induced fission

Recent years have witnessed renewed activities in the study of heavy-ion induced fission, that is, fusion–fission reactions in which the fissioning compound systems are highly excited (hot nuclei). The fission is generally accompanied by light-particle evaporation and  $\gamma$ -radiation. These secondary processes may occur both before and after the scission point is reached where the fission fragments begin to separate, and it has now become possible to distinguish experimentally between pre- and post-scission particle emission.

Of special interest have been the data on the energy dependence of pre-scission neutron multiplicities (i.e. the number of pre-scission neutrons emitted per scission event), measured simultaneously with the fission probabilities. These experiments have revealed that it is no longer adequate to treat fission of hot nuclei along the lines of the statistical model for compound-nucleus decay discussed in Section 10.4.3. It has been found, in particular, that it is not possible to reproduce simultaneously the measured pre-scission neutron multiplicities and fission probabilities in the statistical model, no matter how much one varies the barrier and level-density parameters within physically

reasonable limits (for a careful analysis cf. Newton *et al.* 1988). Further difficulties with the statistical model have to do with reproducing the giant dipole  $\gamma$ -spectra measured in coincidence with fission (cf. Thoennessen *et al.* 1987).

General reviews of the experiments and surveys of theoretical models for their interpretation can be found in Newton (1990), Hilscher and Rossner (1992), Hinde (1993), and, with emphasis on giant dipole  $\gamma$ -emission, in Paul and Thoennessen (1994). The general conclusion is that the fission rates calculated in the statistical model are too large. It is natural to invoke *friction* as a mechanism for slowing down the fission process. Friction in fission has been introduced before in order to describe the behaviour of the kinetic energies of the fission fragments (cf., e.g. Davies *et al.* 1976). If the fission rate is lowered, the relative probability of emission of light particles and  $\gamma$ -rays is enhanced, so that their pre-scission multiplicities are increased.

Various dynamical models have been proposed to incorporate frictional effects in fission via Fokker–Planck equations (cf., e.g. Adeev *et al.* 1988, and references therein). These equations have also been considered in conjunction with light-particle emission (cf., e.g. Strumberger *et al.* 1991, and references therein). Another approach makes use of Langevin equations for fission with the elongation and neck parameters as dynamical fission variables (cf. Wada *et al.* 1993, Gontchar *et al.* 1992, Bao *et al.* 1992, 1995, Tillack 1992, and Tillack *et al.* 1992). This ‘two-dimensional’ Langevin treatment is needed, for example, for the calculation of the kinetic-energy distribution of the fission fragments. However, as far as fission probabilities and pre-scission light-particle and  $\gamma$  multiplicities are concerned, an approach involving a one-dimensional Langevin equation appears to be sufficient (cf. Fröbrich *et al.* 1993, Fröbrich and Gontchar 1993a).

This one-dimensional Langevin approach is the topic of the present section. The Monte Carlo sampling of the Langevin trajectories for fission with account of light-particle and giant-dipole  $\gamma$ -ray emission is carried out either up to the final time when scission or evaporation-residue formation has occurred, or up to some point where the fission rate has become constant (stationary regime). In the latter case one continues the calculation by switching over from the dynamical to the conventional statistical treatment in a modified form. The method is applied to the interpretation of measured pre-scission neutron multiplicities and fission probabilities.

#### 12.4.1 The dynamical phase of fission

In Section 10.4.2 we discussed fission in terms of a fission coordinate  $q$  which describes the motion of the fissioning nucleus along a one-dimensional fission path in the space of deformation variables. There we did not define this coordinate explicitly, but in a dynamical approach its precise meaning must be explained. In the present model the fission coordinate is defined as half the distance  $R$  between the centres of mass of the two ‘halves’ of the fissioning nucleus which become the future fission fragments, normalized to the radius  $R_0$  of the initial compound system,  $q = R/2R_0$ .

Whereas the statistical treatment of Section 10.4.2 was based on phase space arguments, we here consider the *dynamics* of the fission process by introducing the following Langevin equations (cf. the analogous equations (11.64) for deep-inelastic scattering)

$$\begin{aligned}\frac{dq}{dt} &= \frac{p}{M}, \\ \frac{dp}{dt} &= \tilde{F}(q) - \gamma \frac{p}{M} + \sqrt{\gamma k_B T} \Gamma(t).\end{aligned}\quad (12.70)$$

The quantity  $\tilde{F}(q)$  is the driving force of fission,  $M$  is an inertia parameter, and the factor  $\gamma$  is a friction coefficient. The driving and friction forces in eqn (12.70) will be discussed in detail below. The Langevin force is given in terms of the Gaussian-distributed  $\delta$ -correlated stochastic variable  $\Gamma(t)$  defined in eqns (11.66) and (11.67); its strength is determined by the product of the friction constant  $\gamma$  and the temperature  $T$  in accordance with eqns (11.58) and (11.59).

#### The driving force of fission

In the discussion of deep-inelastic scattering the driving force  $\tilde{F}(q)$  was identified with the derivative of a conservative potential (cf. eqns (11.22) and (11.23)). It was mentioned in Section 11.3.2 that this driving force is in general modified by the heating of the system. We disregarded this effect in DIC because it is usually masked there by the uncertainties in the phenomenological potential. However, in damped fission it is taken into account. This is done as follows.

Let us begin by considering very slow changes of the fissioning system so that it always remains in equilibrium. The energy of the system is then a function of its natural variables, the entropy  $S$  and the fission coordinate  $q$ ,  $E = E(S, q)$ , and we can write

$$dE = \frac{\partial E}{\partial S} dS + \frac{\partial E}{\partial q} dq.\quad (12.71)$$

The first partial derivative on the right-hand side is identified with the temperature,

$$T = \left. \frac{\partial E}{\partial S} \right|_{q=\text{const}},\quad (12.72)$$

while the other defines the force which drives the system

$$\tilde{F} = -\left. \frac{\partial E}{\partial q} \right|_{S=\text{const}}.\quad (12.73)$$

Equation (12.71) then becomes

$$dE = T dS - \tilde{F} dq.\quad (12.74)$$

The energy is conserved during the slow changes of the system,  $dE = 0$ , so that we can define the driving force by the alternative formula

$$\tilde{F} = T \left. \frac{\partial S}{\partial q} \right|_{E=\text{const}}.\quad (12.75)$$

It is now expressed in terms of the entropy of the system, which will play an important role in the further development.

The entropy  $S$  appearing in eqn (12.75) is in the simplest approximation given by the Fermi gas expression (10.86), where the internal excitation energy  $E^*$  is equal to the difference between the energy  $E$  and the deformation energy, or fission potential,  $V(q)$

of the fissioning system,  $E^* = E - V(q)$ . The entropy then has the form

$$S(E, q) = 2k_B \sqrt{a(q)[E - V(q)]}. \quad (12.76)$$

The fission potential, and therefore also the entropy, depend parametrically on the angular momentum  $l$  of the system,  $S = S(E, l; q)$ .

The potential  $V(q)$  can be calculated in the framework of the angular-momentum-dependent liquid-drop model (cf. Myers and Swiatecki 1966), using the parametrization of Brack *et al.* (1972) for the elongation, neck, and asymmetry of the fissioning nucleus. In the applications below we restrict ourselves to symmetric fission, and obtain the one-dimensional potential  $V(q)$  from the two-dimensional potential landscape of the liquid-drop model by following the bottom of the fission valley. This procedure is justified if we consider fission to be an overdamped process, as we shall do presently.

The single-particle level density parameter  $a(q)$  appearing in the expression (12.76) for the entropy is not a constant as in the Fermi gas model but depends on the geometrical shape of the system, that is, it is a function of the fission coordinate  $q$ . An appropriate semi-phenomenological choice for the  $q$ -dependence is

$$a(q) = a_V A + a_S A^{2/3} B_S(q), \quad (12.77)$$

where  $A$  is the mass number and  $B_S(q)$  is the surface area of the fissioning nucleus normalized to a spherical surface (cf. Gontchar *et al.* 1993). The values of the coefficients are taken from Ignatyuk *et al.* (1975),  $a_V = 0.073$  and  $a_S = 0.095$ .

Substituting expression (12.76) in formula (12.75), performing the  $q$ -differentiation, and then setting (cf. eqn (10.81))

$$E - V(q) = a(q)(k_B T)^2, \quad (12.78)$$

we find for the driving force

$$\tilde{F} = -\frac{dV(q)}{dq} + \frac{da(q)}{dq}(k_B T)^2. \quad (12.79)$$

It is seen that the driving force  $\tilde{F}$  is not simply the negative gradient of the fission potential,  $-dV(q)/dq$  but contains a thermodynamical correction proportional to the square of the temperature. The strength of this term is given by the derivative of the level density parameter with respect to the fission coordinate,  $da(q)/dq$ .

The role of the fission potential  $V(q)$  is here taken over by the entropy  $-S(q)$  whose derivative  $\partial S(q)/\partial q$ , multiplied by the temperature  $T$ , yields the driving force (cf. (12.75)). A comparison of the quantities  $-S$  and  $V/T$  as functions of the fission coordinate  $q$  is made in Fig. 12.23a for various compound systems with angular momentum  $l = 0$  and energy  $E = 50$  MeV.

◊ The driving force can also be expressed in terms of the free energy  $F$  which is related to the energy by

$$F = E - TS. \quad (12.80)$$

Writing  $E = a(q)(k_B T)^2 + V(q)$  (cf. eqn (12.78)) and  $S = 2a(q)k_B^2 T$  (cf. eqns (12.76) and (12.78)), we have

$$F(T, q) = V(q) - a(q)(k_B T)^2. \quad (12.81)$$

This corresponds to a reduction of the fission potential  $V(q)$  by the deformation- and temperature-dependent term  $-a(q)(k_B T)^2$ .

Expressing the energy in relation (12.74) through the free energy we find that the driving force can also be written as

$$\tilde{F} = -\left.\frac{\partial F}{\partial q}\right|_{T=\text{const}}, \quad (12.82)$$

i.e. as the negative derivative of the free energy at fixed temperature. In view of eqn (12.81) we obtain for the driving force again expression (12.79). ◇

### Overdamped motion

In the present model we regard fission as an overdamped process, which appears to be well justified by a number of phenomenological studies summarized, for example, in Hilscher and Rossner (1992). That is, we assume that the friction is so strong that the motion is governed by the forces alone, while the effects of the inertia can be neglected. We then omit the term  $dP/dt = M d^2q/dt^2$  on the left-hand side of the second equation (12.70) and obtain the one-dimensional Langevin equation

$$\frac{dq}{dt} = \frac{T}{\gamma} \frac{\partial S}{\partial q} + \sqrt{\frac{k_B T}{\gamma}} \Gamma(t), \quad (12.83)$$

where we have inserted expression (12.75) for the driving force. It is usual to introduce the reduced friction parameter  $\beta = \gamma/M$ , which is the ratio of the friction and inertia parameters, and we therefore replace  $\gamma$  with  $\beta M$  in the following, although eqn (12.83) is in fact independent of the inertia  $M$ .

The term  $T \partial S / \partial q = \tilde{F} = -dV/dq + (da/dq)(k_B T)^2$  (cf. eqns (12.75) and (12.79)), inasmuch as the deformation force  $-dV/dq$  dominates, is negative in the region between the deformation ground state and the scission point. It acts against the growth of  $q$ , i.e. the motion towards fission. It is the fluctuating Langevin force which actually drives the fission.

### The friction coefficient

A universal parametrization of the reduced friction coefficient  $\beta$  as a function of  $q$  is given by the constant value  $\beta = 2 \times 10^{21} \text{ s}^{-1}$  for  $q_{\text{gs}} < q < q_{\text{neck}}$ , followed by a linear increase up to the value  $\beta = 30 \times 10^{21} \text{ s}^{-1}$  at  $q = q_{\text{sc}}$  (cf. Fröbrich *et al.* 1993; Fröbrich and Gontchar 1993a). Here  $q_{\text{gs}} = 0.375$  is the value of the fission coordinate characterizing the compound nucleus in its initial state, i.e. in the deformation ground state;  $q_{\text{neck}} = 0.6$  is the value of the fission coordinate at the point where the fissioning system begins to neck in, and  $q_{\text{sc}} = 1.19$  is its value at the scission point, where the fragments begin to separate (the numerical values of the fission coordinate at these points are those obtained in the shape parametrization of Brack *et al.* 1972). The reduced friction coefficient as a function of  $q$ , together with the shapes of the fissioning nuclei, is shown in Fig. 12.23b.

The reduced friction coefficient employed in the present calculations is phenomenological and has been given a schematic form. The strength of the friction and its variation along the fission path, as well as its possible temperature dependence, are not

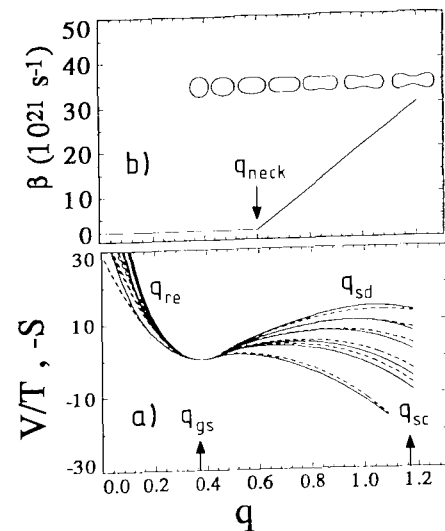


**Figure 12.23** The dynamics of fission. (a) The fission potential  $V$  divided by the temperature  $T$  (dashed curves) in comparison with the negative entropy  $-S$  (solid curves) for the compound systems  $^{178}\text{W}$ ,  $^{188}\text{Pt}$ ,  $^{200}\text{Pb}$ ,  $^{213}\text{Fr}$ ,  $^{224}\text{Th}$ , and  $^{251}\text{Es}$  with angular momentum  $l = 0$  and energy  $E = 50$  MeV (from top to bottom); the entropy is normalized to zero at the ground-state position. (b) The shape of the fissioning nuclei as a function of the fission coordinate  $q$ , and the universal reduced friction coefficient  $\beta$  used in the calculations (solid curve). See text for the meaning of the values  $q_{gs}$ ,  $q_{sc}$ ,  $q_{sd}$ ,  $q_{neck}$ , and  $q_{re}$ .

well known, neither experimentally nor theoretically (cf. the discussion in Hilscher and Rossner 1992).

We note further that the present universal parametrization of the reduced friction coefficient  $\beta$  could only be achieved with the choice (12.77) of the level density parameter. Other level density parameters (e.g. those of Töke and Swiatecki 1981) failed in this respect.

#### Light-particle evaporation and $\gamma$ -radiation rates

The fission process is generally accompanied by the emission of light particles (neutrons, protons, deuterons, and  $\alpha$ -particles) as well as by  $\gamma$ -radiation. The light-particle evaporation is governed by the rates  $R_v$  ( $v = n, p, d, \alpha$ ) given by formula (10.148). The emission of  $\gamma$ -radiation occurs predominantly via the giant dipole resonance, and the corresponding width is given by (cf. Lynn 1968, p. 325)

$$\Gamma_\gamma = \hbar R_\gamma = \frac{4}{3\pi} \frac{NZ}{A} \frac{1+\kappa}{m_N c^2} \frac{e^2}{\hbar c} \frac{1}{\rho_C(E^*, J)} \sum_{I=|J-1|}^{J+1} \int_0^\infty d\epsilon_\gamma \rho_C(E^* - \epsilon_\gamma, I) \frac{\Gamma_G \epsilon_\gamma^4}{(\epsilon_\gamma^2 - E_G^2)^2 + (\Gamma_G \epsilon_\gamma)^2}, \quad (12.84)$$

where  $E_G = 80 A^{-1/3}$  MeV is the position and  $\Gamma_G = 5$  MeV a typical width of the giant-dipole resonance;  $\kappa$  is a parameter connected with deviations from the classical dipole sum rule due to the existence of nuclear exchange forces. Finally,  $\rho_C$  is the level density of the fissioning compound nucleus, and  $E^*$  its excitation energy.

#### The solution of the Langevin equation

The solution of the Langevin equation (12.83) with account of light-particle evaporation and  $\gamma$ -radiation can be carried out using the procedure outlined by Fröbrich *et al.* (1993). One begins by calculating the fusion spin distribution  $\sigma_F(l)$  in the entrance channel of the system (cf. Section 12.3.4), which represents the probability of formation of the compound system as a function of the orbital angular momentum  $l$ . This function determines the distribution of the angular momenta of the fissioning system and fixes the normalization of the fusion–fission process. The initial value of the coordinate  $q$  is its value  $q_{gs}$  corresponding to the compound nucleus in the deformation ground state. The temperature in the initial state is calculated via eqn (12.50) from the excitation energy of the fused system, which is equal to the total energy of the system  $E = \mathcal{E} + Q$  (where  $\mathcal{E}$  is the centre-of-mass energy in the entrance channel and  $Q$  is the fusion  $Q$ -value) minus the deformation energy at the deformation ground state (normalized to zero,  $V(q_{gs}) = 0$ ).

The Langevin equation (12.83) is now discretised and solved by using constant time steps of size  $\tau$ . Simultaneously one calculates the pre-scission emission of a light particle or  $\gamma$ -ray by the following Monte Carlo procedure simulating the radioactive decay for particle emission. One begins by computing the total emission rate  $R = \sum_v R_v$ , where the partial rates  $R_v$  with  $v = n, p, d, \alpha, \gamma$  are the stationary evaporation and  $\gamma$ -radiation rates (cf. eqns (10.148) and (12.84), respectively). The total rate determines the lifetime  $\tau_{\text{em}} = 1/R$  of these decays, which is a measure of the time during which the emission takes place on the average. The ratio  $\tau/\tau_{\text{em}}$  is equal to the probability that particle emission occurs during the time interval  $\tau$ . If this ratio is larger than a random number  $\xi$  ( $0 \leq \xi \leq 1$ ), the emission of one particle (or  $\gamma$ -ray) is registered. The partition into particle types  $v$  is determined by a subsequent Monte Carlo selection with the weights  $R_v/R$ . After each emission act the kinetic energy of the emitted particle is calculated again by a Monte Carlo procedure and counted as energy loss for the Langevin trajectory. Angular momentum is accounted for only roughly by assuming that the emission of a neutron, proton, or  $\gamma$  reduces the angular momentum of the residual nucleus by one unit, and the emission of an  $\alpha$ -particle or deuteron, by two units of  $\hbar$ . These values correspond to upper estimates of statistical-model calculations. One makes an appropriate adjustment of the energy and angular momentum variables in the Langevin equation, and goes on to the next time step. A resetting of the energy must also be carried out on account of friction. The latter causes an energy loss along the fission trajectory which appears as an energy gain in the internal excitation energy  $E^*$ .

The calculation is continued in this fashion step by step, and terminated with one of two alternative outcomes. In the first alternative the fission trajectory reaches the scission point at  $q = q_{sc}$ , in which case a fission event is registered. In the second alternative the internal excitation energy of the system has dropped to a value  $E^* < \min\{B_f, B_v\}$  before the trajectory has reached the saddle point at  $q = q_{sd}$ , where  $B_f = V(q_{sd})$  is the height of the fission barrier and  $B_v$  the binding energy of the particle  $v$ . Then neither

fission nor particle emission can occur any longer, the calculation is terminated, and an evaporation-residue event is registered. Thus one ends up with fission or the formation of an evaporation-residue in coincidence with the corresponding number of particles emitted during the evolution of the fission trajectory. Either of these two events must eventually occur, but along some of the Langevin trajectories this may take a rather long time, when numerical instabilities begin to affect the results of the calculations.

Fortunately, however, before the numerical difficulties set in the dynamical rate becomes constant. This is illustrated in Fig. 12.24 which shows the time dependence of the fission rate  $R_f(t)$  calculated by Monte Carlo sampling of fission trajectories, where for simplicity the evaporation channels have been omitted. Here the fission rate is calculated

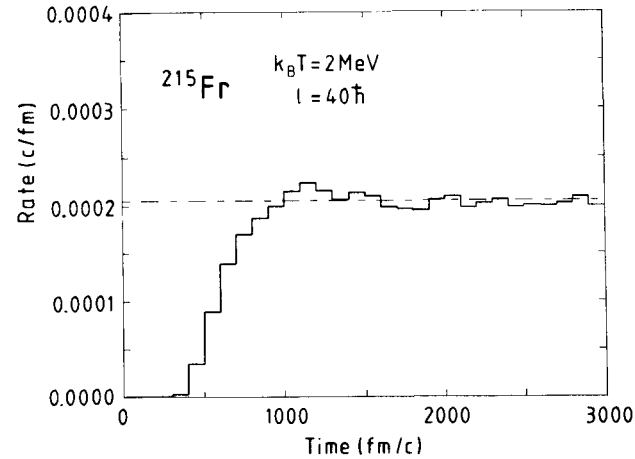


**Figure 12.24** The time dependence of the fission rate for the nucleus  $^{215}\text{Fr}$  at  $k_B T = 2 \text{ MeV}$  and  $l = 40\hbar$ , as calculated by Monte Carlo sampling of fission trajectories. The delay time  $\tau_d$  after which the rate becomes constant is here equal to about  $\tau_d = 1200 \text{ fm}/c \approx 4 \times 10^{-21} \text{ s}$ .

by the formula

$$R_f(t) = \frac{1}{N_0 - N_f(t)} \frac{dN_f(t)}{dt}, \quad (12.85)$$

where  $N_0$  is the number of initial trajectories, and  $N_f(t)$  is the number of trajectories which have terminated with a fission event at time  $t$ . In the Monte Carlo procedure one evaluates formula (12.85) in the form

$$[R_f]_i = \frac{1}{N_0 - \sum_{j=1}^i N_j} \frac{N_i}{\Delta t}, \quad (12.86)$$

where  $N_i$  is the number of trajectories which have fissioned in the  $i$ -th time bin of width  $\Delta t$ .

When the fission rate turns constant fission becomes stationary, so that one reaches the region of validity of the statistical model. Therefore, one may terminate the dynamical calculation at some time  $\tau_d$  after this has happened, and switch over to the conventional calculational procedure in terms of stationary rates (cf. Section 10.4.3); in actual calculations one uses  $\tau_d \approx 100 \times 10^{-21} \text{ s}$ . However, the fission rate to be used in this scheme is now given by the stationary limit of the dynamical rate, not by the Bohr–Wheeler formula (10.154).

The limiting rate can be obtained at the end of the dynamical Langevin calculation just described. However, this rate is needed at varying energies and angular momenta in the subsequent cascade calculations. Therefore, it is mandatory to have available an explicit formula for the calculation of stationary fission rates. In the following we shall show how such a formula can be derived.

### 12.4.2 The stationary phase of fission

#### *The Smoluchowski equation*

In order to explain the procedure we begin by transforming the Langevin equation (12.83) into the corresponding Fokker–Planck equation (using the prescription of Section 11.4.2). The Fokker–Planck equation in the overdamped limit is called the *Smoluchowski equation* and has the form

$$\frac{\partial}{\partial t} d(q; t) = \left( -\frac{\partial}{\partial q} v(q) + \frac{\partial^2}{\partial q^2} D(q) \right) d(q; t) \quad (12.87)$$

with

$$v(q) = \frac{T}{\beta M} \frac{\partial S}{\partial q}, \\ D(q) = \frac{k_B T}{\beta M}. \quad (12.88)$$

We now consider the conditional probability density  $P(q, t; q', t')$ , i.e. the probability for the fission trajectory to be at the point  $q$  at time  $t$  when it is known that it has passed the point  $q'$  at time  $t'$ . It is identical with the transition probability defined in Section 11.4.1. It is clear from eqn (11.76) that the usual (forward) Fokker–Planck equation, in this case the Smoluchowski equation, satisfied by the distribution function  $d(q; t)$  is also satisfied, with respect to the set of variables  $q, t$ , by the conditional probability density  $P(q, t; q', t')$ ,

$$\frac{\partial}{\partial t} P(q, t; q', t') = \left( -\frac{\partial}{\partial q} v(q) + \frac{\partial^2}{\partial q^2} D(q) \right) P(q, t; q', t'). \quad (12.89)$$

Since the coefficients  $v(q)$  and  $D(q)$  are time-independent, the probability density  $P(q, t; q', t')$  is a function of the time difference  $t - t'$  only, so that we have  $P(q, t; q', t') = P(q, t - t'; q', 0)$ .

It is convenient to write eqn (12.89) in the form of a continuity equation,

$$\frac{\partial}{\partial t} P = \frac{\partial}{\partial q} J, \quad (12.90)$$

where

$$J = -vP + \frac{\partial}{\partial q}(DP) \quad (12.91)$$

is the probability current density.

*Boundary conditions.* The probability density  $P(q, t; q', t')$  must satisfy certain boundary conditions in conformance with the behaviour of the fission trajectories. The fission trajectories are reflected at the inner flank of the barrier at a point  $q_{re}$  to the left of the ground-state position  $q_{gs}$ , and they leave the region  $q_{re} < q < q_{sc}$  at the scission point  $q = q_{sc}$ , i.e. they are ‘absorbed’ there. The derivation of the corresponding boundary conditions for the probability density is not a simple matter. We present a heuristic approach, following Goel and Richter-Dyn (1974), Section 3.2 (cf. also van Kampen 1981, Sections VI.7, VI.10, and VIII.5; Szabo *et al.* 1980).

We transform the Smoluchowski equation into a master equation for one-step processes by discretizing the fission coordinate in the form  $q = q_n = q_{re} + nh$  (and similarly  $q' = q_m = q_{re} + mh$ ), where the small parameter  $h$  defines the step size from one value of  $q$  to the next, and the indices  $n, m = 0, \dots, N$  characterize the ‘states’ of the system for the corresponding values of the coordinate  $q$ . We have  $q_0 = q_{re}$  and  $q_N = q_{sc}$ . With the notation  $P(q_n, t; q_m, t') = P_n^m(t - t')$ ,  $v(q_n) = v_n$ , and  $D(q_n) = D_n$  we obtain from eqn (12.89) the discrete master equation

$$\begin{aligned} \frac{\partial P_n^m}{\partial t} = & -\frac{1}{2} \left( \frac{v_{n+1} P_{n+1}^m - v_n P_n^m}{h} + \frac{v_n P_n^m - v_{n-1} P_{n-1}^m}{h} \right) \\ & + \frac{1}{h} \left( \frac{D_{n+1} P_{n+1}^m - D_n P_n^m}{h} - \frac{D_n P_n^m - D_{n-1} P_{n-1}^m}{h} \right) \end{aligned} \quad (12.92)$$

or

$$\frac{\partial P_n^m}{\partial t} = \lambda_{n-1} P_{n-1}^m - (\lambda_n + \mu_n) P_n^m + \mu_{n+1} P_{n+1}^m, \quad (12.93)$$

where

$$\begin{aligned} \lambda_n &= (D_n/h + v_n/2)/h, \\ \mu_n &= (D_n/h - v_n/2)/h. \end{aligned} \quad (12.94)$$

Inspection of eqn (12.93) shows that the coefficient  $\lambda_n$  is the rate of the transition from the state  $n$  to the state  $n + 1$ ; analogously, the coefficient  $\mu_n$  is the transition rate for  $n \rightarrow n - 1$ .

(i) At the reflection point  $n = 0$  the master equation (12.93) reads

$$\frac{\partial P_0^m}{\partial t} = \lambda_{-1} P_{-1}^m - \mu_0 P_0^m - \lambda_0 P_0^m + \mu_1 P_1^m. \quad (12.95)$$

The state  $n = -1$  beyond the reflection point cannot influence the states  $n \geq 0$ , so that the term  $\lambda_{-1} P_{-1}^m$  should vanish. Furthermore, no transitions from the state  $n = 0$  to the state  $n = -1$  are allowed, which would require  $\mu_0 = 0$ . However, since the rates  $\lambda_n, \mu_n$  in eqn (12.93), or rather the transport coefficients  $v(q_n), D(q_n)$ , are derived from the analytic expressions (12.88), the value of  $\mu_0$  is not at our disposal (nor that of  $\lambda_{-1}$ ). We therefore do not implement the boundary condition in the coefficients  $\lambda_n, \mu_n$  but in

the solution  $P_n^m$ . Recognizing that the effect of the reflecting boundary condition is to make the contribution of the first two terms on the right-hand side of eqn (12.95) vanish, we set

$$\mu_0 P_0^m - \lambda_{-1} P_{-1}^m = 0. \quad (12.96)$$

Using the relations (12.94) we can write this equation as

$$\begin{aligned} 0 &= h(\mu_0 P_0^m - \lambda_{-1} P_{-1}^m) \\ &= \frac{1}{2}h[(\mu_0 - \lambda_0)P_0^m + (\mu_{-1} - \lambda_{-1})P_{-1}^m + (\lambda_0 + \mu_0)P_0^m - (\lambda_{-1} + \mu_{-1})P_{-1}^m] \\ &= -\frac{1}{2}(v_0 P_0^m + v_{-1} P_{-1}^m) + \frac{D_0 P_0^m - D_{-1} P_{-1}^m}{h}. \end{aligned} \quad (12.97)$$

In the limit  $h \rightarrow 0$  we find

$$\left( -v(q)P(q, t; q', t') + \frac{\partial}{\partial q}[D(q)P(q, t; q', t')] \right)_{q_{re}} = 0, \quad (12.98)$$

or, using eqn (12.91),

$$J(q_{re}, t; q', t') = 0. \quad (12.99)$$

This relation is easily understood: the fission trajectories turn around at the reflection point so that the probability current vanishes there.

(ii) At the scission point  $n = N$  the trajectories are ‘absorbed’: once the state  $n = N$  has been reached no transitions back to the state  $n = N - 1$  can occur. Therefore, in the master equation (12.93) for  $n = N - 1$ ,

$$\frac{\partial P_{N-1}^m}{\partial t} = \lambda_{N-2} P_{N-2}^m - (\lambda_{N-1} + \mu_{N-1}) P_{N-1}^m + \mu_N P_N^m, \quad (12.100)$$

the term  $\mu_N P_N^m$  on the right-hand side should vanish. Again, we do not apply the boundary condition to the rate, requiring  $\mu_N = 0$ , but to the solution, setting  $P_N^m = 0$  or

$$P(q_{sc}, t; q', t') = 0. \quad (12.101)$$

After setting  $P_N^m = 0$  we can no longer interpret  $P_N^m (= 0)$  as the probability that the system is in the state  $n = N$ . But we may define the probability  $P_*^m$  that the system has left the states  $n = 0, \dots, N - 1$ , i.e. the region between the reflection and absorption points, by

$$P_*^m = 1 - \sum_{n=0}^{N-1} P_n^m. \quad (12.102)$$

For the rate at which the system leaves this region we then have

$$\frac{dP_*^m}{dt} = - \sum_{n=0}^{N-1} \frac{\partial P_n^m}{\partial t} = \lambda_{N-1} P_{N-1}^m; \quad (12.103)$$

here we have made use of eqn (12.93) summed from  $n = 0$  to  $n = N - 1$ , taking into account eqn (12.96) and  $P_N^m = 0$ . The rate (12.103) is seen to be equal to the rate for the transition from the last state before the absorption point,  $n = N - 1$ , to the ‘absorptive’ state  $n = N$  from which it never returns.

### The backward Smoluchowski equation

The probability density  $P(q, t; q', t')$  can also be calculated from a differential equation with respect to the set of the earlier variables  $q', t'$ ; this equation is called the backward Fokker–Planck equation, or in the case of overdamped motion, the backward Smoluchowski equation. It is derived along similar lines as the forward equation.

Consider the law of composition of conditional probability densities for times  $t \geq t' + \tau \geq t'$  (cf. the equivalent equation (11.76)),

$$P(q, t; q', t') = \int dx P(q, t; x, t' + \tau) P(x, t' + \tau; q', t'). \quad (12.104)$$

We write

$$P(x, t' + \tau; q', t') = \int dy \delta(y - x) P(y, t' + \tau; q', t') \quad (12.105)$$

and expand the  $\delta$ -function into a Taylor series,

$$\delta(y - x) = \delta(q' - x + y - q') = \sum_{n=0}^{\infty} \frac{1}{n!} (y - q')^n \left( \frac{\partial}{\partial q'} \right)^n \delta(q' - x); \quad (12.106)$$

then we have

$$P(x, t' + \tau; q', t') = \sum_{n=0}^{\infty} \frac{1}{n!} M_n(q'; t', \tau) \left( \frac{\partial}{\partial q'} \right)^n \delta(q' - x) \quad (12.107)$$

with the moments

$$M_n(q'; t', \tau) = \int dy (y - q')^n P(y, t' + \tau; q', t') \quad (12.108)$$

already defined in eqn (11.80).

Insertion of expression (12.107) in eqn (12.104) yields

$$\begin{aligned} P(q, t; q', t') - P(q, t; q', t' + \tau) &= M_1(q'; t', \tau) \frac{\partial}{\partial q'} P(q, t; q', t' + \tau) \\ &+ \frac{1}{2} M_2(q'; t', \tau) \frac{\partial^2}{\partial q'^2} P(q, t; q', t' + \tau) + \dots \end{aligned} \quad (12.109)$$

Dividing this equation on both sides by  $\tau$  and taking the limit  $\tau \rightarrow 0$ , we obtain the backward Fokker–Planck equation with the time derivative  $-\partial P/\partial t'$  on the left-hand side. Recalling the relation  $P(q, t; q', t') = P(q, t - t'; q', 0)$ , we have  $-\partial P/\partial t' = \partial P/\partial t$ , and obtain

$$\frac{\partial}{\partial t} P(q, t; q', t') = \left( v(q') \frac{\partial}{\partial q'} + D(q') \frac{\partial^2}{\partial q'^2} \right) P(q, t; q', t'), \quad (12.110)$$

where the coefficients  $v(q')$  and  $D(q')$  are the drift and diffusion coefficients defined in eqns (11.88) and (11.89). In the case of overdamped fission eqn (12.110) becomes the backward Smoluchowski equation with the coefficients  $v(q')$  and  $D(q')$  given by eqn (12.88).

*Boundary conditions.* The boundary conditions for  $P(q, t; q', t')$  in the variable  $q'$  are determined by discretizing eqn (12.110), which results in the master equation corresponding to the backward Smoluchowski equation,

$$\begin{aligned} \frac{\partial P_n^m}{\partial t} &= v_m \frac{1}{2} \left( \frac{P_n^{m+1} - P_n^m}{h} + \frac{P_n^m - P_n^{m-1}}{h} \right) \\ &+ D_m \frac{1}{h} \left( \frac{P_n^{m+1} - P_n^m}{h} - \frac{P_n^m - P_n^{m-1}}{h} \right) \end{aligned} \quad (12.111)$$

or

$$\frac{\partial P_n^m}{\partial t} = \mu_m P_n^{m-1} - (\mu_m + \lambda_m) P_n^m + \lambda_m P_n^{m+1}, \quad (12.112)$$

where the coefficients  $\mu_m$  and  $\lambda_m$  are given by the relations (12.94). For the interpretation of the backward master equation we write eqn (12.112) in the form

$$\begin{aligned} P_n^m(t - t') &= (1 - \mu_m dt - \lambda_m dt) P_n^m[t - (t' + dt)] \\ &+ \mu_m dt P_n^{m-1}[t - (t' + dt)] + \lambda_m dt P_n^{m+1}[t - (t' + dt)]. \end{aligned} \quad (12.113)$$

In this equation the conditional probability  $P_n^m(t - t')$  for the system to be in the state  $n$  at time  $t$  when it has been in the state  $m$  at the initial time  $t'$  is expressed as a sum of conditional probabilities  $P_n^{m,m\pm 1}[t - (t' + dt)]$  with initial time  $t' + dt$ . If the system has been in the state  $m$  at time  $t'$ , the states  $m \mp 1$  at time  $t' + dt$  are populated with the probabilities  $\mu_m dt$  and  $\lambda_m dt$ , respectively, which determine the strength of the contributions of the probabilities  $P_n^{m\pm 1}[t - (t' + dt)]$  on the right-hand side of eqn (12.113). Correspondingly, the strength of the contribution of the probability  $P_n^m[t - (t' + dt)]$  is diminished by  $-\mu_m dt - \lambda_m dt$ .

(i) At the reflection point ( $m = 0$ ) the master equation (12.112) yields

$$\frac{\partial P_n^0}{\partial t} = \mu_0 P_n^{-1} - \mu_0 P_n^0 + \lambda_0 (P_n^1 - P_n^0). \quad (12.114)$$

Since the system cannot start at the state  $m = -1$  beyond the reflection point, the probability  $P_n^{-1}$  should vanish in eqn (12.114). Furthermore, the term  $\mu_0 P_n^0$  represents the rate at which the initial state  $m = 0$  populates the state  $m = -1$  and should also be omitted. As before, we implement these requirements in eqn (12.114) via a boundary condition on the solution, leaving  $\mu_0$  untouched. Thus we set

$$P_n^{-1} - P_n^0 = 0. \quad (12.115)$$

Dividing this relation by  $h$  and taking the limit  $h \rightarrow 0$  yields for the boundary condition at the reflection point

$$\left. \frac{d}{dq'} P(q, t; q', t') \right|_{q' = q_{re}} = 0. \quad (12.116)$$

(ii) At the scission point the fission trajectory is absorbed. This means that if the fissioning system is at the point of absorption  $q' = q_{sc}$  at the initial time  $t'$  the probability for it to recede to a point in the region  $q_{re} < q < q_{sc}$  at a later time  $t > t'$  is zero,

$$P(q, t; q_{sc}, t') = 0. \quad (12.117)$$

### The mean fission time

Next we introduce the *mean first-passage time*  $\tau_p(q', t')$ , defined as the mean time after which a trajectory starting at a position  $q'$  at the time  $t'$  has passed the scission point  $q_{sc}$  for the first time (actually, this is the only time the trajectory passes the scission point, because there it is absorbed and leaves the region  $q_{re} < q < q_{sc}$  altogether). It is given by the integral (cf. Pontryagin *et al.* 1933; for a review see Hänggi *et al.* 1990)

$$\tau_p(q', t') = \int_{t'}^{\infty} dt' P_*(t'), \quad (12.118)$$

where  $dP_*(t) = [dP_*(t)/dt]dt$  is the probability of absorption in the time interval  $dt$  (cf. eqn (12.103)). We use the continuous form of eqn (12.102) in the integral, integrate by parts, and set  $P(q, \infty; q', t') = 0$  because after a sufficiently long time the trajectory has surely left the region  $q_{re} < q < q_{sc}$ . We then find

$$\tau_p(q', t') = \int_{t'}^{\infty} dt \int_{q_{re}}^{q_{sc}} dq P(q, t; q', t'). \quad (12.119)$$

In conformance with eqns (12.116) and (12.117), and taking account of the fact that  $P(q, t; q', t) = P(q, t - t'; q', 0)$ , the mean first-passage time satisfies the boundary conditions

$$\frac{d}{dq'} \tau_p(q', t') \Big|_{q' = q_{re}} = 0 \quad (12.120)$$

and

$$\tau_p(q_{sc}, t') = 0. \quad (12.121)$$

From expression (12.119) we can derive an equation for the mean first-passage time in the following way. We write the backward Smoluchowski equation (12.110) as

$$\frac{\partial}{\partial t} P(q, t - t'; q', 0) = L^+(q') P(q, t - t'; q', 0), \quad (12.122)$$

where we have introduced the adjoint Smoluchowski operator

$$L^+(q') = v(q') \frac{\partial}{\partial q'} + D(q') \frac{\partial^2}{\partial q'^2}. \quad (12.123)$$

We apply this operator on both sides of eqn (12.119) and use eqn (12.122) (it now becomes clear why we have to consider the *backward* Smoluchowski equation acting on the early variables  $q', t'$ ). We find

$$\begin{aligned} L^+(q') \tau_p(q', t') &= \int_{t'}^{\infty} dt \int_{q_{re}}^{q_{sc}} dq L^+(q') P(q, t - t'; q', 0) \\ &= \int_{t'}^{\infty} dt \int_{q_{re}}^{q_{sc}} dq \frac{\partial}{\partial t} P(q, t - t'; q', 0) \\ &= \int_{q_{re}}^{q_{sc}} dq [P(q, \infty; q', 0) - P(q, 0; q', 0)]. \end{aligned} \quad (12.124)$$

### 12.4 Dynamical effects in heavy-ion induced fission

Since  $P(q, \infty; q', 0) = 0$  and  $P(q, 0; q', 0) = \delta(q - q')$  by definition, eqn (12.124) becomes

$$L^+(q') \tau_p(q', t') = -1. \quad (12.125)$$

From now on we normalize the time to  $t' = 0$ ; we write for the mean first-passage time  $\tau_p(q', 0) = \tau_p(q')$  and identify it with a *mean fission time*. For the latter we then obtain from eqns (12.88), (12.123), and (12.125)

$$\left( \frac{dS}{dq'} \frac{d}{dq'} + k_B \frac{d^2}{dq'^2} \right) \tau_p(q') = -\frac{\beta M}{T}. \quad (12.126)$$

Here we have replaced the partial derivatives with ordinary derivatives since we are now dealing with a single variable.

Introducing  $w(q') = d\tau_p/dq'$  we find from eqn (12.126)

$$w(q') = \frac{\beta M}{k_B T} e^{-S(q')/k_B} \int_{q_{re}}^{q'} dz e^{S(z)/k_B}, \quad (12.127)$$

which is consistent with the boundary condition of reflection (12.120). For the mean first passage time we then have

$$\tau_p(q') = \frac{\beta M}{k_B T} \int_{q'}^{q_{sc}} dy e^{-S(y)/k_B} \int_{q_{re}}^y dz e^{S(z)/k_B}, \quad (12.128)$$

which satisfies the boundary condition of scission (12.121).

Since the initial state of the fissioning nucleus is the deformation ground state where  $q' = q_{gs}$  (the fission trajectories start out there) we obtain the mean fission time as

$$\tau_f = \frac{\beta M}{k_B T} \int_{q_{gs}}^{q_{sc}} dy e^{-S(y)/k_B} \int_{q_{re}}^y dz e^{S(z)/k_B}. \quad (12.129)$$

### The fission rate

For stationary fission the fission rate can be defined as the inverse of the mean fission time

$$R_f = \frac{1}{\tau_f}. \quad (12.130)$$

We are now in the position to write down the explicit formula for the fission rate asked for at the end of Section 12.4.1. It is derived by expanding the entropy up to quadratic terms in the inner integral in formula (12.129) around the ground-state position  $q_{gs}$  and in the outer integral around the saddle-point position  $q_{sd}$ . The inner integration is taken from  $-\infty$  to  $\infty$ , and the limit of integration  $q_{gs}$  of the outer integral is replaced with  $-\infty$ . One then obtains the explicit formula

$$R_f(E) = \frac{\tilde{\omega}_{gs} \tilde{\omega}_{sd}}{2\pi\beta} \frac{2 \exp \{[S(E, q_{sd}) - S(E, g_{gs})]/k_B\}}{1 + \text{erf}[(q_{sc} - q_{sd})\tilde{\omega}_{sd}\sqrt{M/(2T)}]}, \quad (12.131)$$

where

$$\text{erf}(x) = \frac{2}{\sqrt{\pi}} \int_0^x dt e^{-t^2}$$

is the error function. Here the saddle point and the ground state are determined by the entropy and not, as in the conventional approach, by the potential. Correspondingly, the

frequencies  $\tilde{\omega}_{\text{gs}}$  and  $\tilde{\omega}_{\text{sd}}$  are calculated from the second derivative of the entropy,

$$\begin{aligned}\tilde{\omega}_{\text{gs}} &= \sqrt{|S''|_{\text{gs}} T/M}, \\ \tilde{\omega}_{\text{sd}} &= \sqrt{S''_{\text{sd}} T/M}.\end{aligned}\quad (12.132)$$

The entropy in formula (12.131) is a function of the energy  $E$  and the angular momentum  $l$  (cf. formula (12.76) and the remark thereafter). The temperature  $T$  and the energy  $E$  are related by eqn (12.78).

Formula (12.131) exhibits the effect of the position of the scission point: the error function becomes equal to unity if the scission point is far away from the saddle point, and vanishes when the two points coincide. In the second instance the fission rate is twice that in the first case.

◇ *The Kramers limit in the overdamped case.* Let us consider the case where the scission point is far away from the saddle point and  $E \gg V(q_{\text{sd}}) > V(q_{\text{gs}})$ , and let us assume that the level density is independent of the coordinate. Expanding the entropies at the ground state and at the saddle point in  $V/E$  and writing  $(E/a)^{1/2} = k_B T$  we find

$$e^{[S(q_{\text{sd}}) - S(q_{\text{gs}})]/k_B} = e^{2\sqrt{a[E - V(q_{\text{sd}})]} - 2\sqrt{a[E - V(q_{\text{gs}})]}} \approx e^{-[V(q_{\text{sd}}) - V(q_{\text{gs}})]/k_B T}. \quad (12.133)$$

Substituting this in eqn (12.131) we obtain the *Kramers formula* for the overdamped case (cf. Kramers 1940),

$$R_f^{\text{Kramers}} = \frac{\omega_{\text{gs}} \omega_{\text{sd}}}{2\pi\beta} e^{-[V(q_{\text{sd}}) - V(q_{\text{gs}})]/k_B T}. \quad (12.134)$$

The frequencies  $\omega_{\text{gs}(\text{sd})} = \sqrt{|V''|_{\text{gs}(\text{sd})}/M}$  are here calculated from the curvatures of the potential.

Formula (12.131) improves on the Kramers formula in two respects: it includes temperature-dependent driving forces by replacing the potential with the entropy, and it takes account of the dependence of the fission rate on the position of the scission point relative to the saddle point. ◇

The explicit formula (12.131) has been derived to obtain an analytic expression describing the numerical stationary rates resulting from the dynamical Langevin calculation. In the course of this derivation we have made simplifying assumptions such as regarding the temperature  $T$  and the reduced friction coefficient  $\beta$  as independent of the fission variable  $q$ . Nevertheless comparison with calculated dynamical rates (cf. Gontchar *et al.* 1993) shows agreement within 20%.

#### 12.4.3 Example. Fission probabilities and neutron multiplicities

Formula (12.131) for the fission rate is used in the statistical cascade calculation of the fission process which has to follow the dynamical calculation if, after the delay time  $t_d = 100 \times 10^{-21}$  s, when the fission rate has become stationary, neither fission nor evaporation-residue formation has yet terminated the decay of the compound nucleus along a particular trajectory. Using this formula (with the energy  $E$ , the angular momentum  $l$ , and the friction coefficient  $\beta$  evaluated at the point where the trajectory calculation ends), together with the particle rates (10.148) (with sharp cut-off transmission coefficients, cf. Blann 1980) and the giant-dipole decay rates (12.84), one now

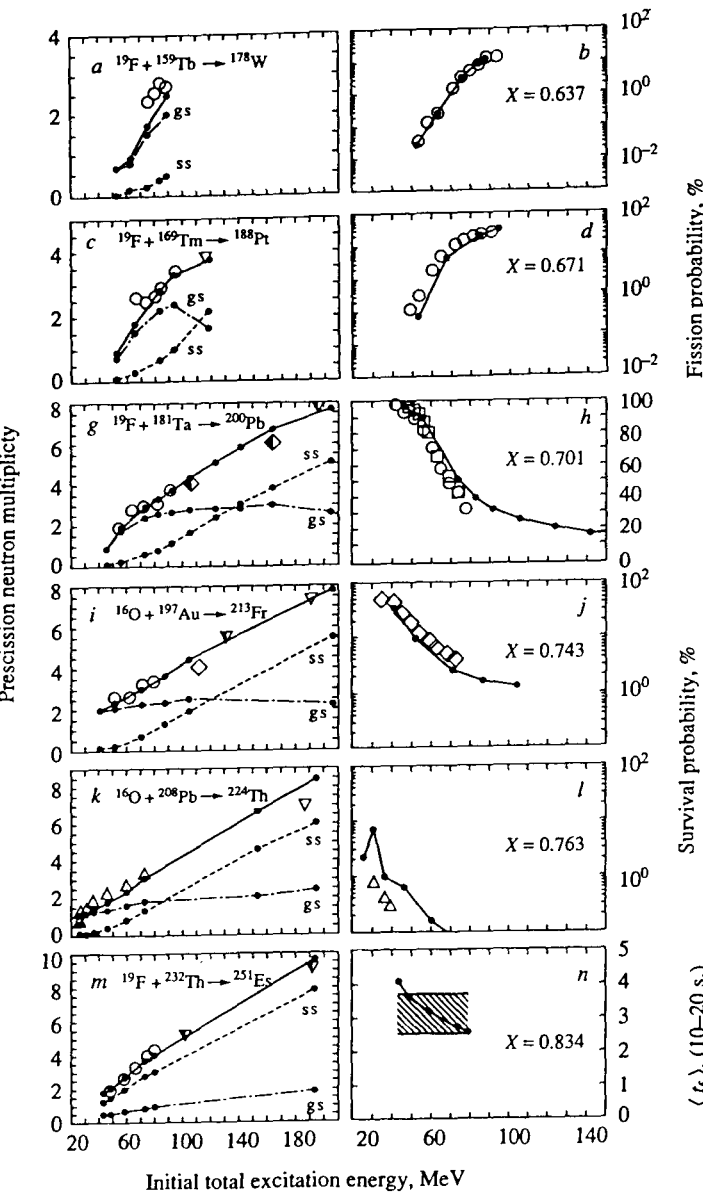


**Figure 12.25** Left side: pre-scission neutron multiplicities in heavy-ion-induced fission for six fusion-fission systems, as functions of the initial excitation energy of the compound nucleus. The ground-state-to-saddle (gs) and saddle-to-scission (ss) contributions are shown separately. Right side: fission probabilities  $P_f$  for three systems, survival probabilities  $P_{\text{surv}} = 1 - P_f$  for two systems, and the mean fission time  $t_f$  for one system. The two figures in a row refer both to the same system. The experimental data are represented by the open symbols.

follows the standard Monte Carlo cascade procedure analogous to that described in Section 10.4.3. Allowance is made for multiple evaporation of light particles and first-, second-, and higher-chance fission after the emission of no, one, two, and more light particles. After each emission act one recalculates the energy and angular momentum, and continues along the cascade until the intrinsic excitation energy has reached a value  $E^* < \min(B_v, B_f)$ , where  $B_v$  is the binding energy of particle  $v$  and  $B_f$  the fission barrier. As in the dynamical calculation, the determination of probabilities and multiplicities reduces again to the counting of events.

As an example we present in Fig. 12.25 the results of a calculation of pre-scission neutron multiplicities and fission probabilities  $P_f$  (the number of fission events divided by the total number of events) or survival probabilities  $P_{\text{surv}} = 1 - P_f$ . In Fig. 12.25n a mean fission time  $t_f$  is shown which has been calculated as the first-passage time at the scission point  $q_{\text{sc}}$  averaged over all Langevin trajectories. These results are compared with the experimental data for a number of fusion–fission systems with fissilities  $x$  in the range  $0.637 < x < 0.834$  (cf. Fröbrich *et al.* 1993; there also the references to the data are given). A satisfactory agreement between theory and experiment is obtained. This has not been possible in the conventional statistical model. We give only this one example for an illustration of the viability of the present phenomenological friction model for fission. The model has also been applied successfully to describe the general trend of the data for pre-scission charged-particle multiplicities, pre-scission giant dipole  $\gamma$ -multiplicities and spectra (cf. Fröbrich *et al.* 1993; Fröbrich and Gontchar 1993a,b; Gontchar and Fröbrich 1994a,b), fission times, energies (temperatures) at scission obtained from an analysis of post-scission neutrons (cf. Hilscher *et al.* 1994) and fission fragment angular distributions (cf. Fröbrich and Rossner 1994). For a review see Fröbrich (1994).

For the description of, for example, the energy distributions of the fission fragments one has to go over from the one-dimensional, overdamped, to the multidimensional, not overdamped, Langevin equations. There the situation is not yet satisfactory. Generally the kinetic-energy distributions come out too narrow. This may be due to the fact that mass asymmetry has not been taken into account or because the scission line has been chosen incorrectly. The omission of the mass-asymmetry degree of freedom is also the reason why, up to now, mass distributions of fission fragments have not been treated in the framework of Langevin equations.

## 12.5 Notes and references

In this chapter we have applied phenomenological Markovian friction and diffusion models in an analysis of fusion, deep-inelastic collisions, and heavy-ion induced fission. The *general trend* of a considerable amount of experimental data for a large variety of observables is well described. The test of the models by experiment does not force us, at the present state of the investigations, to abandon the simple Markovian description. On the other hand, microscopic theories disclose non-Markovian effects (cf. Berdichevsky *et al.* 1989; Hofmann 1992; and references therein).

A few refinements must certainly be added. For example, in order to reproduce the details of the heavy-ion fusion data (like the scatter of the barriers and of the widths of measured fusion probabilities) one must take nuclear shell effects into account (cf., e.g. Berdichevsky *et al.* 1989). This also holds for the description of fission at low

temperatures, where in calculating the entropy one has to go beyond the Fermi gas approximation discussed in Section 12.4. First steps in this direction have been undertaken by Gontchar and Fröbrich (1994a), who include shell effects and the collective rotational enhancement in the level densities.

An important point to clarify is to what extent quantal effects have to be added to the classical Langevin description. In particular, in the low energy regime quantal tunnelling and quantal fluctuations should play a role. It is, for instance, not yet settled whether statistical fluctuations alone can explain the observed barrier fluctuations in fusion probabilities (cf. Marten and Fröbrich 1992). Also, when the distribution function bifurcates into the fusion and deep-inelastic branches for large-mass heavy ions, the limit of the classical Langevin description will be reached at energies below the static barrier, where dissipative tunnelling must be taken into account. A theory for this process has not yet been developed to such a degree to be applicable to sub-barrier fusion of heavy ions. For attempts in this direction, see Fröbrich *et al.* (1990).

In the case of fission it has been shown by the influence functional method of Feynman, using the saddle-point approximation with complex trajectories (cf. Fröbrich and Tillack 1992) or real-time techniques (cf. Hofmann and Ingold 1991), that quantal effects do play a role, even at quite high temperatures. However, it will be difficult to identify the quantal effects in the experimental data, although they affect the fission rates appreciably. For example in the fission of  $^{224}\text{Th}$  at an excitation energy corresponding to a temperature of  $T = 1.5$  MeV the fission rate is enhanced by 20%. Unfortunately the same effect could be obtained by a reduction of the fission barrier by 0.3 MeV, which is less than the uncertainty with which the fission barriers of hot nuclei are known anyhow.

Finally, the Langevin description reproduces the measured spin distributions above the barrier using the Einstein relation for the determination of the diffusion coefficient. However, at energies below the dynamical barrier this coefficient has to be enhanced in order to account systematically for fusion cross sections as well as for spin distributions (cf. Fröbrich and Richert 1990). Therefore, more detailed investigations concerning modifications of the Einstein relation at low energies are called for (cf., e.g. Hofmann *et al.* 1989).

## References

- Adamyan, G. G., Nasirov, A.K., Antonenko, N.V. and Jolos, R.V. (1994). *Phys. Part. Nucl.* **25** 583.
- Adeev, G. D., Gontchar, I. I., Pashkevich, V. V. and Serdyuk, O. I. (1988). *Sov. J. Part. Nucl.* **19** 529.
- Agassi, D., Ko, C. M. and Weidenmüller, H. A. (1978). *Phys. Rev.* **C18** 22.
- Armbruster, P. (1985). *Ann. Rev. Nucl. Part. Sci.* **35** 135.
- Ayik, S., Wolschin, G. and Nörenberg, W. (1978). *Z. Physik* **A286** 271.
- Backe, H. (1984). In *New trends in atomic physics, Les Houches, Session XXXVIII, 1982*, eds. Grynberg, G. and Stora, R., North-Holland, Amsterdam, p. 597.
- Bao, J. D., Zhuo, Y. Z. and Wu, X. Z. (1992). *Commun. Theor. Phys.* **18** 249.
- Bao, J. D., Zhuo, Y. Z. and Wu, X. Z. (1995). *Z. Physik* **A352** 321.
- Bass, R. (1980). *Lecture notes in physics*, vol. 117, Springer, Berlin, p. 281.

- Berdichevsky, D., Lukasiak, A., Nörenberg, W. and Rozmeij, P. (1989). *Nucl. Phys.* **A499** 609.
- Berlanger, M., Grange, P., Hofmann, H., Ngô, C. and Richert, J. (1978). *Z. Physik* **A286** 207.
- Birkelund, J., Tubbs, L. E., Huizenga, J. R., De, J. N. and Sperber, D. (1979). *Phys. Rep.* **56C** 107.
- Blann, M. (1980). *Phys. Rev.* **C21** 1770.
- Blocki, J., Feldmeier, H. and Swiatecki, W.J. (1986). *Nucl. Phys.* **A459** 145.
- Bock, R., Chu, Y. T., Dakowski, M., Gobbi, A., Grosse, E., Olmi, A., Sann, H., Schwalm, D., Lynen, U., Müller, W., Bjørnholm, S., Esbensen, H., Wölfli, W. and Morenzoni, E. (1982). *Nucl. Phys.* **A388** 334.
- Bohne, W., Fröbrich, P., Grabisch, K., Hartmann, K., Lehr, H., Morgenstern, H. and Stöffler, W. (1983). *Z. Physik* **A313** 19.
- Brack, M., Damgaard, J., Jensen, A. S., Pauli, H. C., Strutinsky, V. M. and Wong, C. Y. (1972). *Rev. Mod. Phys.* **44** 320.
- Broglia, R. A., Dasso, C. H. and Winther, A. (1981). *Proc. int. school of physics 'Enrico Fermi', Varenna Course 1979*, North-Holland, Amsterdam, p. 327.
- Brosa, U., Grossmann, S. and Müller, A. (1990). *Phys. Rep.* **C197** 167.
- Dasso, C. H. and Pollarolo, G. (1989). *Phys. Rev.* **C39** 2073.
- Davies, K. T. R., Sierk, A.J. and Nix, J. R. (1976). *Phys. Rev.* **C13** 2385.
- Duchêne, G. and Haas, B. (1990). Private communication.
- Feldmeier, H. (1987). *Rep. Progr. Phys.* **50** 915.
- Feldmeier, H. and Spangenberger, H. (1985). *Nucl. Phys.* **A435** 229.
- Freiesleben, H. and Kratz, J. V. (1984). *Phys. Rep.* **C106** 1.
- Fröbrich, P. (1984a). *Phys. Rep.* **C116** 337.
- Fröbrich, P. (1984b). *J. de Physique* **C6**, **45** 425.
- Fröbrich, P. (1988). *Phys. Lett.* **B215** 36.
- Fröbrich, P. (1990). *Proc. int. school seminar on heavy-ion physics*, ed. Ivashkevich, E. W., Dubna, p. 637.
- Fröbrich, P. (1991). *Springer proc. in phys.* **58** 93.
- Fröbrich, P. (1994). In *Heavy-ion fusion: exploring the variety of nuclear properties*, eds. Stefanini, A. M. et al., World Scientific, Singapore, p. 229.
- Fröbrich, P. and Gontchar, I. I. (1993a). *Nucl. Phys.* **A563** 326.
- Fröbrich, P. and Gontchar, I. I. (1993b). *Proc. int. school seminar on heavy-ion physics*, eds. Oganessian, Yu. Ts. et al., Dubna, p. 344.
- Fröbrich, P. and Richert, J. (1990). *Phys. Lett.* **B237** 328.
- Fröbrich, P. and Rossner, H. (1994). *Z. Physik* **A349** 99.
- Fröbrich, P. and Stroth, J. (1990). *Phys. Rev. Lett.* **64** 629.
- Fröbrich, P. and Tillack, G.-R. (1992). *Nucl. Phys.* **A540** 353.
- Fröbrich, P. and Xu, S. Y. (1988). *Nucl. Phys.* **A477** 143.
- Fröbrich, P., Strack, B. and Durand, M. (1983). *Nucl. Phys.* **A406** 557.
- Fröbrich, P., Lipperheide, R. and Möhring, K. (1990). *Z. Physik* **B78** 325.
- Fröbrich, P., Gontchar, I. I. and Mavlitov, N. D. (1993). *Nucl. Phys.* **A556** 281.
- Goel, N. S. and Richter-Dyn, N. (1974). *Stochastic models in biology*, Academic Press, New York.
- Gontchar, I. I. and Fröbrich, P. (1994a). *Proc. 2nd int. conf. on dynamical aspects of nuclear fission, Smolenice, Slovakia*, eds. Kristiak, J. and Pustyl'nik, B., Dubna, p. 182.
- Gontchar, I. I. and Fröbrich, P. (1994b). *Yad. Fiz.* **57** 1249.
- Gontchar, I. I., Kosenko, G. I., Pischašov, N. I. and Serdyuk, O. I. (1992). *Sov. J. Nucl. Phys.* **55** 514.
- Gontchar, I. I., Fröbrich, P. and Pischašov, N. I. (1993). *Phys. Rev.* **C47** 2228.
- Gross, D. H. E. and Kalinowski, H. (1978). *Phys. Rep.* **C45** 175.
- Gross, D. H. E., Nayak, R. C. and Satpathy, L. (1981). *Z. Physik* **A299** 63.
- Halbert, M. L., Beene, J. R., Hensley, D. C., Honkanen, K., Semkow, T. M., Abenante, V., Sarantites, D. G. and Li, Z. (1989). *Phys. Rev.* **C40** 2558.
- Hänggi, P., Talkner, P. and Borkovec, M. (1990). *Rev. Mod. Phys.* **62** 251.
- Hilscher, D. and Rossner, H. (1992). *Ann. Phys. (Paris)* **17** 471.
- Hilscher, D., Gontchar, I. I. and Rossner, H. (1994). *Yad. Fiz.* **57** 1255.
- Hinde, D. J. (1993). *Nucl. Phys.* **A553** 255c.
- Hofmann, H. (1992). *Proc. int. conf. on nuclear structure and nuclear reactions at low and intermediate energies*, eds. Ivanova, S. P. and Ershov, S. N., Dubna, p. 292.
- Hofmann, H. and Ingold, G. R. (1991). *Phys. Lett.* **B264** 253.
- Hofmann, H., Samhammer, R. and Ockenfuss, G. (1989). *Nucl. Phys.* **A496** 269.
- Hofmann, S. (1993). *Proc. int. school seminar on heavy ion physics*, eds. Oganessian, Yu. Ts. et al., vol. 1, Dubna, p. 125.
- Hofmann, S., Armbruster, P., Folger, H., Hessberger, F. P., Leino, M., Lütgen, A., Münzenberg, G., Ninov, V., Popeko, A., Poppensieker, K., Saro, S., Schädel, M., Schött, H. J., Sümerer, K. and Wirth G. (1992). *GSI-Nachrichten* 08-92, p.6.
- Hofmann, S., Ninov, V., Hessberger, F. P., Armbruster, P., Folger, H., Münzenberg, G., Schött, H. J., Popeko, A., Yeremin, A. V., Andreyev, A. N., Saro, S., Janik, R. and Leino, M. (1995). *Z. Physik* **A350**, 277, 281.
- Ignatyuk, A. V., Itkis, M. G., Okolovich, V. N., Smirenkin, G. N. and Tishin, A. S. (1975). *Yad. Fiz.* **21** 1185.
- Kelly, L. G. (1967). *Handbook of numerical methods*, Addison-Wesley, Cambridge, MA.
- Kramers, H. A. (1940). *Physica* **7** 284.
- Kühn, W., Ruckelshausen, A., Fischer, R. D., Breitbach, G., Henrich, H. J., Metag, V., Novotny, R., Janssens, R. V. F., Khoo, T. L., Habs, D., Schwalm, D., Haas, B. and Simon, R. S. (1989). *Phys. Rev. Lett.* **62** 1103.
- Lynn, J. E. (1968). *Theory of neutron resonance reactions*, Clarendon, Oxford.
- Marten, J. and Fröbrich, P. (1992). *Nucl. Phys.* **A545** 854.
- Meyer, W. G., Viola Jr., V. E., Clark, R. G., Read, S. M. and Theus, R. W. (1979). *Phys. Rev.* **C20** 1716.
- Morse, P. M. and Feshbach, H. (1953). *Methods of theoretical physics*, McGraw-Hill, New York.
- Müller-Nehler, U. and Soff, G. (1994). *Phys. Rep.* **C246** 101.
- Myers, W. D. and Swiatecki, W. J. (1966). *Nucl. Phys.* **81** 60.
- Newton, J. O., Hinde, D. J., Charity, R. J., Leigh, R. J., Bokhorst, J. J. M., Chatterjee, A., Foote, G. S. and Ogaza, S. (1988). *Nucl. Phys.* **A483** 126.
- Newton, J. O. (1990). *Sov. J. Part. Nucl.* **21** 349.

- Ngô, C. and Hofmann, H. (1977). *Z. Physik* **A282** 83.
- Oganessian, Yu. (1994). *Cern Courier* **34** nr. 9, p. 16.
- Paul, P. and Thoennessen, M. (1994). *Ann. Rev. Part. Nucl. Sci.* **44** 65.
- Pontryagin, L. A., Andronov, A. and Vitt, A. (1933). *Zh. Eksp. Teor. Fiz.* **3** 165.
- Preston, M. A. and Bhaduri, R. K. (1975). *Structure of the nucleus*, Addison-Wesley, Cambridge, MA.
- Reinhardt, J., Müller, B., Greiner, W. and Soff, G. (1979). *Z. Physik* **A292** 211.
- Reisdorf, W. and Schädel, M. (1992). *Z. Physik* **A343** 47.
- Rhein, M., Barth, R., Ditzel, E., Feldmeier, H., Kankeleit, E., Lips, V., Müntz, C., Nörenberg, W., Oeschler, H., Piechaczek, A., Polai, W. and Schall, I. (1994). *Phys. Rev.* **C49** 250.
- Satchler, G. R. (1989). *Proc. int. nucl. phys. conf., São Paulo, Brasil*, vol. II, World Scientific, Singapore, p. 541.
- Schiff, L. I. (1968). *Quantum Mechanics*, 3rd edn, McGraw-Hill, New York.
- Schmidt, R. and Teichert, J. (1981). *J. Phys.* **G7** 1523.
- Stefanini, A. M., Corradi, L., Moreno, H., Mueller, L., Napoli, D. R., Spolaore, P., Adamides, E., Beghini, S., Segato, G. F., Soramel, F. and Signorini, C. (1990). *Phys. Lett.* **252B** 43.
- Strumberger, E., Dietrich, K. and Pomorski, K. (1991). *Nucl. Phys.* **A529** 522.
- Swiatecki, W. J. (1981). *Phys. Scr.* **24** 113.
- Szabo, A., Schulen, K. and Schulen, Z. (1980). *J. Chem. Phys.* **72** 4350.
- Thoennessen, M., Chakrabarty, D.R., Herman, M.G., Butsch, R. and Paul, P. (1987). *Phys. Rev. Lett.* **59** 2860.
- Tillack, G.-R. (1992). *Phys. Lett.* **B278** 403.
- Tillack, G.-R., Reif, R., Schülke, A., Fröbrich, P., Krappe, H. J. and Reusch, H. G. (1992). *Phys. Lett.* **B296** 296.
- Töke, J. and Swiatecki, W. J. (1981). *Nucl. Phys.* **A372** 141.
- Van den Berg, A. M., Henning, W., Lee, L. L., Lesko, K. T., Rehm, K. E., Schiffer, J. P., Stephans, G. S. F. and Wolfs, F. L. H. (1988). *Phys. Rev.* **C37** 178.
- Van Kampen, N. G. (1981). *Stochastic processes in physics and chemistry*, North-Holland, Amsterdam.
- Vandenbosch, R. (1992). *Ann. Rev. Nucl. Part. Sci.* **42** 447.
- Wada, T., Abe, Y. and Carjan, N. (1993). *Phys. Rev. Lett.* **70** 3538.
- Wilczynski, J. (1973). *Phys. Lett.* **47B** 484.
- Wolfs, F. L. H. (1987). *Phys. Rev.* **C36** 1359.
- Wolfs, F. L. H., Henning, W., Rehm, K. E. and Schiffer, J. P. (1987). *Phys. Lett.* **196B** 113.
- Wollersheim, H. J., Wilcke, W. W., Birkeland, J. R., Huijzen, J. R., Schröder, W. U., Freiesleben, H. and Hilscher, D. (1981). *Phys. Rev.* **C24** 2114.
- Yadav, H.L. and Nörenberg, W. (1982). *Phys. Lett.* **B115** 179.

## INDEX

- Abelian limit 98
- absorption cross section 13, 170
- absorption factor 303
- action, classical 54, 56
- Airy approximation
- primitive 62
  - uniform 63
- Airy function 53, 62
- analytical continuation
- of classical equations of motion 67
  - of WKB wave function 51, 293, 297
- angle-dependent phase shift method 266
- angular distribution
- in deep-inelastic collisions 368, 409, 427
  - Coulomb-like 368
  - focusing 368
  - orbiting 369
  - in (d,p) stripping 209
- angular momentum
- critical 287, 293
  - for evaporation 279
  - for fission 278, 279, 290
  - grazing 79, 80, 83, 283, 287, 293, 365, 418
  - limiting
    - for DIC 365
    - for fusion 365
    - for quasi-elastic scattering 365
    - see also* impact parameter  - angular momentum loss 407, 410
  - angular momentum operator 8
  - arrangement channel 122
  - asymmetry parameter 276, 396
  - atomic clock for DIC 439
- Baker–Campbell–Hausdorff formula 312
- barrier
- Coulomb-plus-nuclear 419
  - dynamical 411, 421
  - fission 278, 353
  - fusion 280
  - radius of 280
  - static 421
  - s-wave height of 281
  - s-wave radius of 281
- barrier fluctuation model for fusion 319
- barrier penetration
- Hill–Wheeler formula 298, 354
  - quantal 302
  - semiclassical 293
- barrier penetration model 303
- one-dimensional, failure of 303
- barrier-top resonances 66
- BCS-wave function 230
- Bessel function 60, 76, 81
- spherical 8, 11
- Bethe formula 337, 340
- Bethe–Weizsäcker formula 275
- bifurcation into fusion and DIC 432
- black nucleus 78
- body-fixed system 240
- transformation to space-fixed system 241
- Bohr’s independence hypothesis 325
- Bohr–Wheeler formula 354
- Born amplitude for nucleon exchange 203
- Born approximation 20
- coupled-channel 146
  - for transfer 260–2
  - distorted-wave 141
  - for transfer 210–23
  - plane-wave 141
  - for transfer 194–210

boundary condition  
 for backward Smoluchowski equation  
 absorbing 453  
 reflecting 453  
 for Coulomb scattering 236  
 ingoing wave 302  
 for scattering solution 5  
 for Smoluchowski equation  
 absorbing 450  
 reflecting 450  
 bound states embedded in the continuum 154  
 Breit–Wigner resonance 168  
 Brockengespenst 44  
 Brownian motion 371, 375, 388  
 Butler radius 208, 216  
 capture 276, 366, 423  
 cascade calculation  
 family-tree like 357  
 JULIAN code for 358  
 Monte Carlo like 357  
 catastrophe theory 72  
 causality 183  
 caustics 72  
 CCBA, *see* coupled-channel Born approximation  
 central-limit theorem 376  
 centre-of-mass motion 5  
 channel  
 energy 123, 145  
 Hamiltonian 124  
 momentum 123  
 spin 136  
 states 123  
 spin-coupled 136  
 channel–channel coupling, direct 156  
 channel wave functions  
 spin-coupled 235  
 completeness 235  
 orthogonality 235  
 charged-particle multiplicities,  
 pre-scission 458  
 charged-particle scattering 16–22

chemical potential 331  
 classical scattering 35–47  
 classical S-matrix theory 72  
 classification of nuclear reactions 291,  
 364  
 Clebsch–Gordan coefficient 136  
 close collisions 291  
 coherence properties of particle beam  
 115  
 complete fusion 274, 292  
 complex angular momentum 69  
 complex potential 12, 67, 151–87, 315  
 complex trajectories 68  
 complex turning points 67  
 compound-elastic cross section 167,  
 170  
 compound nucleus 273–9  
 decay modes of 273, 343–58  
 evaporation 273, 349  
 fission 274, 354  
 stability of  
 in angular momentum 278, 285  
 in mass 274, 285  
 role of barrier 277  
 temperature of 346  
 compound-nucleus reactions 322–59  
 compound reaction cross section  
 323–31  
 angle-differential 324, 327  
 angle-integrated 325, 328  
 energy-differential 329  
 Hauser–Feshbach formula 325  
 partial 325  
 compound resonances 167  
 compound states 160, 273  
 computer simulation of Langevin process 396  
 continuity equation 12  
 correlation function 377  
 correlation time 377  
 Coulomb  
 deflection function 39  
 excitation  
 multiple 247  
 semiclassical treatment of 266

function  
 irregular 23  
 outgoing 23, 236  
 regular 21, 236  
 monopole–quadrupole interaction  
 412  
 phase shift 19, 21  
 polarization potential 251–60  
 equivalent local 253  
 imaginary part of 257  
 real part of 256  
 potential  
 deformed 242  
 spherical part of 243  
 in surface friction model 412  
 of uniform charge distribution 22  
 radius 22, 247  
 rainbow 61, 65, 71  
 scattering amplitude 19  
 stationary-phase approximation  
 59  
 S-function 22  
 Coulomb–nuclear interference 25  
 Coulomb-plus-nuclear potential,  
 multipole expansion of 244  
 Coulomb-plus-nuclear scattering 22  
 coupled-channel Born approximation  
 146  
 one-nucleon transfer 261  
 two-nucleon transfer 261  
 coupled channels 143–9, 232–67  
 algorithms for solution 237  
 coupling matrix element 236  
 for rotations 246  
 spin-coupled 244  
 for vibrations 250  
 deep-inelastic collisions 267  
 fusion 306, 313  
 inelastic scattering 144, 233–51  
 partial-wave expansion 233  
 rotational excitations 245  
 spin–orbit coupling 238  
 vibrational excitations 248  
 coupled reaction channels 147, 262–5  
 inelastic scattering 264

non-orthogonality terms 148  
 one-neutron transfer 265  
 one-proton transfer 264  
 covariance in Fokker–Planck description 389  
 CRC, *see* coupled reaction channels  
 critical angular momentum 287, 293  
 for evaporation 279  
 for fission 278, 279, 290  
 critical distance model 287  
 cross section  
 absorption 13, 170  
 angle-differential 327  
 from asymptotic wave packets 114  
 classical 37  
 for multiple trajectories 43  
 compound reaction 323–31  
 compound-elastic 167  
 differential 6, 39, 115  
 energy-differential 329  
 evaporation 344  
 fluctuation 169, 323  
 fusion 172, 322  
 classical 279, 282  
 geometric 282  
 inelastic 236  
 reaction 13  
 differential 133  
 energy-averaged 170  
 Rutherford 19, 40  
 shape-elastic 168  
 total 15  
 total elastic 6, 10  
 cut-off angular momentum  
 for complex potential 15  
 for Coulomb-plus-nuclear potential  
 24  
 for short-range potential 11

de Broglie wave length 370  
 decay law, exponential 356  
 decay modes of compound nucleus  
 273, 343–58  
 decay probability 325  
 decay rates 346–58

deep-inelastic collisions 292, 363–401  
 charge and mass diffusion 428  
 energy–angle correlation 369, 415  
 energy loss in 367, 370, 375  
 phenomena 364–71  
 spin distribution of, by Monte Carlo sampling 435  
 temperature in 380  
 theoretical framework 370  
 theories of,  
 classical friction model 400  
 diabatic dissipative dynamics 401  
 linear response theory 401  
 proximity theory of friction 400  
 random matrix model 400  
 surface-friction model 404–40  
 TDHF 401  
 deep-inelastic cross section  
 differential  
 in Gaussian approximation 395, 427  
 by Monte Carlo sampling 432  
 total 428  
 by Monte Carlo sampling 434  
 deflection angle 36, 410  
 negative 370  
 relation to scattering angle 37  
 deflection function 36, 416  
 connection with WKB phase shift 56  
 Coulomb 39  
 in surface-friction model 409  
 deformation parameter 240  
 $\delta$ -electrons 439  
 density matrix of wave packets 116  
 density of states and entropy 333  
 detailed balance, principle of 135  
 for compound reaction cross section 326  
 for partial reaction cross section 141, 325  
 deuteron  
 amplitude 206  
 wave function 207, 215  
 diabatic dissipative dynamics 401

DIC, *see* deep-inelastic collisions  
 differential cross section 4  
 classical 39  
 elastic 6  
 differential reaction cross section 133  
 diffraction  
 by black nucleus 80  
 Fraunhofer 76, 80  
 Fresnel 76  
 in nuclear scattering 78  
 in optics 76  
 sharp-cut-off model 81  
 smooth-cut-off model 88  
 diffusion coefficient 378, 384  
 for charge transfer 426  
 diffusion constant 386  
 diffusion equation 385  
 direct reactions 193–230, 232–67  
 coupled channels 232–67  
 single-step approximations 193–230  
 to unbound states 230  
 dispersion relations 181–6  
 causality 183  
 for GOP 181  
 for optical potential 182  
 subtracted 185  
 dispersion theory of nuclear reactions 204, 230  
 dissipative phenomena 364–71  
 distance of closest approach 36, 39  
 distant collisions 291  
 distorted channel states 124, 155  
 distorted-wave Born approximation 141, 210–23  
 for (d,p) reaction 214  
 for nucleon transfer 210–23  
 post form 143  
 prior form 143  
 distorted wave function 210  
 distorting potential 210  
 distribution function 382  
 doorway states 160  
 double differential cross section  
 deep-inelastic 367

Wilczynski plot 427  
 (d,p) stripping cross section  
 in DWBA 216  
 in PWBA 207  
 drift coefficient 384  
 driving force of fission  
 from entropy 443  
 from free energy 444  
 driving potential for mass and charge 276, 388  
 from liquid-drop model 426  
 with shell effects 396  
 DWBA, *see* distorted-wave Born approximation  
 effective potential 36, 280  
 eigenchannels 306  
 Einstein relation 378, 391  
 modification of 437, 459  
 elastic scattering 3–32  
 elastic transfer 149  
 energy–angle correlation in deep-inelastic collisions 369, 415  
 energy average of cross sections and amplitudes 167  
 energy fluctuations 341  
 energy loss 367, 370, 375, 408, 410  
 energy release 275  
 energy shift 159  
 ensemble, grand-canonical 331  
 entrance channel effects 287, 290  
 entrance-channel model 418  
 entropy 333, 444  
 and density of states 333  
 equilibration of heat bath 376  
 equilibration time 380  
 equipartition theorem  
 classical 377  
 quantal 378  
 equivalent local potential 174–81  
 Ericson fluctuations 359  
 Euler angles 241, 245  
 evaporation  
 cascades 357  
 competition with fission 354  
 cross section 344  
 rate 349  
 residue 273, 346, 357  
 spectrum 346  
 excitation probability for Coulomb excitations 247  
 extra-extra push 422  
 extra push 417, 420, 433  
 at the barrier 421  
 farside scattering 38, 58  
 fast fission 276, 292, 366, 423  
 Fermi energy 334, 337  
 Fermi gas model 331–8  
 excitation energy 336  
 level density parameter 336  
 occupation number 333  
 temperature 336  
 Fermi's golden rule 349  
 Feynman graph 198  
 finite-range calculation 220  
 fissility parameter 278, 421  
 fission  
 barrier 278, 353  
 Bohr–Wheeler formula 354  
 competition with evaporation 354  
 coordinate 351, 442  
 dynamical phase 442–9  
 energies at scission 458  
 Fokker–Planck approach for 442  
 fragments  
 angular distribution of 458  
 kinetic-energy distribution of 442  
 Langevin approach for 442  
 mean fission time 454  
 path 351  
 potential 352, 444  
 probability 441, 456  
 prompt 279  
 rate 351  
 connection with mean first-passage time 455  
 dynamical 448  
 stationary 449

saddle point 352  
scission point 351, 441, 445, 447, 451, 453  
stationary phase 449–56  
temperature in 443  
times 458  
transition state 352  
fluctuation cross section 169, 323  
fluctuation-dissipation theorem 378  
fluctuation strength coefficient 378  
Fokker–Planck description 382–96  
covariance 389  
mean value 385, 389  
variance 385, 389  
Fokker–Planck equation  
connection with Langevin equation 383  
examples  
Brownian motion 388  
charge transfer 426  
with constant coefficients 385  
with linear drift term 387  
Wilczynski plot 426  
Gaussian approximation 392  
moment expansion method 392  
quasi-linear approximation 392  
folding potential 162, 406  
formal theory  
of potential scattering 93–119  
of reactions 121–49  
form factor  
in DWBA 213  
friction 413  
in zero-range 218  
Fourier–Bessel transform 254  
Fraunhofer  
condition 76, 79  
differential cross section 82  
diffraction 30, 76, 80  
free energy 444  
Fresnel  
condition 77, 79  
differential cross section 86  
diffraction 30, 76, 83  
as Coulomb rainbow 66

function 78  
integral 85  
friction  
coefficient 374  
temperature dependence of 445  
in fission 442  
form factor 406  
internal-vibrational 413  
radial 413  
tangential 413  
hypothesis 370  
parameters, universal  
for DIC 415  
for fission 445  
quantal effects 459  
radial 406  
tangential 406  
frictional coupling 413  
frictional force  
energy loss due to 375  
Markovian 375  
non-Markovian 374  
fusion 271–319  
above barrier 279–93  
in surface-friction model 417–23  
barrier 280, 351  
dynamical 421  
static 421  
barrier fluctuation model for 319  
complete 274, 292  
coupled channels 306, 313  
critical distance model 287  
cross section 172, 322, 328  
classical 279, 282, 289  
by Monte Carlo sampling 434  
partial 326, 328  
and reaction cross section 282  
with friction 419  
without friction 418  
incomplete 274, 292  
and nuclear excitations 304, 306  
optical model for 315  
rate 349  
spin distribution of 292, 318  
by Monte Carlo sampling 435

in stars 271  
sub-barrier 293–319  
two-channel model for 306  
in TDHF 319  
fusion–evaporation 276  
fusion–fission 276  
fusion-absorption model 315–8  
fusion-absorption potential 315  
 $\gamma$ -multiplicities 367  
 $\gamma$ -radiation rate 355  
Gamow factor 20  
Gaussian ansatz, multidimensional 392, 426  
generalized optical potential (GOP), 152–64  
giant dipole  $\gamma$ -emission 441, 446  
giant dipole  $\gamma$ -multiplicities 458  
glory  
classical 40, 43  
meteorological 44, 71  
semiclassical 60  
grand-canonical ensemble 331  
grand partition sum 332  
grazing angle 78  
grazing angular momentum 79, 80, 83, 283, 287, 293, 365, 418  
grazing collisions 291  
grazing impact parameter 280  
Green function 103, 253  
Coulomb 257  
free, coordinate representation 201  
free, momentum representation 201

Hamiltonian  
channel 124  
internal 124  
rotational 246  
in shell model 154  
total 125  
vibrational 249  
Hamilton–Jacobi equation 178  
Hauser–Feshbach formula 325  
including direct reactions 327

heat bath 375  
temperature of 377  
Heun method 430  
Hill–Wheeler formula 298, 354  
hot nuclei 441  
hypergeometric function 18, 256  
asymptotic behaviour of 18  
identical particle scattering  
classical 25  
quantal 27  
with spin 28  
impact parameter 36,  
grazing 79, 80, 83, 280  
*see also* angular momentum  
incomplete fusion 274, 292, 420  
index of refraction 13  
inelastic scattering state 144  
inertia parameter 443  
influence functional method 401, 459  
ingoing-wave boundary condition 302  
interaction time 397, 440  
interference of trajectories 59  
inverse scattering problem 31  
use in strong absorption model 89  
knock-out reactions 230  
K-quantum number 245  
Kramers formula 456  
Kramers–Moyal expansion 383  
Langer modification 51, 53  
Langevin description 371–81  
Langevin equation  
applicability to DIC 379  
computer simulation of Langevin process 396  
higher-order algorithms for 400  
connection with Fokker–Planck equation 383  
discretization 380  
of Itô 381  
of Stratonovich 381  
examples  
angular distribution 432

mass transfer 396  
 Wilczynski plot 431  
 for fission 447  
 frictional force 373  
 Langevin force 375  
 Monte Carlo sampling in  
     surface-friction model 429–40  
     multidimensional 379  
     renormalized potential 373  
 Laplace transform 338  
     inverse 339  
 Legendre polynomials 8  
     asymptotic form 56  
     relation to Bessel function 60  
 level density 329, 331–43  
     collective enhancement of 343  
     in Fermi gas model 331  
 formula  
     constant-temperature 342  
     degeneracy of spin states 342  
     derivation of 340  
     practical 342  
 in nuclear shell model 338  
 parameter 336  
     deformation dependence of 444  
     empirical value of 337  
     of Fermi gas 337  
 lifetime 356  
 linear response theory 401  
 Lippmann–Schwinger equation 102,  
     127  
 liquid-drop model 276, 444  
 local momentum 223, 294  
 logarithmic phase factor 19, 22  
 Markovian process 382  
 Maslov index 72  
 mass density 406  
 mass operator 187  
 mean first-passage time 454  
 mean fission time 454  
 mean lifetime 356  
 mean value in Fokker–Planck  
     description 385, 389  
 memory time 374

micro-reversibility, principle of 107,  
     134  
 Møller operator 99, 126  
 Monte Carlo sampling 396  
 Mott formula 28  
 multifragmentation 274, 292  
 multi-nucleon transfer 230  
 multiple excitation  
     Coulomb 247  
     Coulomb and nuclear 247  
 multiple reflections 296  
 multipole coefficient in DWBA  
     T-matrix 212  
 multipole expansion 242  
 nearside scattering 37, 58  
 neck rupture 429  
 negative deflection angle 370  
 Neumann function, spherical 11  
 neutron multiplicity, pre-scission 355,  
     441, 456  
 neutron optics 89  
 Nilsson states 245  
 non-local potential 163  
     of Frahn–Lemmer type 180  
 non-Markovian friction 440  
 no-recoil approximation 223  
 nose-to-nose geometry 411  
 no-spin-flip selection rule 229  
 nuclear contact time 440  
 nuclear rainbow 61, 70  
 nuclear reactions, classification of  
     291, 364  
 occupation number in Fermi gas model  
     333  
 off-energy-shell  
     nucleon 198, 201  
     T-matrix 106  
 on-energy-shell  
     S-matrix 109  
     T-matrix 106  
 one-step processes 450  
 optical model 151–87  
     for fusion 315

S-matrix  
     compound part 167  
     direct part 165  
 T-matrix  
     compound part 167  
 optical potential 13  
     absorptive part 183  
     analyticity of 161  
     for bound states 187  
     dynamical part 153  
     equivalent local 174–81  
         in WKB 175  
         trivially 174  
     generalised (GOP), 152–64  
     non-locality of 162  
     in nuclear matter 187  
     and Pauli principle 163  
     polarization part 183  
     in proper sense 164, 170  
     in schematic model 154  
     static part 153, 157  
     theories of 187  
     time-dependent 183  
 optical theorem 16, 110  
     for charged particles 32  
     generalized 132  
 orbiting 40, 43  
     barrier-top resonances 66  
     classical 44  
     in deep-inelastic collisions 369  
 overdamped motion 414, 445  
 pairing vibration 230  
 parabolic barrier, tunnelling through  
     297  
 parabolic coordinates 17  
 parity 205  
     change in nucleon transfer 212  
     non-normal change of 220  
     normal change of 219  
     selection rule 226  
 partial fusion cross section 328  
 partial rate 356  
 partial-wave expansion 8  
     for Coulomb scattering 21  
     for coupled channels 233  
 partial width 159, 166, 356  
 particle beam  
     coherence properties of 115  
     model for 117  
 particle current density 7  
 particle emission  
     post-scission 441  
     pre-scission 441, 446, 447  
 particle number fluctuations 341  
 Pauli principle 149  
     and optical potential 163  
 Pawula lemma 384  
 Perey factor 179  
 phase shift 9  
     calculation of 11, 25  
     complex 14  
     Coulomb 19, 21  
     nuclear 24  
     in semiclassical approximation  
         48–56  
 phonons  
     annihilation operator for 249  
     creation operator for 249  
     excitation of 249  
 physical sheet on Riemann surface  
     154, 161  
 pick-up reactions 194  
 plane-wave Born approximation 141,  
     194–210  
     for (d,p) reaction 206  
     for nucleon transfer 194–210  
     projectile amplitude 197  
     target structure factor 197  
     T-matrix, interpretation of 198  
 Poisson sum formula 56  
 population line 287  
 post-scission particles 274  
 potential  
     Coulomb  
         deformed 242  
         spherical part of 243  
     Coulomb-plus-nuclear, multipole  
         expansion of 244  
     distorting 142

folding 162, 406  
 fusion-absorption 315  
 non-local 163  
   of Frahn–Lemmer type 180  
 nuclear, deformed 241  
 nucleon–nucleus 406  
 optical 151–87  
   short-range 4  
 potential scattering 3  
   example of 29  
   formal theory of 93–119  
   quantum theory of 3–32  
 time-dependent formalism 93–100  
 time-independent formalism  
   100–10  
   wave-optical description 75–89  
 pre-compound reactions 346, 359  
 pre-equilibrium particle emission 274  
 pre-scission particles 274  
 probability current density 6  
 probability current, physical, structure  
   of 115  
 projectile break-up 274  
 projectile disintegration 198  
 prompt fission 279  
 propagator of nucleon 201  
 proximity theory of friction 400  
 PWBA, *see* plane-wave Born  
   approximation  
 quarter point recipe 86  
 quasi-elastic collisions 291  
 quasi-elastic scattering 433  
   and the reaction cross section 259  
 quasi-linear approximation 394  
 $Q$ -value 125  
   effective 226  
   for fusion 287  
 $Q$ -window 219, 225  
 radius, expansion in spherical  
   harmonics 240  
 rainbow 40  
   in  $\alpha$ -scattering 72  
   bright side 63

classical 44  
 Coulomb 61, 65, 71  
 dark side 63  
 meteorological 44, 71  
 nuclear 61, 70  
 semiclassical 61  
   singularity 42  
 random matrix model 400  
 random numbers  
   Gaussian-distributed 381, 398  
   generation of 398  
   uniformly distributed 398  
 random variables 376  
 rate 346–58  
   evaporation 349  
   fission 351  
   fusion 349  
    $\gamma$ -radiation 355  
   giant dipole  $\gamma$ -emission 446  
   partial 356  
   reaction 347  
   relation to width 356  
 Rayleigh dissipation function 406,  
   408, 413  
 reaction cross section 13–15, 364  
   angle-differential  
    direct part 324  
    fluctuating part 324  
   angle-integrated 140  
   compound 323–31  
   differential 133, 136  
    unpolarized 138  
   and fusion cross section 282  
   partial 14, 140, 364  
   and quasi-elastic scattering 259  
 reaction rate 347  
 reactions  
   compound-nucleus 322–59  
   direct 193–230, 232–67  
   formal theory of 121–49  
   knock-out 230  
   nuclear, classification of 291, 364  
   pick-up 194  
   stripping 194

reaction states 125  
   completeness 129  
   orthogonality 127  
   stationary 127  
     asymptotic form of 133  
   time-dependent 126  
   time-reversed 127  
 recoil effects 221  
 reduced amplitude  
   in DWBA 213  
   in finite-range 220  
   in zero-range 218, 222  
 reduced friction parameter 445  
 reduced local wavelength 49  
 reduced mass 5  
 reduced matrix element 244  
   for rotational excitations 246  
   for vibrational excitations 251  
 reduced transition probability 247  
 reflection coefficient 15  
 refractive scattering 70  
 re-orientation effect 247  
 residual interaction  
   for coupled channels 233  
   in (d,p) reaction 214  
   in DWBA 142, 210  
   in shell model 156  
 Riemann surface, physical sheet on  
   154, 161  
 $R$ -matrix theory 358  
 rotational excitations, coupled-channel  
   treatment 245  
 rotational states 246  
 rotation matrix 241  
 Rutherford cross section 19, 40  
 saddle point for fission 352  
 saddle-point method 69, 339  
 scattering  
   charged-particle 16–22  
   classical 35–47  
   Coulomb-plus-nuclear 22  
   deep-inelastic 363–401  
   elastic potential 3–32  
   inelastic 144, 233–51  
 quantum 3–32  
 semiclassical 34–72  
 scattering amplitude  
   connection with  $T$ -matrix 111  
   Coulomb 19  
     in stationary-phase approximation 59  
   elastic 5, 8  
   nuclear 22  
   in WKB 56  
 scattering states  
   completeness 105  
   inelastic 144  
   orthogonality 105  
 stationary 100  
   asymptotic form of 111  
   relation to time-dependent states 101  
 time-dependent 97  
   time-reversed 99  
 Schrödinger equation  
   many-body 126  
   non-local 176  
   stationary 5, 101  
   time-dependent 94, 97  
     in optical model 184  
 scission point 351, 441, 445, 447, 451,  
   453  
 screening of Coulomb field 19  
 selection rules  
   classical, in transfer 223  
   no-spin-flip 229  
   parity 226  
 semiclassical approximation  
   for complex potentials 67  
   for phase shift 48–56  
   of the partial wave function 50  
   uniform 71  
   validity of 49  
   *see also* WKB, 47–72  
 semiclassical method 55  
 semiclassical scattering 34–72  
 $S$ -function for elastic scattering 10  
 shape-elastic cross section 168

sharp-cut-off model  
for diffraction 81  
for fusion 282, 292  
shell effects 285, 396  
shell-model  
elastic  $S$ -matrix 164  
ground state 154  
Hamiltonian 154  
states 154, 204  
shell-model theory of nuclear reactions 154, 359  
shift operator 222  
single-nucleon transfer 227  
single-particle density of states 335, 338  
single-step approximations 193–230  
 $6$ - $j$  symbol 244  
 $S$ -matrix 132  
connection with  $T$ -matrix 108  
for elastic scattering 10  
energy-averaged 323  
fluctuating part of 323  
on-shell 109, 132  
partial-wave representation 112  
for potential scattering 108  
relation to phase shift 112  
spin-coupled 138  
unitarity of 109, 132  
Smoluchowski equation 449  
backward 452  
smooth-cut-off model for diffraction 88  
Sommerfeld parameter 17, 39  
space-fixed system 240  
transformation to body-fixed system 241  
spectroscopic amplitude 204  
spectroscopic coefficient 213  
spectroscopic factor 204  
spin cut-off parameter 342  
spin distribution  
of fusion 292  
by Monte Carlo sampling  
of DIC 435  
of fusion 435

of nuclear reactions 364  
unitarity limit 436  
spin flip 226  
stationary-phase approximation 57  
stationary point 57  
stationary reaction states 127  
asymptotic form of 133  
stationary scattering states 100  
asymptotic form of 111  
stationary Schrödinger equation 101  
sticking limit 440  
stripping angle 209  
stripping reactions 194  
strong absorption model 87  
sub-barrier fusion 293–319  
sudden limit 306, 308  
superheavy elements 285, 438  
surface-friction model  
Coulomb potential in 412  
for deformable nuclei 410–40  
equations of motion 414  
Rayleigh dissipation function 413  
Fokker–Planck equation, Gaussian  
solution of 425  
friction parameters, universal 415  
Monte Carlo sampling of  
trajectories 429  
nuclear potential in 412  
for rigid nuclei 405–10  
equations of motion 407

target structure factor 204

TDHF  
for deep-inelastic collisions 401  
for fusion 319

temperature  
of compound nucleus 346  
in DIC 380  
of Fermi gas 336  
in fission 443  
of heat bath 377

$3$ - $j$  symbol 244

threshold, inelastic 158, 159

time reversal invariance 108

time reversal operator 134

$T$ -matrix 130  
connection with scattering  
amplitude 111  
off-shell 106  
on-shell 106, 131  
post form 105, 130  
for potential scattering 105  
prior form 106  
spin-coupled 137  
 $T$ -operator 106, 131  
total cross section 15  
deep-inelastic 366  
elastic 6  
energy-averaged 171  
fusion 366  
quasi-elastic 367  
total Hamiltonian 125  
total width 166  
trajectories  
complex 68  
multiple 40, 43  
interference of 59  
transition probability 382  
transition rate 160  
transition state 352  
transmission  
complete 293  
near the barrier top 296  
partial 293  
transmission coefficient 14–15  
absorption factor 303  
barrier penetrability factor 303  
for black nucleus 81  
in Hauser–Feshbach formula 330  
Hill–Wheeler formula 298, 354  
optical 171, 327  
for parabolic barrier 298  
for partial waves 300  
in two-channel model 307  
in WKB 293, 296

tunnelling through parabolic barrier 297

turning point 36, 40  
complex 67

turning-point branch 68

two-channel model for fusion 306  
two-nucleon transfer in CCBA 261  
two-potential formula 143  
unitarity limit of spin distribution 436  
van der Waals potential 256  
variance  
of energy 341  
of particle number 341  
variance in Fokker–Planck description 385, 389  
vertex  
function 200  
interaction 202  
vibrational excitations,  
coupled-channel treatment 248  
vibrational Hamiltonian 249  
vibrational states 250  
wave-optical description of potential  
scattering 75–89  
wave packet  
asymptotic form of 112  
free 93  
of scattering state 98  
size of 95  
spherical 113  
spreading of 95, 119  
for two particles 96  
Weisskopf estimate 355  
Weisskopf–Ewing formula 346  
width 356  
relation to rate 356  
Wigner–Eckart theorem 246, 251  
Wigner transform 176  
Wilczynski plot 368, 415  
WKB  
for complex potentials 69  
connecting formula 51  
for free wave 53  
phase shift, connection with  
deflection function 56  
scattering amplitude 56  
solution for equivalent local  
potential 175

- validity of 180
- wave function 50, 51, 293
- see also* semiclassical approximation
- Wong formula 300
- Woods–Saxon potential 30
  - deformed 241, 247
  - singularities of 67
- Wronskian 294
- yrast line 286
  - statistical 287
- Yukawa potential 203
- Z-coefficient 139
- zero-point fluctuation formula 308
  - rotational excitations 311
  - vibrational excitations 311
- zero-point fluctuations 312, 379
- zero-range approximation 217